Assessment of Regional Earthquake Hazards and Risk Along the Wasatch Front, Utah

U.S. GEOLOGICAL SURVEY PROFESSIONAL PAPER 1500–A–J

Contributions from Utah Geological and Mineral Survey, University of Utah, and Utah State University

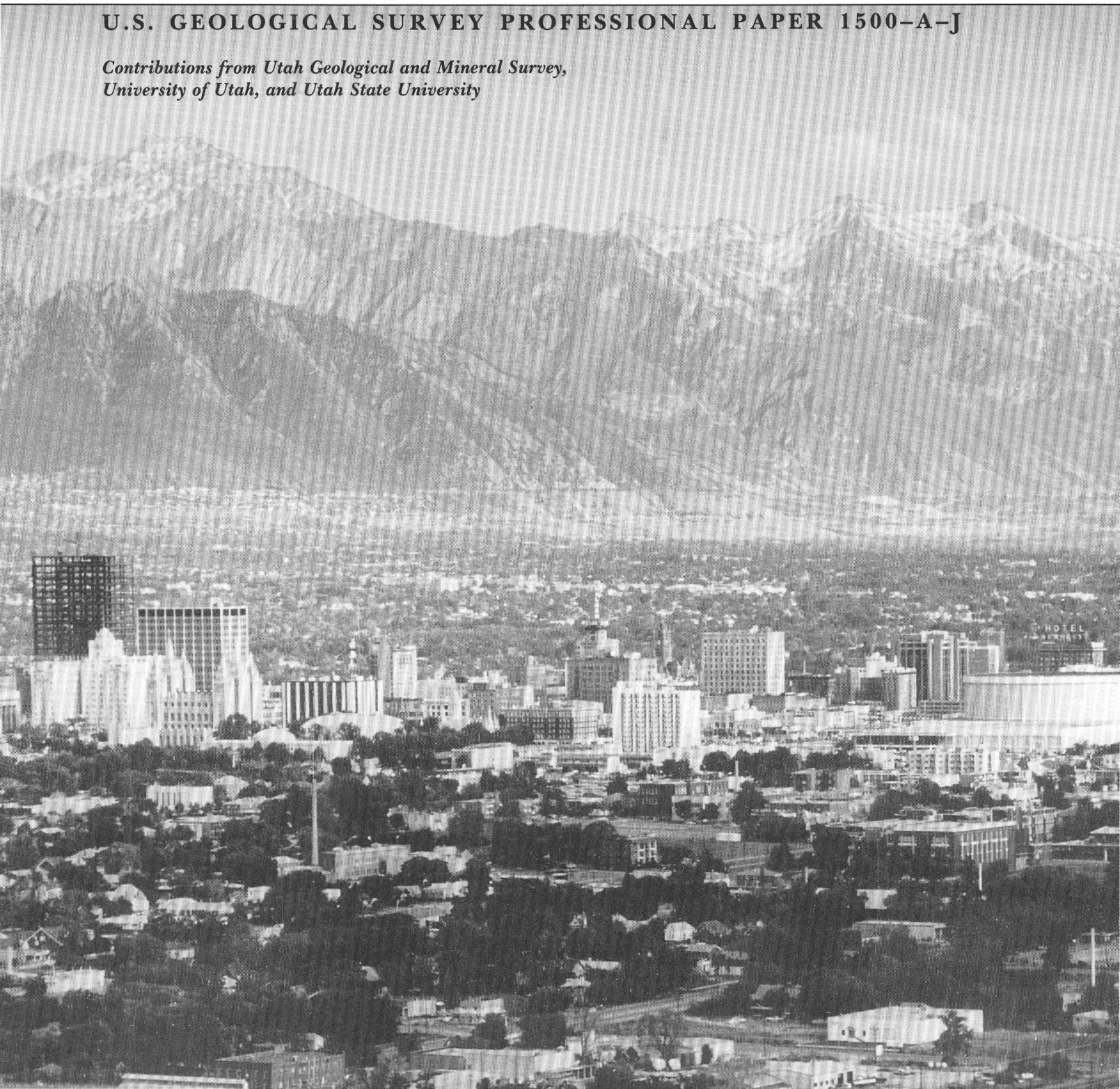

AVAILABILITY OF BOOKS AND MAPS OF THE U.S. GEOLOGICAL SURVEY

Instructions on ordering publications of the U.S. Geological Survey, along with prices of the last offerings, are given in the current-year issues of the monthly catalog "New Publications of the U.S. Geological Survey." Prices of available U.S. Geological Survey publications released prior to the current year are listed in the most recent annual "Price and Availability List." Publications that are listed in various U.S. Geological Survey catalogs (**see back inside cover**) but not listed in the most recent annual "Price and Availability List" are no longer available.

Prices of reports released to the open files are given in the listing "U.S. Geological Survey Open-File Reports," updated monthly, which is for sale in microfiche from U.S. Geological Survey Book and Open-File Report Sales, Box 25425, Denver, CO 80225. Reports released through the NTIS may be obtained by writing to the National Technical Information Service, U.S. Department of Commerce, Springfield, VA 22161; please include NTIS report number with inquiry.

Order U.S. Geological Survey publications **by mail** or **over the counter** from the offices given below.

BY MAIL

Books

Professional Papers, Bulletins, Water-Supply Papers, Techniques of Water-Resources Investigations, Circulars, publications of general interest (such as leaflets, pamphlets, booklets), single copies of Earthquakes & Volcanoes, Preliminary Determination of Epicenters, and some miscellaneous reports, including some of the foregoing series that have gone out of print at the Superintendent of Documents, are obtainable by mail from

U.S. Geological Survey, Book and Open-File Report Sales
Box 25425
Denver, CO 80225

Subscriptions to periodicals (Earthquakes & Volcanoes and Preliminary Determination of Epicenters) can be obtained ONLY from the

Superintendent of Documents
Government Printing Office
Washington, D.C. 20402

(Check or money order must be payable to Superintendent of Documents.)

Maps

For maps, address mail orders to

U.S. Geological Survey, Map Sales
Box 25286
Denver, CO 80225

Residents of Alaska may order maps from

U.S. Geological Survey, Map Sales
101 Twelfth Ave. - Box 12
Fairbanks, AK 99701

OVER THE COUNTER

Books

Books of the U.S. Geological Survey are available over the counter at the following U.S. Geological Survey Public Inquiries Offices, all of which are authorized agents of the Superintendent of Documents:

- **ANCHORAGE, Alaska**—Rm. 101, 4230 University Dr.
- **ANCHORAGE, Alaska**—Federal Bldg., Rm. E–146, 701 C St.
- **DENVER, Colorado**—Federal Bldg., Rm. 169, 1961 Stout St.
- **LAKEWOOD, Colorado**—Federal Center, Bldg. 810
- **MENLO PARK, California**—Bldg. 3 (Stop 533), Rm. 3128, 345 Middlefield Rd.
- **RESTON, Virginia**—503 National Center, Rm. 1C402, 12201 Sunrise Valley Dr.
- **SALT LAKE CITY, Utah**—Federal Bldg., Rm. 8105, 125 South State St.
- **SAN FRANCISCO, California**—Customhouse, Rm. 504, 555 Battery St.
- **SPOKANE, Washington**—U.S. Courthouse, Rm. 678, West 920 Riverside Ave.
- **WASHINGTON, D.C.**—Main Interior Bldg., 2600 corridor, 18th and C Sts., NW.

Maps

Maps may be purchased over the counter at the U.S. Geological Survey offices where books are sold (all addresses in above list) and at the following U.S. Geological Survey offices:

- **ROLLA, Missouri**—1400 Independence Rd.
- **DENVER, Colorado**—Map Distribution, Bldg. 810, Federal Center
- **FAIRBANKS, Alaska**—New Federal Bldg., 101 Twelfth Ave.

Assessment of Regional Earthquake Hazards and Risk Along the Wasatch Front, Utah

PAULA L. GORI *and* WALTER W. HAYS, *Editors*

U.S. GEOLOGICAL SURVEY PROFESSIONAL PAPER 1500–A–J

Contributions from
Utah Geological and Mineral Survey,
University of Utah, and
Utah State University

Chapters A–J are issued as a single volume and are not available separately. Chapter titles are listed in the volume table of contents.

UNITED STATES GOVERNMENT PRINTING OFFICE, WASHINGTON : 1992

U.S. DEPARTMENT OF THE INTERIOR

MANUEL LUJAN, Jr., *Secretary*

U.S. GEOLOGICAL SURVEY

Dallas L. Peck, *Director*

Library of Congress Cataloging in Publication Data

Assessing regional earthquake hazards and risk along the Wasatch Front, Utah / Paula L. Gori and Walter W. Hays, editors.
p. cm. — (U.S. Geological Survey professional paper ; 1500)
Supt. of Docs. no.: I 19.16:1500A–J
1. Earthquake hazard analysis—Wasatch Range (Utah and Idaho) 2. Seismology—Wasatch Range (Utah and Idaho) 3. Natural disasters—Utah. 4. Faults (Geology)—Wasatch Range (Utah and Idaho) 5. Geology, Stratigraphic. 6. Geology—Wasatch Range (Utah and Idaho) I. Gori, Paula. II. Hays, Walter W. III. Series.
QE535.2.U6A84 1991
551.2'2'097922—dc20 90-26385
CIP

For sale by Book and Open-File Report Sales, U.S. Geological Survey, Federal Center, Box 25425, Denver, CO 80225

CONTENTS

[Letters designate the chapters]

(A) Paleoseismology of the Wasatch Fault Zone: A Summary of Recent Investigations, Interpretations, and Conclusions, by Michael N. Machette, Stephen F. Personius, and Alan R. Nelson

(B) Persistent and Nonpersistent Segmentation of the Wasatch Fault Zone, Utah: Statistical Analysis for Evaluation of Seismic Hazard, by Russell L. Wheeler and Katherine B. Krystinik

(C) Subsurface Geology Along the Wasatch Front, by Don R. Mabey

(D) Observational Seismology and the Evaluation of Earthquake Hazards and Risk in the Wasatch Front Area, Utah, by W.J. Arabasz, J.C. Pechmann, and E.D. Brown

(E) Superimposed Late Cenozoic, Mesozoic, and Possible Proterozoic Deformation Along the Wasatch Fault Zone in Central Utah, by Mary Lou Zoback

(F) Neotectonic Framework of the Central Sevier Valley Area, Utah, and Its Relationship to Seismicity, by R. Ernest Anderson and Theodore P. Barnhard

(G) Neotectonics of the Hansel Valley-Pocatello Valley Corridor, Northern Utah and Southern Idaho, by James McCalpin, Robert M. Robison, and John D. Garr

(H) Structure of the Salt Lake Segment, Wasatch Normal Fault Zone: Implications for Rupture Propagation During Normal Faulting, by R.L. Bruhn, P.R. Gibler, W. Houghton, and W.T. Parry

(I) Late Quaternary Displacement on the Morgan Fault, a Back Valley Fault in the Wasatch Range of Northeastern Utah, by J. Timothy Sullivan and Alan R. Nelson

(J) Late Quaternary History of the James Peak Fault, Southernmost Cache Valley, North-Central Utah, by Alan R. Nelson and J. Timothy Sullivan

ASSESSMENT OF REGIONAL EARTHQUAKE HAZARDS
AND RISK ALONG THE WASATCH FRONT, UTAH

INTRODUCTION

By PAULA L. GORI and WALTER W. HAYS

THE EARTHQUAKE THREAT

> There are many geologists who are very wise, but even they do not understand the forces which produce mountains. And yet it must be admitted, not only that mountains have been made, but that some mountains are still rising. The mysterious forces appear to act in different ways in different places, and it is possible that their nature is not universally the same. Suffice it to say that in the Great Basin the movements they cause are vertical. It is as though something beneath each mountain was slowly, steadily, and irresistibly rising, carrying the mountain with it.

So began an article in 1883 by Grove Karl Gilbert, the first Chief Geologist of the U.S. Geological Survey (USGS), warning the citizens of the Great Basin about the potential for damaging earthquakes in their region. Describing the damage and loss of life in a small town in California that he had just visited after an earthquake, Gilbert cautioned that a similar earthquake could occur in Salt Lake City. "It is useless to ask when this disaster will occur. Our occupation of the country has been too brief for us to learn how fast the Wasatch grows; and indeed, it is only by such disasters that we can learn. By the time experience has taught us this, Salt Lake City will have been shaken down...." (Gilbert, 1883, p. 4).

After more than a century of research, geologists and other scientists have increased their understanding of the tectonic processes at work in the Wasatch Front and are now beginning to answer the questions about the seismicity and tectonics of the Wasatch Front that Gilbert and others first posed. Scientists, engineers, architects, urban planners, and emergency managers are not waiting for a major earthquake disaster to learn that measures must be implemented to mitigate an earthquake's effects. They are taking actions now to prepare for and to mitigate the physical effects of such an earthquake.

The majority of Utah's population lives adjacent to the Wasatch fault zone (fig. 1), an active, north-trending zone of normal faulting that extends approximately 370 km at the western foot of the Wasatch Range. Earthquakes have been reported since the arrival of the Mormon pioneers in 1847. During the last two centuries, eight earthquakes of magnitude[1] greater than or equal to 6 have occurred in Utah. The two largest were the magnitude (M_L) 6.6 Hansel Valley earthquake of 1934 (fig. 2) and the M_L 6.5 Richfield earthquake of 1901.

The historical record of seismicity in Utah has been broadened by incorporating geologic evidence and monitoring small earthquakes. Although no large earthquakes (M>7.0) have occurred since Utah was settled, clear geologic and geomorphic evidence (Hamblin, 1976) demonstrates that large earthquakes have occurred repeatedly throughout the late Pleistocene (2 million years before present) and Holocene (last 10,000 years) on segments within the Wasatch fault zone. For this reason and because of the continuing low level of seismicity, scientists believe that some parts of segments of the Wasatch fault zone are overdue for a damaging earthquake (Schwartz and Coppersmith, 1984). Machette and others (this report) have identified 10 segments of the Wasatch fault that have produced large earthquakes on the average of every several hundred to 1,000 years.

[1]Magnitude is a "number that characterizes the size of an earthquake, based on measurement of the maximum motions recorded by a seismograph for earthquake waves of a particular frequency. Scales most commonly used in the Western United States are (1) local magnitude (M_L) (commonly referred to as "Richter magnitude"), (2) surface-wave magnitude (M_S), and (3) body-wave magnitude (m_b). None of these scales satisfactorily measures the largest possible earthquakes because each relates to only certain frequencies of seismic waves and because the spectrum of radiated seismic energy changes with earthquake size. The recently devised moment magnitude (*M*) scale, based on the concept of seismic moment, is uniformly applicable to all sizes of earthquakes" (Ziony, 1985, p. 18).

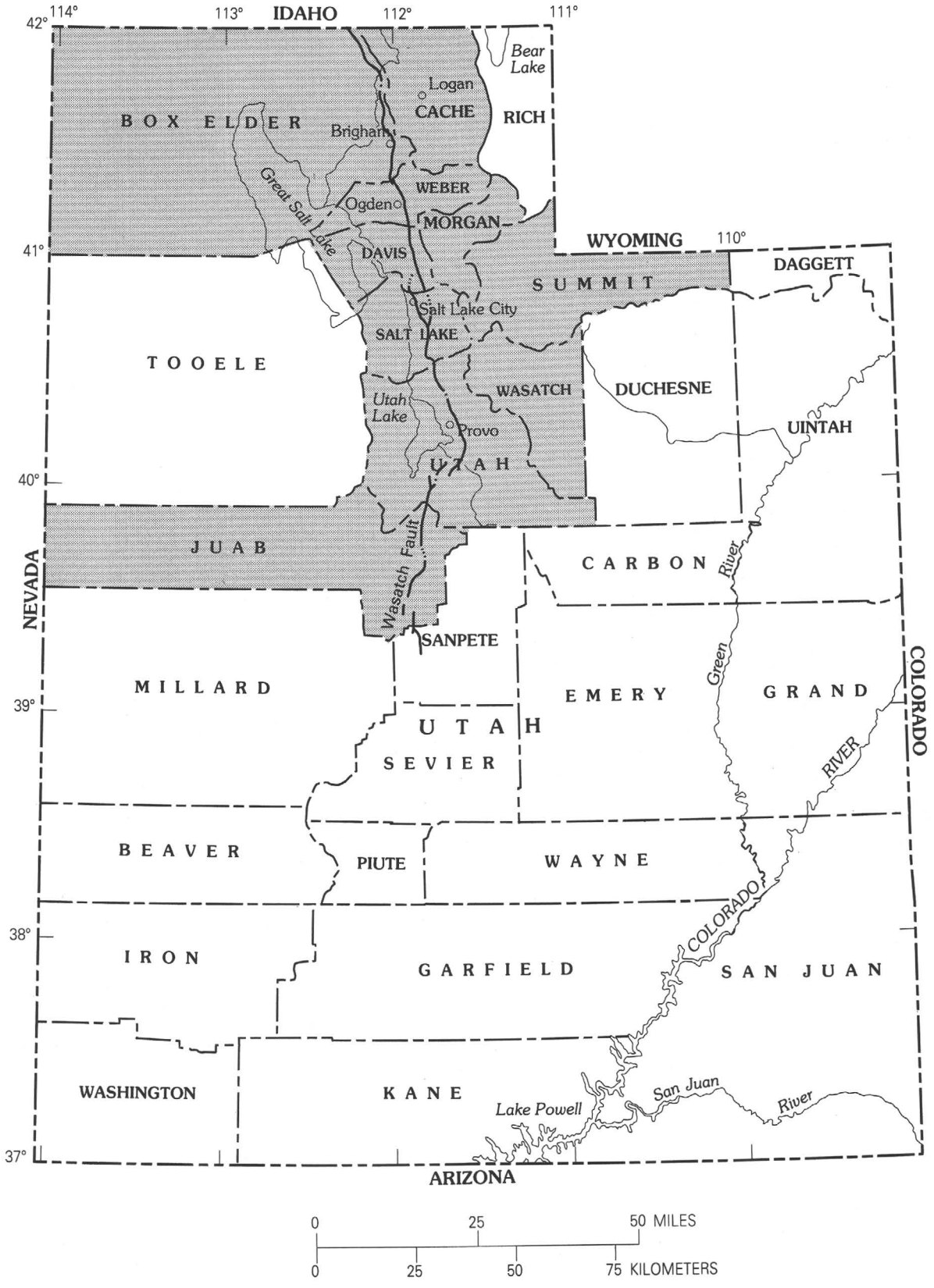

FIGURE 1.—Location map of the Wasatch Front study area (shaded), northern Utah. Generalized fault locations are also shown.

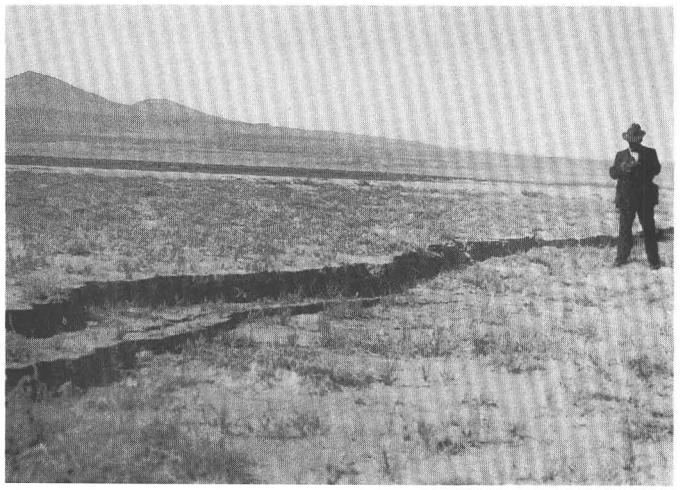

FIGURE 2.—Fault scarp formed in Utah's Hansel Valley north of Great Salt Lake in the 1934 Hansel Valley earthquake.

Utah's largest urban centers, where more than 80 percent of the State's 2 million people live, are located along the Wasatch Front. A large earthquake centered near Salt Lake City has the potential to cause extensive damage to buildings, lifelines, and public facilities. The expected level of peak ground acceleration would be in the range of 0.2 to 0.4 *g* or greater. Surface-fault rupture and tectonic deformation (fig. 3) as well as landslides and liquefaction would be expected to occur in many areas (fig. 4). Death and injury rates could be high, depending on the time of day that the earthquake struck and the nature and extent of pre-event mitigation actions.

The October 28, 1983, Borah Peak, Idaho, magnitude (M_S) 7.3, earthquake reminded scientists and policymakers that large earthquakes will recur in the Intermountain Seismic Belt (fig. 5). Scientists believe that the Borah Peak earthquake is a model of what might happen on the Wasatch Front (Smith and Richins, 1984). A magnitude 7.0 to 7.5 earthquake is now being considered as a scenario earthquake for emergency response planning in Utah.

PURPOSE AND SCOPE OF THIS VOLUME

In 1983, the USGS proposed the Wasatch Front of Utah as the target of a 5-year program of focused research on earthquake hazards and hazards reduction. The goals were to (1) accelerate the development of the knowledge base on seismic sources, size, frequency of occurrence, and physical effects of earthquakes in a 10-county area along the Wasatch Front, including Salt Lake, Davis, Juab, Weber, Wasatch, Summit, Morgan, Cache, Utah, and Box Elder Counties and (2) foster implementation of earthquake hazards mitigation measures.

The USGS earthquake hazards program in the Wasatch Front area was conducted under the auspices of the "Regional Earthquake Hazards Assessment" element, one of five elements in the USGS' Earthquake Hazards Reduction Program. The element was established to provide concentrated and coordinated attention to geographic regions containing large urban areas at risk from earthquakes by utilizing past research and fostering partnerships with universities, the private sector, local government, and State and Federal agencies. The effort provides a technical basis for devising and implementing mitigation and loss reduction measures.

The five interrelated goals in the Utah comprehensive research and implementation program were:

Information systems.—To produce quality data along with a comprehensive information system, available to both USGS and non-USGS users, for use in earthquake hazards evaluations, risk assessment, and implementation of loss reduction measures.

Synthesis of geological and geophysical data.—To prepare synthesis reports describing the nature, extent, frequency of occurrence, and physical effects of the earthquake hazards of ground shaking, surface faulting, earthquake-induced ground failure, and tectonic deformation and recommend future research to increase the knowledge base required for the creation and implementation of mitigation and loss-reduction measures.

Ground-motion modeling.—To produce deterministic and probabilistic ground-motion models and maps of the ground-shaking hazard and commentaries on their use in building codes and land use regulations.

Loss estimation models.—To devise economical methods for acquiring inventories of structures and lifeline systems in urban areas, to create a standard model for loss estimation, to produce loss and casualty estimates for urban areas, and to prepare commentaries giving guidelines for use by agencies of State and local governments.

Implementation.—To foster the creation and implementation of measures to mitigate the earthquake hazards of ground shaking, surface-fault rupture, earthquake-induced ground failure, and tectonic deformation in urban areas and to provide high-quality scientific information that can be used by local government decisionmakers as a basis for implementing and enforcing loss-reduction measures.

This report provides a comprehensive treatment of the knowledge gained by the research and implementation program in the Wasatch Front area. The two volumes are divided into three sections dealing with individual components of the program that collectively define the nature of the earthquake hazards in the Wasatch Front area. The first volume deals with tectonic framework and

FIGURE 3.—Interested bystanders studying fault rupture formed in the 1934 Hansel Valley, Utah, earthquake. From the Thomas Adams Collection; courtesy of the Department of Geology and Geophysics, University of Utah, Provo.

earthquake potential. The second volume covers (1) ground-shaking hazards and aspects of loss estimation and (2) use of earthquake hazards information for urban and regional planning and development. The research results came from studies conducted by scientists and engineers of the USGS, the Utah Geological and Mineral Survey, universities, and private consulting firms. Funding was provided primarily by the USGS in the form of grants to non-USGS scientists and engineers.

TECTONIC FRAMEWORK AND EARTHQUAKE POTENTIAL OF THE WASATCH FRONT AREA

The first volume of Professional Paper 1500 contains chapters devoted to geologic and geophysical studies aimed at improving the fundamental understanding of the potential for the occurrence of large, damaging earthquakes in the Wasatch Front area. In some cases, researchers have drawn on studies of other parts of Utah and the Intermountain Seismic Belt to gain an understanding of the large-magnitude earthquakes that may occur in the Wasatch Front. The geologic and seismological/geophysical studies comprising this section are described in Chapters A through J:

Chapter A: Paleoseimology of the Wasatch Fault Zone: A Summary of Recent Investigations, Interpretations, and Conclusions, by Michael N. Machette, Stephen F. Personius, and Alan R. Nelson. Ten discrete segments have been identified on the Wasatch fault zone. The fact that eight of these segments have demonstrable Holocene movement increases the possible number of separate localities where earthquakes may occur.

Chapter B: Persistent and Nonpersistent Segmentation of the Wasatch Fault Zone, Utah: Statistical Analysis for Evaluation of Seismic Hazard, by Russell L. Wheeler and Katherine B. Krystinik. The Wasatch fault zone has been segmented at four salients—Pleasant View, Salt Lake, Traverse Mountains, and Payson—throughout much or all of its 10-m.y. history and will likely continue to be segmented there throughout the next several millenia, which is the time span of interest for hazard evaluation.

Chapter C: Subsurface Geology Along the Wasatch Front, by Don R. Mabey. Magnetic data suggest segment boundaries of the Wasatch fault zone that are generally consistent with segment boundaries inferred from surface mapping of the fault zone.

Chapter D: Observational Seismology and the Evaluation of Earthquake Hazards and Risk in the Wasatch Front Area, Utah, by W.J. Arabasz, J.C. Pechmann, and E.D. Brown. Background seismicity predominates on second-order faults in the Wasatch Front area.

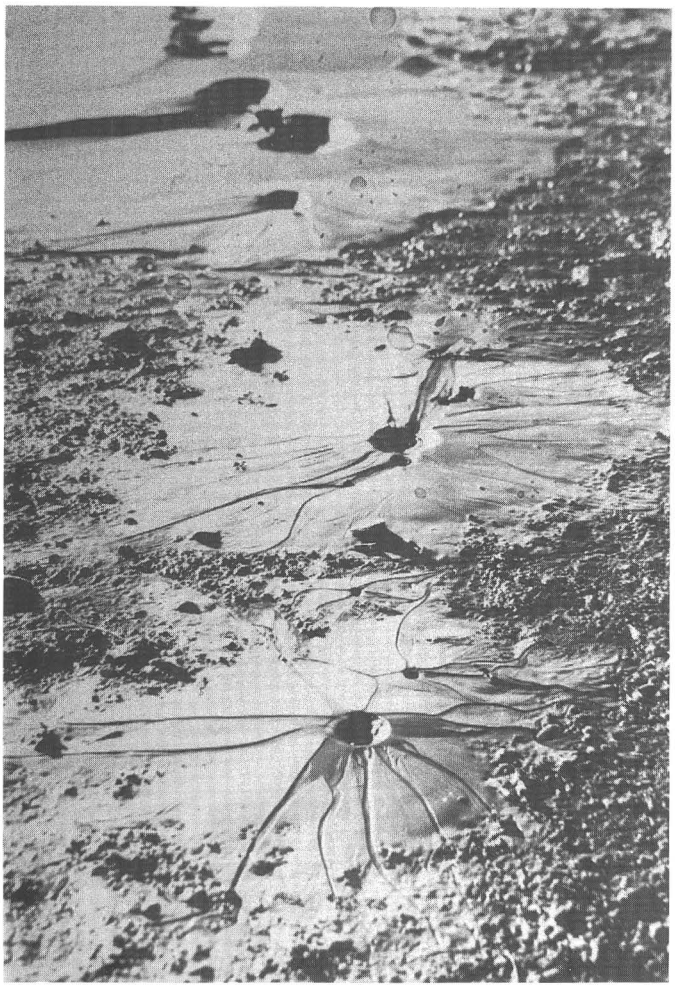

FIGURE 4.—Sand boils caused by liquefaction associated with the 1934 Hansel Valley, Utah, earthquake.

Small to moderate earthquakes are the largest contributor to the probabilistic ground-shaking hazard for exposure periods of 50 years or less. The earthquake data imply an average return period of 24±10 years for potentially damaging earthquakes of magnitude 5.5 or greater along the Wasatch Front.

Chapter E: Superimposed Late Cenozoic, Mesozoic, and Possible Proterozoic Deformation Along the Wasatch Fault Zone in Central Utah, by Mary Lou Zoback. Thrust ramping and late Cenozoic normal faulting may be localized by a major west-dipping normal fault zone formed during the early phases of late Precambrian rifting of the western Cordillera.

Chapter F: Neotectonic Framework of the Central Sevier Valley Area, Utah, and Its Relationship to Seismicity, by R. Ernest Anderson and Theodore P. Barnhard. Normal faults in the Wasatch fault zone such as the Sevier fault probably cut one or more levels of potential structural detachment and penetrate to the base of the seismogenic part of the crust. Such faults are more likely to be the source of infrequent large earthquakes than are faults in the complex structural junctures where late Quarternary deformation is concentrated.

Chapter G: Neotectonics of the Hansel Valley-Pocatello Valley Corridor, Northern Utah and Southern Idaho, by James McCalpin, Robert M. Robison, and John D. Garr. The 1934 M_L 6.6 earthquake may be a typical interpluvial maximum event (that is, long recurrence time and small displacement in comparison with the larger, more frequent surface-faulting events that are triggered by pluvial lake water loading).

Chapter H: Structure of the Salt Lake Segment, Wasatch Normal Fault Zone: Implications for Rupture Propagation During Normal Faulting, by R.L. Bruhn, P.R. Gibler, W. Houghton, and W.T. Parry. There are two potential sites of rupture initiation for large earthquakes at the central and southern ends of the Salt Lake fault segment of the Wasatch normal fault zone. The central site may have been the most common position for repetitive rupture initiation during the last 17 million years.

Chapter I: Quaternary Displacement on the Morgan Fault, a Back Valley Fault in the Wasatch Range of Northeastern Utah, by J. Timothy Sullivan and Alan R. Nelson. Paleoearthquakes having magnitudes in the range of 6.5 to 7 have occurred on the Morgan fault.

Chapter J: Late Quaternary History of the James Peak Fault, Southernmost Cache Valley, North-Central Utah, by Alan R. Nelson and J. Timothy Sullivan. The James Peak fault may be a westerly splay of the East Cache fault rather than a separate valley-bounding fault.

THE GROUND-SHAKING HAZARD AND ASPECTS OF LOSS ESTIMATION IN THE WASATCH FRONT AREA

The second volume of Professional Paper 1500, which will be published under separate cover, is concerned with predicting the effects of local site conditions on ground shaking in the Wasatch Front area and developing loss (risk) estimation procedures. Ground-motion and loss estimation studies comprising this section are described in Chapters K through T:

Chapter K: Site Amplification in the Salt Lake City-Ogden-Provo, Utah, Corridor and the Implications for Earthquake-Resistant Design, by Walter W. Hays. Evaluation of site amplification effects in Utah indicates that soil deposits in the Salt Lake City-Ogden-Provo urban corridor should amplify earthquake ground motions, especially when the level of shear strain induced in the soil column is less than about 0.5 percent.

FIGURE 5.—Graben formed in the fault rupture of the 1983 Borah Peak, Idaho, earthquake.

Chapter L: Predicting Strong Ground Motion in Utah, by Kenneth W. Campbell. Near-source attenuation relationships for predicting peak horizontal acceleration and velocity in terms of earthquake magnitude, source-to-site distance, and several sources and site parameters are used to estimate strong ground motion in north-central Utah.

Chapter M: Probabilistic Analysis of Earthquake Ground-Shaking Hazards Along the Wasatch Front, Utah, by R.R. Youngs, F.H. Swan, M.S. Power, D.P. Schwartz, and R.K. Green. The ground-shaking hazard along the Wasatch Front urban corridor has been assessed by using the geologic and seismologic data base that has been developed for the region.

Chapter N: Relative Ground Response in Salt Lake City and Areas of Springville-Spanish Fork, Utah, by Kenneth W. King, Robert A. Williams, and David L. Carver. To predict the ground-shaking intensity

potential for the Wasatch Front urban corridor, a better understanding of how shallow underlying geology affects ground shaking was developed.

Chapter O: In Situ Poisson's Ratio Measurements Near Provo, Utah, by Richard D. Miller, Don W. Steeples, Kenneth W. King, and Ralph W. Knapp. Classification of sites according to their response to earthquake energy enables engineers to accurately determine structural requirements for individual sites in high- to moderate-risk earthquake zones.

Chapter P: Earthquake Losses in Central Utah, by T.S. Algermissen, Edward P. Arnold, Karl V. Steinbrugge, Margaret G. Hopper, and Philip S. Powers. Estimates of losses in central Utah have been made for a series of simulated earthquakes. Expected maximum losses in the Salt Lake City urban corridor in 50 years at a 10-percent chance of exceedance were also found. The losses range from $830 million for a M_L 5.5 shock on the Provo segment to $5.5 billion for a M_S 7.5 quake on the Salt Lake segment.

Chapter Q: Isoseismals of Some Historical Earthquakes Affecting the Wasatch Front Area, Utah, by Margaret G. Hopper. Isoseismals were drawn for 13 historical earthquakes that caused damage-level intensities (MMI>VI)[2] in the four Wasatch Front counties of Weber, Davis, Salt Lake, and Utah. The highest historical intensity within any of the four counties was MMI VII.

Chapter R: Effects of Six Damaging Earthquakes in Salt Lake City, Utah, by Sherry D. Oaks. Modified Mercalli intensities of historical earthquakes indicate that intensity increases across Salt Lake City from the Wasatch fault zone to the Jordan River Valley by 2 to 3 intensity units and from east of the Utah State Capitol building south to 17th Street by 1½ intensity units (increase in ground-shaking from east to west and from north to south).

Chapter S: Seismic Risk Methods and Estimates for Utility Systems and State-Owned Buildings Along the Wasatch Front, by Craig E. Taylor, Delbert B. Ward, and Jerold M. Haber. Results of seismic risk projects on Utah facilities reaffirm the iterative nature of these projects.

Chapter T: Earthquake Hazards to Domestic Water Distribution Systems in Salt Lake County, Utah, by Lynn M. Highland. In a magnitude 7.5 earthquake occurring along the Wasatch Front in Utah, significant damage may occur to Salt Lake County's domestic water system.

[2]Intensity is "a subjective numerical index describing the severity of an earthquake in terms of its effect on the Earth's surface and on humans and their structures" (Ziony, 1985, p. 18).

USE OF EARTHQUAKE HAZARDS INFORMATION FOR URBAN AND REGIONAL PLANNING AND DEVELOPMENT IN THE WASATCH FRONT AREA

Chapters U through Z describe the use of earthquake hazards information to reduce potential loss of life and damage to property after a damaging earthquake.

Chapter U: Making the Implementation Process of the National Earthquake Hazards Reduction Program Work in Utah, by Walter W. Hays. Utah has the necessary elements of a program to implement loss reduction measures designed to mitigate earthquake hazards.

Chapter V: Reducing Earthquake Risk in Utah: Past Trends and Future Opportunities, by Genevieve Atwood and Don R. Mabey. Utah's political and social structure produces factors that both enhance and impede programs to reduce earthquake risk.

Chapter W: Emergency Management in Utah for Earthquakes, by James L. Tingey and Ralph F. Findlay. The major challenge facing the Utah State Division of Comprehensive Emergency Management has been to provide leadership for the implementation of preparedness and other mitigation strategies within the cities, counties, and State agencies of Utah.

Chapter X: Utah Geological and Mineral Survey Excavation and Inspection Program: A Tool for Earthquake Hazard Recognition in Utah, by Harold E. Gill. Results of the Utah Geologic and Mineral Survey excavation inspection program have shown the zone of deformation along the Wasatch fault to be highly variable and, in some locations, up to several hundred meters wide.

Chapter Y: Fall Hazard Susceptibility Due to Earthquakes, Central Wasatch Front, Utah, by William F. Case. Loss of life and property along a widespread area of the Wasatch Front could result from rock falls triggered by nearby earthquakes.

Chapter Z: Legal Issues Related to Hazard Mitigation Policies, by James E. Slosson. Professionals involved in the design, construction, and maintenance of structures and facilities may be held to the high standards of practice established outside of Utah. Also, planners and public officials may become targets in future litigation and share the burden of court-imposed penalties.

SUMMARY

Efforts to assess regional earthquake hazards and risk along the Wasatch Front in Utah are dynamic and multidisciplinary. This report reflects the nature of that program and the research conducted before 1988. Not only are the topics varied—geology, seismology,

engineering geology, urban planning, law, economics, and so on—but the level of complexity is also varied. Seismologists and geologists can draw upon many years of research in their disciplines in Utah, whereas researchers in engineering, land use planning, and implementation have had to be pioneers in their fields.

The timeliness and importance of the research contained herein have made it desirable to publish this report before the completion of all the research conducted during the 5 years of the program. The results from ongoing research in Utah will be included in a second professional paper (Professional Paper 1519) published as a sequel to this one. Eventually, the tectonic processes and their physical and social effects in the Wasatch Front will be truly understood and documented.

REFERENCES CITED

Gilbert, G.K., 1883, Earthquakes: *Salt Lake Daily Tribune*, Sept. 16, 1883, p. 4.

Hamblin, W.K., 1976, Patterns of displacement along the Wasatch fault: Geology, v. 4, p. 619–622.

Schwartz, D.P., and Coppersmith, K.J., 1984, Fault behavior and characteristic earthquakes: Examples from the Wasatch and San Andreas fault zones: Journal of Geophysical Research, v. 89, no. B7, p. 5681–5698.

Smith, R.B., and Richins, W.D., 1984, Seismicity and earthquake Hazards of Utah and the Wasatch Front: Paradigm and paradox, *in* Hays, W.W., and Gori, P.L., eds., Proceedings of Conference XXVI, a workshop on Evaluation of regional and urban earthquake hazards and risk in Utah: U.S. Geological Survey Open-File Report 84–763, p. 73–112.

Ziony, J.I., ed., 1985, Evaluating earthquake hazards in the Los Angeles region—An earth-science perspective: U.S. Geological Survey Professional Paper 1360, 505 p.

Paleoseismology of the Wasatch Fault Zone: A Summary of Recent Investigations, Interpretations, and Conclusions

By MICHAEL N. MACHETTE, STEPHEN F. PERSONIUS, *and* ALAN R. NELSON

ASSESSMENT OF REGIONAL EARTHQUAKE HAZARDS AND RISK ALONG THE WASATCH FRONT, UTAH

U.S. GEOLOGICAL SURVEY PROFESSIONAL PAPER 1500–A

CONTENTS

	Page
Abstract	A1
Introduction	1
Trenching Along the Wasatch Fault Zone	2
Age Determinations	6
Acknowledgments	7
Regional Quaternary Geologic Framework	7
Segmentation of the Wasatch Fault Zone	10
Segments and Segment Boundaries	10
Types of Segment Boundaries	11
Segmentation Models for the Wasatch Fault Zone	11
Segment Lengths	13
Historical Earthquakes and Surface Ruptures	14
Northern Wasatch Fault Zone	17
Segments Along the Malad Range	17
Collinston Segment	19
Central Wasatch Fault Zone	20
Brigham City Segment	20
Weber Segment	23
Salt Lake City Segment	29
Provo Segment	34
American Fork Part	34
Central Part	39
Spanish Fork Part	40
Central Wasatch Fault Zone—Continued	
Nephi Segment	A42
Southern Wasatch Fault Zone	45
Levan Segment	45
Fayette Segment	47
Summary of Segmentation of the Wasatch Fault Zone	48
Chronology of Recent Movement on the Central Wasatch Fault Zone: A Synopsis	48
Recurrence of Large Earthquakes on the Wasatch Fault Zone	50
Discussion of Slip-Rate Data for the Wasatch Fault Zone	51
Possible Causal Relation Between Deep Cycles of Lake Bonneville and High Rates of Slip on the Wasatch Fault Zone	53
Conclusions	54
References Cited	55
Appendix	61
Dating Techniques and Methodology	63
Radiocarbon Calibration	63
Apparent Mean Residence ^{14}C Ages of Soils	68
Dating the Formation of an A Horizon	69
References Cited	71

ILLUSTRATIONS

		Page
FIGURE 1.	Map showing location of sites along segments of the Wasatch fault zone	A3
2.	Schematic diagram showing probable levels of Lake Bonneville during the past 150,000 years	9
3.	Diagrams showing four types of structural features at some suggested segment boundaries of the Wasatch fault zone	12
4, 5.	Nomograms showing:	
4.	Lengths of the surface traces of proposed segments on some major faults in the northern Basin and Range province	15
5.	Proposed segment lengths for prehistoric faults less than 100 km long and more than 100 km long in the northeastern part of the Basin and Range province	16
6, 7.	Maps showing:	
6.	Northern part of the Wasatch fault zone between Malad City, Idaho, and Honeyville, Utah	18
7.	Brigham City segment of the Wasatch fault zone between Honeyville and North Ogden, Utah	21
8.	Part of the log of trench BC–1 near Brigham City, Utah	22
9, 10.	Maps showing:	
9.	Weber segment of the Wasatch fault zone between North Ogden and Bountiful, Utah	24
10.	Vertical exposure across a fault scarp at the mouth of Garner Canyon near Ogden, Utah	25
11, 12.	Diagrams showing:	
11.	Amounts of displacement and times of fault events recorded in five trenches at the East Ogden site	26
12.	Fault displacements and times of fault events derived from trenching and dating studies at three sites along the Weber segment of the Wasatch fault zone	28

Page

FIGURE 13. Map showing the traces of the Salt Lake City segment A30
14. Aerial photograph showing the surficial geology at the South Fork of Dry Creek site, Salt Lake City segment of the Wasatch fault zone 31
15. Map showing the main trace of the Provo segment of the Wasatch fault zone between the Traverse Mountains and Dry Mountain 35
16. Part of the log of trench AF–1 at the American Fork Canyon site, Provo segment of the Wasatch fault zone 37
17. Schematic diagram showing times of faulting deciphered from three trenches at the American Fork Canyon site, Wasatch fault zone 38
18, 19. Maps showing:
18. Nephi segment of the Wasatch fault zone 43
19. Levan and Fayette segments of the Wasatch fault zone 46
20. Histogram showing estimated timing of major surface ruptures on segments of the Wasatch fault zone during the past 6,000 years 49
21. Schematic diagram showing some slip rates on the Wasatch fault zone for different time intervals as determined from deposits of Holocene to middle Quaternary age 52

TABLES

Page

TABLE 1. Trench and natural exposures along the Wasatch fault zone, Utah A4
2. Lengths of segments and position of boundaries proposed for the Wasatch fault zone, Utah 13
3. Lengths of surface rupturing from recent M_S 6.5 or larger earthquakes in the northern Basin and Range province 17
4. Timing and number of surface-faulting earthquakes and recurrence intervals for Holocene movement on the Wasatch fault zone 33
A1. Data for radiocarbon and thermoluminescence analyses cited in the text 64

ASSESSMENT OF REGIONAL EARTHQUAKE HAZARDS
AND RISK ALONG THE WASATCH FRONT, UTAH

PALEOSEISMOLOGY OF THE WASATCH FAULT ZONE: A SUMMARY OF RECENT INVESTIGATIONS, INTERPRETATIONS, AND CONCLUSIONS

By MICHAEL N. MACHETTE, STEPHEN F. PERSONIUS, and ALAN R. NELSON

ABSTRACT

The Wasatch fault zone forms the core of the structural transition zone between the Basin and Range province to the west and the Colorado Plateaus and Middle Rocky Mountains provinces to the east. The fault zone extends from Malad City, Idaho, on the north, to Fayette, Utah, on the south, a distance of about 343 km (383 km along its irregular trace). Previous studies of the fault zone suggested that it is composed of six discrete segments, each of which tends to rupture independently during major earthquakes (M>7). Since 1983, we have been mapping the surficial geology along the Wasatch Front at a publication scale of 1:50,000. The results of this mapping and synthesis of recent topical studies have led us to modify the positions of some of the previously defined boundaries between segments, suggest new boundaries, and subdivide several of the segments originally defined along the Wasatch fault zone.

We now recognize 10 segments along the Wasatch fault zone. Repeated Holocene movement has been documented along five adjacent segments (the central two-thirds) of the fault zone, and a sixth segment moved once in the Holocene. The heavily urbanized part of the Wasatch Front—between Ogden and Provo, Utah—coincides with the part of the fault zone that shows the highest slip rates, the shortest recurrence intervals for faulting events, and the most recent fault activity.

The 10 segments that we propose have lengths (along surface trace) that are as short as 11 and 17 km for the northernmost and southernmost segments, respectively, to as long as 61 and 70 km for the centrally located Weber and Provo segments, respectively; the average trace length of all the segments is about 37 km. The segments exhibiting Holocene movement, which comprise the central part of the fault zone, average 48 km in length. In comparison, the proposed segment lengths of late Quaternary normal faults in the northeastern part of the Basin and Range province typically average 20 to 30 km.

There have been three large historical earthquakes in nearby parts of the northeastern Basin and Range province and the Intermountain Seismic Belt. These earthquakes had magnitudes (M_S) of 6.6 to 7.5 and produced surface ruptures 11.5 to 36 km in length. Although the correlation between magnitude and the surface rupture lengths of earthquakes on historical normal faults is clearly nonlinear, we infer that major surface-rupturing earthquakes that broke entire segments of the Wasatch fault zone would be similar in magnitude to the major historical earthquakes in the northern Basin and Range province. One implication of our new segmentation scheme is that the expected length of surface rupturing during a major earthquake on the Wasatch fault zone could be as much as 60 to 70 km. Because length of surface rupturing is generally dependent on earthquake magnitude, the largest earthquake on a single segment could be M 7.5 or greater.

Recent trenching of fault scarps and detailed mapping of Quaternary geology along the Wasatch Front show that the Wasatch fault zone has been active repeatedly through the Holocene (past 10,000 years). In addition, the recognition of 10 discrete segments of the Wasatch fault zone, 6 of which have demonstrable Holocene movement, increases the possible number of separate localities where earthquakes and their associated surface ruptures may occur along the Wasatch Front. Although recurrence intervals for individual segments are still being analyzed, we now think that major earthquakes have struck the central, densely urbanized part of the Wasatch fault zone on an average of once every 395 years (this value is termed the composite recurrence interval of faulting).

This estimate is similar to the preferred composite recurrence interval of 444 years calculated by Schwartz and Coppersmith (1984). Dating of paleoseismic events along the Wasatch fault zone indicates that large earthquakes (those that cause significant surface faulting and major ground-shaking damage) have occurred more frequently in the late Holocene than the average value would suggest; thus, we consider that some process of temporal clustering of earthquakes may be active. Recent surface faulting involved at least six faulting events between about 400 and 1,500 yr B.P., or about one event every 220 years. This average is about twice as frequent as that calculated from the paleoseismic record of the past 6,000 years. A lack of movement on the Brigham City segment during the past 3,600 years suggests that it may be the next segment to undergo movement on the Wasatch fault zone.

Manuscript approved for publication November 20, 1990.

INTRODUCTION

In Utah, the Wasatch fault zone is the most obvious and continuous structural element of a prominent transition zone between the Basin and Range province and

the Colorado Plateaus and Middle Rocky Mountains provinces. The late Quaternary trace of the Wasatch fault zone extends from Malad City in southern Idaho to Fayette in central Utah, a straight-line distance of about 343 km (fig. 1). The Wasatch fault zone is nearly 383 km long along its irregular surface trace and, as such, is the longest continuous and active normal fault zone in the Western United States. Other fault zones, such as the one associated with the Central Nevada Seismic Belt, approach this length but have discrete gaps in surface rupturing or seismicity.

Although the Wasatch fault zone has been the subject of much scientific interest since G.K. Gilbert's pioneering studies (Gilbert, 1890, 1928), the first comprehensive study of the Wasatch fault zone was not completed until the 1970's. Cluff and others (1970, 1973, 1974) used low-sun-angle photographs to map ruptures along the entire length of the Wasatch fault zone from Malad City to Gunnison, which is about 15 km south of Fayette, Utah. Although their 1:24,000-scale maps show the most detailed trace of the Wasatch fault zone, they sometimes confused other faultlike features (such as landslide scars and shorelines) with bona fide fault scarps. As a logical extension of this reconnaissance work, other geologists at Woodward-Clyde Consultants made detailed investigations of the surficial geology at four trench sites along the Wasatch fault zone during the period 1978 to 1982. This work resulted in many important preliminary reports and culminated in two major reports that focused on paleoseismological aspects of the Wasatch fault zone.

Recent U.S. Geological Survey (USGS) mapping along the Wasatch Front in central and northern Utah has focused on differentiating middle to upper Quaternary deposits (those younger than 750,000 years) that record long- to short-term slip rates on the Wasatch fault zone. Studies of historical earthquakes on major normal faults in the Basin and Range province and studies of paleoseismicity on prehistoric faults in the Western United States have shown that surface rupturing tends to occur on discrete sections of long faults or fault zones. These discrete elements, called fault segments, are generally defined as portions of the fault that tend to move independently of one another during large earthquakes. Our scenario of segmentation of the Wasatch fault zone is based on apparent recency of fault movement as determined from geomorphic, stratigraphic, and dating evidence, on amounts of displacement of faulted deposits, on geometric patterns of surface ruptures and their relations to bedrock geology of the fault zone, and on the overall history of movement of the Wasatch fault zone during the Holocene and latest Pleistocene.

Our mapping along the Wasatch Front has allowed us to further divide the six segments of the Wasatch fault zone (fig. 1) proposed by Swan and others (1980) and Schwartz and Coppersmith (1984). In addition to our detailed mapping studies, the USGS and the Utah Geological and Mineral Survey (UGMS) are engaged in a cooperative study of specific sites along the Wasatch fault zone, where trenching will reveal the time of the most recent ruptures and permit further characterization of major faulting events, such as determinations of recurrence intervals and displacements per event. Although this trenching work continues, summaries of published reports and preliminary results from our trench studies are discussed in this report. Readers should be aware that many of the values reported here for recurrence intervals, timing of fault movement, and slip rates are provisional and may change as further results become available from the cooperative program of trenching and isotopic dating. In addition, recent reports on some of the new major trenching sites (for example, Forman and others, 1991; Personius, 1991a, b) along the Wasatch fault zone include more detailed discussions of age determinations, amounts of fault offset, slip rates, and interpretations of faulting history. Much of the work reported here has been summarized in a recent paper by Machette and others (1991).

TRENCHING ALONG THE WASATCH FAULT ZONE

The Wasatch fault zone has been the focus of extensive trenching efforts since the initial investigations of Cluff and others (1970, 1973, 1974). The results of early (1978–83) trenching have been summarized by Swan and others (1980) and Schwartz and Coppersmith (1984). As of 1987, 47 trenches and 4 natural exposures have been logged and described from 20 sites on 6 segments of the Wasatch fault zone and the associated West Valley fault zone (table 1). Most of the trenches have provided some control on the time of most recent faulting, but only a few have set limits on recurrence intervals and slip rates for faulting events. Our new dating control helps to refine recurrence intervals and times of most recent faulting at the trench sites as well as to highlight changes in slip rates through time.

As an extension of our geologic mapping, the USGS and the UGMS undertook a study of several trench sites along previously unstudied parts of the Wasatch fault zone (fig. 1). In September 1986, 13 trenches were excavated at 3 sites on the Wasatch fault zone near Brigham City, East Ogden, and American Fork Canyon (sites 1, 4, and 9, table 1). The history of faulting that is being developed from these and additional trenches has helped to test our earlier suggestion (Machette and others, 1986) that the Wasatch fault zone has at least 10 to as many as 12 discrete segments, each of which may act independently during major earthquakes (see "Fault Segmentation"). From 1985 to 1987, various

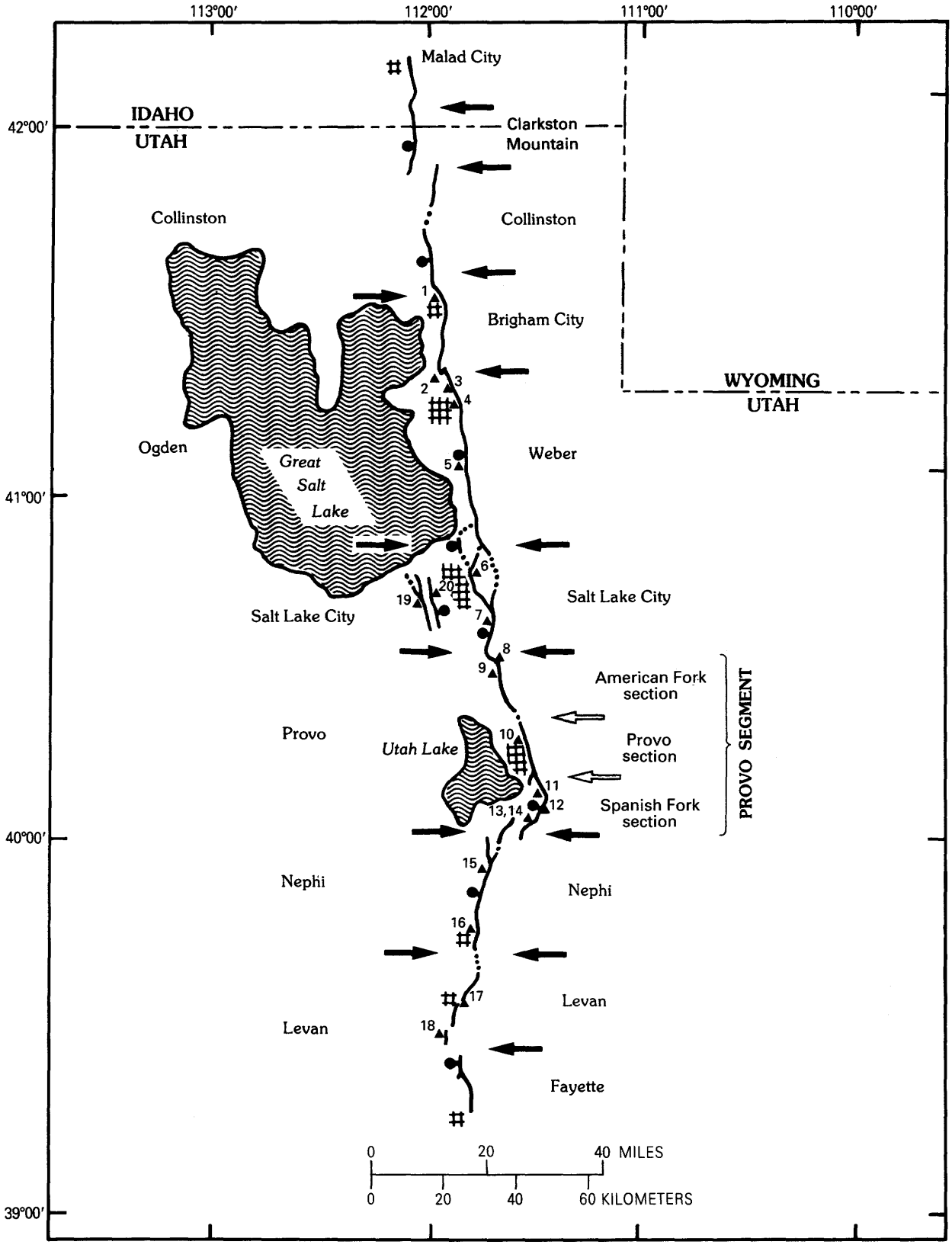

FIGURE 1.—Location of sites along segments of the Wasatch fault zone. Segments proposed by Schwartz and Coppersmith (1984) are shown to the left (west) of the fault zone, and those proposed in this study are to the right (east) of the fault zone. The main trace of the Wasatch fault zone is shown by a heavy line having a ball and bar on the downthrown side. Solid arrows indicate segment boundaries. Major towns are shown by hachures. Study sites, shown by numbered triangles, are listed in table 1.

TABLE 1.—*Trench and natural exposures along the Wasatch fault zone, Utah*

[Trench sites and natural exposures are listed by fault segment from north to south on the Wasatch fault zone and along the West Valley fault zone to the west]

Site		Principal investigator[1]	Dates of investigation	Trench/natural exposures (number logged)	Age of faulted deposits	Number of datable samples			Parameters determined[2]		
						Organic carbon	Charcoal sample	Thermolumi-nescence	Most recent event	Recurrence interval of faulting	Slip rate[3] (interval, in 1,000 years)
No.	Name										
Brigham City segment											
1	Brigham City	S.F. Personius (USGS, Denver).	September 1986	5/0 (1)	Early to middle Holocene	5	0	2	Yes	Yes	Yes (3.6–4.7, 0–14)
2	Pole Patch	S.F. Personius (USGS, Denver).	September 1985	1/0 (1)	Latest Pleistocene	2	0	0	Yes	AV	Yes (0–15)
Weber segment											
3	Garner Canyon	A.R. Nelson (USGS, Denver).	July 1985	0/1 (1)	Middle to late Holocene	3	0	0	Yes	Yes	No
4	East Ogden	A.R. Nelson (USGS, Denver).	September 1986	5/0 (5)	Middle to late Holocene	16	3	11	Yes	Yes	Yes (0.5–4.2, 0–15)
5	Kaysville	Woodward-Clyde Associates.	Summer 1978	7/0 (7)	Latest Pleistocene	0	1	0	MN	AV	Yes (0–8)
Salt Lake City segment											
6	Dresden Place	John Garr (Delta Engineering).	November 1986	2/0 (2)	Latest Pleistocene	0	0	6	No	No	Yes (0–15)
7	Little Cottonwood Canyon.	Woodward-Clyde Associates.	Summer 1979	3/0 (3)	Latest Pleistocene	0	3	0	No	AV	Yes (0–19)
8	Dry Creek	D.P. Schwartz (USGS, Menlo Park), W.R. Lund (UGMS).	Summer 1985	5/0 (5)	Middle to late Holocene	5	0	0	Yes	Yes	Yes (0–5)
Provo segment											
9	American Fork Canyon.	M.N. Machette (USGS, Denver).	September 1986	3/0 (3)	Middle to late Holocene	3	3	10	Yes	Yes	Yes (0.5–5.3, 0–15)
10	Rock Creek	M.N. Machette (USGS, Denver).	July 1985	0/1 (1)	Late Holocene	2	0	0	Yes	No	No
		W.E. Lund (UGMS), D.P. Schwartz (USGS, Menlo Park).	May 1988	1/2 (3)	Late Holocene	7	3	3	Yes, DP	No	No
11	Hobble Creek (Deadmans Hollow)	Woodward-Clyde Associates.	Summer 1978	3/0 (3)	Latest Pleistocene, middle to late Holocene.	0	0	0	MN	AV	Yes (0–14, 0–17)
12	Mapleton	W.E. Lund (UGMS)	Summer 1978	5/0 (3)	Latest Pleistocene to late Holocene.	8	1	1	Yes	Yes	Yes (0–3)
13	Water Canyon	D.A. Ostenaa (USBR, Denver).	Spring 1987	3/0 (3)	Holocene (plus snails and artifacts).	7	18	5	Yes	AV	Yes (0–8)
14	Woodland Hills	M.N. Machette (USGS, Denver).	November 1986	2/0 (1)	Late Pleistocene to Holocene(?).	1	0	6	MN	AV	Yes (0–150)

Site No.	Site Name	Principal investigator[1]	Dates of investigation	Trench/natural exposures (number logged)	Age of faulted deposits	Number of datable samples: Organic carbon	Number of datable samples: Charcoal sample	Number of datable samples: Thermoluminescence	Parameters determined[2]: Most recent event	Parameters determined[2]: Recurrence interval of faulting	Parameters determined[2]: Slip rate[3] (interval, in 1,000 years)
					Nephi segment						
15 . . .	North Creek	Woodward-Clyde Associates.	September 1980	3/0 (2)	Middle to late Holocene	2	2	0	MN	Yes	Yes (0–5)
16 . . .	Red Canyon	M.E. Jackson (University of Colorado).	June 1987	1/0 (1)	Latest(?) Pleistocene and Holocene.	4	0	12	MX	Yes	Yes (0–5)
					Levan segment						
17 . . .	Deep and Pigeon Creeks.	Woodward-Clyde Associates.	Summer 1980	0/2 (0)	Holocene	0	1	0	MX	MN	No
	Deep Creek	M.E. Jackson (University of Colorado).	June 1987	0/1 (1)	Holocene	0	0	4	Yes	MN	No
18 . . .	Skinner Peaks	M.E. Jackson (University of Colorado).	June 1987	1/0 (1)	Holocene	5	7	10	MX	MN	Yes
					West Valley fault zone						
19 . . .	Granger fault	J.R. Keaton (Dames and Moore, Salt Lake City).	1985–86, 1987–88	2/0 (2)	Late Pleistocene to Holocene.	0	0	4	MN	AV	Yes (0–12, 0–58, 0–140).
20 . . .	Taylorsville fault	J.R. Keaton (Dames and Moore, Salt Lake City).	1985–86, 1987–88	2/0 (2)	Latest Pleistocene and Holocene.	0	0	0	MN	AV	Yes (0–12)

[1]USGS, U.S. Geological Survey; UGMS, Utah Geological and Mineral Survey; USBR, U.S. Bureau of Reclamation.
[2]AV, average value; MN, minimum value; MX, maximum value; DP, data pending.
[3]Calculated over intervals before present.

governmental agencies and private contractors excavated several additional trenches (Machette, 1987). Three sites were excavated along the Salt Lake City segment—at Dresden Place (site 6, table 1) along the East Bench fault by Delta Engineering; at the South Fork of Dry Creek (site 8, table 1) along the main Wasatch fault by the USGS and UGMS; and at the Forestdale Golf Course site (not logged) along the East Bench fault by the UGMS. To the south on the Provo segment, a trench site on the Woodland Hills fault (site 14, table 1) was excavated by the U.S. Bureau of Reclamation (USBR). In addition, two sites off the Wasatch fault zone that supplied information pertinent to this report have been excavated—the West Valley fault zone (sites 19 and 20, table 1) studies by Keaton and others (1987) and Keaton and Currey (1989) and the East Cache fault zone (no fault number) study by McCalpin (1987) and McCalpin and Forman (1991).

Starting in the spring of 1987, new trenches along the Wasatch fault zone were opened by the UGMS and USGS at Rock Creek, east of Provo, and at a site southeast of Mapleton on the Provo segment (sites 10 and 12, table 1); by the USBR at Water Canyon near the southern end of the Provo segment (site 13, table 1); and by Michael Jackson of the University of Colorado at sites west of Red Canyon on the Nephi segment (site 16, table 1) and north of Skinner Peaks on the Levan segment (site 18, table 1). As a result of the recent flurry of trenching operations (36 trenches or new exposures in 2 years), we now have data from at least one major trenching site on each of the heavily populated segments and from as many as three major sites on the Provo and Weber segments. Because the areas of the northernmost and southernmost fault segments are sparsely populated and show little or no evidence of Holocene movement, no trenching operations have been conducted there.

Displacement values and slip rates cited throughout this report refer only to the vertical component of tectonic displacement or slip (NVTD of Schwartz and Coppersmith, 1984), which includes compensation for backtilting, antithetic faults, and warping. However, in many cases, a lack of good exposures or poor preservation of the faulted surfaces allowed us to determine displacement only across a narrow zone or exposure rather than across a wider zone that may reflect the far-field effects of tectonism. In such cases, cited values of displacement are crude approximations of the common maximum vertical displacement.

It is our practice to use metric units, both in the field and in this report, for measurements of length and height. However, because most of the geologic and geomorphic features decribed herein have been mapped on USGS 1:24,000-scale topographic-quadrangle maps, we report the altitudes of important map-oriented features, such as shorelines, in both metric (meters) and English (feet) units.

AGE DETERMINATIONS

We cite 36 new ^{14}C ages that we have obtained for this study. The procedures that we have developed for using these age determinations to estimate the ages of faulted soil materials and the times of faulting are discussed in detail in the appendix, along with the limitations involved in their interpretations. However, we use a number of terms (in acronym form) in the text to describe different procedures or elements of dating techniques. The following list describes these acronyms.

AMRT	Apparent mean residence time (age) of soil organic carbon
AMS	Accelerator mass spectrometry (a measurement technique)
cal yr B.P.	Calendar years before present (1950 A.D.)
^{14}C	Carbon 14 or, more commonly, radiocarbon
ka	Thousands of years (ago)
Ma	Millions of years (ago)
LHC	Lower horizon contact (usually the base of a deposit, such as fault-scarp colluvium)
MRC	Mean residence correction (AMRT at time of burial of sampled unit); UMRC refers to upper contact, LMRC refers to lower contact
CAS	Carbon age span (the total time interval represented by different ages of carbon in the soil sample)
UHC	Upper horizon contact (usually the surface of a buried soil and its associated deposit)
yr B.P.	Years before present (1950 A.D.)

The ^{14}C ages are of two main types: conventional gas-proportional and AMS ages on charcoal samples and AMRT ages on organic concentrates from the A horizons of surface and buried soils. Although both types of ages are measured in ^{14}C years (^{14}C yr B.P.) and converted to calendric dates (cal yr B.P.), the geologic interpretation of AMRT ages is complex, and the associated errors (both analytical and geologic) commonly are much larger than those for charcoal samples (see discussion in appendix).

In addition to the ^{14}C ages, we obtained 18 thermoluminescence (TL) age estimates for materials associated with faulting (see appendix). The TL technique directly dates the last exposure of a mineral to sunlight and, as such, reflects the time of its burial.

ACKNOWLEDGMENTS

This study could not have been completed without the able assistance of many others. We thank the staff of the UGMS for funding the trenching program and some of the ^{14}C ages; we especially acknowledge the assistance of William Lund, who coordinated much of the trenching operations. Genevieve Atwood (former Director of the UGMS) authorized the excavation of 13 trenches and allowed us to employ her technical staff during exploration of the trenches. Genevieve was an ardent supporter throughout the course of this study and is particulary memorable for her "Science is Fun" admonition. Many thanks are extended to UGMS staff members William Mulvey, Suzanne Hecker, William Case, Bob Klauk, and Hal Gill, each of whom spent considerable time in the trenches.

As part of the National Earthquake Hazards Reduction Program, the State of Utah sponsors a County Geologist Program. In this capacity, Robert Robison (Utah County), Craig Nelson (Salt Lake County), and Michael Lowe (Weber and Davis Counties) each contributed to the investigation of trenches and provided information about land ownership at potential trenching sites. The U.S. Bureau of Reclamation (Provo office) provided hydraulic shoring and the manpower to install it. John Garr (Delta Engineering, Salt Lake City, Utah) helped with trench logging at East Ogden, and Donald Currey (University of Utah) and John Garr provided unpublished information for the Dresden Place site.

We appreciate the cooperation of the following landowners who permitted us to excavate trenches during the fall of 1986: at Brigham City, Elbert Beecher and George Anderson; at East Odgen, the Fife Equipment and Investment Company of Brigham City; and, at American Fork Canyon, the Hayes brothers (John K., Robert D., and David R.) of Provo, Utah. Pat Cashman (then at Weber State College) provided storage facilities for research equipment during our excursions to Utah.

We appreciate the forthright and stimulating discussions of Basin and Range faulting with our colleague David Schwartz (formerly of Woodward-Clyde Associates) and are particularly grateful to him for sharing his knowledge of paleoseismology. David continues to be involved with all aspects of research along the fault zone.

Accurate chronologic dating has been the crux of many former studies and a critical element of this study. We are indebted to the following persons and laboratories for ^{14}C analyses: Stephen Robinson and Deborah Trimble of the USGS at Menlo Park, Calif.; Robert Stuckenrath of the University of Pittsburgh; Irene Stehle of Dicarb Radioisotope Co., Norman, Okla.; and A.J.T. Jull and colleagues at the University of Arizona-National Science Foundation Accelerator Facility for Radioisotope Analysis, Tuscon. Thermoluminescence analyses were provided under a USGS-sponsored research grant to Steve Forman, Michael Jackson, and Paula Mott of the Institute for Arctic and Alpine Research (INSTAAR) of the University of Colorado and James McCalpin of Utah State University. Rolf Kihl, also of INSTAAR, and Kathleen Haller of the USGS prepared most of the samples of soils and organic-rich sediment for ^{14}C analysis.

We appeciate the helpful comments of participants on Wasatch fault zone field trips and at earthquake hazard conferences that we have attended. This manuscript was improved by the critical reviews and comments of Russell Wheeler, Donald R. Nichols, and R. Ernest Anderson, all of the USGS.

REGIONAL QUATERNARY GEOLOGIC FRAMEWORK

Much of our mapping along the Wasatch Front utilizes stratigraphy based on relatively new interpretations of the late Quaternary (past 130,000 years) history of Lake Bonneville. The results of research from the 1970's and the 1980's have yielded a simplified stratigraphic framework (see Scott and others, 1983; Currey and Oviatt, 1985; Currey and Burr, 1988) compared with that developed in the 1950's and 1960's (see Morrison's (1965) discussion of pre-1970 stratigraphic concepts). The new stratigraphic interpretations of the lake's history hinge on strategic ages coupled with careful discrimination of transgressive and regressive lacustrine sediments deposited before, during, and after isostatic adjustments in the lake basin.

Deposition of Quaternary deposits along the Wasatch Front appears to be closely associated with climatic cycles—cool periods of greater effective moisture (glacial or pluvial intervals) or warm periods of restricted moisture (interglacial or interpluvial intervals). We suspect that depositional or erosional cycles along the Wasatch Front are stimulated by rapid changes in climate and vegetation; that is, these changes may cause dynamic thresholds in surface processes to be exceeded and thereby trigger periods of erosion or deposition.

Stratigraphic and paleontologic evidence suggests that the climate in the eastern Basin and Range province was conducive to forming large and relatively deep lakes (Lake Bonneville, for example) at least three times since 200 ka (200,000 years ago) (Scott and others, 1983). In addition, scant evidence has been found for middle (130–750 ka) and early (750 ka–2.0 Ma) Pleistocene predecessors of Lake Bonneville. Deposits of well-dated airfall volcanic ash interbedded with lacustrine sediments in the Bonneville Basin show that several

ancestral Lake Bonnevilles existed intermittently in the past 2 Ma. Near Beaver, Utah (about 280 km south of Salt Lake City), basin-fill sediments record a major freshwater lake (Lake Beaver) during late Pliocene and early Pleistocene time (Machette, 1985). Lake Bonneville and Lake Beaver are but two examples of the many lakes that must have been present in the eastern Basin and Range province during Quaternary time (past 2 Ma).

Unfortunately, lake deposits older than late Pleistocene are only sparsely exposed in the Basin and Range province because much of the area, including the Bonneville drainage basin, is still relatively undissected. Young lacustrine and alluvial sediments related to Lake Bonneville largely obscure the record of all but the most recent lacustrine and fluvial cycles. Nevertheless, there are some exposures of fluvial and lacustrine deposits along the Wasatch Front that may be middle Pleistocene (750–130 ka) in age. For example, extensive alluvial-fan deposits in the Loafer Mountain area of the southeastern part of Utah Valley have thick, red argillic B (clay-rich) horizons and thick Stage III to IV calcic (calcium-carbonate-rich) horizons that suggest ages of at least several 100 ka (see Birkeland's (1984) review of soils and Quaternary geology). The highest and oldest of these fans contain two volcanic ash beds, which have been identified by Izett and others (1970) as the Lava Creek B (0.62 Ma) (Izett, 1981) and the Bishop (0.74 Ma) (Izett, 1982). Also, in the Salt Lake Valley, there is a small remnant of fan alluvium or glacial outwash of middle Pleistocene age exposed south of Bells Canyon (Scott and Shroba, 1985; Personius and Scott, 1990, in press) that has a uranium trend age of 250±90 ka (J.N. Rosholt, written commun. to W.E. Scott, 1984).

The sparsely preserved surficial deposits that predate the last deep cycle of Lake Bonneville (Bonneville lake cycle, 32–10 ka) (see fig. 2) include lacustrine deposits associated with the Little Valley lake cycle (latest middle Pleistocene) (Scott and others, 1983) and till of the largely contemporaneous Dry Creek glacial advance. Deposits of the intervening Cutler Dam lake cycle (middle late Pleistocene) (Oviatt and others, 1987), also known as the Hansel Valley lake cycle of McCalpin and others (this volume), are also present along the Wasatch Front. These two pre-Bonneville glacial-pluvial cycles most likely correlate with marine isotope stages 6 and 4, respectively (Martinson and others, 1987, fig. 18; Richmond and Fullerton, 1987, fig. 2). Till of Madsen and Currey's (1979) penultimate Dry Creek advance is exposed locally at the mouths of large canyons that cut deeply into the Wasatch Range. Scott and Shroba (1985) suggested that this till may be about 150 ka on the basis of its weathering characteristics. The outwash and alluvial-fan deposits of this same general age, which are more widespread than the till, are preserved as remnants of formerly widespread geomorphic surfaces at many places along the Wasatch Front. Although Scott and others (1983) considered the Little Valley lake cycle to have culminated about 150 ka, the lake cycle (and associated glaciation) probably persisted for several tens of thousands of years and ended about 130 ka (McCoy, 1987), as determined from stratigraphic, soil morphologic, and amino-acid-ratio evidence.

As previously mentioned, Oviatt and others (1985), McCalpin (1986), and Keaton and others (1987) found evidence of a major intermediate-level lake cycle that predates the Bonneville lake cycle and postdates the Little Valley lake cycle. Oviatt and others (1987) reported ^{14}C dates and amino-acid analyses from sediments exposed along the Bear River north of Brigham City that suggest an age of more than 40 ka for deposits of the Cutler Dam lake cycle; however, these lake deposits must be significantly younger than those of the Little Valley lake cycle, as the development of soils on relict surfaces of the deposits demonstrates. McCalpin (1986) reported TL age estimates of 76 and 82 ka for deposits of his Hansel Valley lake cycle in the northwestern part of the Bonneville Basin. In addition, Keaton and others (1987, table 2) reported amino-acid-racemization age estimates of 45 to 80 ka for sediments of an intermediate lake cycle (that is, the Cutler Dam lake cycle) in the Salt Lake Valley and preferred an age of 58 ka for the end of the cycle. If we assume that the intermediate-age lake sediments from these three distant areas of the Bonneville Basin all were deposited during a pluvial cycle associated with marine isotope stage 4, then 60 to 75 ka seems to be a reasonable time for most sediment of the Cutler Dam lake cycle of Lake Bonneville.

Most of the units that we have mapped along the Wasatch Front were deposited during the transgression (rise) and regression (fall) of the latest cycle of Lake Bonneville (the Bonneville lake cycle) and the largely contemporaneous glaciation in the Wasatch Range between 32 and 10 ka and as alluvial fans during the Holocene. The following summary of the geologic history during the latest Pleistocene and Holocene is abstracted largely from reports by Madsen and Currey (1979), Currey and others (1983), Scott and others (1983), and Currey and Oviatt (1985) and from evidence uncovered during our geologic mapping and dating investigations.

In the latest Pleistocene (35–10 ka), valley glaciers were extensive in the Wasatch Range and high-elevation mountains of northeastern and central Utah. Along the Wasatch Front, valley glaciers advanced beyond the precipitous front of the Wasatch Range and into the eastern parts of the Salt Lake Valley and Utah Valley before 22 ka, while Lake Bonneville stood at a low to intermediate level (fig. 2). Till from these glaciers was

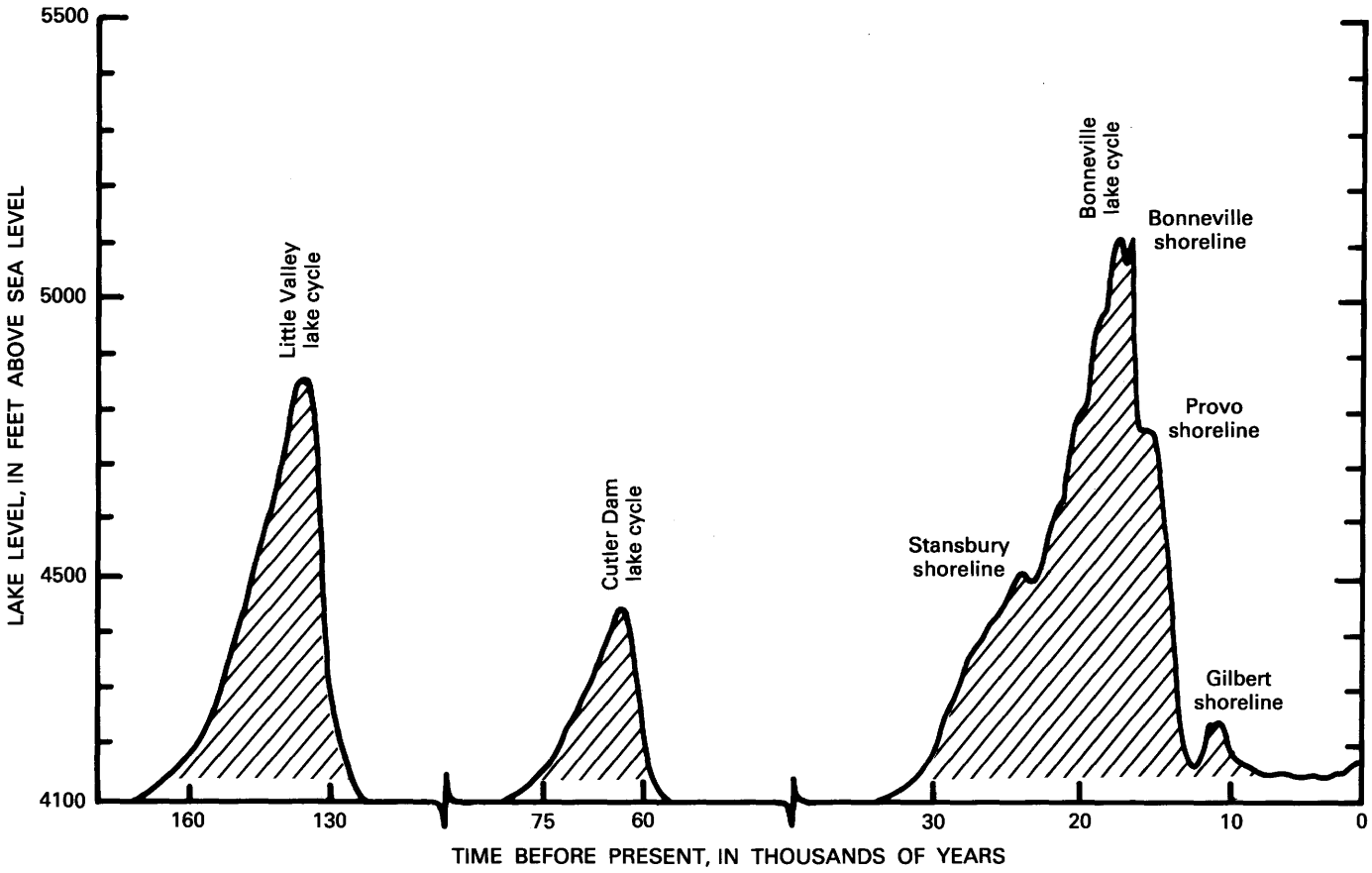

FIGURE 2.—Probable levels of Lake Bonneville during the past 150,000 years. Modified from Currey and Oviatt (1985); extended past 30,000 years on the basis of recent stratigraphic studies of pre-Bonneville lake cycle deposits by Scott and others (1983), McCoy (1987), Oviatt and others (1987), and McCalpin and others (this volume).

deposited as large end moraines that extended as much as 1 km beyond the mountain front at Little Cottonwood Canyon and Bells Canyon southeast of Salt Lake City and at Dry Creek east of Alpine in the northern part of Utah Valley. Meltwater streams from these glaciers and others higher in the Wasatch Range deposited gravelly outwash in large alluvial fans along the Wasatch Front and, farther basinward, as fan-delta complexes that were graded to a transgressing Lake Bonneville. The lake's expansion, which started about 32 ka, was interrupted by several pauses and minor regressions (such as the one that formed the Stansbury shoreline) (fig. 2) and culminated about 15 ka at the highest of the Bonneville shorelines (post-rebound altitudes of 1,573–1,584 m or 5,160–5,200 ft above sea level along most of the Wasatch Front). The outwash and alluvial fans along the mountain front were inundated by the lake and, except for small areas near the canyon mouths that stood above the level of the lake, were covered by a veneer of relatively fine grained lake sediment.

Although most workers agree that the Bonneville lake cycle culminated in a major high stand that eventually overtopped its natural sill at Red Rock Pass in southern Idaho, Currey and Oviatt (1985) found evidence of a drop in lake level and a readvance to the overflow level (the Keg Mountain oscillation) at about 16 to 15 ka. Some workers remain skeptical about this oscillation, but Machette's (1988, 1989) mapping near the American Fork Canyon and Scott's reconnaissance of the northern Oquirrh Mountains west of Salt Lake City (W.E. Scott, oral commun., 1987) tend to support an oscillation near the end of the final transgressive phase of the Bonneville lake cycle. Gravel pits in the fan-delta complex at the mouth of the American Fork Canyon record two closely timed series of transgression and regression at the Bonneville level (Machette, 1988), which Machette inferred to be the physical manifestation of the Keg Mountain oscillation.

After Lake Bonneville attained an altitude of about 1,552 m (5,092 ft), it overtopped its natural sill near Red Rock Pass and rapidly downcut about 108 m (355 ft) to an altitude of about 1,444 m (4,737 ft), where the outlet was stabilized and the lake formed the highest of the Provo shorelines. This fall, which occurred about 14.5 ka

(Scott and others, 1983; Currey and Burr, 1988) marked the end of the transgressive phase of the Bonneville lake cycle and initiated rapid stream erosion of unconsolidated lake sediment along former shoreline areas and in mountain canyons. Much of the eroded sediment was deposited in deltas, bars, and spits graded to the Provo shoreline of the Bonneville lake cycle. Modeling of isostatic rebound by Currey and Burr (1988) suggests that Lake Bonneville may have occupied the main Provo level for only about 300 years (14.5–14.2 ka). As the lake began to retreat below the Provo shoreline (about 14 ka), streams cut into the higher delta and shore complexes to form new terraces and deltas graded to successively lower shorelines of the regressing Lake Bonneville. The lake's retreat from the Provo shoreline level was caused by additional (but minor) downcutting of the outlet at Red Rock Pass, by continued rapid isostatic uplift of the deeper parts of the Lake Bonneville basin, and by lake evaporation caused by a progressively warmer climate that marked the end of the Pleistocene Epoch.

By 11 ka, the lake had fallen to a level at or below that of the present Great Salt Lake (altitude 1,283 m or about 4,210 ft in 1987). After reaching a low, extremely dessicated level, the lake rose briefly at 10.3 to 10.5 ka (Currey and others, 1983, fig. 13) to form the Gilbert shoreline at about 1,294 m altitude (4,246 ft); we consider this final rise to be the culmination of the Bonneville lake cycle. Since the beginning of the Holocene (10 ka), Great Salt Lake (a saline remnant of Lake Bonneville) has remained within about 10 m of its present level (Scott and others, 1983; Currey and Oviatt, 1985).

In contrast to the late Pleistocene, the Holocene is marked by climatic conditions similar to those of the present and by deposition of local alluvial fans close to the mountain front. Most of the deposition occurs near the mouths of steep canyons, which are sites of intermittent debris flows and floods. Away from the mountain front, reduced flow in streams prevents transport of gravels more than a few kilometers, whereas, farther downstream, the flood plains are depositional centers for sandy to silty alluvium.

One of the significant stratigraphic results from our ^{14}C dating and TL analyses is recognition of a major episode of debris-flow deposition and fan formation that began after about 8 ka and ended about 5 ka (details of dating are discussed later in this report). Because similar sequences of landscape destabilization and stripping of upland hillslopes during the early Holocene have been recognized over wide regions of the Basin and Range province (Dohrenwend, 1987, p. 307), there is probably a regional, perhaps climatic cause for the activity. This time interval generally correlates with the Altithermal (warm) climatic period of Antevs (1948, 1955), which originally was defined from the pollen record in Europe.

SEGMENTATION OF THE WASATCH FAULT ZONE

Swan and others (1980) were the first investigators to suggest that movement on the Wasatch fault zone was naturally divided among segments—portions of the fault that tend to move independently of one another during large-magnitude earthquakes. In their report, they speculated on the number of possible segments for the Wasatch fault zone. They suggested at least 6 segments on the basis of historical microseismicity on the Wasatch fault zone to as many as 10 segments on the basis of geometric variations along the fault zone and a 30- to 40-km rupture length associated with large-magnitude earthquakes on normal faults worldwide. In the second report, Schwartz and Coppersmith (1984) used geomorphic, geophysical, paleoseismic, and geodetic data to propose that the Wasatch fault zone is composed of six major segments (fig. 1).

These two papers introduced the concept that individual slip events from large-magnitude earthquakes associaed with surface ruptures on major normal-slip fault zone, such as the Wasatch, are largely confined to discrete parts. These parts—or segments, as they were called—represent only a fraction of the fault's total length; the location of individual segments may be controlled by local geometric and structural properties of the fault zone. However, the term "segment" was not defined explicitly and has since been used in contexts that range from "a portion" (that is, a geometric part) to "a structural entity" (that is, a structural segment). dePolo and others (1989, 1991) have discussed this problem of nomenclature and suggested that the term "earthquake segment" be used for those parts of a fault or faults that "rupture as a unit during an earthquake." We use the term "segment" with the same meaning, although our determination of segments of the Wasatch fault zone is based on paleoseismological data rather than seismological data. Nevertheless, the segments defined herein indicate the extent of surface rupturing that we would expect during large-magnitude earthquakes that nucleate on the Wasatch fault zone.

SEGMENTS AND SEGMENT BOUNDARIES

We now recognize 10 segments along the Wasatch fault zone (fig. 1). Boundaries between these segments represent persistent (long-term) structural features. However, some apparent boundaries may be geologically transient (short-term or nonpersistent) features (see Wheeler and Krystinik (this volume) for a discussion of nonpersistent and persistent segment boundaries). Some nonpersistent boundaries occur along long segments, and these boundaries may be the initiation or termination

points for some surface ruptures, depending on stress conditions and the size of the causative earthquake. For example, a magnitude 5.5 to 6.5 earthquake could rupture only a portion of a long segment.

If segment boundaries are persistent and repeated barriers to lateral propagation of surface faulting, they should cause structural anomalies along fault zones. The anomalies may present themselves as either abrupt changes in structural relief between segments (owing to different long-term slip rates) or more likely as areas where structural relief is less than it is in adjacent parts of the range (see Wheeler, 1989; Wheeler and Krystinik, this volume). Changes in structural relief may be expressed as (1) subsurface ridges between deep structural basins (that is, gravity saddles), (2) depressed structural levels in the range, (3) bedrock blocks (salients) stranded at intermediate structural levels between parallel strands of the fault zone, or (4) any combination of these three.

TYPES OF SEGMENT BOUNDARIES

As a result of our detailed mapping along the central and southern parts of the Wasatch fault zone (Honeyville to Fayette, Utah), we recognize four features that mark persistent and nonpersistent segment boundaries (Machette and others, 1987) (fig. 3):

1. Major bedrock blocks (spurs) or salients that extend into the basin at intermediate structural levels. These features are commonly bound by Quaternary faults that are less active than the range-bounding faults. The bedrock spurs north of Salt Lake City and Ogden are salients, as are the Transverse Mountains. Salients can persist as barriers for millions of years.
2. Major lateral (echelon) steps in the fault zone that cross bedrock-cored ranges, such as at Dry Mountain south of Payson (a variety of a salient) and between the Levan and Fayette segments, or are within bedrock, such as at Provo Canyon. Lateral steps can be either persistent or nonpersistent barriers; dePolo and others (1989, 1991) found many examples of historical faulting where echelon steps in a fault failed to stop propagating ruptures.
3. T-junction fault boundaries that involve the oblique intersection of two fault traces. One of the traces extends either basinward as a branching fault (Springville fault in the Utah Valley) or as a cross fault into bedrock (the northern part of the Brigham City segment). These features have been classified as geometric segment boundaries by dePolo and others (1989, 1991); they are not usually associated with reduced structural relief in either the ranges or the basin and thus are largely nonpersistent in the geologic record.
4. Long (10–15 km) gaps in the fault zone. These features in the fault zone probably reflect the reduction of structural relief across boundaries. These features must occur on a time scale of hundreds of thousands of years (that is, long cycles of slip versus no slip). Through time, gaps may move in response to changes in stress accumulation or orientation. The Nephi-Levan segment boundary is marked by an obvious gap of 15 km in Holocene and latest Pleistocene faulting, but ancient scarps on middle(?) Pleistocene deposits in the gap attest to the presence of a throughgoing, albeit inactive, fault.

SEGMENTATION MODELS FOR THE WASATCH FAULT ZONE

The six segments proposed by Schwartz and Coppersmith (1984) are shown on the left-hand side of figure 1. Although they ended their northernmost segment (Collinston) at the Bear River, they followed Cluff and others' (1970) belief that movement on the Wasatch fault zone continued much farther to the north. The southern end of their Collinston segment has been moved 5 km north on the basis of mapping north of Brigham City by Personius (1988a, 1990), and its northern end has been extended about 11 km past the Bear River (Machette and others, 1987). In addition, we recognize another 41 km of the Wasatch fault zone that extends north along the Malad Range to Malad City, Idaho. This extension of the Wasatch fault zone has been tentatively divided into the Clarkston Mountain and Malad City segments (fig. 1), which are separated by the 6-km-wide Woodruff spur (Machette and others, 1987). The original Ogden segment, which extended from north of Brigham City to North Salt Lake City, is now divided into the 40-km-long Brigham City segment and the 61-km-long Weber segment.

The Provo segment, which borders the eastern margin of Utah Valley, appears to be a single segment, as evidenced by similarities in the timing of the most recent and the penultimate events determined from major trenching investigations at the American Fork Canyon and Mapleton sites (table 1). Schwartz and Coppersmith (1984) originally proposed a single Provo segment, but Machette and others (1986, 1987) tentatively subdivided the Wasatch fault zone into three shorter segments named American Fork, Provo (restricted sense), and Spanish Fork.

In our 10-segment model for the Wasatch fault zone, the Malad City-Clarkston Mountain segments and the Levan-Fayette segments are differentiated somewhat arbitrarily, mainly because we lack dating control to prove that these segments have different histories. As the following discussion of segments will show, there has

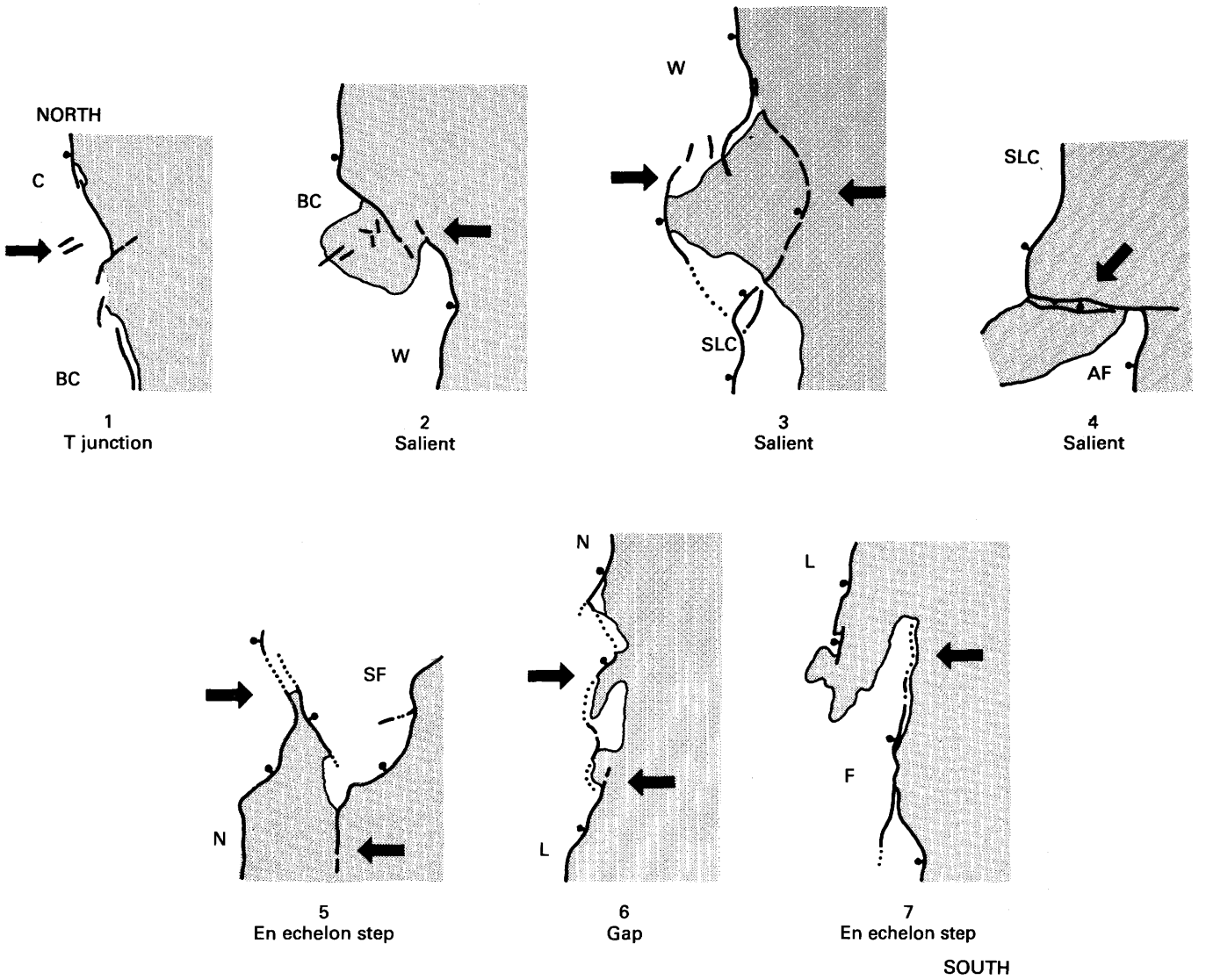

FIGURE 3.—Four types of structural features at some suggested segment boundaries of Wasatch fault zone. Examples 1 through 7 are from north to south; segment names are abbreviated as follows: C, Collinston; BC, Brigham City; W, Weber; SLC, Salt Lake City; SF, Spanish Fork; N, Nephi; L, Levan; F, Fayette. The main trace of the Wasatch fault zone is shown by a heavy line having a ball and bar on the downthrown side. Solid arrows mark the ends of rupture segments or the centers of overlaps or gaps. Bedrock areas are indicated by shading.

TABLE 2.—*Lengths of segments and position of boundaries proposed for the Wasatch fault zone, Utah*
[Length rounded to 0.5 km]

Fault segment or part[1]	Length of segment (km)		Comments
	Surface trace	Straight line	
Malad City segment	17	16.5	No latest Quaternary movement. Length does not include 6-km-wide Woodruff spur at southern end.
Clarkston Mountain segment	19	17	No latest Quaternary movement. Extends from Woodruff spur south to Malad River. Has 7-km left step to east and 2-km north-south overlap with Collinston segment to south.
Collinston segment	30	29.5	No movement later than 15 ka. Northern end at Short Divide; fault's position in Bear River area uncertain.
Brigham City segment	40	35.5	Repeated Holocene movement. Has 1-km left step and 1.5-km north-south overlap at southern end; includes most of Pleasant View salient.
Weber segment	61	56	Repeated Holocene movement. Length to where fault loses evidence of Holocene movement, east of Bountiful and 2 km north of Salt Lake salient (11 km wide).
Salt Lake City segment	46	39	Repeated Holocene movement. East Bench and main Wasatch fault south to Corner Canyon, at Traverse Range. Length excludes 7.5-km left step across Traverse Range salient and 4- to 6-km-long Warm Springs fault west of Salt Lake salient.
Provo segment	69.5	59	Repeated Holocene movement extends from Chipman Creek to Payson Canyon. Includes the American Fork, Central, and Spanish Fork parts.
American Fork part	(22.5)	(21)	Repeated Holocene movement. Extends from Chipman Creek near Alpine south to Provo River. Has 2-km-wide left step into bedrock at southern end. No north-south overlap at southern end.
Central part	(18.5)	(17)	Repeated Holocene movement. Extends from Provo River Canyon to Springville. Includes Springville fault. Overlaps 3 km with Spanish Fork part.
Spanish Fork part	(31.5)	(24)	Repeated Holocene movement. Pronounced concave-to-west trace. Has 4-km right step and more than 6 km of north-south overlap with Nephi segment.
Nephi segment	42.5	37.5	Repeated Holocene movement. Extends from Payson to Nephi. Has major right step 8.5 km in bedrock between eastern (Santaquin Canyon) and western (Juab Valley) strands. Separated from Levan segment by a 15-km gap in faulting to south.
Levan segment	30	25.5	Single(?) Holocene movement. Length includes two major gaps (6 km net) in faulting within segment. Steps 3.5 km left and 5 km south to Fayette segment.
Fayette segment	11	10.5	No Holocene movement. Has a western strand (4 km long) and major range-bounding eastern strand (9 km long). Ends just west of Fayette Cemetery.
Total length of segments	366	326	Total length of segments; excludes gaps, overlaps, and salients.
Average length of segments	36.6	32.6	Total length divided by 10 segments.
Total length of Holocene segments	289	252.5	
Average length of Holocene segments	48.2	42.1	Total length of Holocene segments divided by six segments.
Total length of Wasatch fault zone	383	343	Including gaps and salients, subtracting overlaps.

[1]Schwartz and Coppersmith (1984) proposed six segments. Their Collinston segment is divided here into the Malad City, Clarkston Mountain, and Collinston (restricted sense) segments. Their Ogden segment is divided into the Brigham City and Weber segments (the Brigham City includes about 5 km of the original Collinston segment). We divided their Provo segment into three parts—American Fork, Central, and Spanish Fork (Machette and others, 1986). However, further study reveals that this division is not warranted. The length values for these parts are shown in parentheses. Their Levan segment is divided into the Levan (restricted sense) and Fayette segments.

been repeated Holocene movement along five segments (the central two-thirds of the Wasatch fault zone), and a sixth (the Levan) shows evidence of a single movement in the late Holocene. The heavily urbanized part of the Wasatch Front—between Ogden and Provo—is the section of the Wasatch fault zone that shows the highest slip rates, the shortest recurrence intervals, and the most recent fault activity.

SEGMENT LENGTHS

The segments that we propose have lengths (along their surface traces) that are as short as 11 and 17 km for the segments at the ends of the fault zone to as long as 61 and 70 km for the centrally located Weber and Provo segments, respectively; the average length is about 37 km (table 2).

The average length along the surface trace for all of the segments of the Wasatch fault zone is 37 km (fig. 4*A*). The central five segments, which show repeated Holocene movement, have an average length of about 48 km along the surface trace (see table 2 for the calculated range in segment lengths). The three northernmost segments and the two southernmost segments have an average length of about 20 km, whereas the inboard two segments (the Collinston and Levan) are each 30 km long.

Segmentation of Basin and Range-style faults is a subject that is receiving broad attention, partly as a result of the 1983 Borah Peak earthquake, which ruptured only a small fraction of the total length of the Lost River fault zone in Idaho, and partly as a result of increased awareness of earthquake hazards and risks. We have found that the lengths of many of our proposed segments of the Wasatch fault zone are generally substantially longer than segments proposed for other major late Quaternary normal faults in the northern Basin and Range province (fig. 4). For example, mapping of the 135-km-long Lost River fault zone (fig. 4*B*) by Crone and others (1987) and reconnaissance by Scott and others (1985) suggest a division into six segments that range in length from 18 to 29 km. Crone and Haller (1989, 1991) have completed reconnaissance studies of the 150-km-long Lemhi and Beaverhead fault zones in east-central Idaho and the 27-km-long Red Rock fault zone in southwestern Montana. Their studies suggest segment lengths of 12 to 43 km (Lemhi) (fig. 4*C*), 20 to 42 km (Beaverhead) (fig. 4*D*), and 11 to 16 km (Red Rock) (fig. 4*E*) for these range-bounding fault zones. A.J. Crone and M.N. Machette (unpub. data, 1988) have measured scarp profiles along the Bear Lake fault, which borders the eastern side of Bear Lake in Utah and Idaho. Analysis of the morphology of scarps along the fault suggests two segments (26 and 32 km long) of distinctly different age (fig. 4*E*). Closer to the Wasatch fault zone, McCalpin (1987, 1989) and McCalpin and Forman (1991) have divided the East Cache fault zone into three segments (greater than 14 to as much as 26 km long) (fig. 4*E*). By comparison, the Wasatch fault zone segments range from 11 to 70 km in length and average 37 km (fig. 4*A*).

The regional studies of paleoseismicity cited above suggest a commonality of segment lengths for range-bounding faults believed to be associated with large-magnitude (M_S 7+) earthquakes in the northern part of the Basin and Range province and the Intermountain Seismic Belt of Smith and Sbar (1974). Figure 5 summarizes the lengths of segments found in two classes of faults: (1) those along major range fronts (Wasatch, Lost River, Beaverhead, Lemhi, and Teton faults) that are typically longer than 100 km and (2) those along lesser range fronts (Red Rock, Star Valley, East Cache, and East Bear Lake faults) that are typically less than 100 km long. The proposed segments of the longer faults commonly range from 20 to 40 km in length and average 25 km (and more for the Wasatch), whereas segments of the shorter faults range from 15 to 30 km and average about 20 km.

HISTORICAL EARTHQUAKES AND SURFACE RUPTURES

Well-documented surface ruptures caused by historical large-magnitude earthquakes have occurred in the Central Nevada Seismic Belt (Wallace and Whitney, 1984) and the Intermountain Seismic Belt (Smith and Sbar, 1974), which form parts of the margins of the Basin and Range province. These data provide a comparative base for surface ruptures formed during prehistoric earthquakes along the Wasatch fault zone. Table 3 shows data for nine M_S 6.5 or larger earthquakes that have struck the northern Basin and Range province since 1915; these events include the 1915 Pleasant Valley, 1932 Cedar Mountain, and 1954 Rainbow Mountain-Dixie Valley-Fairview Peak sequence of earthquakes in west-central Nevada; the 1934 Hansel Valley earthquake in northern Utah; the 1959 Hebgen Lake earthquake in western Montana; and the 1983 Borah Peak earthquake in central Idaho.

The Central Nevada Seismic Belt defines a north-northeast- to south-southwest-trending band of historically active faults. Major earthquakes have produced surface ruptures once every 15 to 20 years (on average) during the past 115 years (Wallace and Whitney, 1984; Pearthree and Demsey, 1987). The Pleasant Valley earthquake of 1915 (Wallace, 1984a) had an estimated magnitude of M_S 7.6 to M 7.75 (table 3) and produced about 62 km of surface rupturing. It is the largest-magnitude earthquake recorded in the Central Nevada Seismic Belt. Seventeen years later, in 1932, a major earthquake (M 7.2) (table 3) struck the Cedar Mountain area and produced about 61 km of distributed surface faulting (Slemmons, 1977).

In the summer of 1954, the Central Nevada Seismic Belt again became the locus of seismic activity as two major earthquakes in the Rainbow Mountain area of western Nevada caused surface rupturing (table 3). On December 16, the Fairview Peak-Dixie Valley earthquakes occurred at two discrete hypocenters separated in time by only 4 minutes (Doser, 1986). Doser's body-wave analysis indicates M_S 7.1 for the Fairview Peak earthquake and M_S 6.8 for the Dixie Valley earthquake. The Fairview Peak-Dixie Valley earthquakes reportedly produced 47- to 62-km-long surface ruptures, although the reported lengths vary by 10 to 14 km, depending on the source (see Slemmons, 1957, 1977; Bonilla and others, 1984; dePolo and others, 1989, 1991). dePolo

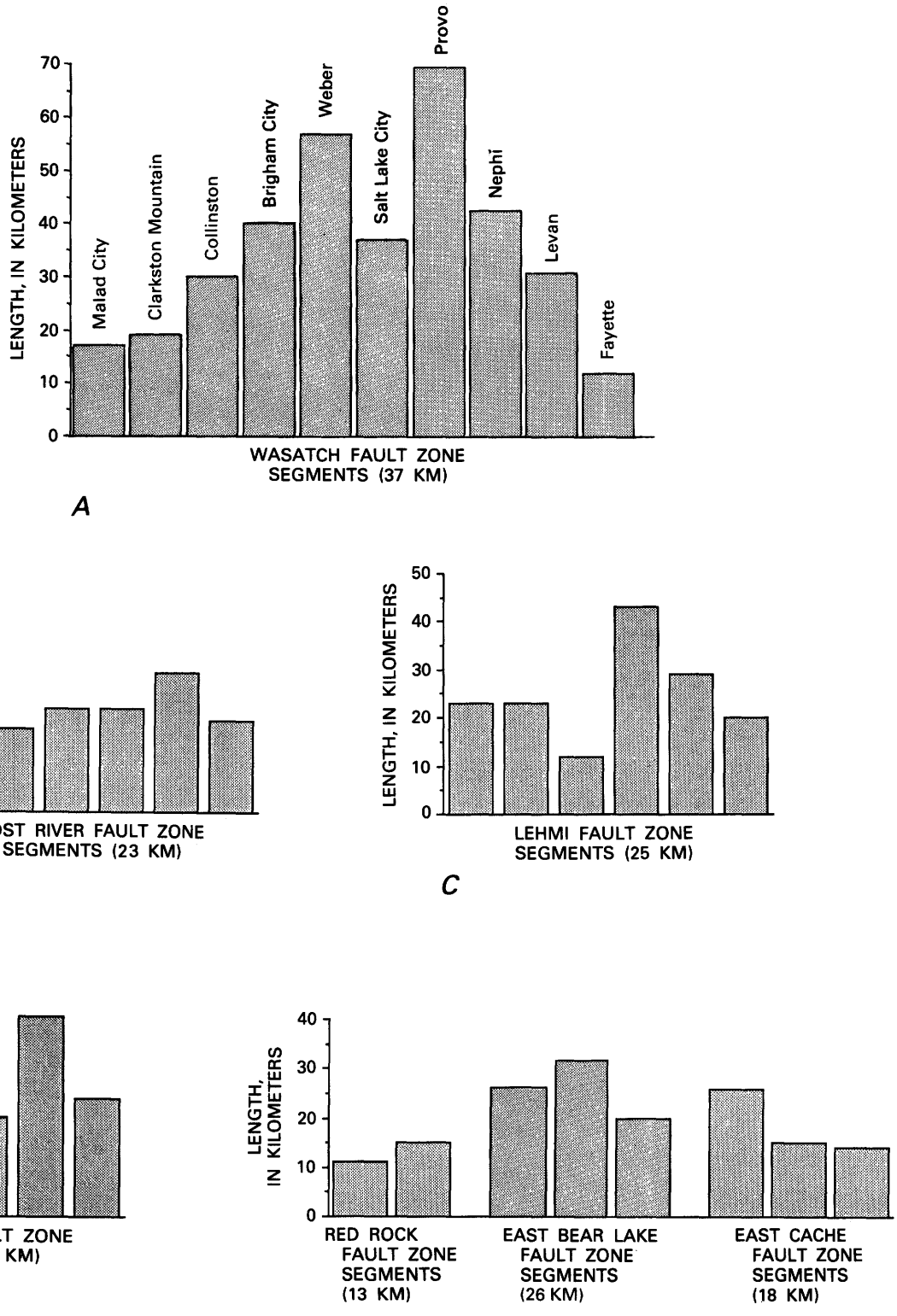

FIGURE 4.—Lengths of the surface traces of proposed segments on some major faults in the northern Basin and Range province. The number in parentheses below each fault name is the average length of all segments in that fault. Sources of data: Wasatch fault zone, this report, table 2; Lost River fault zone, Scott and others (1985), Crone and others (1987); Lemhi, Beaverhead, and Red Rock fault zones, Crone and Haller (1989, table 1; 1991); East Bear Lake fault zone, A.J. Crone and M.N. Machette (unpub. data, 1988); East Cache fault zone, McCalpin (1989) and McCalpin and Forman (1991).

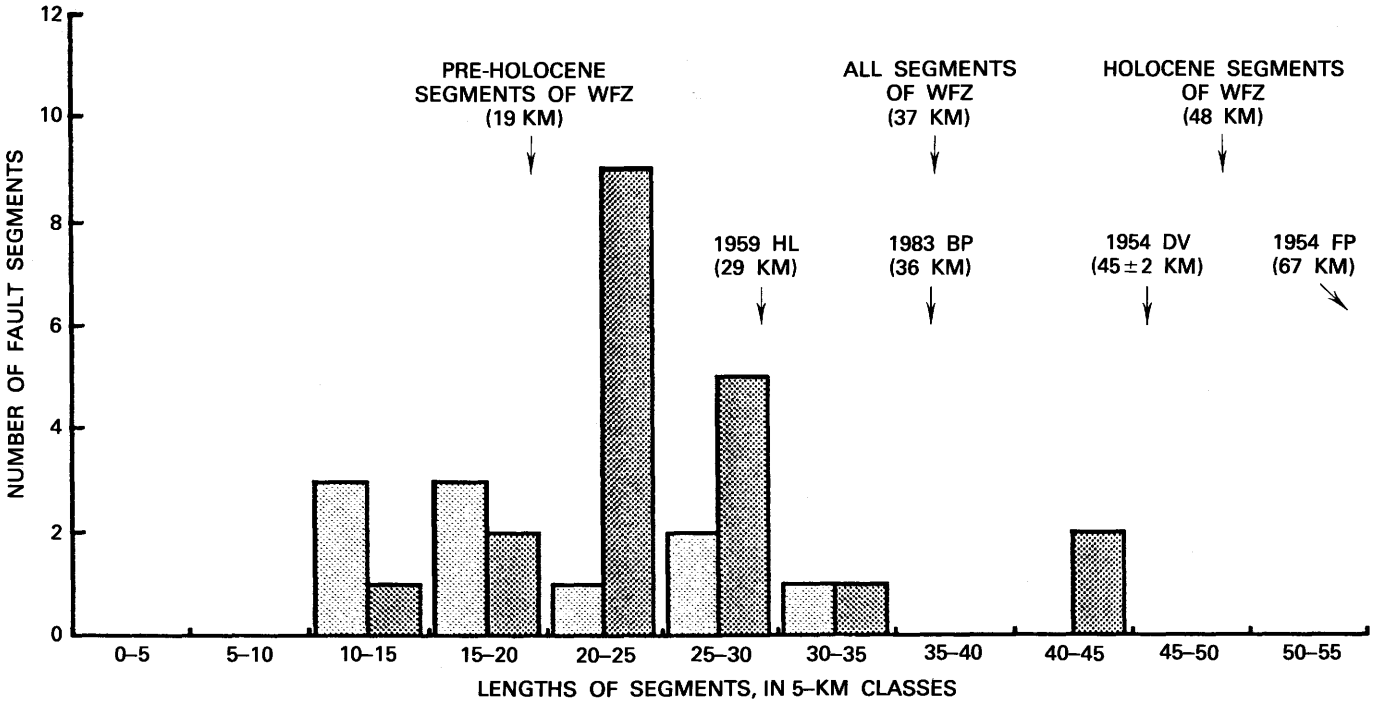

FIGURE 5.—Proposed segment lengths for prehistoric faults less than 100 km long (light shading) and more than 100 km long (dark shading) in the northeastern part of the Basin and Range province. The lengths of proposed prehistoric segments along the Wasatch fault zone (WFZ) and the lengths of historical surface ruptures produced during four $M_S \geq 6.5$ earthquakes are shown by arrows. HL, Hebgen Lake, Mont.; BP, Borah Peak, Idaho; DV, Dixie Valley, Nev.; FP, Fairview Peak, Nev.

and others' (1989, 1991) recent compilation of historical faulting in the Basin and Range province listed rupture lengths of 67 km for the Fairview Peak earthquake and 45±2 km for the Dixie Valley earthquake. We prefer to use these latter rupture lengths because they are based on surface mapping and a systematic treatment of all the historical earthquake data. Motion on all of these historical faults has been either normal dip slip or oblique-normal slip.

Table 3 also shows the magnitudes and lengths of surface rupturing associated with M≥6.5+ earthquakes in the northeastern part of the Basin and Range province. In 1934, a M 6.6 earthquake struck Hansel Valley about 45 to 50 km west of the northern end of the Wasatch fault zone (Shenon, 1936; Doser, 1989; McCalpin and others, this volume). This earthquake produced about 11.5 km of ruptures (Slemmons, 1977) and is the only earthquake to have ruptured the ground surface in Utah in historical time (see Arabasz and others, this volume). In 1959, a M_S 7.5 earthquake struck Hebgen Lake in Montana (Doser, 1985) and caused extensive ground deformation (surface rupturing and differential subsidence). Movement occurred along along two major fault systems (Witkind, 1964): the Red Canyon and Kirkwood faults, which lie mainly in bedrock, and the range-bounding Hebgen Lake fault. Surface rupture on the two overlapping fault systems (24 and 13 km, respectively) produced 29.1 km of surface rupturing as measured from end to end (Slemmons, 1977; as measured from Witkind, 1964, pl. 2).

Some small-displacement surface ruptures may not be included in the measurements discussed above. For example, Crone and others (1987) recorded 36±3 km of surface rupturing as a result of the 1983 M_S 7.3 Borah Peak earthquake (Doser and Smith, 1985; Stover, 1987), although only 26 km of the 1983 ruptures on the Lost River fault zone had more than 25 cm of offset. Scarps less than 25 cm high on the Lost River fault zone may not have been identified if the earthquake had occurred several decades ago, before geologists began using low-altitude low-sun-angle photography to help map surface rupture. This point is important, because most investigations of prehistoric faulting (paleoseismology) have not found evidence for small-displacement (less than 25 cm) surface-rupturing events.

In summary, historical large-magnitude earthquakes in the northern Basin and Range province have been associated with surface ruptures that range in length from as little as 11 km (Hansel Valley) to as much as 62 km (Fairview Peak); generally, as magnitude increases, so do length of rupture and amount of displacement. Although this statement seems intuitively correct, we cannot be more specific, because the empirical relation between magnitude and length for normal and normal-

TABLE 3.—*Lengths of surface rupturing from recent M_S 6.5 or larger earthquakes in the northern Basin and Range province*

[—, not determined]

Earthquake location (Reference from column C)	Date	Fault type[1]	A Slemmons (1977, table 16)		B Bonilla and others (1984, table 2)		C Doser (1985, 1986), Crone and others (1987)	
			M[2]	Length of surface faulting (km)[2]	M_S[3]	Length of surface faulting (km)[4,5]	M_S[6]	Length of surface faulting (km)[4]
Pleasant Valley, Nev.	10/03/15	NS	7.75	62	7.6	61±1	—	—
Cedar Mountain, Nev.	12/20/32	OS	7.2	61	—	—	—	—
Hansel Valley, Utah	03/12/34	OS	6.6	11.5	—	—	—	—
Rainbow Mountain, Nev. (Doser, 1986)	07/06/54	NS	6.6	17.7	6.3	20±2	6.6 (6.2)	16
	08/24/54	NS	6.8	30.6	7.0	26±5	6.8 (6.5)	25
Fairview Peak, Nev. (Doser, 1986)	12/16/54	OS	7.1	58.0	7.2	48±5	7.1 (7.2)	62
Dixie Valley, Nev. (Doser, 1986)	12/16/54	NS	6.8	61.2	—	47±4	6.8 (6.7)	36
Hegben Lake, Mont. (Doser, 1985)	08/17/59	NS	7.25	29.1	7.6	26±2	7.5 (7.3)	[7]29
								[8]30
Borah Peak, Idaho (Crone and others, 1987)	10/28/83	OS	—	—	—	—	7.3 (7.0)	[9]36

[1]NS, normal dip slip; OS, oblique dip slip.

[2]Unspecified Richter magnitude.

[3]Mean of surface-wave magnitude determinations.

[4]Single value for length of surface faulting generally conforms with length along surface trace.

[5]Range of values described by error limits indicates maximum and minimum lengths owing to uncertainties as described by Bonilla and others (1984, p. 2380).

[6]Values in parentheses indicate maximum moment magnitudes calculated from seismic moment (Stein and Bucknam, 1985).

[7]Length of fault having more than 10 cm (0.3 ft) of offset. Total length of surface faulting may be several kilometers longer.

[8]Length estimated from geodetic modeling (Savage and Hastie, 1966).

[9]Includes gaps and long sections exhibiting less than 25 cm of offset. Length of faulting displaying more than 25 cm of offset is about 26 km (Crone and others, 1987, fig. 4).

oblique faults has so much scatter that Bonilla and others (1984, p. 2391) recommended against using this relation for estimating earthquake magnitude. In addition, Doser's studies of the historical earthquakes of the Central Nevada Seismic Belt and the Intermountain Seismic Belt indicate that most large earthquakes are complex events, often composed of discrete but closely spaced earthquake subevents. Thus, some large-magnitude earthquakes and surface ruptures may be multiple-segment-rupturing events.

One implication of our segmentation model is that the anticipated length of surface rupturing during a major earthquake along some parts of the Wasatch fault zone could be less—by as much as a factor of 2—than previously reported. If we assume that length of surface rupturing and amount of slip are dependent on the energy released during an earthquake (that is, moment magnitude), then the largest earthquake that could be expected along an entire single segment would be somewhat less for our revised segments. Another implication is that our finer subdivision (10 segments versus 6) increases the number of possible segments on which discrete surface rupturing could occur along the Wasatch fault zone.

For convenience of discussion we have divided the Wasatch fault zone into northern, central, and southern sections on the basis of their fault activity during the Holocene. The northern section shows no evidence of Holocene faulting, the central section shows evidence of repeated Holocene faulting, and the southern section shows evidence of one or no Holocene faulting events.

NORTHERN WASATCH FAULT ZONE

Segmentation of the northern section of the Wasatch fault zone is difficult to recognize because there is little evidence of faulting in deposits younger than the Bonneville lake cycle. Our primary criteria for delineating segments and segment boundaries on the more active parts of the Wasatch fault zone are changes in latest Pleistocene and Holocene fault behavior, but, because the northern section of the Wasatch fault zone lacks fault scarps of this age, we have instead used geomorphic and structural relations to identify probable fault segments and boundaries. Although we are less confident of these segments, the structural and geomorphic patterns suggest that the 70-km-long northern section of the Wasatch fault zone is composed of a 17-km-long Malad City segment, a 19-km-long Clarkston Mountain segment, and a 30-km-long Collinston segment (figs. 1, 6).

SEGMENTS ALONG THE MALAD RANGE

The northern end of the Wasatch fault zone, which commonly has been mapped along the western flank of the Malad Range, dies out 4 km northeast of Malad City, Idaho (Cluff and others, 1974). On the basis of our aerial photographic analysis and brief field reconnaissance of

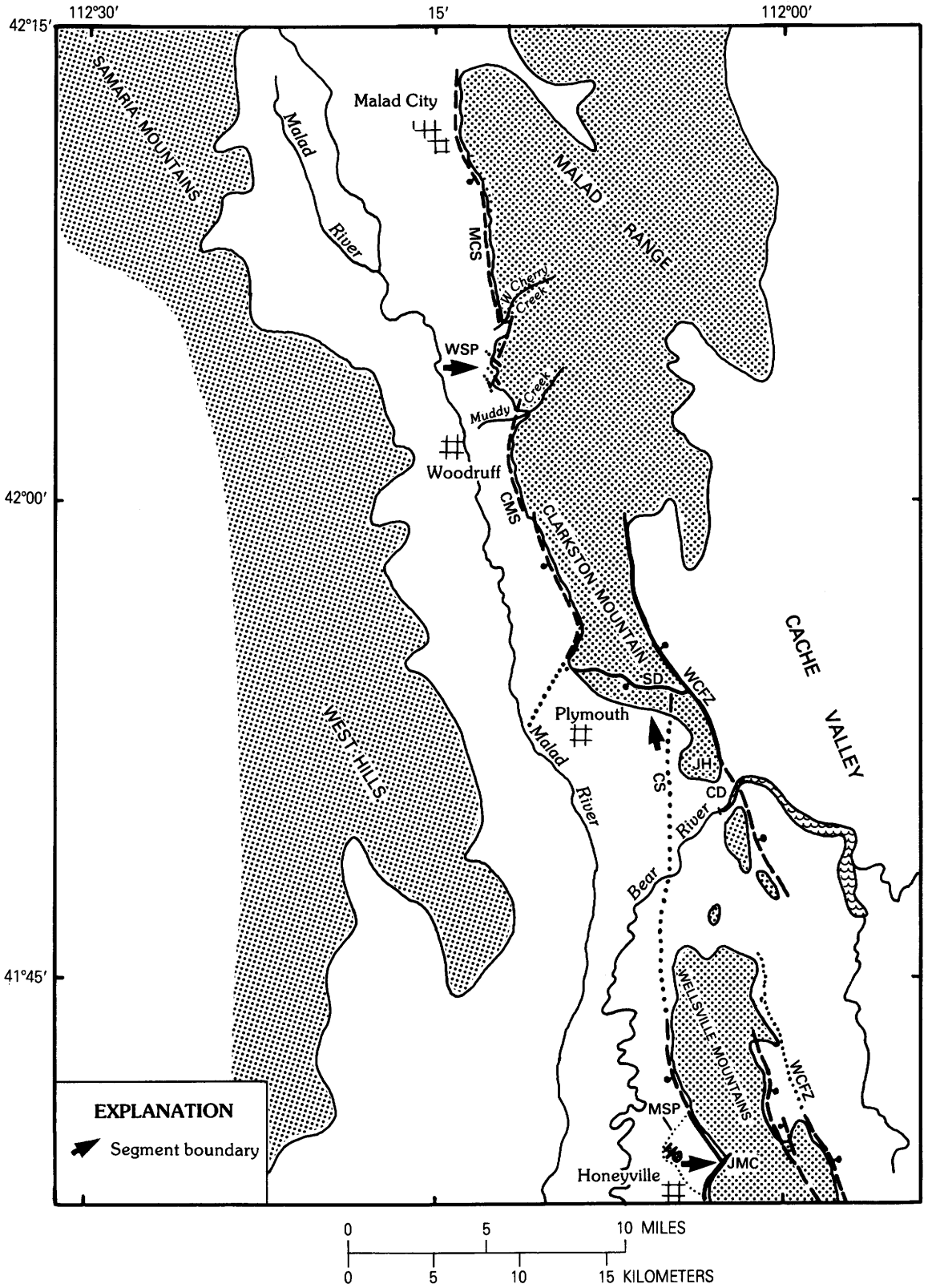

FIGURE 6.—Northern part of the Wasatch fault zone between Malad City, Idaho, and Honeyville, Utah, showing the Malad City (MCS), Clarkston Mountain (CMS), and Collinston (CS) segments. Other geographic and tectonic features mentioned in the text are the Woodruff spur (WSP), Short Divide (SD), Junction Hills (JH), Cutler Dam (CD), the Madsen spur (MSP), Jim May Canyon (JMC), and part of the West Cache fault zone (WCFZ). The dotted contact shows the near-surface limit of bedrock on the Madsen spur.

this region, we have divided the Wasatch fault zone along the western flank of the Malad Range into the Malad City and Clarkston Mountain segments.

The Malad City segment is expressed as a steep, relatively continuous escarpment along the western base of the Malad Range, from 4 km northeast of Malad City south to the vicinity of West Cherry Creek, Idaho (fig. 6). Photographic reconnaissance by us and by Cluff and others (1974) has shown that younger lacustrine deposits of the Bonneville lake cycle lie undisturbed across most of this section of the fault zone. The presence of steep escarpments and steep, linear gravity gradients parallel to the fault zone (Peterson, 1974; Zoback, 1983) and the possible presence of fault scarps on "older" alluvium (Cluff and others, 1974) suggest that the Malad City segment has been active during the late Pleistocene.

The boundary between the Malad City and the Clarkston Mountain segments is expressed as a bedrock spur that extends 6 km along the front of the Malad Range, northeast of Woodruff, Idaho. Just south of West Cherry Creek, the front of the Malad Range changes from the steep, linear escarpment that characterizes the Malad City segment to an irregular zone (the Woodruff spur) that extends southward to Muddy Creek. The Woodruff spur is coincident with a prominent saddle in the gravity data (Peterson, 1974; Zoback, 1983); this relation indicates that net slip across the Wasatch fault zone decreases at this point. Photographic reconnaissance by Cluff and others (1974) suggests that the spur is fractured by numerous faults rather than by a single well-defined fault or narrow fault zone. Fractured bedrock in the spur may have dispersed and absorbed energy as ruptures approached from the north or south, thereby decoupling the two adjacent fault segments (King and Nabelek, 1985; Wheeler and Krystinik, this volume). The Woodruff spur is shown as a major transverse structural feature on Zoback's (1983, figs. 3, 5) gravity map.

The Clarkston Mountain segment is expressed as a steep, linear escarpment that extends from the vicinity of Muddy Creek at the southern end of the Woodruff spur southward along the western flank of the southern Malad Range (Clarkston Mountain) and dies out near the Malad River, 4 km west of Plymouth, Utah. The southern 4 km of the Clarkston Mountain segment are expressed as a linear escarpment covered by sediment of the Bonneville lake cycle; however, regressional (Provo) shorelines clearly wrap sharply around this escarpment and suggest that it is a fault scarp that slightly predates the Bonneville lake cycle. Thus, the latest movement on the Clarkston Mountain segment probably occurred in late Pleistocene time, during or before the end of the Bonneville lake cycle.

Near the southern end of Clarkston Mountain at Short Divide, a prominent down-to-the-south east-striking normal fault places Tertiary lacustrine sediment (Salt Lake Group of Williams (1958)) against lower Paleozoic sedimentary rock. This fault crosses the Cenozoic structural grain in the region and appears to have been active in late Tertiary and Quaternary time. It marks the boundary between the Clarkston Mountain segment and the northern end of the Collinston segment (fig. 6). The two segments are separated by a 7-km left step and gap in late Pleistocene faulting. This pattern of faulting differs from that of Cluff and others (1974), who mapped the Wasatch fault zone as a continuous feature around the southern end of Clarkston Mountain by connecting the fault on the western side of the Malad Range (our Clarkston Mountain segment) with the fault along the western side of the Junction Hills (our Collinston segment). From our photographic and map interpretations, we believe their presumed connecting fault to be an escarpment formed by the Bonneville shoreline. The Clarkston Mountain-Collinston segment boundary also appears as a major transverse structural feature on Zoback's (1983, figs. 3, 5) gravity map.

COLLINSTON SEGMENT

The surface trace and geologic history of the Collinston segment are poorly defined because our surface mapping and photographic reconnaissance have revealed no evidence of surface faulting in deposits younger than the Bonneville lake cycle along most of its length. The northern end of the segment is probably near Short Divide, where the Wasatch fault zone appears to intersect the previously discussed east-striking fault near the southern end of Clarkston Mountain. Farther south, the Bear River flows southwest from Cache Valley through a major topographic saddle between the southern end of Clarkston Mountain and the northern end of the Wellsville Mountains. This saddle is marked by a gradual decrease in height of the mountains to the north and south, and the southern margin of the saddle coincides with the northerly plunge of bedrock at the northern end of the Wellsville Mountains (Oviatt, 1986a, b). The topography of this region suggests that the total throw on the Collinston segment decreases from south to north. However, the steep escarpment along the western side of Junction Hills (north of the Bear River) and a north-trending gravity gradient (Zoback, 1983) suggest that normal faulting probably extends continuously along the western flank of Junction Hills, across the Bear River, and south to the western flank of the Wellsville Mountains.

One possible explanation for the decrease in throw on the central and northern parts of the Collinston segment is the presence of the West Cache fault zone. This down-to-the-east normal fault forms the western margin

of Cache Valley and lies at the eastern base of the Wellsville Mountains and the Malad Range (fig. 6). Cluff and others (1974) and Oviatt (1986a) have mapped several fault scarps on the West Cache fault zone that cut Bonneville lake cycle deposits in the topographic saddle between Junction Hills and the eastern side of the Wellsville Mountains. The presence of these scarps and the steeper topography of the eastern side of the northern Wellsville Mountains and Malad Range suggest that the northern part of the West Cache fault zone has been the most active part of this fault zone. Perhaps the apparent eastward transfer of extension from the Wasatch fault zone to the West Cache fault zone in both the long (Quaternary) and the short (Holocene) term may help explain the geomorphic patterns on the Collinston segment.

Near the southern boundary of the Collinston segment, Personius (1988a, 1990) mapped a 2-km-long fault scarp on gravel of the Bonneville lake cycle and on lower Holocene fan alluvium. This short Holocene scarp (shown on fig. 6 as a solid line at the southern end of the segment) is considered part of the Collinston segment, although it probably formed in response to surface faulting originating on the more active, adjacent Brigham City segment. This relation is similar to the pattern of surface faulting that accompanied the 1983 Borah Peak earthquake in Idaho. Near the northern end of the Lost River fault, the 1983 surface faulting jumped over the segment boundary at the northern end of the Thousand Springs Valley and ruptured a small part of the Warm Springs segment (Crone and others, 1987). Sympathetic or subsidiary rupturing is a reasonable explanation for the short Holocene scarp at the southern end of the Collinston segment, because no evidence of Holocene faulting is found on the remainder of the segment to the north. Although the most recent faulting on most of the Collinston segment occurred before the Bonneville lake cycle, the steep escarpments along the Wellsville Mountains and the Junction Hills suggest that the segment has probably been active in late Pleistocene time.

The boundary between the Collinston and Brigham City segments is placed at a reentrant on the western flank of the Wellsville Mountains near the mouth of Jim May Canyon, 2 km northeast of Honeyville, Utah. The boundary is marked by a change in the trend of the fault, differences in the amount of displacement of similar aged pre-Bonneville lake cycle deposits, and a general lack of geomorphic evidence for Holocene movement on most of the Collinston segment (Personius, 1986, 1988a, b, 1990). Directly west of the reentrant at Jim May Canyon, a topographic bench known as the Madsen spur (Gilbert, 1928) has been mapped by Oviatt (1986b) and Personius (1988a, 1990). Oviatt (1986b) interpreted the entire spur as a huge bedrock landslide, but we believe that exposed landslide deposits are restricted to small bedrock erratics at the surface near the mountain front (Personius, 1988a, 1990). The large bedrock outcrop mapped by Oviatt (1986b) and Personius (1988a, 1990) near the western edge of the spur (fig. 6) dips to the northeast, into the southern end of the Collinston segment. We believe that the size and geometry of this deposit suggest that it is an outcrop of intact bedrock, suspended at an intermediate structural level between the active trace of the Wasatch fault zone and a buried fault (Davis, 1985) that forms the western margin of the Madsen spur (Personius, 1988a, b, 1990). Just north of the bedrock exposure (fig. 6), two short faults offset Bonneville lake cycle gravels (Personius, 1988a, b, 1990); the presence of these faults may indicate that the structural complexities within the spur have absorbed and dispersed fault ruptures on the Brigham City and (or) Collinston segments of the Wasatch fault zone.

CENTRAL WASATCH FAULT ZONE

The central section of the Wasatch fault zone is composed of recently active fault segments, all of which have experienced repeated movement in the Holocene. From north to south, the five segments are Brigham City, Weber, Salt Lake City, Provo, and Nephi (fig. 1). The following discussion highlights evidence from recent investigations along each segment. Final determination of revised slip rates and recurrence intervals along this section of the Wasatch fault zone awaits analysis of dated samples from recently excavated trenches.

BRIGHAM CITY SEGMENT

The Brigham City segment (fig. 7) is the northernmost segment of the Wasatch fault zone that exhibits clear evidence of recurrent Holocene faulting along its entire length (fig. 7). Slip rates on the northern part of the segment (north of Brigham City to Honeyville) appear to have been lower than those on the southern part of the segment. However, near the segment's northern boundary, evidence from Personius (1988a, b, 1990) clearly indicates that two or more faulting events occurred after Lake Bonneville fell below the Provo shoreline (14 ka).

Trench studies conducted in September and October 1986 near Brigham City (fig. 7) (Personius and Gill, 1987; Personius, 1991a) revealed evidence for three surface-faulting events in lower or middle Holocene alluvial-fan deposits. The timing of the two most recent events evident in the Brigham City trench (BC–1) are constrained by ^{14}C analysis of buried A horizons on fault-scarp colluvium (fig. 8). The results of AMRT ages

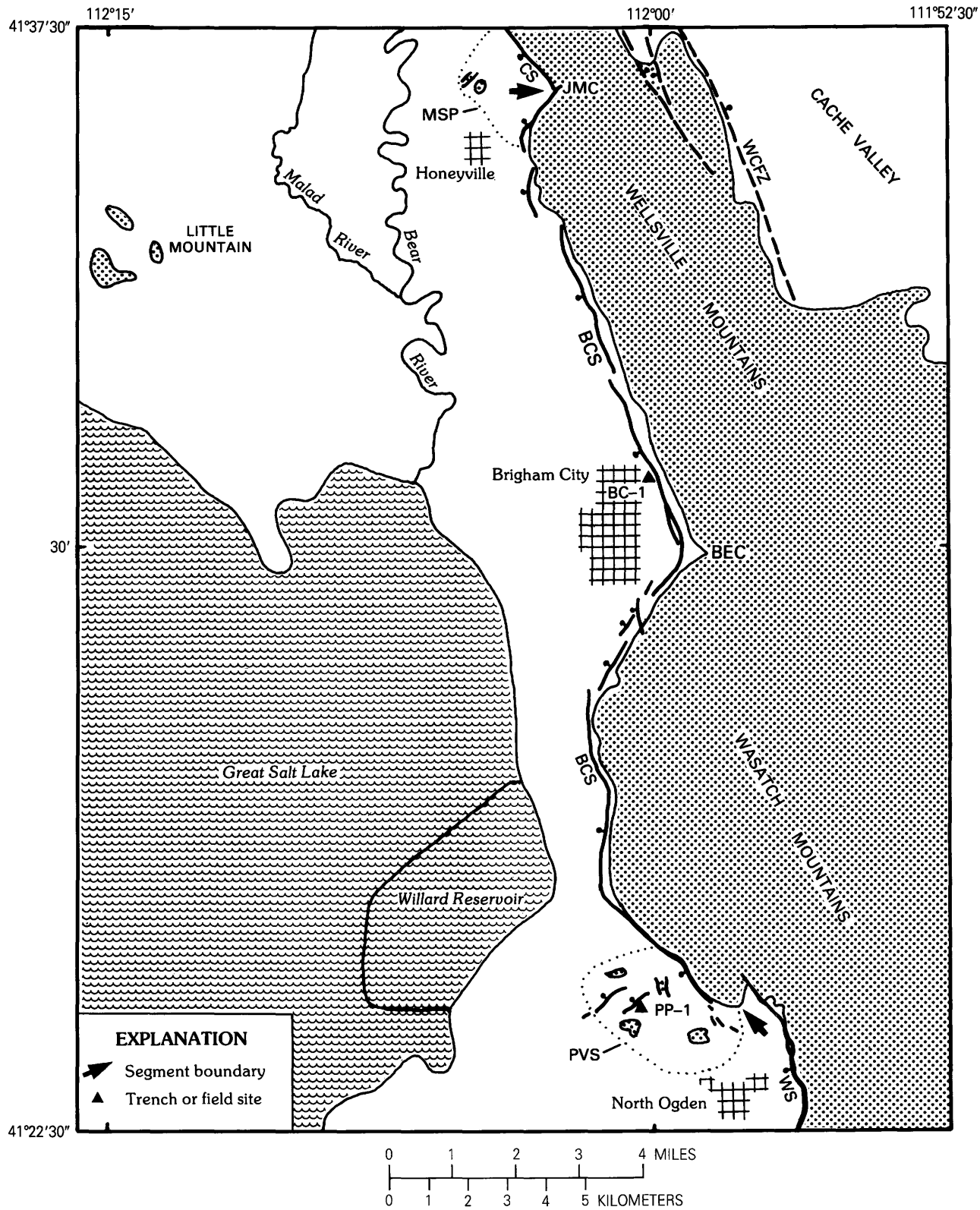

FIGURE 7.—Brigham City segment (BCS) of the Wasatch fault zone between Honeyville and North Ogden, Utah; also shown are the southern part of the Collinston segment (CS) and the northern part of the Weber segment (WS). Other geographic and tectonic features mentioned in the text are the Madsen spur (MSP), Jim May Canyon (JMC), part of the West Cache fault zone (WCFZ), Box Elder Canyon (BEC), and the Pleasant View salient (PVS). Sites are labeled as follows: BC–1, Brigham City trench 1; PP–1, Pole Patch trench 1. The dotted contacts show the near-surface limit of bedrock on the Madsen spur and the Pleasant View salient.

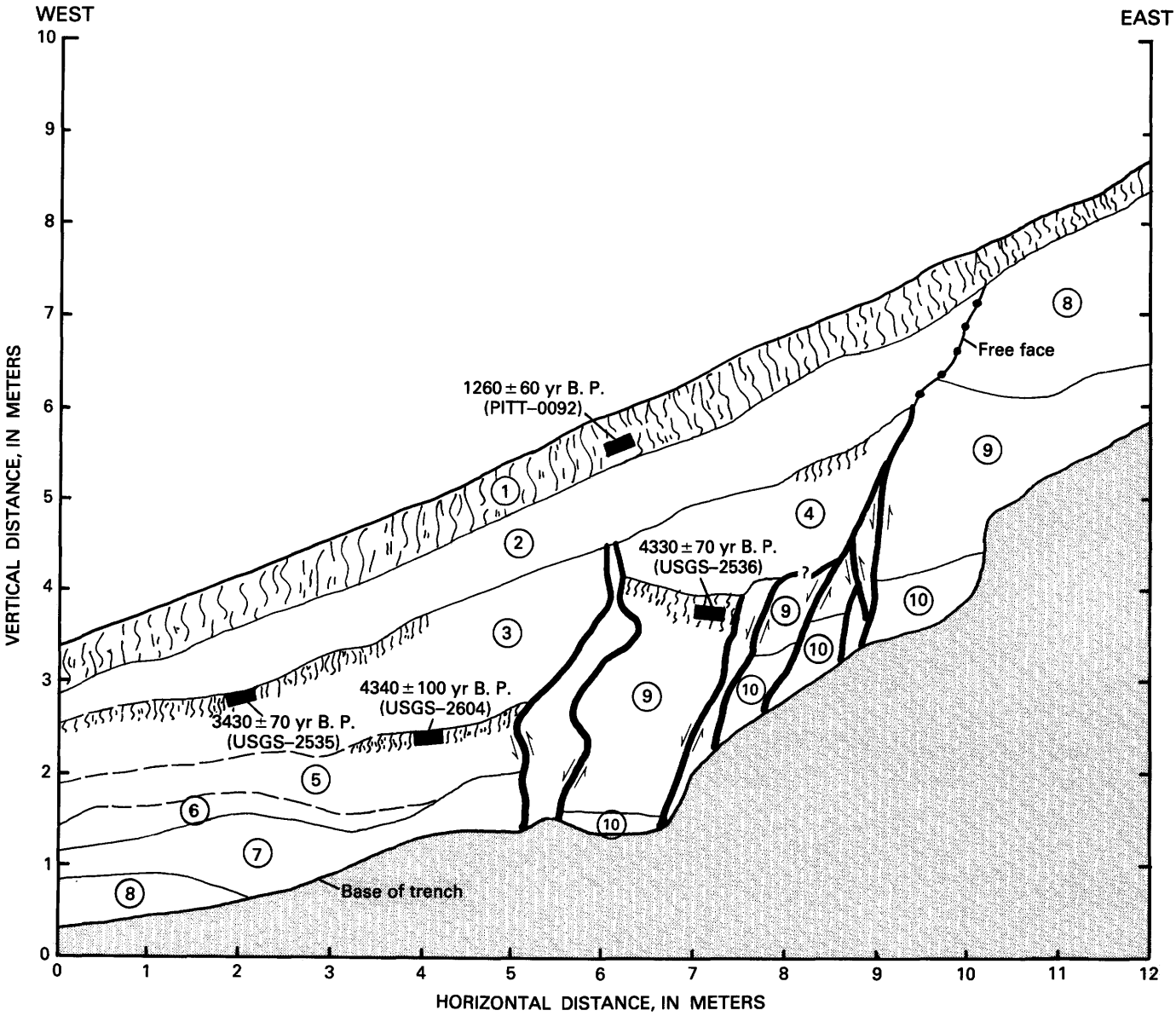

FIGURE 8.—Part of the log of trench BC–1 near Brigham City, Utah. The figure shows the relations of faults (heavy lines), scarp colluvial deposits (units 1–5), and Holocene alluvial-fan deposits (units 6–10) in the northern wall of the trench. The solid rectangles show the locations of organic-rich sediment sampled for ^{14}C dating; ages are labeled with laboratory sample numbers (see table A1). Wavy vertical lines indicate A horizons. Horizontal and vertical distances on axes are arbitrary.

on organic matter concentrated from soils buried by the two youngest colluvial wedges (table A1) suggest that these events occurred about 4.7±0.5 and 3.6±0.5 ka. The resulting recurrence interval between the two youngest events is 1,100±1,000 years (Personius, 1991a). A colluvial wedge from an earlier event that occurred about 5 to 7 ka lacks suitable material for ^{14}C analysis and therefore has not been dated. Although the size of individual faulting events at this site is difficult to determine, the total vertical offset of the fan deposits (6 m) and the number of events (three) exposed in trench BC–1 indicate an average of 2 m of displacement per surface-faulting event and a post-middle Holocene slip rate of 0.75±0.3 mm/yr on the central part of the Brigham City segment.

Just south of the trench site, there are large scarps (15–20 m high) on the Provo-level delta at the mouth of Box Elder Canyon and elsewhere along the southern part of the segment (Personius, 1988a, 1990). These scarps and the 2 m of average displacement recorded in trench BC–1 indicate that as many as 6 to 10 surface-faulting events may have occurred on the central part of

the Brigham City segment since 14 ka. The distribution of fault scarps on latest Pleistocene and Holocene deposits indicates that the entire Brigham City segment has remained active throughout most of the early and middle Holocene. However, only a few small, short, discontinuous scarps near the southern segment boundary have been mapped on what could be upper Holocene deposits (Personius, 1988a, 1990). The general lack of fault scarps on young deposits and evidence in the Brigham City trench for only one faulting event in the past 3,000 to 4,000 years are in sharp contrast to the abundance of fault scarps on upper Holocene deposits along the Weber segment and evidence for multiple faulting events in the same general time period (Nelson and others, 1987; Nelson and Personius, 1990, in press) (see following discussion of the Weber segment).

The boundary between the Brigham City and Weber segments is near the northeastern corner of the Pleasant View salient, 3 km north of North Ogden, Utah (fig. 7) (Personius, 1986, 1988a, b, 1990; Nelson and Personius, 1987, 1990, in press). This salient, which was first recognized by Gilbert (1928), seems to be bounded on most sides by normal faults (Davis, 1985). The Pleasant View salient is a foundered block of Proterozoic and lower Paleozoic rock (Crittenden and Sorenson, 1985) that has been stranded at an intermediate structural level. The salient is broken by a network of short normal faults that are subsidiary to the main trace of the Wasatch fault zone. At least five of these faults offset deposits of the Bonneville lake cycle. Results from a trench excavated across one of these faults (PP–1, fig. 7) show about 5 m of vertical offset and evidence for three faulting events in the past 10 to 15 ka. Radiocarbon analysis of soil organics deposited in a tectonic crack in the penultimate colluvial wedge indicates that the most recent event occurred 4.6±0.5 ka (table A1) (Personius, 1991b). Analysis of ^{14}C ages suggests that the most recent event exposed in trench PP–1 is probably the same as the penultimate event recorded in trench BC–1 discussed above.

WEBER SEGMENT

The 61-km-long Weber segment of the Wasatch fault zone extends from Barrett Canyon, 3 km north of North Ogden, to the Salt Lake salient, a major footwall spur of bedrock that extends westward between Bountiful and northern Salt Lake City. The Weber segment comprises the southern two-thirds of Schwartz and Coppersmith's (1984) 70-km-long Ogden segment; we place the northern boundary of the Weber segment at the Pleasant View salient, well south of their boundary for the Ogden segment (fig. 9).

Rates of faulting differ along the Brigham City and Weber segments of the main fault on either side of the salient. Surface offset recorded by scarps and trench data from the Brigham City segment suggest that high rates of surface faulting occurred in latest Pleistocene to middle Holocene time but that tectonic activity must have slowed or ceased along the Brigham City segment in late Holocene time (Personius, 1988b). In contrast, fault scarps having 2 to 5 m of surface offset are common on deposits of late Holocene age on the northern part of the Weber segment. These differences in fault activity confirm that the Pleasant View salient is a Holocene boundary between two fault segments (Nelson and Personius, 1987).

Recent mapping (Nelson and Personius, 1990, in press) shows that the Weber segment of the Wasatch fault zone is expressed at the surface by almost continuous scarps on Holocene deposits from its northern end to as far south as North Canyon, south of Bountiful (fig. 9). Most of these scarps are formed on Holocene alluvial-fan and debris-flow deposits.

Upper Holocene alluvial fans composed of stream and debris-flow sediment are of at least two different ages along the Weber segment, but the degree of soil development and fan surface morphology cannot be used consistently to differentiate two or more ages of fans. Radiocarbon ages from the East Ogden site (discussed below and listed in table A1) indicate that even the older (Holocene) fan remnants exposed along the fault are less than 6 ka. Fault scarps of differing heights on the upper Holocene fans provide the only practical way of distinguishing fans of two ages, and such evidence is available at only a few stream drainages. Distinguishing fans by differing scarp heights assumes a uniform slip rate along the segment throughout the late Holocene.

Surface offsets measured along the fault indicate slip rates of 0.9 to 1.9 mm/yr over the past 15 ka for the central three-quarters of the Weber segment. Slip rates decrease as one approaches both ends of the segment. This relation was demonstrated by making topographic profiles of 77 scarps in the field and by using the USGS's computer-assisted PG–2 photogrammetric plotter to make an additional 298 profiles from 1:10,000-scale photographs (Nelson and Personius, 1990, in press). Comparison of field and plotter profiles of the same scarps (97 profiles) shows that the computer-assisted profiles generally yield surface offset values within ±10 percent of values measured from field profiles. This measurement error is similar to errors in estimating offsets from field-measured profiles, especially for scarps more than 5 m in height. In some areas, pre-1960 aerial photography has been used to measure profiles across scarps that were destroyed as much as 30 years ago by urbanization.

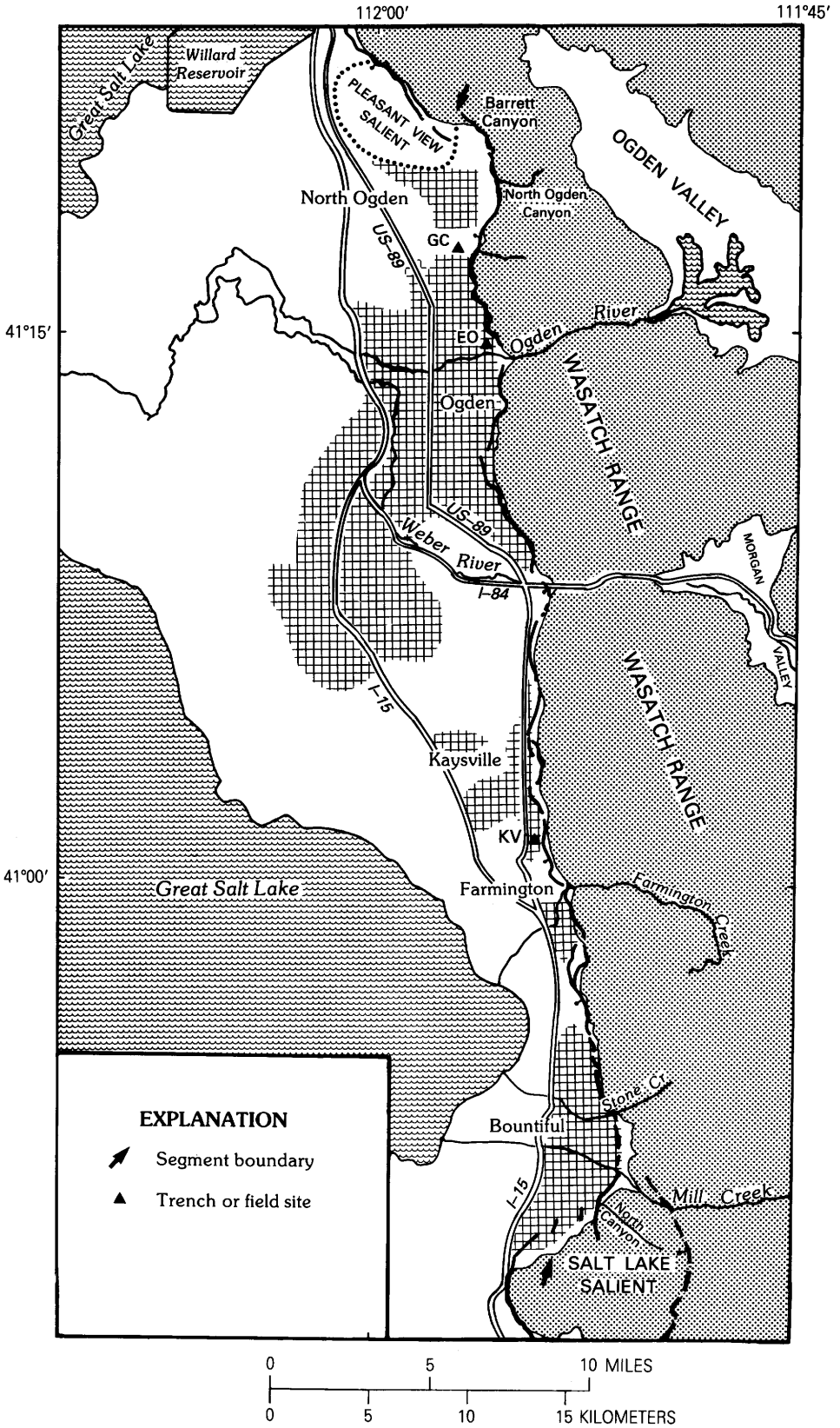

FIGURE 9.—Weber segment of the Wasatch fault zone between North Ogden and Bountiful, Utah, showing the main trace of the fault. Trench exposure sites are abbreviated as follows: GC, Garner Canyon; EO, East Ogden; KV, Kaysville.

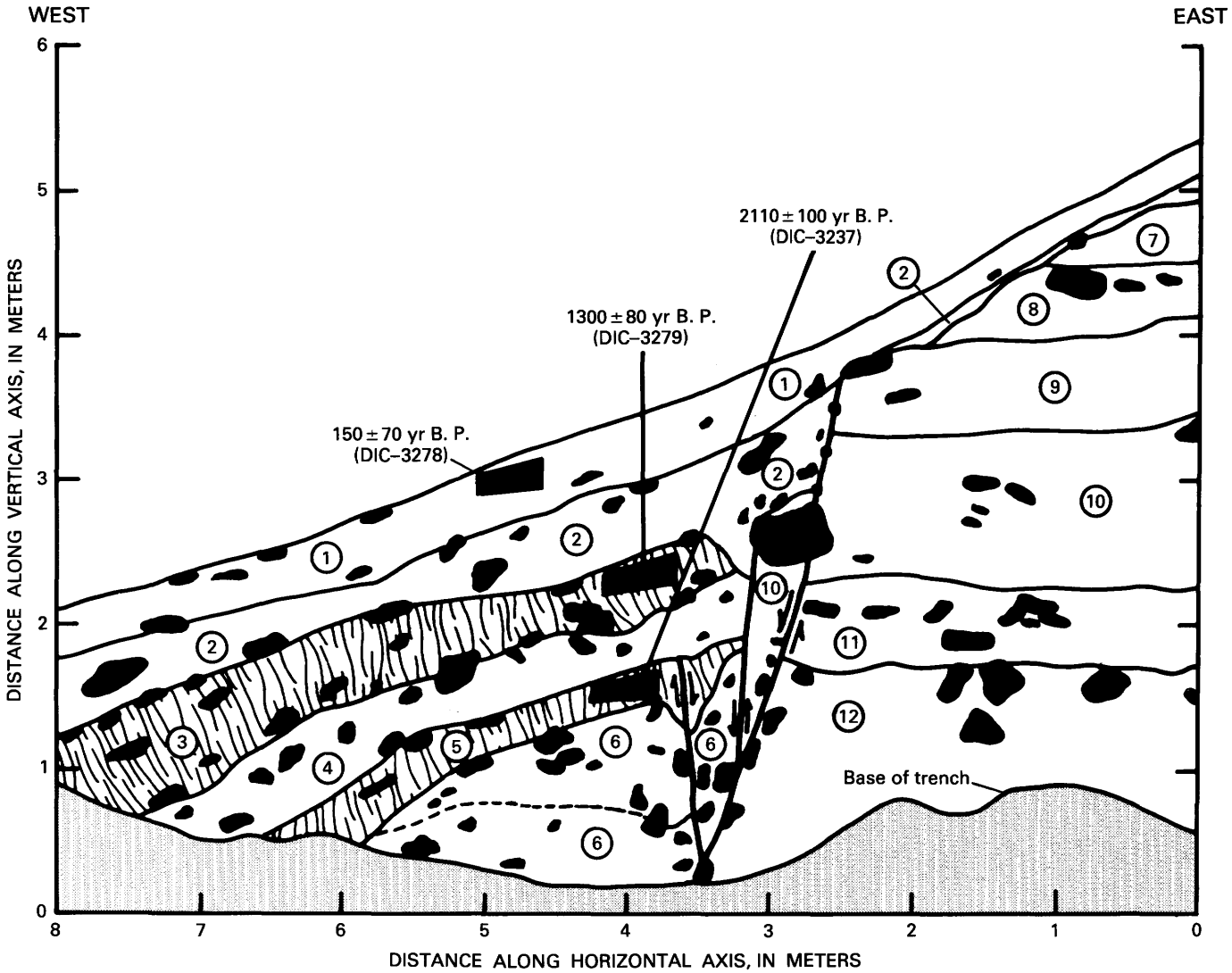

FIGURE 10.—Vertical exposure across a fault scarp at the mouth of Garner Canyon (Weber segment) near Ogden, Utah, showing the fault zone and colluvium produced by faulting events. The scarp (6 m high, 4.4-m vertical displacement) was produced by three or four earthquakes during the middle to late Holocene. Solid patches show boulders and large cobbles. Buried A horizons (units 3, 5) overlie cobbly debris wedges (units 4, 6) derived from a free face formed in stream and debris-flow material (units 7–12). Unit 5 has been displaced by a small antithetic fault. Radiocarbon dates (and laboratory numbers) (table A1) for A horizons are shown. Interpretation of these AMRT ages and correlations with estimated times of events at the East Ogden site suggest that the three most recent events occurred at more than 2.2 ka, 1.5 to 2.0 ka, and 0.8 to 1.2 ka.

The exposures at the East Ogden and Garner Canyon sites, near the northern end of the Weber segment (fig. 9), reveal a detailed middle and late Holocene fault history (Nelson and others, 1987; Nelson, 1988). Colluvial wedges, which were found in six exposures at these two sites, were deposited following the last three or four events on the fault. The vertical displacements measured in all exposures are similar to values of surface offset calculated from topographic profiles across the scarps. At the Garner Canyon site on the northern edge of Ogden, the last two events, each having about 1.0-m displacement, occurred about 1.5 to 2.0 ka and 0.8 to 1.2 ka. These ages are based on correlations with the East Ogden site and on ^{14}C AMRT ages on organic matter concentrated from soil A horizons (calibrated AMRT's) (fig. 10; ARN85–03 and ARN85–05, table A1). At the East Ogden site, two scarps on middle Holocene fan deposits (dated at about 5–6 ka) (ARN86–21, table A1) record about 5.3 and 8.1 m of total displacement. Where these scarps cross two upper Holocene fan deposits, the displacements are only about 1.2 and 1.8 m. Trenches across the 5- and 8-m scarps exposed deltaic deposits beneath fan deposits in the faults' hanging-wall block. The deltaic deposits probably formed at the Provo level

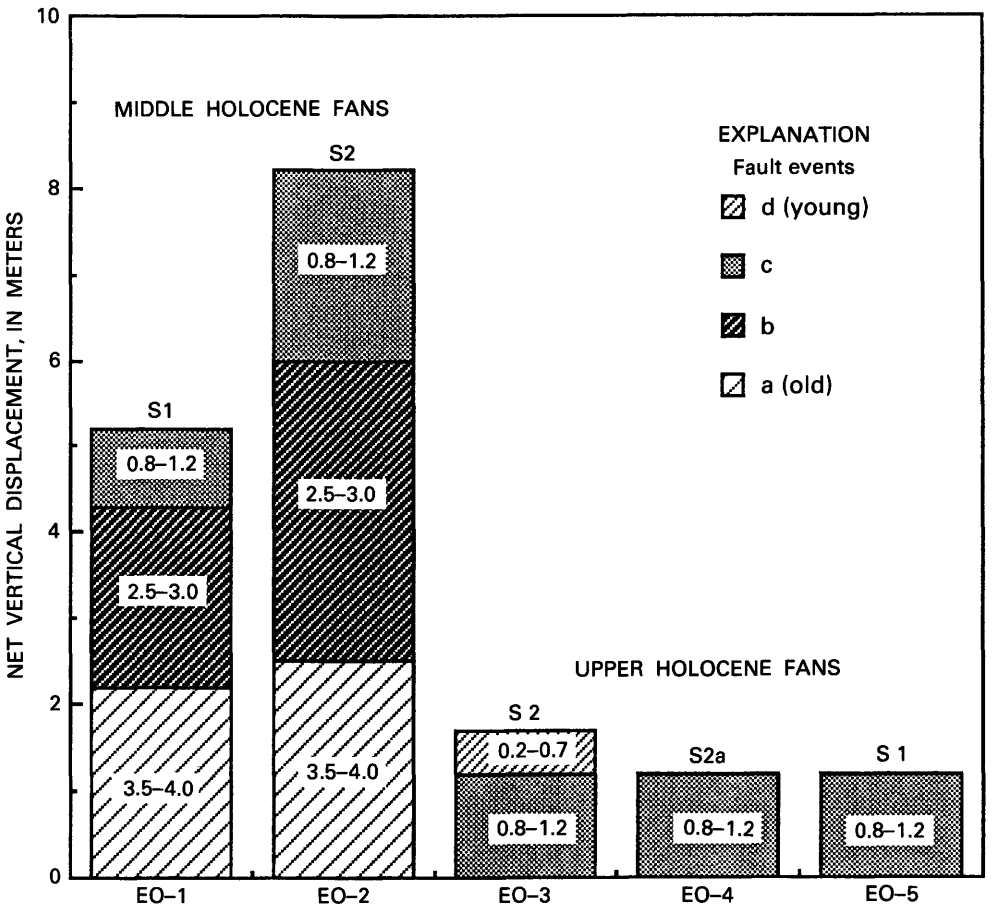

FIGURE 11.—Amounts of displacement and times of fault events recorded in five trenches at the East Ogden site (see fig. 9 for location of site). Correlation of faulting events is shown by patterned boxes. Event c is recorded in five trenches that cross both the 8-m scarp (S2) and the 5-m scarp (S1). Scarp S2a (trench EO–4) is antithetic to scarp S2 (trench EO–2), so most of the displacement for event c in trench EO–4 should be subtracted from the displacement for this event on the adjacent main scarp S2 (trench EO–2) to obtain the net displacement for this event near the 8-m (S2) scarp. Trench EO–3 contains evidence of a small young event (event d), for which no evidence was recognized in trenches EO–2 and EO–5 on the 8-m (S2) scarp.

of the Bonneville lake cycle about 14 ka. The stratigraphy and lithology of colluvium exposed in a trench across the 5-m scarp suggest two events, each of about 2.2-m displacement during the middle Holocene, followed by a 0.9-m event in the late Holocene (fig. 11) (ARN86–19, table A1). The colluvial sediments exposed in an adjacent 8-m scarp reveal two middle or late Holocene events of about 2.5- and 3.5-m displacement, followed by a 2.2-m event during the late Holocene (ARN86–06 and ARN86–13, table A1).

Thermoluminescence analyses of fine-grained distal colluvium in trenches EO–1 and EO–2 (Forman and others, 1991) help to constrain the age of the East Odgen fault events, particularly the earlier events that are poorly dated by ^{14}C analyses. A TL age estimate of 2,700±300 years (ITL–24, table A1) is probably a minimum for the second event in trench EO–1. Five age estimates from samples above ITL–24 (ITL–72, ITL–75, ITL–112, ITL–47, and ITL–113, table A1) suggest a nonuniform sedimentation rate for the distal colluvium adjacent to the 5-m scarp. Distal sediment was deposited in pulses in response to the two most recent faulting events. A TL age estimate of 3,200±300 years (ITL–74, table A1) also constrains the minimum time for the first event in trench EO–2 and the maximum time for the second event. This age estimate agrees well with a calibrated AMRT age of about 3.5 ka on a sample having a very low organic content from an equivalent stratigraphic position in trench EO–2 (ARN86–06, table A1). Thus, the TL age estimates suggest that the second

rupture event in both trenches (EO–1 and EO–2) is probably the same event—a conclusion that we could not draw solely from our ^{14}C ages.

The results of ^{14}C analyses of 3 charcoal samples and 16 samples of concentrated A-horizon sediment from the five trenches at the East Ogden site (see table A1) highlight many of the problems with using AMRT ages to estimate the time of faulting events on normal faults. Of the 10 samples collected within 1 m of the present surface, two pairs of samples have inverted ages (lower sample younger than a stratigraphically higher sample) (ARN86–23, ARN86–24 and ARN86–03, ARN86–04, table A1), and 3 samples yielded more than 112 percent modern carbon (ARN86–08, ARN86–14, and ARN86–15, table A1). These results are probably due to the incorporation of modern bomb (thermonuclear-blast-induced) carbon into modern A horizons by mixing of surface sediment into lower parts of the A horizon through unrecognized animal burrowing and, possibly, translocation of fine organic matter within coarse-grained horizons. Several of the AMRT ages may also reflect a reworking of old A-horizon sediment exposed in fault scarps into newly developing soils on colluvial debris wedges adjacent to the scarps (ARN86–24 and possibly ARN86-19, table A1). Comparison of all TL age estimates and ^{14}C ages shows that ^{14}C ages for deeper (buried) horizons are more consistent than those for shallower samples. Thus, fault events recorded by near-surface units (less than 1-m depth) are difficult to date accurately by means of AMRT ages, at least at sites like East Ogden, where most units are pervious sand or gravel.

Stratigraphic relations indicate that at least three, and probably four, faulting events have been recorded in trenches at the East Ogden site since the debris-flow units were deposited 5 to 6 ka (fig. 11). Both of the main faults probably ruptured to the ground surface during the three largest events (a, b, and c, fig. 11). Displacement at East Ogden during event c seems to have been only about half that during events a and b. On the basis of our interpretation of all the ^{14}C and TL analyses currently available, we estimate the timing of event a at 3.5 to 4.0 ka, that of event b at 2.5 to 3.0 ka, and that of event c at 0.8 to 1.2 ka. Mixing of near-surface stratigraphic units by burrowing, possible pedogenic translocation of carbon, and the interpretive problems with the AMRT ages on these units make it difficult to determine if the 8-m scarp at the site has been offset by a small-displacement event within the past 500±200 years (ARN86–04 and ARN86–43, table A1). If so, then the displacement was probably less than 0.8 m. These conclusions raise questions about the minimum size of displacement events that can be recognized in trenches, about whether large later events destroy evidence of small earlier events, and about the limits of AMRT ages in resolving faulting events spaced only 500 to 1,000 years apart.

Our studies show that the general history of faulting at the Garner Canyon and East Ogden sites is similar to the history determined from the Kaysville site (23 km to the south) (figs. 9, 12) by Swan and others (1980). They demonstrated at least three surface-faulting events during the past 8 ka (±2 ka), although the timing of each event was poorly constrained. Discrete colluvial wedges and correlative faulted and back-tilted graben deposits in the trenches were the basis for recognizing three faulting events. The two latest events occurred within the past 1.6 ka, and stratigraphic and geomorphic evidence suggests that the most recent event occurred within the past 500 years but before settlement of the area in 1847. Swan and others' (1980) best estimate for the elapsed time between faulting events is 500 to 1,000 years, the longer interval being preferred. The long-term record at Kaysville is recorded by a lower Holocene alluvial fan displaced 10 to 11 m. Because displacements produced by the two most recent events were 1.7 and 1.8 m, the prior 6.5 to 7.5 m of displacement may have occurred during the older third event. However, it seems more likely that the remaining fan displacement represents the cumulative displacement from two or more events that were not recognized in the trench.

Our limited age control at the trench sites prevents us from drawing more detailed conclusions about the history of faulting along the northern two-thirds of the Weber segment (fig. 12). Except for the last event, displacements at Garner Canyon are less than half the size of displacements at East Ogden for the same events, as would be expected for a site near (6 km) the end of a major fault segment. Even less dating control is available at the Kaysville site near the center of the Weber segment. A ^{14}C date of 1,580±150 ^{14}C yr B.P., which limits the maximum time of the two youngest events at Kaysville, suggests that event c and possibly event d (East Ogden site) are recorded here. If so, displacements during event c were comparable at the two sites, but displacement during event d was twice as large at Kaysville as it was at East Ogden. Possibly, event d is the result of an earthquake that ruptured only the central part of the Weber segment within the past 500±200 years. Other alternatives could be that evidence for event d at East Ogden has been misinterpreted and no event occurred or that a small youngest event ruptured the surface at the East Ogden site but did not reach or was not recorded at the Garner Canyon and Kaysville sites.

The southern end of the Weber segment is bounded by one of the most prominent salients along the Wasatch Front (Personius and Scott, 1990, in press; Nelson and

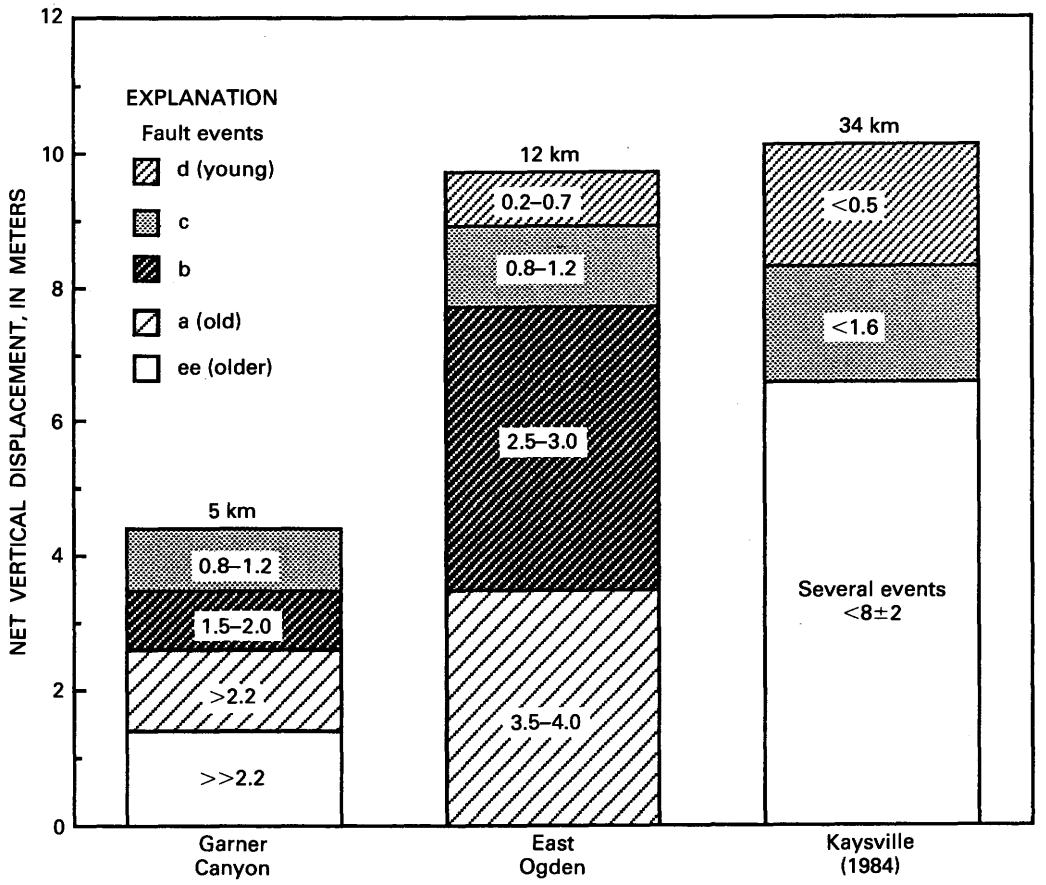

FIGURE 12.—Fault displacements and times of fault events (in thousands of years) derived from trenching and dating studies at three sites along the Weber segment of the Wasatch fault zone (fig. 9). Timing at the East Odgen site is summarized from data in table A1 and figure 11. Letter designations for events and shading for the East Ogden (EO) site match those shown in figure 11. Age estimates based on ^{14}C and TL analyses for faulting events are shown within patterned boxes. Shading patterns indicate only one of several reasonable event correlations from site to site. Because of limited age control, we cannot correlate events from site to site with certainty. If a small-displacement event d occurred at the East Ogden site, it may correlate with the last event at the Kaysville site, as suggested here. However, the last event at Kaysville (d) may also correlate with the last large event at East Ogden (event c). The last event at Garner Canyon is almost certainly the same event as the last large event at East Ogden (c). TL analyses from distal colluvium in trench EO–1 suggest that event b on that scarp is older than the penultimate event at Garner Canyon. Thus, the penultimate event at Garner Canyon does not seem to be recorded at East Ogden. Event a at East Ogden probably correlates with the first event (a) at Garner Canyon. In summary, at least three and probably four major fault events have occurred at each site in the past 5 ka, but uncertainties in correlation prevent us from determining whether the fault ruptured each site during each event.

Personius, 1990, in press). However, fault scarps in this area are easily confused with nontectonic features such as shorelines, scarps related to large lateral spreads, and small landslide headscarps. For this reason, the distribution of Holocene and latest Pleistocene scarps is less certain here than it is elsewhere along the segment. The main trace of the fault extends south of North Canyon (fig. 9). Other prominent north-south fault scarps also cross the Bonneville and lower shorelines along the middle portion of the northern edge of the salient. These faults extend into the Tertiary bedrock of the salient and have moved since the fall of the lake from the Bonneville shoreline. Other smaller scarps south of Stone Creek that parallel the shorelines on the salient's northern edge indicate that northeast-southwest-oriented latest Pleistocene or Holocene faults also bound the northern edge of the salient. Although all fault scarps may not have been identified in this area, we conclude (1) that the northern part of the Salt Lake salient contains many small faults with both north-south and northeast-southwest orientations; (2) that some of these faults have had significant displacements in the past 15 ka but that many have not

moved during the late Holocene; and (3) that, on the basis of scarp heights, latest Pleistocene and Holocene slip rates on faults near the salient are much lower than rates for the main trace of the fault along the remainder of the segment (Nelson and Personius, 1990, in press). As with the Pleasant View salient, which bounds the northern end of the Weber segment, these characteristics are typical of segment boundaries.

SALT LAKE CITY SEGMENT

The Salt Lake City segment of the Wasatch fault zone traverses the most populous part of Utah's Wasatch Front. Detailed mapping along the segment by Scott and Shroba (1985) and by Personius and Scott (1990, in press) indicated that most of the recent faulting is concentrated on the Warm Springs fault (west-bounding fault of the Salt Lake salient), on the East Bench fault (intrabasin fault and possible east-bounding fault of the Salt Lake salient), and on the main strand of the Wasatch fault zone (Cottonwood section of Personius and Scott, 1990, in press) that bounds the range front from Olympus Cove south to Corner Canyon on the northern flank of the Traverse Mountains (fig. 13).

Scott and Shroba (1985), Scott (1988), and Personius and Scott (1990, in press) summarized evidence for Holocene movement along the Warm Springs fault. The prominent north-trending scarps of the Warm Springs fault crossed young fans along the western edge of the Salt Lake salient near Beck's Hot Springs before gravel mining destroyed the surface evidence of this part of the fault. Gilbert (1928) noted that these scarps were 10 to 14 m high on two adjacent Holocene (post-Bonneville lake cycle) alluvial fans just south of Beck's Hot Springs (see Hunt, 1981, p. 27–29; Scott and Shroba, 1985, p. 6). The north-south trend of the scarps, their continuity (as shown on 1952 aerial photographs and old geologic maps), and their suspected Holocene age suggest that the Warm Springs fault is the main trace of the Wasatch fault zone in this area. Discontinuous scarps on the northwestern end of the salient appear to step eastward around the salient, filling a 2-km-wide gap between the northern end of the Warm Springs fault and the southern end of the Weber segment (Personius and Scott, 1990, in press; Nelson and Personius, 1990, in press). Between the southern end of the Warm Springs fault and the East Bench fault to the southeast (fig. 13), there is a 4-km gap in Holocene faulting, which coincidently is the location of downtown Salt Lake City.

The East Bench fault is the northeastward extension of the range-bounding Wasatch fault zone, which departs from the range front just south of Olympus Cove and extends basinward into the southern part of Salt Lake City. Farther north, the East Bench fault turns sharply to the northeast near the Dresden Place site (DP, fig. 13) and trends toward the mountain front, where it loses definition in surficial deposits. The northern end of the East Bench fault may coincide with bedrock faults that bound the eastern side of the Salt Lake salient (fig. 13) as mapped by Davis (1983a). From Olympus Cove north to downtown Salt Lake City, there is no evidence of active range-front faulting, whereas Holocene movement is concentrated on the East Bench fault.

In the fall of 1986, two deep exploratory trenches were excavated at the Dresden Place site in eastern Salt Lake City (DP, fig. 13; site 6, table 1). Although these trenches were open for inspection for only about 2 weeks, they have greatly increased our knowledge of this poorly studied part of the Wasatch fault zone. Inspection of the trenches by D.R. Currey (University of Utah) and M.N. Machette and mapping of the excavations by John Garr (written commun., 1987) revealed at least 7 m of deformation in sediment deposited during the transgressive phase of the Bonneville lake cycle (about 26–15 ka at this site). Of the 7 m of deformation, 3 m is expressed as monoclinal warping (plastic deformation) of deep-water sediment (laminated silt and clay). Currey suggested that, because plastic deformation probably requires saturation of the sediment, this deformation must have occurred before Lake Bonneville fell far enough below the altitude of the site (about 1,326 m or 4,350 ft) to cause dewatering of the sediment. The falling lake reached this altitude about 12.5 ka, as estimated from the hydrograph of Lake Bonneville that was constructed by Currey and Oviatt (1985, fig. 2). The rapid drawdown in Lake Bonneville and its successor's (Great Salt Lake) low level have caused the ground-water table at the Dresden Place site to be low throughout the Holocene. Therefore, the plastic deformation of the Lake Bonneville sediment must have occurred in latest Pleistocene time (15–10 ka, regressive phase of the Lake Bonneville cycle). At this site, the absence of colluvium within the plastically deformed lake beds suggests that the deformation occurred in a single tectonic event near or after deposition of the lake sediment but before dewatering occurred.

Plastic deformation was followed by at least 4 m of brittle deformation, as indicated by planar fault ruptures extending to the top of the undisturbed sediment in the trenches. Although the brittle deformation must be younger than 12.5 ka, it seems likely that it corresponds with one or more episodes of Holocene movement on the East Bench fault, as indicated by mapping of faulted Holocene sediment in areas immediately south of Dresden Place (Scott and Shroba, 1985; Personius and Scott, 1990, in press).

South of Salt Lake City, results of detailed mapping, exploratory trenching, and ^{14}C dating by Swan and

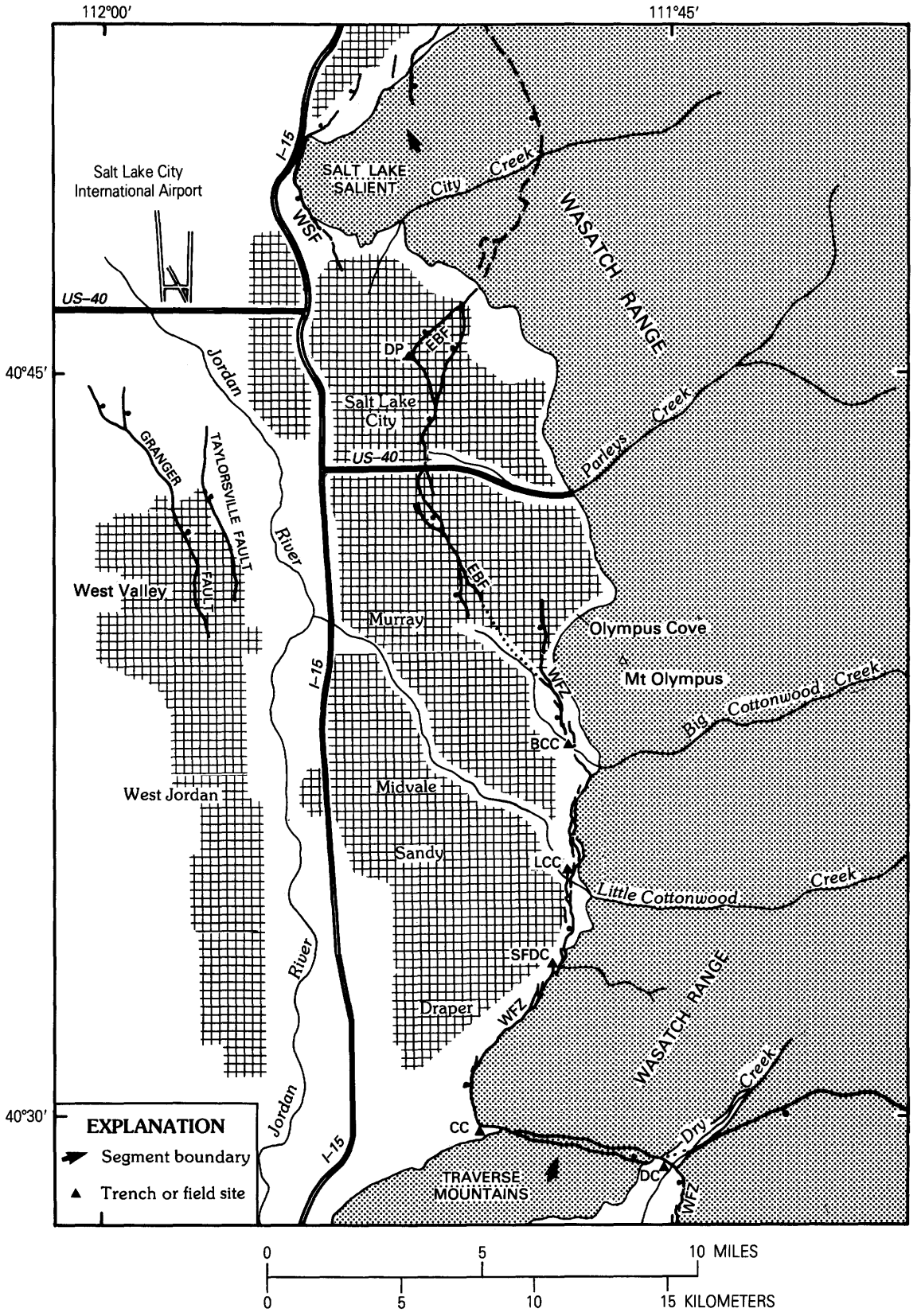
112°00'
111°45'
40°45'
40°30'
Salt Lake City International Airport
SALT LAKE SALIENT
I-15
WSF
US-40
DP
EBF
Salt Lake City
Jordan River
GRANGER
TAYLORSVILLE FAULT
FAULT
West Valley
West Jordan
Murray
Midvale
Sandy
Draper
WASATCH RANGE
City Creek
Parleys Creek
Olympus Cove
Mt Olympus
Big Cottonwood Creek
BCC
LCC
Little Cottonwood Creek
SFDC
WFZ
CC
DC
Dry Creek
TRAVERSE MOUNTAINS
EXPLANATION
Segment boundary
Trench or field site
0 5 10 MILES
0 5 10 15 KILOMETERS

others (1980) at the mouth of Little Cottonwood Canyon (LCC, fig. 13; site 7, table 1) indicated several surface-faulting events during the past 19 ka (assumed age of faulted till) and at least one event within the past 8 ka. Their study suggested an average slip rate of 0.76 mm/yr (+0.6 mm/yr, −0.2 mm/yr), an average displacement of 2 m per event and an average recurrence interval of 2,400 to 3,000 years since the culmination of the transgressive phase of the Bonneville lake cycle (15 ka). However, the complex pattern of deformation in this part of the Wasatch fault zone prevented an accurate determination of the timing of the most recent event at the Little Cottonwood Canyon site.

In 1985, at the South Fork of Dry Creek (SFDC, fig. 13; site 8, table 1), the UGMS and USGS began a program of aerial photograph interpretation, scarp profiling, exploratory trenching, and ^{14}C dating to obtain additional paleoseismic information on the Salt Lake City segment. (This site is referred to as the South Fork of Dry Creek because there is a second, larger Dry Creek northeast of Alpine, Utah, along the Provo segment of the Wasatch fault zone.) Interpretations of the stratigraphic and structural relations of the site (South Fork of Dry Creek) have been finalized by Lund and Schwartz (1987), but they have not yet published their final analysis of recurrence intervals and slip rates or data for the timing of the faulting events.

The site at the South Fork of Dry Creek is about 2.5 km south of Little Cottonwood Canyon, between the steep front of the Wasatch Mountains and the highest of the Bonneville shorelines. Here, the Wasatch fault zone has as many as six west-facing scarps that form a complex en echelon zone of deformation as much as 305 m wide (fig. 14). Unconsolidated surficial deposits between the mountain front and the Bonneville shoreline include (from youngest to oldest) Holocene debris-flow deposits, late Pleistocene or early Holocene alluvial-fan and debris-flow deposits, and small remnants of middle Pleistocene alluvial-fan deposits (Scott and Shroba, 1985; Lund and Schwartz, 1987; Personius and Scott, 1990, in press). Geomorphic surfaces associated with these deposits are dropped progressively down to the west across the fault zone. The cumulative displacement of these surfaces and their deposits becomes greater with increasing age and thus indicates a history of recurrent faulting in the late Pleistocene and Holocene.

The youngest deposits at the trench site are two upper Holocene debris flows; the northern one flowed several hundred meters downslope (west) from the mouth of the South Fork of Dry Creek, and a second one deposited a lobe at the mouth of Dry Gulch, the next canyon to the south (fig. 14). The debris flow along the South Fork of Dry Creek formed distinct levees, which were later

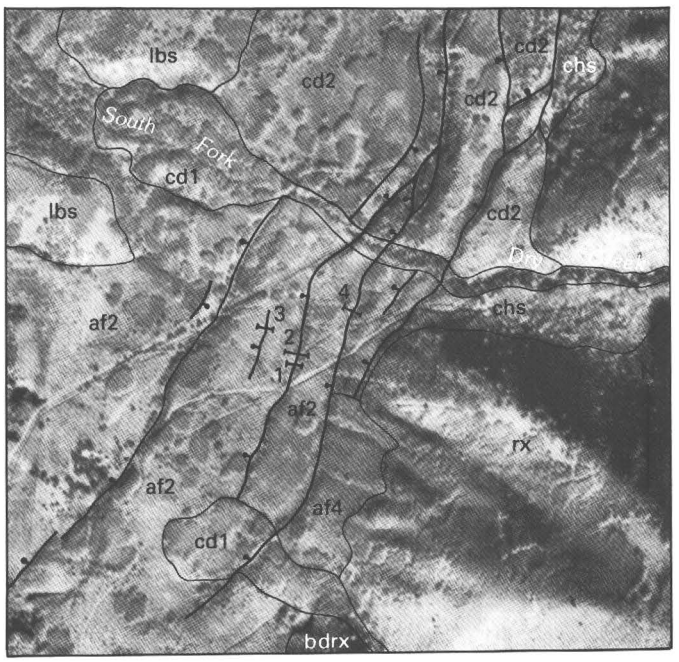

FIGURE 14.—Surficial geology at the South Fork of Dry Creek site, Salt Lake City segment of the Wasatch fault zone (Lund and Schwartz, 1987). Geology modified from Scott and Shroba (1985) by W.R. Lund and D.P Schwartz (written commun., 1988). Figure 13 shows the location of this site (SFDC). (Photograph courtesy of W.R. Lund, Utah Geological and Mineral Survey.)

◀ FIGURE 13.—Traces of the Salt Lake City segment, including the main Wasatch fault zone (WFZ), the East Bench fault (EBF), and the Warm Springs fault (WSF). Traces of the Taylorsville and Granger faults of the West Valley fault zone are also shown. Faults are shown by heavy lines having a bar and ball on the downdropped side. Also shown are important geographic features and towns. Trench and field sites are abbreviated as follows: DP, Dresden Place; BCC, Big Cottonwood Canyon; LCC, Little Cottonwood Canyon; SFDC, South Fork of Dry Creek; CC, Corner Canyon; DC, Dry Creek.

displaced by movement on five of the six faults that form laterally continuous scarps in the study area (fig. 14). The sixth, most basinward fault does not displace the levees but is buried by them, an indication that at least two discrete episodes of surface faulting occurred at the site. This relation is consistent with the results of Lund and Schwartz's exploratory trenching, which shows that both single- and multiple-event scarps are present along the faults at this site but that no more than two surface-rupture events were recognized in any trench (W.R. Lund and D.P. Schwartz, oral commun., 1987). By comparing the amount of displacement in the levees with that in the trenches, Lund and Schwartz have shown that, for multiple-event scarps, only the most recent event displaced the levee; hence, the earlier faulting event must have occurred before deposition of the debris flow. In addition, the displacement observed on single-event faults in the trenches corresponds closely with that measured from scarps on the levees.

In 1985, W.R. Lund and D.P. Schwartz collected organic matter from buried A horizons exposed in the trenches. So far, they have obtained three AMRT ages from a buried soil that is formed on the older of two colluvial wedges exposed in the trenches. The older wedge was downdropped during the most recent faulting event and subsequently buried by a younger colluvial wedge. The first age obtained from the buried soil was 1,890 ^{14}C yr B.P. (Lund and Schwartz, 1987). A second sample from the same soil (age) yielded an age that is significantly younger than the first determination (Schwartz and others, 1988) but in accord with a minimum age estimate of 900 years (Lund and Schwartz, 1987) as determined from diffusion modeling of the morphology of the single-event fault scarp. Calendar (but not AMRT) calibration of these two ^{14}C ages constrains the most recent event to between 1,130 and 1,830 cal yr B.P. (Schwartz and others, 1988). The third sample from the buried soil has recently yielded an AMRT date of about 1,500 ^{14}C yr B.P. (D.P Schwartz and W.R. Lund, written commun., 1989), which is near the midpoint of the earlier range of dates. Schwartz and Lund currently interpret the most recent faulting at the South Fork of Dry Creek to have occurred about 1.5±0.3 ka.

We have found that ^{14}C dating of organic matter from modern (surface) A horizons along the Wasatch fault zone commonly yields AMRT ages of several hundred years (see discussion in appendix); these ages reflect the accumulation and cycling of carbon in A horizons over time. Thus, AMRT ages from buried A horizons should predate the time of A horizon burial.

The maximum time for the older event at the site is constrained by calendar-corrected ^{14}C ages from soil organics of 5,455 and 5,975 cal yr B.P. (Schwartz and others, 1988) and a TL age estimate of 5,525±390 cal yr from the soil on the older, twice-faulted alluvial-fan deposits. These ^{14}C dates (which do not consider the age of the soils at the time of burial) show that the faulted deposits are middle Holocene rather than latest Pleistocene and thus are similar in age to many other remnants of alluvial fans along the Wasatch Front.

The site at the South Fork of Dry Creek records two large displacements (each about 4.5 m) during the past 5.5 ka and a Holocene slip rate that exceeds 1 mm/yr (4.5-m displacement in as little as 3,700–4,400 years). At present, the recurrence interval on this segment of the Wasatch fault zone appears to be rather long (that is, 3,500–4,000 years) if one assumes that the younger event is 1.5±0.3 ka and the earlier event is middle Holocene (5.0–5.5 ka, the preferred range). An important conclusion of Schwartz and Lund's trenching is that the fault scarps are the product of either one or two large displacements rather than many small displacements closely spaced in time. In addition, the observation that similar-sized displacements were repeated at this site on the Wasatch fault zone fits Schwartz and Coppersmith's (1984) model of characteristic fault behavior.

Keaton and others (1987) and Keaton and Currey (1989) have completed a study of the West Valley fault zone (fig. 13), part of which lies about 5 km west of Salt Lake City. Although this fault zone is 8 to 10 km west of the East Bench fault of the Wasatch fault zone, discussion of the West Valley fault zone is included here because it is a major (down-to-the-east) fault zone that may be related to the adjacent Wasatch fault zone.

The West Valley fault zone strikes north-northwest of the Jordan River in the north-central part of Salt Lake County (fig. 13) (Personius and Scott, 1990, in press). Two principal surface traces of the fault zone—the Granger and Taylorsville faults—were identified in the early 1960's by Marsell and Threet (1964). Keaton and others (1987) found that the two principal faults each have evidence of Holocene movement. Numerous previously unmapped but suspected fault scarps and lineaments were found as far as 9 km north of the limits of the fault zone as recognized by Marsell and Threet (1964) (see Keaton and others, 1987, figs. 2, 18). These suspect features extend the West Valley fault zone north to the vicinity of Salt Lake City International Airport (fig. 13); as such, the fault zone forms an area of deformation about 7 km in width and 16 km in length.

The Granger fault (site 19, table 1) forms the westernmost of the two scarps of the West Valley fault zone and shows evidence of 4.5 to 12.2 m of normal slip (down to the east) within the past 12 ka; these data yield a minimum slip rate of 0.4 to 1.0 mm/yr (Keaton and others, 1987). Faulted sediment of a previous lake cycle (probably the Cutler Dam lake cycle of Oviatt and others (1987)) was found by Keaton and others (1987) on the

TABLE 4.—*Timing and number of surface-faulting earthquakes and recurrence intervals for Holocene movement on the Wasatch fault zone*

[All values for age and time are rounded to the nearest 50 years]

Segment (no.)	Site	A Age of oldest faulting event or datum (cal yr B.P.)	B Estimated time of most recent faulting (cal yr B.P.)	C Time between A and B (yr)[1]	D Number of faulting events and intervals	
					Events	Intervals
Brigham City (1)	Trench BC–1	[2]4,700±500	3,600±500	1,100±1,000	2	1
Weber (2)	East Ogden	[2]3,750±250	500±300	3,250±550	4	3
Salt Lake City (3)	Dry Creek	[2]5,250±250	1,500±300	3,750±550	2	1
Provo (American Fork part) (4)	AF–1, AF–2	[2]5,300±300	500±200	4,800±500	3	2
Nephi (5)	North Creek	[3]5,300±200	[4]400	4,900±200	3	2
Levan (6)	Deep Creek	[3]7,300	1,000	[5]—	1	0
Total (based on segments 1–5)				17,800±2,800	15	9

Calculated recurrence interval[6] (yr)	
Average recurrence[7] on:	
Single segment of the Wasatch fault zone	1,980±310
All segments of Wasatch fault zone having repeated Holocene movement (CRI)[8]	395±60

[1]Time intervals for some sites include time between the oldest event at a site and the age of the datum; thus, some values in this column are maximums.

[2]Age of oldest recorded faulting event.

[3]Age of faulted datum estimated from dating and stratigraphic and tectonic considerations.

[4]No error limits assigned to this estimate.

[5]Not applicable. Only one faulting event was recorded, so no recurrence interval can be calculated.

[6]Three significant figures are used to compute average values of recurrence from the mean of the sum of column C. Reported values are rounded to the nearest 5 years.

[7]Average recurrence interval is determined by dividing the sum of time in column C by the sum of intervals between faulting events in column D.

[8]Composite recurrence interval (the recurrence interval for movement on any of segments 1–5).

footwall of an exploratory trench and in drill holes on the hanging wall. The calculated displacement of the sediment ranges from 12.2 to 19.8 m; Keaton and others (1987) assigned an age of 58 ka to the lacustrine beds on the basis of correlation with the end of marine isotope stage 4, which should have been represented by a pluvial episode in the Bonneville Basin. The resulting average slip rates for the Granger fault since the end of the Cutler Dam lake cycle are 0.21 to 0.34 mm/yr. In addition, Keaton and others (1987) suggested that slip rates on the Granger fault may have been about 0.1 mm/yr since the culmination of the last major pre-Bonneville lake cycle (about 130 ka). These estimates are derived from the projected offset of lacustrine beds penetrated by drill holes on both sides of the fault.

The markedly different average slip rates recorded by pre-Bonneville lake cycle and post-Bonneville lake cycle (less than 12 ka) suggested to Keaton and others (1987, p. 25) that the deep water of Lake Bonneville may have suppressed strain release along the West Valley fault zone, whereas strain release may have been accelerated after Lake Bonneville started to drain at about 14.5 ka. Similar evidence and interpretations of large changes in average slip rates before and after Lake Bonneville's culmination have been suggested for a number of points along the Wasatch fault zone (Machette, 1984; Machette and others, 1986) by comparing the net displacement in late Pleistocene and Holocene deposits of different ages (see "Discussion of Slip-Rate Data for the Wasatch Fault Zone" and the accompanying fig. 21).

The Taylorsville fault (site 20, table 1), the easternmost of the two topographic escarpments of the West Valley fault zone, was formed by 1.5 m of monoclinal flexure (down to the east) and laterally discontinuous faulting in the past 5 to 7 ka (Keaton and others, 1987; Keaton and Currey, 1989). The resulting uplift (deformation) rate across the Taylorsville fault has been 0.21 to 0.30 mm/yr, which is comparable to the longer term (58 ka) values determined from the adjacent Granger fault. Keaton and others (1987) speculated that the Taylorsville fault may be the surface expression of a fault that has earthquakes just slightly above the threshold magnitude (taken as M_S 6.5) that would create a continuous surface rupture along a discrete fault plane. Their seismological analysis (table 4) suggests that earthquakes as large as M_S 7.0 could be reasonable for a surface rupture having a displacement of as much as 1.5 m along the West Valley fault zone. Such faulting would have had an average recurrence interval of 1,000 to 4,000 years on the Granger fault and 5,000 to 7,000 years on the Taylorsville fault during the past 15,000 years.

The west-trending Traverse Mountains form a major bedrock salient at the southern end of the Salt Lake Valley and are the boundary between the Salt Lake City and Provo segments of the Wasatch fault zone. The Traverse Mountains are one of four such salients that

form major structural barriers along the Wasatch fault zone (Wheeler and Krystinik, this volume).

Scott and Shroba (1985) and Personius and Scott (1990, in press) traced surface ruptures of the Salt Lake City segment along the Wasatch Front as far south as Corner Canyon on the northern side of the Traverse Mountains, where the fault scarps turn from a south to an east-southeast strike. In this area, the Wasatch fault zone forms a broad gouge zone into which Corner Canyon has been excavated. From Corner Canyon (CC, fig. 14), the Wasatch fault zone turns eastward and dips shallowly to the south (Bruhn and others, 1987), where it separates intrusive rock of the Little Cottonwood stock (middle Tertiary) from late Tertiary fanglomerate (Salt Lake Formation), extrusive volcanic rock (middle Tertiary), and the underlying platform of the upper Paleozoic Oquirrh Formation (Personius and Scott, 1990, in press). This geology differs from the mapping done by Davis (1983a), who mapped the fanglomerates as Oquirrh Formation), and indicates more structural relief than previous work had suggested. Machette (1989, in press) has traced the Wasatch fault zone continuously across the salient from Corner Canyon to the mouth of Dry Creek (DC, fig. 15), where uppermost Pleistocene glacial outwash is displaced 3 to 5 m (this Dry Creek is about 3 km northeast of Alpine, Utah). Upper Quaternary alluvium at the head of the Traverse Mountains (salient) has been offset by the Wasatch fault zone, an indication that the salient is being actively deformed, albeit at an appreciably slower rate than the segments to the north and south. The major bend in the Wasatch fault zone in this area, named the Fort Canyon fault by Bruhn and others (1987), corresponds to the westward projection of the south-dipping Deer Creek fault (DCF, fig. 15), which is the northern limb of an east-vergent Laramide thrust fault. These transverse structures allow the Wasatch fault zone to step 8.5 km to the east (left) across the Traverse Mountains.

PROVO SEGMENT

Schwartz and Coppersmith (1984) suggested that the section of the Wasatch fault zone from the Traverse-Mountains south to Payson Canyon is a single segment and named it the Provo segment. This segment, reported as 55 km long, was one of the longest of the fault zone. In 1986, as a result of his preliminary mapping and scarp morphology studies in the Utah Valley, Machette tentatively subdivided the original Provo segment (which he measured at 70 km long) into the American Fork, Provo (restricted sense), and Spanish Fork segments (Machette and others, 1986). Since then, detailed mapping and trenching at three new sites have indicated that Schwartz and Coppersmith's (1984) suggestion of one segment is probably correct. Thus, in the following discussions, the American Fork, Provo (restricted sense), and Spanish Fork segments of the fault are considered to be parts of the Provo segment for the purpose of discussion. In this sense, they are much like the geometrically defined segments of de Polo and others (1989, 1991).

All of the data from exploratory trenching along the Provo segment are compatible with earthquakes that rupture the whole 70-km-long segment. Although this length of rupture seems long from historical and paleoseismic perspectives, we cannot disprove complete rupturing during M>7 earthquakes.

AMERICAN FORK PART

The American Fork part of the Provo segment forms the northeastern border of the Utah Valley and is short in comparison with most of the proposed segments along the central, active part of the Wasatch fault zone (about 22.5 km as opposed to an average of 48 km) (table 2). The Wasatch fault zone has an en echelon 2-km left step at the Provo River, which Machette considered to be the probable southern boundary of the proposed American Fork segment. This proposed segment boundary was partly supported by Zoback's (1983) compilation of gravity for the region, which shows a prominent gravity saddle (a local high) within the Utah Valley adjacent to Provo River Canyon, between strong lows to the north and south that probably represent subbasins of the Utah Valley.

Most of the paleoseismic data for this part of the Provo segment comes from a trenching site near American Fork Canyon, where the Quaternary geology had been mapped at a scale of 1:10,000 by Machette (1989, in press). The American Fork Canyon site (AFC, fig. 15) is characterized by a large, well-preserved fan-delta complex that was constructed during the transgressive phase of the Bonneville lake cycle.

A widespread but thin mantle of calcareous loess was deposited across the landscape as newly exposed sediment of the Bonneville lake cycle was eroded by the

FIGURE 15.—Main trace of the Provo segment of the Wasatch fault zone (WFZ) between the Traverse Mountains and Dry Mountain, showing the American Fork part (to the north), the central part, and the Spanish Fork part (to the south). Faults are shown by heavy lines having a bar and ball on the down-dropped side (dotted where uncertain). Also shown are important geographic features and towns. Trench and field sites are abbreviated as follows: CC, Corner Canyon; DC, Dry Creek; AFC, American Fork Canyon; RC, Rock Creek; HC, Hobble Creek; MN, Mapleton North; MS, Mapleton South; WC, Water Canyon. Faults are abbreviated as follows: WH, Woodland Hills splay; SF, Springville (near the middle of the Provo segment); BF, Benjamin (northern end of Nephi segment). ▶

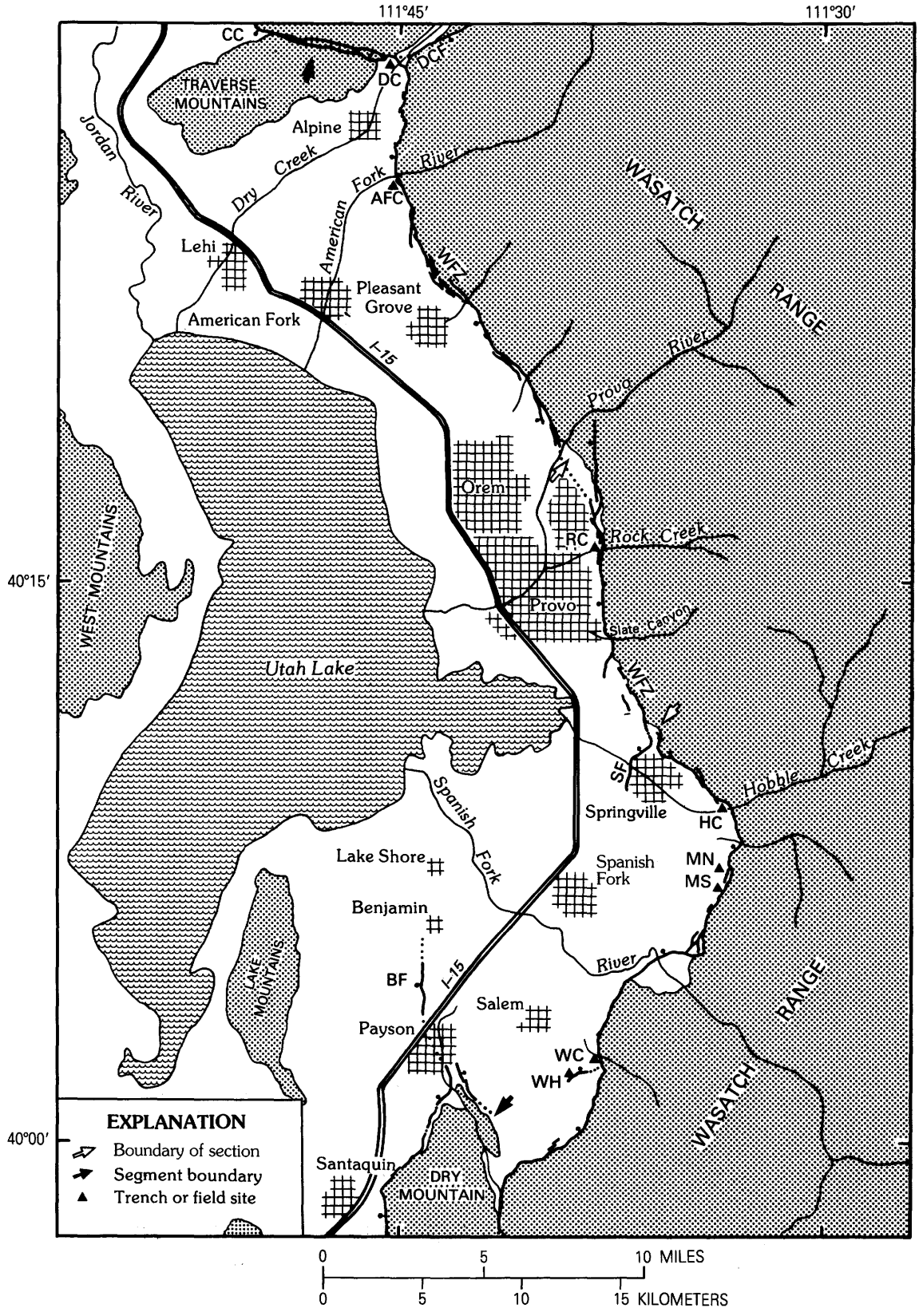
111°45′
111°30′
40°15′
40°00′
CC
DC
DCF
TRAVERSE MOUNTAINS
Alpine
Jordan River
Dry Creek
American Fork River
AFC
WASATCH RANGE
Lehi
American Fork
Pleasant Grove
WFZ
I-15
Provo River
Orem
RC
Rock Creek
Provo
Slate Canyon
WEST MOUNTAINS
Utah Lake
SF
Hobble Creek
Springville
HC
Spanish Fork
Lake Shore
Spanish Fork
MN
MS
Benjamin
BF
I-15
Salem
Payson
LAKE MOUNTAINS
WC
WH
Santaquin
DRY MOUNTAIN
EXPLANATION
Boundary of section
Segment boundary
Trench or field site
0 5 10 MILES
0 5 10 15 KILOMETERS

wind. This process probably continued from about 13 ka well into the early Holocene. Overlying the loess are local alluvial fans that consist mainly of coalesced debris-flow deposits and alluvium of early(?) to middle Holocene age. Textural analysis of the matrix of the debris flows (M.N. Machette, unpub. data, 1987) shows that they were derived from the loess mantle, which now has been completely eroded from the mountainous slopes. An age of 7,290±100 ^{14}C yr B.P. (AA–2268, table A1) was obtained from charcoal in the loess in trench AF–3 (see following trench discussion), whereas an age of 4,740±90 ^{14}C yr B.P. (AA–2266, table A1) was obtained from charcoal in debris flows that overlie the loess. These two age determinations correspond to calendar-calibrated dates of 8,061 and 5,518 cal yr B.P. (the respective one-sigma error limits are generally ±200 years) (table A1). The younger date comes from charcoal in a burn layer between flows about 1 m below the surface of the debris-flow package and may predate the surface of the alluvial fan by 100 years or less (there are no intervening soils). Therefore, the ^{14}C dates constrain the timing of a major phase of debris-flow deposition and associated fan building at the American Fork site from about 8.0 to 5.4 ka—that is, from early to middle Holocene.

The American Fork part of the Provo segment is marked by a prominent set of scarps at the foot of the Wasatch Range, both north and south of American Fork Canyon (Machette, 1989, in press). Repeated movement across the fault zone has produced progressively more net displacement in middle to late Pleistocene deposits than it has in latest Pleistocene (Bonneville lake cycle) and Holocene deposits. The fan-delta complex at American Fork Canyon was abandoned about 14.5 ka during the fall to the Provo shoreline level. South of the canyon, gravel of the highest Bonneville shoreline is displaced 15 to 20 m across a 50-m-wide graben. North of the canyon, gravel at the same level is displaced 26 m across a large scarp lacking a graben. Maximum and minimum values of net displacement of the gravel yield maximum and minimum slip rates of 1.7 and 1.0 mm/yr for the past 14.5 ka. In contrast, the long-term slip rates recorded by 130- to 250-ka alluvium along this part of the Provo segment and other segments of the central Wasatch fault zone are only 0.1 to 0.3 mm/yr (Machette, 1984). These long-term slip rates are almost an order of magnitude less than slip rates recorded since Lake Bonneville fell from its highest level 14,500 years ago (see "Discussion of Slip-Rate Data for the Wasatch Fault Zone").

In 1986, Machette and Lund excavated three 25- to 50-m-long trenches across the Wasatch fault zone at the American Fork Canyon site. All three trenches were located on faulted alluvial fans that consist primarily of debris-flow deposits, the surface of which we consider to have become stabilized by about 5.4 ka on the basis of the previously mentioned ^{14}C ages (table A1). The trenches showed conclusively that the middle Holocene deposits commonly are displaced 7 to 8 m by three faulting events where the fault zone has a simple geometry of single or multiple parallel normal faults (Machette and Lund, 1987).

Trench AF–1, the deepest and longest of the trenches, was placed across the 8-m-high main fault scarp and penetrated a relatively simple stack of three colluvial wedges, each of which was derived from erosion of material newly exposed in the scarp during faulting (fig. 16). In turn, each wedge is separated by thick, well-developed A horizons and weakly developed calcic A horizons (Ak) or Ck horizons. The uppermost buried soil in trench AF–1 (sample F86–U8, fig. 16) yielded a TL age estimate of 400±100 cal yr (ITL–23, table A1). Organic carbon from the upper part of the A horizon of the same soil (sample AF–1C, fig. 16) yielded a ^{14}C age of 980±70 ^{14}C yr B.P. (USGS–2532, table A1). The calibrated AMRT age for the A horizon sample is 713 cal yr B.P. (the range is 620–830 yr B.P.). This date and the TL age estimate place a maximum limit on the time of most recent faulting. However, we estimate an age of about 0.5 ka for the burial of the upper horizon contact (UHC) of the soil (see table A1) by inferring a mean-residence correction (MRC) of 200 years at the time of burial. In addition, charcoal within the youngest fault-scarp colluvium (sample AF–1A, fig. 16) was dated at 140±120 ^{14}C yr B.P. (AA–2267, table A1); it has a permissible calendric age range of modern (post-1950) to 480 cal yr B.P. owing to three possible dendrochronologic dates. We consider 207 cal yr B.P. (the mean value of the three dates) as an absolute minimum time limit for the most recent event, owing to the position of the charcoal within the wedge and to the possibility of contamination by modern carbon (see prior discussion of "Weber Segment").

Dating of samples from trench AF–2 also yielded a combination of TL and ^{14}C ages that places additional constraints on the time of most recent faulting (fig. 17). Trench AF–2 crossed an east-facing scarp that is antithetic to the main fault scarp, which here is nearly 10 m high. These two scarps form a graben that is about 25 m wide and 50 m long. Faulted sag-pond silt that is buried by the youngest fault-scarp colluvium has a TL age estimate of 500±200 cal yr (ITL–3, table A1), whereas the upper 5 cm of a thick organic-rich buried A horizon immediately below the silt has an age of 620±150 ^{14}C yr B.P. (USGS–2533, table A1).

The lack of coarse clasts in the silt layer in the sag pond indicates that it is an eolian accumulation; therefore, the sediment must have been fully exposed to sunlight and should have had no TL signal at the time of burial by the youngest colluvial wedge. The age determined for the silt

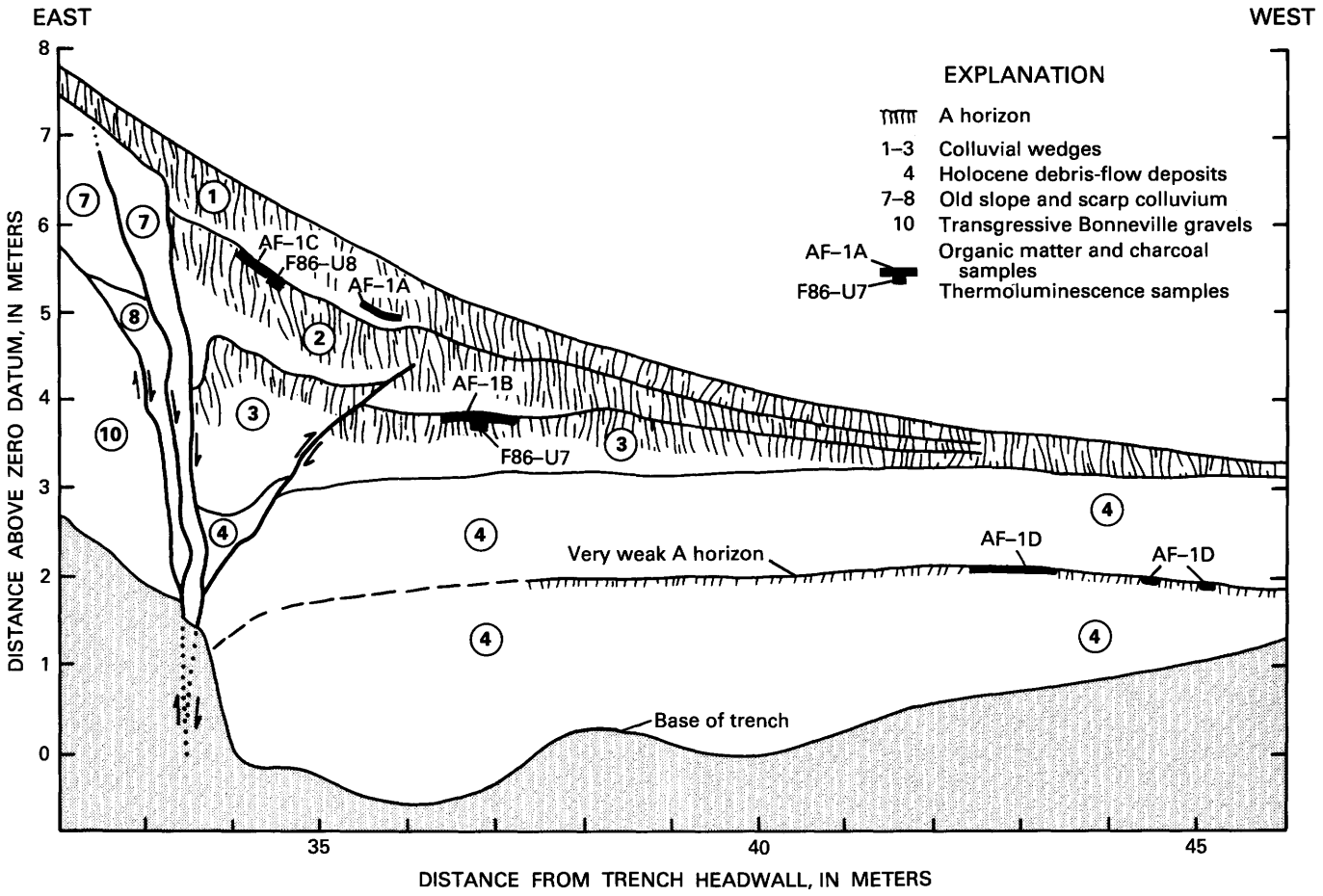

FIGURE 16.—Part of the log of trench AF–1 at the American Fork Canyon site, Provo segment of the Wasatch fault zone. Diagram shows the relation of three colluvial wedges and soils (units 1–3) to units on the upthrown and downdropped fault blocks on the southern wall of the trench. Field sample numbers refer to dating control shown in table A1.

should approximate the time at which the sag pond was buried and, thus, date the time of the most recent faulting event. The buried A horizon has a thick accretionary profile that must have required a long time to form (that is, probably many hundreds to perhaps a thousand years). However, we estimate that the carbon in the upper 5 cm of the accretionary A horizon has an estimated age span (CAS) of only about 150 years (table A1). The AMRT age of the A horizon sample is 620±150 ^{14}C yr B.P. (USGS–2533, table A1), which yields a calibrated date of 612 cal yr B.P. (the age range is 360–830 cal yr B.P.). Because we sampled only the uppermost 5 cm of the buried A horizon, we subtract 100 years for the MRC of the upper soil contact (table A1). Using the calibrated AMRT date and MRC, we estimate an age of about 0.5 ka for the UHC of the buried A horizon.

The combination of two ^{14}C ages and two TL age estimates from trenches AF–1 and AF–2 provides four constraints on the time of the most recent faulting at the American Fork Canyon site. The calibrated AMRT ages of 713 and 612 cal yr B.P. provide maximum limits. The TL age estimates, which should also provide close maximum dates for the time of faulting, are 400±100 and 500±200 cal yr (fig. 17). Thus, our age estimates for the buried soil and silt suggest a probable age of 0.5 ka for the UHC of the soil formed on colluvial wedges that were downfaulted and buried during the most recent faulting event.

Interpretation of the error limits for the AMRT ages is problematic, owing to corrections for the MRC of the upper soil contact. The analytical errors associated with the determinations carry over to the UHC age estimates, but all of the ages appear to fall within overlapping error limits. However, the accuracy of TL age estimates of less than 1,000 years is suspect (S.L. Forman, oral commun., 1988) because of low light levels measured in the laboratory and potential errors in determining equivalent doses (see discussion in appendix). Therefore, in this young age range, we place less importance on the TL age estimates (400 and 500 yr) and more importance on the two UHC age estimates of 500 cal yr B.P. On this basis, we

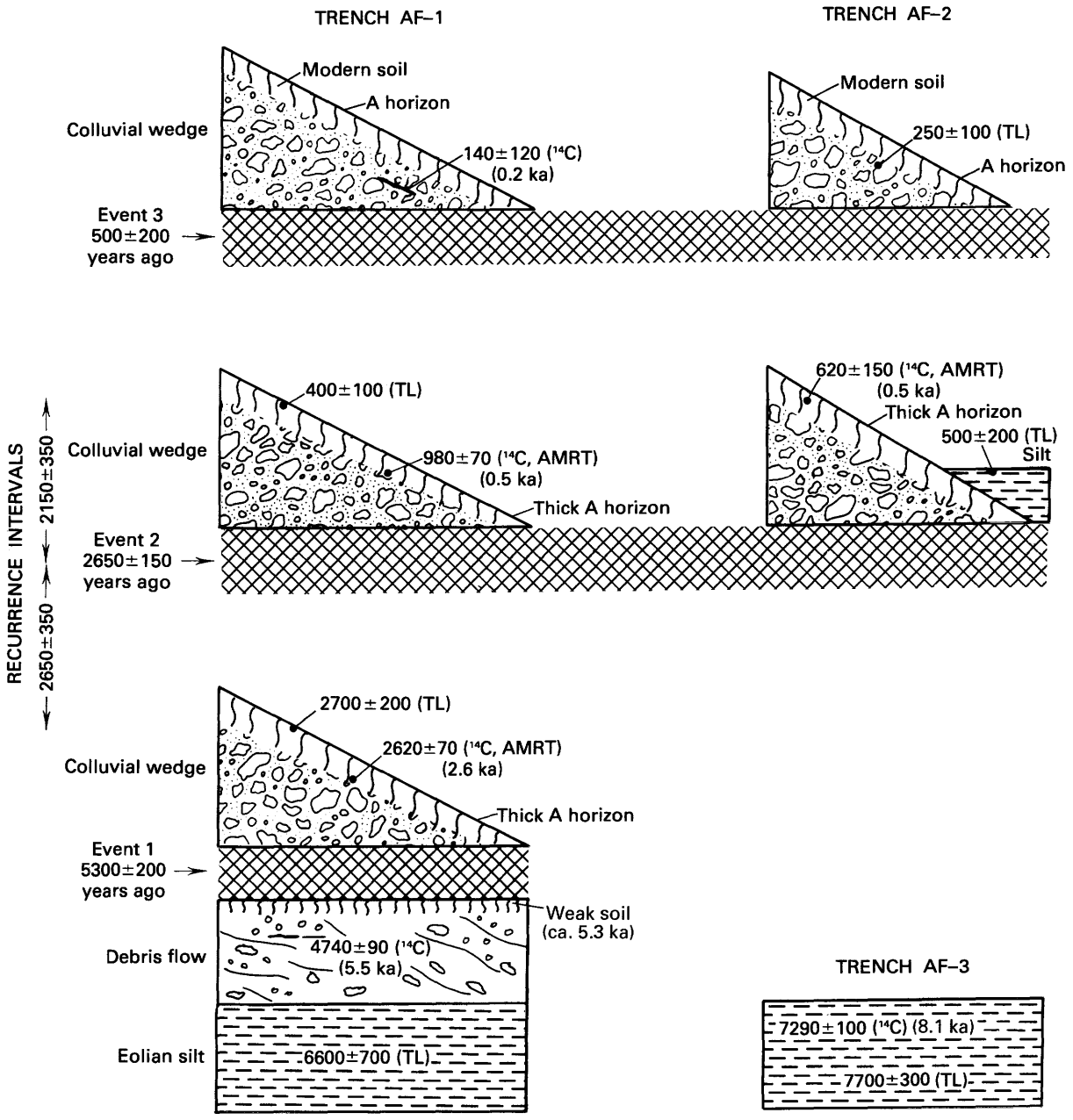

FIGURE 17.—Times of faulting deciphered from three trenches at the American Fork Canyon site, Wasatch fault zone. Cited age estimates (in thousands of years) are derived from thermoluminescence (TL) and radiocarbon (^{14}C) ages listed in table A1. AMRT, apparent mean residence time of soil organic carbon.

suggest using 500±200 years as the probable time of the most recent faulting at American Fork Canyon (fig. 17).

Evidence for and dating of the penultimate faulting event is clearest in trench AF–1 (fig. 16). Samples for TL and ^{14}C analysis were collected from the upper part of the buried soil that formed on the third (and oldest exposed) colluvial wedge in the trench. These samples provided maximum limiting dates on the time of burial of the soil. Sample F86–U7 yielded a TL age estimate of 2,700±200 cal yr (ITL–16, table A1), whereas the ^{14}C AMRT age from the same soil (sample AF–1B) is 2,620±70 ^{14}C yr B.P. (USGS–2531, table A1). This AMRT determination results in a calibrated date of 2,777 cal yr B.P. (the range is 2,549–2,879 cal yr B.P.). We estimate an age of about 2.6±0.2 ka for the ^{14}C-dated UHC by subtracting 200 years (MRC at the time of burial) (see table A1). Because these two age estimates (2.6 and 2.7 ka) are so close and fall within concordant error limits (about 200 years each), we use the midpoint of the two age estimates to place the second faulting

event at 2,650 yr B.P. (see fig. 17). We use an error limit of 250 years (2,400–2,900 yr B.P.), which includes errors associated with both the TL and the ^{14}C ages. The recurrence interval for the most recent faulting event (500±200 yr B.P.) and the second faulting event (2,650±250 yr B.P.) is 2,150±450 years.

The timing of the first (oldest) faulting event recorded in trench AF–1 is constrained by a ^{14}C accelerator date on charcoal from within debris-flow deposits, which are buried by the third and stratigraphically lowest colluvial wedge. Calibration of the charcoal's age determination of 4,740±90 yr B.P. (AA–2266, table A1) resulted in three possible calendar dates: 5,467, 5,534, and 5,553 cal yr B.P. The mean of these dates is 5,518 cal yr B.P., but the associated errors create a possible range of from 5,289 to 5,721 cal yr B.P. Assuming an age of 5.5±0.2 ka for the charcoal, we infer that the surface of the overlying debris flow was buried by a wedge of fault-scarp colluvium about 5.3±0.3 ka. This age estimate includes 200 years for the burial of the charcoal (a surface burn layer), deposition of the overlying 1.2-m-thick debris-flow surface, and formation of a very weak (incipient) A horizon on its surface (the oldest colluvial wedge buried nearly fresh debris-flow material). If our estimate of timing is reasonable for the first (oldest) event recorded in AF–1, then the recurrence interval between the first (5.3±0.3 ka) and the second (2.65±0.25 ka) events is about 2,650 years; as in the younger interval, 450 years seems to be a reasonable (cumulative) error limit.

Trenching of the fault scarps on Holocene deposits shows that three surface-faulting events contributed to the 7 to 8 m of net displacement recorded since 5.3 ka. Reconstructing the volume of each colluvial wedge indicates that these events had similar (2.2–2.7 m) amounts of displacement. The three Holocene events each produced discrete colluvial wedges, although only trench AF–1 showed evidence of all three events. Trench AF–2 records the most recent (0.5 ka) and probably the second (2.65 ka) faulting events, whereas trench AF–3 records the second and an earlier (greater than 5.3 ka, less than 0.8 ka) event not seen in trenches AF–1 or AF–2. The amount of displacement and distribution of this faulting event (in the other trenches) is unknown.

The preliminary analysis of paleoseismicity at the American Fork Canyon site relies on both conventional and accelerator-method ^{14}C dating of charcoal and soil-organic carbon (AMRT dates), TL analysis, and detailed mapping of lithologic and stratigraphic units. The results form the basis for an interpretation of three Holocene fault events at about 0.5, 2.65, and 5.3 ka. The strength of development of the soils on each colluvial wedge in the trenches (fig. 16) supports the early suggestion by Machette and Lund (1987) that faulting must have occurred over long intervals (that is, thousands rather than hundreds of years). If the most recent surface-faulting event is correctly dated at 0.5 ka and if 5 to 6 m of displacement occurred since 5.3±0.3 ka (estimated time of burial of unit 4) (fig. 16), then two major faulting events occurred during an interval of 4,800±500 years. The resulting slip rate since middle Holocene time is between 1.0 and 1.4 mm/yr (5–6 m/4,800±500 yr), which is consistent with the range of slip rates (1.0–1.7 mm/yr) determined for the past 15 ka from the adjacent faulted Bonneville lake cycle deposits. These values confirm that the rate of slip on the Wasatch fault zone in the northern part of the Utah Valley has been relatively high since the culmination of the Bonneville lake cycle and especially during the later part of the Holocene.

CENTRAL PART

The central part of the Provo segment is the middle of three segments that Machette and others (1986, 1987) subdivided from the original Provo segment of Schwartz and Coppersmith (1984). The central part extends from Provo Canyon (where its most recent scarps are in bedrock) south to and including the Springville fault (SF, fig. 15) at Springville, Utah, a distance of 18.5 km. South of Little Rock Creek (3 km north of Rock Creek) (RC, fig. 15), the active trace of the Wasatch fault zone is primarily in surficial deposits along the western base of the Wasatch Range.

Between the canyons of the Provo River and Little Rock Creek, the western front of the Wasatch Range is characterized by numerous large but poorly recognized Quaternary landslides. We believe that Davis' (1983b) compilation of the geology of this area incorrectly shows large blocks of upper Paleozoic rock (Oquirrh Formation) thrust eastward and uplifted in the Wasatch mountain block. In contrast, Machette (1989, in press) indicated that exposures in much of the "Oquirrh-like" material are comprised of fanglomerate facies of the Salt Lake Formation (upper Tertiary) or of large landslide masses of Oquirrh Formation that have slid on upper Paleozoic Manning Canyon Shale along steep parts of the range front. Extensive upper Tertiary(?) and Quaternary landslide deposits that predate the Bonneville lake cycle also are present in this area; these deposits have been derived largely from the catastrophic landslide failure of the Manning Canyon Shale. These landslide deposits and the Salt Lake Formation are locally preserved in an overlapping left step of the Wasatch fault zone at an intermediate structural level; usually, these deposits are deeply buried in the basins and eroded from the ranges.

Only one exposure along the central part of the Provo segment of the Wasatch fault zone has been studied in detail. In 1986, Machette and William Mulvey of the

UGMS mapped a natural exposure of a single fault on the southern bank of the modern drainage from Rock Canyon, which is at about the midpoint of the central part, and measured about 2 m of net displacement (1.5 m of tectonic displacement, 0.5 m of drag) in middle(?) to upper Holocene debris flows and alluvium. The resulting scarp has been partly buried by later debris flows and alluvium. Radiocarbon dating of soil-organic matter in the fault-scarp colluvium yielded an AMRT age of 1,110±50 ^{14}C yr B.P (DIC–3236, table A1). Two factors need to be considered before interpreting this date. First, soil organics in the colluvium that was dated may span several hundred years, so this amount of time should be considered in estimating the time of faulting. Second, some of the organic matter was derived from the soil on the upthrown fault block and thus may have added a significant amount of old carbon to the sample; this reworked carbon may have increased the ^{14}C age by several hundred years. Thus, the calibrated AMRT age of 1,005 cal yr B.P. (range is 950–1,150 cal yr B.P.) (see table A1) could reflect the approximate time of faulting. However, this date probably has a much larger uncertainty owing to reworking or accumulation of soil organics.

Control on the minimum time of faulting at the natural exposure was provided by a ^{14}C age from a soil that had formed on the fault-scarp colluvium before burial by upper Holocene fluvial and debris-flow deposits. This organic-rich soil postdates the faulting and predates the burial of the fault scarp. Organic carbon from this A horizon yielded an AMRT date of 455±35 ^{14}C yr B.P. (PITT–0091, table A1), which corresponds to a calibrated AMRT age of 512 cal yr B.P. (the range in age is 457–552 cal yr B.P.). We estimate a MRC of 100 years for the soil at the time of burial (see table A1) and suggest an age, although poorly constrained, of about 0.4 ka for burial of the UHC of the soil and the adjacent fault scarp. These preliminary investigations suggested that the most recent faulting at Rock Canyon occurred since about 1.0 ka and that the resultant scarp was buried by alluvium at about 0.4 ka.

The poor dating control described above and the possibility of nonsynchronous movement on three short parts of the Provo segment prompted further studies at the Rock Canyon site. In the spring of 1988, W.R. Lund (UGMS) and D.P. Schwartz (USGS) trenched a 4.5-m-high scarp on alluvium just north of Rock Canyon Road, about 100 m south of the stream exposure. In addition, they cleaned off the stream embankment with a backhoe and exposed a previously unmapped splay of the fault. These two fault splays merge to the south to form the scarp that was trenched by Lund and Schwartz.

Preliminary mapping of the trench (W.R. Lund and D.P. Schwartz, oral commun., 1989) revealed a single colluvial wedge and, thus, evidence for only one faulting event. Although the size of this scarp (4.5 m) had suggested two or three faulting events (Machette and others, 1987), Lund and Schwartz found that backtilting and graben formation account for the 2-m difference between stratigraphic offset (about 2.5 m) and scarp height. Although no charcoal was found in the trench, they sampled several organic soils for bulk (AMRT) ^{14}C dating, all of which should predate the most recent faulting. At the new exposure along the stream channel, ^{14}C dating of both charcoal from above and soil organics from below the colluvial wedge should allow them to place tighter limits on the time of most recent faulting.

The central part of the Provo segment is characterized by multiple parallel to anastomosing strands of the fault zone, and rarely is there a single fault strand on which most of the movement has taken place. The pattern of ground rupture is complicated south of Slate Canyon (due east of Provo) (fig. 15), where the Wasatch fault zone offsets transgressive gravel of the Bonneville lake cycle and regressive gravel at and below the Provo level. The gravel is draped across steeply sloping alluvial-fan deposits that predate the Bonneville lake cycle. The history of faulting in this area is difficult to decipher for three reasons: (1) existing fault scarps (pre-Bonneville lake cycle) were modified by shore processes during the rise and fall of Lake Bonneville, (2) most of these faults were reactivated by Holocene movement, and (3) much of the gravel cover has been disturbed by quarrying or by regrading of abandoned gravel pits or has been covered by homes.

The southern end of the central part is considered to be the Springville fault (SF, fig. 15), a basinward splay of the Wasatch fault zone that forms a 3-km-long fault scarp on Holocene alluvium of Hobble Creek. The fault extends from just east of the State Fish Hatchery (1 km north of the northern edge of Springville) southward to Utah Highway 77. Scarps along this fault are less than 2 m high and, within Springville, have been extensively modified. Bissell's (1963) map shows another fault scarp about 1 km south of Springville. However, we agree with Miller's (1982) decision not to map the feature as a fault; it appears to be both a part of a young Provo shoreline and the head of a massive lateral spread (see Machette 1989, in press).

SPANISH FORK PART

The Spanish Fork part of the Provo segment is restricted to the Wasatch fault zone between Springville and Payson Canyon. It is the southernmost of three segments that Machette and others (1986, 1987) subdivided from Schwartz and Coppersmith's (1984) original

Provo segment. The Spanish Fork part forms a major concave-to-the-west bend in the Wasatch fault zone, the only such prominent bend along the entire fault zone. The Spanish Fork part is bounded on the north and west by the central part of the Provo segment, which extends into the basin as the Springville fault (SF, fig. 15). The lack of a salient or a spur at the intersection of the Provo and Spanish Fork parts indicates that there is no prominent deficit or change in structural throw along the fault zone. Thus, if this intersection is a structural boundary, it must be a nonpersistent feature—one that may only intermittently or occasionally control the starting or stopping points of surface rupturing. On the south, the Spanish Fork part of the Provo segment is bounded by the Payson salient (Dry Mountain) and the northward extension of the Nephi segment (the Benjamin fault of Hintze (1973)) (BF, fig. 15). The Payson salient represents a persistent structural barrier. The Benjamin and Springville faults both have down-to-the-west displacement, which suggests that they could connect in the subsurface of the southern Utah Valley. However, Zoback's (1983) gravity data suggest that the deep part of the basin extends, uninterrupted, from east of Spanish Fork northwest into the area of Utah Lake across the alignment of the two faults. Thus, it appears that the Springville and Benjamin faults must die out as they extend into Utah Valley.

The Spanish Fork part has been the focus of detailed mapping and trenching studies, especially during 1987. In the past 10 years, four major trenching sites have been investigated on this part of the Provo segment: three on the main Wasatch fault zone and a fourth on a splay of the Wasatch fault zone (fig. 15; sites 11–14, table 1). Swan and others' (1980) study of tectonic, stratigraphic, and geomorphic relations at Hobble Creek (HC, fig. 15), coupled with trenching at Deadmans Hollow about 1 km to the west, provided the first evidence of repeated Holocene movement on the Provo segment of the Wasatch fault zone. They found evidence for six or seven surface-faulting events that resulted in 11.5 to 13.5 m of net vertical tectonic displacement since formation of the Provo fan-delta complex at the mouth of Hobble Canyon. The three youngest events were defined on the basis of colluvial deposits observed in trenches across a sequence of faulted alluvial fans at Deadmans Hollow. Three or four earlier events were inferred from tectonic strath terraces preserved on the upthrown fault block along Hobble Creek. The number of post-Provo surface-faulting events is probably reasonable, but the absence of organic material in exposures of the terrace alluvium or in the trenches prevented determination of individual recurrence intervals. The average interval between faulting events for the past 14 ka is 1,700 to 2,600 years (as revised by Schwartz and Coppersmith, 1984). The age of the most recent event was estimated to be at least 1 ka on the basis of relatively degraded fault scarps, although more recent trenching shows that the most recent faulting is younger than this estimate. Individual amounts of displacement for post-Provo events were not well constrained, but the average value ranges from 1.6 to 2.3 m for each of the six or seven inferred events.

Scarps on sediment of the Bonneville lake cycle south of Hobble Creek are both steep and large. However, the true net displacement in transgressive sediment of the Bonneville lake cycle is difficult to determine because of extensive backtilting, graben formation, and colluviation. Swan and others (1980, table 1) preferred a displacement value of 30±0.5 m for the trangressive sediment, whereas we estimate 40 to 45 m on the basis of the geometry of backtilting that is proportional to the adjacent well-preserved Provo alluvial surface. If one assumes that the faulted lake sediment is 17±2 ka (permissible age range for sediment at this altitude), then the resulting average slip rate at Hobble Creek has been between 1.8 mm/yr (Swan and others, 1980, table 1) and 2.5 mm/yr. The latter value is based on the midpoints of our displacement and age values. Because the net displacement recorded by offset of transgressive deposits (30–45 m) is two to three times greater than that recorded by regressive deposits (11.5–13.5 m) of the Bonneville lake cycle and the potential difference in age (1–4 ka) is only slight, we suspect that faulting at this site occurred at very high rates (perhaps as much as 10 mm/yr) during and after the catastrophic fall of Lake Bonneville 15,000 years ago (see "Possible Causal Relation Between Deep Cycles of Lake Bonneville and High Rates of Slip on the Wasatch Fault Zone").

In June 1987, W.R. Lund and D.P. Schwartz dug six exploratory trenches at two sites east and south of Mapleton, Utah, to determine recurrence intervals and to further refine the time of most recent faulting along this part of the Provo segment of the Wasatch fault zone. The trenching sites (fig. 15, MN, Mapleton North; MS, Mapleton South) are 4 and 5.5 km south of the Hobble Creek site, respectively. Lund and Schwartz's investigations (Schwartz and others, 1988; Lund and others, 1991) indicated two surface-faulting events in the past 3 ka, the most recent being bracketed by ^{14}C ages on charcoal of 445±75 and 770±100 ^{14}C yr B.P., which correspond to calendar dates of 512 and 689 cal yr B.P., respectively. They believe that the most recent faulting event at Mapleton probably occurred about 0.6±0.1 ka and, thus, could well be the same event recorded at the American Fork Canyon site (0.5±0.2 ka). In addition, Lund and Schwartz obtained a preliminary TL age estimate of 3.3±0.3 ka and a ^{14}C date of 2,810±95 yr B.P. (which yields possible calendar dates of 2,890, 2,900, and 2,930 cal yr B.P.) from a soil buried by the older of two

colluvial wedges (Schwartz and others, 1988). These TL and ^{14}C dates suggest that the second event occurred at 3.0±0.3 ka (Lund and others, 1991) or about 2,400 years before the most recent faulting event. Given the problems involved in dating, the timing of the second event is essentially the same as the 2.65±0.25 ka estimate for the penultimate event at the American Fork Canyon site. The coincidence in dating from these two sites demands that they are on a master (Provo) segment whose last two faulting events have ruptured its entire length.

Dean Ostenaa of the USBR (Denver) is investigating recent movement on the Spanish Fork part of the Provo segment at the Water Canyon site (WC, fig. 15), which is about 14 km southwest of Hobble Creek. This investigation is part of a study for the USBR's Central Utah Project. In 1986, before trenching began at the Water Canyon site, the USBR excavated two trenches across a 1.5- to 3-m-high fault scarp parallel to and above the prominent high shoreline of Lake Bonneville (altitude 5,095 ft, or 1,553 m) about 1.5 km southwest of Water Canyon at the southeastern end of Utah Valley. This fault scarp is herein named the Woodland Hills splay (WH, fig. 15; site 14, table 1). The larger, western trench was mapped by Machette, Robert Robison (Utah County Geologist), Craig Nelson (Salt Lake County Geologist), Rodney Weisser (USBR, Provo), and James McCalpin (Utah State University, Logan). Their interpretations suggest three or four major surface-faulting events in the past 150 ka and a total of about 3 m of net vertical displacement. Radiocarbon AMRT dates of 1,190±50 ^{14}C yr B.P. (USGS–2500, table A1) and 1,380±60 ^{14}C yr B.P. (BETA–19594, table A1) were obtained from two splits of organic matter in a buried A horizon. These dates correspond to calibrated AMRT ages of 1,102 and 1,306 cal yr B.P., respectively. The error limits on the AMRT dates are generally about 80 to 130 years (table A1), and the two calibrated AMRT ages are concordant at about 1,200±200 cal yr B.P. From this estimate, we subtracted 200 years to compensate for MRC at the time of burial (see table A1). Thus, we suspect that the most recent faulting event occurred about 1.0±0.2 ka. The timing of the most recent movement on the Woodland Hills splay of the Wasatch fault zone and of that on the main segment dated at Mapleton would be compatible only if one argues for subtracting a much larger MRC (about 600 years) from the age of the buried A horizon at Woodland Hills.

Inasmuch as movement on the Woodland Hills splay produced small amounts of displacement and has only a short rupture length, faulting along this splay probably was triggered by movement on the main Wasatch fault zone. However, based on recurrence intervals, it appears that the Woodland Hills splay is an active participant in Wasatch fault zone rupturing only a fraction of the time, perhaps once for every 5 to 10 events that occur on the Provo segment.

The USBR's study was expanded in 1987 with the excavation of three trenches at Water Canyon (WC, fig. 15; site 13, table 1). Two trenches were excavated in Holocene fan-head terraces at the mouth of the canyon, and a third trench was excavated in slope colluvium several hundred meters south of Water Canyon. Although final analysis of the trenching investigations awaits accelerator-method ^{14}C dating of charcoal samples, Dean Ostenaa (oral and written communs., 1987) suspects three or possibly four faulting events in the past 6 to 8 ka. If his estimate of the number of events and the time range holds, there would be a conflict between the fault chronology determined here and that determined at Mapleton, 14 km to the north-northeast. For example, Dean Ostenaa (written commun., 1987) interpreted two events in the past 0.8 ka at Water Canyon, whereas W.R. Lund and D.P. Schwartz have evidence for one event about 0.6 ka.

Between the Mapleton and Water Canyon sites, the trace of the Spanish Fork part makes a spectacular 100° clockwise bend at the mouth of Spanish Fork Canyon. This geometry is suggestive of a potential segment boundary. However, detailed mapping of this area by Machette (1989, in press) reveals continuous Holocene faults around the bend and several prominent antithetic faults that crosscut the bend. The apparent displacement recorded in deposits of the Bonneville lake cycle decreases at the bend in comparison with sites to both the north and the west. This decrease in displacement probably results from drag in the bend (that is, the confining geometry created by perpendicular basinward-dipping fault planes). The continuity of faulting and the evidence of repeated Holocene faulting all along this part of the segment suggest that it is continuous from just north of Springville to Payson Canyon, where the fault turns southward and is concealed by massive Quaternary landslide deposits. We suspect that recent faulting continues several kilometers up Payson Canyon, but evidence for faulting is hidden by landsliding and tree cover.

NEPHI SEGMENT

The Nephi segment, which extends from Payson to Nephi, is comprised of a main western strand and an eastern strand. The western strand bounds the Wasatch Range in northern Juab Valley, and the eastern strand bounds the western side of Dry Mountain, east of Santaquin Creek (fig. 18). Holocene ruptures on the western strand continue as far north as Mendenhall Creek; from there, they turn northeast and strike into the bedrock of the range. Northward-striking scarps persist north of Mendenhall Creek, but they are discontinuous and more

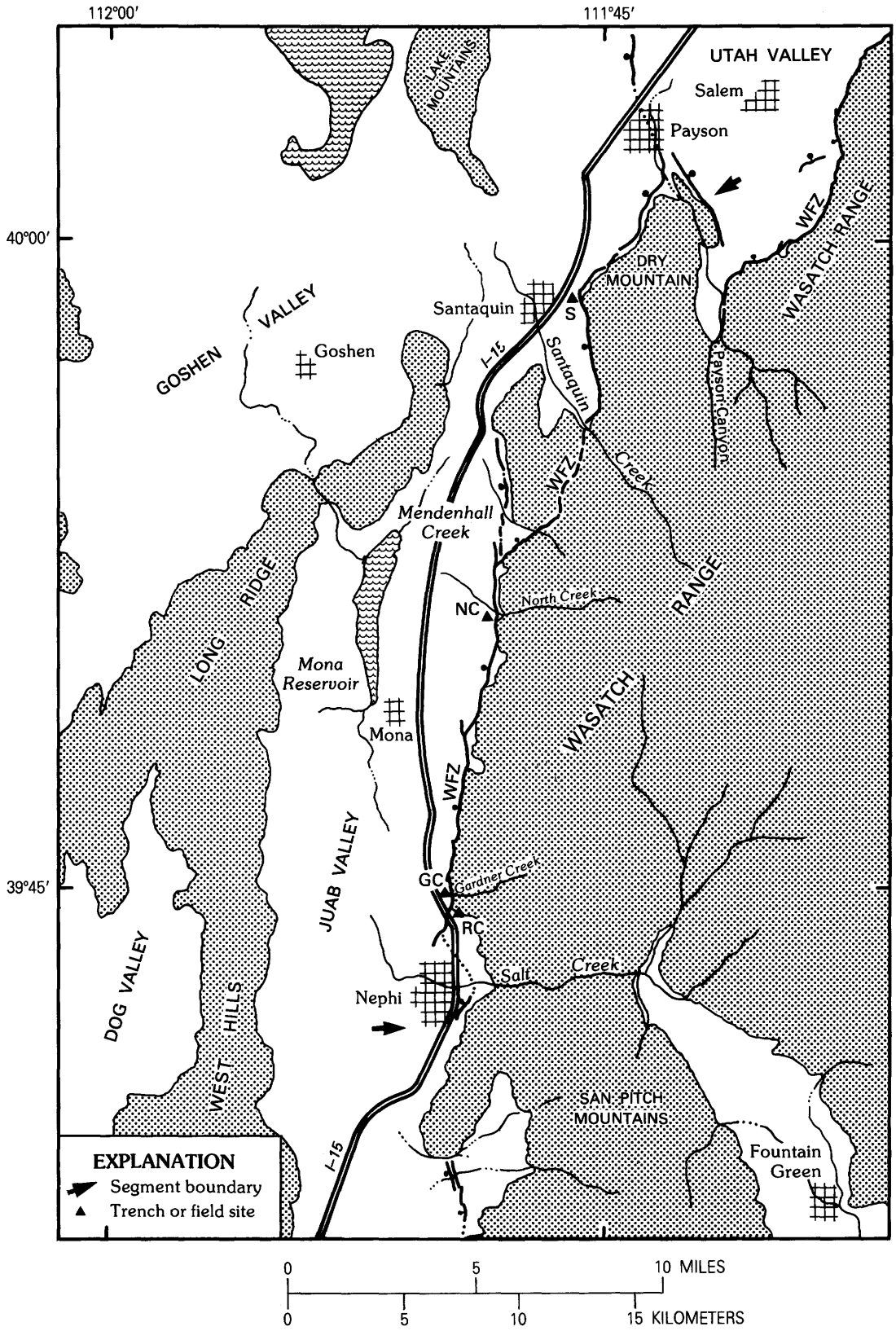

FIGURE 18.—Nephi segment of the Wasatch fault zone (WFZ), which extends from just north of Payson to Nephi, Utah. Faults are shown by heavy lines having a bar and ball on the downdropped side. The area south of the segment boundary lacks evidence of Holocene faulting. Also shown are important geographic features and towns. Trench and field sites are abbreviated as follows: S, Santaquin; NC, North Creek; GC, Gardner Creek; RC, Red Canyon.

degraded (older) than those to the south. Although evidence of recent faulting between the two strands in the Wasatch Range is obscured by vegetation and extensive landslides, we suspect that the two strands of the Wasatch fault zone are connected by a major down-to-the-north bedrock fault that strikes northeast toward the canyon of Santaquin Creek (Davis, 1983b). The Manning Canyon Shale, an incompetent unit susceptible to landsliding and intraformational faulting, is nearly vertical and strikes in a northeasterly direction between Mendenhall Creek and the end of the eastern north-striking strand at Santaquin Creek. We suspect that the Manning Canyon Shale is a convenient pathway for transferring near-surface movement between the two en echelon strands of the Nephi segment.

At the northwestern end of Dry Mountain (about 2 km east of Santaquin), the eastern strand of the Nephi segment turns northeastward and becomes discontinuous in post-Bonneville lake cycle sediment. Young fault scarps (originally mapped by Cluff and others (1973)) continue across Payson Canyon, turn northward, and bound a narrow bedrock-cored horst block. This horst is the northern extension of the Payson salient and is mantled by beach gravel (Bonneville lake cycle) north of Tithing Mountain. At Payson, the Nephi segment loses definition and is largely coincident with fluvial terrace scarps graded to regressional (Provo) levels of Lake Bonneville (Machette, 1989, in press).

The Wasatch fault zone continues another 3.5 km north of Payson to the vicinity of the Benjamin Cemetery, which is on a low north-south elongated hill underlain by sediment of the upper Tertiary Salt Lake Formation (Davis, 1983b). This hill is bounded on the west by the Benjamin fault (BF, fig. 15) of Hintze (1973), which forms a 1- to 2-m-high fault scarp on Bonneville lake cycle silt and clay of the regressive (Provo) phase. The scarp extends about 2 km south of the hill to within 1.5 km of Payson. Hintze (1973) reported that the fault forms a series of aligned hot springs that extends almost 4.5 km north of the Benjamin Cemetery to near Lake Shore, Utah, 8 km north of Payson (fig. 15). We consider the Benjamin fault to be a northward, less active part of the Nephi segment of the Wasatch fault zone.

The Nephi segment is one of two of Schwartz and Coppersmith's (1984) segments that we have not modified except for the postulated cross-range fault that extends from Mendenhall Creek northeast to the canyon of Santaquin Creek. The surface trace of the Nephi segment is 42.5 km long (Payson to Nephi); if the Benjamin fault and its subsurface projection to the north are included, the total length is about 50 km. Detailed maps of Cluff and others (1973) show a number of linear features within the city limits of Nephi, but our reconnaissance (M.N. Machette, unpub. mapping, 1987) could not confirm them as faults. They show up as sharp changes in tone on aerial photographs but are not associated with topographic escarpments. They may, however, have exhibited topographic relief before settlement of the town. The southern limit of continuous faulting on the Nephi segment is at Utah Highway 41, about 2 km north of the center of Nephi. There are discontinuous fault scarps on alluvial fans of pre-Holocene(?) age as far as 2 km south of Salt Creek (fig. 18), but there is no evidence that recent faulting has displaced the intervening upper Holocene alluvial fan of Salt Creek.

Schwartz and others (1983) excavated three trenches at North Creek, the fourth major site excavated by Woodward-Clyde geologists along the Wasatch fault zone. At North Creek, the Wasatch fault zone offsets an alluvial fan that contained charcoal dated at 4,580±250 ^{14}C yr B.P. (USGS W–4057) (Bucknam, 1978), which corresponds to a calibrated date of 5,300 cal yr B.P. (range is 4,869–5,589 cal yr B.P.). Topographic profiles across the fan show that the surface has been offset 7.0±0.5 m. Schwartz and others (1983) reported that this displacement is the result of three surface-faulting events, the most recent and penultimate events being represented by scarp-derived colluvium. An older, third event is inferred from a tectonic strath terrace, which is incised in an uplifted part of the North Creek fan.

The timing of the most recent event at North Creek is constrained by two ^{14}C dates and from age estimates based on scarp morphology. Age determinations of 1,110±60 and 1,350±70 ^{14}C yr B.P. from charcoal and organic matter in the trenches provide a maximum age for the most recent event. These two ^{14}C age determinations correspond to calibrated dates of 975 or 1,048 and 1,289 cal yr B.P., respectively, although the latter date has not been corrected for the AMRT effect. Thus, the youngest event at North Creek could have occurred as much as 1,000 cal yr B.P. However, the steep scarp angles (40°−42°) along this segment of the fault, the lack of upstream migration of knickpoints in many stream channels above the fault scarp, and a generally continuous 15-km-long fault scarp that lacks vegetation suggested very recent movement (400±100 years ago) to Schwartz and others (1983). They estimated 2.0 to 2.2 m of displacement per event on the basis of the thickness of scarp-derived colluvial wedges, topographic profiles of the faulted surface, and the height of the tectonic strath terrace.

Constraint on the minimum time since the penultimate event at North Creek was provided by a ^{14}C age of 3,640±75 ^{14}C yr B.P. from a buried soil on the second colluvial wedge. The ^{14}C age corresponds to calendar dates between 3,930 and 3,980 cal yr B.P. (the one-sigma error describes a range of 3,841–4,088 cal yr B.P.) or about 4.0±0.2 ka. This maximum estimate, however,

does not include an MRC for the soil, which could be several hundred years. Hanson and Schwartz (1984) reported several other conventional and accelerator ^{14}C dates from the North Creek site that are considerably younger but argued that the above mentioned ^{14}C date provided the most reliable time constraint. The displacement during the second event was 2.0 to 2.5 m.

The first (oldest) event occurred between 4.0±0.2 and 5.3±0.3 ka (see previous discussion of charcoal in the alluvial fan) and produced 2.6 m of displacement, as indicated by the depth of inset of the strath terrace just above the fault. Although the ages listed above provide general limits on the times of faulting at North Creek, none of the determinations come from samples that are in stratigraphically definitive positions (for example, charcoal at the buried surface of a proximal colluvial wedge).

In June 1987, Michael Jackson (University of Colorado) excavated a trench on the distal portion of the alluvial fan of Red Canyon at the southern end of the Nephi segment. His site (RC, fig. 18) is just east of Interstate Highway 15, about 3.5 km north of Nephi. However, because the trench is close to the end of the Nephi segment, not all of the faulting events at North Creek (near the center of the segment) may have ruptured as far south as the Red Canyon site. Jackson's trench crossed a 5-m-high fault scarp and exposed interbedded, distal alluvial-fan sediment (pebbly sand) and thin, silty, debris-flow deposits. Three discrete but thin colluvial wedges were recognized along the main fault, and an additional wedge was recognized along a subsidiary fault.

A TL age estimate of 14.6±1.2 ka from what appears to be nonbleached material in the oldest colluvial wedge suggests that the faulted alluvial-fan sequence at Red Canyon is latest Pleistocene in age (Jackson, 1988, in press). Relations between the stratigraphic and tectonic units exposed in the Red Canyon trench and Jackson's (1988) ^{14}C dates suggest three or four major surface-faulting events during the middle and late Holocene. Jackson (1988, fig. 5-4), inferring synchroneity with faulting at the North Creek site, suggested that the "most probable" times for faulting events at Red Canyon are 1,200, 3,000 to 3,500, and 4,000 to 4,500 cal yr B.P.

The southern end of the Nephi segment and the northern end of the Levan segment are separated by a 15-km-long gap in recent faulting. M.N. Machette (unpub. data, 1987) found no evidence of latest Pleistocene or Holocene faulting in this gap, although older fault scarps are preserved on middle Pleistocene alluvial fans that emanate from the northeastern side of the San Pitch Mountains (see lower part of fig. 18). Zoback's (1983) gravity map shows a deep, continuous gravity trough in the valley adjacent to the gap in recent faulting; together, these data suggest that the Wasatch fault zone is a continuous structural feature beneath the gap.

The middle Pleistocene alluvial fans in the gap are part of a broad, extensive alluvial cone (known informally as Levan Ridge) that forms a drainage divide within the Juab Valley. Inspection of topographic maps of the northern San Pitch Mountains and the adjacent Juab Valley suggests that the streams supplying sediment to Levan Ridge are grossly underfit. There is a prominent north-south valley within the San Pitch Mountains that projects north to the Salt Creek drainage (several kilometers east of Nephi) and south to the head of Levan Ridge. Machette suspects that the ancient course of Salt Creek formed the aforementioned valley in the San Pitch Mountains and that Salt Creek deposited the bulk of alluvium that underlies Levan Ridge. If so, then headward incision of the lower reach of Salt Creek, perhaps as recently as the late Pleistocene, resulted in capture of the upper Salt Creek drainage and subsequent entrenchment of Salt Creek Canyon. This stream capture would explain the deposition of a young fan complex at the mouth of Salt Creek Canyon.

SOUTHERN WASATCH FAULT ZONE

The southern section of the Wasatch fault zone comprises segments of the fault zone that do not exhibit repeated Holocene movement, in contrast to the more active central section of the Wasatch fault zone. The southern section of the fault zone consists of the Levan segment, which Schwartz and Coppersmith (1984) defined as extending from near Pigeon Creek (PC, fig. 19) east of Levan, south to near Gunnison. Machette and others (1986, 1987) suggested that the Levan segment should be subdivided into the Levan segment (restricted sense) and the Fayette segment (fig. 19). The intervening segment boundary is located at the left step that the fault trace takes from the Juab Valley to Flat Canyon (the south-trending canyon headed by Maple Creek, north of Fayette). We make this subdivision on the basis of apparent recency of movement (late Holocene movement on the Levan segment versus no evidence of Holocene movement on the Fayette segment) and on the basis of the major left step and gap in faulting (Machette and others, 1986, 1987).

LEVAN SEGMENT

Our aerial photographic reconnaissance, geologic mapping, and analysis of scarp morphology indicate that the Levan segment has Holocene ruptures from Hartley's Creek, 3.8 km northeast of Levan (fig. 19) to as far south as Botham Road, 18 km south of Levan. Near Botham

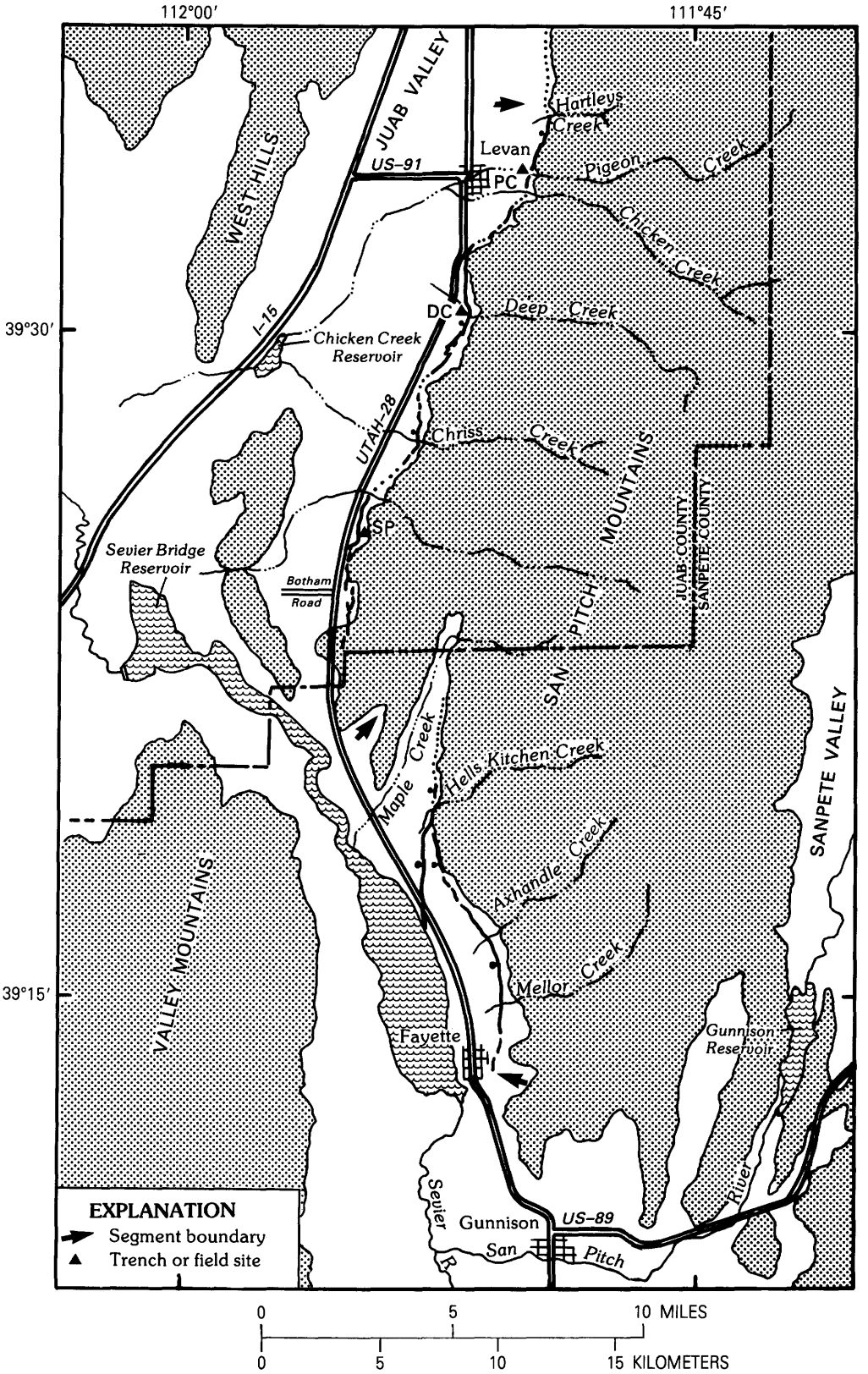

FIGURE 19.—Levan (northern) and Fayette (southern) segments of the Wasatch fault zone. Faults are shown by heavy lines having a bar and ball on the downdropped side (dotted where uncertain). Also shown are important geographic features and towns. Trench and field sites are abbreviated as follows: PC, Pigeon Creek; DC, Deep Creek; SP, Skinner Peaks.

Road, the Levan segment steps left about 0.5 km and enters bedrock. However, there is clear evidence of Quaternary faulting for another 3 km south of Botham Road, but we cannot tell if the most recent movement is Holocene. The southern end of the Levan segment (including the part of uncertain age) is about 0.5 km east of Utah State Highway 28 at the southern jog in the Juab-Sanpete County line. From this point south, the trace of the late Quaternary Wasatch fault zone makes a 3.5-km step to the left (to the east) and 5 km to the south to the vicinity of Flat Canyon. We suspect that the western front of the San Pitch Mountains between Maple Creek and Hells Kitchen Creek also is fault controlled, but there is no evidence of young fault scarps on alluvial fans in this area. The morphology of fault scarps along the Fayette segment, which extends from Hells Kitchen Creek south to Fayette, shows no evidence of Holocene movement (M.N. Machette, unpub. data, 1986).

Most of the fault scarps on Holocene deposits along the Levan segment are less than 3 m high and probably are the result of a single late Holocene faulting event. Fault scarps on upper to middle Pleistocene alluvium are commonly 5 to 10 m high or higher; this height suggests recurrent late Quaternary faulting.

At Pigeon Creek (PC, fig. 19), 2 km north and due east of Levan, two samples of charcoal from faulted alluvium in a natural exposure were dated by the accelerator method at 1,750±350 and 2,100±300 ^{14}C yr B.P. by geologists from Woodward-Clyde and Associates (see Crone, 1983, p. 15; Schwartz and Coppersmith, 1984). These ages placed a maximum limit on the time of most recent faulting. Extensive flooding in 1984 and the subsequent construction of flood-control levees have prevented us from restudying the Pigeon Creek site. However, a second natural exposure at Deep Creek, about 5 km south of Levan, has provided datable material. Here the fault forms a 2.5-m-high scarp and is exposed in the north wall of the creek. Schwartz and Coppersmith (1984) and M.N. Machette (unpub. mapping, 1984–86) studied this exposure and concluded that the scarp was produced by a single faulting event. Machette measured a net vertical displacment of about 1.75 m, which is comprised of 2.3 m of displacement on the main fault and 0.55 m of offsetting displacement on a graben-bounding antithetic fault about 15 m to the west. Charcoal from an unspecified position in the faultedalluvium at this site has been dated at 7,300±1,000 ^{14}C yr B.P. (Schwartz and Coppersmith, 1984).

Michael Jackson also mapped the Deep Creek exposure and measured 2.3 to 2.4 m of displacement on the main fault. Jackson also determined a TL age estimate of about 1,000±100 cal yr for the soil on alluvium that is buried by fault-scarp colluvium (Jackson, 1988, in press). This TL age suggests that the most recent faulting event is about 1.0±0.1 ka.

Jackson (1988, in press) also excavated a 5-m-deep trench across a 3.3-m-high fault scarp on middle Holocene alluvial-fan sediment near the southern end of the Levan segment at the Skinner Peak site (SP, fig. 19; site 18, table 1). The site is about 1.5 km northwest of Skinner Peaks and about 200 m east of Utah State Highway 28. Jackson (1988, in press) found only one colluvial wedge, but there was at least twice as much alluvium (about 5 m) on the downdropped block as on the upthrown block. These relations suggest that the alluvium must have been deposited across or, more likely, against a preexisting escarpment. Thus, there appears to have been one faulting event after formation of the alluvial fan and one event during or before deposition of the fan. A combination of ^{14}C dates and TL age estimates from this trench provides a maximum time for the most recent event of less than 3.1 to 3.9 ka, which supports Schwartz and Coppersmith's (1984) earlier interpretation of a young (less than 1,750 yr B.P.) faulting event and is consistent with results from the Deep Creek site. The stratigraphic and structural relations exposed in Jackson's trench suggest to us that the penultimate faulting event on the Levan segment could have occurred in latest Pleistocene or early Holocene time. If this speculation is correct, then distal segments of the Wasatch fault zone (such as the Levan) may have recurrence intervals on the order of 10,000 years, or about one-fifth that of the more active central segments.

FAYETTE SEGMENT

The Fayette segment is the southernmost segment of the 383-km-long Wasatch fault zone (fig. 1). It is similar in many ways to the segments of the northern Wasatch fault zone, except that Lake Bonneville was shallower here and remained below (west of) the main trace of the fault zone. Fault scarps on latest Pleistocene and early(?) Holocene alluvial fans are present from Hells Kitchen Creek south to the Fayette Cemetery, about 1 km east of Fayette (fig. 19). The Fayette segment has two strands: a 6-km-long western strand that strikes north-south and a concave-to-the-west, 11-km-long eastern strand that strikes southeast and south. These two strands join near the northern end of the segment, about 1 km south of Hells Kitchen Canyon. The fault scarps along this segment are commonly eroded at the mouths of canyons but preserved on terraces that are elevated 2 to 5 m above stream level. Profiles were measured across a number of scarps on faulted stream terraces along both strands to determine the relative ages of the scarps. The morphometric data (scarp height and maximum slope angle)

from these profiles plot between the regression lines for data from the Drum Mountains fault scarps in west-central Utah (early Holocene) (Crone, 1983; Pierce and Colman, 1986) and the highest shoreline of the Bonneville lake cycle (14.5 ka) (Bucknam and Anderson, 1979). These morphometric relations and the degree of scarp dissection suggest that the most recent movement on the Fayette segment occurred between 10 and 15 ka and, thus, is substantially older than and clearly different in age from the Levan segment to the north and west.

SUMMARY OF SEGMENTATION OF THE WASATCH FAULT ZONE

Our studies show that the Wasatch fault zone has 10 discrete fault segments, each of which is capable of generating large-magnitude earthquakes. Four of these segments (the northern three and the southern one) have not been active in the past 10 to 15 ka. The slip rates for these distal segments are lower, and recurrence intervals are at least five times longer than those of the six active segments along the central part of the Wasatch fault zone. Five of these six segments show evidence of multiple surface ruptures during the Holocene. Trenches across these segments generally reveal evidence for two, three, or four faulting events since the middle Holocene (5–6 ka).

Schwartz and Coppersmith's (1984) studies of segmentation suggested 6 segments for the Wasatch fault zone; our segmentation scheme increases to 10 the number of segments that are likely to have discrete surface rupturing (see "Recurrence of Large Earthquakes on the Wasatch Fault Zone") but slightly reduces the length of expected surface rupturing during major earthquakes along the Wasatch Front. However, we cannot discount the possibility that major earthquakes will rupture more than one adjacent segment or that some earthquakes will rupture only part of a long segment, such as Provo or Weber.

The average length of all of the Wasatch fault zone segments is about 37 km (table 2, fig. 4). However, the six Holocene segments, which comprise three-fourths of the fault zone, average about 48 km in length. This length is almost twice that suggested from paleoseismicity studies in the northeastern part of the Basin and Range province and in the Intermountain Seismic Belt. Because the prehistoric earthquakes along the Wasatch fault zone have typically caused about 2 m of surface displacement (see Schwartz and Coppersmith's (1984) discussion of characteristic displacement), we expect large-magnitude (M_S 7–7.5) earthquakes to occur along the Wasatch fault zone in the future.

CHRONOLOGY OF RECENT MOVEMENT ON THE CENTRAL WASATCH FAULT ZONE: A SYNOPSIS

The Wasatch fault zone has been the focus of extensive trenching efforts since Cluff and others' (1970, 1973, 1974) initial investigations in the 1970's. Including the trench studies that were completed in 1987, 43 trenches and 4 natural exposures have been logged and described from the 18 sites on the Holocene segments of the Wasatch fault zone (table 1). As such, the Wasatch fault zone may be the most studied normal fault zone in the world.

Most of the trenches across the Wasatch fault zone have provided some control on the times of most recent faulting or provided limits for recurrence intervals and slip rates for faulting events. In the past 2 years, we have obtained 36 ^{14}C dates (both conventional and accelerator methods on charcoal and soil organic matter) and 17 experimental TL age estimates (see table A1). The combination of these new ages, trenching investigations, and published data is the basis for our estimates of the timing of Holocene surface-faulting events (paleoearthquakes) and recurrence intervals on segments of the Wasatch fault zone (fig. 20). More importantly, differences in the timing of the most recent and older events along the length of the Wasatch fault zone are the most diagnostic criteria for determining the lengths, validity, and persistence of segments.

Several interesting patterns evolve from the chronology depicted in figure 20. The most striking pattern is one of temporal clustering of large earthquakes—that is, a strong grouping of surface-rupturing earthquakes on the Wasatch fault zone over a geologically short time interval. If one assumes that the most recent event on the Salt Lake City segment occurred about 1.5 ka (rather than closer to the 1.8-ka limit shown in fig. 20), then faulting occurred between about 400(?) and 1,500(?) years ago on five of the six segments of the Wasatch that have Holocene movement. On the basis of the Wasatch fault zone's behavior since the middle Holocene, we estimate that a major earthquake occurred about once every 395 years (see table 4) on the central part of the Wasatch fault zone between Brigham City and Nephi. However, the recent episode of movement on the Wasatch fault zone (six faulting events during a 1,100-year interval) indicates one major surface-rupturing event every 220 years, or about twice as often as we would expect from the longer (Holocene) record. In addition, we have no evidence for a major surface-rupturing earthquake on the Wasatch fault zone during the past 400 to 500 years (our best estimate for the most recent event on the Nephi segment and the youngest time that we allow for the Weber segment). Although these relations point strongly to a process of temporal

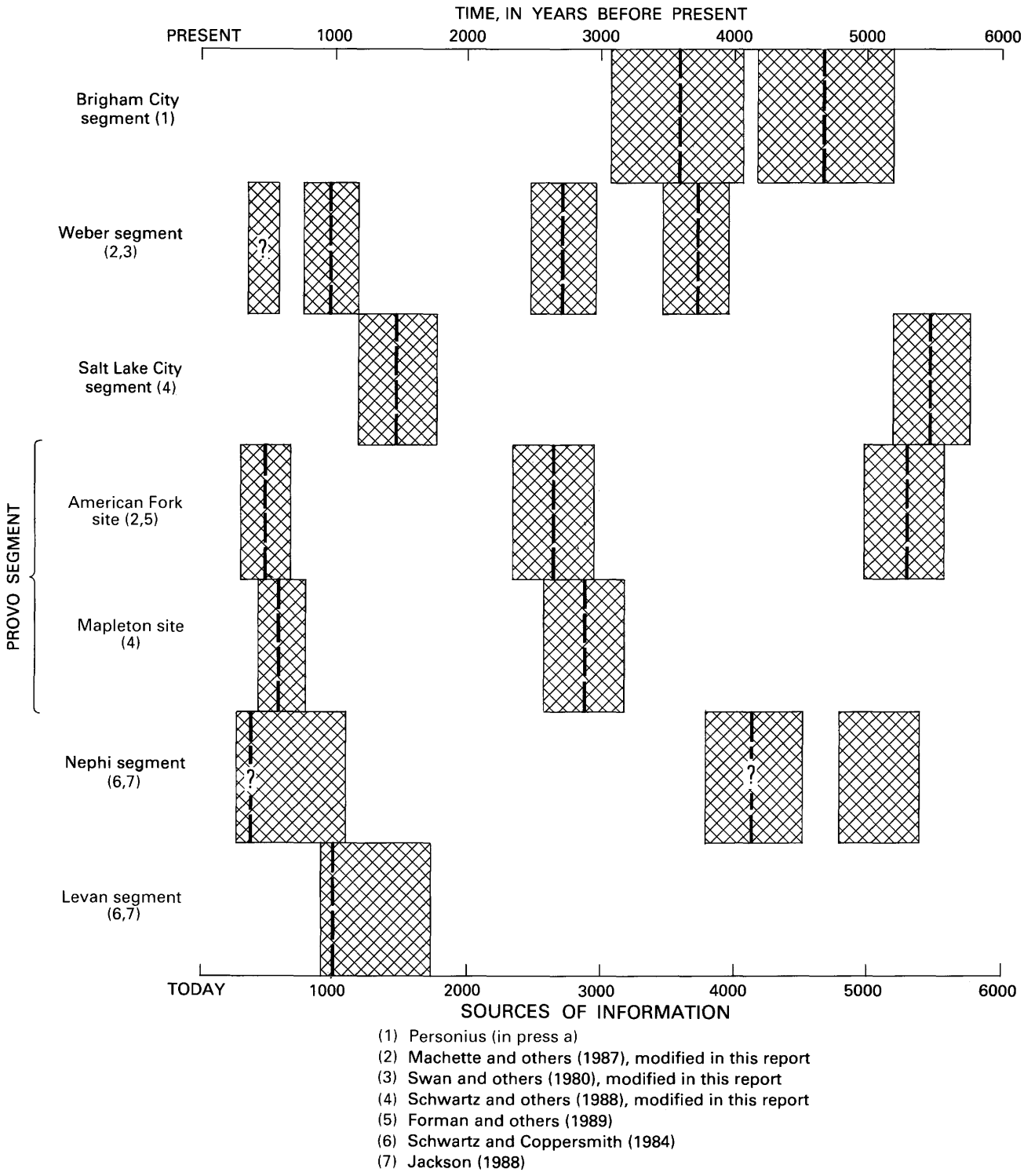

FIGURE 20.—Estimated timing of major surface ruptures on segments of the Wasatch fault zone during the past 6,000 years. Dashed vertical lines indicate our estimates of the most probable time of faulting (queried or missing where timing is uncertain). Cross-hachure patterns indicate permissible limits for faulting events as determined from a combination of calibrated ^{14}C ages and TL age estimates listed in table A1.

clustering of large-magnitude earthquakes, the process seems to be intermittent through time.

Second, there seems to be a significant difference in the average recurrence intervals for the active segments from south to north along the Wasatch fault zone. The segments from Salt Lake City to Nephi have fairly long intervals, typically 2,000 to 4,000 years, whereas the Weber and Brigham City segments are characterized by shorter intervals (about 1,100 years). However, the lack of movement on the Brigham City segment during the past 3,600 years is striking (fig. 20). Personius (1991a) suggested a total of three faulting events between 3,600 and 7,000(?) years ago (an interval of approximately 3,400 years). Thus, the recent 3,600-year period of tectonic quiescence stands in marked contrast to earlier recurrence intervals on this segment.

Third, the lack of surface faulting along the Brigham City segment since 3.6 ka suggests that this segment is a likely candidate for future surface faulting. No other segment of the central Wasatch fault zone has been dormant as long in the late Holocene. On the other hand, this segment may be in a dormant phase if its movement history is related (spatially) to other extensional faults to the northeast. Studies of Quaternary faulting in northeastern Utah and southern Idaho indicate that the East Cache fault (McCalpin, 1989; McCalpin and Forman, 1991), the Morgan fault (Sullivan and Nelson, this volume), and the East Bear Lake fault (A.J. Crone and M.N. Machette, unpub. data, 1988) have been active during the Holocene. These faults form the southern part of an extensive right-stepping en echelon pattern of active faulting that extends to the Yellowstone area of northwestern Wyoming and westward to the north of the Snake River Plain (see Smith and others, 1985; Pierce and Scott, 1986; Smith, 1988; Anders and others, 1989). This system of faults may be preferentially transferring extension to the northeast, thereby decoupling the northern three segments (Malad City, Clarkston Mountain, and Collinston) of the Wasatch fault zone from its more active portions to the south (Machette and others, 1991).

RECURRENCE OF LARGE EARTHQUAKES ON THE WASATCH FAULT ZONE

Schwartz and Coppersmith (1984) estimated that a major surface-faulting event should occur on average once every 615 to 666 years on one of their six proposed segments of the Wasatch fault zone, although their preferred value was 444 years. These values were based on estimates of 12 or 13 (minimum) to 18 (probable) faulting events in the past 8,000 years. We refer to this interval (444 years) as the composite recurrence interval (CRI) of faulting. The main usefulness of CRI values is in estimating the influence of earthquakes from adjacent or nearby segments. For example, the damaging effects of ground shaking and liquefaction are known to occur hundreds of kilometers away from the epicenter of large-magnitude earthquakes. Thus, for hazards assessment, one must consider the effects of an earthquake on any one of the populated central segments of the Wasatch fault zone.

Our calculations of CRI are based on the Wasatch fault zone segments that show recurrent Holocene movement and, therefore, have determinable recurrence intervals. We should, however, qualify the use of CRI values. Inspection of our data on the timing of events on the Wasatch fault zone will show that recurrence intervals vary widely, from as little as 500 to 1,000 years on some segments to as much as 4,000 years on others. In addition, we have strong evidence that some, but not all, earthquakes tend to occur in clusters and that recurrence intervals between earthquakes on adjacent segments during a temporal clustering episode may be as short as several hundred years. Thus, values for recurrence on a single segment of the Wasatch fault zone and on the entire Wasatch fault zone may have little significance other than to characterize the general activity of the fault zone.

There are several problems inherent in Schwartz and Coppersmith's (1984) method of estimating recurrence intervals, although these problems arise mainly from a lack of information on the age of faulted datums and the timing of the most recent event. They chose to estimate the number of earthquakes over a set time interval rather than to use intervals defined by dated earthquakes. The first problem is the result of including time for undefined recurrence intervals. For example, if the most recent event on a segment was 1.5 ka, then an additional 1,500 years is included in the observational window for calculating the recurrence interval of that segment. Ideally, one should discard incomplete recurrence intervals by removing the time since the most recent event (column B, table 4) and the time between the faulted datum and the oldest event (footnote 3, table 4). Even for our calculations, the latter value is not always known or determinable, but, where it is known, we use the time of the oldest event in column A of table 4. In such cases, a calculated recurrence interval is more accurate because it includes only the time between the oldest recorded event and the beginning of the period being considered (that is, the age of the faulted stratigraphic unit). Our estimate of the total time encompassed by the segments showing recurrent Holocene movement (17,800 years) (column C, table 4) may include a total of several hundred years between the oldest fault event and the dated materials for the Nephi segment and

thus represents only 1 to 2 percent of potential error. Alternatively, one can argue that the deletion of at least 3,600 years for the current recurrence interval on the Brigham City segment leads us to underestimate the composite recurrence interval. If such an unconstrained value is included, then the minimum values should be included for all segments, and the method of calculation will be similar to that used by Schwartz and Coppersmith. Nevertheless, if we had included an additional 3,600 years and one additional (but incomplete) recurrence interval in our calculations (table 4), the CRI value would increase about 35 years for a value of 430 years.

The chronology of faulting that we have constructed so far (fig. 20) suggests that at least 15 faulting events occurred in the past 3,500 to 5,500 years on the central six segments of the Wasatch fault zone (table 4). Our model for recurrence calculations considers the five segments that have recurrent Holocene movement. These data yield a CRI of 395±60 years (this value is based on 15 faulting events and 9 recurrence intervals on a total of 5 segments of the Wasatch fault zone during 17,800±2,800 cumulative years).

The chronology of faulting along the central Wasatch fault zone (fig. 20) suggests that all the segments except Brigham City have been active in the past 1,500 years and that none have been active in the past 400 to 500 years. The average time between faulting events on the whole fault zone in the most recent episode of faulting was about 220 years (six events between 400 and 1,500 years ago). The shortness of intervals between recent events, the recent period of fault quiescence, and the long average recurrence intervals for individual segments (1,980±310 years) (table 4) lead us to suspect that major earthquakes and surface faulting along the Wasatch fault zone may have occurred in clusters interspersed with less-frequent random events between clusters.

A historical analog for the Holocene faulting on the Wasatch fault zone may be the Central Nevada Seismic Belt (Wallace and Whitney, 1984) of the western Basin and Range province. This belt is characterized by a concentration of historical large-magnitude earthquakes and associated surface ruptures that occurred on an average of once every 15 to 20 years. The pattern of rupturing suggests that the belt is composed of a series of active segments and seismic gaps, which correspond to inactive fault segments. Through time, these gaps have been filled sequentially by faulting events and, as such, represent a historical example of temporal clustering (Wallace, 1984b, 1987). If and when rupturing is completed by filling the two remaining seismic gaps in the belt, activity might shift to another major fault zone in the region. Pearthree and Demsey's (1987) morphometric analysis of prehistoric fault scarps of the Central Nevada Seismic Belt suggests that its individual faults have recurrence intervals of many thousands of years, much like those of the Wasatch fault zone (table 4). However, the Central Nevada Seismic Belt and the Wasatch fault zone may differ in one major respect: the average times between major earthquakes during temporal clustering are 15 to 20 years and about 220 years, respectively.

The process of earthquake clustering, which is physically manifested as a temporal linking of movement from one fault or fault segment to another, has been termed "contagion" by Perkins (1987), after the analogy with contagious illness. The implications of a clustering process are significant for analyses of earthquake risk along the Wasatch fault zone and other fault zones. For example, assuming a Poisson distribution of nonclustered earthquakes (the commonly accepted distribution), one would expect a major earthquake somewhere on the central section of the Wasatch fault zone once every 395±60 years on the basis of our timing model (fig. 18, table 4). Such a short recurrence interval poses a significant risk for the densely populated part of the Wasatch fault zone, where many critical structures and facilities have expected lifespans of 100 years or more. If the case of the recent temporal clustering of earthquakes on the Wasatch fault zone having CRI of about 220 years is valid and if the most recent episode ended about 400 to 500 years ago, then one might argue that the recent episode has been completed. In this case, one may expect a long period of relative tectonic quiescence (perhaps 1,000 to 2,000 years long) before the next episode of temporal clustering on the Wasatch fault zone. Complicating this scenario is the seeming random distribution of faulting events that occurred before 1,500 years (fig. 20). Although our data present compelling evidence of a non-Poisson distribution of earthquakes on the Wasatch fault zone, especially during late Holocene time, we do not understand what causes the variability in earthquake recurrence on individual segments, what controls the pattern of rupturing on segments during clustered episodes of earthquakes, and what mechanisms control the process of temporal clustering. Proving that the process was or is active and representative of long-term behavior of the Wasatch fault zone will require an extensive and well-dated record that extends at least 15,000 years into the past.

DISCUSSION OF SLIP-RATE DATA FOR THE WASATCH FAULT ZONE

Sediment that predates the Bonneville lake cycle (more than 35 ka) is rarely exposed on both sides of the Wasatch fault zone along its northern and central

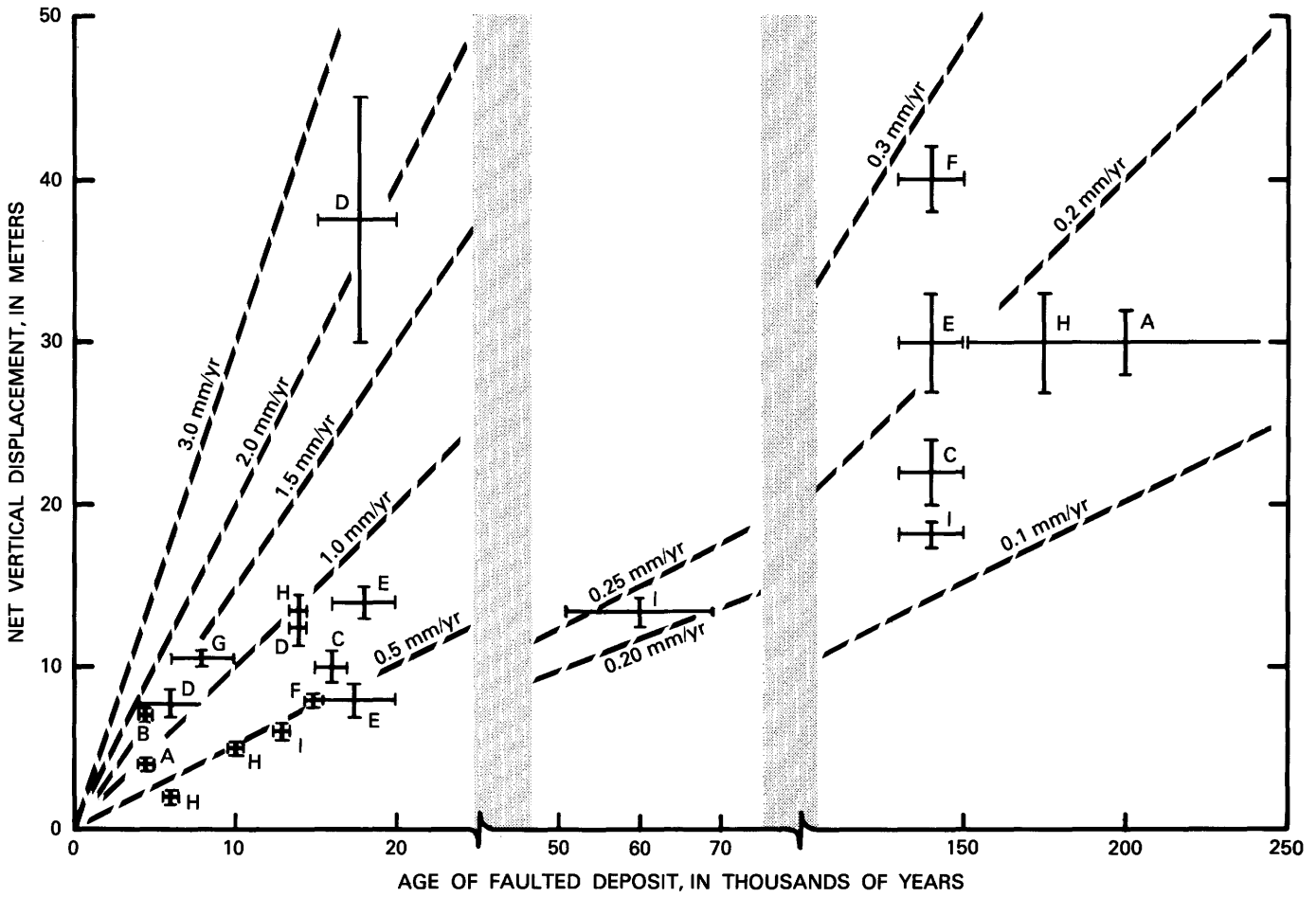

FIGURE 21.—Some slip rates on the Wasatch fault zone for different time intervals as determined from deposits of Holocene to middle Quaternary age. Letters A through I (listed below) indicate locations of slip-rate determinations. Abbreviated site names (in parentheses) are the same as those used on cited figures. Vertical and horizontal bars indicate the range in probable amounts of displacement and ages of deposits. Dashed lines indicate different rates of slip. Note changes in scale at the breaks in horizontal axes (25/40 ka and 80/100 ka). A, Gardner Creek (GC, fig. 18), Nephi segment, Wasatch fault zone; B, North Creek (NC, fig. 18), Nephi segment, Wasatch fault zone; C, canyon of Santaquin Creek (S, fig. 16), Nephi segment, Wasatch fault zone; D, Hobble Creek (HC, fig. 15), Provo segment, Wasatch fault zone; E, canyon of Dry Creek (DC, fig. 15), Provo segment, Wasatch fault zone; F, canyons of Big and Little Cottonwood Creeks (BCC and LCC, fig. 13), Salt Lake City segment, Wasatch fault zone; G, Kaysville (KV, fig. 9), Weber segment, Wasatch fault zone; H, Jim May Canyon (JMC, fig. 8), Brigham City segment, Wasatch fault zone; I, Granger fault (fig. 13), West Valley fault zone (Keaton and others, 1987).

sections. However, south of Santaquin, Utah (fig. 18), the Wasatch fault zone generally is above the highest shoreline of the Bonneville lake cycle; here we can measure and compare the net slip in alluvial deposits that both postdate and predate the Bonneville lake cycle. In addition, several exposures of pre-Bonneville age deposits on fault segments to the north of Santaquin provide data on longer term rates of slip. We have studied these and other sites in detail to compare slip rates for the time intervals before and after the Bonneville lake cycle (fig. 21). The slopes of the dashed lines shown in figure 21 delineate slip rates of 0.1 to 3.0 mm/yr for different parts of the time scale as recorded by faulted deposits. In order to plot the amount of displacement of deposits of middle Pleistocene to Holocene age on one diagram, two breaks were made in the time scale, one between 25 and 40 ka and a second between 80 and about 100 ka. Only the slip-rate lines for the youngest interval project through the axis, and the time axis has a different scale for each of the three intervals. However, by plotting the slip-rate data in this manner, we can make direct comparisons of average slip rates over much different time intervals.

At Gardner Creek near Nephi, 150- to 250-ka alluvial-fan deposits that have well-developed calcic soils are displaced about 30 m across the fault zone (Machette, 1984). The Wasatch fault zone at this site has had an average slip rate of 0.12 to 0.20 mm/yr during the past 150 to 250 ka. At the same site, middle(?) Holocene

sediment is displaced 3.9 m, indicating an average slip rate of 0.8 to 1.0 mm/yr for the past 4 to 5 ka. These two averages (labeled as points A, fig. 21), which reflect an appropriate fivefold increase in slip rate sometime during the latest Quaternary, are typical of the central part of the Wasatch fault zone. Large temporal changes in slip rate (fig. 21) have been documented at sites near Santaquin (northern part of Nephi segment), at Dry Creek northeast of Alpine (northern part of Provo segment), at Big and Little Cottonwood Canyons (Salt Lake City segment), at Jim May Canyon (near Honeyville on the Brigham City segment), and on the Granger fault (West Valley fault zone) (Keaton and others, 1987).

Along the central Wasatch fault zone, sediment of or related to the Bonneville lake cycle (10–32 ka) commonly has been deposited against or across preexisting scarps of the fault zone. This sediment and the subsequent Holocene deposits record relatively high rates of fault slip. For example, Swan and others (1980) calculated slip rates for three separate geologic units at the Hobble Creek site (point D, fig. 21). The slip rates range from a maximum of 1.8 to 2.5 mm/yr in sediment at the highest Bonneville shoreline level (17±2 ka) to 0.85 to 1.0 mm/yr in alluvium graded to the Provo level (13.5–14 ka) to 1 to 2 mm/yr in middle to lower(?) Holocene stream sediment (4.5–9 ka).

With the exception of the Hobble Creek site, most slip rates along the Wasatch fault zone (fig. 21) have been between 0.5 and 1.5 mm/yr since culmination of the Bonneville lake cycle. As figure 21 illustrates, the slip rates during the past 15 ka have been distinctly higher (2–3 times) than the average rates of 0.1 to 0.3 mm/yr recorded by deposits older than the Bonneville lake cycle. If we examine the average slip rates recorded between the time of deposition of the older deposits and the culmination of the Bonneville lake cycle, the difference in long- and short-term slip rates is even greater. For example, if 200-ka alluvium records an average slip rate of 0.2 mm/yr (40-m net slip) and adjacent 15-ka lake sediment records an average slip rate of 1.0 mm/yr (15-m net slip), then the apparent increase in slip rates is fivefold. However, the displacement recorded between deposition of the older unit and that of the younger unit is only 25 m, whereas the time interval for slip is 185,000 years . The resulting interim (185,000 years) slip rate is about 0.14 mm/yr, or about 30 percent less than the long-term (200,000 years) average slip rate. As we discuss later, our observation of large and systematic changes in slip rate through time suggests a causal relation between hydrologic cycles of Lake Bonneville and large changes in slip rates on the adjacent Wasatch fault zone.

POSSIBLE CAUSAL RELATION BETWEEN DEEP CYCLES OF LAKE BONNEVILLE AND HIGH RATES OF SLIP ON THE WASATCH FAULT ZONE

The pattern, magnitude, and regularity of change in slip rates that we have seen along the Wasatch fault zone are of regional extent and, thus, are probably related to processes acting on a regional rather than a local scale. The basic evidence for this conclusion comes from the relatively low average slip rates (0.1–0.3 mm/yr) recorded in alluvium deposited before the culmination of the transgressive phase of the most recent and deepest Quaternary lake cycle in the Bonneville Basin and the high slip rates (typically 0.4–1.8 mm/yr) recorded in sediment deposited since 15 ka (fig. 21). This relation strongly suggests that the presence of a large, deep lake may have influenced the timing of movement on the Wasatch fault zone.

Several aspects of Lake Bonneville's history may be related to the recent relatively high slip rates along the Wasatch fault zone. During the highest stand of the lake (15 ka) (fig. 2), most basins in northwestern Utah were flooded to a maximum depth of 300 m. This depth of water imposes the same load as 130 to 160 m of sedimentary rock. Almost all of this load was on the downthrown block of the Wasatch fault zone. The lake was fairly deep (200–250 m) just a few kilometers west of localities where high slip rates have been measured. The hydrologic and lithostatic loads imposed by Lake Bonneville and its sediment may have significantly increased the confining pressure on the westward-dipping Wasatch fault zone and thereby inhibited faulting. If increased pore pressure reached seismogenic depths, the effective confining pressure on the fault zone could have been reduced. Nevertheless, if we envision the Earth's crust as a gently upwarped beam over a viscous mantle, then the beam could be shortened (compressed) during deep lake cycles owing to isostatic depression in the lake basin; as much as 60 m of depression occurred at the high stand of the Bonneville lake cycle. In an east-west extensional regime such as the Basin and Range province, this compression would tend to increase horizontal forces across steeply dipping, north-striking normal faults and perhaps retard normal faulting (Keaton and others, 1987).

As mentioned previously, beginning about 14.5 ka, the level of Lake Bonneville rapidly fell 108 m (to the Provo level) by overflow and rapid downcutting of the lake's sill. An additional almost 200 m of fall occurred in the next several thousand years owing to the onset of the Holocene Epoch. These geologically rapid changes in Lake Bonneville were accompanied by (1) rapid isostatic uplift of the basin (Crittenden, 1963a, b; Currey and Burr, 1988), (2) deposition of thick fan-delta complexes and lacustrine spits on the downdropped blocks of the

Wasatch fault zone during the lake's regression, and (3) a probable decrease in the lateral compression that may have previously retarded faulting during the deep (transgressive) phase of the lake cycle.

This well-documented but geologically short-lived episode of isostatic rebound represents upward arching and lengthening of the crust and may have allowed the east-west extension that formed the Basin and Range province to become predominant again. Thus, we speculate that several aspects of the most recent and deepest cycle of Lake Bonneville may have stimulated the recent acceleration of slip rate and (by inference) paleoseismic activity along the Wasatch fault zone. Similar causal relations have been suggested for seismicity in other continental regions. For example, rapid glacio-isostatic rebound after the retreat of late Pleistocene icecaps in Scotland, Finland, and Sweden was associated with both new and renewed tectonic deformation and (by inference) seismicity (Morner, 1978). Morner (1978, p. 45) concluded that "intense faulting, fracturing, and seismic activity are shown to be linked to the deglaciation phase because of the initiation of *changes* [our emphasis] in stress and strain when the rate of glacio-isostatic uplift is near its maximum." Along the same lines, Johnston (1987) proposed that the weight of extensive continental ice sheets suppresses seismic activity in the interior regions of both Greenland and Antarctica. If thick (2-km) ice sheets can have such an effect, it seems reasonable that Lake Bonneville (which at its highest stand was nearly 1 km deep) also may have suppressed seismic activity and slip on the Wasatch fault zone. In addition, rapid changes in water level during either filling or draining are known to have induced seismicity under moderate to large reservoirs in various parts of the world (see Simpson's (1986) review of induced seismicity).

Recent studies of lake sediment that predates the Bonneville lake cycle (for example, Scott and others, 1983; McCalpin, 1986; McCoy, 1987; Oviatt and others, 1987; McCalpin and others, this volume) suggest that the Bonneville Basin may have been occupied by shallow to moderately deep pluvial lakes during most glacial episodes. Oxygen-isotope data from the deep marine record suggest that major glaciations occur about every 120,000 years and minor interglaciations at intervals of 40,000 to 50,000 years (Martinson and others, 1987). If the filling or presence of a deep lake adjacent to the Wasatch fault zone was a suppressor of strain release (slip) on the Wasatch fault zone, then older lake cycles of somewhat lesser extent (such as the Cutler Dam and Little Valley lake cycles shown in fig. 2) also may have influenced cyclic episodes of movement on the Wasatch fault zone.

We do not mean to infer that periods of high lake level were times of seismic quiescence on the fault zone but rather that, during these periods, the Wasatch fault zone may have had lower slip rates—rates similar to those determined from late Quaternary faults in the eastern Basin and Range province and backvalleys of the eastern Wasatch Range (rates of 0.1–0.2 mm/yr are common for these faults). The late Cenozoic uplift rate for the central part of the Wasatch Range is about 0.4 to 0.8 mm/yr as determined by fission-track studies (Naeser and others, 1983; Parry and Bruhn, 1986, 1987). These long-term rates are intermediate—slower than the Holocene-late Pleistocene rate and faster than the post-middle Pleistocene rate on the Wasatch fault zone.

If this postulated causal relation between water depth and slip rates is correct, one might view the Wasatch fault zone as having four modes of slip or tectonic activity: (1) low rates during the maxima of deep-lake cycles (perhaps approaching the long-term rates), (2) very low (suppressed) rates during the transgressive phase of a lake cycle, (3) very high (accelerated) rates during the regressive phase of a lake cycle, and (4) high rates during interpluvials (shallow or dry lake levels). A thorough testing of the hypothesis would require long and detailed (150,000 years) records of paleoseismicity at one or more sites on the Wasatch fault zone. Trenches that could expose such a record would probably be tens of meters deep, have sloping or stair-stepped walls, be costly to construct, and require several man-years to log and interpret. In addition, dating methods whose age capabilities are greater than those of ^{14}C analyses (less than 40 ka) would have to be employed.

Although there have been relatively few detailed studies of paleoseismicity in the eastern Basin and Range province (Nelson and Weisser, 1985; Nelson and VanArsdale, 1986; Foley and others, 1986; Keaton and others, 1987; Sullivan and others, 1988; West, 1989; Nelson and Sullivan, this volume), regional studies (Bucknam and Algermissen, 1984; Wallace, 1984b) show that slip rates on other major faults in the province have been as much as an order of magnitude less than rates documented for the Wasatch fault zone during the latest Pleistocene and Holocene. These studies include some major range-bounding faults in the transition zone between the Colorado Plateaus and the Basin and Range provinces. Many of these faults are considered to be fundamental, deeply penetrating structures capable of generating large-magnitude earthquakes. Because these faults have lower slip rates (and, by inference, longer recurrence intervals) than the Wasatch fault zone and generally do not show evidence of vastly different short- versus long-term slip rates, the Wasatch fault zone may present a special case for assessment of earthquake risk.

CONCLUSIONS

[T]he filling of the Bonneville Basin with water added a very considerable weight to the valleys, and therefore to the down-

> thrown blocks, and made no corresponding addition to the uplifted blocks represented in the mountain ranges.... It is therefore theoretically conceivable that during the presence of the lake the process of faulting along the mountain bases was stimulated, and that after the evaporation of the water the process was correspondingly retarded [G.K. Gilbert (1890, p. 357)].

We are struck by Gilbert's astute observations about Lake Bonneville stratigraphy and the Wasatch fault zone and his inference of a causal relation between the lake and the fault zone, made almost 100 years ago (Machette, 1988b). In contrast, however, our investigations suggest, somewhat meagerly, that movement on the Wasatch fault zone may have been stimulated by the catastrophic overflow and lowering of Lake Bonneville, whereas its transgression actually may have supressed or slowed the faulting process. Evidence from recent trenching investigations and mapping of Quaternary geology along the Wasatch Front suggests that the Wasatch fault zone was very active during the regressive phase of the Bonneville lake cycle (15,000–10,000 years ago) and during the subsequent low lake stand (Holocene interpluvial).

The sparse data now available on fault activity during the transgressive phase of the Bonneville lake cycle suggest suppression of faulting on the West Valley fault zone (Keaton and others, 1987) but inducement of faulting in Hansel Valley (McCalpin and others, this volume). The apparent nonsynchroneity of movement on these fault systems may be related to their structural and geographic settings. The Hansel Valley earthquake was associated with an intra-Bonneville Basin fault that does not seem to be a fundamental structure of the northern Basin and Range, whereas the West Valley fault zone may be a major basin-margin fault that is sympathetic to the Wasatch fault zone.

Our recognition of 10 discrete segments of the Wasatch fault zone, 6 of which have demonstrable Holocene movement, increases the possible number of separate localities where earthquakes may nucleate and where associated surface ruptures may occur along the Wasatch Front. Although the average recurrence interval for the active segments is about 2,000 years, we think that major earthquakes have struck the central, heavily urbanized section of the Wasatch fault zone on an average of once every four centuries (395 years) during the past 5,500 years. This estimate is only slightly shorter than Schwartz and Coppersmith's (1984) preferred composite recurrence interval of 444 years. We have no firm evidence that large earthquakes (those that cause significant surface faulting) have occurred in the past 400 to 500 years, as the average would demand. However, the abundance of faulting events (one every 220 years) between 400 and 1,500 years ago—at about twice the average Holocene rate—suggests that a form of temporal clustering of earthquakes has been (and may still be) active along the Wasatch fault zone.

One of the most important questions remaining to be answered is whether the recent temporal cluster has been completed. The lack of movement along the Brigham City segment during the past 3,600 years is somewhat ominous in view of evidence for movement during the past 1,500 years on the other four segments of the central Wasatch fault zone to the south.

REFERENCES CITED

Anders, M.H., Geissman, J.W., Piety, L.A., and Sullivan, J.T., 1989, Parabolic distribution of circum-eastern Snake River Plain seismicity and latest Quaternary faulting—Migratory pattern and association with the Yellowstone hotspot: Journal of Geophysical Research, v. 94, no. B2, p. 1589–1621.

Antevs, E., 1948, The Great Basin, with emphasis on glacial and postglacial times, pt. III, Climate changes and pre-white man: University of Utah Bulletin 38, no. 20, p. 168–191.

———1955, Geologic-climatic dating in the west: American Antiquity, v. 20, p. 317–335.

Birkeland, P.W., 1984, Soils and geomorphology: New York, Oxford University Press, 372 p.

Bissell, H.J., 1963, Lake Bonneville—Geology of southern Utah Valley, Utah: U.S. Geological Survey Professional Paper 257-F, p. B101–B130.

Bonilla, M.G., Mark, R.K., and Lienkaemper, J.J., 1984, Statistical relations among earthquake magnitude, surface rupture length, and surface fault displacement: Bulletin of the Seismological Society of America, v. 74, no. 6, p. 2379–2411.

Bruhn, R.L., Gibler, P.R., and Parry, W.T., 1987, Rupture characteristics of normal faults—An example from the Wasatch fault zone, Utah, *in* Coward, M.P., Dewey, J.F., and Hancock, P.L., eds., Continental extensional tectonics: Geological Society of London Special Publication 28, p. 337–353.

Bucknam, R.C., 1978, Northwestern Utah seismotectonic studies, *in* Seiders, W., and Thomson, J., compilers, Summaries of technical reports, v. VII: Menlo Park, Calif., U.S. Geological Survey Office of Earthquake Studies, p. 64.

Bucknam, R.C., and Algermissen, S.T., 1984, A comparison of geologically determined rates of late Quaternary seismic activity and historic seismicity data in the Great Basin, western United States, *in* A collection of papers of International Symposium on Continental Seismicity and Earthquake Prediction (Sept. 8–14, 1982, Beijing, China): Beijing, Seismological Press, p. 169–176.

Bucknam R.C., and Anderson, R.E., 1979, Estimation of fault-scarp ages from a scarp-height—slope-angle relationship: Geology, v. 7, p. 11–14.

Cluff, L.S., Brogan, G.E., and Glass, C.E., 1970, Wasatch fault, northern portion—Earthquake fault investigation and evaluation, prepared for the Utah Geological and Mineral Survey: Oakland, Calif., Woodward-Clyde and Associates, 27 p., 21 maps, scale 1:24,000.

———1973, Wasatch fault, southern portion—Earthquake fault investigation and evaluation, prepared for the Utah Geological and Mineral Survey: Oakland, Calif., Woodward-Lundgren and Associates, 79 p., 23 maps, scale 1:24,000.

Cluff, L.S., Glass, C.E., and Brogan, G.E., 1974, Investigation and evaluation of the Wasatch fault north of Brigham City and Cache Valley faults, Utah and Idaho—A guide to land-use planning with recommendations for seismic safety (prepared for the U.S. Geo-

logical Survey under contract 14-08-001-13665): Oakland, Calif., Woodward-Lundgren and Associates, 147 p., 35 maps, scale 1:24,000.

Crittenden, M.D., Jr., 1963a, New data on the isostatic deformation of Lake Bonneville: U.S. Geological Survey Professional Paper 454-E, p. E1-E31.

———1963b, Effective viscosity of the Earth derived from isostatic loading of Pleistocene Lake Bonneville: Journal of Geophysical Research, v. 68, no. B19, p. 5517-5530.

Crittenden, M.D., Jr., and Sorenson, M.L., 1985, Geologic map of the North Ogden quadrangle and part of the Ogden and Plain City quadrangles, Box Elder and Weber Counties, Utah: U.S. Geological Survey Miscellaneous Investigations Series Map I-1606, scale 1:24,000.

Crone, A.J., 1983, Amount of displacement and estimated age of a Holocene surface faulting event, eastern Great Basin, Millard County, Utah, *in* Gurgel, K.D., ed., Geologic excursions in neotectonics and engineering geology in Utah, guidebook—Part IV: Utah Geological and Mineral Survey Special Studies 62, p. 49-54.

Crone, A.J., and Haller, K.M., 1989, Segmentation of basin-and-range normal faults—Examples from east-central Idaho and southwestern Montana, *in* Schwartz, D.P., and Sibson, R.H., eds., Proceedings of Conference XLV; a workshop on fault segmentation and controls on rupture initiation and termination: U.S. Geological Survey Open-File Report 89-315, p. 110-130.

———1991, Segmentation and the coseismic behavior of Basin-and-Range normal faults—Examples from east-central Idaho and southwestern Montana, U.S.A., *in* Hancock, P.L., Yeats, R.S., and Sanderson, D.J., special eds., Characteristics of active faults (special issue): Journal of Structural Geology, v. 13, no. 2, p. 151-164.

Crone, A.J., Machette, M.N., Bonilla, M.G., Lienkaemper, J.J., Pierce, K.L., Scott, W.E., and Bucknam, R.C., 1987, Surface faulting accompanying the Borah Peak earthquake and segmentation of the Lost River fault, central Idaho: Bulletin of the Seismological Society of America, v. 77, no. 3, p. 739-770, 3 pls., scale 1:24,000.

Currey, D.R., and Burr, T.N., 1988, Linear model of threshold-controlled shorelines of Lake Bonneville, *in* Machette, M.N., ed., In the footsteps of G.K. Gilbert—Lake Bonneville and neotectonics of the eastern Basin and Range Province (Geological Society of America Guidebook to Field Trip 12): Utah Geological and Mineral Survey Miscellaneous Publication 88-1, p. 104-110.

Currey, D.R., and Oviatt, C.G., 1985, Durations, average rates, and probable causes of Lake Bonneville expansion, still-stands, and contractions during the last deep-lake cycle, 32,000 to 10,000 yrs ago, *in* Kay, P.A., and Diaz, H.F., eds., Problems of and prospects for predicting Great Salt Lake levels—Proceedings of a NOAA Conference held March 26-28, 1985: Salt Lake City, Center for Public Affairs and Administration, University of Utah, p. 9-24.

Currey, D.R., Oviatt, C.G., and Plyler, G.B., 1983, Lake Bonneville stratigraphy, geomorphology, and isostatic deformation in west-central Utah, *in* Gurgel, K.D., ed., Geologic excursions in neotectonics and engineering geology in Utah, guidebook—Part IV: Utah Geological and Mineral Survey Special Studies 62, p. 63-82.

Davis, F.D., 1983a, Geologic map of the central Wasatch Front, Utah: Utah Geological and Mineral Survey Map 54-A, scale 1:100,000.

———1983b, Geologic map of the southern Wasatch Front, Utah: Utah Geological and Mineral Survey Map 55-A, scale 1:100,000.

———1985, Geologic map of the northern Wasatch Front, Utah: Utah Geological and Mineral Survey Map 53-A, scale 1:100,000.

dePolo, C.M., Clark, D.G., Slemmons, D.B., and Aymard, W.H., 1989, Historical basin and range province surface faulting and fault segmentation, *in* Schwartz, D.P., and Sibson, R.H., eds., Proceedings of Conference XLV; a workshop on fault segmentation and controls on rupture initiation and termination: U.S. Geological Survey Open-File Report 89-315, p. 131-162.

dePolo, C.M., Clark, D.G., Slemmons, D.B., and Ramelli, A.R., 1991, Historical surface faulting in the Basin and Range province, Western North America—Implications for fault segmentation, *in* Hancock, P.L., Yeats, R.S., and Sanderson, D.J., special eds., Characteristics of active faults (special issue): Journal of Structural Geology, v. 13, no. 2, p. 123-136.

Dohrenwend, J.C., 1987, Basin and Range, *in* Graf, W.L., ed., Geomorphic systems of North America: Geological Society of America Centennial Special Volume 2, ch. 9, p. 303-342.

Doser, D.I., 1985, Source parameters and faulting processes of the 1959 Hebgen Lake, Montana, earthquake sequence: Journal of Geophysical Research, v. 90, no. B6, p. 4537-4555.

———1986, Earthquake processes in the Rainbow Mountain-Fairview Peak-Dixie Valley, Nevada, region 1954-1959: Journal of Geophysical Research, v. 91, no. B12, p. 12572-12586.

———1989, Extensional tectonics of northern Utah-southern Idaho, U.S.A., and the 1934 Hansel Valley sequence: Physics of the Earth and Planetary Interiors, v. 54, p. 120-134.

Doser, D.I., and Smith, R.B., 1985, Source parameters of the 28 October, 1983, Borah Peak, Idaho, earthquake from body wave analysis: Bulletin of the Seismological Society of America, v. 75, p. 1041-1051.

Foley, L.L., Martin, R.A., Jr., and Sullivan, J.T., 1986, Seismotectonic study for Joes Valley, Scofield, and Huntington North dams, Emery County and Scofield projects, Utah: U.S. Bureau of Reclamation Seismotectonic Report 86-7, 302 p.

Forman, S.L., Nelson, A.R., and McCalpin, J.P., 1991, Thermoluminescence dating of fault-scarp-derived colluvium—Deciphering the timing of paleoearthquakes on the Weber segment of the Wasatch fault zone, north-central Utah: Journal of Geophysical Research, v. 96, no. B1, p. 595-606.

Gilbert, G.K., 1890, Lake Bonneville: U.S. Geological Survey Monograph 1, 438 p.

———1928, Studies of Basin-Range structure: U.S. Geological Survey Professional Paper 153, 89 p.

Hanson, K.L., and Schwartz, D.P., 1984, Guidebook to Late Pleistocene and Holocene faulting along the Wasatch Front and vicinity—Little Cottonwood Canyon to Scipio, Utah: American Geophysical Union, Chapman Conference on Fault Behavior and the Earthquake Generation Process, Snowbird, Utah, 1982, 40 p., 34 figs., 1 pl.

Hintze, L.F., 1973, Geologic road log of western Utah and eastern Nevada, pt. 1: Brigham Young University Geology Studies, v. 20, pt. 2, p. 10.

Hunt, C.B., ed., 1982, Pleistocene Lake Bonneville, ancestral Great Salt Lake, as described in the notebooks of G.K. Gilbert, 1875-1880: Brigham Young University Geology Studies, v. 29, pt. 1, p. 1-225.

Hunt, C.B., Varnes, H.D., and Thomas, H.E., 1963, Lake Bonneville—Geology of northern Utah Valley, Utah: U.S. Geological Survey Professional Paper 257-A, 99 p.

Izett, G.A., 1981, Volcanic ash beds—Recorders of upper Cenozoic silicic pyroclastic volcanism in the Western United States: Journal of Geophysical Research, v. 86, no. B11, p. 10,200-10,222.

———1982, The Bishop ash bed and some older compositionally similar ash beds in California, Nevada, and Utah: U.S. Geological Survey Open-File Report 82-582, 44 p., 3 oversized sheets.

Izett, G.A., Wilcox, R.E., Powers, H.A., and Desborough, G.A., 1970, The Bishop ash bed, a Pleistocene marker bed in the western United States: Quaternary Research, v. 1, p. 121-132.

Jackson, M.E., 1988, Thermoluminescence dating of Holocene paleoseismic events on the Nephi and Levan segments, Wasatch fault

zone, Utah: Boulder, University of Colorado, unpublished M.Sci. thesis, 149 p.

———in press, Number and timing of paleoseismic events on the Nephi and Levan segments of the Wasatch fault zone, Utah, *in* Lund, W.R., ed., Paleoseismology of Utah, v. 3: Utah Geological and Mineral Survey Special Studies 78.

Johnston, A.C., 1987, Suppression of earthquakes by large continental ice sheets: Nature, v. 330, p. 467 (December 3, 1987).

Keaton, J.R., and Currey, D.R., 1989, Earthquake hazards evaluation of the West Valley fault zone, Salt Lake City urban area, Utah (report sponsored by U.S. Geological Survey under contract 14-08-0001-G1397, September 15, 1989): Salt Lake City, Utah, Dames and Moore, 68 p.

Keaton, J.R., Currey, D.R., and Olig, S.J., 1987, Paleoseismicity and earthquake hazards evaluation of the West Valley fault zone, Salt Lake City urban area, Utah (report sponsored by U.S. Geological Survey under contract 14-08-0001-22048, March 6, 1987): Salt Lake City, Utah, Dames and Moore, 55 p., 33-p. app.

King, G., and Nabelek, J., 1985, Role of fault bends in the initiation and termination of earthquake rupture: Science, v. 228, p. 984–987.

Lund, W.R., and Schwartz, D.P., 1987, Fault behavior and earthquake recurrence at the Dry Creek site, Salt Lake segment, Wasatch fault zone, Utah: Geological Society of America Abstracts with Programs, v. 19, no. 5, p. 317.

Lund, W.R., Schwartz, D.P., Mulvey, W.E., Budding, K.E., and Black, B.D., 1991, Fault behavior and earthquake recurrence on the Provo segment of the Wasatch fault zone at Mapleton, Utah Co., Utah, *in* Lund, W.R., ed., Paleoseismology of Utah, v. 1: Utah Geological and Mineral Survey Special Studies 75, 41 p.

Machette, M.N., 1984, Preliminary investigations of late Quaternary slip rates along the southern part of the Wasatch fault zone, *in* Hays, W.W., and Gori, P.L., eds., Proceedings of Conference XXVI—A workshop on evaluation of regional and urban earthquake hazards and risk in Utah: U.S. Geological Survey Open-File Report 84-763, p. 391–406.

———1985, Late Cenozoic geology of the Beaver basin, southwestern Utah: Brigham Young University Geology Studies, v. 32, pt. 1, p. 19–37.

———1987, Recent studies of the Wasatch fault zone, Utah—A review: Geological Society of America Abstracts with Programs, v. 19, no. 5, p. 317.

———1988a, American Fork Canyon—Holocene faulting, the Bonneville fan-delta complex, and evidence for the Keg Mountain oscillation, *in* Machette, M.N., ed., In the footsteps of G.K. Gilbert—Lake Bonneville and neotectonics of the eastern Basin and Range province (Geological Society of America Guidebook to Field Trip 12): Utah Geological and Mineral Survey Miscellaneous Publication 88-1, p. 89–95.

———1988b, ed., In the footsteps of G.K. Gilbert—Lake Bonneville and neotectonics of the eastern Basin and Range Province (Geological Society of America Guidebook to Field Trip 12): Utah Geological and Mineral Survey Miscellaneous Publication 88-1, 120 p.

———1989, Preliminary surficial geologic map of eastern Utah Valley, Utah County and parts of Salt Lake and Juab Counties, Utah: U.S. Geological Survey Miscellaneous Field Studies Map MF-2109, scale 1:50,000, 30-p. text.

———in press, Surficial geologic map of eastern Utah Valley, Utah County and parts of Salt Lake and Juab Counties, Utah: U.S. Geological Survey Miscellaneous Investigations Map I-2095, scale 1:50,000.

Machette, M.N., and Lund, W.R., 1987, Trenching across the American Fork segment of the Wasatch fault zone, Utah: Geological Society of America Abstracts with Programs, v. 19, no. 5, p. 317.

Machette, M.N., Personius, S.F., and Nelson, A.R., 1986, Late Quaternary segmentation and slip-rate history of the Wasatch fault zone, Utah: EOS [Transactions of the American Geophysical Union], v. 67, no. 44, p. 1107.

———1987, Quaternary geology along the Wasatch fault zone—Segmentation, recent investigations, and preliminary conclusions, *in* Gori, P.L., and Hays, W.W., eds., Assessment of regional earthquake hazards and risk along the Wasatch Front, Utah: U.S. Geological Survey Open-File Report 87-585, p. A1–A72.

Machette, M.N., Personius, S.F., Nelson, A.R., Schwartz, D.P., and Lund, W.R., 1991, The Wasatch fault zone, Utah—Segmentation and history of Holocene earthquakes, *in* Hancock, P.L., Yeats, R.S., and Sanderson, D.J., special eds., Characteristics of active faults (special issue): Journal of Structural Geology, v. 13, no. 2, p. 137–150.

Madsen, D.B., and Currey, D.R., 1979, Late Quaternary glacial and vegetation changes, Little Cottonwood Canyon area, Wasatch Mountains, Utah: Quaternary Research, v. 12, p. 254–270.

Marsell, R.E., and Threet, R.L., 1964, Geologic map of Salt Lake County, Utah, *in* Crawford, A.L., ed., Geology of Salt Lake County: Utah Geological and Mineral Survey Bulletin 69, scale 1:63,360.

Martinson, D.G., Pisias, N.G., Hays, J.D., Imbrie, J., Moore, T.C., Jr., and Shackleton, N.J., 1987, Age dating and the orbital theory of the Ice Ages—Development of a high-resolution 0 to 300,000-year chronostratigraphy: Quaternary Research, v. 27, p. 1–29.

McCalpin, J., 1986, Thermoluminescence (TL) dating in seismic hazard evaluations—An example from the Bonneville basin, Utah, *in* Symposium on Engineering Geology and Soils Engineering, 22d, Boise, Idaho, 1986, Proceedings: p. 156–176.

———1989, Surficial geologic map of the Cache Valley, Cache County, Utah: U.S. Geological Survey Miscellaneous Field Studies Map MF-2107, scale 1:50,000.

McCalpin, J., and Forman, S.L., 1991, Quaternary faulting and thermoluminescence dating of the East Cache fault zone, north-central Utah: Bulletin of the Seismological Society of America, v. 81, no. 1, p. 139–161.

McCoy, W.D., 1987, Quaternary aminostratigraphy of the Bonneville basin, Western United States: Geological Society of America Bulletin, v. 98, p. 99–112.

Miller, R.D., 1982, Surficial geologic map along part of the Wasatch Front, Great Salt Lake and Utah Valleys, Utah: U.S. Geological Survey Miscellaneous Field Studies Map MF-1477, scale 1:100,000.

Morner, N.-A., 1978, Faulting, fracturing, and seismicity as functions of glacio-isostasy in Fennoscandia: Geology, v. 6, p. 41–45.

Morrison, R.B., 1965, Quaternary geology of the Great Basin, *in* Wright, H.E., Jr., and Grey, D.G., eds., Quaternary geology of the United States: Princeton, N.J., Princeton University Press, p. 265–285.

Naeser, C.W., Bryant, B., Crittenden, M.D., Jr., and Sorensen, M.L., 1983, Fission-track ages of apatite in the Wasatch Mountains, Utah—An uplift study, *in* Miller, D.M., Todd, V.R., and Howard, K.A., eds., Tectonic and stratigraphic studies in the eastern Great Basin: Geological Society of America Memoir 157, p. 29–36.

Nelson, A.R., and Personius, S.F., 1987, A nonconservative barrier to Holocene rupture propagation in the northern Wasatch fault zone, Utah, USA: International Union for Quaternary Research International Congress, 12th, Ottawa, 1987, Programme with Abstracts, p. 231.

———1990, Preliminary surficial geologic map of the Weber segment, Wasatch fault zone, Weber and Davis Counties, Utah: U.S. Geological Survey Miscellaneous Field Studies Map MF-2132, scale 1:50,000.

———in press, Surficial geologic map of the Weber segment, Wasatch fault zone, Weber and Davis Counties, Utah: U.S. Geological Survey Miscellaneous Investigations Map I–2199, scale 1:50,000.

Nelson, A.R., and Weisser, R.R., 1985, Quaternary faulting on Towanta Flat, northwestern Uinta Basin, *in* Picard, M.D., ed., Geology and energy resources, Uinta Basin, Utah: Utah Geological Association Publication 12, p. 147–158.

Nelson, A.R., Klauk, R.H., Lowe, M., and Garr, J.D., 1987, Holocene history of displacement on the Weber segment of the Wasatch fault zone at Ogden, northern Utah: Geological Society of America Abstracts with Programs, v. 19, no. 5, p. 322.

Oviatt, C.G., 1986a, Geologic map of the Cutler Dam quadrangle, Box Elder and Cache Counties, Utah: Utah Geological and Mineral Survey Map 91, scale 1:24,000.

———1986b, Geologic map of the Honeyville quadrangle, Box Elder and Cache Counties, Utah: Utah Geological and Mineral Survey Map 88, scale 1:24,000.

Oviatt, C.G., McCoy, W.D., and Reider, R.G., 1985, Quaternary lacustrine stratigraphy along the lower Bear River, Utah—Evidence for a shallow early Wisconsin lake in the Bonneville basin: Geological Society of America Abstracts with Programs, v. 17, no. 4, p. 260.

———1987, Evidence for a shallow early or middle Wisconsin-age lake in the Bonneville basin, Utah: Quaternary Research, v. 27, p. 248–262.

Parry, W.T., and Bruhn, R.L., 1986, Pore fluid and seismogenic characteristics of fault rock at depth on the Wasatch fault, Utah: Journal of Geophysical Research, v. 91, no. B1, p. 730–744.

———1987, Fluid inclusion evidence for minimum 11 km vertical offset on the Wasatch fault, Utah: Geology, v. 15, p. 67–70.

Pearthree, P.A., and Demsey, K., 1987, Patterns of Holocene faulting and the rate of extension in central Nevada: Geological Society of America Abstracts with Programs, v. 19, no. 7, p. 802.

Perkins, D.M., 1987, Contagious fault rupture, probabilistic hazard, and contagion observability, *in* Crone, A.J., and Omdahl, E.M., eds., Proceedings of Conference XXXIX—Directions in paleoseismology: U.S. Geological Survey Open-File Report 87–673, p. 428–439.

Personius, S.F., 1986, The Brigham City segment—A new segment of the Wasatch fault zone, northern Utah: Geological Society of America Abstracts with Programs, v. 18, no. 5, p. 402.

———1988a, Preliminary surficial geologic map of the Brigham City segment and adjacent parts of the Weber and Collinston segments, Wasatch fault zone, Box Elder and Weber Counties, Utah: U.S. Geological Survey Miscellaneous Field Studies Map MF–2042, scale 1:50,000.

———1988b, A brief summary of the surficial geology along the Brigham City segment of the Wasatch fault zone, Utah, *in* Machette, M.N., ed., In the footsteps of G.K. Gilbert—Lake Bonneville and neotectonics of the eastern Basin and Range Province (Geological Society of America Guidebook to Field Trip 12): Utah Geological and Mineral Survey Miscellaneous Publication 88–1, p. 26–32.

———1990, Surficial geologic map of the Brigham City segment and adjacent parts of the Weber and Collinston segments, Wasatch fault zone, Box Elder and Weber Counties, Utah: U.S. Geological Survey Miscellaneous Investigations Map I–1979, scale 1:50,000.

———1991a, Paleoseismic analysis of the Wasatch fault zone at the Brigham City trench site, Brigham City, Utah, *in* Lund, W.R., ed., Paleoseismology of Utah, v. 2: Utah Geological and Mineral Survey Special Publication 76, p. 1–18.

———1991b, Paleoseismic analysis of the Wasatch fault zone at the Pole Patch trench site, Pleasant View, Utah, *in* Lund, W.R., ed., Paleoseismology of Utah, v. 2: Utah Geological and Mineral Survey Special Publication 76, p. 19–39.

Personius, S.F., and Gill, H.E., 1987, Holocene displacement on the Brigham City segment of the Wasatch fault zone near Brigham City, Utah: Geological Society of America Abstracts with Programs, v. 19, no. 5, p. 326.

Personius, S.F., and Scott, W.E., 1990, Preliminary surficial geologic map of the Salt Lake City segment and parts of adjacent segments of the Wasatch fault zone, Davis, Salt Lake, and Utah Counties, Utah: U.S. Geological Survey Miscellaneous Field Studies Map MF–2114, scale 1:50,000.

———in press, Surficial geologic map of the Salt Lake City segment and parts of adjacent segments of the Wasatch fault zone, Davis, Salt Lake, and Utah Counties, Utah: U.S. Geological Survey Miscellaneous Investigations Map I–2106, scale 1:50,000.

Peterson, D.L., 1974, Bouguer gravity map of part of the northern Lake Bonneville basin, Utah and Idaho: U.S. Geological Survey Miscellaneous Field Studies Map MF–627, scale 1:250,000.

Pierce, K.L., and Colman, S.M., 1986, Effect of height and orientation (microclimate) on geomorphic degradation rates and processes, late-glacial terrace scarps in central Idaho: Geological Society of America Bulletin, v. 97, p. 869–885.

Pierce, K.L., and Scott, W.E., 1986, Migration of faulting along and outward from the tract of thermo-tectonic activity in the eastern Snake River Plain region during the last 15 m.y.: EOS [Transactions of the American Geophysical Union], v. 67, no. 44, p. 1225.

Richmond, G.M., and Fullerton, D.S., 1987, Introduction to Quaternary glaciation in the United States of America: Quaternary Science Reviews, v. 5, p. 3–10.

Savage, J.C., and Hastie, L.M., 1966, Surface deformation associated with dip-slip faulting: Journal of Geophysical Research, v. 71, no. B20, p. 4897–4904.

Schumm, S.A., 1977, The fluvial system: New York, John Wiley, 338 p.

Schwartz, D.P., and Coppersmith, K.J., 1984, Fault behavior and characteristic earthquakes—Examples from the Wasatch and San Andreas fault zones: Journal of Geophysical Research, v. 89, no. B7, p. 5681–5698.

Schwartz, D.P., Hanson, K.L., and Swan, F.H., III, 1983, Paleoseismic investigations along the Wasatch fault zone—An update, *in* Gurgel, K.D., ed., Geologic excursions in neotectonics and engineering geology in Utah, guidebook—Part IV: Utah Geological and Mineral Survey Special Studies 62, p. 45–48.

Schwartz, D.P., Lund, W.R., Mulvey, W.E., and Buddington, K.E., 1988, New paleoseismicity data and implications for space-time clustering of large earthquakes on the Wasatch fault zone, Utah [abs.]: Seismological Research Letters, v. 59, no. 1, p. 15.

Scott, W.E., 1988, G.K. Gilbert's observations of post-Bonneville movement along the Warm Springs fault, Salt Lake County, Utah, *in* Machette, M.N., ed., In the footsteps of G.K. Gilbert—Lake Bonneville and neotectonics of the eastern Basin and Range province (Geological Society of America Guidebook to Field Trip 12): Utah Geological and Mineral Survey Miscellaneous Publication 88–1, p. 44–46.

Scott, W.E., and Shroba, R.R., 1985, Surficial geologic map of an area along the Wasatch fault zone in the Salt Lake Valley, Utah: U.S. Geological Survey Open-File Report 85–448, pamphlet, 2 pls., scale 1:24,000.

Scott, W.E., McCoy, W.D., Shroba, R.R., and Rubin, M., 1983, Reinterpretation of the exposed record of the last two cycles of Lake Bonneville, Western United States: Quaternary Research, v. 20, no. 3, p. 261–285.

Scott, W.E., Pierce, K.L., and Hait, M.H., Jr., 1985, Quaternary tectonic setting of the 1983 Borah Peak earthquake, central Idaho: Bulletin of the Seismological Society of America, v. 75, no. 4, p. 1053–1066.

Shenon, P.J., 1936, The Utah earthquake of March 12, 1934 (extracts from a report), *in* Neumann, F., United States earthquakes, 1934:

Washington, D.C., U.S. Coast and Geodetic Survey Serial 593, p. 43–48. (Reissued in 1968 by National Earthquake Information Center as United States Earthquakes, 1928–1935.)

Simpson, D.W., 1986, Triggered earthquakes: Annual Review of Earth and Planetary Science Letters, v. 14, p. 21–42.

Slemmons, D.B., 1957, Geological effects of the Dixie Valley–Fairview Peak, Nevada, earthquakes of December 16, 1954: Bulletin of the Seismological Society of America, v. 47, p. 353–375.

———1977, Faults and earthquake magnitude, *in* State-of-the-art for assessing earthquake hazards in the United States: U.S. Army Corps of Engineers, Waterways Experiment Station Miscellaneous Paper S–73–1, rept. 6, p. 1–129.

Smith, R.B., 1988, Seismicity and earthquake hazards of the Borah Peak–Hebgen Lake–Yellowstone–Teton region—Implications for earthquakes in extensional and active volcanic regimes: Geological Society of America Abstracts with Programs, v. 20, no. 7, p. A12.

Smith, R.B., and Sbar, M.L., 1974, Contemporary tectonics and seismicity of the western United States with emphasis on the Intermountain Seismic Belt: Geological Society of America Bulletin, v. 85, no. 8, p. 1205–1218.

Smith, R.B., Richins, W.D., and Doser, D.I., 1985, The 1983 Borah Peak, Idaho, earthquake—Regional seismicity, kinematics of faulting, and tectonic mechanism, *in* Stein, R.S., and Bucknam, R.C., eds., Proceedings of Workshop XXVIII on the Borah Peak, Idaho, earthquake: U.S. Geological Survey Open-File Report 85–290, p. 236–263.

Stein, R.S., and Bucknam, R.C., 1985, Basin and Range viewed from Borah Peak: EOS, Transactions of the American Geophysical Union, v. 66, no. 34, p. 603–604.

Stover, C.W., ed., 1987, United States earthquakes, 1983: U.S. Geological Survey Bulletin 1698, 196 p.

Sullivan, J.T., Nelson, A.R., LaForge, R.C., Wood, C.K., and Hansen, R.A., 1988, Central Utah regional seismotectonic study for USBR dams in the Wasatch Mountains: U.S. Bureau of Reclamation Seismotectonic Report 88–5, 338 p.

Swan, F.H., III, Schwartz, D.P., and Cluff, L.S., 1980, Recurrence of moderate to large magnitude earthquakes produced by surface faulting on the Wasatch fault zone, Utah: Bulletin of the Seismological Society of America, v. 70, p. 1431–1462.

Wallace, R.E., 1984a, Faulting related to the 1915 earthquakes in Pleasant Valley, Nevada: U.S. Geological Survey Professional Paper 1274–A, 33 p.

———1984b, Patterns and timing of late Quaternary faulting in the Great Basin province and relation to some regional tectonic features: Journal of Geophysical Research, v. 89, no. B7, p. 5763–5769.

———1987, Variations in slip rates, migration, and grouping of slip events on faults in the Great Basin province: Bulletin of the Seismological Society of America, v. 77, no. 3, p. 868–876.

Wallace, R.E., and Whitney, R.A., 1984, Late Quaternary history of the Stillwater seismic gap, Nevada: Bulletin of the Seismological Society of America, v. 74, no. 1, p. 301–314.

West, M.W., 1989, Neotectonics of Derby Hogsback and Absaroka thrust plates, Uintah County, Wyoming, and Summit County, Utah, with applications to earthquake hazard assessment: Golden, Colorado School of Mines, unpublished Ph.D. thesis, v. 1, 358 p.; v. 2, 142-p. appendix, 17 pls.

Wheeler, R.L., 1987, Boundaries between segments of normal faults—Criteria for recognition and interpretation, *in* Crone, A.J., and Omdahl, E.M., eds., Proceedings of Conference XXXIX—Directions in paleoseismology: U.S. Geological Survey Open-File Report 87–673, p. 385–398.

———1989, Persistent segment boundaries on basin-range normal faults, *in* Schwartz, D.P., and Sibson, R.H., eds., Proceedings of Conference XLV; a workshop on fault segmentation and controls on rupture initiation and termination: U.S. Geological Survey Open-File Report 89–315, p. 432–444.

Wheeler, R.L., and Krystinik, K.B., 1987, Evaluating coinciding anomalies along a fault trace or traverse—Simulations and statistical procedures: U.S. Geological Survey Bulletin 1802, 12 p.

———1988, Segmentation of the Wasatch fault zone, Utah—Summaries, analyses, and interpretations of geological and geophysical data: U.S. Geological Survey Bulletin 1827, 47 p.

Williams, J.S., 1958, Geologic atlas of Utah, Cache County: Utah Geological and Mineral Survey Bulletin 64, 104 p.

Witkind, I.J., 1964, Reactivated faults north of Hebgen Lake, *in* The Hebgen Lake, Montana, earthquake of August 17, 1959: U.S. Geological Survey Professional Paper 435–G, p. G37–G50.

Zoback, M.L., 1983, Structure and Cenozoic tectonism along the Wasatch fault zone, Utah: Geological Society of America Memoir 157, p. 3–27.

APPENDIX

DATING TECHNIQUES AND METHODOLOGY

This appendix contains a discussion of the methods that we used to estimate the timing of depositional or tectonic events from new ^{14}C ages and thermoluminescence (TL) age estimates cited in the main body of this report and listed in table A1. The ^{14}C ages are of two types: (1) conventional gas-proportional and accelerator-mass-spectrometer (AMS) ages on charcoal samples and (2) apparent mean residence time (AMRT) ages (gas-proportional counters) on organic concentrates from the A horizons of soils. Although both types of age are measured in radiocarbon years (^{14}C yr B.P.) and converted to calendric (calendar year) dates, the geologic interpretation of AMRT ages is a complex process, and their associated total errors are larger than the errors on ages from charcoal.

Ages derived from the TL method (Aitken, 1985; Forman and others, 1988, 1989) are based on the property of some minerals to emit light when heated. Although widely used in archeologic investigations, thermoluminescence has been applied only recently to problems in Quaternary geology (Wintle and Huntley, 1982). Exposing mineral grains to sunlight for periods of as little as 8 hours drains their inherited or acquired TL signal; if a mineral has been exposed to sunlight during transport, its TL signal is zeroed. In turn, burial allows acquisition of a new TL signal, which restarts the TL clock. Thermoluminescence directly dates the last exposure of a mineral to sunlight and, as such, reflects the time of its burial by any number of surficial processes—in this case, by colluviation in response to surface faulting. TL ages are reported in years (assumed to be calendar years), and we know of no systematic deviation of reported TL ages from calendric dates (Forman and others, 1988, 1989). However, the methodology of TL analysis is still evolving, and the values of several parameters used in calculating TL ages for most sites are not well known. The relation between ^{14}C age and calendric date, on the other hand, is known to be nonlinear owing to variable rates of ^{14}C production in the upper atmosphere; that is, ^{14}C years do not necessarily correspond with calendar years (Stuiver and Quay, 1979). Extensive studies on tree rings of known ages in Europe and North America show that ^{14}C ages in the 2,000-year age range can be as much as 100 years too young, whereas those in the 4,000- to 5,000-year range may be several hundreds of years too young (Stuiver and Kra, 1986). ^{14}C ages of less than 1,000 years may be either older or younger than the corresponding calendric date.

The ages in this report fall into two categories: numerical ages and calibrated ages as defined by Colman and others (1987). Radiocarbon and TL ages are numerical ages, but estimates of the times of the beginning and end of soil formation for A horizons are, at best, calibrated ages. Note that Colman and others' (1987) use of the term "calibrated" does not refer to the calibration of ^{14}C dates, which is the topic of much of the following discussion. We follow the suggestions of the North American Commission on Stratigraphic Nomenclature (1983) (see also Stuiver and Kra, 1986; Colman and others, 1987) in reserving the noun "date" for ^{14}C ages that can be accurately calibrated to the calendric time scale. Most of our ^{14}C ages from charcoal can be calibrated, and the resulting dates are reported in calendar years (cal yr B.P.). Although we use the ^{14}C calibration procedure to improve the accuracy of our AMRT ages, we do not consider the resulting "corrected ages" to be accurate enough to be termed "dates" (they represent intervals of time, not points in time); thus, we refer to them as calibrated AMRT ages. We choose to highlight the large uncertainties in our estimates of the ages of the beginning and ending times of A horizon formation by calling them "age estimates." This usage helps to distinguish these soil formation ages, which have large uncertainties, from "numerical ages" (^{14}C and TL), which are more precise and accurate. Because estimates of soil formation ages are derived from ^{14}C ages that have been calibrated to the calendric time scale (explained below), the age estimates are measured in years. In this report, we refer to approximate ages, groups of ages, and estimates derived from such ages in terms of thousands of years (ka) (complete listing of ages are reported in table A1). This abbreviation is used only for ages, not for time intervals, which are spelled out (3,000 years) (North American Stratigraphic Code, 1983).

RADIOCARBON CALIBRATION

To directly compare our ^{14}C ages with TL ages, we must convert the ^{14}C ages to the calendric time scale. This calibration procedure allows us to estimate the times of soil formation and fault events and to estimate earthquake recurrence intervals in calendar years rather than in ^{14}C years. The calibration of ^{14}C ages is much simpler and more accurate than it was a few years ago, owing to the development of high-precision calibration curves for the past 9,000 years (Stuiver and Kra, 1986) and the distribution of computer software that performs the calibration calculations (Stuiver and Reimer, 1986).

The calibration procedure requires making several decisions about the analyzed samples: a laboratory error multiplier must be estimated, the type of reference data (decadal or bidecadal) must be selected, and the age span of the carbon in the sample must be estimated. The error reported with ^{14}C ages from most laboratories is based

TABLE A1.—*Data for radiocarbon and thermoluminescence analyses cited in the text*

[Published or unpublished data from other workers not included. —, not applicable]

Trench[1]	Laboratory number (field sample number)[2]	Material sampled (preparation)[3]	Geologic material and map unit (sampling depth, in m)	Age[4]				Remarks
				Radiocarbon age (in ^{14}C yr B.P.) or TL age estimate (in cal yr)	Calibrated charcoal and AMRT ^{14}C ages (range of one-sigma error) [$\bar{x}$ of ages]	MRC and CAS (in yr)[5]	Estimated age of soil horizon contacts[6]	
Brigham City trench 1 (S.F. Personius, September 1986)								
BC–1	PITT–0092 (BC–7).	A horizon (B).	Scarp slope colluvium, unit 1–2A (0.35).	1,260±60 ^{14}C	—	—	—	Minimum time since youngest event.
	USGS–2535 (BC–5).	A horizon (B).	Scarp slope colluvium, unit 3A (1.35).	3,430±70 ^{14}C	3,700 (3,529–3,889)	200 CAS 100 MRCU	3,600 UHC	Maximum time since most recent event.
	USGS–2536 (BC–4).	A horizon (B).	Soil on debris flow, unit 9–2A (2.6).	4,330±70 ^{14}C	4,910 (4,759–5,079)	200 CAS 200 MRCU	4,700 UHC	Maximum time since second event.
	USGS–2604 (BC–8).	A horizon (B).	Scarp slope colluvium, unit 5–1A (2.6).	4,340±100 ^{14}C	4,915 (4,659–5,249)	200 CAS 200 MRCU	4,700 UHC	Maximum time since second event.
Pole Patch trench 1 (S.F. Personius, September 1985)								
PP–1.....	PITT–0093 (SP–85–4–1).	Organic matter (B).	Soil debris in tectonic crack; unit c (0.60).	4,190±125 ^{14}C	4,760 (4,419–5,029)	200 CAS 200 MRCU	4,600 AMRT	Near time of most recent event.
Garner Canyon exposure (A.R. Nelson, July 1985)								
	DIC–3278 (ARN85–04).	A horizon (B).	Scarp slope colluvium, unit 1–1A (0.25).	150±70 ^{14}C	161 (160–350)	200 CAS 200 MRCL	350 LHC	Modern soil on slope.
	DIC–3279 (ARN85–05).	A horizon (B).	Scarp slope colluvium, unit 3–1A (1.20).	1,300±80 ^{14}C	1,234 (1,050–1,370)	200 CAS 100 MRCU 200 MRCL	1,150 UHC 1,450 LHC	Maximum time since most recent event.
	DIC–3237 (ARN85–03).	A horizon (B).	Scarp slope colluvium, unit 5A (1.90).	2,110±100 ^{14}C	2,106 (1,880–2,369)	200 CAS 100 MRCU 200 MRCL	2,000 UHC 2,250 LHC	Maximum time since second event.
East Ogden trenches (A.R. Nelson, September 1986)								
EO–1	PITT–0100 (ARN86–26).	A horizon (B).	Scarp slope colluvium, unit 1–3A (0.15).	285±30 ^{14}C	346 (300–388)	200 CAS 100 MRCL	450 LHC	Modern soil near fault scarp.
	PITT–0098 (ARN86–19)	A horizon (B).	Scarp slope colluvium, unit 3–2A (0.72).	1,365±40 ^{14}C	1,294 (1,214–1,357)	250 CAS 200 MRCU 200 MRCL	1,100 UHC 1,500 LHC	Maximum time since most recent event.
	ITL–113 (EO1TL11).	A horizon (C).	Scarp slope colluvium, unit 1–3A (0.25).	1,200±100 TL	—	—	—	Shows nonuniform sedimentation rate in colluvium.
	ITL–47 (EO1TL10).	A horizon (C).	Distal scarp colluvium, unit 1–5A (0.40).	1,200±20 TL	—	—	—	Probably postdates most recent event.
	ITL–112 (EO1TL9).	A horizon (C).	Distal scarp colluvium, unit 1–5A (0.65).	2,000±200 TL	—	—	—	Shows nonuniform sedimentation rate in colluvium.
	ITL–75 (EO1TL8).	A horizon (C).	Distal scarp colluvium, unit 1–5A (0.84).	2,500±300 TL	—	—	—	Predates(?) most recent event.
	ITL–72 (EO1TL7).	A horizon (C).	Distal scarp colluvium, unit 3–1A (1.28).	3,100±300 TL	—	—	—	Shows nonuniform sedimentation rate in colluvium.
	ITL–24 (EO1TL6).	A horizon (C).	Distal scarp colluvium, unit 3–1A (1.65).	2,700±300 TL	—	—	—	Maximum time since second event.
	ITL–138 (EO1TL3).	A horizon (C).	A horizon sediment, unit 7–1A (1.85).	4,600±400 TL	—	—	—	Maximum time since earliest event.

TABLE A1.—*Data for radiocarbon and thermoluminescence analyses cited in the text*—Continued

Trench[1]	Laboratory number (field sample number)[2]	Material sampled (preparation)[3]	Geologic material and map unit (sampling depth, in m)	Age[4]				Remarks
				Radiocarbon age (in ^{14}C yr B.P.) or TL age estimate (in cal yr)	Calibrated charcoal and AMRT ^{14}C ages (range of one-sigma error) [$\bar{x}$ of ages]	MRC and CAS (in yr)[5]	Estimated age of soil horizon contacts[6]	
East Ogden trenches (A.R. Nelson, September 1986)—Continued								
EO–2	ITL–115 (EO2TL3).	A horizon (C).	Distal scarp colluvium, unit 3–1A (0.75).	1,500±200 TL	—	—	—	Maximum time since most recent event.
	ITL–114 (EO2TL2).	A horizon (C).	Distal scarp colluvium, unit 3–1A (1.05).	1,800±200 TL	—	—	—	Maximum time since most recent event.
	ITL–74 (EO2TL4).	A horizon (C).	Distal scarp colluvium, unit 8–1A (1.35).	3,200±300 TL	—	—	—	Probably minimum time since first (oldest) event.
	ITL–80 (EO2TL5).	A horizon (C).	A horizon sediment, unit 7A (2.35).	4,000±400 TL	—	—	—	Maximum time since first event.
	PITT–0097 (ARN86–14).	A horizon (B).	Scarp slope colluvium, unit 1–3A (0.05).	122 percent modern.	—	—	—	Top of modern soil on scarp; shows extent of burrowing.
	PITT–0106 (ARN86–15).	A horizon (B).	Scarp slope colluvium, unit 1–4A (0.45).	122 percent modern.	—	—	—	Bottom of modern soil on scarp; shows extent of burrowing.
	PITT–0096 (ARN86–13).	A horizon (B).	Scarp slope colluvium, unit 3–1A (1.30).	1,065±30 TL	989 (941–1,032)	200 CAS 100 MRCU 200 MRCL	850 UHC 1,150 LHC	Maximum time since most recent major event.
	PITT–0104 (ARN86–06).	A horizon (B).	Scarp slope colluvium, unit 5–1A (2.65).	3,295±130 ^{14}C	3,518 (3,259–3,859)	100 CAS 50 MRCU 50 MRCL	3,450 UHC 3,550 LHC	Minimum time since first event. Horizon may be eroded. Maximum time since second event.
	USGS–2499 (ARN86–20).	Charcoal (A).	Top of soil on debris flow, unit 7A (2.50).	4,100±180 ^{14}C	4,568, 4,589, 4,606, 4,773, 4,804. (4,240–4,972) [$\bar{x}$=4,668]	—	—	May be close to time of first event.
	PITT–0094 (ARN86–05).	A horizon (B).	Soil on debris flows, unit 7A (2.35).	4,505±65 ^{14}C	5,131 (4,939–5,349)	200 CAS 400 MRCU 200 MRCL	4,750 UHC 5,350 LHC	Maximum AMRT of first event.
	AA–2270 (ARN86–21).	Charcoal (A).	Scarp slope colluvium, unit 5–1A (2.67).	4,780±100 ^{14}C	5,484, 5,521, 5,571 (5,299–5,729) [$\bar{x}$=5,528]	—	—	Collected 20 cm west of PITT–104; charcoal is reworked.
EO–3	PITT–0101 (ARN86–17).	A horizon (B).	Weak soil on debris flow, unit 6–1A (0.60).	290±60 ^{14}C	325 (7–490)	100 CAS 50 MRCU 50 MRCL	250 UHC 350 LHC	Maximum age on one of most recent debris flows across scarp.
	PITT–0095 (ARN86–10).	A horizon (B).	Slopewash, unit 9–2A (1.00).	1,340±95 ^{14}C	1,274 (1,060–1,420)	200 CAS 200 MRCU	1,050 UHC	Maximum time since most recent event. Thick soil on slopewash above scarp.
	PITT–0107 (ARN86–18).	A horizon (B).	Base of soil on debris flow, unit 10–1A (1.80).	2,820±65 ^{14}C	2,933 (2,819–3,119)	200 CAS 300 MRCU 100 MRCL	2,650 UHC 3,050 LHC	Minimum age for extensive upper Holocene debris flow not found in EO–1 and EO–2.
	PITT–0105 (ARN86–08).	A horizon (B).	Soil on alluvium, unit 5–1A (0.80).	112 percent modern ^{14}C	—	—	—	Shows extent of animal burrowing. Youngest alluvium at site.
	AA–2269 (ARN86–43).	Charcoal (A).	Sandy alluvium, unit 9–1 (0.80).	580±70 ^{14}C	555, 617, 622 (510–680) [$\bar{x}$=598]	—	—	Within tectonically(?) deformed unit. Maximum time since possible small, most recent event.

TABLE A1.—*Data for radiocarbon and thermoluminescence analyses cited in the text*—Continued

Trench[1]	Laboratory number (field sample number)[2]	Material sampled (preparation)[3]	Geologic material and map unit (sampling depth, in m)	Age[4]: Radiocarbon age (in ^{14}C yr B.P.) or TL age estimate (in cal yr)	Age[4]: Calibrated charcoal and AMRT ^{14}C ages (range of one-sigma error) [$\bar{x}$ of ages]	Age[4]: MRC and CAS (in yr)[5]	Age[4]: Estimated age of soil horizon contacts[6]	Remarks
East Ogden trenches (A.R. Nelson, September 1986)—Continued								
EO–4	PITT–0103 (ARN86–04).	A horizon (B).	Scarp colluvium, unit 2–1A (0.35).	460±65 ^{14}C	514 (357–570)	100 CAS 50 MRCU 50 MRCL	450 UCH 550 LHC	Minimum time since possible small, most recent event. Proximal colluvium.
	PITT–0102 (ARN86–03).	A horizon (B).	Crotovinas in scarp colluvium, unit 4–1A (0.60).	105±55 ^{14}C	—	—	—	Shows extent of animal burrowing in coarse-grained alluvium.
EO–5	PITT–0108 (ARN86–24).	A horizon (B).	Scarp slope colluvium, unit 1–1A (0.05).	815±45 ^{14}C	—	—	—	Modern A horizon; must include older reworked A horizon sediment.
	PITT–0099 (ARN86–23).	A horizon (B).	Organic-rich distal colluvium, unit 1–2A (0.30).	390±25 ^{14}C	481 (439–506)	50 CAS 400 MRCL	800 LHC	Organic-rich lens near base of modern A horizon adjacent to fault.
	PITT–0109 (ARN86–25).	A horizon (B).	Scarp slope colluvium, unit 3–1A (1.20).	1,040±75 ^{14}C	971 (800–1,110)	250 CAS 200 MRCU 200 MRCL	750 UHC 1,150 LHC	Maximum time since most recent major event.
American Fork Canyon trenches (M.N. Machette, September 1986)								
AF–1	AA–2267 (AF–1A).	Charcoal (A).	Fault-scarp colluvium, unit 1 (0.55).	140±120 ^{14}C	142, 214, 264 (post-1950 to 480) [$\bar{x}$=207]	25 CAS	—	Minimum time since most recent event. Excludes calendric dates of less than 0 and 20 yr B.P.
	ITL–23 (F86–U8).	A horizon (C).	Fault scarp colluvium, unit 2 (0.55).	400±100 TL	—	—	—	Near time of most recent event.
	USGS–2532 (AF–1C).	A horizon (B).	Fault-scarp colluvium, unit 2 (0.80).	980±70 ^{14}C	713 (620–830)	300 CAS 200 MRCU	500 UHC	Near time of most recent event.
	USGS–2531 (AF–1B).	A horizon (B).	Fault-scarp colluvium, unit 3 (0.75).	2,620±70 ^{14}C	2,777 (2,549–2,879)	300 CAS 200 MRCU	2,650 UHC	Near time of second event.
	ITL–16 (F86–U7).	A horizon (C).	Fault-scarp colluvium, unit 3 (0.75).	2,700±200 TL	—	—	—	Near time of second event.
	AA–2266 (AF–1D).	Charcoal (A).	Burn layer in debris flow, unit 4 (1.50).	4,740±90 ^{14}C	5,467, 5,534, 5,553 (5,289–5,721) [$\bar{x}$=5,518]	25 CAS 200 MRCU	5,300 UHC	Near time of first event. MRCU includes 100 years for deposition and 100 years to form weak soil.
	ITL–2 (F86–U4)	Silt (C)	Loess below debris flow, unit 9 (1.62).	6,600±700 TL	—	—	—	Time near end of loess deposition; predates debris flow (unit 4).
AF–2	ITL–18 (F86–U14).	Silt (C)	Modern sag-pond deposit, unit 1 (0.50).	250±100 TL	—	—	—	Minimum time since most recent event.
	ITL–3 (F86–U9).	Silt (C)	Sag-pond deposit under colluvium, unit 3 (1.00).	500±200 TL	—	—	—	Near time of most recent event.
	USGS–2533 (AF–2A).	A horizon (B).	Fault-scarp colluvium, unit 2 (1.00–1.05).	620±150 ^{14}C	612 (360–830)	150 CAS 100 MRCU	500 UHC	Maximum time since most recent event.
AF–3	ITL–46 (F86–U11).	Silt (C)	Loess under debris flow, unit 6 (2.25).	7,700±300 TL	—	—	—	Time near end of loess deposition; predates debris-flow sequence.
	AA–2268 (AF–3A).	Charcoal (A).	Loess under debris flow, unit 6 (2.80).	7,290±100 ^{14}C	8,061 (7,919–8,336)	25 CAS	—	Time near end of loess deposition; predates debris-flow sequence.

TABLE A1.—*Data for radiocarbon and thermoluminescence analyses cited in the text*—Continued

Trench[1]	Laboratory number (field sample number)[2]	Material sampled (preparation)[3]	Geologic material and map unit (sampling depth, in m)	Age[4]: Radiocarbon age (in ^{14}C yr B.P.) or TL age estimate (in cal yr)	Age[4]: Calibrated charcoal and AMRT ^{14}C ages (range of one-sigma error) [$\bar{x}$ of ages]	Age[4]: MRC and CAS (in yr)[5]	Age[4]: Estimated age of soil horizon contacts[6]	Remarks
Rock Canyon natural exposure (M.N. Machette, October 1986)								
RC	DIC–3236 (RC–1)	Organic matter (B).	Fault-scarp colluvium, unit 3 (1.20).	1,110±50 ^{14}C	1,005 (950–1,150)	200 CAS	—	Approximate time of most recent event.
	PITT–0091 (RC–2).	A horizon (B).	Postfault debris flow, unit 5A (1.50).	455±35 ^{14}C	512 (457–552)	150 CAS 100 MRCU	400 UHC	Minimum time since burial of fault scarp.
Woodland Hills trench 2 (M.N. Machette, November 1986)								
WH–2.....	USGS–2500 (WH–2–1).	A horizon (B).	Block in scarp-slope colluvium, unit 8A (90–160).	1,190±50 ^{14}C	1,102 (1,020–1,220)	300 CAS 200 MRCU	900 UHC	Near time of most recent event; same sample as BETA–19594.
	BETA–19594 (WH–2–1).	A horizon (B).	Block in scarp-slope colluvium, unit 8A (90–160).	1,380±60 ^{14}C	1,306 (1,180–1,400)	300 CAS 200 MRCU	1,100 UHC	Near time of most recent event; same sample as USGS–2500.

[1]Sites are listed from north to south by trench number and then by increasing age (stratigraphic depth).

[2]AA, University of Arizona-National Science Foundation Accelerator Facility for Radioisotope Analysis (TAMS method); BETA, Beta Analytic, Inc.; DIC, Dicarb Radioisotope Company; PITT, University of Pittsburgh Applied Research Center Radiocarbon Laboratory; USGS, U.S. Geological Survey Radiocarbon Laboratory, Menlo Park, Calif.; ITL, thermoluminescence analyses by S.L. Forman, Institute for Arctic and Alpine Research, University of Colorado.

[3]A, root hairs removed; B, root hairs removed, HCl and NaOH extracted, and organics concentrated by sedimentation or centrifugation; C, sample is sieved and split, and calcium and organic matter are removed in darkness.

[4]yr B.P., years before present (1950); ^{14}C, radiocarbon; TL, thermoluminescence; AMRT, apparent mean residence time (age) of carbon in sample. Error limits for ^{14}C are one-sigma standard deviation, but we use an error multiplier of twice the reported laboratory error for calibration; error limits for TL are means ($\bar{x}$) of errors (one-sigma standard deviation from each measurement).

[5]MRC, estimated mean residence correction to AMRT age for estimates on upper (U) and lower (L) soil contacts (estimated AMRT age of sample before burial); CAS, estimated span for age of carbon in sample at time of burial.

[6]UHC, upper horizon contact; LHC, lower horizon contact; AMRT, apparent mean residence time (age) of sample.

only on counting statistics of the sample and reference standards. To estimate the true laboratory error in an age, the reported one standard deviation should be multiplied by an error multiplier for samples of a particular type analyzed by a particular laboratory (International Study Group, 1982; Long, 1990). Because we have no error multipliers for the laboratories that dated our samples, we use an error multiplier of 2 for all of our samples (see Scott and others, 1983; Stuiver and Pearson, 1986). The long estimated age spans and large errors for most of our ages indicate that the bidecadal (20-year interval) data set is the appropriate one for our samples (see Stuiver and Reimer, 1986).

The calibration program treats ages derived from samples containing carbon in plants that grew over short spans of time (less than 30 years) differently than it does samples containing carbon that accumulated over longer intervals (Stuiver and Reimer, 1986). We suspect that our charcoal samples from the Wasatch Front are mostly burned sagebrush or other shrubs that grew in less than 30 years. For these samples, the calibration program uses the curve based on tree-ring data grouped into 20-year intervals. Because the detailed curve has many small fluctuations, a ^{14}C age and the two-sigma error limits about the age (one-sigma error times error multiplier of 2) will usually intersect the calibration curve in several places, yielding several possible calendric dates (or calendric ages for our calibrated AMRT ages) (Stuiver and Pearson, 1986). We can rarely determine which of these calibrated dates represents the true age of the sample, so we report each date and the total one-sigma error limits of the calibration procedure (that is, the error limits in table A1 cover the range from the minimum one-sigma limit on the youngest calibration date to the maximum one-sigma limit on the oldest date). For samples that are judged to contain carbon that spans more than 30 years, the calibration program calculates a moving average of the calibration curve based on the estimated age span of the sample (to the nearest 20 years). Most of our AMRT samples contain soil organic carbon that accumulated over a span of more than 100 years. When we use the moving-average procedure of the program to calibrate our AMRT ages, many of the fluctuations in the calibration curve are smoothed out or eliminated. This smoothing of the curve can result in the AMRT age's intersecting the curve at only one point; it gives a single calendric age (calibrated AMRT age) and a modest error for each AMRT age. Thus, even though the AMRT ages are much more difficult to interpret than the charcoal ages (discussed below), the calibration procedure yields calibrated AMRT ages that can appear more precise than the charcoal ages; however, the following discussion will show that they are not.

APPARENT MEAN RESIDENCE ^{14}C AGES OF SOILS

The concept of an AMRT age of a soil is the most effective and widely used way to interpret the laboratory-reported ^{14}C age of organic matter in soil horizons (Scharpenseel and Schiffmann, 1977). However widely used, the interpretation of AMRT ages is complicated by a number of factors (Matthews, 1980). The gradual accumulation of the many components of organic matter in the upper (A) horizon of a soil profile, the removal of less resistant components of organic matter through decay and oxidation in the horizon, the penetration and decay of all ages of plant roots into the horizon, the mixing of organics within the horizon by animals, both small (for example, insects and worms) and large (rodents), and the continual translocation of insoluble as well as soluble organic compounds from higher to lower parts of the horizon result in a diverse mixture of carbon of different ages throughout the horizon.

Organic matter is a combination of humus (or humic substances) and other organic components (such as protein, carbohydrates, and amino acids), each of which responds differently upon burial. Generally, humic substances will resist decay and oxidation and are relatively inert with respect to biologic and chemical attack, whereas other organic substances decay quickly (some in a matter of years or decades). Hence, humic acids are often selected for dating the oldest carbon in a soil sample. These processes of carbon accumulation and decay, transport, and removal are highly dependent on the topographic setting of the soil (slope, aspect, and drainage), the type and rate of biologic activity in the soil, the inorganic sedimentation rate, the type of vegetation (for example, grassland versus forest), and climate (Martel and Paul, 1974; Scharpenseel and Schiffmann, 1977).

An AMRT age is calculated from the total ^{14}C activity measured on all the carbon-containing components in a pretreated soil sample. The age distribution of carbon in the sample is a function of the turnover rate of carbon in the soil (O'Brien, 1984). Thus, for example, even the upper few centimeters of modern A horizons could yield an AMRT age of a few tens to a few hundreds of years, depending on the importance of the factors listed above. An AMRT age from the upper part of an A horizon is usually younger than the mean age of carbon in a soil because A horizons contain much more young carbon (such as the other organics discussed above) than old carbon (Geyh and others, 1971). For old, deeply buried A horizons, the alternate can be true—younger, less resistant organic components may be destroyed, and the more resistant, older (humic) organic components may remain. Thus, depending on the organic constituents, the time and depth of burial, and the sample's position in a soil, an

AMRT age could theoretically be as old as the time of soil inception to as young as the time of burial.

To interpret and calibrate AMRT ages, we need to estimate the total amount of time represented by the ages of the carbon-containing compounds in the soil sample. We term this time parameter the carbon age span (CAS) of a soil sample. The CAS is very dependent on but quite different from the length of time that it took for the organic matter in an A horizon sample to accumulate because of the carbon-cycling processes mentioned above. Two samples from A horizons might have similar AMRT ages but very different CAS values, depending, for example, on their position on a slope (Martel and Paul, 1974). CAS is used in the calibration program as an estimate of the age span of the carbon in our samples. These estimates are based on the general form of AMRT age versus depth relations reported by others (see Matthews, 1980; Brown, 1986), thickness of the sampling interval, organic content of the sample, rate of organic matter turnover (bioturbation and organic cycling), slope position, sample thickness, vegetation, and, more importantly, our interpretation of AMRT ages on a small number of A horizon samples from sites in central Utah (discussed below).

A further problem in interpreting AMRT ages is that the procedures for treatment of samples before ^{14}C analysis are not standardized. The many different procedures used to isolate different components of soil organic matter yield different AMRT ages, depending on the objectives of each study (for example, see Stuckenrath and others, 1979; Goh and Molloy, 1978; Matthews, 1980). No single procedure is recognized as optimal, but consistent pretreatment of all samples is mandatory for meaningful interpretation of AMRT ages. We followed many previous studies in using physical methods to isolate the fine organic fraction (less than 125 μ) of the A horizon (Scharpenseel and others, 1968; Kihl, 1975) and then asked the dating laboratories to centrifuge this fraction during HCl and NaOH treatments to recover as much of the finest organic fraction as possible before analysis. Thus, although our soil concentrates were analyzed by three different laboratories (USGS, Dicarb, and University of Pittsburgh), pretreatment procedures were the same for all samples; thus, all AMRT ages should be as comparable as possible, although we cannot fully evaluate differences in each ^{14}C laboratory's analytical procedures (for example, Scott and others, 1990).

In contrast, procedures for the pretreatment of charcoal samples are standardized, and ages for samples analyzed by different laboratories can be compared directly (Stenhouse and Baxter, 1983). Major uncertainties involved in interpreting charcoal ages are (1) the length of time between the formation of the charcoal and its deposition (including possible reworking), (2) the relation of the charcoal to the stratigraphic unit in which it is found (for example, a burned root or filled animal burrow), and (3) contamination by rootlets.

Because the interpretation of AMRT ages is so complex and total errors of ages are large, some authors argue that the basic procedure for calibrating AMRT ages is questionable. For example, as Geyh and others (1971) pointed out, the proportions of carbon of different ages in a typical horizon sample vary greatly, so most of the carbon often dates from the younger portion of the CAS. The dominance of younger carbon in the sample and the exponential decay rate of ^{14}C cause the relations between AMRT ages and CAS values from the upper and lower parts of a soil horizon to vary significantly with the mean calendric age of the soil. We agree that AMRT ages cannot be calibrated with the same accuracy as dates from charcoal. However, there are systematic and geologically important deviations between the ^{14}C time scale and the calendric time scale, particularly for samples less than 1,000 years old. Including averaged estimates of this deviation (through use of the smoothed curve) in our age corrections improves the accuracy of our estimates of the timing of faulting events.

DATING THE FORMATION OF AN A HORIZON

A major limitation of AMRT ages is that they are composite ages (combined activity of all ^{14}C in the sample); for this reason, most AMRT ages cannot accurately date geologic events represented by depositional units above and below the sampled horizons. The time of the beginning of soil formation on a particular deposit can rarely be dated with AMRT methods (Geyh and others, 1971). Similarly, an AMRT age on the upper 1 cm of an organic-rich buried A horizon still provides only a maximum limit on the time of the soil's burial (Matthews, 1980).

Despite these problems, we need to estimate as accurately as possible the times of faulting events at our trench sites. In pursuit of this goal, we use calibrated AMRT ages (and other parameters used to estimate CAS values) to derive age estimates for the upper horizon contact (UHC) and sometimes for the lower horizon contact (LHC) of selected A horizons. The estimated CAS for each sample and AMRT ages on modern A horizons from these and similar sites help us estimate how divergent the sample's calibrated AMRT age is from the time of deposition of the unit on which the A horizon is developed and from the date of burial of the A horizon.

We probably could have improved the accuracy of our UHC and LHC age estimates though an extensive program of ^{14}C analysis of various organic fractions in the samples of surface and buried soils that we submitted

for ARMT dating (for example, Matthews, 1980). However, time and budget constraints prevented this type of approach in a project of such broad scope. Although the analysis of many more samples of modern A horizons at different depths might have improved our age estimates, our results from the East Ogden trench site highlight a major problem in measuring AMRT ages on modern soils. Some AMRT ages from East Ogden (from depths of as much as 60 cm) have greater ^{14}C activity than modern samples (that is, they date in the future). Such ages indicate that burrowing has introduced significant amounts of carbon produced during thermonuclear explosions (bomb carbon) into the lower parts of some of the more permeable, sand-rich A horizons. It is difficult to estimate how much of the carbon in the modern A horizons on these fault scarps is bomb carbon, which horizons have been burrowed and which have not, and whether reworked organic sediment from older A horizons farther up the scarp has been incorporated into modern horizons. For these reasons, even a very extensive program of ^{14}C dating of modern A horizons might not significantly improve our estimates of the AMRT age of modern A horizons from sites such as East Ogden.

Our AMRT data on modern A horizons are limited to a small number of samples from middle to lower slope positions on fault scarps at trench sites along the Wasatch fault zone. These data suggest that samples from the upper 3 to 20 cm of a typical modern 10- to 40-cm-thick A horizon would yield AMRT ages of about 100 to 400 years if no bomb carbon were present. Bomb carbon has clearly influenced some near-surface samples, but AMRT ages from upper and lower parts of thick A horizons buried by the last major faulting event at the East Ogden site also differ by about 50 to 300 years. The ages from these buried horizons have not been influenced by bomb carbon (because they are deeply buried and are prehistoric), and they therefore suggest that our estimates of the AMRT in modern horizons are reasonable. For the thicker horizons, there must be some age-depth effect (see for example, Matthews, 1980), but we have too few samples to determine the influence of this effect. A horizons developed under scrub oak forests probably give younger AMRT ages than horizons developed at sagebrush or grassland sites, because organic material is generated and accumulates much faster at wooded sites. AMRT ages of as much as 1.5 to 2.7 ka have been obtained from a drier, higher altitude grassland site, which has a low rate of organic productivity, 50 km to the east of the Wasatch fault zone (Nelson and Van Arsdale, 1986). Samples from distal-slope positions on scarps probably give younger ages than those from midslope positions from the same depth because organic-rich sediment (for example, accretionary A horizons) accumulates fastest near the base of a slope. A horizons on steep scarps appear to yield younger ages than those on gentle scarps. Thus, because a scarp broken by repeated Holocene displacements becomes higher and steeper with each succeeding event, an A horizon buried during the first fault event at a site would generally yield an older AMRT age immediately after burial (MRC, mean residence correction) than would a comparably developed A horizon on the steepened scarp formed after the second or third fault event.

We use the above generalizations, estimated values for CAS, the sample parameters used to estimate the CAS, and modern AMRT ages of 100, 150, 200, or 300 years to estimate UHC and, in some cases, LHC ages from the calibrated AMRT ages. UHC age estimates are calculated by considering horizon and sample thicknesses and then subtracting an appropriate MRC (based on modern AMRT value) from the calibrated AMRT age. Modern AMRT values were generally added to calibrated AMRT ages where minimum estimates of LHC age were needed. We deal with the problems inherent in determining UHC and LHC age estimates from such a limited database by assigning large errors to our age estimates. The myriad uncertainties in interpreting AMRT ages and the even larger errors introduced by estimating UHC and LHC ages suggest errors on the final age estimates of from ±200 to ±400 years. Regardless of the one-sigma error ranges listed in table A1 for AMRT and calibrated AMRT ages and the UHC and LHC age estimates, this magnitude of total error should be assumed for all horizon contact age estimates. For these reasons, we also round all calibrated soil ages to the nearest 50 years and report them in units of thousands of years (ka). The errors in ^{14}C ages introduced by isotopic fractionation of ^{14}C in terrestrial organic matter are small (probably less than 50 years) relative to these total errors. Therefore, we did not attempt to correct our ages for isotopic fractionation.

The following example will illustrate our method of deriving an upper horizon contact (UHC) age estimate from a laboratory-reported AMRT age of 2,000±100 ^{14}C yr B.P. of the upper 10 cm of a tectonically buried A horizon that is 35 cm thick. For this example, we estimate that the carbon in the sampled part of the A horizon had a 300-year age span (CAS) and a MRC of 200 years (AMRT at the time of burial). In addition, we apply a multiplier of 2 to the reported laboratory error. The resulting calibrated AMRT age is 1,963 cal yr B.P. (the one-sigma error limits are +236 and −237 years). From this date, we subtract the MRC of 200 years to obtain an age estimate of 1,763 cal yr B.P. for the UHC (buried surface of the A horizon). After rounding the estimate to the nearest 50 years, we estimate that this A horizon was buried by fault-scarp colluvium about 1.75±0.2 ka. As can be seen from this example, the reported AMRT age

of 2,000 yr B.P. is almost 250 years (12 percent) greater than the estimated time of faulting.

REFERENCES CITED

Aitken, M.J., 1985, Thermoluminescence dating: New York, Academic Press, 291 p.

Brown, R.H., 1986, ^{14}C depth profiles as indicators of trends in climate and $^{14}C/^{12}C$ ratio: Radiocarbon, v. 28, no. 2A, p. 350–357.

Colman, S.M., Pierce, K.L., and Birkeland, P.W., 1987, Suggested terminology for Quaternary dating methods: Quaternary Research, v. 28, p. 314–319.

Forman, S.L., Jackson, M.E., McCalpin, J., and Maat, P., 1988, The potential of using thermoluminescence to date buried soils developed on colluvial and fluvial sediments from Utah and Colorado, U.S.A.—Preliminary results: Quaternary Science Reviews, v. 7, no. 3/4, p. 287–294.

Forman, S.L., Machette, M.N., Jackson, M.E., and Maat, P., 1989, An evaluation of thermoluminescence dating of paleoearthquakes on the American Fork segment, Wasatch fault zone, Utah: Journal of Geophysical Research, v. 94, no. B2, p. 1622–1630.

Geyh, M.A., Benzler, J.-H., and Roeschmann, G., 1971, Problems of dating Pleistocene and Holocene soils by radiometric methods, *in* Yaalon, D.H., ed., Paleopedology—Origin, nature and dating of paleosols: Jerusalem, International Society of Soil Science, Israel University Press, p. 63–75.

Goh, K.M., and Molloy, B.P.J., 1978, Radiocarbon dating of paleosols using soil organic matter components: Journal of Soil Science, v. 29, p. 567–573.

International Study Group, 1982, An inter-laboratory comparison of radiocarbon measurements in tree rings: Nature, v. 298, p. 619–623.

Kihl, R., 1975, Physical preparation of organic matter samples for ^{14}C dating (app.), *in* Andrews, J.T., Radiocabon date list II from Cumberland Peninsula, Baffin Island, N.W.T., Canada: Arctic and Alpine Research, v. 7, p. 90–91.

Long, A., 1990, A quality assurance protocol for radiocarbon dating laboratories: Radiocarbon, v. 32, p. 393–397.

Martel, Y.A., and Paul, E.A., 1974, The use of radiocarbon dating of organic matter in the study of soil genesis: Soil Science Society of America Proceedings, v. 38, p. 501–506.

Matthews, J.A., 1980, Some problems and implication of ^{14}C dates from a podzol buried beneath an end moraine at Haugabreen, southern Norway: Geografiska Annaler, v. 62A, p. 185–208.

Nelson, A.R., and Van Arsdale, R.B., 1986, Recurrent Late Quaternary movement on the Strawberry normal fault, Basin and Range—Colorado Plateau transition zone, Utah: Neotectonics, v. 1, p. 7–37.

North American Commission on Stratigraphic Nomenclature, 1983, North American stratigraphic code: Bulletin of the American Association of Petroleum Geologists, v. 67, p. 841–875.

O'Brien, B.J., 1984, Soil organic carbon fluxes and turnover rates estimated from radiocarbon enrichments: Soil Biology and Biochemistry, v. 16, p. 115–116.

Scharpenseel, H.W., and Schiffmann, H., 1977, Radiocarbon dating of soils—A review: Zeitschrift fur Pflanzenernahrung Dungung und Bodenkunde, v. 140, p. 159–174.

Scharpenseel, H.W., Pietig, F., and Tamers, M.A., 1968, Bonn radiocarbon measurements 1: Radiocarbon, v. 10, p. 8–28.

Scott, E.M., Baxter, M.S., and Aitchison, T.C., 1983, ^{14}C dating reproducibility—Evidence from a combined experimental and statistical programme, *in* Mook, W.G., and Waterbolk, H.T., eds., Proceedings of the First International Symposium, ^{14}C and Archaeology: PACT Journal of the European Study Group on Physical, Chemical and Mathematical Techniques Applied to Archaeology, v. 8, p. 133–146.

Scott, E.M., Aitchison, T.C., Harkness, D.D., Cook, G.T., and Baxter, M.S., 1990, An overview of all three stages of the International Radiocarbon Intercomparison: Radiocarbon, v. 32, p. 309–320.

Stenhouse, M.J., and Baxter, M.S., 1983, ^{14}C dating reproducibility—Evidence from routine dating of archaeological samples, *in* Mook, W.G., and Waterbolk, H.T., eds., Proceedings of the First International Symposium, ^{14}C and Archaeology: PACT Journal of the European Study Group on Physical, Chemical and Mathematical Techniques Applied to Archaeology, v. 8, p. 147–166.

Stuckenrath, R., Miller, G.H., and Andrews, J.T., 1979, Problems of radiocarbon dating Holocene organic-bearing sediments, Cumberland Peninsula, Baffin Island, N.W.T., Canada: Arctic and Alpine Research, v. 11, p. 109–120.

Stuiver, M., and Kra, R., eds., 1986, Calibration issue—Proceedings of the 12th International Radiocarbon Conference, Trondheim, Norway, 1985: Radiocarbon, v. 28, 225 p.

Stuiver, M., and Pearson, G.W., 1986, High-precision calibration of the radiocarbon time scale, AD 1950–500 BC: Radiocarbon, v. 28, p. 805–838.

Stuiver, M., and Quay, P.D., 1979, Changes in atmospheric carbon-14 attributed to a variable sun: Science, v. 207, p. 11–19.

Stuiver, M., and Reimer, P.J., 1986, A computer program for radiocarbon age calibration (ver. 2.0): Radiocarbon, v. 28, no. 2B, p. 1022–1030 (Rev 2.0).

Wintle, A.G., and Huntley, D.J., 1982, Thermoluminescence dating of sediments: Quaternary Science Reviews, v. 1, p. 31–53.

Persistent and Nonpersistent Segmentation of the Wasatch Fault Zone, Utah: Statistical Analysis for Evaluation of Seismic Hazard

By RUSSELL L. WHEELER *and* KATHERINE B. KRYSTINIK

ASSESSMENT OF REGIONAL EARTHQUAKE HAZARDS AND RISK ALONG THE WASATCH FRONT, UTAH

U.S. GEOLOGICAL SURVEY PROFESSIONAL PAPER 1500–B

Confirmation that the Wasatch fault zone is segmented into lengths that tend to rupture independently and implications for hazard evaluation in the population centers of Utah and in other normal fault zones

CONTENTS

	Page
Abstract	B1
Introduction	1
Segmentation	1
Purpose	2
Acknowledgments	4
Methods	4
Anomalies	4
Data	4
Causes of Coincident Anomalies	7
Geologic Causes of Anomalies other than Segmentation	7
Simulation and Statistical Procedures	8
Locational Uncertainties of Anomaly Edges	9
Descriptive Results	10
Observed Pattern of Anomalies	10
Anomalous Sections of the Fault Zone	10
Associated Data Types	10
Diagnostic and Characteristic Data Types	13
Summary of Descriptive Results	13
Results from Simulation and Statistical Testing	15
One-Dimensional Comparisons of Observed and Simulated Patterns	15
Results from Simulation and Statistical Testing—Continued	
Three-Dimensional Comparisons of Observed and Simulated Patterns	B16
Quantitative Comparisons of Observed and Simulated Patterns	16
Interpreting a Single Anomalous Part of the Fault Zone	20
Discussion	22
Segmented Ruptures	22
Persistent and Nonpersistent Segment Boundaries	24
Bedrock Ridges	25
Applications to Large Historical Earthquakes	31
Borah Peak, Idaho—October 28, 1983	31
Hebgen Lake, Montana—August 17, 1959	33
Rainbow Mountain, Nevada—July 6 and August 24, 1954	35
Fairview Peak-Dixie Valley, Nevada—December 16, 1954	35
Pleasant Valley, Nevada—October 2, 1915	39
Summary	42
Conclusions	43
References Cited	43

ILLUSTRATIONS

		Page
FIGURE 1.	Index map of the Wasatch fault zone in northern central Utah and selected towns and cities along the Wasatch Front	B3
2.	Graph showing observed distribution of anomalies along the Wasatch fault zone	6
3, 4.	Diagrams showing:	
3.	Three-dimensional geometry of comparison of the observed anomaly pattern to simulated patterns	9
4.	Axes of figure 3, showing a serial section	9
5.	Graphs showing observed anomaly pattern of figure 2 redrawn to give minimum and maximum widths allowed for each anomaly by locational uncertainties of its edges	11
6.	Histograms of anomaly widths	12
7.	Graphs showing pairs and m-tuplets of coincident anomalies in the observed anomaly pattern along the Wasatch fault zone	14
8.	Diagram representing coincidings between anomalies at km 130 of the Wasatch fault zone	15
9.	Histograms of values of the Jaccard coefficient J for the 15 possible pairs of 6 data types	17
10.	Graphs showing the constancy and fidelity of the six data types in the four anomalous parts of the Wasatch fault zone	18
11.	Histograms comparing numbers of m-tuplets in observed and simulated patterns	19
12.	Diagrams comparing numbers of m-tuplets in observed and simulated patterns	22
13.	Graphs showing summaries of serial sections	26
14–20.	Maps showing:	
14.	Four sets of segment boundaries for the Wasatch fault zone	28
15.	Segment boundary at the Traverse Mountains salient	29
16.	Fault network in a hypothetical nonconservative barrier on a normal fault	30

Page

17. October 28, 1983, Borah Peak, Idaho, earthquake B32
18. August 17, 1959, Hebgen Lake, Mont., earthquake 34
19. July–December 1954, Rainbow Mountain, Fairview Peak, and Dixie Valley, Nev., earthquakes 36
20. October 2, 1915, Pleasant Valley, Nev., earthquake 40

TABLES

Page

TABLE 1. Locations of transverse anomalies B5
2. Coincidings of anomalies 16
3. Constancy and fidelity for anomalous and nonanomalous parts of the Wasatch fault zone 18
4. Total counts of m-tuplets produced by all simulations together 24

ASSESSMENT OF REGIONAL EARTHQUAKE HAZARDS
AND RISK ALONG THE WASATCH FRONT, UTAH

PERSISTENT AND NONPERSISTENT SEGMENTATION OF THE WASATCH FAULT ZONE, UTAH: STATISTICAL ANALYSIS FOR EVALUATION OF SEISMIC HAZARD

By RUSSELL L. WHEELER and KATHERINE B. KRYSTINIK

ABSTRACT

The Wasatch fault zone of central Utah might be divided into segments that tend to rupture independently of one another. If so, ruptures of sufficiently large earthquakes would tend to start and stop at segment boundaries and would tend not to cross boundaries. The validity of the segmentation hypothesis will affect how seismic hazard is estimated for the Wasatch Front urban corridor, the severity of the estimated hazard, and the degree to which the estimated hazard is concentrated in the State's population centers along the central part of the Wasatch fault zone.

To test the segmentation hypothesis, we examined Bouguer gravity data, earthquake epicenters, fault zone geometry, and aeromagnetic, topographic, and structural data along the fault zone. In each of the six data types, we sought the kinds of anomalies (characteristic expressions) that a long-lasting segment boundary should produce. Anomalies in fault zone geometry are large footwall salients, at which the eastern (upthrown) wall of the north-striking normal fault zone projects westward into the hanging wall and the fault trace bows westward around the projections. Of 26 anomalies in the 6 data types, 4 are salients—from north to south, the Pleasant View, Salt Lake, Traverse Mountains, and Payson salients. Salients appear to be the most fundamental anomalies. Seventeen of the other 22 anomalies coincide with the salients; at each salient, anomalies in three to five other data types coincide; no other anomalies coincide elsewhere. Geologic processes other than segmentation might have produced any of the anomalies, but only segmentation or chance could produce such coincidings of anomalies in a way that is consistent with the geologic evolution of central Utah. By using simulation experiments and statistical tests of the results of those simulations, we show that the observed degree of anomaly coinciding should not be attributed to chance.

Formation of the salients occupied much or all of the history of the Wasatch fault zone. Fault scarps of late Pleistocene and Holocene age tend to end or change age at the salients, an indication that scarps also are segmented there. We conclude that the Wasatch fault zone has been persistently segmented at the four salients throughout much or all of its 10-m.y. history and will likely continue to be segmented there through at least the next several millenia, which is the time span of interest for hazard evaluation.

From mapping of late Quaternary deposits along the fault zone, other workers detected these four persistent segment boundaries, plus five other boundaries that are little expressed or poorly expressed in our six data types. The five others might be nonpersistent boundaries, alternating between active states, in which they control several successive ruptures, and inactive states, in which they do not. Although recently active, such boundaries might change state and so are less likely to affect the next few large ruptures than the persistent boundaries are. For the estimation of seismic hazard, it is fortunate that most of the segment boundaries in the populous central part of the Wasatch fault zone are persistent, so that their past behavior is a reasonable guide to their expected future behavior.

From our consideration of the persistent boundaries, we conclude that others should exist on other normal fault zones where exposed or shallowly buried transverse bedrock ridges, some having salients, indicate accumulated slip deficits and where two or more individual large historical or prehistoric rupture zones have started or stopped. Testing this model against five historical earthquake sequences in and near the Basin and Range province indicates the existence of two persistent boundaries on the Lost River fault zone of Idaho (which broke in 1983), one persistent boundary between the Dixie Valley and Fairview faults of Nevada (December 1954), and one persistent boundary and one nonpersistent boundary in the Pleasant View rupture zone of Nevada (1915). The northern end of the Dixie Valley fault is not a segment boundary, persistent or otherwise. Both ends of the Rainbow Mountain rupture zone of Nevada (July-August 1954), the southern end of the Fairview Peak rupture zone, and the northern end of the Pleasant Valley rupture zone provide too little information to test the model. The Hebgen Lake earthquake in Montana (1959) occurred on a fault zone that is too young for the model to apply.

Manuscript approved for publication November 20, 1990.

INTRODUCTION

SEGMENTATION

Swan and others (1980) and Schwartz and Coppersmith (1984) hypothesized that the Wasatch fault zone is

divided into six segments that are mostly or wholly independent of one another structurally and seismogenically. The proposed segments range in length from at least 30 to about 70 km (fig. 1). Schwartz and Coppersmith (1984) also hypothesized that seismic energy release on a given segment occurs mostly as earthquakes of a size that is characteristic of the segment. These characteristic earthquakes would rupture the whole segment but would not rupture across segment boundaries into adjacent segments. This report concentrates on the segmentation hypothesis.

If the segmentation hypothesis is valid for the Wasatch fault zone, the consequences for hazard evaluation in Utah would be twofold. First, segmentation would affect the geographic distribution of expected large earthquakes along the Wasatch fault zone. Scarp-forming earthquakes over the last 8,000 years have been concentrated in the four central and most heavily populated proposed segments (Schwartz and Coppersmith, 1984, table 2). When the data of Schwartz and Coppersmith (1984) are compared with the frequencies that would be expected in the central segments if scarp-forming earthquakes were distributed uniformly along the fault zone, the implication is that segmentation could nearly double the frequency of scarp-forming earthquakes in the Salt Lake City and Nephi segments by maintaining the number of large earthquakes in the fault zone as a whole but concentrating them into the middle segments.

Second, segmentation would change probabilistic maps of seismic hazard. Producing such maps requires estimates of three elements: the magnitude of the largest expected earthquake, the frequency distribution of earthquakes of various magnitudes, and the geographic area (seismic source zone) over which the estimates of magnitude and frequency apply (Algermissen and others, 1982; Thenhaus, 1983). Segmentation of the Wasatch fault zone would change all three estimates because each segment would become a separate source zone having its own maximum expected magnitude and frequency distribution. Estimates of magnitudes and frequencies would probably have larger uncertainties than they would if the whole Wasatch fault zone were treated as a single, unsegmented source zone, because each segment would have to be evaluated by using only the comparatively sparse data from within its source zone. The estimated maximum magnitude might decrease because earthquakes large enough to rupture more than one segment (multisegment earthquakes) might be precluded. Then the estimated frequency of single-segment earthquakes might increase because the strain that would have been released by one multisegment earthquake would have to be released in several smaller, single-segment earthquakes.

PURPOSE

Following Schwartz and Coppersmith (1984), our study area is the Wasatch fault zone between lat 39° N. and lat 42° N. (the Utah-Idaho border), a north-south distance of 332 km. For this area, we examined several types of geologic and geophysical data that might contain anomalies (characteristic expressions of long-lasting segment boundaries). For each kind of data, we expanded or contracted the study area to whatever width was needed to characterize pertinent aspects of the data at the fault zone.

Wheeler (1984) examined the aims of hazard evaluation and analyses of temporal variations in the long historical record of seismicity in a tectonically analogous part of northeastern China. He concluded that the geologic records most likely to be useful in evaluating segmentation are those that formed during, or can be shown to bear on, the Holocene and late Pleistocene. The importance of Holocene and late Pleistocene records would increase if the degree of independence between segments and the level of seismic activity on single segments change over a period of centuries to millenia (Machette, 1984; Smith and Richins, 1984, p. 79; Personius, 1985; Machette and others, this volume). In fact, examining different parts of the Quaternary geologic record led Maclean (1985), Machette and others (1986, this volume), Mayer and Maclean (1986), Personius (1986), and Nelson and Personius (1987) to delineate segment boundaries, some of which differ from boundaries recognized in the Holocene record by Schwartz and Coppersmith (1984). These differences might indicate that different segment boundaries have persisted for different lengths of time.

Schwartz and Coppersmith's (1984) segmentation hypothesis was based mostly on data from trenches that were dug across scarps of the Wasatch fault zone at only four sites (fig. 1). Although the trench data are sufficient to suggest the segmentation hypothesis, one trench site per segment is not enough to evaluate that hypothesis. Schwartz and Coppersmith (1984) observed several apparent spatial associations of the proposed segment boundaries with anomalies in topographic, geophysical, and other data and suggested that these spatial associations are stronger than those that would be expected to occur by chance. Wheeler (1984) noted that an appropriately formulated statistical test could provide a rigorous evaluation of these and other spatial associations and therefore of the segmentation hypothesis itself.

Thus, to evaluate the segmentation hypothesis as it applies to the Wasatch fault zone, we must answer two questions. First, do segments exist along the Wasatch Front, or are they artifacts of subjective perception and a small sample, being indistinguishable from patterns

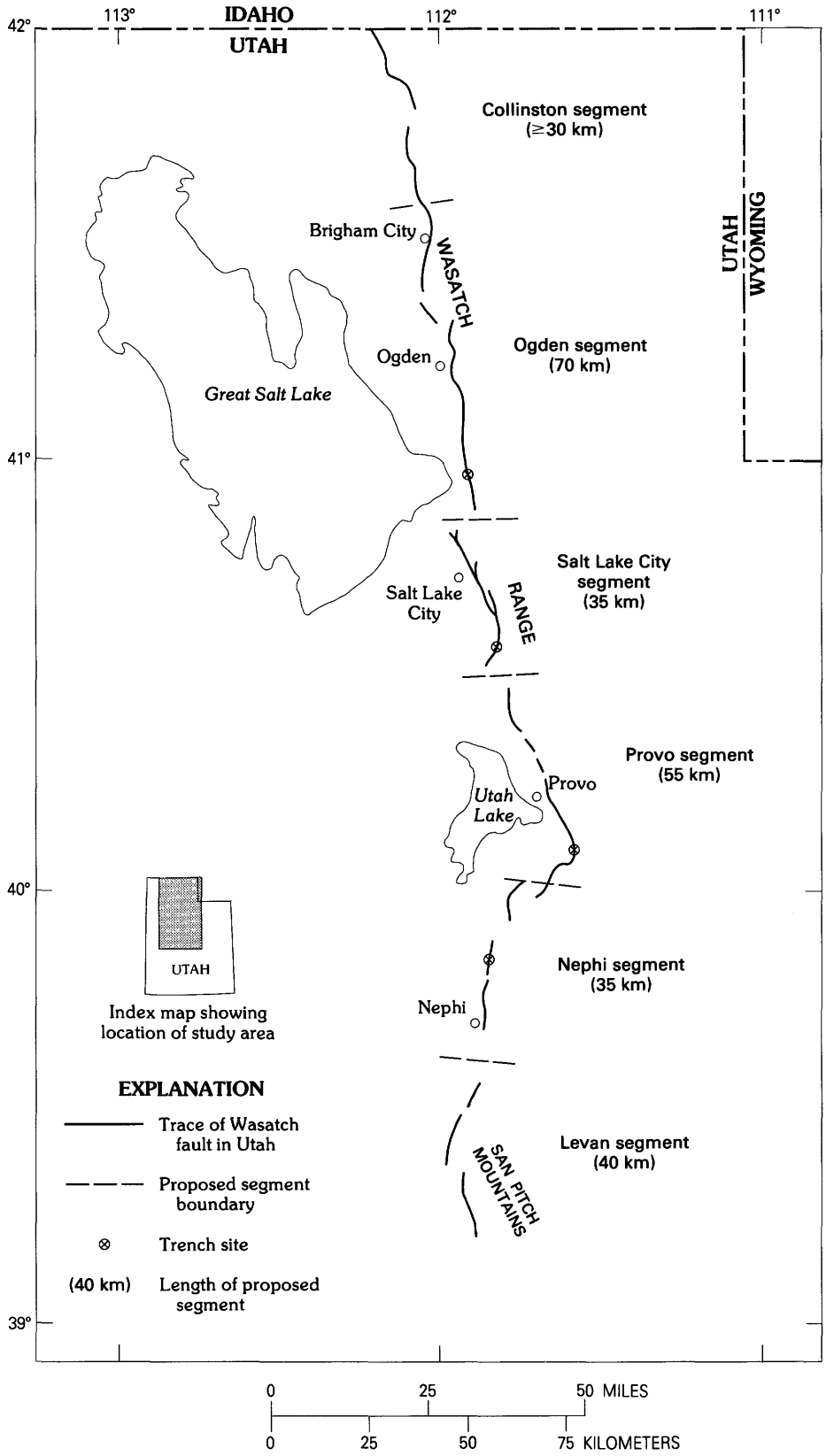

FIGURE 1.—Wasatch fault zone in northern central Utah and selected towns and cities along the Wasatch Front. The Wasatch Front is usually taken to include the populated valleys that lie along and immediately west of the trace of the Wasatch fault zone (Mabey, this volume) and that include most of the population of Utah. The trace of the fault zone, proposed segment boundaries, and trench sites are those of Schwartz and Coppersmith (1984), from whose figure 1 this map is modified. Investigations in progress by several workers have added trench sites and natural fault exposures and have changed some segment boundaries and mapped fault traces. Inset shows the location of the map area within Utah.

that could arise by chance? Second, if segments exist, have they affected uplift and seismicity along the fault zone both during the Holocene and far enough back in geologic time that the segments can be expected to continue to affect seismicity for the next decades to millenia?

ACKNOWLEDGMENTS

Because of the diversity of information that we analyzed and interpreted, we are especially indebted to topical and regional specialists for discussions, corrections, preprints, and sharing of unpublished materials. These generous colleagues include W.J. Arabasz and R.L. Bruhn (University of Utah), D.R. Mabey (Utah Geological and Mineral Survey), Larry Mayer (Miami University, Ohio), and A.J. Crone, S.K. Goter, M.N. Machette, A.R. Nelson, S.F. Personius, W.E. Scott, D.P. Schwartz, and R.S. Stein (U.S. Geological Survey). The entire manuscript benefited from comments by Machette, Nelson, K.M. Shedlock, and M.L. Zoback (U.S. Geological Survey).

METHODS

ANOMALIES

Wheeler and Krystinik (1988) examined six kinds of data along the length of the Wasatch fault zone in Utah for the kinds of anomalies that a long-lasting segment boundary might produce. Each data type and its anomalies satisfy seven criteria (Wheeler and Krystinik, 1988) insuring that the anomalies (1) pertain to the identification of segment boundaries and the evaluation of seismic hazard, (2) are reliable, and (3) can be analyzed by the statistical and related methods of Wheeler and Krystinik (1987a).

At several places along the fault zone, anomalies in two or more data types coincide. (Anomalies in the same data type cannot coincide because they would merge into a single anomaly.) Two anomalies form a coincident pair if either overlaps the center of the other (Wheeler and Krystinik, 1987a). Three anomalies can form as many as three coincident pairs. If all three pairs exist, the three anomalies form a triplet. Similarly, m anomalies define an m-tuplet if the anomalies overlap enough to form all of the possible $m(m-1)/2$ coincident pairs (Wheeler and Krystinik, 1987a). For example, 6 anomalies that form 15 coincident pairs form a sextuplet.

DATA

The gravity data show transverse anomalies G1 through G10 (table 1, fig. 2) as groups of east-trending zones of gravity saddles, east-trending gradients, and ends of north-trending gradients and gravity lows. The transverse gravity anomalies match those derived independently by Zoback (1983) and include those of Mabey (this volume). All of us interpreted G1 through G10 to record changes along the normal fault zone in the depths to the bottoms of adjoining basins in the hanging (western) wall. Wheeler and Krystinik (1988) argued that basin subsidence probably occurred as a result of seismic slip on the fault zone, so that adjoining hanging-wall basins displaying different amounts of subsidence would abut parts of the fault zone having different seismic histories. Thus, a transverse gravity anomaly that separates such basins could be a segment boundary. We do not claim that G1 through G10 must represent segment boundaries. We merely observe that long-lasting segment boundaries or their effects should produce transverse anomalies like G1 through G10; therefore, examination of the gravity data and of G1 through G10 is justified. We make similar observations for the other five data types.

The total magnetic intensity data show transverse anomalies M1 through M3 (table 1, fig. 2) as east-trending belts of east-trending gradients and of narrow, high-amplitude magnetic highs (Zietz and others, 1976). Mabey and others (1964) attributed M1 to uplifted and exposed Precambrian metamorphic rocks and M2 and M3 to buried and exposed intrusive and volcanic rocks of Tertiary age and associated mineral deposits. Wheeler and Krystinik (1988) suggested that M1 is bounded on the south and perhaps on the north by cross faults along which the metamorphic rocks were uplifted, perhaps on lateral ramps in Cretaceous thrust faults. They also suggested that M2 and M3 might be localized by fracture systems that extend to depths at which magma was generated. Pre-existing faults or other fracture zones that cross the late Tertiary (Naeser and others, 1983) Wasatch fault zone might segment it by separating and decoupling adjoining blocks of one fault wall or both.

Seismological data show anomalies Se1 through Se4 (table 1, fig. 2) as changes along the fault zone in the abundance of epicenters of small earthquakes that occurred near the trace of the fault zone from 1962 to 1986 (Arabasz and others, 1980; Arabasz, 1984; Smith and Richins, 1984; W.J. Arabasz, oral communs., 1986). The changes could represent differences between present-day rates of seismic slip on adjacent lengths of the fault zone. Such differences could represent different rates of long-term seismic slip, different ratios of seismic to aseismic slip, or different magnitudes and frequencies of the earthquakes that caused seismic slip to occur; any of these differences could arise from independent slip of two fault segments separated by a change in epicentral

TABLE 1.—*Locations of transverse anomalies*

[Study area is 332 km long, north to south, the northern end being at Utah-Idaho border. Values are from Wheeler and Krystinik (1988)]

Transverse anomaly number	Distance south of Utah-Idaho border (km): Northern end of transverse anomaly[1]	Distance south of Utah-Idaho border (km): Southern end of transverse anomaly	Transverse anomaly width (km)[2]	Distance to next transverse anomaly to south (km)[3]
Gravity data				
G1	−10	2	2	10
G2	12	17	5	40
G3	57	63	6	5
G4	68	78	10	45
G5	123	135	12	13
G6	148	157	9	9
G7	166	175	9	11
G8	186	192	6	19
G9	211	237	26	42
G10	279	292	13	40
Aeromagnetic data				
M1	54	130	76	18
M2	148	173	25	54
M3	227	246	19	86
Seismological data				
Se1	59	78	19	42
Se2	120	133	13	8
Se3	141	151	10	62
Se4	213	226	13	106
Fault geometry (salients)				
Sa1	70	76	6	48
Sa2	124	134	10	31
Sa3	165	169	4	48
Sa4	217	230	13	102
Topographic data				
T1	130	140	10	107
T2	247	254	7	78
Structural data				
St1	112	138	26	8
St2	146	167	21	53
St3	220	245	25	87

[1]Zoback (1983, fig. 2) showed that transverse anomaly G1 extends 10 km north of the Utah-Idaho border. Data north of the border lie outside the study area and are not used here, so the width of G1 is taken as 2 km.

[2]For each data type, the sum of these values is the length of the study area that is occupied by transverse anomalies.

[3]For each data type, the last entry is the distance from the southernmost transverse anomaly to the southern end of the study area at lat 39° N. For each data type, the sum of the values in this column is the length of the study area not occupied by transverse anomalies.

abundance. Then Se1 through Se4 could be segment boundaries.

The geometry of the fault zone shows anomalies Sa1 through Sa4 (table 1, fig. 2). At each anomaly, the footwall projects westward into the hanging wall as a large salient, and the mapped trace of the fault zone or one of its strands bends west around the tip of the salient (Hintze, 1980; Davis, 1983a, b, 1985). The trace of the fault zone also forks or steps en echelon at the salients. Sa1, Sa2, Sa3, and Sa4 are the Pleasant View, Salt Lake, Traverse Mountains, and Payson salients, respectively (Wheeler and Krystinik, 1987b, c, 1988). If slip vectors change orientation across the salients, then, by definition, the salients are nonconservative barriers as described by King (1983). King (1983), King and Yielding (1984), and King and Nabelek (1985) suggested a mechanism by which large ruptures would tend to start and stop at nonconservative barriers. Briefly, if two adjacent parts of a fault slip along different vectors, the slip geometry at the junction of the two parts requires the formation of a network of many subsidiary faults surrounding the junction. This network is the process zone of King and Nabelek (1985). The energy of an incoming rupture is absorbed by the process zone and dispersed into small slips on many of its faults. Large ruptures that propagate toward the process zone tend to stop there, so that the zone is a barrier. The shattered process zone has low strength but high fracture toughness; thus, it also acts as an asperity, and large ruptures tend to start there and propagate away along the main fault. Accordingly, ruptures tend not to cross the process zone, so that it becomes a segment boundary. Bruhn and others (this volume, 1987) concluded from structural measurements and geometric arguments that slip vectors change orientation across the Salt Lake and Traverse Mountains salients. Nelson and Personius (1987) noted that young fault scarps end or change age at the Pleasant View salient, as would be expected of a nonconservative barrier. If the mechanism of King and Nabelek (1985) operates at the salients, they would be segment boundaries.

Transverse topographic anomalies T1 and T2 (table 1, fig. 2) are formed where the height of the uplifted mountains or their width or both change abruptly northward or southward. Choosing anomalies is a more subjective process for topographic data than it is for the other five data types and the least likely to give reproducible results. To insure reproducibility, Wheeler and Krystinik (1988) used only those topographic anomalies that were recognized by a majority of 12 independent interpreters. Of 14 suggested topographic anomalies, 2 were chosen by at least 9 interpreters; no others were chosen by more than 5. A topographic anomaly could mark a place along the fault zone where a footwall block has been uplifted more than its neighbor across the anomaly. Because much or all uplift has occurred seismically, a topographic anomaly could separate lengths of

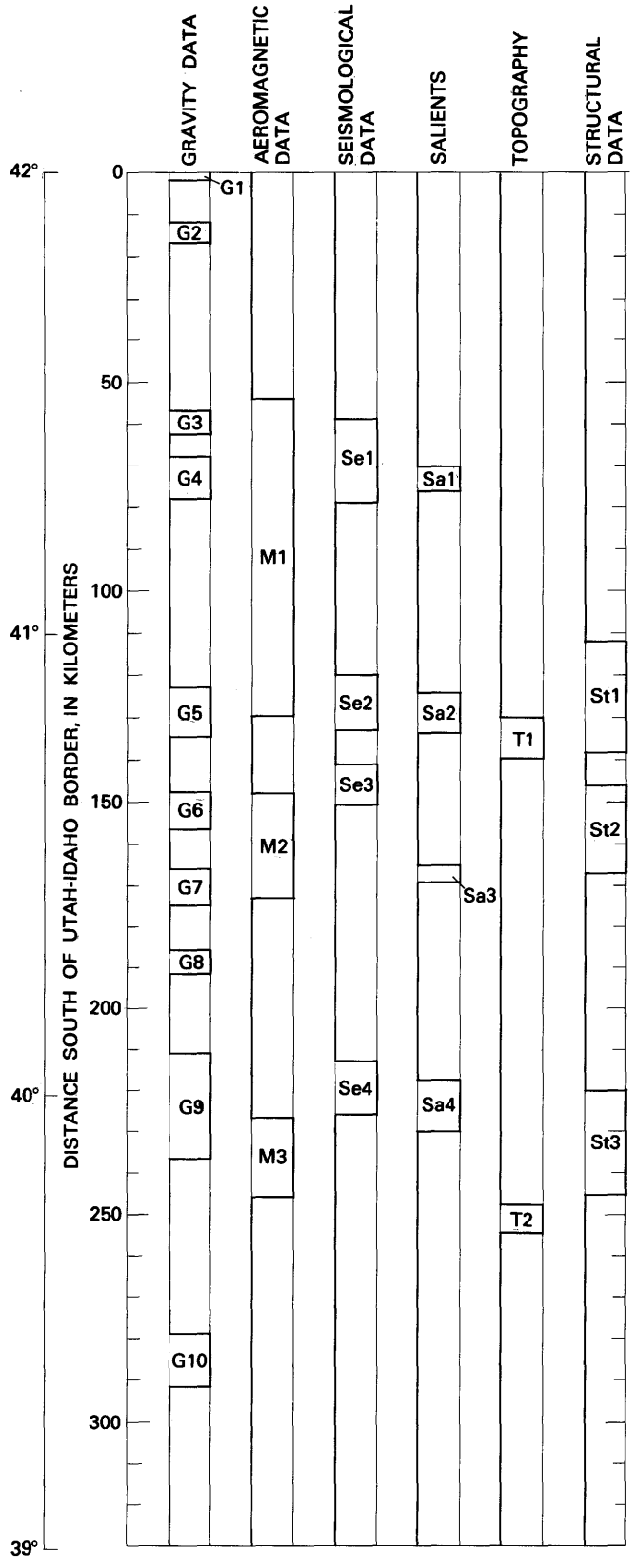

the fault zone that have different seismic histories and could be a segment boundary.

Structural anomalies St1 through St3 (table 1, fig. 2) were chosen by considering the depths at which large normal faults of the Basin and Range province typically nucleate (about 15 km, at or near the base of the brittle upper crust) (Smith and Richins, 1984, p. 97, figs. 9, 11). Large cross faults that extend to this depth could decouple adjoining lengths of the Wasatch fault zone from each other and could act as segment boundaries. Wheeler and Krystinik (1988) reviewed the structural evolution of central Utah and found three large east-striking faults or fault zones (St1–St3) that could serve as structural anomalies and could extend to depths of about 15 km. St1 is a buried lateral ramp in thrust sheets that moved eastward into north-central Utah mostly in Cretaceous time (Armstrong and Oriel, 1965; Oriel and Armstrong, 1966; Armstrong, 1968; Royse and others, 1975). The ramp is nowhere exposed, but Smith and Bruhn (1984), Schirmer (1985), and Wheeler and Krystinik (1988) used geometric arguments to conclude that it must dip north. St3, a similar north-dipping lateral ramp at the southern end of a more southerly thrust sheet, also formed in Cretaceous time (Crittenden, 1961; Armstrong, 1968; Lawton, 1985; Bryant and Nichols, 1988). The top of the ramp is exposed in the southern end of the Wasatch Range northeast of Nephi (Hintze, 1980). St2 is the buried fault system that is inferred to bound and underlie the Uinta aulacogen, a long-lasting trough (Forrester, 1937) that extends more than 200 km eastward from the Salt Lake City segment (fig. 1). The aulacogen probably formed as an east-trending continental rift in Middle Proterozoic time (Hansen, 1965; Wallace and Crittenden, 1969; Burke and Dewey, 1973). Its existence is inferred from a long stratigraphic record of repeated, superimposed, eastward-elongated uplifts and downwarps from Middle Proterozoic and perhaps Archean through Oligocene time (Bryant, 1985; Wheeler and Krystinik, 1988) and from young, inward-dipping reverse faults that bound the inferred aulacogen along its northern and southern edges (Bruhn and others, 1983; Gries, 1983; Stone, 1986). However, we found no evidence that the reverse faults penetrate as deeply as 15 km or that they were active when the aulacogen formed during Middle Proterozoic time. Accordingly, Wheeler and Krystinik (1988) took anomaly St2 to represent the entire system of deep,

◀ FIGURE 2.—Observed distribution of anomalies along the Wasatch fault zone. The length of the anomaly pattern is 332 km, from the Utah-Idaho border at lat 42° N. to the southern edge of the study area at lat 39° N. Each of the six data types is represented by a vertical line that steps to the right at one end of an anomaly and back to the left at the other end. Anomaly locations and letter-number names are from Wheeler and Krystinik (1988).

east-striking, unexposed faults that are inferred to underlie the aulacogen, from the northern edge of the aulacogen to the southern edge inclusive.

CAUSES OF COINCIDENT ANOMALIES

Segmentation and other geologic processes might each produce single anomalies of the kinds described above. Coincident anomalies might be produced by segmentation, by some other geologic process that affects more than one data type, or by chance in the form of the spatially random operation of independent geologic processes that each affect only one data type. We will attribute coincident anomalies to segmentation if we can eliminate the two alternative causes. Geologic processes other than segmentation must be eliminated by considering the geologic evolution and characteristics of central Utah. Chance must be eliminated statistically before coincident anomalies can be considered worth interpreting, either as segment boundaries or as manifestations of any other geologic processes.

GEOLOGIC CAUSES OF ANOMALIES OTHER THAN SEGMENTATION

Transverse anomalies G1 through G10 in Bouguer gravity data can be interpreted as separating sediment-filled hanging-wall basins (Zoback, 1983). Such anomalies would reflect segment boundaries because they would separate parts of the fault zone that have slipped separately and perhaps independently. Overlaying an enlarged version of Zoback's (1983) Bouguer gravity map on Hintze's (1980) geologic map indicates that G5 through G7 can be tentatively attributed partly to large lateral ramps in thrust sheets. The ramps could act as segment boundaries by decoupling adjacent parts of the Wasatch fault zone so that the parts could slip independently of each other. Other kinds of east-striking cross faults might also cause transverse gravity anomalies, such as east-trending gravity gradients, by juxtaposing rocks of different densities. Deeply penetrating cross faults could also decouple adjacent parts of the Wasatch fault zone and act as segment boundaries. For example, east-striking faults in the Uinta aulacogen or at its edges could cause G6 and G7. Edges of high-density igneous rocks could produce transverse gravity anomalies, but intrusive and extrusive igneous rocks at and near the Wasatch fault zone generally have low densities, some comparable to those of surrounding sedimentary rocks (Zoback, 1983, p. 5, 11). Also, most edges of gravity highs near the fault zone follow the contact between bedrock and basin-filling sediments more faithfully than they follow contacts between igneous rocks and other rocks (Zoback, 1983; Hintze, 1980) and so appear to outline shapes of basins instead of igneous bodies. Facies changes within the sediments that fill some basins could produce lateral density contrasts (Mabey, this volume), but these contrasts are likely to be too small to produce the 10 to 40 mGal of gravity relief that occurs across several of anomalies G1 through G10. Thus, segment boundaries of one form or another are the most likely explanation for most of G1 through G10.

Mabey and others (1964) attributed transverse anomalies in the aeromagnetic field to exposed Precambrian rocks (M1) and to east-trending belts of igneous rocks (M2, M3). The Precambrian rocks form the main mass of a thrust sheet, the southern edge of which is a lateral ramp (Wheeler and Krystinik, 1988). The magma that fed the igneous belts could have risen along east-trending systems of fractures. Both lateral ramps and deeply penetrating fracture systems could decouple adjacent parts of the Wasatch fault zone and thus cause its segmentation. Of the various ways to emplace magnetic rock into nonmagnetic surroundings, only thrusting and igneous activity are consistent with the geologic history of north-central Utah. For example, sedimentary processes do not produce magnetic anomalies having the magnetic relief of M1 through M3 (200–800 γ) (Zietz and others, 1976), and uplift of magnetic rock in mantled gneiss domes would have been restricted to the more westerly parts of the orogen whose eastern parts are preserved along the Wasatch Front. The only reasonable explanations for M1 through M3 are consistent with the notion that these transverse anomalies are expressions of segment boundaries.

By definition, seismological anomalies Se1 through Se4 are segment boundaries for the small earthquakes that were recorded from 1962 through 1986.

Sa1 through Sa4 are salients occurring where the Wasatch fault splits and rejoins itself to enclose a partly downdropped block (Sa1, Sa2), bends sharply (Sa1, Sa3), or steps en echelon to the east or west (Sa4) (Wheeler and Krystinik, 1988). Our inspection of fault patterns and bedrock lithologies near Sa1 through Sa4 (Hintze, 1980) suggests two possible causes for such splits, sharp bends, and steps. In the upper few kilometers of the crust, a massive, unlayered or irregularly layered rock mass might have sufficient fracture toughness that a rupture propagating toward the mass might go partly or entirely around it more easily than it would go straight through it. This scenario might have happened at the southern end of the Archean migmatites, schists, and gneisses of the Farmington Canyon Complex (Bryant, 1984) at Sa2 and along the margin of the quartz monzonite of the Little Cottonwood stock (Crittenden, 1965) at Sa3. Alternatively, two ruptures that nucleate independently of each other and propagate toward each other are

unlikely to meet in perfect alignment. Their tips would probably propagate past each other for some distance before each rupture curved to join the other. The result could be a sharp bend in the combined fault trace (Sa1, Sa3), a fault trace that appears to split and rejoin itself (Sa1, Sa2), or en echelon steps in the fault trace (Sa4). Whether a salient originates and grows at a tough rock mass, whether two rupture tips barely miss each other, or whether both occur, each of the four salients has hundreds to thousands of times more structural relief that it could have acquired during one large earthquake. Each salient must have grown over many recurrence intervals of such earthquakes. A salient that grows through similar behavior of many large ruptures is a segment boundary.

Topographic anomalies T1 and T2 could be produced by (1) differences in rates or amounts of uplift across a segment boundary, (2) irregular fault geometry, (3) lithologic variation, (4) variation in the geometries of the thrust sheets and related folds that are exposed throughout most of the eastern wall of the Wasatch fault zone, or (5) variations in erosion rates and stream sizes. Factors 2 through 4 might be related to segment boundaries but need not be. Later, we will show that topographic anomalies are poorly associated with inferred segment boundaries. Perhaps the plethora of possible causes of topographic anomalies is the reason for this poor association. T1 is a topographic low (Wheeler and Krystinik, 1988) that coincides with Mesozoic rocks in and near the Parleys Canyon syncline (Crittenden, 1974). The Mesozoic rocks are bounded on the north and south by more resistant Precambrian rocks (Hintze, 1980). T2 is also a topographic low (Wheeler and Krystinik, 1988) that coincides with a river that cuts through easily erodible Mesozoic strata (Hintze, 1980). These strata pass northward under the resistant Paleozoic rocks of a thrust sheet, which form a tall mountain at the northern edge of T2 (Hintze, 1980). Thus, both topographic anomalies might arise from lithologic variations that need not be related to segment boundaries.

Anomalies in pre-Cenozoic structures are large lateral ramps that dip moderately northward (St1, St3) and an inferred system of east-striking faults (of unknown geometry) of the Uinta aulacogen (St2) (Wheeler and Krystinik, 1988). St1 through St3 are inferred to cut the upper crust. All three could act as segment boundaries by decoupling adjacent parts of the Wasatch fault zone and allowing the parts to operate as independent segments. No other similar structures are known along the fault zone. The best candidate for a similar structure is the north-dipping Willard fault (Crittenden, 1972), which dips too gently to be considered a segment boundary (Wheeler and Krystinik, 1988).

In summary, transverse anomalies in aeromagnetic and seismological data, salients, and pre-Cenozoic structures can be reasonably explained only as expressions of segment boundaries or of faults and other fractures that could act as segment boundaries. Topographic anomalies can have causes other than segment boundaries, but they are the anomalies that are least involved in the inferred segment boundaries of the Wasatch fault zone. There are so many transverse gravity anomalies that one might expect some to have causes other than segment boundaries. Some of the other causes are geologically reasonable; in fact, as we will show later, 4 of the 10 transverse gravity anomalies do not coincide with other anomalies (G1, G2, G8, G10) (fig. 2). However, the striking grouping of most anomalies into a few anomalous parts of the fault zone (fig. 2) can be reasonably attributed only to the operation of segment boundaries or to chance.

SIMULATION AND STATISTICAL PROCEDURES

Wheeler and Krystinik (1987a) described or derived several procedures for summarizing and evaluating how anomalies are distributed along the fault zone. They illustrated these procedures by applying them to an artificial data set that resembles a simple version of the real data of figure 2. Among these procedures is modification and use of the Jaccard coefficient J (Cheetham and Hazel, 1969) to identify strongly associated data types or those that tend to have and lack anomalies at the same places along the fault zone. One nonnegative value of J can be calculated for each pair of data types. Values of J near or larger than 1 identify pairs of data types that are comparatively strongly associated. These data types might be more useful together than they are separately for interpreting the observed pattern of anomalies. Conversely, values of J near 0 identify pairs of data types that are comparatively unassociated and that tend to have and lack anomalies without regard to each other. We chose all data types and their anomalies with an eye to identifying segment boundaries, so that any data type that tends to be unassociated with the others (and particularly with data types of most interest for identification of segment boundaries) probably can be dropped from further consideration.

Simulations and appropriately designed statistical tests aid in deciding whether anomalies in the observed pattern (fig. 2) coincide more than should be attributed to chance. Each simulation takes the observed number and widths of anomalies in each data type, locates those anomalies randomly along the fault zone, and produces a simulated anomaly pattern that resembles figure 2 to some degree. For the anomalies in figure 2, we performed 300 simulations. This number was chosen because it was large enough to smooth out the peculiar-

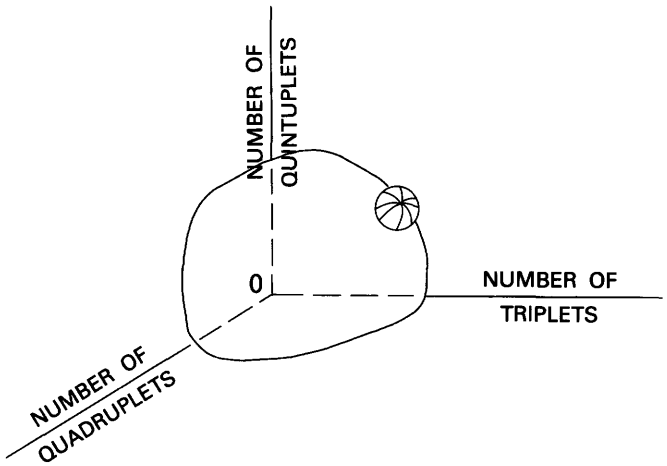

FIGURE 3.—Three-dimensional geometry of comparison of the observed anomaly pattern to simulated patterns. Each pattern plots in this graph according to its numbers of triplets, quadruplets, and quintuplets of coincident anomalies, which are identified according to the rules given in the text. Axes are mutually perpendicular, so the quadruplet axis rises out of the page. The red line outlines the cloud of points, one from each simulated pattern. Dashed parts of axes and origin 0 lie behind the cloud. The center of the small ball enclosing an asterisk represents the single observed pattern. A statistical test determines whether this ball is significantly distinct from the cloud of points.

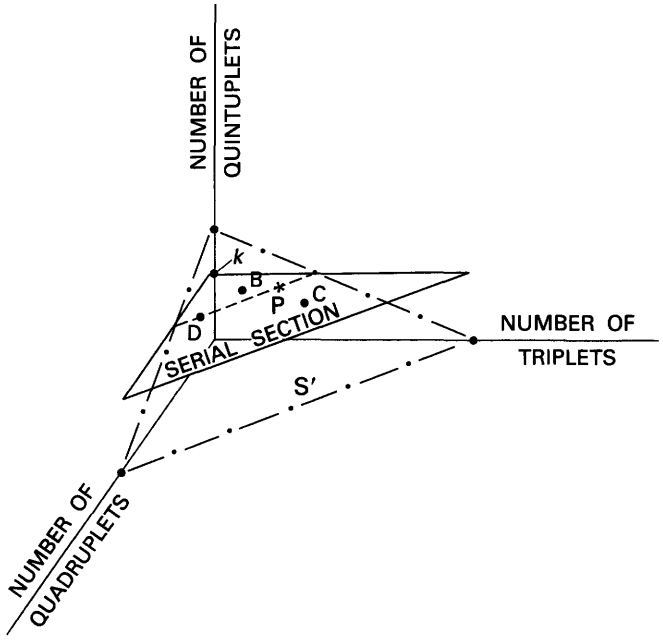

FIGURE 4.—Axes of figure 3, showing a serial section (red lines). The serial section lies parallel to the triplet and quadruplet axes and intercepts the quintuplet axis perpendicularly at k, so that all observed or simulated patterns of anomalies that contain k quintuplets plot in this serial section (for example, as points B–D). S′ is called the significance plane (dash-dot line) and intercepts all three axes obliquely. There is one serial section for each value of k, $k=0$, 1, 2,.... The section shown here is the one on which the observed pattern plots (point P, shown as an asterisk). S′ intersects the serial section in the thin dashed line and is constructed so that the dashed line passes through P. Modified from Wheeler and Krystinik (1987a).

ities of any small group of simulated patterns but small enough for the simulations to be computationally feasible.

Each anomaly pattern plots in a three-dimensional graph according to its numbers of triplets, quadruplets, and quintuplets (fig. 3). Only one simulation produced a sextuplet, so this single simulated pattern will be treated individually. Wheeler and Krystinik (1987a) described a simple way to perform the statistical test by counting the numbers of patterns that plot in serial sections through figure 3 (fig. 4). Each observed or simulated pattern plots on one of a few serial sections. For example, the patterns for the data from the Wasatch fault zone all plot on the first three sections, because each pattern has $k=0$, 1, or 2 quintuplets. The significance plane S′ intersects each section in a dashed line (fig. 4), although only one section and one dashed line contain the point P that corresponds to the observed pattern. $N(e)$ is the number of simulated patterns that plot on or outside (farther from the origin than) the dashed lines, summed over all serial sections. Points C and D (fig. 4) contribute to $N(e)$. $N(p)$ is the total number of simulated patterns in all the sections; thus, points B through D (fig. 4) all contribute to $N(p)$. The level of significance of the statistical test is $N(e)/N(p)$ (Wheeler and Krystinik, 1987a).

LOCATIONAL UNCERTAINTIES OF ANOMALY EDGES

The northern and southern edges of each anomaly have locational uncertainties. Most uncertainties are ±1 to 5 km (Wheeler and Krystinik, 1988). We investigated the effects of uncertainties by analyzing two observed patterns in addition to the pattern in figure 2, which shows the measured width of each anomaly (table 1). One of the other patterns, which shows the minimum anomaly widths that are allowed by the locational uncertainties, was tested against 300 simulations of the locations of these narrowed anomalies. The other pattern, which shows maximum allowable widths, was tested against only 100 simulations because the wider anomalies generated more and larger coincidings, and the greatly increased computation time made more simulations infeasible. Thus, we did three statistical tests instead of one. We tested for significance with each of these three sets of simulations. The principles of simultaneous infer-

ence (Miller, 1981, p. 8) require that each of the three tests use a level of significance of 0.05/3=0.0167 instead of the habitual 0.05.

DESCRIPTIVE RESULTS

OBSERVED PATTERN OF ANOMALIES

Gravity, aeromagnetic, seismological, and topographic data, salients, and pre-Cenozoic structures together define a total of 26 anomalies along the Wasatch fault zone (fig. 2). Locational uncertainties of anomaly edges define minimum and maximum widths for each anomaly (fig. 5). Most anomalies occupy only a small fraction of the fault's length of 332 km (fig. 6).

ANOMALOUS SECTIONS OF THE FAULT ZONE

Most of the 26 anomalies (figs. 2, 5) fall in four narrow, well-demarcated, anomalous sections of the fault zone (fig. 7). Only five anomalies occur singly or elsewhere (fig. 7*A*). This striking concentration of anomalies into four distinct parts of the fault zone is robust, being weakened little even if each anomaly takes on its extreme widths (figs. 7*B*, *C*).

Triplets, quadruplets, and quintuplets of coincident anomalies are built up from coincident pairs. For example, about at km 70, five anomalies in four data types are involved in eight pairs (fig. 7*A*). These 5 anomalies could define as many as 10 pairs. Of these 10 possible pairs, the one between anomalies G3 and G4 is forbidden because 2 anomalies in the same data type cannot coincide. Anomalies G3 and Sa1 do not overlap and so cannot form a pair. The other eight possible pairs are all present. A triplet is present if and only if all three possible pairs between its three anomalies also are present. At km 70, pair lines define five triplets: G3–M1–Se1, G4–M1–Se1, G4–Se1–Sa1, G4–M1–Sa1, and M1–Se1–Sa1. Similarly, a quadruplet is formed by six pairs among four anomalies. At km 70, the only quadruplet is G4–M1–Se1–Sa1. No quintuplet can link these four anomalies with G3 because the G3–G4 pair is forbidden and the G3–Sa1 pair is not present. If anomalies take on their maximum widths, no change occurs in this list of pairs and m-tuplets (fig. 7*C*). However, using minimum widths breaks the pair G3–Se1, which causes the triplet G3–M1–Se1 to degenerate into its two remaining pairs (fig. 7*B*).

The six coincident anomalies at km 160 and the five at km 230 can be examined similarly. The six anomalies in six data types at km 130 are linked more complexly (fig. 8). Consideration of figure 8 will reveal the 12 pairs, 11 triplets, 5 quadruplets, and 1 quintuplet that are summarized at the right edge of figure 7*A*. Narrowing anomalies to their minimum widths breaks the pairs G5–M1, G5–T1, M1–Se2, and M1–Sa2 and causes some m-tuplets to degenerate (fig. 7*B*). Widening anomalies to their maximum widths produces all possible pairs except M1–T1, and some m-tuplets are added (fig. 7*C*).

Some of these pairs and m-tuplets duplicate each other. A quintuplet comprises five quadruplets, which duplicate it. Similarly, a quadruplet comprises four triplets, and a triplet comprises three pairs. For measured widths, the observed pattern contains one quintuplet, one quadruplet, eight triplets, and one pair after duplicates have been omitted (table 2). For minimum widths, the observed pattern contains two quadruplets, two triplets, and seven pairs. For maximum widths, it contains two quintuplets, six quadruplets, one triplet, and one pair.

Anomalies G1, G2, G8, G10, and T2 are singlets (figs. 2, 7*A*); none coincides with any other anomaly. As widths decrease to their minimums, several things occur: anomalies overlap less, coincident anomalies become scarcer, and these five singlets are joined by G7 and Se3 (figs. 5*A*, 7*B*). As widths increase to their maximums, the reverse occurs, but the original five singlets do not join any pairs or m-tuplets (figs. 5*B*, 7*C*).

ASSOCIATED DATA TYPES

The 15 possible pairings of the 6 data types give 15 values of the Jaccard coefficient J (fig. 9). Increased anomaly widths will tend to increase the number of coincident anomalies and the degree of association between any two data types. Decreased anomaly widths will tend to produce the opposite effect. Both effects can be seen by comparing median values of J and histogram shapes in figure 9.

The most highly associated data types overall are aeromagnetic data (M) and pre-Cenozoic structure (St). This high association also holds for maximum and minimum anomaly widths. Each structural anomaly coincides with one and only one aeromagnetic transverse anomaly and vice versa, regardless of whether anomalies take on their measured, minimum, or maximum widths (fig. 7). The data type that is most highly associated with seismological data (Se) is footwall salients (Sa). This association is also robust under the effect of width but is only moderately strong (J=0.60) (fig. 9*A*). Each seismological anomaly coincides with one and only one salient and vice versa, except Se3 and Sa3, which do not coincide with each other (fig. 7*A*). No change occurs for minimum widths (fig. 7*B*), but for maximum widths Se2 and Se3 both coincide with Sa2 (fig. 7*C*).

Each type of data can combine with five others to produce five J values (fig. 9). The median of these five J values indicates how well the data type is associated with the other five types of data overall. Aeromagnetic data

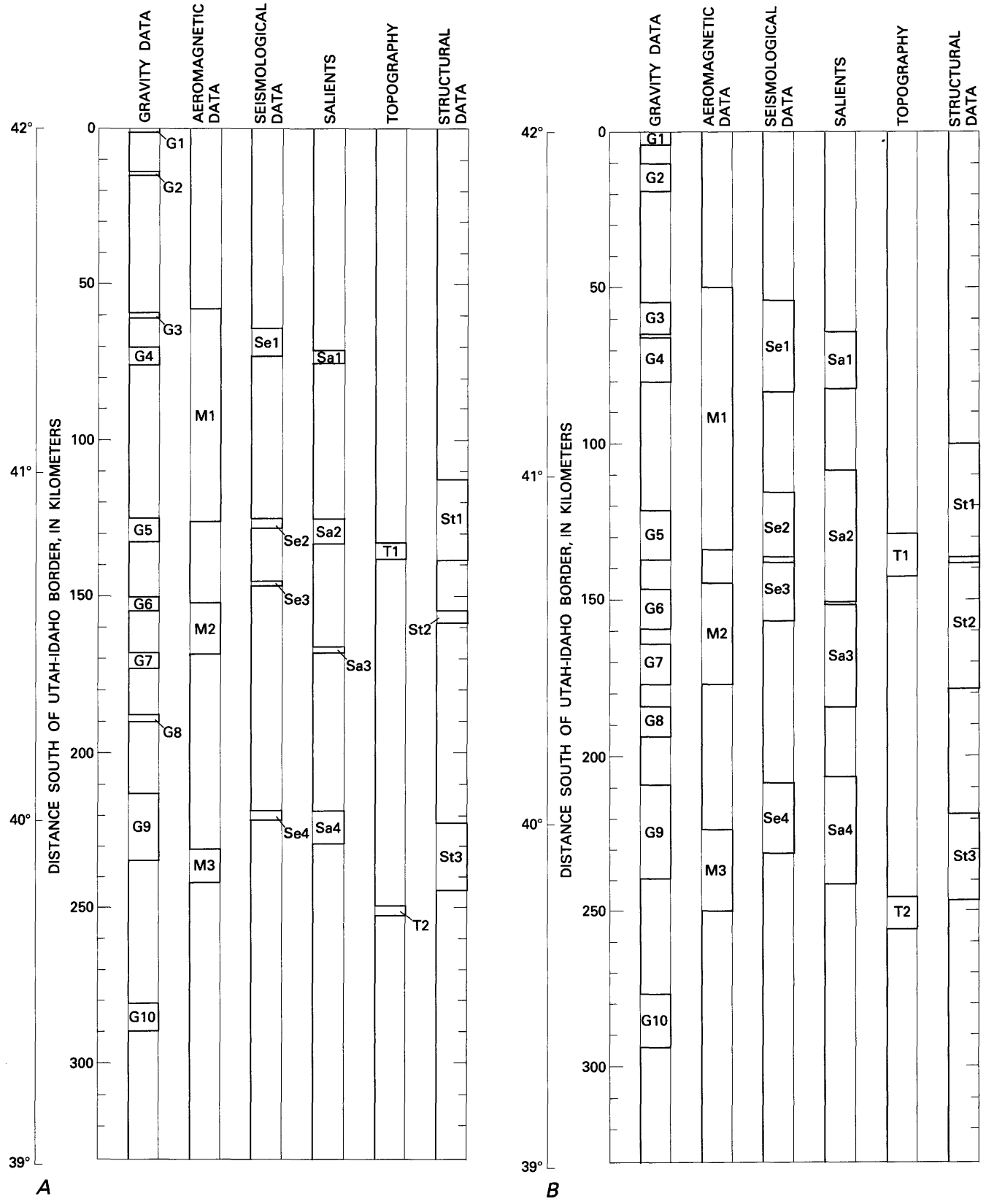

FIGURE 5.—Observed anomaly pattern of figure 2 redrawn to give (*A*) minimum and (*B*) maximum widths allowed for each anomaly by locational uncertainties of its edges. Uncertainties are from Wheeler and Krystinik (1988). In figure 5*A*, this procedure would give anomaly Se3 a width of 0 km. Its minimum width is arbitrarily set at 1 km. In figure 5*B*, Se2 and Se3 overlap by 2 km, as do St1 and St2.

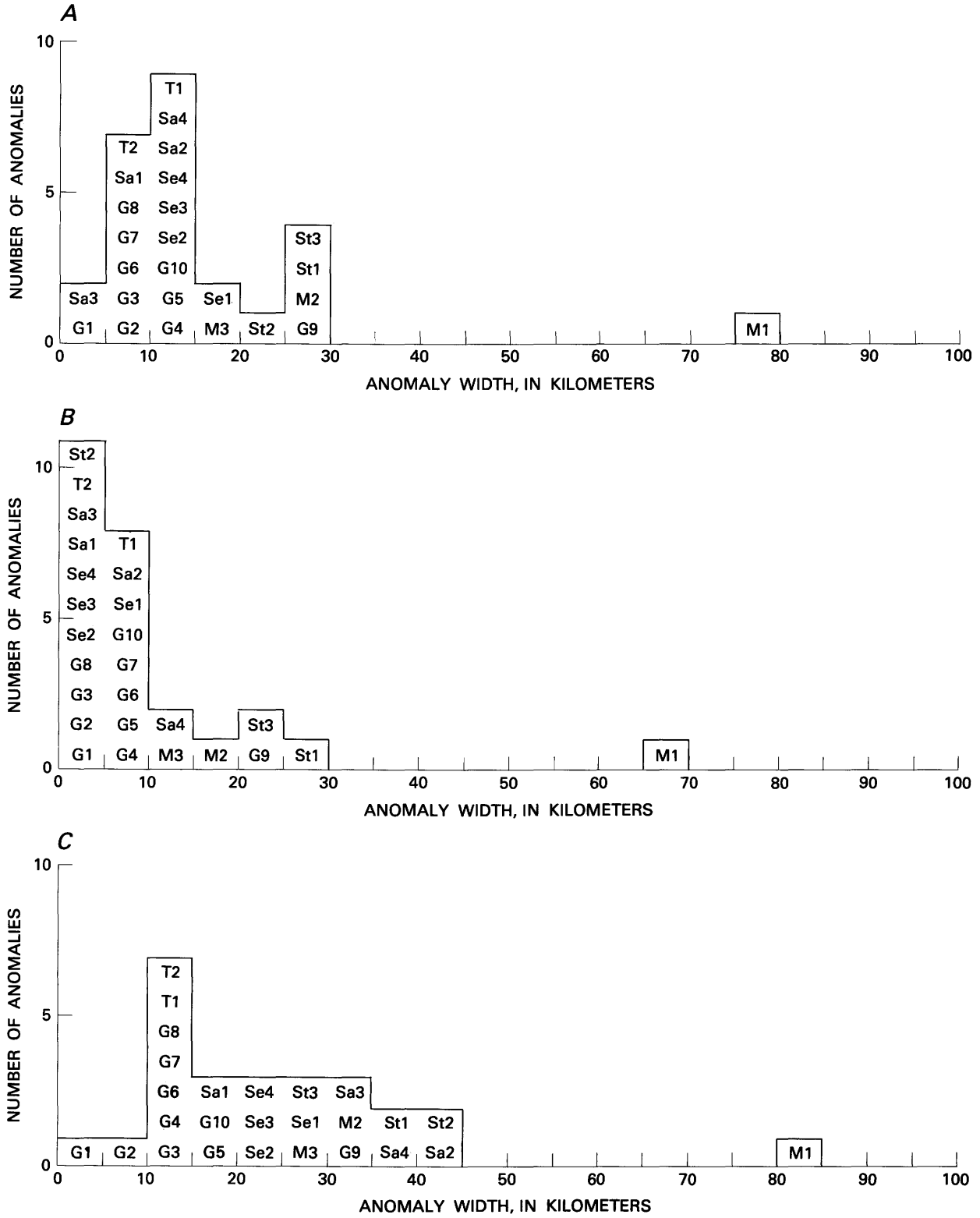

FIGURE 6.—Anomaly widths. Each anomaly is identified by its letter-number name. G denotes Bouguer gravity data; M, aeromagnetic data; Se, seismologic data; Sa, salients; T, topographic data; St, pre-Cenozoic structures. Widths are from Wheeler and Krystinik (1988). *A*, Measured anomaly widths (fig. 2). The median of 26 widths is 11 km, about 3 percent of the 332-km length of the fault zone in the study area. The widest anomaly after M1 spans 8 percent of the fault zone length. *B*, Minimum widths that are allowed by locational uncertainties of anomaly edges (fig. 5*A*). The median is 6 km. The widest anomaly after M1 spans 8 percent of the fault zone length. *C*, Maximum allowable widths (fig. 5*B*), the median being 19 km. The widest anomaly after M1 spans 13 percent of the fault zone length.

are the most strongly associated with other data types overall (median $J=0.75$, 0.33, and 0.86 in fig. 9*A*, *B*, and *C*, respectively). Most of the aeromagnetic transverse anomalies are connected by pair lines to several other anomalies (fig. 7). In contrast, topographic anomaly T1 is sparsely connected, and T2 is not connected to other anomalies. Topographic data are the least strongly associated overall (median $J=0.00$, 0.00, and 0.20 in fig. 9*A*, *B*, and *C*, respectively).

DIAGNOSTIC AND CHARACTERISTIC DATA TYPES

Does any one data type identify anomalous parts of the fault zone particularly well? This question can be answered by using techniques that are associated with cluster analysis. The four anomalous parts of the fault zone divide the zone into nine parts (fig. 7), which group naturally into two clusters. The anomalous cluster contains four parts (those around kms 70, 130, 160, and 230). The nonanomalous cluster contains five parts (the three intervening parts of the fault zone and the two ends, where anomalies are scarce and coincident anomalies are absent).

The entries in a presence-absence matrix (table 3) allow calculation of two measures called constancy (*C*) and fidelity (*F*) (Hazel, 1970). Each is expressed as an integer between 0 and 10. Constancy expresses the degree to which the anomalies of a data type characterize a cluster. Structural anomalies characterize the anomalous cluster moderately well ($C=8$, table 3), because one or more of these anomalies are present in most of the fault zone parts that are in the anomalous cluster. Fidelity expresses the degree to which the anomalies of a data type are diagnostic of a cluster. Structural anomalies are perfectly diagnostic of the anomalous cluster ($F=10$, table 3) but undiagnostic of the nonanomalous cluster ($F=0$). The occurrence of a structural anomaly in a particular part of the fault zone indicates that the part belongs in the anomalous cluster.

For most data types, the *C* and *F* values for the nonanomalous cluster are lower than those for the anomalous cluster (table 3). This difference is reassuring, because the data types were chosen and the anomalies were defined to be likely to reflect the presence of segment boundaries (which should correspond to anomalous parts of the fault zone) instead of segment interiors (which should correspond to nonanomalous parts).

We seek data types that are both diagnostic and characteristic of anomalous parts of the fault zone and that will plot at the upper right-hand corner of a graph of *C* plotted against *F* (fig. 10). For measured anomaly widths, salients (Sa) and seismological anomalies (Se) are perfectly characteristic and perfectly diagnostic of anomalous parts of the Wasatch fault zone (fig. 10*A*). When uncertainty in anomaly widths is considered (fig. 10*B*, *C*), seismological anomalies become slightly worse indicators of anomalous parts of the fault zone, but salients remain perfect one-to-one indicators. Aeromagnetic transverse anomalies (M) are perfectly characteristic ($C=10$) but only moderately diagnostic ($F=8$), and this result is not affected by the uncertainties in anomaly widths. Every anomalous part of the fault zone contains an aeromagnetic transverse anomaly, but such an anomaly can also occur in a nonanomalous part of the fault. Because the unusually wide anomaly M1 spans two anomalous parts of the fault zone and the intervening nonanomalous part (fig. 7), $F=8$.

Recall that the two most highly associated data types are aeromagnetic (M) and pre-Cenozoic structural (St) data. Anomalies in these two data types correspond in parts A2, A3, and A4 of the fault zone but not in part A1 (table 3), producing $C=8$ and $F=10$ for coincident structural and aeromagnetic transverse anomalies in the anomalous cluster. These values do not change with uncertainty in anomaly widths. Thus, the coinciding of structural and aeromagnetic transverse anomalies is perfectly diagnostic but only moderately characteristic of anomalous parts of the fault zone. Coincident transverse anomalies in aeromagnetic and structural data identify parts of the fault zone as anomalous, but one anomalous part of the fault zone (A1) lacks such a coincident pair.

SUMMARY OF DESCRIPTIVE RESULTS

With one exception, the 26 anomalies found in the Wasatch fault zone are of similar widths, the median being 3 percent of the length of the fault zone. Most anomalies coincide with one another in four narrow, anomalous parts of the fault zone.

For the fault zone as a whole, aeromagnetic transverse anomalies are the most highly associated with anomalies of other kinds, especially those in structural data. Topographic anomalies are the least well associated with other kinds. The data type that is most highly associated with seismological anomalies is salients, although only moderately so.

For anomalous parts of the fault zone, salients are perfectly diagnostic and perfectly characteristic; seismological anomalies are the second best such one-to-one indicator. Aeromagnetic transverse anomalies are perfectly characteristic but only moderately diagnostic, and coincident structural and aeromagnetic transverse anomalies are perfectly diagnostic but only moderately characteristic.

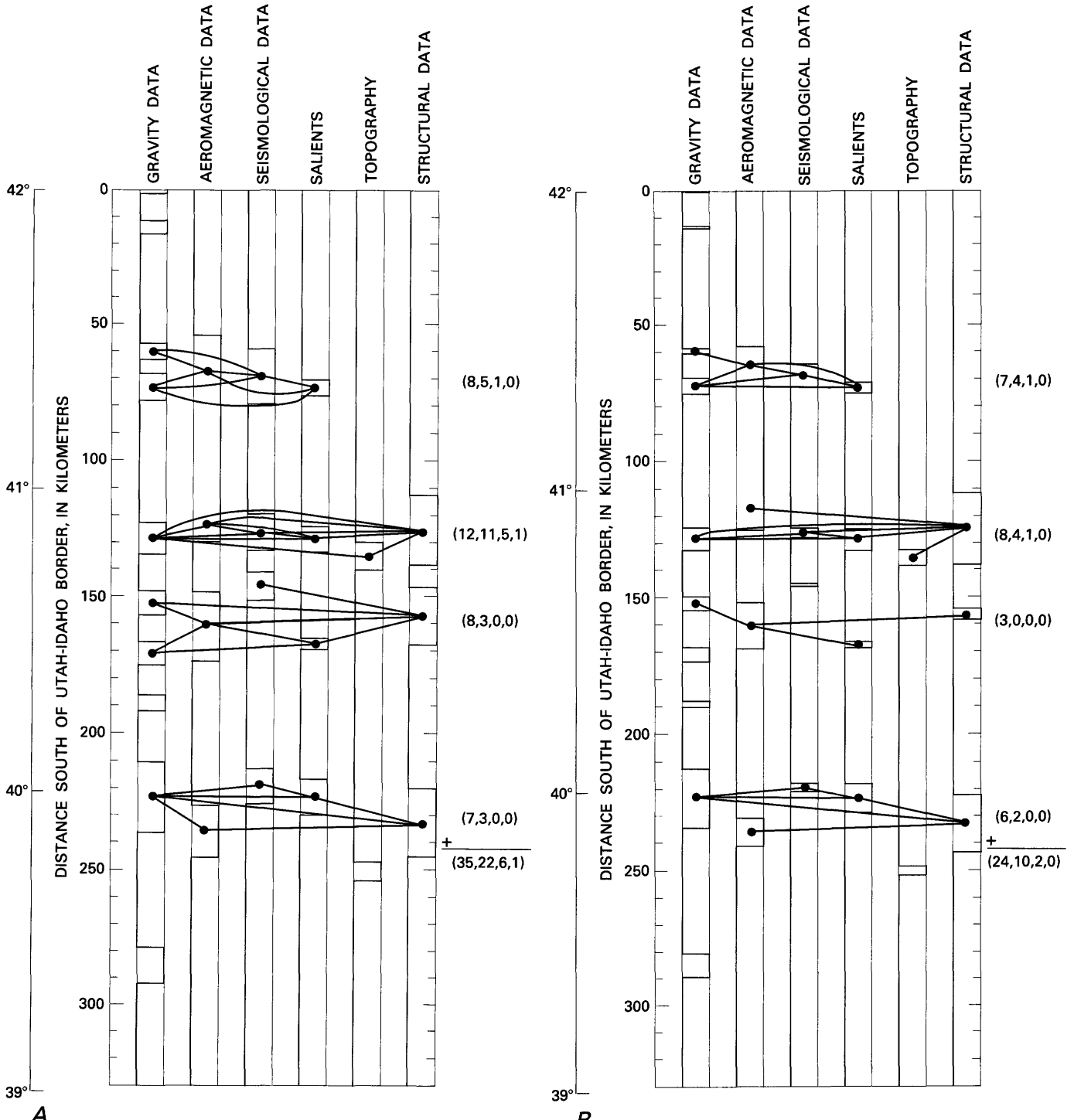

FIGURE 7.—Pairs and m-tuplets of coincident anomalies in the observed anomaly pattern along the Wasatch fault zone. Figures 2 and 5 name each anomaly. Solid circles identify anomalies that are involved in pairs and m-tuplets. Only anomaly M1 has two solid circles, because only it is long enough to span two groups of coincident anomalies. Solid pair lines that connect these solid circles link anomalies that are paired according to the rule that either anomaly contains the center of the other. An m-tuplet is present wherever all $m(m-1)/2$ of the possible pairs of the m anomalies are also present (Wheeler and Krystinik, 1988). In parentheses to the right of each group of paired anomalies are the numbers of pairs, triplets, quadruplets, and quintuplets in the group, in that order. There are no sextuplets or larger m-tuplets. Below the plus sign are the totals of pairs and m-tuplets for the whole anomaly pattern. *A*, Each anomaly is given its measured width (fig. 2). *B*, Each anomaly is given the minimum width that is allowed by the locational uncertainties of its edges (fig. 5*A*). *C*, Each anomaly is given its maximum allowable width (fig. 5*B*). Numbers in square brackets to the right summarize the single pair between anomalies Se3 and Sa2.

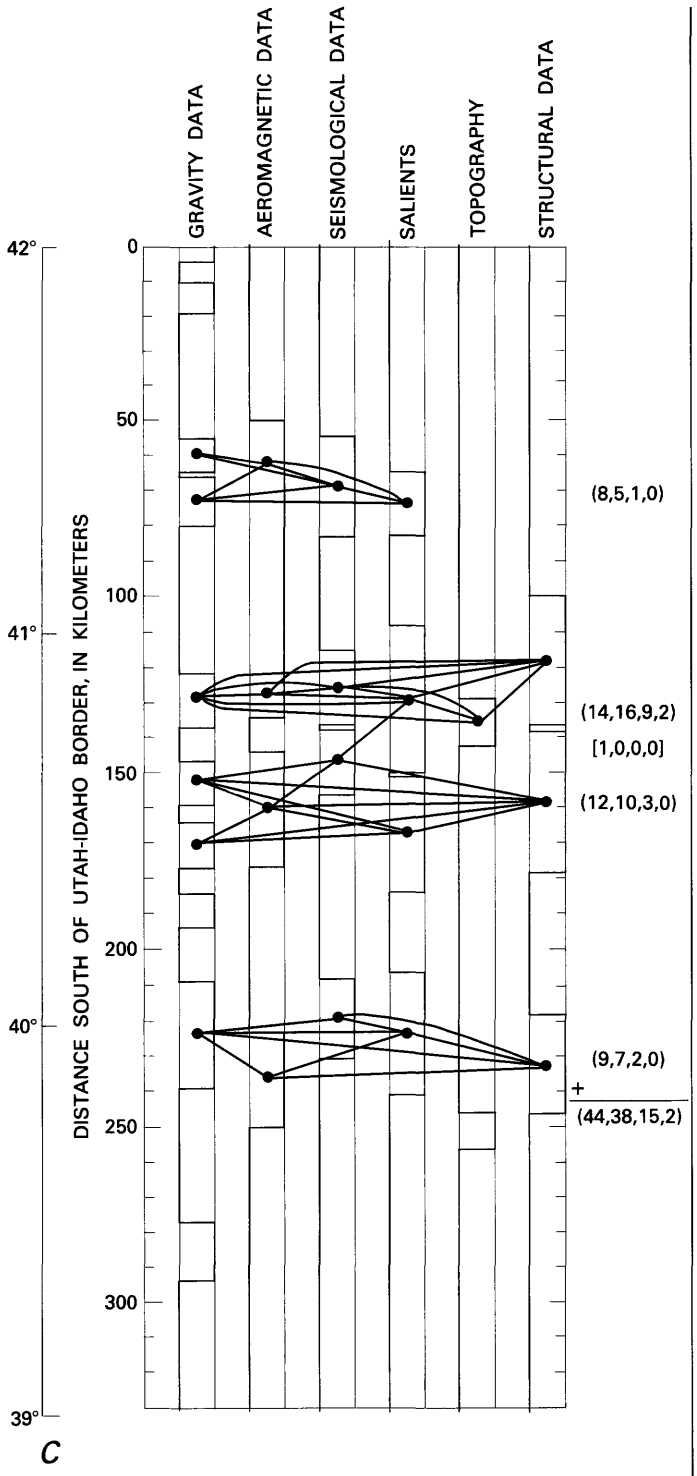

FIGURE 7.—Continued.

RESULTS FROM SIMULATION AND STATISTICAL TESTING

Is the observed concentration of anomalies into four parts of the fault zone worth interpreting, or should it be dismissed as a likely result of a random scattering of anomalies in unrelated variables along the Wasatch fault zone? The most direct way to answer this question is to compare the observed anomaly pattern with simulated patterns that have been produced by such a random scattering of anomalies, as Wheeler and Krystinik (1987a) illustrated by using an artificial data set.

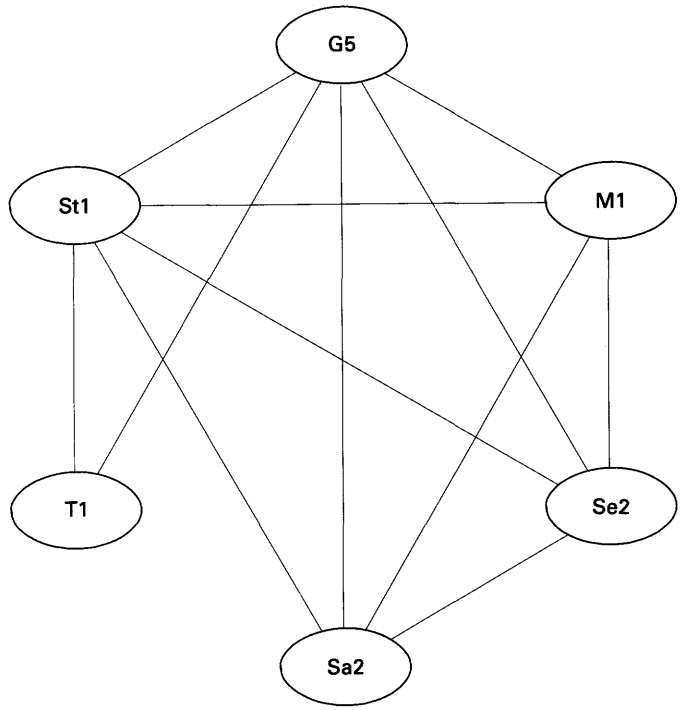

FIGURE 8.—Coincidings between anomalies at km 130 of the Wasatch fault zone. Six ellipses represent anomalies that coincide there (figs. 2, 7*A*). G denotes Bouguer gravity data; M, aeromagnetic data; Se, seismologic data; Sa, salients; T, topographic data; St, pre-Cenozoic structure. Lines joining ellipses represent the pair lines that identify coincident pairs (fig. 7*A*). A triplet appears here as three pair lines that form a triangle (G5–M1–Se2 or M1–Sa2–St1). The triplet Sa2–T1–St1 is absent because the pair Sa2–T1 is absent (fig. 7*A*). A quadruplet appears as four ellipses linked by six pair lines that form a closed quadrilateral and its two internal diagonals (G5–Se2–Sa2–St1). A quintuplet appears as five ellipses, each connected to the others by four pair lines (G5–M1–Se2–Sa2–St1).

ONE-DIMENSIONAL COMPARISONS OF OBSERVED AND SIMULATED PATTERNS

For measured widths, few of the simulations produced as many triplets or quintuplets as those observed, and the observed pattern has more quadruplets than most simulated patterns do (fig. 11*A*). For minimum widths, the observed pattern has unusually many quadruplets but not unusually many triplets, and there are no quintuplets in any simulated or observed pattern (fig. 11*B*). For maximum widths, the observed pattern has unusually many quadruplets and quintuplets but unusually few triplets (fig. 11*C*). Also, one simulation for maximum widths produced the only sextuplet encountered in any

TABLE 2.—*Coincidings of anomalies (duplicating pairs and m-tuplets deleted)*

[Pairs and m-tuplets (triplets, quadruplets, and quintuplets) are among those shown in fig. 7. Entries are lists of anomaly names from figs. 2 and 5. —, none of the indicated kinds of pairs or m-tuplets is present, except as duplicates of parts of larger m-tuplets that might be listed farther to the left for the same location]

Location[1]	Quintuplets	Quadruplets	Triplets	Pairs
Measured widths				
70	—	G4–M1–Se1–Sa1	G3–M1–Se1	—
130	G5–M1–Se2–Sa2–St1	—	G5–T1–St1	—
160	—	—	G6–M2–St2 G7–M2–Sa3 M2–Sa3–St2	Se3–St2
230	—	—	G9–Se4–Sa4 G9–M3–St3 G9–Sa4–St3	—
Minimum widths				
70	—	G4–M1–Se1–Sa1	—	G3–M1
130	—	G5–Se2–Sa2–St1	—	M1–St1 T1–St1
160	—	—	—	G6–M2 M2–Sa3 M2–St2
230	—	—	G9–Sa4–St3 G9–Se4–Sa4	M3–St3
Maximum widths				
70	—	G4–M1–Se1–Sa1	G3–M1–Se1	—
130	G5–Se2–Sa2–T1–St1 G5–M1–Se2–Sa2–St1	—	—	—
140	—	—	—	[2]Se3–Sa2
160	—	G7–M2–Sa3–St2 G6–M2–Sa3–St2 G6–M2–Se3–St2	—	—
230	—	G9–Se4–Sa4–St3 G9–M3–Sa4–St3	—	—

[1]Approximate distance south of the Utah-Idaho border, in kilometers.

[2]This pair links two anomalous parts of the fault zone by spanning a nonanomalous part and is indicated by square brackets at the right-hand edge of figure 7*C*.

anomaly pattern. Thus, these one-dimensional comparisons suggest that anomalies in the observed pattern coincide more than those in the simulated patterns, but the difference is not striking enough to distinguish clearly the observed degree of coinciding from the effects of chance.

THREE-DIMENSIONAL COMPARISONS OF OBSERVED AND SIMULATED PATTERNS

Histograms of m-tuplet frequencies (fig. 11) are easy to understand, but information is lost when a pattern's number of triplets is separated from its numbers of quadruplets and other m-tuplets and similarly for other combinations of m-tuplets. We retain this information by representing each pattern's triplets, quadruplets, quintuplets, and sextuplets together (fig. 12).

For measured widths (fig. 12*A*), 294 of the 300 simulated patterns lack quintuplets and plot in the plane of the page. Five simulated patterns and the observed pattern have one quintuplet each and plot one unit above the page, and a sixth simulated pattern plots two units above the page. Viewed this way, the observed pattern plots near the outside of the group of all points that represent simulated patterns. Accordingly, when all m-tuplets are examined together the anomalies of the observed pattern are seen to coincide strongly when they are compared with the anomalies of the simulated patterns.

For minimum and maximum anomaly widths, the picture is similar but less clear cut. For minimum widths, no pattern has m-tuplets larger than quadruplets, so all plot in the plane of the page (fig. 12*B*). The asterisk lies on the edge of the cloud of plotted points from the simulations. At least two simulated patterns have anomalies that coincide at least as strongly as is observed. For maximum widths, the observed pattern plots to the right and above the page from the envelope that encloses the plotted locations of all simulated patterns (fig. 12*C*). The sextuplet is much rarer than the quintuplets, so this simulated pattern probably should be considered to have anomalies that are at least as strongly coincident as those of the observed pattern.

Therefore, examining all sizes of m-tuplets together shows that the observed pattern has anomalies that coincide more strongly than those of nearly all simulated patterns. This difference holds whether anomalies take on their measured, minimum, or maximum widths.

QUANTITATIVE COMPARISONS OF OBSERVED AND SIMULATED PATTERNS

For the statistical test of figures 3 and 4, a concise statement of the null hypothesis of Wheeler and Krystinik (1987a) is that the observed pattern was drawn

FIGURE 9.—Values of the Jaccard coefficient J for the 15 possible pairs of 6 data types. For each entry, the value of J is written above the letters identifying the two data types whose degree of association is summarized by J. G denotes Bouguer gravity data; M, aeromagnetic data; Se, seismologic data; Sa, salients; T, topographic data; St, pre-Cenozoic structures. For example, in figure 9*A*, structural and aeromagnetic data are highly associated (J=1.00). *A*, Measured widths of anomalies (figs. 2, 7*A*). The median value of J is 0.40. *B*, Minimum widths that are allowed by locational uncertainties of anomaly edges (figs. 5*A*, 7*B*). The median decreases to 0.22. *C*, Maximum allowable widths (figs. 5*B*, 7*C*). The median increases to 0.56. ▶

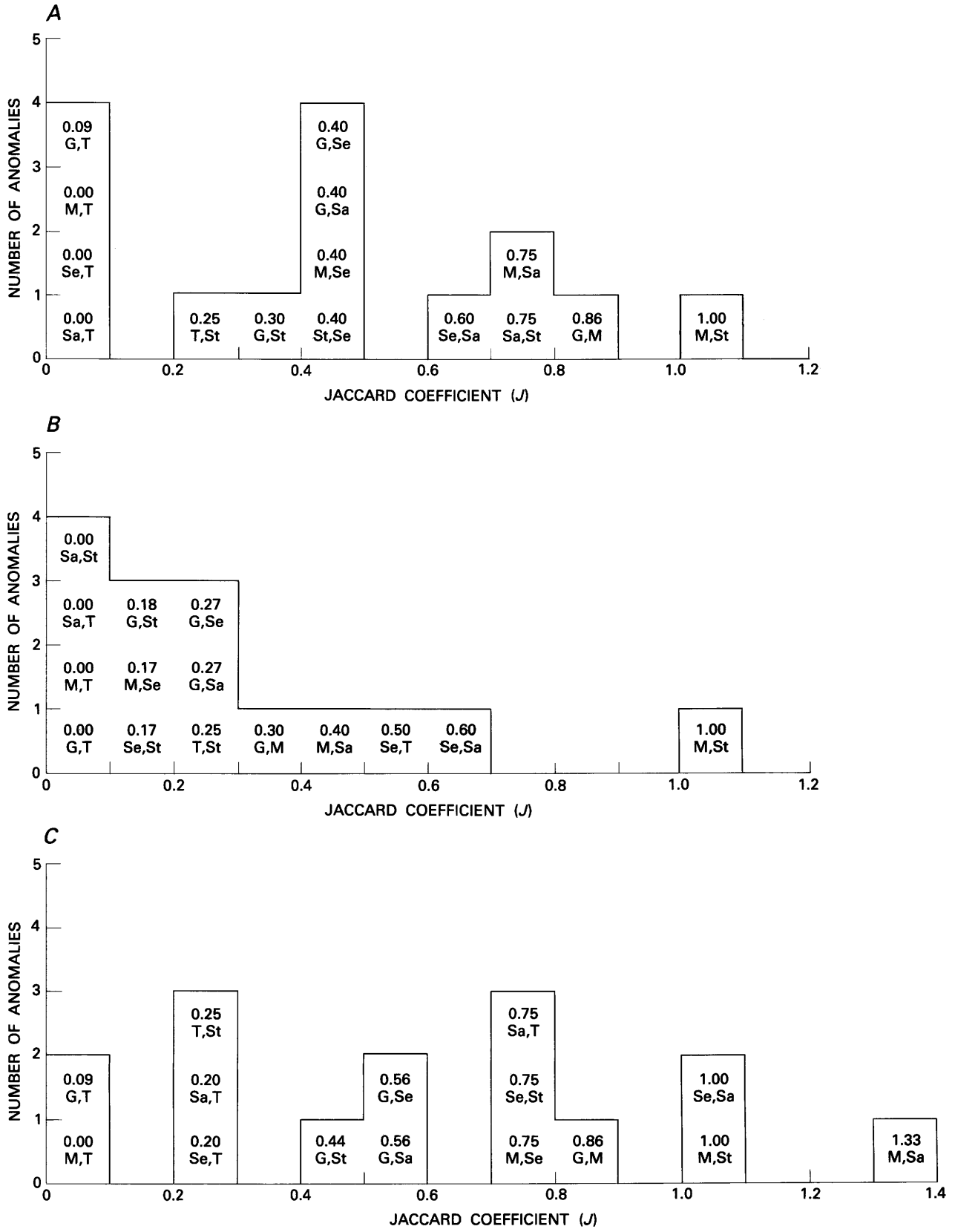
A
NUMBER OF ANOMALIES
0.09 G,T
0.00 M,T
0.00 Se,T
0.00 Sa,T
0.25 T,St
0.30 G,St
0.40 St,Se
0.40 G,Se
0.40 G,Sa
0.40 M,Se
0.60 Se,Sa
0.75 Sa,St
0.75 M,Sa
0.86 G,M
1.00 M,St
JACCARD COEFFICIENT (J)
B
NUMBER OF ANOMALIES
0.00 Sa,St
0.00 Sa,T
0.18 G,St
0.27 G,Se
0.00 M,T
0.17 M,Se
0.27 G,Sa
0.00 G,T
0.17 Se,St
0.25 T,St
0.30 G,M
0.40 M,Sa
0.50 Se,T
0.60 Se,Sa
1.00 M,St
JACCARD COEFFICIENT (J)
C
NUMBER OF ANOMALIES
0.09 G,T
0.00 M,T
0.25 T,St
0.20 Sa,T
0.20 Se,T
0.44 G,St
0.56 G,Se
0.56 G,Sa
0.75 Sa,T
0.75 Se,St
0.75 M,Se
0.86 G,M
1.00 Se,Sa
1.00 M,St
1.33 M,Sa
JACCARD COEFFICIENT (J)

TABLE 3.—*Constancy and fidelity for anomalous and nonanomalous parts of the Wasatch fault zone (measured anomaly widths)*

[—, column not applicable]

Cluster[1]	Part[2]	Data type[3] G	M	Se	Sa	T	St
Presence-absence matrix[4]							
N.....	N1	1	0	0	0	0	0
A.....	A1	1	1	1	1	0	0
N.....	N2	0	1	0	0	0	0
A.....	A2	1	1	1	1	1	1
N.....	N3	0	0	0	0	0	0
A.....	A3	1	1	1	1	0	1
N.....	N4	1	0	0	0	0	0
A.....	A4	1	1	1	1	0	1
N.....	N5	1	0	0	0	1	0
Constancy							
A.....	—	10	10	10	10	2	8
N.....	—	6	2	0	0	2	0
Fidelity							
A.....	—	6	8	10	10	5	10
N.....	—	4	2	0	0	5	0

[1]A is the cluster of four anomalous parts of the fault zone, which are about 70, 130, 160, and 230 km south of the Utah-Idaho border (fig. 7*A*). N is the cluster of five intervening and surrounding nonanomalous parts of the fault zone, including the northern and southern ends.

[2]Part of the fault zone. In each cluster, parts are numbered consecutively from north to south.

[3]G, gravity data; M, aeromagnetic data; Se, seismologic data (epicenters); Sa, salients in fault zone geometry; T, topographic data; St, pre-Cenozoic structures.

[4]1 means that the indicated data type has one or more anomalies in the indicated part of the fault zone. 0 means that no such anomaly is present in the indicated part. Values of entries were determined by inspection of figure 7*A*.

from a population in which anomalies do not tend to coincide more strongly than anomalies of the simulated patterns. Analogously, the alternative hypothesis is that anomalies in the population do tend to coincide more strongly than those in the simulations. Each serial section contains a dashed line, the position and slope of which are calculated from the total counts of m-tuplets in

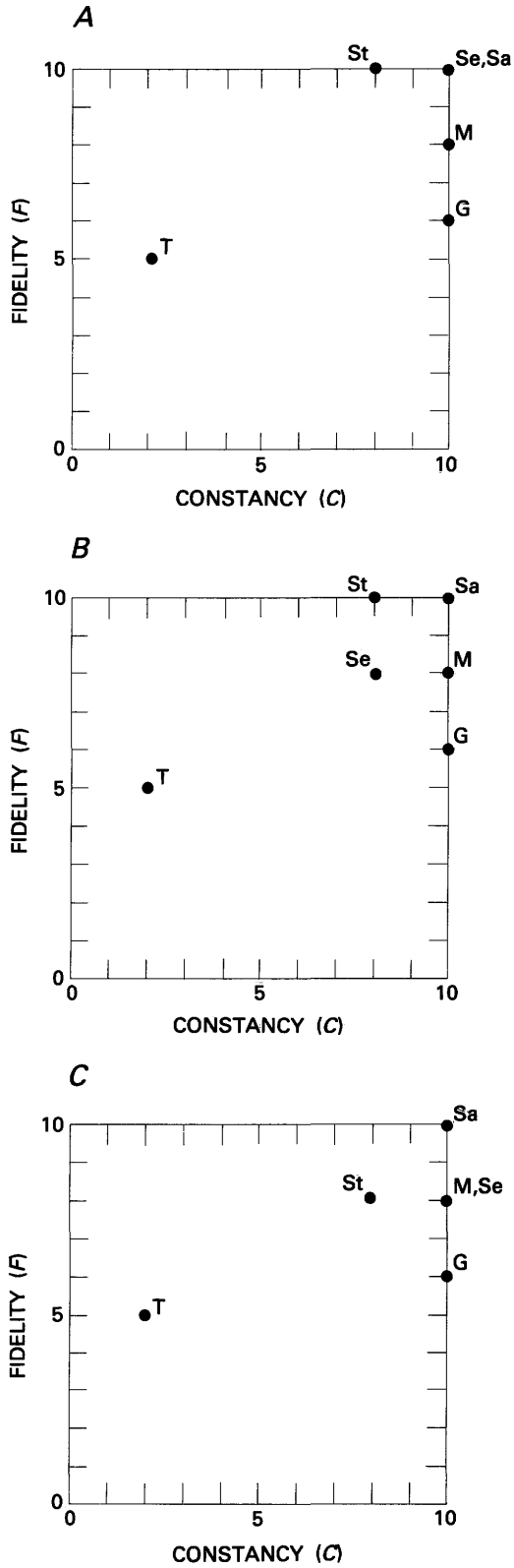

FIGURE 10.—Constancy and fidelity of the six data types in the four anomalous parts of the Wasatch fault zone. High values of constancy C identify data types in which the presence of an anomaly characterizes the cluster of four anomalous parts of the fault zone. High values of fidelity F identify data types in which the presence of an anomaly is diagnostic of the cluster of anomalous parts of the fault zone. G denotes gravity data; M, aeromagnetic data; Se, seismologic data; Sa, salients; T, topographic data; St, pre-Cenozoic structures. *A*, Measured widths of anomalies (figs. 2, 7*A*). Plotted values are from the bottom two parts of table 3. *B*, Minimum widths that are allowed by locational uncertainties of anomaly edges (figs. 5*A*, 7*B*). Plotted values are from tables like table 3 and derived from figure 7*B*. *C*, Maximum allowable widths (figs. 5*B*, 7*C*). Plotted values are derived by a method analogous to that used in figure 10*B*. ▶

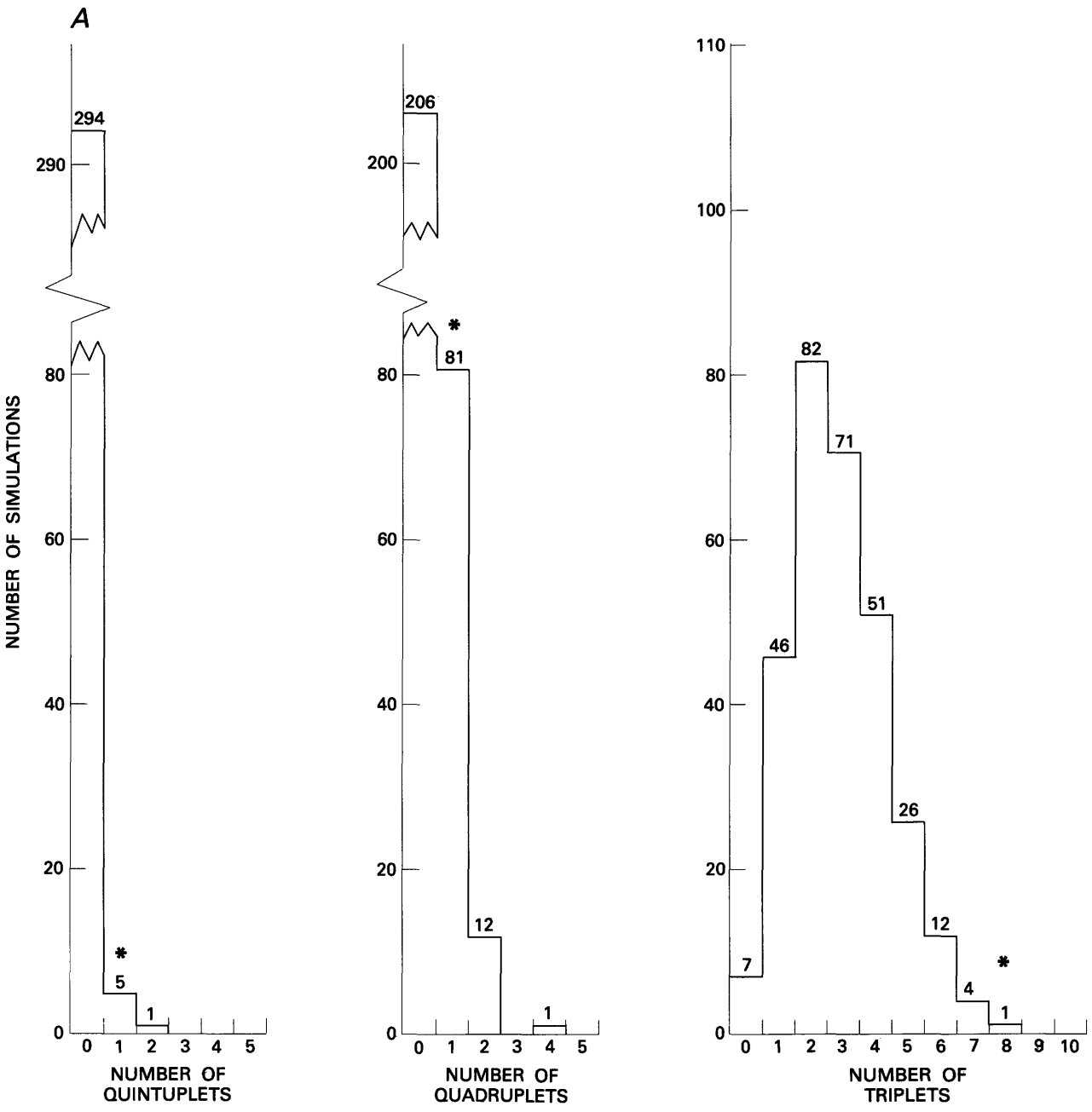

FIGURE 11.—Comparison of numbers of m-tuplets in observed and simulated patterns. Histograms summarize simulated patterns. The number atop each bar shows its height, in numbers of simulations. Asterisks indicate the numbers of m-tuplets in the observed pattern of figure 7. All patterns have had duplicate m-tuplets removed, as they are in table 2. Pairs are ignored. *A*, Measured anomaly widths. 300 simulations. No patterns have any sextuplets or larger m-tuplets. *B*, Minimum widths that are allowed by locational uncertainties of anomaly edges. 300 simulations. No patterns have any quintuplets or larger m-tuplets. *C*, Maximum allowable widths. 100 simulations. No patterns have any m-tuplets larger than sextuplets.

all simulations taken together (table 4) and from the value of k that identifies the serial section (fig. 4) (fig. 10 of Wheeler and Krystinik (1987a) shows equations for the calculations). Any simulated pattern that plots on or outside the dashed line in the appropriate serial section is taken to have anomalies that are at least as strongly coincident as those of the observed pattern. We performed three tests—one each of measured, minimum, and maximum anomaly widths—so, as described previously, we will reject the null hypothesis if $N(e)/N(p)$ is less than 0.0167 for all three tests. $N(p)$ is 300, 300, and 100 for measured, minimum, and maximum widths, respectively. Comparisons of figures 12 and 13 allow counting of $N(e)$. Scale differences preclude combining

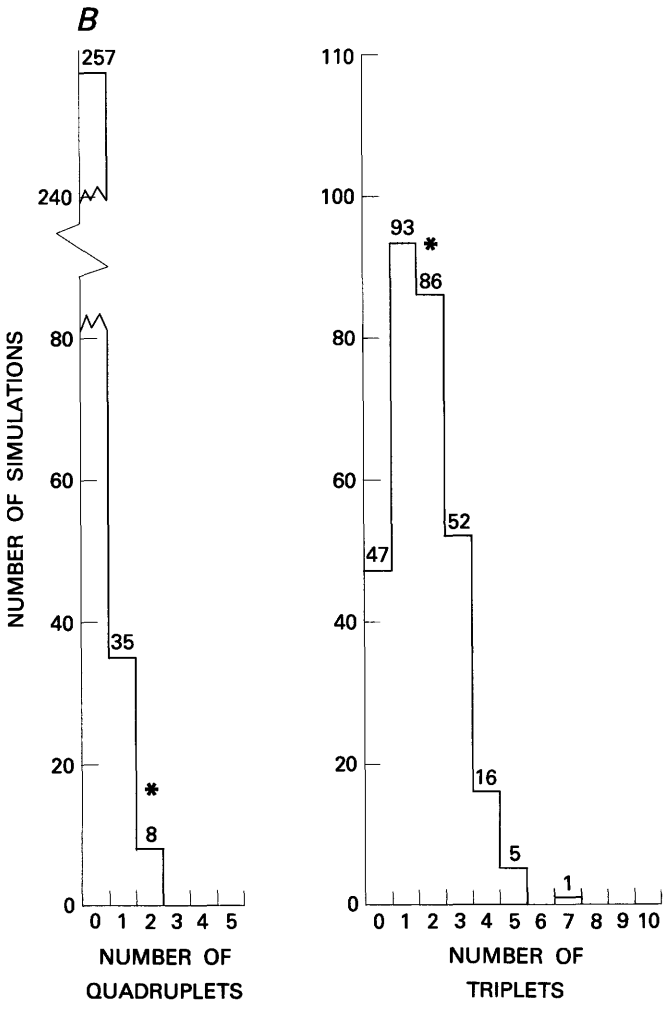

FIGURE 11.—Continued.

figures 12 and 13 without sacrificing needed detail, but the observed pattern is represented in both figures by an asterisk to facilitate comparison.

For measured widths, the upper right-hand cell of figure 12*A* has 5 quadruplets and 10 triplets and would plot at $q=5$, $t=10$ in figure 13*A*. Comparison of the two figures is aided by observing that no simulated patterns can plot above or to the right of this cell in either figure. For $k=0$ (no quintuplets), all simulated patterns plot to the left of the appropriate dashed line and so cannot contribute to $N(e)$. The same is true for the five simulated patterns having $k=1$, all of which have $q=0$. However, the one simulated pattern that has $k=2$ plots at (0,1) (fig. 12*A*), which falls to the right of the appropriate dashed line (fig. 13*A*). $N(e)$ comprises the following contributions: 0 from $k=0$, 0 from $k=1$, and 1 from $k=2$. The level of significance is $1/300=0.0033$. This value is smaller than the prechosen level of significance 0.0167; so, for measured widths, we reject the null hypothesis that the observed pattern has anomalies located by random scattering.

For minimum widths, the dashed line of figure 13*B* passes through the center of the cell (2,2) in figure 12*B*. Because the dashed line slopes steeply down to the right, only two simulated patterns plot in cells whose centers lie to the right of the dashed line (fig. 12*B*). Since $N(e)=2$, the level of significance is $2/300=0.0067$. This value is less than 0.0167, so, for minimum widths, we also reject the null hypothesis.

For maximum widths, the upper right-hand cell of figure 12*C* would plot at $q=10$, $t=15$ in figure 13*C*. The point (10, 15) lies to the left of the dashed lines for $k=0$ and $k=1$ (fig. 13*C*), so, for these two serial sections, no simulated patterns can plot to the right of the corresponding dashed lines or contribute to $N(e)$. For $k=2$, two simulations plot at (0, 3) and (1, 3) (fig. 12*C*). Both points lie to the left of the dashed line for $k=2$ (fig. 13*C*). So far, no serial section has contributed to $N(e)$. However, we consider that the simulated pattern having the sextuplet (fig. 12*C*) has more strongly coincident anomalies than the observed pattern does. Then $N(e)=1$, so the level of significance is $1/100=0.01$. This value is less than 0.0167, so, for maximum widths, we again reject the null hypothesis.

The result of the statistical testing is that, regardless of uncertainties in anomaly widths, the observed pattern contains anomalies that coincide significantly more strongly than we would expect if the anomalies had been scattered randomly along the Wasatch fault zone.

INTERPRETING A SINGLE ANOMALOUS PART OF THE FAULT ZONE

The degree of coinciding among anomalies in the observed pattern is statistically significant because there are unusually many places where unusually many anomalies coincide. All four anomalous parts of the fault zone and all of their component anomalies are required to support this conclusion of significance. No one anomalous part of the fault zone can be singled out as significant in itself. For example, random processes occasionally produced a single quintuplet and commonly produced a single quadruplet (fig. 11*A*). Thus, our analyses allow interpretation of the observed pattern as a whole but not of any one part of it in isolation. Interpretation of a single anomalous part of the fault zone could be based on a geologic description of the history and present state of that part of the fault zone to demonstrate that the individual anomalies coinciding there are genetically linked instead of randomly coincident. Such description and demonstration lie beyond the scope of this report.

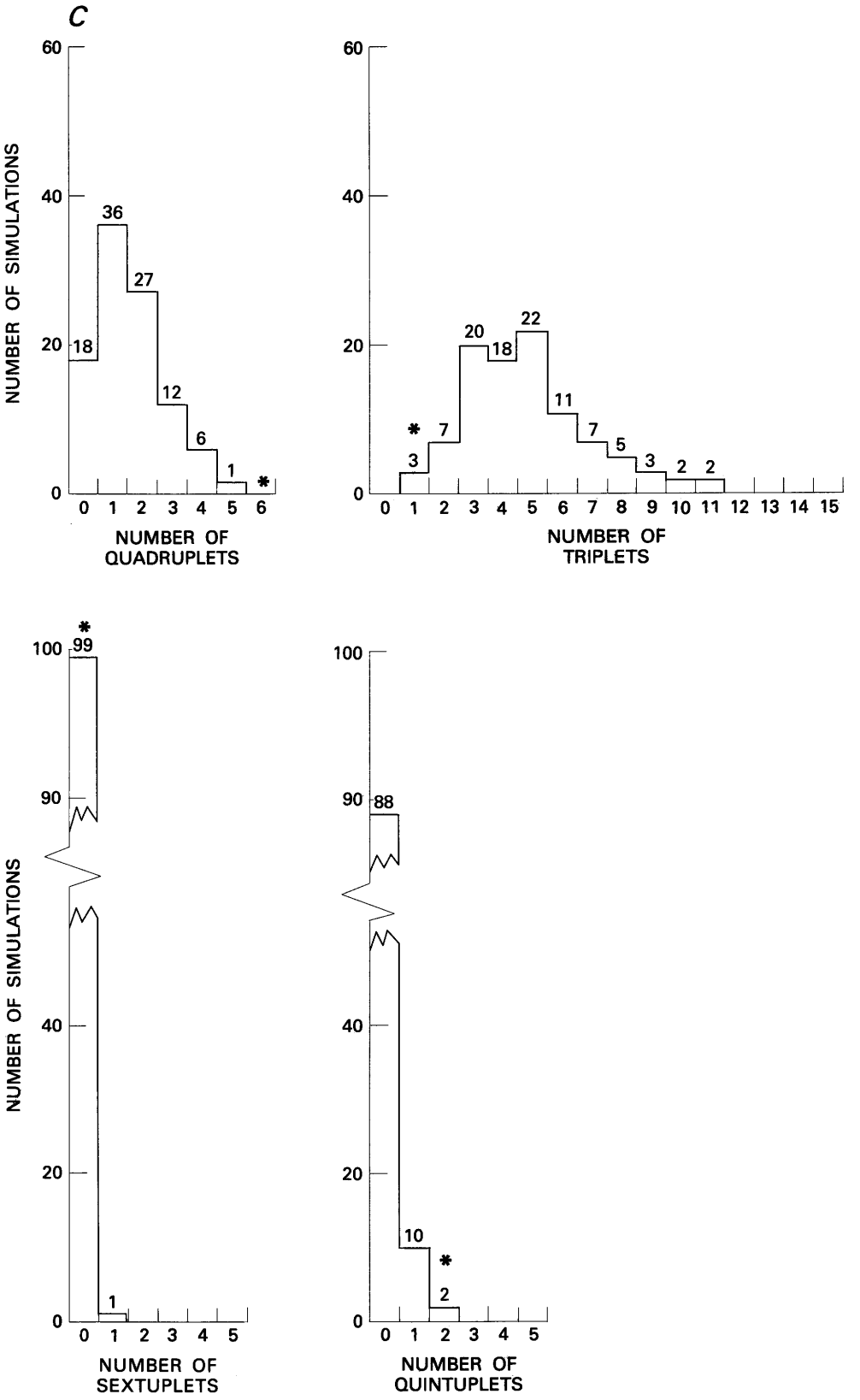

FIGURE 11.—Continued.

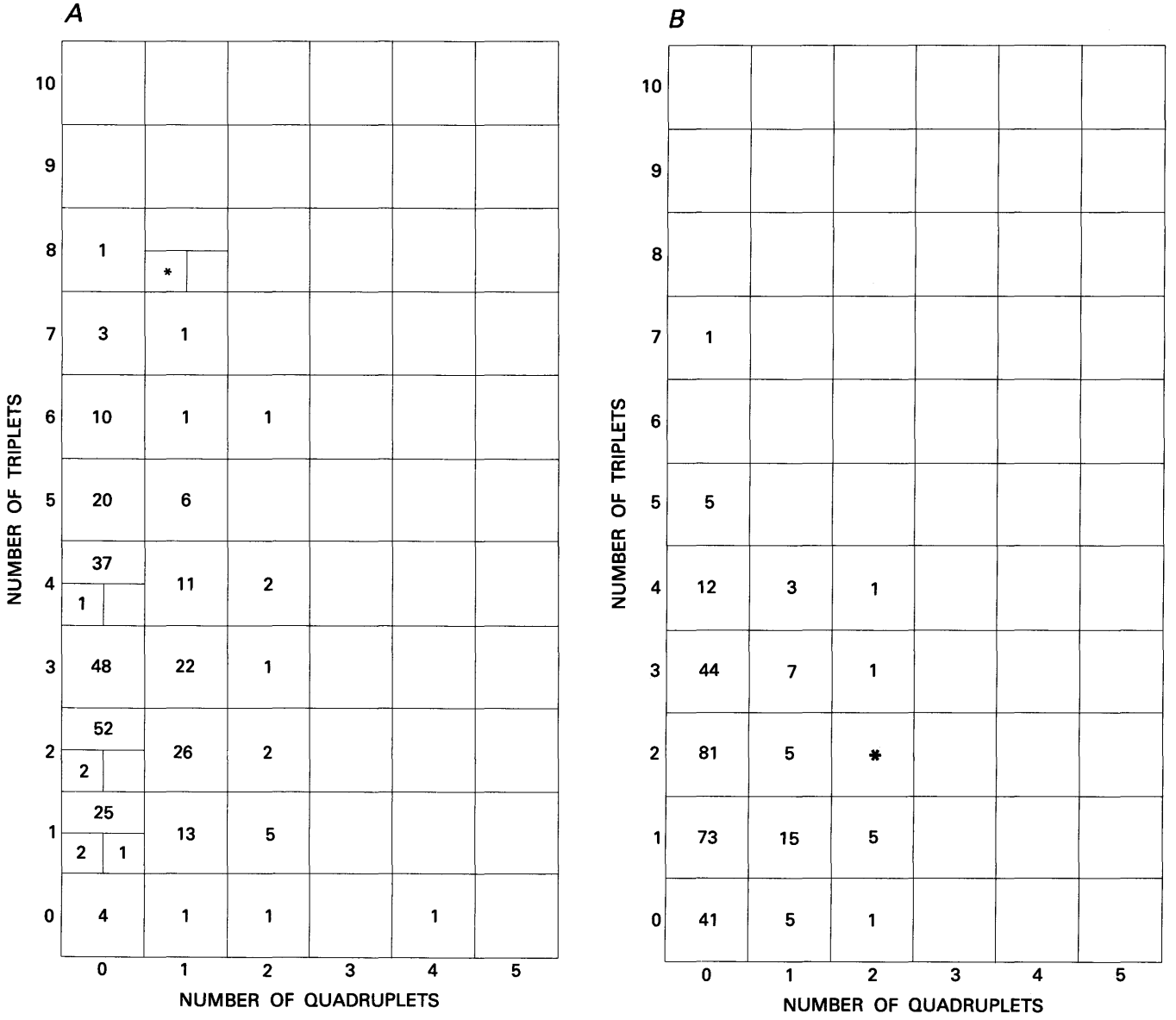

FIGURE 12.—Comparison of numbers of m-tuplets in observed and simulated patterns. Asterisks represent observed patterns. Numerical entries are the numbers of simulated patterns that have the indicated numbers of triplets and quadruplets. Cells that are divided into three subcells record patterns having quintuplets. Upper, lower left-hand, and lower right-hand subcells give the numbers of patterns having zero, one, and two quintuplets, respectively. Zero-valued entries are omitted for clarity. Numbers of quintuplets are plotted along a third axis that rises perpendicularly out of the page. For example, in figure 12*A*, 28 simulated patterns have 1 triplet but no quadruplets; of these patterns, 25 lack quintuplets and plot in the plane of the page, 2 have 1 quintuplet each and plot 1 unit above the page, and 1 has 2 quintuplets and plots 2 units above the page. *A*, Measured anomaly widths. 300 simulations. *B*, Minimum widths that are allowed by locational uncertainties of anomaly edges. 300 simulations. *C*, Maximum allowable widths. 100 simulations. Circled entry at (1, 2) indicates that one of these two simulated patterns also has a sextuplet.

DISCUSSION

SEGMENTED RUPTURES

We have shown that the Wasatch fault zone has been segmented persistently through much of the late Cenozoic. We still need to show that ruptures from large earthquakes on the fault zone are segmented at the same places. The Wasatch Range and San Pitch Mountains and the valleys that border them on the west (fig. 1) form a crustal block that is segmented gravitationally, magnetically, seismologically, and structurally. The Wasatch fault zone, which traverses this block, is itself segmented geometrically by salients. These expressions of segmen-

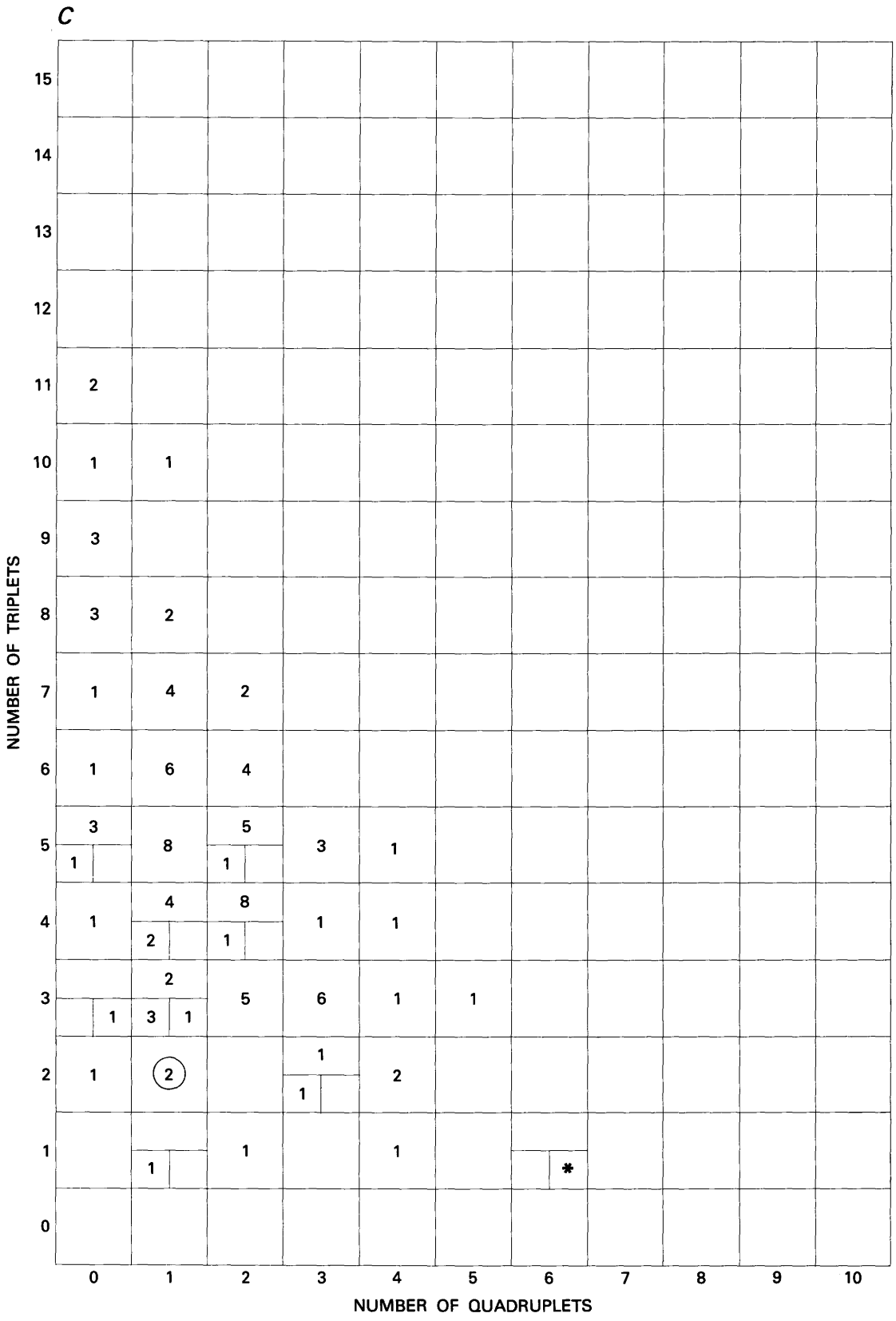

FIGURE 12.—Continued.

TABLE 4.—*Total counts of* m-*tuplets produced by all simulations together*

Width	Triplets	Quadruplets	Quintuplets	Sextuplets
Measured	817	109	7	0
Minimum	517	51	0	0
Maximum	483	155	14	1

tation coincide at salients and only there. We conclude that the coinciding takes place not by chance but because salients have the same cause as the other expressions of segmentation. We consider the salients to be segment boundaries.

The salients have map widths and structural reliefs that are measured in kilometers (Davis, 1983a, b, 1985; Zoback, 1983, fig. 6). Such structural relief presumably accumulated by seismic rupture. The structural relief of a salient is many hundreds to thousands of times larger than the few meters of relief that would be produced by one rupture. For example, values given by Zoback (1983) and Schwartz and Coppersmith (1984) show the salients to have structural reliefs of about 2.6 to 4.0 km, which were produced about 2 m at a time by ruptures recurring at intervals of about 2,000 to 8,000 years. Such structural relief would have taken about 2.6 to 16 m.y. to accumulate, or much or all of the history of the Wasatch fault zone (the past 10 m.y. or more) (Naeser and others, 1983). Thus, the Wasatch fault zone and the rocks adjacent to it are segmented, and this segmentation has persisted through much or all of the fault's evolution.

However, none of the six data types of this report records properties of individual large seismic ruptures or groups of large ruptures. The moderate association of the four segment boundaries with seismological anomalies (figs. 7, 9) indicates that the salients affect the seismicity of the fault zone, at least for the small earthquakes that define the seismological anomalies. However, the segmentation hypothesis of Schwartz and Coppersmith (1984) states that large ruptures will tend to start, stop, or do both at segment boundaries and that no ruptures are likely to cross boundaries into adjacent segments. Results so far are consistent with the possibility that large ruptures might start at salients and propagate in both directions along the fault zone, so that ruptures would span salients and extend simultaneously into both adjacent segments. The nature of the association between the segmented fault zone and the behavior of large seismic ruptures cannot be inferred from information presented so far.

The logical jump from a geometrically segmented fault zone to segmented ruptures requires information about the ruptures. Such information comes from recent U.S. Geological Survey mapping of the late Quaternary history of the Wasatch fault zone (Machette and others, 1986, this volume; Nelson and Personius, 1987; Personius, 1985, 1986; Scott and Shroba, 1985). From field mapping, analyses of profiles of fault scarps, maps of trenches dug across scarps, and related chronological and stratigraphic information, these workers concluded that Holocene and latest Pleistocene surface-rupturing events on the fault zone have been segmented. They infer the existence of 12 segments and subsegments separated by 11 boundaries.

Four of these segment boundaries in Holocene to latest Pleistocene surface ruptures occur at the Pleasant View, Salt Lake, Traverse Mountains, and Payson salients. At these four places where the fault zone is geometrically segmented, the surface ruptures that represent the last few large increments of the fault's growth caused by seismic activity are also segmented. If one assumes that earlier (Pleistocene) surface ruptures behaved like the younger ruptures, then the older ruptures were also segmented at the four salients. We make that assumption and conclude that the four salients of the Wasatch fault zone were persistent boundaries for individual large seismic ruptures through most or all of the evolution of the fault zone.

PERSISTENT AND NONPERSISTENT SEGMENT BOUNDARIES

Three studies have inferred segment boundaries from examinations of geologic records younger than those that we used (fig. 14). Schwartz and Coppersmith (1984) divided the Wasatch fault zone into six segments. Most of their information came from the Holocene record that was exposed in and near trenches at four sites along the fault zone (fig. 1). Maclean (1985) studied morphology and morphometry of 98 drainage basins that evolved throughout the Quaternary in the footwall of the fault zone. For this time span, Maclean (1985) and Mayer and Maclean (1986) divided the fault zone into nine segments. M.N. Machette and his coworkers have mapped and examined the late Quaternary history of the fault zone. Their partly published studies cover nearly all the length of the fault zone in Utah and record numerous aspects of the single- and multiple-event scarps that form the most striking expression of the late Quaternary seismic history of the fault zone. They divided the fault zone into 10 segments, 8 of which and a part of a ninth are within the area covered by this study. The nine late Quaternary segment boundaries of Machette and others (this volume) represent the most complete and uniform description of segmentation of the last few large seismic ruptures on the various parts of the fault zone.

Each of these three studies of a young geologic record recognized the four persistent segment boundaries, although Schwartz and Coppersmith (1984) did not iden-

tify the Pleasant View boundary (fig. 14). Each study also interpreted several additional segment boundaries. Agreement on these other boundaries, however, was much poorer than it was on the four persistent boundaries. Other boundaries were inferred at eight or nine places in the study area, but only two or three of these boundaries were chosen by two of the three studies, and none was chosen by all three (fig. 14).

Our preferred interpretation of these discrepancies is that most represent real changes through time instead of error by one or more studies, including ours. A segment boundary that is recognized in one young geologic record but not in another and not in the pre-Quaternary record might be nonpersistent. A nonpersistent boundary is one that nucleates or stops several successive seismic ruptures but that does not do so before or after the time spanned by these several ruptures. The location, time of turning on, and duration of a nonpersistent boundary might be controlled by older structures, but this control might be so subtle or complex that it cannot be distinguished from the operation of random processes. Then the location, appearance, and disappearance of a nonpersistent boundary could be observed but not predicted.

A useful guide to considering these hypothetical nonpersistent boundaries is the idea of nonconservative barriers (King, 1983; King and Yielding, 1984; King and Nabelek, 1985). Faults contain geometric irregularities such as bends, forks, and bumps. Where an irregularity is extreme enough that the orientation of the slip vector cannot be conserved across it, the irregularity is a nonconservative barrier. Geometric consequences of this change in slip vector orientation cause ruptures to tend to start and stop at nonconservative barriers. Bruhn and others (this volume, 1987) analyzed the Salt Lake and Traverse Mountains salients and interpreted them as nonconservative barriers. Nelson and Personius (1987) interpreted the Pleasant View boundary similarly. Geometric irregularities such as salients are large enough and extreme enough that they likely will endure considerable slip and likely will persist through much or all of the history of a fault zone like the Wasatch. Narrower forks, gentler bends, and smaller bumps might force the slip vector to change orientation across them for a few successive ruptures but then might be smoothed out by abrasion of the bumps and insides of the bends and by abandonment of one branch of each fork. Such lesser geometric irregularities could be formed where lithology, strength, and other rock properties vary along the fault zone. The interactions of these lesser variations with the rupture processes are likely to be complex enough that nonpersistent boundaries could appear to be scattered randomly along the fault zone and to form and disappear randomly through the history of the fault zone. The idea of nonconservative barriers suggests reasonable explanations for the appearance and disappearance of a nonpersistent boundary, for its expected duration over several successive ruptures, and for any inability to predict its location, time of appearance, or duration.

If nonpersistent boundaries exist, as they appear to, they would pose a problem for hazard evaluation. The past behavior of a persistent boundary is a guide to its likely behavior in the coming decades to millenia, which is the time span of interest to hazard evaluation. A nonpersistent boundary might be the starting or ending point of a rupture, might limit the maximum length of a rupture and therefore the maximum size of the earthquake, or might do neither, without much regard for the recent behavior of the boundary. It is fortunate that most recent boundaries appear to be persistent (three of four) in the populous central part of the Wasatch Front between Brigham City and Provo (fig. 14). Most of the suggested boundaries that might be nonpersistent are farther north or south, where fewer people and engineered structures are at risk.

BEDROCK RIDGES

Each salient coincides with one or two transverse gravity anomalies (fig. 7*A*). Although each transverse gravity anomaly is built up from several components (gradients and their ends, the ends of elongate highs and lows, and the like), each also has the general form of a gravity saddle—a local interruption in the long gravity low that trends northward along the western side of the Wasatch fault zone (Zoback, 1983). Four of the five saddles having the greatest gravity relief are those that coincide most closely with the salients—transverse anomalies G4, G5, G7, and G9 (fig. 7*A*). Zoback (1983), Mabey (this volume), and we interpret each gravity saddle as the expression of a bedrock ridge, partially or wholly buried by the low-density Cenozoic fillings of the valley basins that underlie the north-trending gravity low. The bedrock ridges trend across the north-trending basins, so that the gravity saddles mark places where the basins are less deep than they are under the adjacent valleys to the north and south. Because the basins formed by slip on the Wasatch fault zone, the gravity saddles also mark places where structural relief and the accumulated slip that created the relief are less than they are to the north and south.

The Traverse Mountains segment boundary is the clearest example of a bedrock ridge and its gravity expression (fig. 15). The ridge, partially exposed as the eastern Traverse Mountains, is at least partly bounded by faults that have slipped during the Quaternary, as the Wasatch fault zone has. The isogals show that the bedrock ridge extends across the valley, although the western part of the ridge is buried. Structural relief on

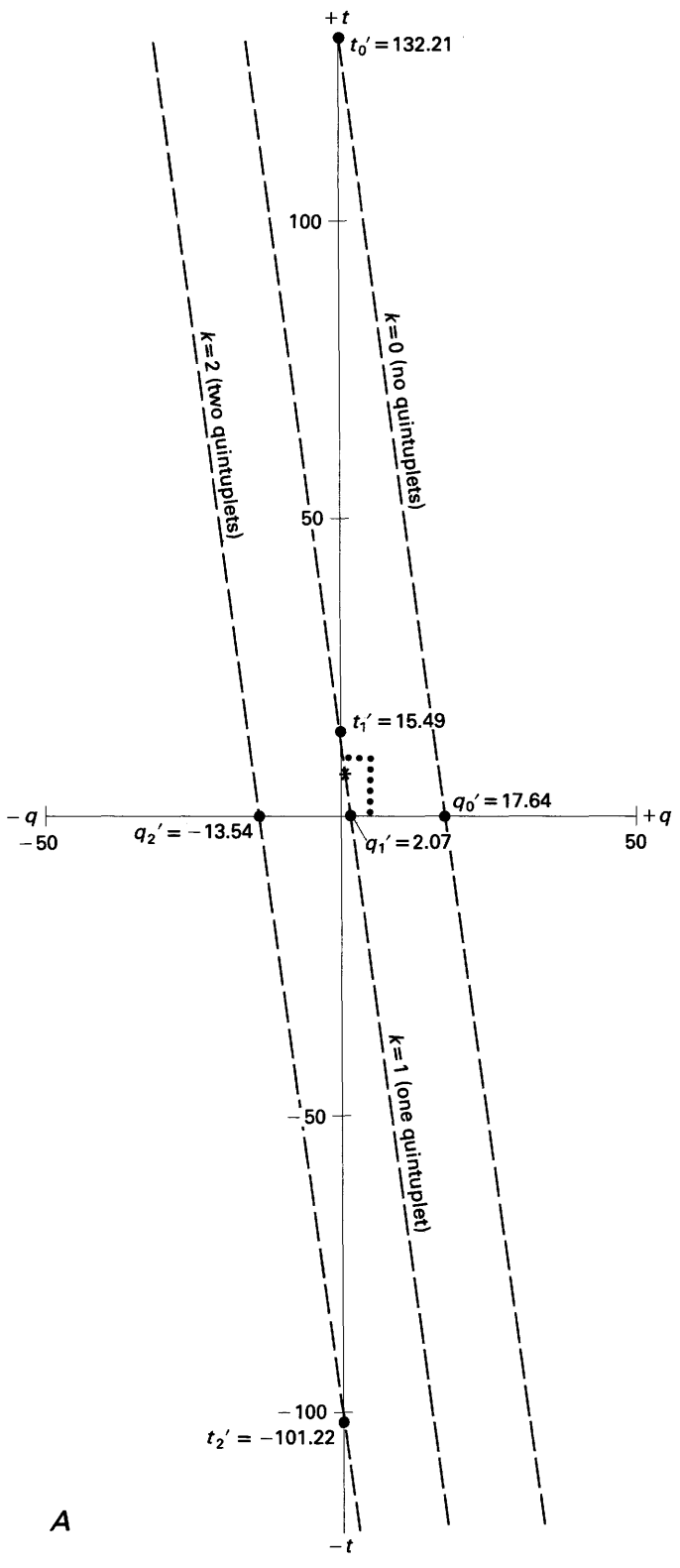

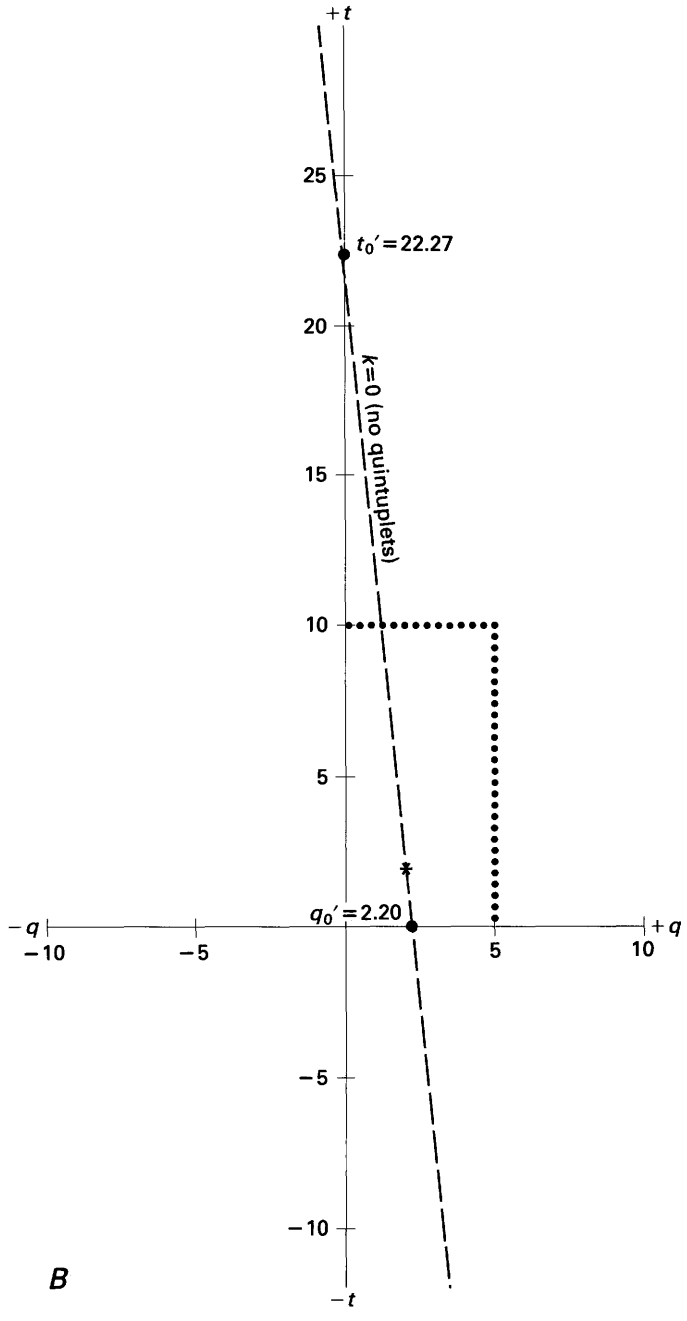

FIGURE 13.—Summaries of serial sections (like the one shown in fig.4). In notation similar to that of Wheeler and Krystinik (1987a), the number of quadruplets per pattern is q, and the number of triplets is t. Dashed lines are traces of significance plane S′ (fig. 4), for various numbers (k) of quintuplets per anomaly pattern. Locations of intercepts q_k' and t_k' are shown by solid circles. To aid comparisons with figure 12, values of intercepts are written near these solid circles; asterisks represent the observed pattern, and the top and right-hand edges of corresponding parts of figure 12 are shown by dotted lines. *A*, Measured anomaly widths (compare with fig. 12*A*). Observed pattern has eight triplets, one quadruplet, and one quintuplet. *B*, Minimum widths that are allowed by locational uncertainties of anomaly edges (compare with fig.12*B*). The observed pattern has two triplets and two quadruplets. No simulated or observed pattern has any quintuplets, so only the dashed line for $k=0$ is shown. *C*, Maximum allowable widths (compare with fig. 12*C*). The observed pattern has one triplet, six quadruplets, and two quintuplets.

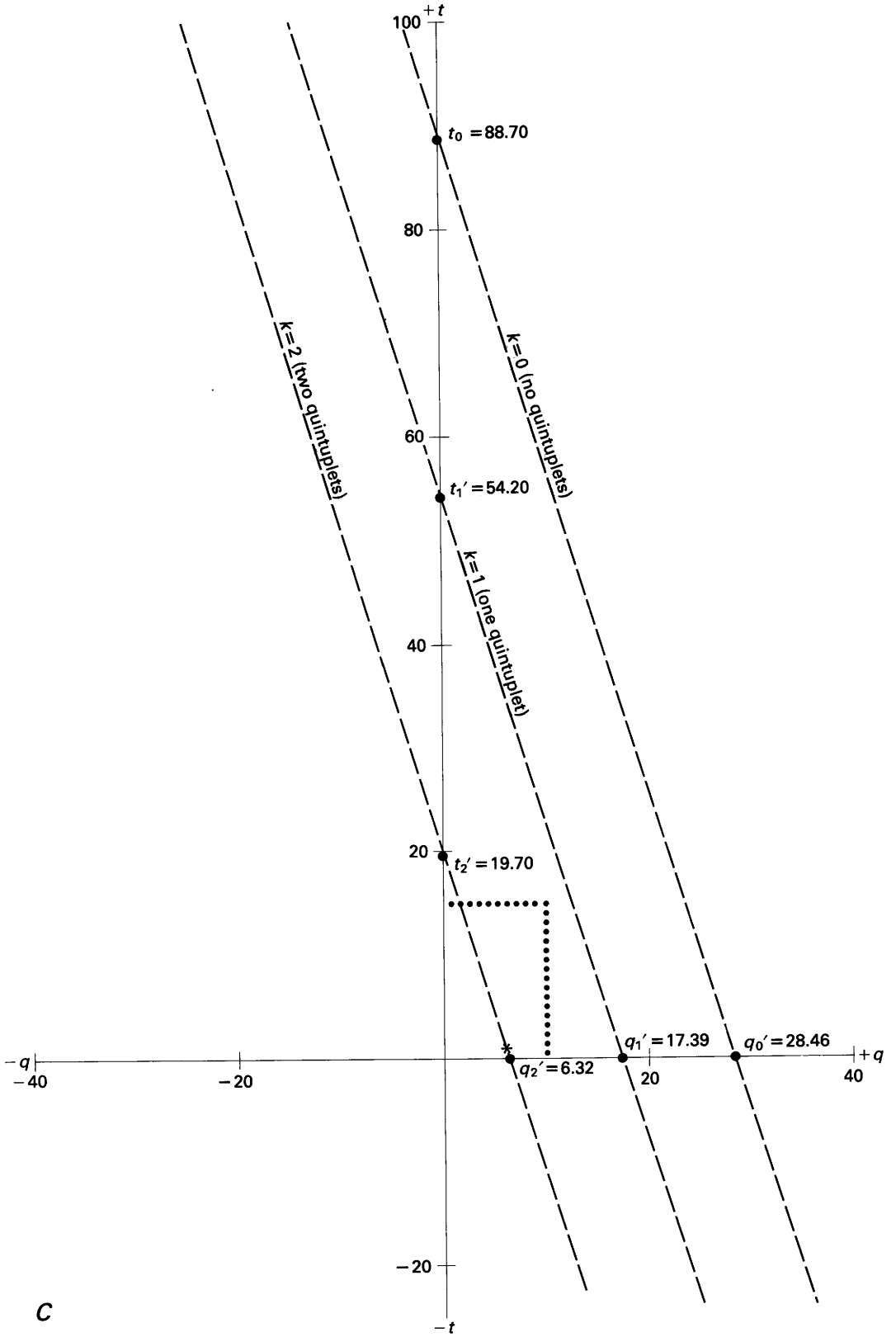

FIGURE 13.—Continued.

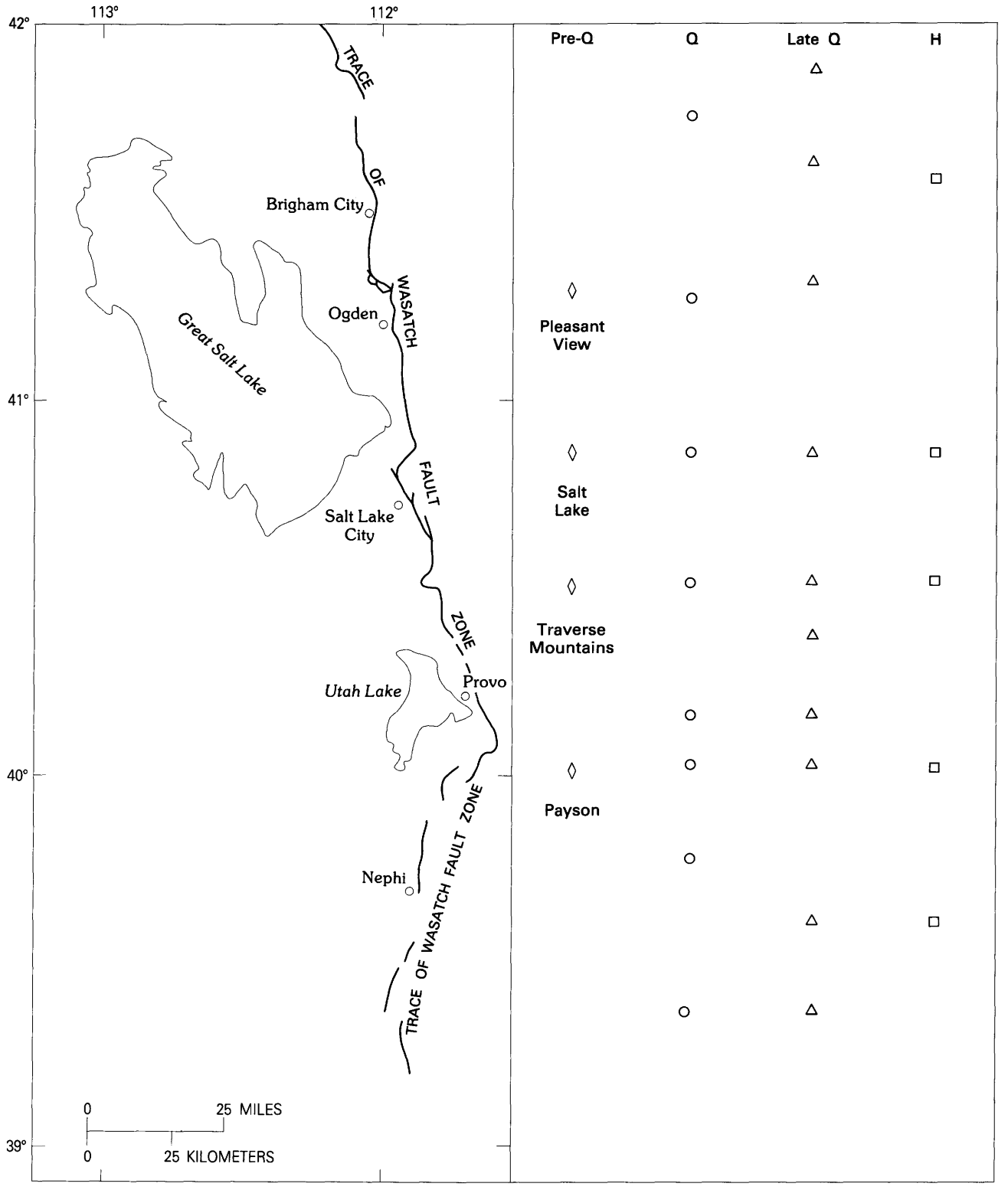

the Wasatch fault zone is much less at the ridge than it is in Salt Lake or Utah Valleys. The relief between the salient and the bottoms of both valleys is partitioned among a network of extensional faults, including the normal fault that separates the salient from the Traverse Mountains (fig. 15), normal faults that are mapped within the eastern Traverse Mountains (Davis, 1983b), normal faults that are mapped as separating the Traverse Moun-

◀ FIGURE 14.—Four sets of segment boundaries for the Wasatch fault zone, derived from different parts of the geologic records. The right-hand side of the figure shows different symbols placed at the latitudes of the suggested boundaries. Four diamonds show names boundaries from this report. The geologic record that we examined to define these boundaries is mostly pre-Quaternary (pre-Q), although we also used earthquake epicenters from 1962 through 1986. Eight circles show segment boundaries proposed by Maclean (1985) and Mayer and Maclean (1986), which are based on the Quaternary (Q) record. Ten triangles locate boundaries determined by M.N. Machette, A.R. Nelson, S.F. Personius, and W.E. Scott (written communs., cited by Anderson, 1985, 1986), Machette and others (1986, this volume), Nelson and Personius (1987), Personius (1986), and Machette, Personius, Scott, and Nelson (written commun., 1986). These boundaries are based on the late Quaternary (late Q) record. An eleventh boundary is north of our study area. Five squares show Schwartz and Coppersmith's (1984) boundaries, which are based mostly on the Holocene (H) record.

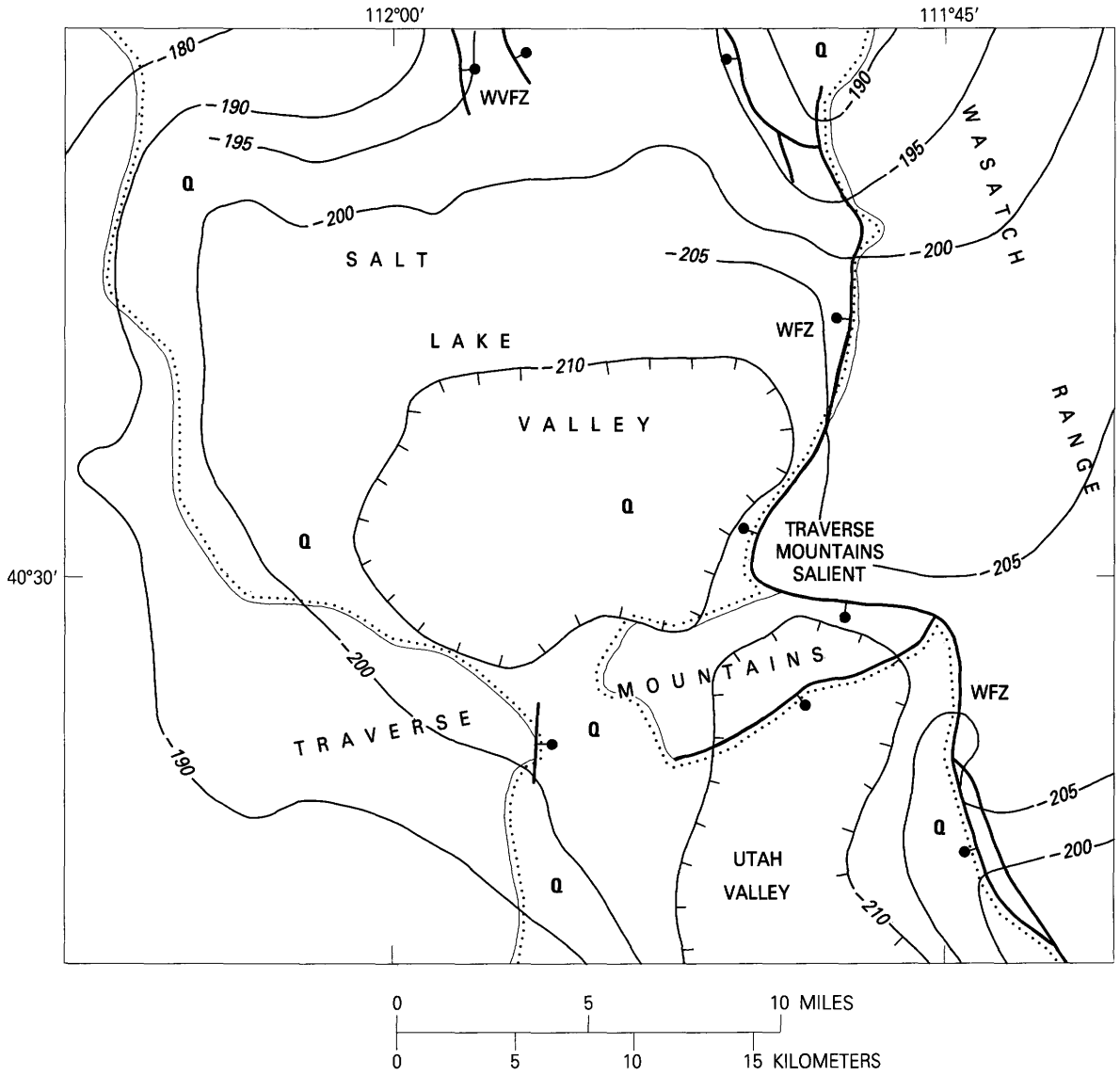

FIGURE 15.—Segment boundary at the Traverse Mountains salient. Heavy lines represent traces of normal faults exhibiting Quaternary or probable Quaternary slip, simplified from Davis (1983b), Scott and Shroba (1985), Keaton and others (1987), and M.N. Machette (oral and written communs., 1987). Bar and ball identify the downthrown side of each fault. Dotted lines show contacts between Quaternary valley-filling sediments (Q) and pre-Quaternary bedrock (dots on Quaternary side of contact) (simplified from Hintze (1980) and Zoback (1983, fig. 4)). Contour lines are selected isogals of the Bouguer gravity field, traced from Zoback (1983, fig. 4). The contour interval is 5 mGal near the northern and eastern edges of map and 10 mGal elsewhere. Single hachures point inward on the lowest contours around local gravity minima. WFZ, Wasatch fault zone; WVFZ, southern end of West Valley fault zone of Keaton and others (1987).

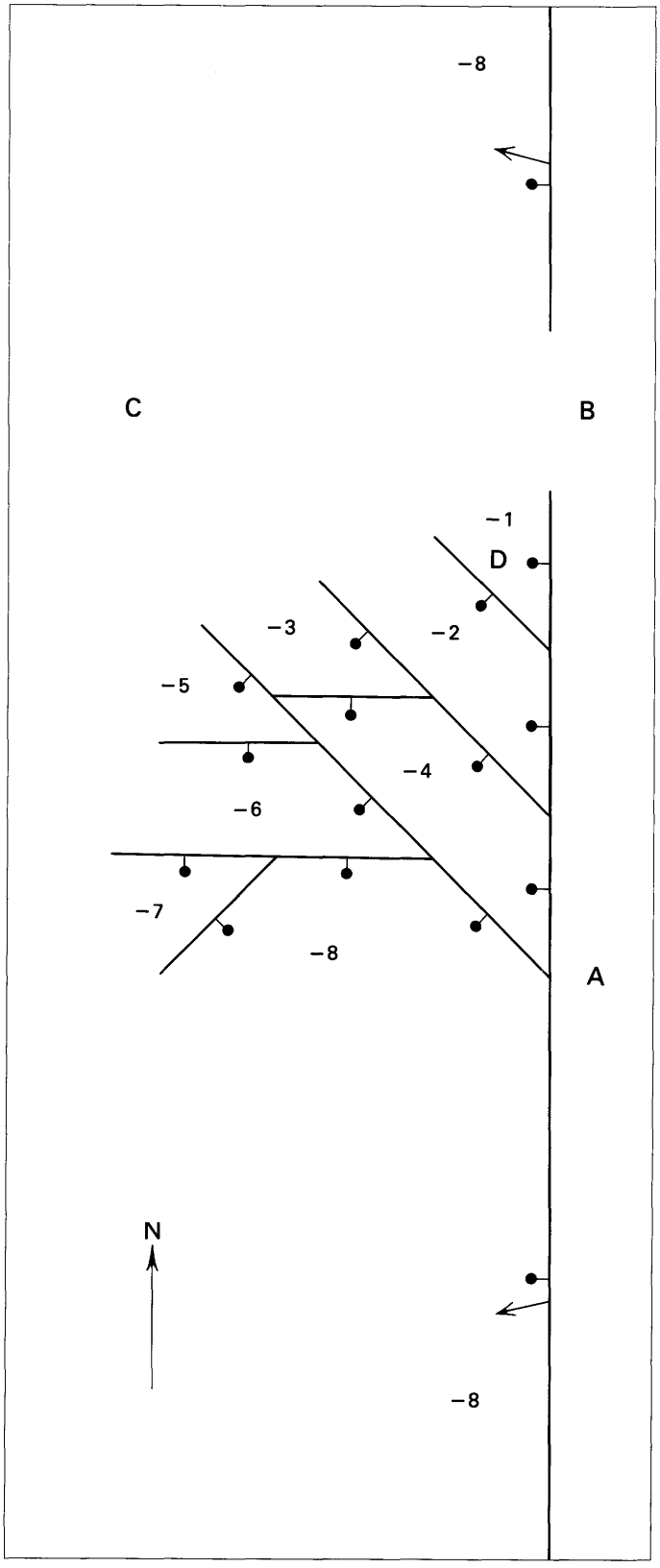

tains from Utah Valley (fig. 15) and are inferred to do the same at Salt Lake Valley (Mattick, 1970; Houghton, 1986, p. 52), and perhaps still other normal and normal-oblique faults that underlie the east-trending gravity gradients at the northern end of Utah Valley and the southern end of Salt Lake Valley. For example, Okaya and Thompson (1985) described three buried normal-faults that step down into the deepest part of a graben and that underlie a gravity gradient in the Dixie Valley of Nevada.

Two processes can explain the observed association of salients with bedrock ridges and small structural relief across the Wasatch fault zone. The first process arises from the requirement that slip for any earthquake must decrease to zero at the edges of the rupture zone. King (1986) postulated that slip measured along the ground rupture of a single earthquake will be largest in the middle and will taper toward the ends of the ground rupture, so that the ends will have a slip deficit in comparison with the middle portion. Measurements on historical ground ruptures of large, normal-faulting earthquakes in and near the Basin and Range province show much local variation along the ruptures but, in general, support King's postulate (Byerly, 1956; Tocher, 1956; Slemmons, 1957; Slemmons and others, 1959; Myers and Hamilton, 1964, pl. 2; Crone and Machette, 1984; Wallace, 1984, fig. 28). Large ruptures on normal faults will tend to have ends (that is, to start, stop, or do both) at persistent segment boundaries, so that, over time, these boundaries will accumulate large slip deficits in comparison with the slips in segment interiors. The slip deficits will be expressed as structural reliefs across the fault zone that are smaller at the boundaries than they are in segment interiors.

The second process is implicit in the model of a nonconservative barrier (King and Nabelek, 1985). Imagine a simple, planar, normal fault zone that strikes north, dips west, and slips an arbitrary eight units (fig. 16). For simplicity, we ignore slip tapering toward rupture ends. Tapering of slip only accentuates the result described later. Suppose that two strands within the fault zone rupture toward each other, not necessarily simultaneously, with slightly divergent slip vectors. Convergent slip vectors would produce a more complex but otherwise similar result. The divergence causes

◀ FIGURE 16.—Fault network (process zone) in a hypothetical nonconservative barrier on a normal fault. Solid lines represent traces of faults; bar and ball are on the downthrown side of each fault. Arrows show trends of slip vectors. Numbers give structural elevations (in arbitrary units) with respect to zero elevation of the eastern wall of the main (north-striking) fault strand. A identifies a fork in the fault trace; B and C, two ends of a bedrock ridge; D, a small fault block (all are discussed in the text).

extension in the hanging wall at the northern end of the southern rupture; arguments analogous to those that follow apply to the southern end of the northern rupture. The southward extension in the hanging wall can be accommodated if the northern end of the main fault strand forks at, say, 45° to the northwest (loc. A, fig. 16). Suppose that the two forks share equally the slip on the single fault strand, so that each branch of the fork slips four units. The geometric requirements of brittle slip force each branch to fork again and so on, down to sizes at which the rock mass no longer acts like distinct rigid blocks (King, 1983). After three forkings, the northern end of the hanging wall is broken into blocks that step downward to the south and west (fig. 16) and form a fault network that is the process zone of the nonconservative barrier (King and Nabelek, 1985). Structural relief of the blocks in the hanging wall decreases northward and eastward across the fault network. If a similar thing happens at the southern end of the northern rupture, the result is a ridge that plunges westward across the barrier, from B to C in figure 16. Slip taper will decrease the westward plunge of the ridge. If the barrier is a persistent segment boundary, then over the course of many ruptures, the ridge will increase its structural relief in comparison with adjacent parts of the footwall.

Suppose that sediment accumulates on the down-dropped blocks, as it has in Salt Lake and Utah Valleys (fig. 15). If the fault pattern of figure 16 were buried to level −0.5, halfway between the top of block D and the top of the footwall block, the result would be a buried bedrock ridge. The low-density sediments would be thinner over the ridge than they would be in the valleys to the north and south, and a gravity saddle would be created. If sediment cover reached only to level −1.5, the eastern fault-bounded end of the ridge would be exposed as a salient like the Pleasant View and Salt Lake salients or like the eastern Traverse Mountains. If cover were thinner still, reaching to levels between −5.5 and −7.5, an exposed bedrock ridge would separate the two valleys, as one does west of the Payson salient (Hintze, 1980).

Consideration of figure 16 suggests a way to estimate the relative persistence of some segment boundaries, averaged over the whole history of the fault zone. If the boundary is perfectly persistent, the fault must end there. If the boundary is so persistent that few ruptures cross it, block D of figure 16 will have no throughgoing fault of large throw on its eastern side and might be part of the footwall block. A bedrock ridge will be exposed across most or all of the valley. This situation occurs at the Traverse Mountains salient (fig. 15), which is cored by the massive Little Cottonwood stock of Oligocene age (Crittenden and others, 1973). If more ruptures cross the boundary, they will tend to drop block D down a bit more in comparison with the footwall, but the bedrock ridge might still be exposed. Both occurrences are present at the Payson salient (Davis, 1983b; Machette and others, this volume). As successively larger proportions of the ruptures cross the boundary, the bedrock ridge will first be buried (as it is at the Salt Lake salient) (Davis, 1983a), then the salient itself will be buried or nearly buried (as it is at the Pleasant View salient) (Crittenden and Sorenson, 1985), and, finally, the gravity saddle will flatten and nearly disappear at boundaries that persist for only a few successive ruptures.

Thus, on the Wasatch fault zone, the most obvious expression of a persistent segment boundary is an exposed salient, but the key to estimating the relative persistence of several boundaries is the relative sizes of the structural reliefs between footwall, salient, bedrock ridge, and adjacent valley bottoms. For segment boundaries of intermediate persistence or for boundaries that have been persistent for only the most recent portion of a fault's history, bedrock ridges might be more diagnostic than salients. Where Bouguer gravity data are abundant, as they are along the Wasatch Front, relative structural relief can be estimated easily, but, along other fault zones where gravity coverage is sparse or nonexistent, relative structural relief must be estimated indirectly.

APPLICATIONS TO LARGE HISTORICAL EARTHQUAKES

The conclusion that bedrock ridges and salients, where coincident with the ends of large individual ruptures, identify persistent segment boundaries on the Wasatch fault zone can be generalized to other normal fault zones in and near the Basin and Range province. We test the generalization by examining the ends of ground ruptures from single large historical earthquakes.

BORAH PEAK, IDAHO—OCTOBER 28, 1983

Crone and others (1987) summarized evidence that the two ends of the main shock rupture zone of the 1983 Borah Peak, Idaho, earthquake occurred at persistent boundaries of the Thousand Springs segment of the Lost River fault zone (fig. 17). At the southeastern boundary, here named the Elkhorn Creek segment boundary, the fault zone cuts the older Borah Peak horst. Geologic mapping and a gravity saddle indicate that the horst extends as a bedrock ridge southwest to the main shock epicenter (Skipp and Harding, 1985). Crone and others (1987) suggested that the horst and its faults extend to the depth of the main shock hypocenter (about 15 km) (Doser, 1985a; Dewey, 1987), because some of the faults have up to 3 km of throw and because a similar horst

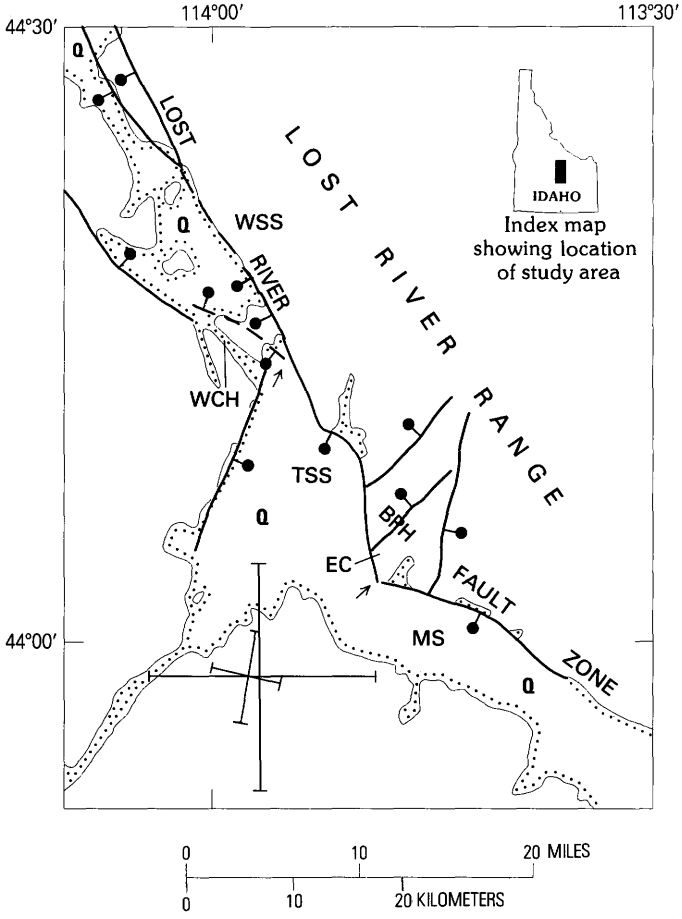

FIGURE 17.—October 28, 1983, Borah Peak, Idaho, earthquake. Heavy lines show ground ruptures from the normal-faulting earthquake; bar and ball are on the downthrown side of each rupture. Solid lines show continuous surface ruptures; dashed lines show discontinuous ruptures. Red lines represent older normal faults. Thin lines show contacts between Quaternary sediments (Q) in valleys and pre-Quaternary bedrock (dots on Quaternary side of contact). Two crosses show the epicentral locations of the main shock and the locational uncertainties of two independent workers (large cross, Richins and others (1987, table 2, p. 704); small cross, Dewey (1987, table 1)). WSS, Warm Spring segment of the Lost River fault zone; TSS, Thousand Springs segment; MS, Mackay segment; WCH, Willow Creek Hills; EC, Elkhorn Creek; BPH, Borah Peak horst; two small arrows, boundaries of TSS. Inset shows the location of the map area within Idaho. Simplified from Bond (1978), Skipp and Harding (1985), and Crone and others (1987).

about 25 km to the south is cored by an Eocene pluton. Surface faulting in 1983 followed Holocene scarps along the Thousand Springs segment (Crone and Machette, 1984). A gap of 4 km separates that faulting and those scarps from evidence of recurrent late Quaternary surface faulting along the entire length of the Mackay segment, an indication that at least two pre-1983 ruptures also had ends at the Elkhorn Creek boundary. About 5 to 10 mGal of gravity relief across the gravity saddle from northwest to southeast (Skipp and Harding, 1985) indicate that many ruptures have had slip deficits, and presumably ends, at the boundary during the evolution of the Lost River fault zone.

At the northwestern boundary of the main rupture zone, here named the Willow Creek Hills segment boundary, a bedrock ridge is exposed most of the way across the valley. Zones of small, discontinuous surface offsets and cracks fork to extend northwestward into the bedrock ridge and northward along the Warm Spring segment. However, the main rupture was confined to the Thousand Springs segment, as determined from geologic (Crone and Machette, 1984), geodetic (Barrientos and others, 1987), and seismological (Doser and Smith, 1985) evidence. The 1983 rupture of the Thousand Springs segment repeated an early Holocene (Hanks and Schwartz, 1987) rupture of the same segment with striking fidelity (Salyards, 1985; Vincent, 1985; especially Schwartz and Crone, 1985). The Warm Spring segment ruptured at about the same time in the early Holocene or more recently, but neither Holocene rupture broke the Willow Creek Hills boundary (Crone and others, 1987). The exposed bedrock ridge indicates that many previous ruptures behaved similarly. Structural relief across the Lost River fault zone there is about half that in the interior of the Thousand Springs segment (Crone and others, 1987).

Thus, both boundaries of the main 1983 rupture have been persistent, and both form bedrock ridges like those along the Wasatch fault zone. There is no fault-bounded salient at the Willow Creek Hills boundary. At the Elkhorn Creek boundary, the sharp bend in the Lost River fault zone is much less sharp than the bends in the Wasatch fault zone at the Salt Lake, Traverse Mountains (fig. 15), and Payson salients but resembles in shape the bend at the Pleasant View salient (Crittenden and Sorensen, 1985). The corner of the footwall block at Elkhorn Creek is broken by several small faults (Susong and Bruhn, 1986) and, in this respect, has a structural character between the unfaulted Traverse Mountains salient (fig. 15) and the moderately faulted Payson salient (Hintze, 1980). The Pleasant View and Salt Lake salients are separated from the main footwall block by normal faults of much larger throw. We choose not to call the bend at Elkhorn Creek a salient because doing so would stretch the term beyond the limit of usefulness.

Both boundaries have been interpreted as barriers to the propagation of the rupture zone (Boatwright, 1985; Crone and others, 1985). We further interpret both as nonconservative barriers. Slip-vector orientations are too sparse to determine whether orientations change across either boundary (A.J. Crone, oral commun., 1987), as Bruhn and others (1987, this volume) have done for the boundaries of the Salt Lake segment. However, at the Elkhorn Creek boundary, many ruptures have had

ends at about the same place, including at least the last three ruptures. The northeast-striking normal faults of the Borah Peak horst form a network with the northwest-striking Lost River fault zone. Within the bend in the range front, the Lost River fault zone expands into a skein of northwest-striking fault strands that cut diagonally across the bend; some of those strands were reactivated in 1983 (Susong and Bruhn, 1986). The 1983 rupture started at the horst and propagated unilaterally northwestward. Crone and others (1987, p. 763) speculated that the faults of the horst "...could create irregularities or obstructions on the Lost River fault plane that might inhibit propagating ruptures...." All of these characteristics are properties that would be expected of a nonconservative barrier (King and Nabelek, 1985).

At the Willow Creek Hills boundary, at least the last three ruptures and many previous ones have had ends. Early aftershocks in 1983 clustered in the boundary and the northern part of the Thousand Springs segment (Richins and others, 1987). After November 1983, aftershocks migrated through the boundary into the Warm Spring segment (Zollweg and Richins, 1985). Aftershocks at and near the boundary tended to have large magnitudes, high stress drops, and focal mechanisms displaying diversely oriented nodal planes (Boatwright, 1985; Richins and others, 1987), as though strain were being accommodated by breaking bit by bit through a network of interlocked faults. Crone and others (1987, p. 764) speculated about intersecting faults there much as they did for the Elkhorn Creek boundary. Geodetic modeling (Barrientos and others, 1987, fig. 14) indicates that rupture in the boundary extended to lesser depths and involved less slip than rupture on the Thousand Springs segment did, as though the boundary at depth had more fracture toughness than the segment interior. All these characteristics are also expected properties of a nonconservative barrier. Thus, although we lack slip orientation data across the Willow Creek Hills and Elkhorn Creek segment boundaries, the 1983–84 earthquake sequence revealed enough characteristics of the two boundaries for us to conclude that they are nonconservative barriers.

HEBGEN LAKE, MONTANA—AUGUST 17, 1959

The main shock of the 1959 Hebgen Lake, Mont., earthquake consisted of two subevents (Ryall, 1962). The first was at a depth of about 10 km; the second, 5 s later, was a much larger subevent at a depth of about 15 km (Doser, 1985b). Epicenters are poorly constrained, but most teleseismic epicenters for the main shock, its subevents, and large aftershocks and the epicenters of small aftershocks determined from a portable network cluster around the southeastern half of the trace of the Red Canyon fault, near the southeastern end of ground ruptures (fig. 18) (Stewart and others, 1964; Trimble and Smith, 1975; Doser, 1985b). Geodetic modeling indicated that rupture occurred on two planes that dip southwest from the traces of the Hebgen and Red Canyon faults; the rupture downdip from the Hebgen fault extended to a greater depth but had about the same length and slip as the rupture downdip from the Red Canyon fault (Barrientos and others, 1987). However, the first subevent was so much smaller than the second that both planes must have slipped during the second subevent (Barrientos and others, 1987). Therefore, it is not known which plane or which outcropping fault slipped first to produce the first subevent and presumably trigger the second.

The results described above can be interpreted in two ways in terms of segment boundaries and barriers. The first interpretation is that the fault-bounded Red Canyon fault block (fig. 18) is a salient and a persistent boundary between the Hebgen and Red Canyon segments of the southwest-dipping Hebgen-Red Canyon fault zone. In this interpretation, the Hebgen Lake earthquake—the largest normal-faulting shock so far recorded in or near the Basin and Range province—was one of the few earthquakes that ruptured past the salient and thus gave it a structural relief intermediate between that of the hanging wall and that of the footwall. If the salient is a nonconservative barrier, its expected high fracture toughness could require an unusually large earthquake to drive a rupture all the way through the process zone. Alternatively, if previous earthquakes had strained the barrier until it was ready to fail, the comparatively small first subevent could have triggered that failure in the form of the much larger second subevent, which had unusually large slip and stress drop (Barrientos and others, 1987).

The second interpretation (which we prefer) is that the Hebgen-Red Canyon fault zone is young and that its still-evolving geometry has not yet stabilized enough to justify interpretation in terms of persistent segment boundaries and long-lasting barriers. The youth of the fault zone has several bases:

1. First, Barrientos and others (1987) summarized evidence that the fault zone is part of a fault system about 0.6 to 2.0 m.y. old, only about 12 to 50 percent the estimated age of the Lost River fault zone.
2. Witkind and others (1962) and Myers and Hamilton (1964, p. 85-87) observed that younger ground ruptures, including those of 1959, tend to extend into unbroken rock beyond the ends of older faulting. Barrientos and others (1987) suggested that the high stress drops inferred for the main shock subevents could reflect fresh breaks of largely intact rock.

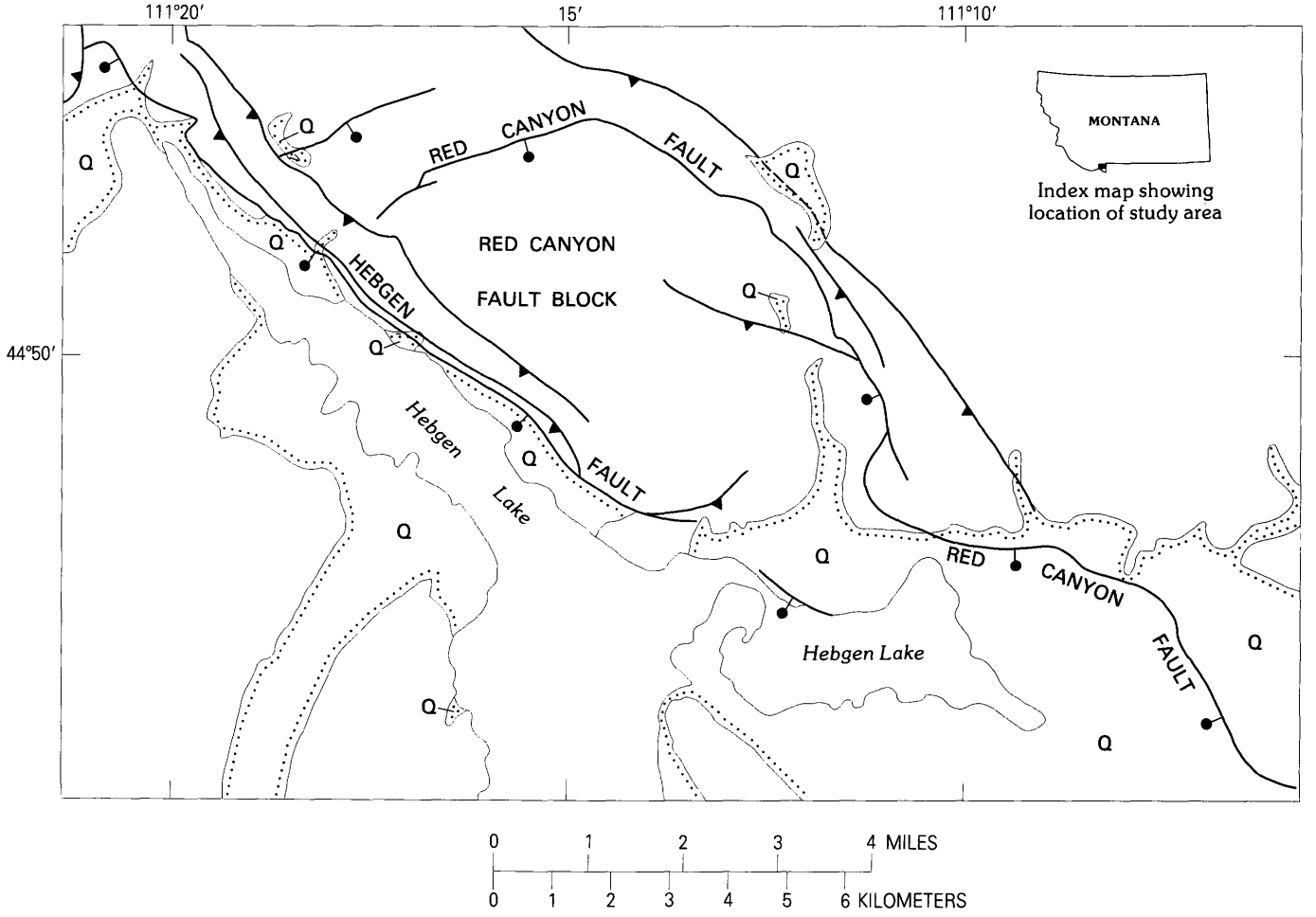

FIGURE 18.—August 17, 1959, Hebgen Lake, Mont., earthquake. Heavy lines show main ground ruptures along the Hebgen and Red Canyon faults and other faults from the normal-faulting earthquake; bar and ball are on the downthrown side of each rupture. Red lines show traces of reverse faults; teeth are on the upthrown sides. Light lines show the shoreline of Hebgen Lake and the contact between Quaternary glacial, landslide, and other deposits (Q) and underlying pre-Quaternary bedrock (dots on Quaternary side of contact). Inset shows the location of the map area in southwestern Montana. Simplified from Myers and Hamilton (1964, pl. 2) and Witkind and others (1964, pl. 5).

3. Witkind and others' (1964, pl. 5) geologic mapping shows that there is little cumulative slip across the ends of the comparatively short traces of the Hebgen and Red Canyon faults and that there is no deep, sediment-filled valley on the downthrown block, indicative of few slip events and presumably a short history in comparison with the Lost River or Wasatch fault zones.
4. In 1959, the largest ground-level slip on the Red Canyon fault was 9 to 15 ft (2.7–4.6 m) after correction for local slumping (Myers and Hamilton, 1964, pl. 2). Near the same place, the fault has its largest cumulative slip of about 1,000 ft (303 m) (Witkind and others, 1964, pl. 5). If slip in 1959 was typical of large events on the Red Canyon fault, such events have occurred no more than 67 to 111 times. Lesser slips in additional smaller earthquakes would decrease this number. If the fault is 0.6 to 2.0 m.y. old, the recurrence interval for slips like that of 1959 is at least 5,400 to 29,800 years, which is consistent with evidence for several late Quaternary scarp-forming events on the Hebgen-Red Canyon fault zone (Myers and Hamilton, 1964).
5. From structural, geomorphic, and geodetic evidence, Myers and Hamilton (1964, p. 91–96) concluded that, through Quaternary time, a new system of east-striking normal faults has been propagating eastward into the region near and south of Hebgen Lake, cutting across and reactivating parts of older, northwest-striking faults. Although the Hebgen and

Red Canyon faults strike northwest, overall subsidence in 1959 formed an east-trending basin (Myers and Hamilton, 1964, pl. 2).

That the geometry of the fault zone is still evolving would be suspected from its youth alone. Additional support comes from the observation that the traces of the Hebgen and Red Canyon faults lie near and in the downdip direction from the traces of older thrust faults (fig. 18). Myers and Hamilton (1964) thus concluded that the normal faults probably reactivated the thrust faults in the shallow subsurface. However, they also noted that the thrust complex is probably only a few kilometers thick, so that the shapes of the normal faults in map view are unlikely to resemble their shapes at hypocentral depths. In particular, the curve of the Red Canyon fault around the Red Canyon fault block is probably a near-surface feature, as the block itself is. The two southwest-dipping rupture planes that were inferred from geodetic data converge downward. We speculate that, eventually, the Hebgen fault will connect with the eastern half of the Red Canyon fault and abandon the Red Canyon fault block to the footwall of the fault zone. At depth, this evolution might have occurred already. If the Red Canyon fault block is shallow and ephemeral, interpretations of the Hebgen-Red Canyon fault zone in terms of persistent segment boundaries and long-lasting barriers are premature by at least several hundred thousand years.

RAINBOW MOUNTAIN, NEVADA—JULY 6 AND AUGUST 24, 1954

Nevada's Rainbow Mountain fault zone produced discontinuous, normal-slip surface ruptures having less than 1 m of surface offset twice within 7 weeks in 1954 (Tocher, 1956). The July main shock (fig. 19*A*, epicenter A) comprised two subevents about 8 s apart, the first and larger occurring at a depth of 10 km in right-normal slip and the second occurring at 7 km in mostly normal slip (Doser, 1986). The August main shock (fig. 19*A*, epicenter C) involved three subevents starting over 22 s, all at depths of about 12 km, of decreasing sizes and involving right-normal slip (Doser, 1986). From epicenters, focal mechanisms, and locations of ground ruptures, Doser (1986) inferred that the fault zone broke in two overlapping sections, the southern portion in July and the northern portion in August, each rupture zone propagating northward. Large aftershocks (Doser, 1986) and small earthquakes in 1969 and 1970 (Ryall and Malone, 1971) clustered near epicenters A and C (fig. 19*A*). The southern part of the surface breaks passed along the straight eastern side of Rainbow Mountain (Slemmons, 1956; Stewart and Carlson, 1978), but otherwise the rupture "...did not in its entirety follow any previously recognized fault..." (Tocher, 1956, p. 10). Sparse gravity data between exposed Cenozoic andesites and basalts of Rainbow Mountain and the southern Stillwater Range indicate a thin cover of sediments there but are too few to support inferences of the shape of the buried bedrock surface (fig. 19*B*) (Erwin and Berg, 1977).

The Rainbow Mountain earthquakes illustrate an important point about inferring segmentation of a fault zone. Despite the geologic, gravity, and seismological investigations of the earthquake sequence and its surroundings, there are too few data to determine whether any previous earthquakes had ends where the 1954 rupture zones started and stopped. The idea of segmentation requires that at least a few ruptures have had ends at about the same place. We cannot demonstrate coincident ends of successive ruptures on the Rainbow Mountain fault, so we cannot show that the 1954 breaks were not randomly distributed along an unsegmented fault zone. As shown by the discussions of other historic earthquakes in this report, the most useful evidence for such a demonstration comes from field investigations of scarps and other records of Holocene and late Pleistocene earthquakes, and from geophysical delineation of changes in structural relief along a fault zone.

FAIRVIEW PEAK-DIXIE VALLEY, NEVADA—DECEMBER 16, 1954

Four months after the Rainbow Mountain earthquake sequence, another sequence on the opposite side of the Stillwater Range produced information from which segmentation can be inferred. Bilateral rupture near the middle of the graben-bounding Fairview fault in Nevada began at a depth of 15 km, involved as many as three subevents starting over 16 s, and also broke the opposite bounding fault of the graben (West Gate fault) and a third fault (Gold King fault) that is on strike north of the Fairview fault but dips opposite to it (fig. 19*A*) (Doser, 1986). Slip was right normal at the hypocenter and at the surface on the Fairview and southern West Gate faults, but the Gold King and northern West Gate faults showed only normal slip at the surface (Larson, 1957; Slemmons, 1957; Slemmons and others, 1959; Doser, 1986). However, the following summer, geodetic measurements detected about 2 m of right slip that had occurred since the summer of 1954 across the southern Gold King and northern West Gate faults (Whitten, 1957), so either coseismic or postseismic right-normal movement characterized all three faults. In 1966 and from 1969 to 1970, small earthquakes mostly clustered between the main shock hypocenter of 1954 and the southern part of the trace of the Fairview fault, which had right-normal slip (Stauder and Ryall, 1967; Westphal and Lange, 1967; Ryall and Malone, 1971).

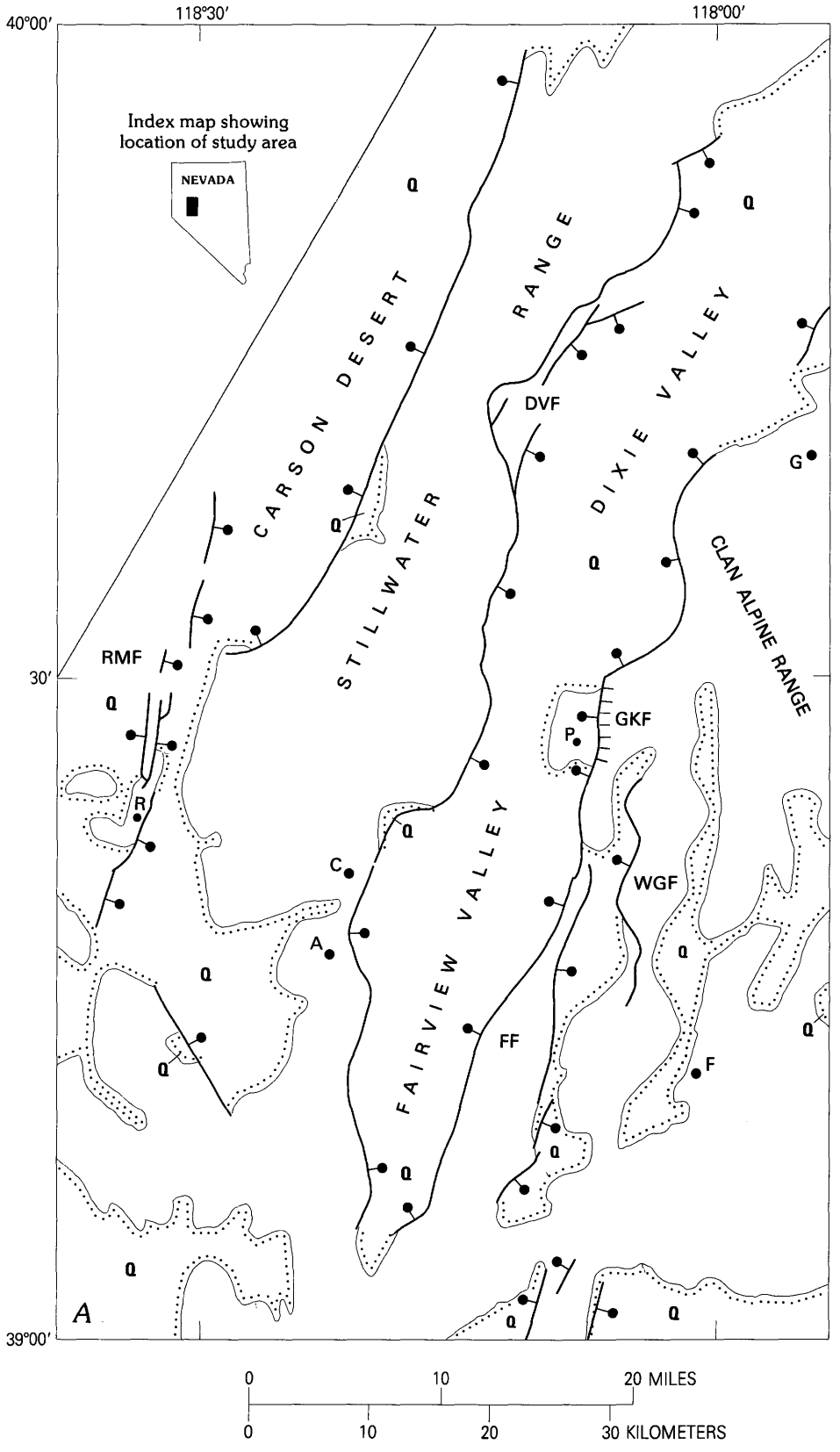

FIGURE 19.—July–December 1954 Rainbow Mountain, Fairview Peak, and Dixie Valley, Nev., earthquakes. *A*, Normal faults and epicenters. Red lines show main surface faulting from 1954; bar and ball are on the downthrown side of each fault. DVF, Dixie Valley fault; FF, Fairview fault; GKF, Gold King fault (hachured part also had ground rupture in 1903); RMF, Rainbow Mountain fault; WGF, West Gate fault. Thin lines with bars and balls represent other late Quaternary faults. Thin lines with dots show contact between Quaternary valley fillings (Q) and pre-Quaternary bedrock, wherever the contact is not a late Quaternary normal fault (dots on Quaternary side of contact). Solid circles locate epicenters of 1954 main shocks, using identifying letters of Doser (1986): A, Rainbow Mountain earthquake, ***M*** (moment magnitude) 6.2, July 6, locational precision about 20 km; C, Rainbow Mountain earthquake, ***M*** 6.5, August 24, precision also about 20 km; F, Fairview Peak earthquake, December 16, ***M*** 6.9 to 7.27, precision about 8 km (Doser (1986) used this event as a master to locate the other three but did not include the effect of its locational uncertainty in the precision of the other locations); G, Dixie Valley earthquake, December 16, ***M*** 6.7, precision about 40 km. P shows Pirouette Mountain; R locates Rainbow Mountain. Inset shows the location of the map area within Nevada. Simplified from Slemmons (1956, 1957), Tocher (1956), Slemmons and others (1959), Stewart and Carlson (1978), and Doser (1986). *B*, Bouguer gravity contours. Dashed lines show the Quaternary-pre-Quaternary contact from figure 19*A*, both faulted and unfaulted (dots on Quaternary side of contact). Solid lines represent isogals at 10-mGal contour intervals. Simplified from Erwin and Bittleston (1977) and Erwin and Berg (1977), who used a contour interval of 5 mGal.

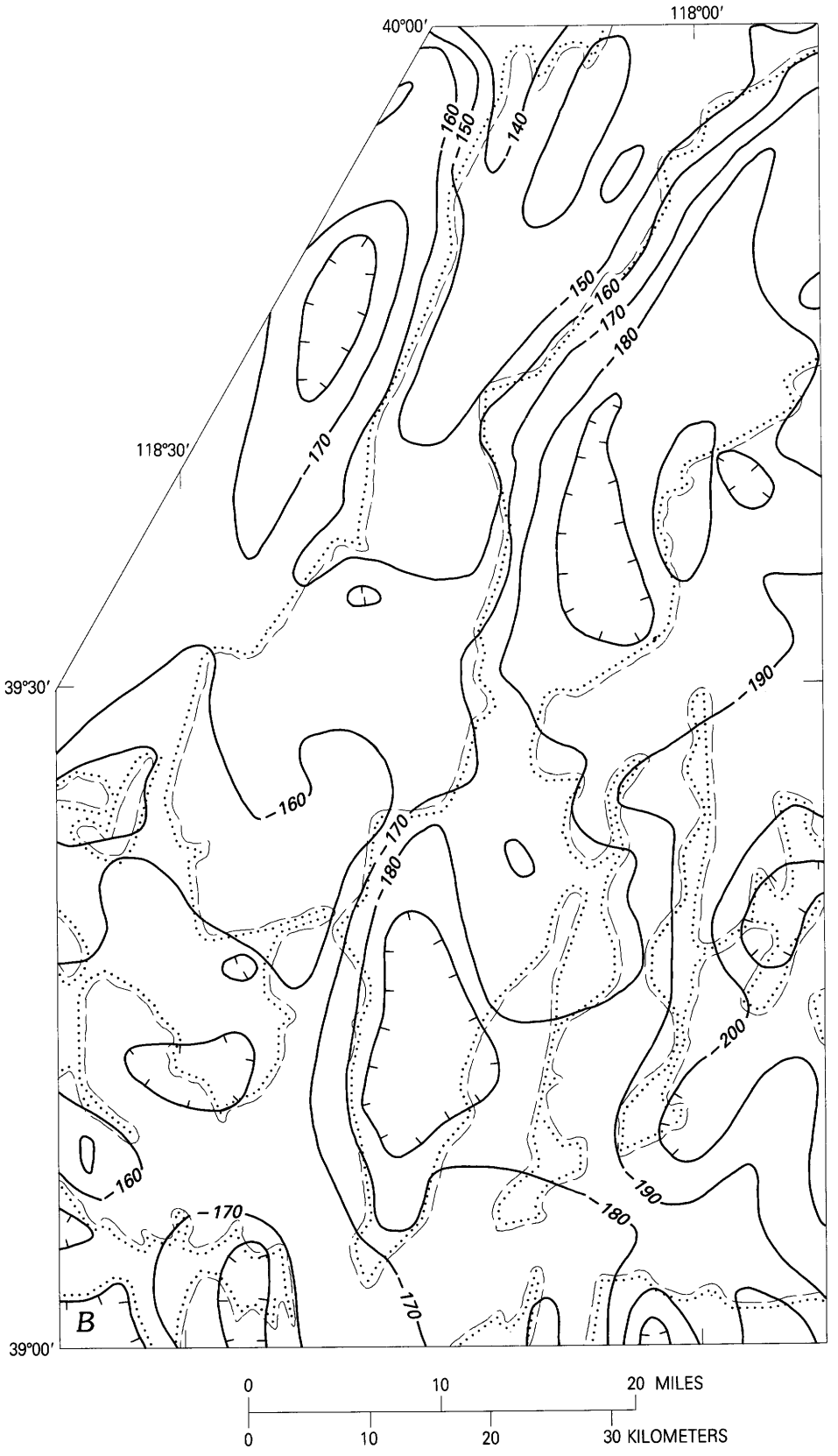

FIGURE 19.—Continued.

Four minutes after the Fairview Peak earthquake, a smaller shock broke the Dixie Valley fault (fig. 19*A*), beginning at a depth of 12 to 15 km in two subevents starting 6 s apart and perhaps propagating bilaterally (Okaya and Thompson, 1985; Doser, 1986). Slip was normal at the hypocenter (Doser, 1986), but, at the surface, it was right normal northeast of a sharp bend in the fault trace (at the letters DVF, fig. 19*A*) and left normal south of the bend (Slemmons, 1957; Slemmons and others, 1969). Small earthquakes from 1969 to 1970 were few, but most clustered between the main shock epicenter and the trace of the Dixie Valley fault (Ryall and Malone, 1971).

The following evidence indicates that the narrow passage between Dixie and Fairview Valleys is a persistent segment boundary of the fault zones on both sides of the valleys, which we named the Pirouette Mountain boundary. On the eastern side of the valley, the Fairview-West Gate-Gold King rupture ended there in 1954. Although surface faulting broke the boundary along the Gold King fault, slip there was small and discontinuous, and its dip was the opposite of that on the Fairview fault (Slemmons, 1957), analogous to surface faulting in 1983 in the Willow Creek Hills boundary on the Lost River fault (fig. 17). The Gold King fault also produced at least 3 mi (5 km) of surface faulting in the fall of 1903 (Slemmons and others, 1959). The 1903 rupture was confined to the Pirouette Mountain boundary, an indication that the boundary differs mechanically or in its strain history from parts of the same fault zone to the north and south. Slemmons (1956, fig. 2) depicted the fault zone on the eastern sides of Dixie and Fairview Valleys as having had late Quaternary slip. In both valleys, the fault zone separates Quaternary sediments from pre-Quaternary bedrock of the Clan Alpine and adjoining ranges (Stewart and Carlson, 1978). Accordingly, the fault zone in both valleys has probably accumulated at least a few tens of meters of structural relief. However, in the Pirouette Mountain boundary the fault zone crosses exposed bedrock as the Gold King fault, and there is little or no accumulated structural relief (Slemmons and others, 1959). Therefore, at least one and probably several pre-1903 faulting events either stopped at the Pirouette Mountain boundary or decreased their slip markedly for 5 to 10 km across the boundary. The latter possibility is unlikely, because maps and longitudinal profiles of slip data measured along surface ruptures of large historical earthquakes in and near the Basin and Range province indicate that slip from single earthquakes varies markedly over distances of 1 to 2 km and can shift from one fault strand to another where their tips overlap, but stretches of small slip that are 5 to 10 km wide usually exist only at the ends of ruptures (Slemmons, 1957; Myers and Hamilton, 1964, pl. 2; Crone and Machette, 1984; Wallace, 1984, fig. 28). We conclude that the Pirouette Mountain boundary has been a late Quaternary segment boundary.

Geophysical evidence indicates that the boundary has been persistent. Gravity modeling across Dixie Valley and seismic reflection profiles, all near the northern end of the 1954 ground ruptures, indicate up to 2 km of Quaternary sediments, thickest in the western half of the valley (Okaya and Thompson, 1985). Seismic refraction studies in Dixie Valley indicate depths to pre–Tertiary bedrock as great as 3.2 km in a central graben about 25 km north of Pirouette Mountain and shallowing southward to 1.1 km in the passage between Dixie and Fairview Valleys (Meister, 1967). Sparse Bouguer gravity data show a poorly defined gravity saddle at the boundary (fig. 19*B*) having about 20 mGal of gravity relief with respect to the centers of Dixie and Fairview Valleys (Erwin and Berg, 1977). A local gravity high, perhaps attributable to exposed Cenozoic and Mesozoic andesites, rhyolites, and tuffs, masks any gravity relief that might exist between the boundary and the narrow valley between the Fairview and West Gate faults (fig. 19*B*) (Erwin and Berg, 1977). Thus, Pirouette Mountain is the exposed eastern end of a largely buried bedrock ridge that separates Dixie and Fairview Valleys. The Pirouette Mountain boundary lacks a fault-bounded salient or a projecting spur like the persistent boundaries of the Wasatch fault zone have and more closely resembles the Willow Creek Hills boundary of the Lost River fault zone (where the bedrock ridge is exposed) and the Elkhorn Creek boundary (where the ridge is buried) (fig. 17). Because pre-Tertiary bedrock is shallower at the bedrock ridge than it is under Dixie and Fairview Valleys, ruptures along the eastern sides of both valleys have tended to lose slip and probably stopped there persistently throughout the evolution of the valleys. The same might be true for the graben and valley between the Fairview and West Gate faults and was true in 1954.

On the western sides of Dixie and Fairview Valleys, the 1954 Dixie Valley rupture ended at the Pirouette Mountain boundary. The gravity saddle indicates that many other ruptures also did so throughout the evolution of both valleys. Accordingly, the bedrock ridge at Pirouette Mountain has persistently segmented the fault zones on both sides of the valleys.

The manner in which the 1954 ruptures jumped from the east-dipping Fairview fault across the Pirouette Mountain boundary to the east-dipping Dixie Valley fault suggests an analogy to the northern end of the 1983 Borah Peak rupture of the Lost River fault zone (fig. 17). At the Willow Creek Hills boundary, the rupture broke discontinuously and with little slip northwestward through the boundary, forming or reactivating faults that dip opposite to the main rupture along the Thousand

Springs segment. Previously, we interpreted results of rupture mapping, aftershock studies, and geodetic modeling to suggest that, at the Willow Creek Hills boundary, the 1983 rupture and its aftershocks broke, bit by bit, through a network of interlocked faults that form the process zone of a nonconservative barrier, after the model of King and Nabelek (1985). For the Dixie Valley and Fairview Peak earthquakes, Snay and others (1985) modeled geodetic data and suggested that slip in 1954 also occurred on a buried fault that strikes north-northwest, dips steeply east-northeast, and underlies southern Dixie Valley, the Pirouette Mountain boundary, and northern Fairview Valley. Perhaps the 1954 and 1983 ruptures represent different expressions of the same phenomenon, in which most large ruptures on the Fairview Valley and Thousand Springs segments stop at the Pirouette Mountain and Willow Creek Hills boundaries, but some break through to rupture the Dixie Valley and Warm Spring segments.

The northern end of the 1954 surface rupture of the Dixie Valley fault is not a segment boundary. The end overlaps by 15 to 20 km the southern ends of Holocene and late Pleistocene scarps (Wallace and Whitney, 1984), and there is no gravity saddle there (fig. 19*B*). Perhaps rupture ends in the central part of the Dixie Valley fault are distributed more or less randomly along the fault, the southern ends being bounded by the Pirouette Mountain boundary and the ruptures extending northward various distances according to the amount of strain that has accumulated on this part of the Dixie Valley fault and adjacent parts. This example shows the need to demonstrate that two or more rupture ends coincide before inferring the presence of a segment boundary, whether persistent or not.

PLEASANT VALLEY, NEVADA—OCTOBER 2, 1915

Because of its early date, little is known seismologically about the 1915 Pleasant Valley, Nev., earthquake, but geologic and gravity evidence and the more recent earthquakes that we have discussed previously allow some interpretation. The main shock, two large foreshocks, or both produced five main scarps (fig. 20*A*) (Wallace, 1984). Wallace (1984) suggested that, of these five, the small Stillwater scarp might have formed by lateral spreading of a ridge instead of by tectonic rupture. We will not consider this scarp further.

Because of its length and large displacements, the Pearce scarp dominates the 1915 surface ruptures and provides 70 percent of the total estimated seismic moment (Wallace, 1984). Glass and Slemmons (1969) concluded from examining low-sun-angle aerial photographs that nearly all the 1915 scarps, including the Pearce scarp, followed still older scarps, although these older scarps could be of diverse ages. From diverse geologic observations, Wallace (1984) concluded that the Pearce scarp had broken in at least one late Quaternary earthquake, the displacement of which was similar to that of the 1915 event, probably between a few thousand and 12,000 years ago. An earthquake producing such displacement would probably have broken most or all of the 30-km length of the Pearce scarp, as happened in 1915. From a trench dug across the northern tip of the Pearce scarp, Bonilla and others (1984) interpreted several Holocene and late Pleistocene displacements, each probably less than 1 m, and suggested that two of them occurred in the 5,000 years before 1915. Therefore, the Pearce scarp probably has broken at least twice, including in 1915, and perhaps more often in the Holocene and latest Pleistocene.

To the south, Wallace and Whitney's (1984) compilation shows no Holocene or late Pleistocene scarps on the Sou Hills scarp or in the Sou Hills, although Wallace (1984, pl. 1) showed a few small pre-1915 scarps on the Sou Hills scarp and along strike to the north (fig. 20*A*). Individual scarps from 1915 are lower, shorter in map view, and less continuous along the Sou Hills scarp than they are along the Pearce scarp. At its southern end, the Pearce scarp splays to form numerous very short, low, east- and west-facing scarps covering an area about 5 km long and 2 km wide and dating from 1915 and earlier (Wallace, 1984, pl. 1). The area resembles the shallowly buried Pleasant View salient of the Wasatch fault zone both in size and in the diffuse style of its faulting. Fonseca (1985) described the Sou Hills similarly, contrasting its late Cenozoic faulting style to that of the Tobin and Stillwater Ranges. At locality C in figure 20*B*, a gravity saddle and the exposed bedrock ridge of the Sou Hills separate Pleasant Valley, where Erwin (1974) inferred 2,000 to 2,500 ft (0.6–0.8 km) of Cenozoic alluvial filling on the basis of gravity data, from northern Dixie Valley, where Speed (1976) estimated 6,000 ft (1.8 km) of Cenozoic filling on the basis of gravity modeling but Erwin (1974) inferred only about 2,000 ft (0.6 km). These observations and inferences support a suggestion that the 1915 rupture and one or more earlier ruptures had slip deficits at the Sou Hills and stopped there, analogous to the model in figure 16.

By analogy to other fault zones discussed previously, the ending of the 1915 rupture at the Sou Hills, the gravity saddle, and the diffuse style of the 1915 and older faulting indicate that the Sou Hills is a persistent segment boundary and perhaps a nonconservative barrier also. Fonseca (1985) drew an analogy to the Borah Peak earthquake, during which low, discontinuous surface ruptures broke into the Willow Creek Hills segment boundary and, a few kilometers farther north, into the Warm Spring segment (fig. 17). Like the Willow Creek

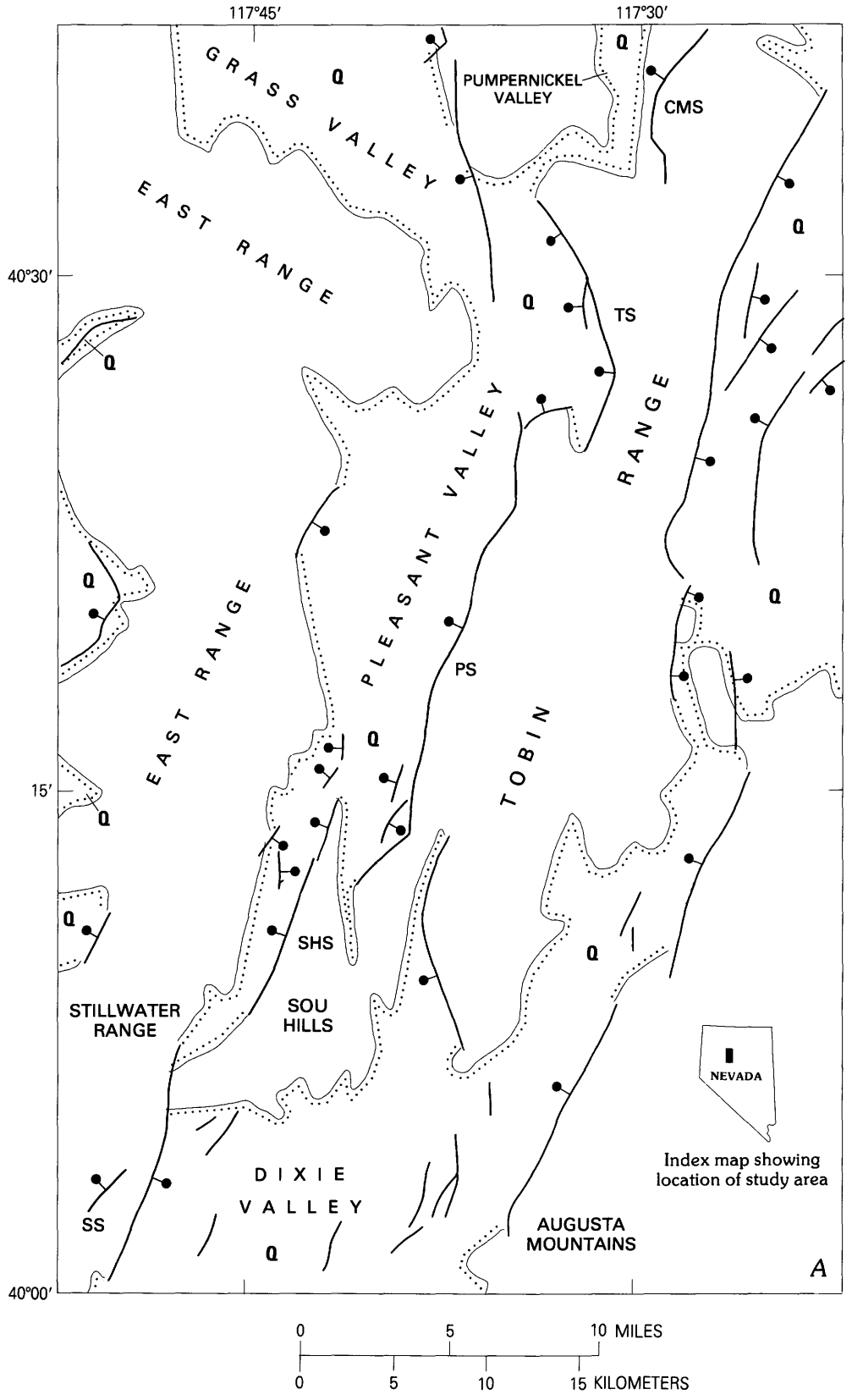

FIGURE 20.—October 2, 1915, Pleasant Valley, Nev., earthquake. *A*, Normal faults. Red lines show main surface faulting from 1915; bar and ball are on the downthrown side of each fault. CMS, China Mountain scarp; TS, Tobin scarp; PS, Pearce scarp; SHS, Sou Hills scarp; SS, Stillwater scarp. Thin lines with bars and balls represent other Quaternary faults (bars and balls omitted where slip sense is not known). Thin lines with dots show contact between Quaternary valley fillings (Q) and pre-Quaternary bedrock, wherever the contact is not a Quaternary fault (dots on Quaternary side of contact). Inset shows the location of the map area within Nevada. Simplified from Muller and others (1951), Speed (1976), Stewart and Carlson (1978), Wallace (1984), and Wallace and Whitney (1984). *B*, Bouguer gravity contours. Dashed lines show Quaternary–pre-Quaternary contact from figure 20*A*, both faulted and unfaulted (dots on Quaternary side of contact). Solid lines represent selected isogals. The contour interval is 5 mGal near gravity saddles A, B, and C and 10 mGal elsewhere. Simplified from Erwin (1974).

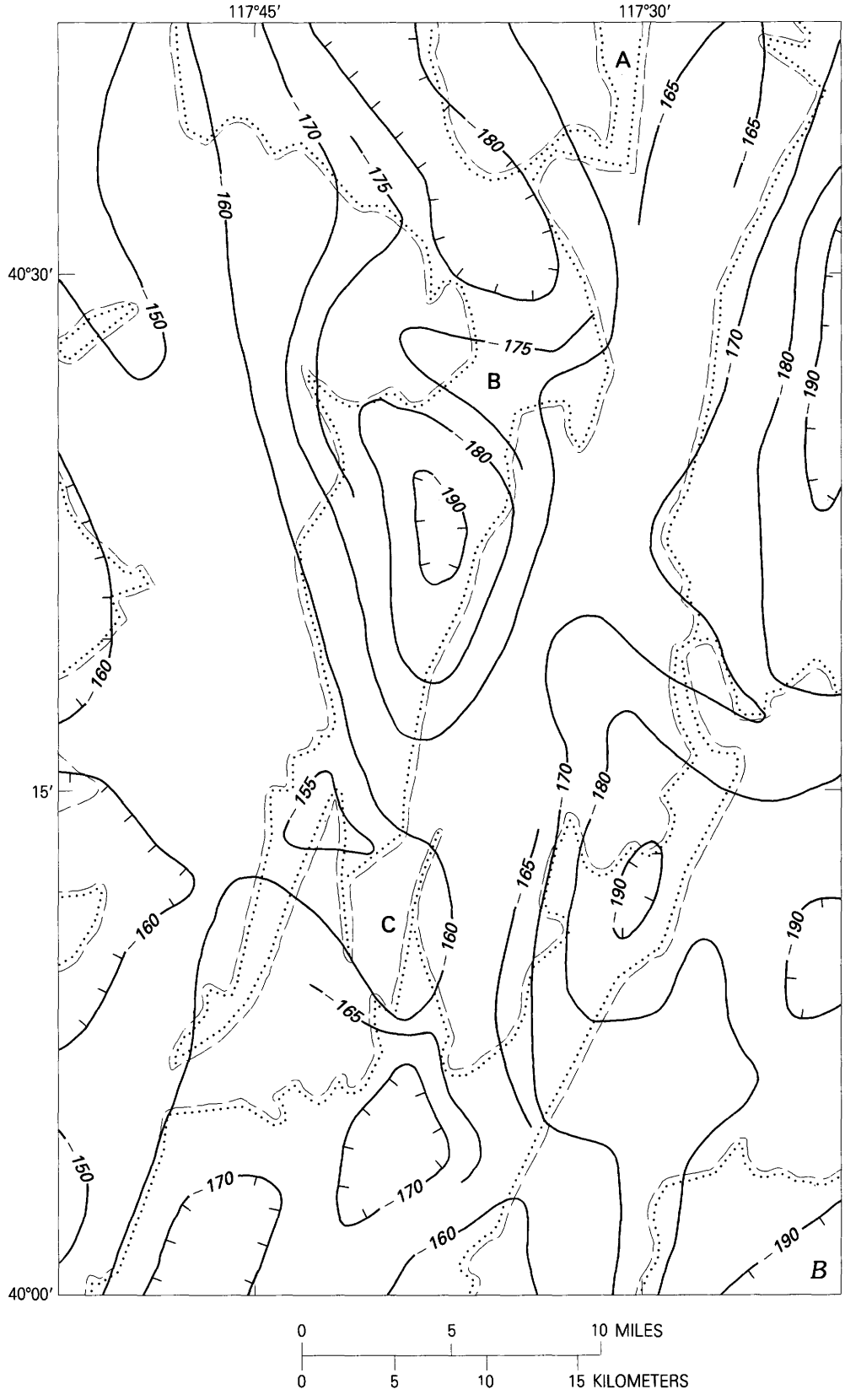

FIGURE 20.—Continued.

Hills, the Sou Hills are fault bounded, juxtaposing Tertiary rocks of the bedrock ridge with the Triassic rocks of the adjacent Stillwater Range and the Triassic and Permian rocks of the southern Tobin Range (Muller and others, 1951). The structural relief of the Sou Hills is intermediate between that of the bounding ranges and that of Pleasant and Dixie Valleys. We follow Fonseca's (1985) usage in defining the Sou Hills segment boundary, which includes the Sou Hills scarp of Wallace (1984).

North of the Pearce scarp, at the gap that separates it from the Tobin scarp, a gravity saddle indicates a buried bedrock ridge (locality B, fig. 20*B*). Erwin (1974) inferred from gravity data that Grass Valley contains about 4,000 ft (1.2 km) of Cenozoic filling at the northern edge of the area shown in figure 20. Throw across the Tobin scarp is at least 2,500 ft (0.8 km), comparable to Erwin's (1974) inference of 2,000 ft (0.6 km) of Cenozoic filling in northern Pleasant Valley. Throw on the Tobin scarp decreases to zero immediately south of the scarp's southern end (Muller and others, 1951). This evidence of accumulated slip deficits at the gap could support a speculation of a persistent segment boundary there.

However, we found no evidence that individual ruptures have had ends there. In 1915, the Tobin scarp broke an older scarp as continuously as the Pearce scarp did and creating displacements as large (Wallace, 1984). Wallace and Whitney's (1984) compilation shows late Pleistocene scarps on both sides of the gap. The compilation shows Holocene scarps along the Pearce scarp but not along the Tobin scarp. However, these Holocene scarps are so few that the difference might be erosional instead of tectonic. Also, gravity relief in both Grass and Pleasant Valleys is about 25 mGal between the valley centers and the ranges to the east and about 40 mGal to the west, whereas relief across the saddle between the valleys is only 10 to 20 mGal (Erwin, 1974). If structural relief increases with gravity relief, then the structural relief across the Tobin and Pearce scarps is almost as large at the saddle as it is to the north or south. There is little accumulated slip deficit at the gap between the Tobin and Pearce scarps. Finally, Wallace (1984) observed that a piedmont surface that spans the gap slopes north and northwest and appears to be oversteepened. He suggested that structural relief might be expressed in the gap as warping. An old scarp strikes northeast partway across the gap (fig. 20*A*) and could be evidence of occasional surface rupture across the gap. Thus, because geologic evidence is insufficient to determine whether prehistoric ruptures crossed the gap, we conclude that the buried bedrock ridge might have been produced by warping and occasional throughgoing ruptures instead of by repeated rupture ends at a segment boundary. If there is a boundary there, it did not persist through 1915.

At the northern end of the 1915 ground ruptures, scarps were few, low, and discontinuous in comparison with those on the Tobin and Pearce scarps. This situation occurred in 1915, probably during the Holocene, and during the late Pleistocene (Wallace, 1984; Wallace and Whitney, 1984). The China Mountain scarp is the only one from 1915 to form within a mountain block instead of along a range front. Wallace (1984) and Wallace and Whitney (1984) showed no scarps of any late Quaternary age in the gap between the China Mountain and Tobin scarps, and Wallace (1984) wondered why the 1915 break jumped across the gap to the China Mountain scarp instead of following the older scarps northwestward along the eastern side of Grass Valley. Which of the two paths was followed by most pre-1915 ruptures is unknown. A wide, gentle gravity saddle centers at locality A in figure 20*B* but is poorly defined by a few stations in its northwestern quarter (Erwin, 1974). The existence of the saddle is determined mostly by lows in Pumpernickel Valley north of the area shown in figure 20 and in Grass Valley. The area of the China Mountain scarp, including the gap between it and the Tobin scarp, might be a segment boundary, perhaps persistent, but we cannot settle the issue without more gravity and geologic evidence. Prehistoric ruptures might have tended to end at the gap north of the Tobin scarp, might have continued preferentially northwest along the edge of Grass Valley, or might have begun to abandon Grass Valley in favor of the China Mountain scarp in response to a hypothesized clockwise rotation of the direction of regional extension (Wallace, 1984). Evidence supporting such a hypothesized rotation can be seen in map relations in the Augusta Mountains (fig. 20*A*). North-striking normal faults within the mountains are truncated by a north-northeast-striking normal fault at the range front (Muller and others, 1951). This range front fault forms the contact between bedrock and Quaternary alluvium and thus has been active during the Quaternary. Similar relations are less clearly evident in the southern Tobin Range.

In conclusion, the Sou Hills are a persistent segment boundary, similar to the Willow Creek Hills boundary on the Lost River fault zone. The gap between the Tobin and Pearce scarps either is not a segment boundary or is one of low persistence, similar to the several gravity saddles on the Wasatch fault zone that lack salients, exposed bedrock ridges, or other evidence of recurrent slip deficits. The area of the China Mountain scarp cannot be evaluated with available evidence.

SUMMARY

A segment boundary exists where two or more large historical or prehistoric ruptures have coincident start-

ing or stopping ends. Analysis of the Wasatch fault zone produced a model in which gravity saddles or other evidence of buried bedrock ridges and footwall salients that separate hanging-wall valleys indicates accumulated slip deficits, which are interpreted as evidence of many coincident starting or stopping ends (that is, as persistent segment boundaries).

The Borah Peak rupture of 1983 started at the Elkhorn Creek boundary and ended at the Willow Creek Hills boundary, both persistent and both probably nonconservative barriers.

The Hebgen Lake earthquake of 1959 occurred on a young fault zone whose geometry is still evolving and which should not yet be interpreted in terms of persistent segment boundaries and long-lasting barriers.

The Rainbow Mountain earthquakes of 1954 occurred on a fault zone where there are too few gravity or geologic data to test the Wasatch model, an indication that descriptions of more than one rupture zone are needed before segmentation can be inferred.

The Fairview Peak-Dixie Valley rupture zones of 1954 were separated by the persistent Pirouette Mountain segment boundary, which tends to control large ruptures on both the eastern and western sides of Fairview and Dixie Valleys and perhaps in the graben between the Fairview and West Gate faults. The Pirouette Mountain boundary might be a nonconservative barrier. The fact that the northern end of the Dixie Valley rupture zone is not a segment boundary, persistent or otherwise, demonstrates that segments need not rupture completely even in large earthquakes. There are too few data to allow evaluation of the southern end of the Fairview Peak rupture zone.

The southern end of the 1915 Pleasant Valley earthquake was at the persistent Sou Hills boundary, which might be a nonconservative barrier. The gap between the Pearce and Tobin scarps is a nonpersistent boundary, which did not end the 1915 rupture zone. The northern end of the 1915 rupture lacks enough data for interpretation.

CONCLUSIONS

The Wasatch fault zone and most or all of the large seismic ruptures that occur on it are segmented. Large ruptures tend to start, stop, or do both at boundaries between segments, tend to be confined within single segments, and tend not to rupture across boundaries into adjacent segments.

Persistent segment boundaries occur at the Pleasant View, Salt Lake, Traverse Mountains, and Payson salients. These boundaries have controlled the seismic evolution of the Wasatch fault zone for much or all of its history and likely will continue to do so into the near future. Most boundaries in the populous central parts of the Wasatch Front are persistent.

Other proposed segment boundaries elsewhere along the fault zone might be nonpersistent, and their locations and times of activity might change unpredictably with time. If boundaries that have affected Holocene and older Quaternary ruptures are not persistent, then these boundaries might not affect the next several ruptures that occur on the Wasatch fault zone. However, the next ruptures might also be affected by nonpersistent boundaries that have not affected the young geologic record. Present boundaries that might be nonpersistent lie mostly in the comparatively sparsely populated areas north of Brigham City and south of Provo.

From 1962 to 1986, epicenters of small earthquakes that occurred near the trace of the Wasatch fault zone changed abundance across the four persistent segment boundaries. In contrast, Arabasz and Julander (1986) suggested that small earthquakes elsewhere along the Wasatch Front can be controlled in complex ways by little-known structures of buried thrust sheets and therefore are unlikely to be clearly associated with exposed structure. The fact that seismicity near the fault zone is associated with the salients is encouraging for efforts to understand earthquake generation along the Wasatch Front.

Analysis of the Wasatch fault zone produced a model that predicts persistent segment boundaries where exposed or shallowly buried transverse bedrock ridges, some with salients, indicate accumulated slip deficits and where two or more individual large rupture zones have started or stopped.

Testing this model against five historical earthquake sequences in and near the Basin and Range province indicates the existence of two persistent segment boundaries on the Lost River fault zone of Idaho, one persistent boundary between the Dixie Valley and Fairview faults of Nevada, and one persistent boundary and one nonpersistent boundary in the Pleasant View rupture zone of Nevada. The northern end of the Dixie Valley fault is not a segment boundary, persistent or otherwise. There is too little information available on both ends of Nevada's Rainbow Mountain rupture zone, the southern end of the Fairview Peak rupture zone, and the northern end of the Pleasant Valley rupture zone to test the model there. The Hebgen Lake earthquake in Montana occurred on a fault zone that is too young for the model to apply.

REFERENCES CITED

Algermissen, S.T., Perkins, D.M., Thenhaus, P.C., Hanson, S.L., and Bender, B.L., 1982, Probabilistic estimates of maximum acceler-

ation and velocity in rock in the contiguous United States: U.S. Geological Survey Open-File Report 82–1033, 99 p., 6 pls.

Anderson, R.E., 1985, Regional and local hazards mapping in the eastern Great Basin, *in* Jacobsen, M.L., and Rodriguez, T.R., comps., National Earthquake Hazards Reduction Program, summaries of technical reports, v. XXI: U.S. Geological Survey Open-File Report 86–31, p. 472–478.

———1986, Regional and local hazards mapping in the eastern Great Basin, *in* Jacobsen, M.L., and Rodriguez, T.R., comps., National Earthquake Hazards Reduction Program, summaries of technical reports, v. XXII: U.S. Geological Survey Open-File Report 86–383, p. 480–483.

Arabasz, W.J., 1984, Earthquake behavior in the Wasatch Front area: Association with geologic structure, space-time occurrence, and stress state, *in* Hays, W.W., and Gori, P.L., eds., Proceedings of Conference XXVI; a workshop on Evaluation of regional and urban earthquake hazards and risk in Utah: U.S. Geological Survey Open-File Report 84–763, p. 310–339.

Arabasz, W.J., and Julander, D.R., 1986, Geometry of seismically active faults and crustal deformation within the Basin and Range–Colorado Plateau transition in Utah: Geological Society of America Special Paper 208, p. 43–74.

Arabasz, W.J., Smith, R.B., and Richins, W.D., 1980, Earthquake studies along the Wasatch Front, Utah: Network monitoring, seismicity, and seismic hazards: Bulletin of the Seismological Society of America, v. 70, p. 1479–1499.

Armstrong, R.C., and Oriel, S.S., 1965, Tectonic development of Idaho-Wyoming thrust belt: Bulletin of the American Association of Petroleum Geologists, v. 49, p. 1847–1866.

Armstrong, R.L., 1968, Sevier orogenic belt in Nevada and Utah: Geological Society of America Bulletin, v. 79, p. 429–458.

Barrientos, S.E., Stein, R.S., and Ward, S.N., 1987, Comparison of the 1959 Hebgen Lake, Montana and the 1983 Borah Peak, Idaho earthquakes from geodetic observations: Bulletin of the Seismological Society of America, v. 77, p. 784–808.

Boatwright, J., 1985, Characteristics of the aftershock sequence of the Borah Peak, Idaho, earthquake determined from digital recordings of the events: Bulletin of the Seismological Society of America, v. 75, p. 1265–1284.

Bond, J.G., 1978, Geologic map of Idaho: Moscow, Idaho Bureau of Mines and Geology, 1 sheet, scale 1:500,000.

Bonilla, M.G., Villalobos, H.A., and Wallace, R.E., 1984, Exploratory trench across the Pleasant Valley fault, Nevada: U.S. Geological Survey Professional Paper 1274–B, p. B1–B14, 1 pl.

Bruhn, R.L., Picard, M.D., and Beck, S.L., 1983, Mesozoic and early Tertiary structure and sedimentology of the central Wasatch Mountains, Uinta Mountains and Uinta Basin, *in* Gurgel, K.D., ed., Geologic excursions in the overthrust belt and metamorphic core complexes of the Intermountain region: Utah Geological and Mineral Survey Special Studies 59, p. 63–105.

Bruhn, R.L., Gibler, P.R., and Parry, W.T., 1987, Rupture characteristics of normal faults: An example from the Wasatch fault zone, Utah, *in* Coward, M.P., Dewey, J.F., and Hancock, P.L., eds., Continental extensional tectonics: Geological Society of London Special Publication 28, p. 337–353.

Bryant, B., 1984, Reconnaissance geologic map of the Precambrian Farmington Canyon Complex and surrounding rocks in the Wasatch Mountains between Ogden and Bountiful, Utah: U.S. Geological Survey Miscellaneous Investigations Map I–1447, 1 sheet, scale 1:50,000.

———1985, Structural ancestry of the Uinta Mountains, *in* Picard, M.D., ed., Geology and energy resources, Uintah basin of Utah: Utah Geological Association Publication 12, p. 115–120.

Bryant, B., and Nichols, D.J., 1988, Late Mesozoic and early Tertiary reactivation of an ancient crustal boundary along the Uinta trend and its interaction with the Sevier orogenic belt, *in* Schmidt, C.J., and Perry, W.J., Jr., eds., Interaction of the Rocky Mountain foreland and the frontal Cordilleran thrust belt: Geological Society of America Memoir 171, p. 411–430.

Burke, K., and Dewey, J.F., 1973, Plume-generated triple junctions: Key indicators in applying plate tectonics to old rocks: Journal of Geology, v. 81, p. 406–433.

Byerly, P., 1956, The Fallon-Stillwater earthquakes of July 6, 1954, and August 23, 1954—Historic introduction: Bulletin of the Seismological Society of America, v. 46, p. 1–3.

Cheetham, A.H., and Hazel, J.E., 1969, Binary (presence-absence) similarity coefficients: Journal of Paleontology, v. 43, p. 1130–1136.

Crittenden, M.D., Jr., 1961, Magnitude of thrust faulting in northern Utah: U.S. Geological Survey Professional Paper 424–D, p. D128–D131.

———1965, Geology of the Dromedary Peak quadrangle, Utah: U.S. Geological Survey Geologic Quadrangle Map GQ–378, 1 sheet, scale 1:24,000.

———1972, Willard thrust and the Cache allochthon, Utah: Geological Society of America Bulletin, v. 83, p. 2871–2880.

———1974, Regional extent and age of thrusts near Rockport Reservoir and relation to possible exploration targets in northern Utah: Bulletin of the American Association of Petroleum Geologists, v. 58, p. 2428–2435.

Crittenden, M.D., Jr., and Sorensen, M.L., 1985, Geologic map of the North Ogden quadrangle and part of the Ogden and Plain City quadrangles, Box Elder and Weber Counties, Utah: U.S. Geological Survey Miscellaneous Investigations Series Map I–1606, 1 sheet, scale 1:24,000.

Crittenden, M.D., Jr., Stuckless, J.S., Kistler, R.W., and Stern, T.W., 1973, Radiometric dating of intrusive rocks in the Cottonwood area, Utah: Journal of Research of the U.S. Geological Survey, v. 1, p. 173–178.

Crone, A.J., and Machette, M.N., 1984, Surface faulting accompanying the Borah Peak earthquake, central Idaho: Geology, v. 12, p. 664–667.

Crone, A.J., Haller, K.M., Guo, S., Liao, Y., Li, Y., and Vincent, K.R., 1985, Late Quaternary faulting along the Mackay segment of the Lost River fault, central Idaho [abs.]: E⊕S, Transactions of the American Geophysical Union, v. 66, no. 46, p. 1067.

Crone, A.J., Machette, M.N., Bonilla, M.G., Lienkaemper, J.J., Pierce, K.L., Scott, W.E., and Bucknam, R.C., 1987, Surface faulting accompanying the Borah Peak earthquake and segmentation of the Lost River fault, central Idaho: Bulletin of the Seismological Society of America, v. 77, p. 739–770.

Davis, F.D., comp., 1983a, Geologic map of the central Wasatch Front, Utah: Utah Geological and Mineral Survey Map 54–A, 2 sheets, scale 1:100,000.

———1983b, Geologic map of the southern Wasatch Front, Utah: Utah Geological and Mineral Survey Map 55–A, 2 sheets, scale 1:100,000.

———1985, Geologic map of the northern Wasatch Front, Utah: Utah Geological and Mineral Survey Map 53–A, 2 sheets, scale 1:100,000.

Dewey, J.W., 1987, Instrumental seismicity of central Idaho: Bulletin of the Seismological Society of America, v. 77, p. 819–836.

Doser, D.I., 1985a, The 1983 Borah Peak, Idaho, and 1959 Hebgen Lake, Montana, earthquakes; models for normal fault earthquakes in the Intermountain seismic belt, *in* Stein, R.S., and Bucknam, R.C., eds., Workshop XXVIII—On the Borah Peak, Idaho, earthquake: U.S. Geological Survey Open-File Report 85–290–A, p. 368–384.

———1985b, Source parameters and faulting processes of the 1959 Hebgen Lake, Montana, earthquake sequence: Journal of Geophysical Research, v. 90, no. B6, p. 4537–4555.

———1986, Earthquake processes in the Rainbow Mountain-Fairview Peak-Dixie Valley, Nevada, region 1954–1959: Journal of Geophysical Research, v. 91, no. B12, p. 12572–12586.

Doser, D.I., and Smith, R.B., 1985, Source parameters of the 28 October 1983 Borah Peak, Idaho, earthquake from body wave analysis: Bulletin of the Seismological Society of America, v. 75, p. 1041–1051.

Erwin, J.W., 1974, Bouguer gravity map of Nevada—Winnemucca sheet: Nevada Bureau of Mines and Geology Map 47, 4-p. pamphlet, 1 sheet, scale 1:250,000.

Erwin, J.W., and Berg, J.C., 1977, Bouguer gravity map of Nevada—Reno sheet: Nevada Bureau of Mines and Geology Map 58, 1 sheet, scale 1:250,000.

Erwin, J.W., and Bittleston, E.W., 1977, Complete Bouguer gravity map of Nevada—Millett sheet: Nevada Bureau of Mines and Geology Map 53, 1 sheet, scale 1:250,000.

Fonseca, J.E., 1985, Barriers to faulting in the Basin-Range province—Evidence from the Sou Hills transverse block: Geological Society of America Abstracts with Programs, v. 17, no. 7, p. 585.

Forrester, J.D., 1937, Structure of the Uinta Mountains: Geological Society of America Bulletin, v. 48, p. 631–666.

Glass, C.E., and Slemmons, D.B., 1969, Restudy of surface faulting from the October 2, 1915, Pleasant Valley area earthquake, Nevada: Geological Society of America Abstracts with Programs, v. 1, no. 5, p. 28.

Gries, R., 1983, North-south compression of Rocky Mountain foreland structures, *in* Lowell, J.D., and Gries, R., eds., Rocky Mountain foreland basins and uplifts: Denver, Colo., Rocky Mountain Association of Geologists, p. 9–32.

Hanks, R.C., and Schwartz, D.P., 1987, Morphologic dating of the pre-1983 fault scarp on the Lost River fault at Doublespring Pass Road, Custer County, Idaho: Bulletin of the Seismological Society of America, v. 77, p. 837–846.

Hansen, W.R., 1965, Geology of the Flaming Gorge area, Utah-Colorado-Wyoming: U.S. Geological Survey Professional Paper 490, 196 p.

Hazel, J.E., 1970, Binary coefficients and clustering in biostratigraphy: Geological Society of America Bulletin, v. 81, p. 3237–3252.

Hintze, L.F., 1980, comp., Geologic map of Utah: Salt Lake City, Utah Geological and Mineral Survey, 2 sheets, scale 1:500,000.

Houghton, W.P., 1986, Structural analysis of the Salt Lake-Provo segment boundary of the Wasatch fault zone: Salt Lake City, University of Utah, unpublished M.Sci. thesis, 64 p.

Keaton, J.R., Currey, D.R., and Olig, S.J., 1987, Paleoseismicity and earthquake hazards evaluation of the West Valley fault zone, Salt Lake City urban area, Utah: Report to U.S. Geological Survey under contract 14–08–0001–22048, 93 p.

King, G., 1983, The accommodation of large strains in the upper lithosphere of the Earth and other solids by self-similar fault systems: The geometrical origin of b-value: Pure and Applied Geophysics, v. 121, p. 761–815.

———1986, Speculations on the geometry of the initiation and termination processes of earthquake rupture and its relation to morphology and geological structure: Pure and Applied Geophysics, v. 124, p. 567–585.

King, G., and Nabelek, J., 1985, Role of fault bends in the initiation and termination of earthquake rupture: Science, v. 228, p. 984–987.

King, G., and Yielding, G., 1984, The evolution of a thrust fault system: Processes of rupture initiation, propagation and termination in the 1980 El Asnam (Algeria) earthquake: Geophysical Journal of the Royal Astronomical Society, v. 77, p. 915–933.

Larson, E.R., 1957, Minor features of the Fairview fault, Nevada: Bulletin of the Seismological Society of America, v. 47, p. 377–386.

Lawton, T.F., 1985, Style and timing of frontal structures, thrust belt, central Utah: Bulletin of the American Association of Petroleum Geologists, v. 69, p. 1145–1159.

Mabey, D.R., Crittenden, M.D., Jr., Morris, H.T., Roberts, R.J., and Tooker, E.W., 1964, Aeromagnetic and generalized geologic map of part of north-central Utah: U.S. Geological Survey Geophysical Investigations Map GP–422, 1 sheet, scale 1:250,000.

Machette, M.N., 1984, Preliminary investigations of late Quaternary slip rates along the southern part of the Wasatch fault zone, central Utah, *in* Hays, W.W., and Gori, P.L., eds., Proceedings of Conference XXVI; a workshop on Evaluation of regional and urban earthquake hazards and risk in Utah: U.S. Geological Survey Open-File Report 84–763, p. 391–406.

Machette, M.N., Personius, S.F., and Nelson, A.R., 1986, Late Quaternary segmentation and slip-rate history of the Wasatch fault zone, Utah [abs.]: E⊕S, Transactions of the American Geophysical Union, v. 67, no. 44, p. 1107.

———1987, Quaternary geology along the Wasatch fault zone—Segmentation, recent investigations, and preliminary conclusions, *in* Gori, P.L., and Hays, W.W., eds., Assessment of regional earthquake hazards and risk along the Wasatch Front, Utah: U.S. Geological Survey Open-File Report 87–585, p. A1–A72.

Maclean, A.F., 1985, Quaternary segmentation of the Wasatch fault zone, Utah, as studied by morphometric discriminant analysis: Oxford, Ohio, Miami University, unpublished M.Sci. thesis, 200 p.

Mattick, R.E., 1970, Thickness of unconsolidated to semiconsolidated sediments in Jordan Valley, Utah: U.S. Geological Survey Professional Paper 700–C, p. C119–C124.

Mayer, L., and Maclean, A., 1986, Tectonic geomorphology of the Wasatch Front, Utah, using morphologic discriminant analysis—Preliminary implications for Quaternary segmentation of the Wasatch fault zone [abs.]: Geological Society of America Abstracts with Programs, v. 18, no. 2, p. 155.

Meister, L.J., 1967, Seismic refraction study of Dixie Valley, Nevada, *in* Thompson, G.A., Meister, L.J., Herring, A.T., Smith, T.E., Burke, D.B., Kovach, R.L., Burford, R.O., Salehi, I.A., and Wood, M.D., Geophysical study of Basin-Range structure, Dixie Valley region, Nevada: Bedford, Mass., U.S. Air Force Cambridge Research Laboratories, final scientific report under contract AF 19(628)–3867, pt. I, 80 p.

Miller, R.G., Jr., 1981, Simultaneous statistical inference (2d ed.): New York, Springer-Verlag, 299 p.

Muller, S.W., Ferguson, H.G., and Roberts, R.J., 1951, Geology of the Mount Tobin quadrangle, Nevada: U.S. Geological Survey Geologic Quadrangle Map GQ–7, 4-p. text, 1 sheet, scale 1:125,000.

Myers, W.B., and Hamilton, W., 1964, Deformation accompanying the Hebgen Lake earthquake of August 17, 1959—The Hebgen Lake, Montana, earthquake of August 17, 1959: U.S. Geological Survey Professional Paper 435–I, p. 55–98, 2 pls.

Naeser, C.W., Bryant, B., Crittenden, M.D., Jr., and Sorensen, M.L., 1983, Fission-track ages of apatite in the Wasatch Mountains, Utah: An uplift study, *in* Miller, D.M., Todd, V.R., and Howard, K.A., eds., Tectonic and stratigraphic studies in the eastern Great Basin: Geological Society of America Memoir 157, p. 29–36.

Nelson, A.R., and Personius, S.F., 1987, A nonconservative barrier to Holocene rupture propagation in the northern Wasatch fault zone, Utah [abs.]: International Union for Quaternary Research International Congress, 12th, Ottawa, Ontario, 1987, Programme with Abstracts, p. 231.

Okaya, D.A., and Thompson, G.A., 1985, Geometry of Cenozoic extensional faulting: Dixie Valley, Nevada: Tectonics, v. 4, p. 107–125.

Oriel, S.S., and Armstrong, F.C., 1966, Times of thrusting in Idaho-Wyoming thrust belt: Reply: Bulletin of the American Association of Petroleum Geologists, v. 50, p. 2614–2621.

Personius, S.F., 1985, Preliminary assessment of late Quaternary displacement along the Wasatch fault zone near Brigham City, Utah [abs.]: Geological Society of America Abstracts with Programs, v. 17, no. 4, p. 261.

———1986, The Brigham City segment—A new segment of the Wasatch fault zone, northern Utah [abs.]: Geological Society of America Abstracts with Programs, v. 18, no. 5, p. 402.

Richins, W.D., Pechmann, J.C., Smith, R.B., Langer, C.J., Goter, S.K., Zollweg, J.E., and King, J.J., 1987, The Borah Peak, Idaho, earthquake and its aftershocks: Bulletin of the Seismological Society of America, v. 77, p. 694–723.

Royse, F., Warner, M.A., and Reese, D.L., 1975, Thrust belt structural geometry and related stratigraphic problems, Wyoming-Idaho-northern Utah, *in* Bolyard, D.W., ed., Deep drilling frontiers of the central Rocky Mountains: Denver, Colo., Rocky Mountain Association of Geologists, p. 41–54.

Ryall, A., 1962, The Hebgen Lake, Montana, earthquake of August 18, 1959—P waves: Bulletin of the Seismological Society of America, v. 52, p. 235–271.

Ryall, A., and Malone, S.D., 1971, Earthquake distribution and mechanism of faulting in the Rainbow Mountain-Dixie Valley-Fairview Peak area, central Nevada: Journal of Geophysical Research, v. 76, no. 29, p. 7241–7248.

Salyards, S.L., 1985, Patterns of offset associated with the 1983 Borah Peak, Idaho, earthquake and previous events, *in* Stein, R.S., and Bucknam, R.C., eds., Proceedings of Workshop XXVIII—On the Borah Peak, Idaho, earthquake: U.S. Geological Survey Open-File Report 85–290–A, p. 59–75.

Schirmer, T.W., 1985, Basement thrusting in north-central Utah: A model for the development of the northern Utah highland, *in* Kerns, G.J., and Kerns, R.L., Jr., eds., Orogenic patterns and stratigraphy of north-central Utah and southeastern Idaho: Utah Geological Association Publication 14, p. 129–143.

Schwartz, D.P., and Coppersmith, K.J., 1984, Fault behavior and characteristic earthquakes: Examples from the Wasatch and San Andreas fault zones: Journal of Geophysical Research, v. 89, no. B7, p. 5681–5698.

Schwartz, D.P., and Crone, A.J., 1985, The 1983 Borah Peak earthquake—A calibration event for quantifying earthquake recurrence and fault behavior on Great Basin normal faults, *in* Stein, R.S., and Bucknam, R.C., eds., Proceedings of Workshop XXVIII—On the Borah Peak, Idaho, earthquake: U.S. Geological Survey Open-File Report 85–290–A, p. 153–160.

Scott, W.E., and Shroba, R.R., 1985, Surficial geologic map of an area along the Wasatch fault zone in the Salt Lake Valley, Utah: U.S. Geological Survey Open-File Report 85–448, 18 p., 2 oversize sheets, scale 1:24,000.

Skipp, B., and Harding, S.T., 1985, Preliminary report on geology of Borah Peak area, Idaho, including interpretation of seismic and gravity data, *in* Stein, R.S., and Bucknam, R.C., eds., Proceedings of Workshop XXVIII—On the Borah Peak, Idaho, earthquake: U.S. Geological Survey Open-File Report 85–290–A, p. 657–671.

Slemmons, D.B., 1956, Geologic setting for the Fallon-Stillwater earthquakes of 1954: Bulletin of the Seismological Society of America, v. 46, p. 4–9.

———1957, Geological effects of the Dixie Valley-Fairview Peak, Nevada, earthquakes of December 16, 1954: Bulletin of the Seismological Society of America, v. 47, p. 353–375, 1 pl.

Slemmons, D.B., McDonald, R.L., and Cluff, L., 1969, Surface faulting from the December 16, 1954, earthquake in Dixie Valley, Nevada: Geological Society of America Abstracts with Programs, v. 1, no. 5, p. 73–74.

Slemmons, D.B., Steinbrugge, K.V., Tocher, D., Oakeshott, G.B., and Gianella, V.P., 1959, Wonder, Nevada, earthquake of 1903: Bulletin of the Seismological Society of America, v. 49, p. 251–265, 2 pls.

Smith, R.B., and Bruhn, R.L., 1984, Intraplate extensional tectonics of the eastern Basin-Range: Inferences on structural style from seismic reflection data, regional tectonics, and thermal-mechanical models of brittle-ductile deformation: Journal of Geophysical Research, v. 89, no. B7, p. 5733–5762.

Smith, R.B., and Richins, W.D., 1984, Seismicity and earthquake hazards of Utah and the Wasatch Front: Paradigm and paradox, *in* Hays, W.W., and Gori, P.L., eds., Proceedings of Conference XXVI; a workshop on Evaluation of regional and urban earthquake hazards and risk in Utah: U.S. Geological Survey Open-File Report 84–763, p. 73–112.

Snay, R.A., Cline, M.W., and Timmerman, E.L., 1985, Dislocation models for the 1954 earthquake sequence in Nevada, *in* Stein, R.S., and Bucknam, R.C., eds., Proceedings of Workshop XXVIII—On the Borah Peak, Idaho, earthquake: U.S. Geological Survey Open-File Report 85–290–A, p. 531–555.

Speed, R.C., 1976, Geologic map of the Humboldt lopolith and surrounding terrane, Nevada: Geological Society of America Map and Chart Series MC–14, 6-p. pamphlet, 1 sheet, scale 1:81,000.

Stauder, W., and Ryall, A., 1967, Spatial distribution and source mechanism of microearthquakes in central Nevada: Bulletin of the Seismological Society of America, v. 57, p. 1317–1345.

Stewart, J.H., and Carlson, J.E., 1978, Geologic map of Nevada: U.S. Geological Survey and Nevada Bureau of Mines and Geology, 3 sheets, scale 1:500,000.

Stewart, S.W., Hofmann, R.B., and Diment, W.H., 1964, Some aftershocks of the Hebgen Lake earthquake—The Hebgen Lake, Montana, earthquake of August 17, 1959: U.S. Geological Survey Professional Paper 435–D, p. 19–24.

Stone, D.S., 1986, Seismic and borehole evidence for important pre-Laramide faulting along the Axial Arch in northwest Colorado, *in* Stone, D.S., ed., New interpretations of northwest Colorado geology: Denver, Colo., Rocky Mountain Association of Geologists, p. 19–36.

Susong, D.D., and Bruhn, R.L., 1986, Structure of an earthquake rupture segment boundary in the Lost River fault zone, Idaho—Implications for rupture propagation during the 1983 Borah Peak earthquake [abs.]: E⊕S, Transactions of the American Geophysical Union, v. 67, no. 44, p. 1107.

Swan, F.H., III, Schwartz, D.P., and Cluff, L.S., 1980, Recurrence of moderate to large magnitude earthquakes produced by surface faulting on the Wasatch fault zone, Utah: Bulletin of the Seismological Society of America, v. 70, p. 1431–1462.

Thenhaus, P.C., ed., 1983, Summary of workshops concerning regional seismic source zones of parts of the conterminous United States, convened by the U.S. Geological Survey 1979–1980, Golden, Colorado: U.S. Geological Survey Circular 898, 36 p.

Tocher, D., 1956, Movement on the Rainbow Mountain fault: Bulletin of the Seismological Society of America, v. 46, p. 10–14, 3 pls.

Trimble, A.B., and Smith, R.B., 1975, Seismicity and contemporary tectonics of the Hebgen Lake-Yellowstone Park region: Journal of Geophysical Research, v. 80, no. B5, p. 733–741.

Vincent, K.R., 1985, Measurement of vertical tectonic offset using longitudinal profiles of faulted geomorphic surfaces near Borah Peak, Idaho—A preliminary report, *in* Stein, R.S., and Bucknam, R.C., eds., Proceedings of Workshop XXVIII—On the Borah Peak, Idaho, earthquake: U.S. Geological Survey Open-File Report 85–290–A, p. 76–96.

Wallace, C.A., and Crittenden, M.D., Jr., 1969, The stratigraphy, depositional environment and correlation of the Precambrian Uinta Mountain Group, western Uinta Mountains, Utah, *in* Lindsay, J.B., ed., Geologic guidebook of the Uinta Mountains, Utah's maverick range: Intermountain Association of Geologists annual field conference, 16th, Evanston, Wyo., 1969, Guidebook, p. 127–141.

Wallace, R.E., 1984, Fault scarps formed during the earthquakes of October 2, 1915, in Pleasant Valley, Nevada, and some tectonic implications: U.S. Geological Survey Professional Paper 1274–A, p. A1–A33, 1 pl.

Wallace, R.E., and Whitney, R.A., 1984, Late Quaternary history of the Stillwater seismic gap, Nevada: Bulletin of the Seismological Society of America, v. 74, p. 301–314.

Westphal, W.H., and Lange, A.L., 1967, Local seismic monitoring—Fairview Peak area, Nevada: Bulletin of the Seismological Society of America, v. 57, p. 1279–1298.

Wheeler, R.L., 1984, A plan for evaluating hypothesized segmentation of the Wasatch fault, *in* Hays, W.W., and Gori, P.L., eds., Proceedings of Conference XXVI; a workshop on Evaluation of regional and urban earthquake hazards and risk in Utah: U.S. Geological Survey Open-File Report 84–763, p. 576–605.

Wheeler, R.L., and Krystinik, K.B., 1987a, Evaluating coinciding anomalies along a fault trace or other traverse—Simulations and statistical procedures: U.S. Geological Survey Bulletin 1802, 12 p.

———1987b, Persistent and nonpersistent segment boundaries on the Wasatch fault, central Utah [abs.]: Seismological Research Letters, v. 58, no. 1, p. 31.

———1987c, Persistent and nonpersistent seismic segmentation of the Wasatch fault zone, Utah [abs.]: Geological Society of America Abstracts with Programs, v. 19, no. 5, p. 342.

———1988, Segmentation of the Wasatch fault zone, Utah—Summaries, analyses, and interpretations of geological and geophysical data: U.S. Geological Survey Bulletin 1827, 47 p.

Whitten, C.A., 1957, Geodetic measurements in the Dixie Valley area: Bulletin of the Seismological Society of America, v. 47, p. 321–325.

Witkind, I.J., Myers, W.B., Hadley, J.B., Hamilton, W., and Fraser, G.D., 1962, Geologic features of the earthquake at Hebgen Lake, Montana, August 17, 1959: Bulletin of the Seismological Society of America, v. 52, p. 163–180.

Witkind, I.J., Hadley, J.B., and Nelson, W.H., 1964, Pre-Tertiary stratigraphy and structure of the Hebgen Lake area—The Hebgen Lake, Montana, earthquake of August 17, 1959: U.S. Geological Survey Professional Paper 435–R, p. 199–207, 1 pl.

Zietz, I., Shuey, R., and Kirby, J.R., Jr., 1976, Aeromagnetic map of Utah: U.S. Geological Survey Geophysical Investigations Map GP–907, 1 sheet, scale 1:1,000,000.

Zoback, M.L., 1983, Structure and Cenozoic tectonism along the Wasatch fault zone, Utah, *in* Miller, D.M., Todd, V.R., and Howard, K.A., eds., Tectonics and stratigraphy of the eastern Great Basin: Geological Society of America Memoir 157, p. 3–27.

Zollweg, J.E., and Richins, W.D., 1985, Later aftershocks of the 1983 Borah Peak, Idaho, earthquake and related activity in central Idaho, *in* Stein, R.S., and Bucknam, R.C., eds., Proceedings of Workshop XXVIII—On the Borah Peak, Idaho, earthquake: U.S. Geological Survey Open-File Report 85–290–A, p. 345–384.

Subsurface Geology Along the Wasatch Front

By DON R. MABEY, UTAH GEOLOGICAL AND MINERAL SURVEY, SALT LAKE CITY, UTAH

ASSESSMENT OF REGIONAL EARTHQUAKE HAZARDS AND RISK ALONG THE WASATCH FRONT, UTAH

U.S. GEOLOGICAL SURVEY PROFESSIONAL PAPER 1500–C

CONTENTS

	Page
Abstract	C1
Introduction	1
Geophysical Data	2
Gravity Data	2
Magnetic Data	6
Interpretations	6
Cenozoic Sediments	6
Interpretations—Continued	
Displacement Along the Wasatch Fault Zone	C11
Dip of the Wasatch Fault	11
Spurs of the Wasatch Range	12
Fault Segments	13
Conclusions	15
References Cited	15

ILLUSTRATIONS

Page

FIGURES 1–4. Maps showing:

1. Complete Bouguer gravity anomalies of the Wasatch Front area and the surface traces of the Wasatch and East Cache fault zones C4
2. Residual total magnetic intensities of the Wasatch Front area and the surface traces of the Wasatch and East Cache fault zones 8
3. Thickness of low-density sedimentary rocks in Wasatch Front valleys and the Cache Valley, inferred from gravity data 10
4. Blocks of contrasting lithology inferred from magnetic anomalies, boundaries of areas of contrasting gravity anomalies, and fault-rupture segment boundaries from Schwartz and Coppersmith (1984) and additional boundaries inferred from geophysical data for the Wasatch Front 14

ASSESSMENT OF REGIONAL EARTHQUAKE HAZARDS
AND RISK ALONG THE WASATCH FRONT, UTAH

SUBSURFACE GEOLOGY ALONG THE WASATCH FRONT

By DON R. MABEY[1]

ABSTRACT

Most of the life and property at risk from an earthquake on the Wasatch fault is in the valley areas west of the fault, where a complete cover of Quaternary sediments obscures the pre-Quaternary geology. A compilation of data from drill holes that provide significant information on the subsurface geology in the valley has been used with regional gravity and magnetic data, supplemented locally by more detailed geophysical surveys, to study the subsurface geology of the Wasatch Front area. Bouguer gravity lows are produced by low-density sediments in a string of Cenozoic basins along the Wasatch Front. These sediments, which are primarily Miocene and Pliocene in age, are up to 4 km thick in grabens that underlie the valleys. Major normal faults are reflected by large linear gravity gradients. Detailed quantitative interpretations of the gravity anomalies require information on the lateral and vertical variations in the density of the Cenozoic sediments. The large eastward decrease in regional Bouguer gravity anomalies across the Wasatch Front reflects isostatic compensation for the high elevations of the Wasatch Range and areas to the east. Individual basins and ranges to the west are not in isostatic equilibrium. The segmentation of the gravity lows and the blocks of contrasting basement lithology indicated by the magnetic data suggest segment boundaries for the Wasatch fault zone that are generally consistent with segment boundaries inferred from surface mapping of the fault zone.

INTRODUCTION

The Wasatch fault zone lies between the north-trending Wasatch Range on the east and a near-continuous string of valleys on the west. At two locations, rocks of Tertiary age and older occur in transverse zones extending between the Wasatch Range and parallel ranges to the west. Elsewhere, Quaternary sediments cover the valley areas. Most of the population and property at risk from an earthquake on the Wasatch fault zone are in these valleys. Knowledge of the subsurface structure of these valleys and the physical properties of the rocks underlying the valley floors is important to both understanding the geologic structure of the Wasatch Front and predicting the ground response and deformation that will occur with an earthquake along the Wasatch fault zone. Most pre-Cenozoic rocks that are exposed in the Wasatch Range and in the parallel ranges to the west are in thrust sheets that moved tens of kilometers eastward relative to underlying rocks during the Sevier orogeny. Exposures of autochthonous pre-Cenozoic rocks are not adequate to reveal the deep subsurface geology or to define major crustal blocks along the Wasatch Front. The primary purposes of the investigations reported here are to examine the data relating to the subsurface geology of the Wasatch Front, to interpret those data in terms of regional subsurface geology related to the earthquake hazard of the area, and to indicate how geophysical data can be used in more detailed studies.

The name Wasatch Front as generally used by the residents of Utah refers to a loosely defined area along the western side of the Wasatch Range, where most of Utah's population resides. In 1983, the National Board of Geographic Names (NBGN), on the recommendation of the Utah State Committee on Place Names, defined the Wasatch Range as extending from Collinston on the north to Nephi on the south and as being the western-most of the several north-trending mountain masses in the Middle Rocky Mountain physiographic province. Wasatch Mountains is not recognized as a geographic name by the NBGN. Stokes (1977) defined the "Wasatch Front valleys" physiographic subdivision as the valley area west of the Wasatch Range (as later defined by the NBGN), excluding the area of maximum historical extent of the Great Salt Lake but including Utah Lake and including the valley area to the north on the western side of Clarkston Mountain. In this study, the eastern part of the Great Salt Lake is included as part of the Wasatch Front valleys. Cache Valley and the other

Manuscript approved for publication November 20, 1990.
[1]Now at Atwood and Mabey, Inc., CVSR Box 2408, Moab, UT 84532.

valleys lying immediately east of the Wasatch Range are not normally considered part of the Wasatch Front. Local concentrations of population and development exist in Cache Valley, as does a significant earthquake hazard. Several lifelines into the Wasatch Front valleys extend through the Wasatch Range, and water storage reservoirs in the Wasatch Range are upstream from major population centers of the Wasatch Front. For these reasons, the Wasatch Range and Cache Valley are included in this study.

Information on the subsurface geology along the Wasatch Front can be obtained from geophysical and drill-hole data. As part of the Wasatch Front Earthquake Hazards Reduction Program, the Utah Geological and Mineral Survey (UGMS) has compiled geophysical data along the Wasatch Front and assembled information on drill holes in the valley areas along the front. The primary sets of geophysical data are regional gravity and magnetic surveys that cover the entire study area and a few refraction and reflection seismic profiles. Thousands of wells have been drilled in the valleys, but only a small percentage provides geologic data of use in this study. All available drill-hole logs were examined, and a computer file was developed from 267 drill holes that either (1) were over 300 m deep, (2) encountered bedrock (usually pre-Tertiary rock or Tertiary volcanic rocks), or (3) had complete and accurate lithologic logs (Case, 1985). The geophysical data, drill-hole data, and surface geology were then interpreted to define (1) the thickness, structure, and composition of the Cenozoic rocks underlying the valley areas, (2) blocks of crust displaying contrasting lithology, and (3) other regional crustal anomalies that might relate to current seismicity.

This study is built on numerous other studies that usually involved only one of the data sets used or that examined only part of the Wasatch Front. The earliest published regional geophysical studies of a major part of the Wasatch Front were the gravity survey by Cook and Berg (1961) and the aeromagnetic survey by Mabey and others (1964). These two studies defined the major regional gravity and magnetic anomalies along the Wasatch Front from Nephi to Farmington and established the sources of the larger regional anomalies. Zoback (1983) used gravity data as the foundation for a study of structure and Cenozoic tectonism in north-central Utah. Arnow and Mattick (1968) reported on a seismic refraction profile to determine the thickness of valley fill in Salt Lake Valley. (Several reports by the U.S. Geological Survey (USGS) and others before 1983 used the name Jordan Valley for the valley area between the Oquirrh Mountains and the Wasatch Range. In 1983, the NBGN rejected the name Jordan Valley in favor of Salt Lake Valley.) Mattick (1970) used seismic refraction data along with gravity, magnetic, and drill-hole data to study the thickness of unconsolidated to semiconsolidated sediments in Salt Lake Valley. Resistivity soundings have been used locally to determine the thickness and resistivity of sediments in the valleys (Zohdy and Jackson, 1969). Seismic reflection profiling has been used extensively by commercial companies to explore for petroleum in the Cenozoic basins and underlying older rocks, but most of these data are not available to the public. Cook and others (1967) presented an interpretive geologic cross section along an east-west profile between Little Mountain and the Wasatch Range in the Ogden area based on a seismic refraction and reflection survey and detailed gravity data. Smith and Bruhn (1984) presented data from several reflection profiles obtained in petroleum exploration, and Glenn and others (1980) reported on one profile across Hill Air Force Base. Recently, high-resolution seismic refraction profiles have been used to study near-surface fault geometry (Crone and Harding, 1984). Several other investigators have used geophysical data, most commonly gravity data, in studies of the subsurface geology of individual valleys or parts of the valleys.

The surface geology of the Wasatch Front has been studied by numerous investigators for over a century. Regional geologic maps that were particularly useful to this study were the geologic map of Utah (Hintze, 1980), geologic maps of the central, southern, and northern Wasatch Front (Davis, 1983a, b, 1985), and the geologic map of the Farmington Canyon complex and surrounding rocks (Bryant, 1984).

GEOPHYSICAL DATA

GRAVITY DATA

Zoback (1983) compiled a gravity map of the Wasatch Front region based on data in USGS files. This data set includes gravity stations from numerous surveys done by the USGS and others. Zoback's compilation was used to prepare a gravity map for this study (fig. 1). After the study reported here was completed, a new complete Bouguer gravity anomaly map of Utah was prepared by the USGS and the UGMS (Cook and others, 1989). This map, which was published by the UGMS at a scale of 1:500,000, is based on a new data set, which includes many gravity stations from a 30-year compilation made by K.L. Cook and his students at the University of Utah and not previously available to the public. The new data set better defines the gravity field throughout Utah and provides data for detailed interpretation of gravity anomalies in the area of the study reported here. The new data do not significantly alter the 5-mGal contours presented in figure 1 or the regional interpretation based on the data used to prepare that map.

The Wasatch Front is coincident with a steep regional Bouguer gravity anomaly gradient between the regional gravity high over the topographic low of the Lake Bonneville basin and the higher terrain of the Middle Rocky Mountain province to the east. At its maximum east of the Great Salt Lake, this gradient averages over 1 mGal/km for a distance of 100 km. This 100-mGal regional Bouguer gravity relief correlates well with the inverse of the regional topography, which involves a change in average elevation of about 800 to 1,100 m (depending on how the average elevation is determined). This correlation of 0.09 to 0.13 mGal/m is approximately equal to the Bouguer correction of 0.11 mGal/m used to compute the Bouguer anomaly and indicates that the regional topography across the Wasatch Front is in approximate isostatic equilibrium. A major part of the mass deficiency under the Wasatch Range and the area to the east relative to the Basin and Range province to the west is likely due to a thicker crust, but part of the deficiency may be due to a less dense crust. The steepest part of the regional gravity gradient is coincident with the western front of the Wasatch Range and indicates that the relief across the range front is, at least in part, an isostatic response. This gravity feature is in marked contrast to that of most ranges in the Basin and Range province to the west, where ranges of average size appear to be supported by the strength of the crust (Eaton and others, 1978). Any explanation of the structure of the western front of the Wasatch Range must involve both the extension associated with basin and range structure and the isostatic response to the contrasting crust on the two sides of the front.

Superimposed on the large regional gravity gradient along the Wasatch Front are local anomalies typical of the Basin and Range province that are produced by the relatively low density rocks of Cenozoic age that underlie the valley areas and by generally smaller amplitude anomalies produced by density variations within pre-Cenozoic rocks. Before a quantitative interpretation of the local anomalies can be made, they must be isolated from the regional anomaly.

In the Wasatch Front valleys is a zone of north-trending gravity lows produced by the Cenozoic rocks. The range in amplitude and form of these anomalies indicates the complexity of the structure underlying the valleys. Although the gravity data have been used by several investigators to infer the structure of the valleys and the thickness of the Cenozoic rocks, important uncertainties exist relative to the interpretation of the gravity data. The two most important uncertainties are (1) the amplitude and form of the regional gravity anomaly produced by deeper sources, which must be inferred before the anomaly caused by the Cenozoic rocks can be analyzed, and (2) the variations in the density of the Cenozoic rocks.

Several methods can be used to isolate the gravity effect of the Cenozoic rocks. A regional gravity anomaly can be computed by fitting a relatively low order surface to the Bouguer gravity anomaly values and removing that regional anomaly from the Bouguer gravity anomaly. The application of this technique is compromised because the local anomalies of interest are so large in both extent and amplitude that they are an important factor in controlling the computed surface. The most commonly used method has been to assume a regional anomaly based on the anomaly values for stations on pre-Cenozoic rocks. This technique is often highly subjective, particularly in the area immediately west of the Wasatch Range. A regional gravity anomaly that correlates with regional elevation can be computed by assuming either an isostatic model or a correlation function between the regional gravity anomaly and the average elevation. The computed regional gravity anomaly is strongly influenced by the isostatic model or correlation function assumed. A technique that works well for two-dimensional modeling of profiles is to model the total Bouguer gravity anomaly, including the regional component. This technique allows all mass anomalies that contribute to the Bouguer gravity profile to be considered in one model, and the uncertainties of all assumptions are apparent to the interpreter.

In computing the Bouguer gravity anomaly and in interpreting the gravity anomalies, the rocks of pre-Cenozoic age in the Wasatch Front area are generally assumed to have a density of 2.67 g/cm^3. The density of the Cenozoic rocks ranges from less than 2.0 g/cm^3 for some of the unconsolidated, fine, well-sorted sediments to over 2.5 g/cm^3 for some of the volcanic rocks and the well-consolidated sedimentary rocks. In general, the older, more deeply buried Cenozoic sedimentary rocks and the volcanic rocks are more dense than the younger sedimentary rocks, but another important factor determining density is sedimentary rock type. The coarse, poorly sorted, fluvial sediments along the margins of the local basins are significantly more dense than the fine, well-sorted, lacustrine sediments in the central parts of the basins. This systematic decrease in density toward the centers of Cenozoic basins in the Basin and Range province was described by Kane and Pakiser (1961) and Mabey (1960) for California basins and by Mabey and Morris (1967) for a Utah basin, but most interpretations of gravity anomalies along the Wasatch Front have assumed a single density contrast for sediments of the same age or depth within a basin. Although this assumption is valid when the gravity data are used only to indicate the general configuration and thickness of the Cenozoic basins, it can lead to incorrect conclusions in

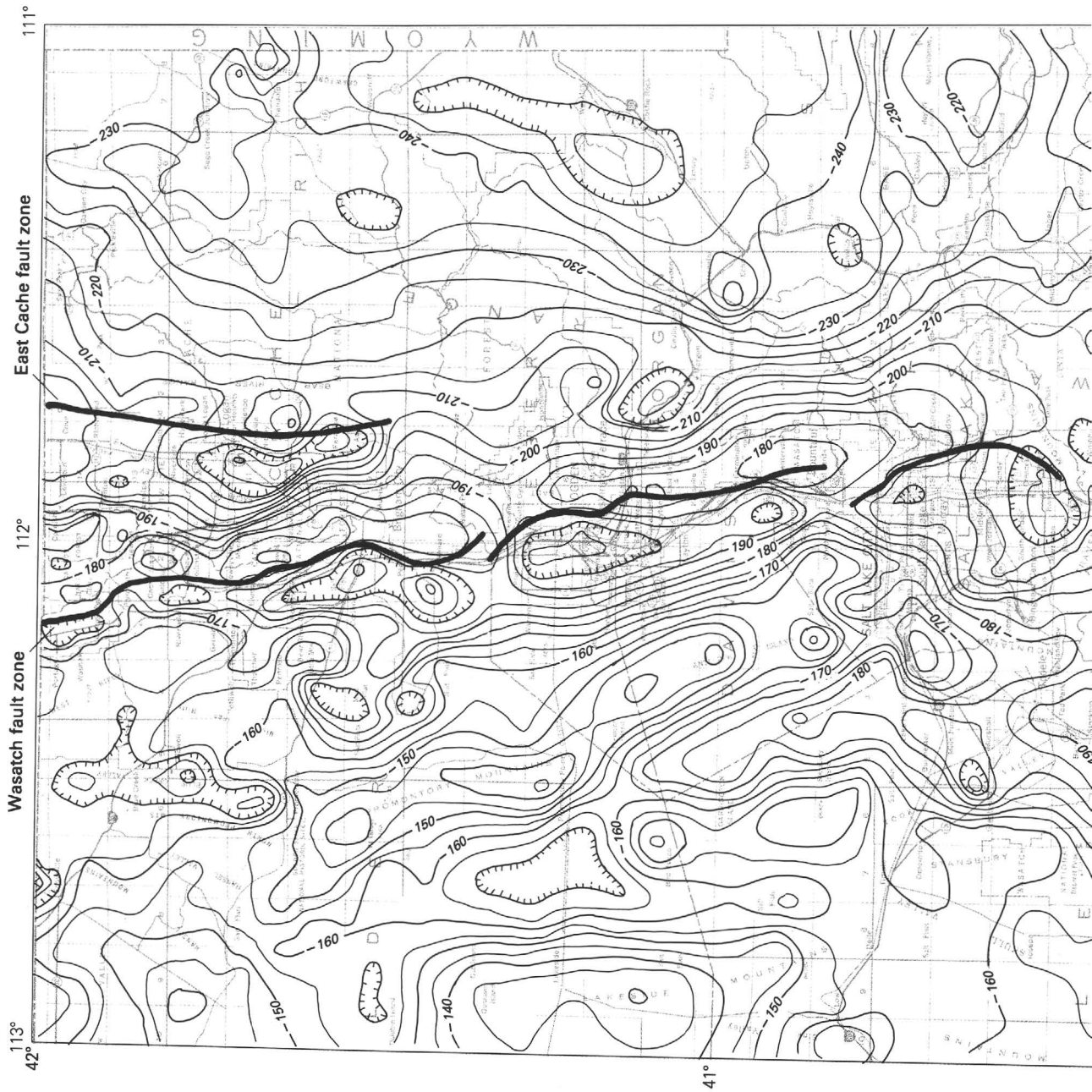
East Cache fault zone
Wasatch fault zone
111°
112°
113°
42°
41°
230
240
220
210
200
190
180
170
160
150
140

FIGURE 1.—Complete Bouguer gravity anomalies of the Wasatch Front area and the surface traces of the Wasatch and East Cache fault zones. Contour interval is 5 mGal. Gravity map is modified from Zoback (1983).

modeling details of basin margins, including location and dip of normal faults bounding the basins.

MAGNETIC DATA

The magnetic map of Utah (Zietz and others, 1976) was prepared by mosaicking magnetic contour maps based on several independent surveys. A new magnetic map of Utah based on merging digital data sets to a common datum and projecting the data to a common level is being prepared and will be published by the UGMS at a scale of 1:500,000. As with the new gravity data set, the new magnetic data set will facilitate a more detailed quantitative analysis of the data than is attempted here. The magnetic map of the Wasatch Front area presented here (fig. 2) is modified only slightly from that of Zietz and others (1976). The two surveys that were used to compile this part of the State map were both flown at 3,700 m above sea level; thus, no flight-level problem exists within the data. The survey in the northern part of the area is based on north-south flight lines 8 km apart; the survey to the south is based on east-west flight lines 3.2 km apart.

The regional residual magnetic field in the Wasatch Front area is dominated by magnetic anomalies from two principal sources: Tertiary igneous rocks and Precambrian crystalline rocks (Mabey and others, 1964). Two west-trending zones of Tertiary igneous rocks are indicated by bands of magnetic highs south of Salt Lake City. The northern zone is here called the Bingham-Park City magnetic zone, and the southern is the Tintic magnetic zone. The major cause of these magnetic highs is Tertiary plutons, although Tertiary volcanic rocks locally contribute to the magnetic anomalies. The magnetic anomalies over Antelope Island and the Wasatch Range north of Salt Lake City are produced by rocks in the Archean Farmington Canyon Complex. Magnetic highs over these Archean rocks are associated with the quartz monzonite granite gneiss and migmatite mapped by Bryant (1984). There is little magnetic expression of the schist and gneiss as mapped by Bryant. A broad magnetic high in Cache Valley and over the range to the west is also probably produced primarily by Precambrian rocks, but Cenozoic volcanic rocks in northeast Cache Valley appear to be contributing to the anomaly (Scheu, 1985).

INTERPRETATIONS

CENOZOIC SEDIMENTS

The Wasatch Formation of Eocene and Paleocene age is exposed in the central Wasatch Range and areas to the east but does not crop out west of the Wasatch fault zone. The sedimentary rocks exposed over much of the Salt Lake salient were once thought to be Wasatch Formation but now appear to be younger (Bryant, 1984). The Wasatch Formation is over 1,000 m thick in the Wasatch Range and may extend west under the Wasatch Front valleys. Sedimentary rocks encountered in several wells in valleys west of the Wasatch fault have been identified as Wasatch Formation primarily on the basis of color (Case, 1985). Some of these rocks may be younger or older than the Wasatch Formation. Paleocene and Eocene rocks of the North Horn Formation, the Flagstaff Limestone, and the Colton Formation occur in the southern Wasatch Range and may occur under adjacent valleys.

Volcanic rocks of late Eocene and Oligocene age are widespread in the ranges over the Wasatch Front area and are reported in some drill holes in the valleys (Case, 1985). The Norwood Tuff, which includes tuff, tuffaceous sandstone, conglomerate, and clay, is over 1,000 m thick in the central Wasatch Range and underlies some of the valley areas. Latite, andesite, and rhyolite flows and tuffs were erupted in the igneous belts producing the Bingham-Park City and Tintic magnetic zones. These rocks are exposed in the ranges and are known to extend under the valleys in the area of these belts.

The pattern of basin and range topography in the Wasatch Front region appears to have developed in Miocene time in response to regional extension (Stewart, 1978). In the Wasatch Front area, Miocene and Pliocene rocks are extensively exposed only around Cache Valley and the City Creek spur; however, they are encountered in most deeper wells in the valleys (Case, 1985) and appear to be the major low-density rock causing the gravity lows in the valleys.

The Miocene and Pliocene history of the Wasatch Front valleys is poorly known, but it appears that local basins of deposition began to subside in Miocene time and have continued subsiding to the present. As the basins evolved, the area, location of maximum subsidence, style of deformation, climate, and source of sediments likely changed, producing a complex distribution of sedimentary rock types in the basins. Igneous flows and sills occur interbedded with Miocene and Pliocene sedimentary rocks in northern Cache Valley (Scheu, 1985) and in the area of the Great Salt Lake.

The subsurface contact between the Tertiary and Quaternary sediments under the valleys often cannot be identified with confidence. In northern Salt Lake County, Arnow and Mattick (1968) correlated a downward increase in resistivity and an increase in seismic velocity with the Tertiary-Quaternary contact. P-wave velocities above this contact were less than 1.8 km/s. They attributed P-wave velocities as high as 3.8 km/s to Tertiary rocks and velocities greater than 4.6 km/s to

consolidated rocks of several ages. They interpreted a seismic refraction profile across the valley north of Salt Lake City and data from three drill holes as indicating that the thickness of the Quaternary sediments ranges from 180 to 770 m and the thickness of Tertiary rock from 0 to 1,040 m. The maximum thickness of the combined Cenozoic units along the profiles is 1,470 m. Arnow and Mattick reported that one well penetrated volcanic rocks, possibly andesites, between 700 and 850 m below the surface. Arnow and others (1970) prepared a contour map (at 500-ft contour intervals) of the base of the Quaternary deposits in Salt Lake Valley south of this profile. This map was based on drillers' logs, and the top of the Tertiary deposits was selected at the first reported beds of lava, conglomerate, hardpan, or various types of cemented or hard materials that were more than 1 m thick. Nowhere did they find Quaternary deposits thicker than those along the seismic profile; over most the valley, Quaternary sediments were less than 300 m thick.

Hunt and others (1953) interpreted well logs in northern Utah Valley as indicating that the Quaternary sediments thickened southward to the Geneva Steel plant, where they were about 150 m thick. Dustin and Merritt (1980), also using well logs, concluded that the Quaternary deposits were approximately 50 to 60 m thick at the northern end of Utah Valley and 135 to 150 m thick at the southern end. Feth and others (1966), in a study of the Weber and Davis County area, reported that a well near Farmington appears to have penetrated the base of the Quaternary at 248 m but that Quaternary sediments are less than 60 m thick at most places in their study area. Williams (1962) reported that most wells in southern Cache Valley do not penetrate the base of the Quaternary sediments but that one well did at about 150 m. In northern Cache Valley, Stanley (1971) found an increase in resistivity at depths ranging from 90 to 150 m. He concluded that this horizon was probably the top of pre-Lake Bonneville sediments of Pleistocene age; however, this horizon could also be interpreted as the base of the Quaternary sediments. Bjorklund and McGreevy (1971) examined the logs of five deep wells in Cache Valley; although they concluded that it was difficult to distinguish the Quaternary-Tertiary contact, they placed the contact at the top of a thick conglomerate at depths of about 335 to 400 m.

Only in one local area of the Wasatch Front valleys—northern Salt Lake County—are Quaternary sediments in excess of 400 m thick indicated; as will be discussed later, this area is characterized by anomalous structure. In most of the valley areas, the Quaternary sediments are reported to be less than 200 m thick. Where seismic velocity and resistivity data are available, the base of the assumed Quaternary deposits appears to correlate with a significant increase in seismic velocity and resistivity. The inferred subsurface boundary between Tertiary and Quaternary sediments in the Wasatch Front valleys has not been dated in most areas. The horizon at which the degree of consolidation of the sediments increases may not everywhere correspond to a time boundary. It is, however, a boundary significant to predicting ground response in an earthquake. Either seismic refraction or resistivity soundings have proven to be practical geophysical techniques for mapping this boundary.

Paleogene and Quaternary rocks do contribute to the large gravity lows under the Wasatch Front valleys, but, in areas where borehole data are available, the largest contribution is from the Miocene and Pliocene sedimentary rocks. Locally, these rocks are very thick. Nearly 4,000 m of these rocks were penetrated in the Gulf Energy and Minerals well in southern Utah Valley, and the base still was not reached (Davis and Cook, 1983).

If the assumption is made that all of the residual Bouguer gravity lows over the Wasatch Front valleys are produced by the density contrast between sediments of Miocene age and younger and the more dense, older rocks, then the gravity anomaly can be analyzed to determine the thickness of the low-density rocks required to produce the gravity low. A computer program was used to determine the thickness of low-density sediments that would produce the Bouguer gravity low along 26 profiles across the Wasatch Front valleys. The computation assumes that the prism of sediments is normal to the profile and extends to considerable distances on each side of the profile. Because of the elongation of the gravity lows and the locations and orientations of the profiles, the assumption does not induce large errors. A density contrast of -0.4 g/cm^3 was assumed. The resulting inversion of the gravity data is shown as a contour map of sediment thickness in figure 3. Zoback (1983), Peterson (1974), Peterson and Oriel (1970), Davis and Cook (1983), and others have interpreted gravity profiles to infer the thickness of low-density sediments along profiles in the same area. Their procedures involved assuming a density model and modifying it until a model was produced that satisfied their chosen geologic constraints and that also produced an acceptable match to the gravity anomaly. The technique used here differs; its only geologic constraint is that the surface extent of the low-density sediments must correspond to the known geology. It is thus an inversion of the gravity data. The thickness of sediments indicated in figure 3 is generally greater than that inferred by Zoback (1983), Peterson (1974), and Peterson and Oriel (1970); they assumed a density contrast of -0.5 g/cm^3, and here a contrast of -0.4 g/cm^3 was assumed. The thicknesses are in general agreement with those of Davis and Cook (1983), who

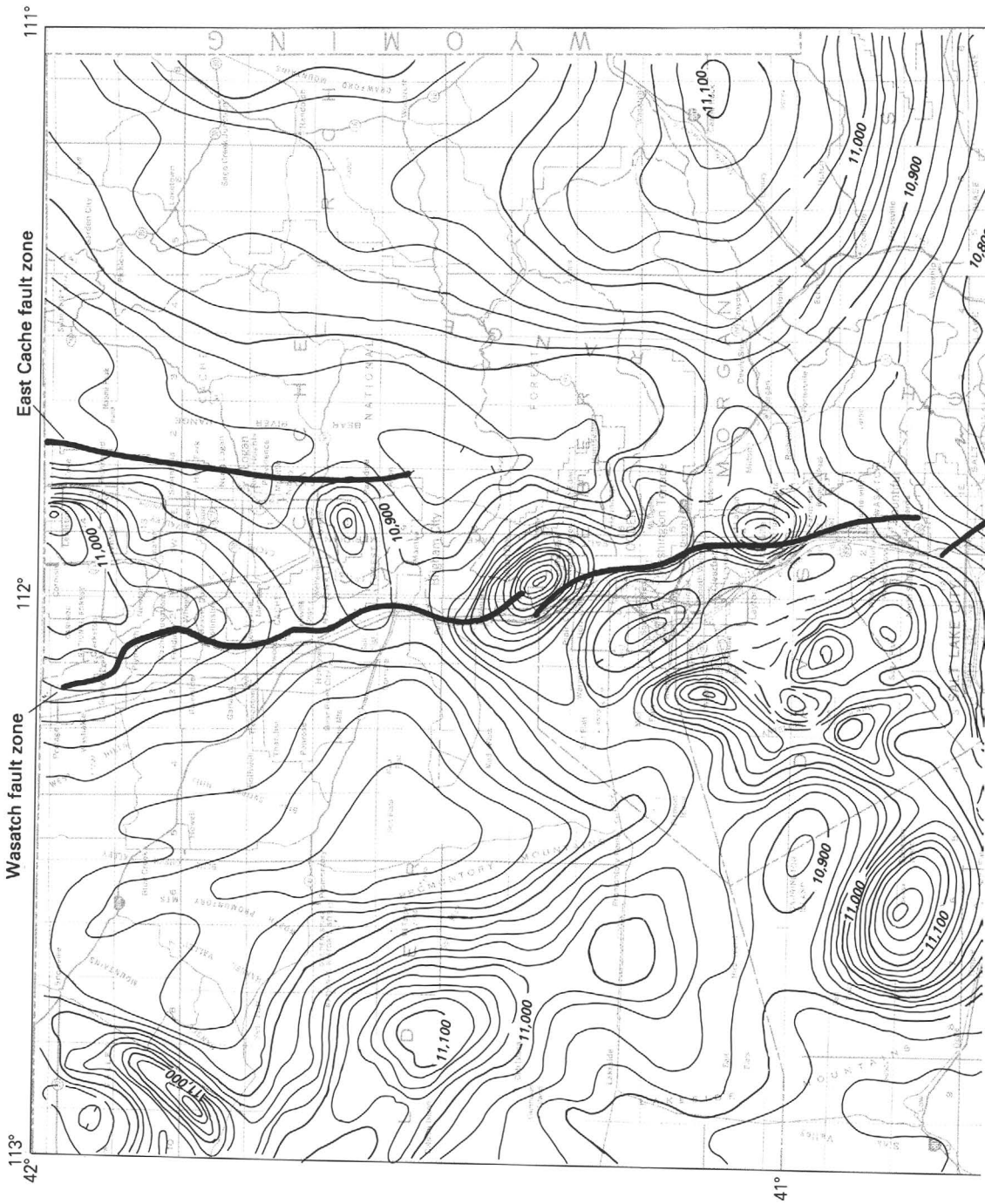
East Cache fault zone
Wasatch fault zone
11,100
11,000
10,900
111°
112°
113°
42°
41°

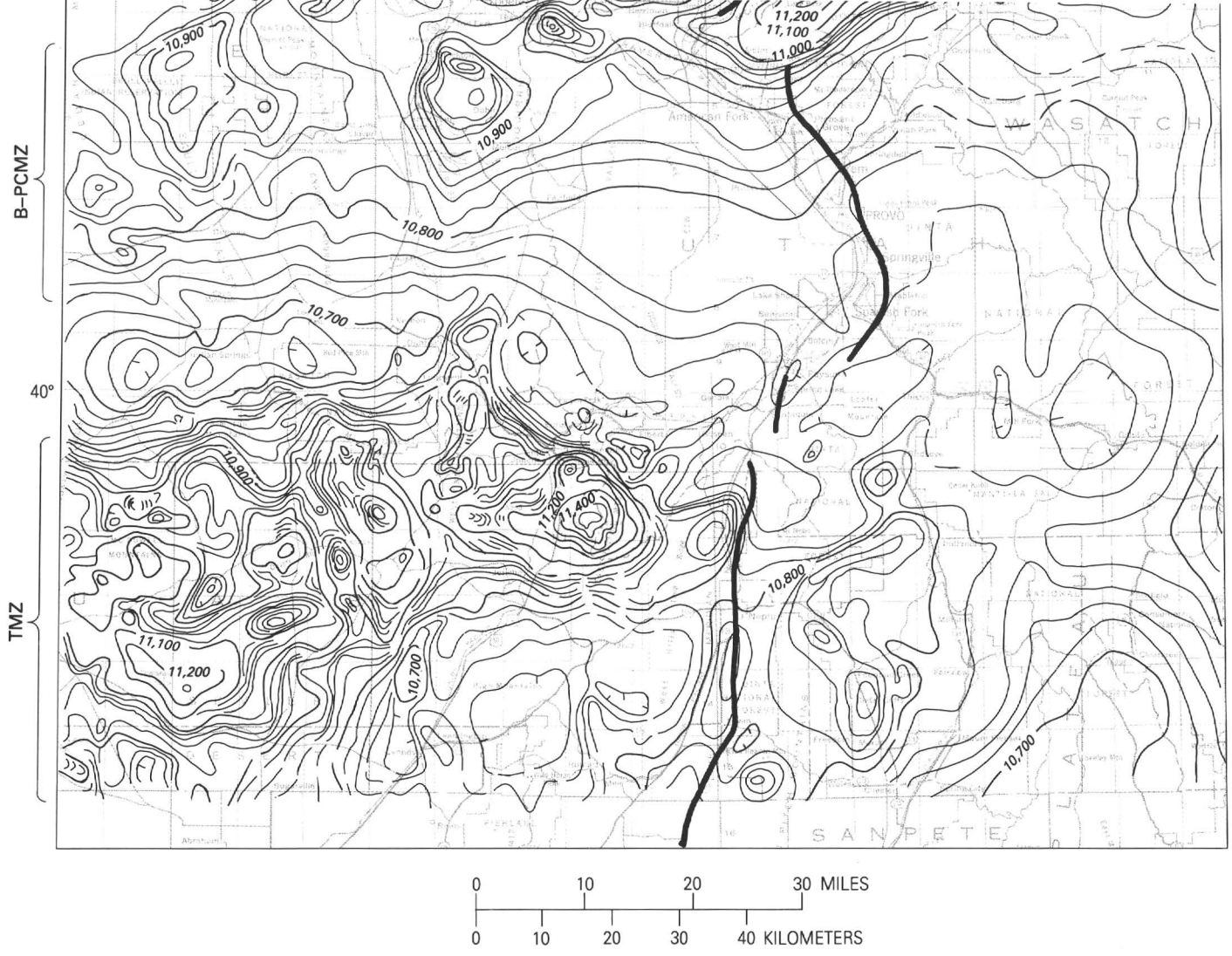

FIGURE 2.—Residual total magnetic intensities of the Wasatch Front area and the surface traces of the Wasatch and East Cache fault zones. B–PCMZ is the Bingham-Park City magnetic zone, and TMZ is the Tintic magnetic zone. Contour interval is 20 γ. Magnetic map is modified from Zietz and others (1976).

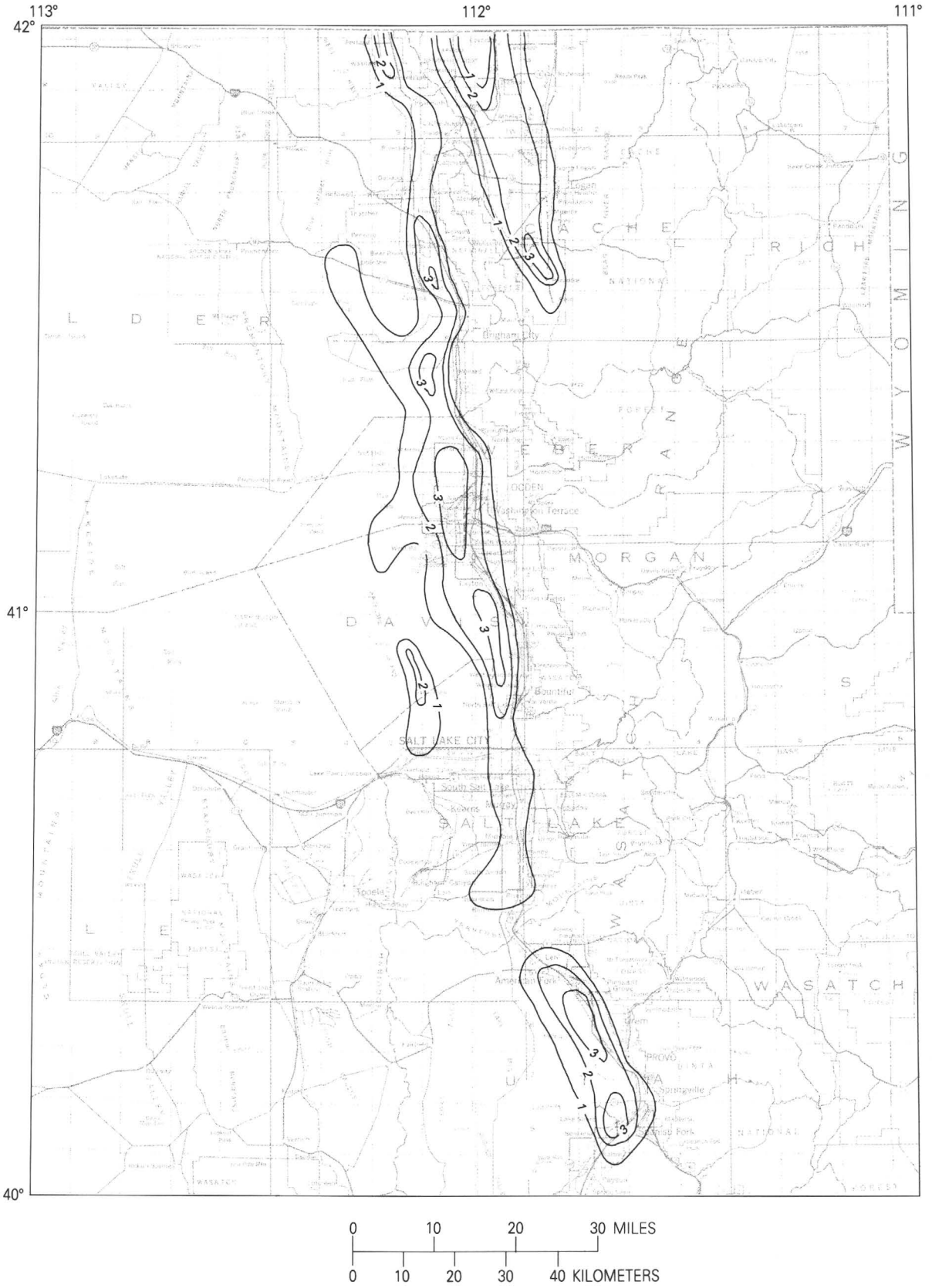

FIGURE 3.—Thickness of low-density sedimentary rocks in Wasatch Front valleys and the Cache Valley, inferred from gravity data. Contour interval is 1 km.

assumed a contrast decreasing with depth from −0.62 to −0.22 g/cm^3. The density of the Cenozoic sediments normally increases with depth; at depths greater than 2 km, the density contrast with the older rocks is likely to be substantially less than the −0.4 g/cm^3 assumed in the inversion of the gravity data. The result is that, in the area of thickest sediments, the calculated thickness may be substantially less than the actual thickness. This situation is known to occur at the southern end of Utah Valley, where a drill hole is reported to have bottomed at 4,000 m in Cenozoic sediments at a location where the inversion of the gravity data indicates that the sediments are less than 4,000 m thick.

Throughout the Wasatch Front valleys, the axis of the gravity low (and, presumably, the axis of the structural low) is east of the center of the valley. The topographic low is generally west of the axis of the valley. Thus, movement along the Wasatch fault zone on the eastern side of the valley tilts the valley floor eastward, but debris derived from the Wasatch Range and the highlands to the east is then deposited along the eastern side of the valley and displaces the topographic low to the west. This scenario is well illustrated in Utah Valley, where the axis of the gravity low lies along the eastern shore of Utah Lake, and on the eastern shore of the Great Salt Lake, where the axis of the gravity low is generally east of the lake. The gravity data support the conclusion that the gross structure of the valleys is eastward-tilting blocks.

DISPLACEMENT ALONG THE WASATCH FAULT ZONE

The crest of the Wasatch Range is generally 1.5 to 2 km above the valley floor to the west. This range of values is often accepted as the minimum vertical displacement of the Wasatch fault. The maximum vertical displacement can be estimated by adding to the range height the maximum depth to the base of the Miocene sediments under the valley (about 4 km) and the estimated thickness of rock removed from the range crest in Miocene and post-Miocene time, which is difficult to estimate but might be as much as 2 km. This process yields a maximum vertical displacement across the Wasatch fault zone of about 8 km. These calculations of maximum and minimum fault displacement both assume that warping has not made a major contribution to the structural relief across the Wasatch Front.

Although local evidence of lateral displacement along the Wasatch fault zone has been identified, there is no evidence that lateral displacement is an important component of total displacement, and the character of the surface trace of the fault is inconsistent with major lateral movement. Displacement of magnetic features that extend across the fault can be used to estimate lateral movement. The Bingham-Park City magnetic zone is nearly normal to the Wasatch fault. If the Oligocene intrusive rocks that are the major cause of the magnetic anomaly were once a continuous linear-sided mass, any post-Oligocene offset of that mass should be apparent in the magnetic data. No major offset is apparent. The approximately 5-km left-lateral offset of the crest of the magnetic high across the fault can be explained by the present topography of the top of the intrusive mass. The Tintic magnetic zone is best defined from the Tintic Mountains west, and it is questionable whether the large volumes of Oligocene intrusive rocks that produce the higher amplitude magnetic highs in the zone occur east of the Wasatch fault. Local magnetic highs in the Wasatch Range east of Nephi appear to be produced by outcropping Tertiary volcanic rocks. Therefore, this magnetic zone is of limited use in detecting lateral offset.

The magnetic anomalies north of Salt Lake City are not continuous but appear to define two zones, one trending north and one trending north-northwest. Three high magnetic closures form a north-northwest-trending zone about 50 km long over Antelope Island and the adjacent valley area to the east. A magnetic low over the structurally low part of the valley separates these anomalies from a magnetic high zone of similar length over the Wasatch Range. The left-lateral offset of these two zones is about 40 km. This evidence of lateral offset of the Precambrian rocks is weak. Even if it is real, the offset could have occurred long before the development of the Wasatch fault zone.

DIP OF THE WASATCH FAULT

Gilbert (1928) measured the dip of the Wasatch fault at several locations and, excluding the dips on spurs and salients, determined an average dip of 33.4°. Zoback (1983) questioned whether some of the dips that Gilbert measured were of the fault surface, and she reported four new measurements for the dip of the fault in bedrock, at locations not on spurs; her values of dip ranged from 44° to 68°. Gilbert's measurements and others in the vicinity of the spurs and the Transverse Range indicate that individual faults of the Wasatch fault zone in near-surface bedrock dip about 70° to the west. Away from the spurs, the near-surface dips vary considerably but are generally less than 70° and in some areas are less than 30°.

A Bouguer gravity anomaly gradient parallels the front of the Wasatch Range and the Wasatch fault zone for most of their lengths. Locally, the steepest gradient is coincident with the active surface trace of the fault, but, along portions of the fault, the gravity data suggest that pre-Tertiary bedrock occurs at relatively shallow

depths on the downthrown side of the mapped traces of the fault. In the Bountiful area, for example, the mapped fault traces are in the area of a gravity high that suggests the presence of bedrock at relatively shallow depths on both sides of the fault. A large gravity gradient that is suggestive of faulting along the northern extension of the Warm Springs fault (Cook and Berg, 1961, pl. 13) lies about 3 km west of the mapped traces. In some places where a gravity gradient occurs in the area of the fault zone, the gradient does not indicate a high-angle fault interface between contrasting density units but can be modeled with an interface sloping about 20° to the west. An example is the East Bench fault in the eastern part of Salt Lake City. These relatively low gravity gradients can be interpreted as reflecting a series of step faults. The decrease in density of basin fill toward the center of the valley will also tend to extend the gravity gradient associated with the edge of a prism of valley fill over a greater distance than it would if fill were one density unit. If a single density contrast is assumed in interpreting such an anomaly, the inferred dip of the density interface will be lower than the actual dip. In some locations, such as at the western end of spurs and in parts of the range front, steep gravity gradients approximately coincident with the surface fault trace indicate considerable concealed displacement along the exposed traces of the Wasatch fault zone. Because the gravity lows in the valleys west of the fault zone are in large part reflecting the distribution of Miocene and Pliocene sediments, the lack of correlation between some of the structures indicated by the gravity data and the surface traces of the Wasatch fault may reflect changes of basin structure with time. The relatively low dip of most of the faults in the Wasatch fault zone and the lateral gradation of density in the basin fill are serious handicaps in using the gravity data to infer the geometry of the Wasatch fault zone.

Using seismic reflection data, Smith and Bruhn (1984) estimated the dip of the Wasatch fault at five locations. At depths from 0.8 to 2.0 km, they estimated apparent dips ranging from 6° to 54° to the west, the average estimate being 30°. At two locations, the apparent dips at depths greater than 2.0 km were estimated to be 4° and 10°.

The geophysical evidence available on the dip of the Wasatch fault zone indicates that the zone and major faults within the zone dip to the west. In the vicinity of the spurs and the Transverse Range, individual faults dip steeply at least near the surface. Elsewhere, the dips are considered to be less and commonly appear to decrease with increasing depth. Accurately determining the dip of the Wasatch fault zone or that of individual faults in the zone at depths of more than a few tens of meters is difficult. The most useful data have been obtained by seismic reflection profiling. Seismic reflection surveys designed to determine fault geometry and supplemented by other geophysical data and perhaps drilling appear to offer the most promise of providing detailed information on subsurface geology of the Wasatch fault zone. When the fault ruptures, measurements of deformation before, during, and after the events, focal mechanism analysis, and the distribution in space of related earthquakes will likely provide information on fault geometry that cannot be obtained before the event.

Linear zones of steep gravity gradients occur on the western sides of most of the major gravity lows in the Wasatch Front valleys. These gradients are generally interpreted as indicating normal faults or fault zones that are the western sides of grabens within the valleys. These fault zones are usually not along mountain fronts but from 4 to 20 km east of the nearest mountains to the west. These gradients cannot usually be correlated with mapped surface faults, but thermal springs coincident with these gradients suggest that they may reflect active fault zones. These gradients are in areas inundated by Lake Bonneville within the last 15,000 years, and evidence of older faulting is difficult to identify in the unconsolidated sediments involved. The areas of lowest Bouguer gravity anomaly values in the Wasatch Front valleys can be interpreted as indicating grabens, but the individual grabens are generally significantly narrower than the valley. Only in a few locations, such as at the ends of some of the spurs of the Wasatch Range, does the inferred location of the faults bounding the grabens correspond to the mapped location of the surface trace of active faults.

In the Cache Valley area, the area of thick, low-density rocks extends beyond the valley over outcropping Tertiary sedimentary rocks. The gravity data suggest that all of southern Cache Valley is underlain by thick, low-density sediments, but, in the north, the area of thick sediments is confined to the western side of the valley. An appended area of thick sediments extends from Cache Valley into Clarkston Valley.

SPURS OF THE WASATCH RANGE

Gilbert (1928) studied the Wasatch fault and named the major spurs of the Wasatch Range; his names are used here. The gravity data provide some indication of the subsurface geology that was not accessible to Gilbert, and geologic mapping since Gilbert's work has better defined the surface geology. Gilbert concluded that the spurs were separated from the main mass of the Wasatch Range and from the valleys by faults. He further concluded that the faults along the valley side of the spurs were likely to dip more steeply than those along the

range front. He noted that hot springs occur along each of the major spurs and that only at two other locations along the Wasatch fault did hot springs occur. He (Gilbert, 1928, p. 32) concluded, "It may be that the outer faults of the spurs are peculiarly favorable for the conveyance of deep penetrating circulation because of the less perfect adjustment there of the fault walls." Geophysical data and recent geologic mapping generally support Gilbert's conclusion, except as they relate to his Traverse spur.

Steep local gravity gradients have been measured along the Wasatch fault zone at the western edges of the Madsen, Pleasant View, and City Creek spurs. This occurrence supports Gilbert's conclusion that the faults here dip more steeply than is normal for the Wasatch fault zone. The faults on the western side of each of these spurs trend a few degrees west of north. Only at the City Creek spur are there data on the thickness of Quaternary sediments under the valley west of the spur, but the 770-m thickness inferred here by Arnow and Mattick (1968) is the thickest reported anywhere in the Wasatch Front valleys. The Tertiary sedimentary rocks in the City Creek spur that had earlier been considered to be of Eocene age are now mapped as Miocene and Pliocene age (Bryant, 1984). If these sediments were deposited in the valley, their presence on the spur supports Gilbert's conclusion that the spur blocks were once so associated with the valley block as to receive the same deposit and have since been lifted with reference to the valley block (Gilbert, 1928, p. 31). In addition, Gilbert (1928, p. 32) noted that the diversities in the history of each spur "show that the conditions determining adhesion to the [Wasatch] range or to the sinking valley were local and variable." There is no evidence in the gravity data of a fault displaying a major vertical displacement on the western side of the Traverse spur as defined by Gilbert. A concealed fault trending a few degrees north of east, at the western end, has been postulated along the hot springs in the area (Gilbert, 1928, p. 29; Cook and Berg, 1961, p. 81). The Tertiary rocks exposed on the spur are Oligocene volcanic rocks and do not provide evidence that the spur is an uplifted part of the valley. The Traverse spur as defined by Gilbert appears to be a part of the Traverse Range and not a spur of the Wasatch Range in the sense that the Madsen, Pleasant View, and City Creek spurs are.

FAULT SEGMENTS

The Wasatch fault zone consists of several segments, each behaving with some degree of independence from adjacent segments. Schwartz and Coppersmith (1984) defined six major rupture segments and proposed that a rupture event will likely be confined to one segment. The gravity and magnetic data were analyzed independently to identify features that might relate to segment boundaries. These maps were then compared with the segments defined by Schwartz and Coppersmith (fig. 4). Because Schwartz and Coppersmith used Zoback's (1983) gravity data along with other data to define their segments, their segments are not completely independent of the geophysical data.

Five blocks of contrasting magnetic properties were identified (fig. 4*A*). Block I is the eastern end of the Tintic magnetic zone. To the west, the zone is dominated by magnetic highs produced by Tertiary intrusive rocks, but, in the Wasatch Range, the amplitude of the anomalies is lower, and most individual magnetic highs relate to Tertiary volcanic rocks. Block III is the Bingham-Park City magnetic zone. Tertiary intrusive rocks appear to make up much of the upper crust. In both of these blocks, but particularly in Block III, Tertiary igneous activity likely modified the crust significantly, so that its response to regional strain is now different from that of the adjacent blocks. Blocks II and IV are characterized by generally low magnetic relief. In these blocks, the Phanerozoic sedimentary rocks appear to be very thick, and there is no evidence of an underlying, strongly magnetized magnetic basement. Block V is characterized by magnetic highs produced by Precambrian crystalline rocks of the Farmington Canyon Complex. There is no indication in the magnetic data that these rocks are allochthonous. Block VI is a region of relatively low magnetic relief, except for two areas of high magnetic intensity in the Cache Valley area. The maximum intensity of the northern magnetic high in Cache Valley occurs a few kilometers north of the Utah-Idaho border in an area where intrusive and extrusive basalts crop out (Scheu, 1985). However, there is no evidence that these rocks underlie the central and southern parts of Cache Valley, and it seems unlikely that the entire area of high magnetic intensity is produced by Tertiary igneous rocks. This zone of high magnetic intensity continues north to the Pocatello area, where Precambrian rocks appear to be the primary cause of the anomaly. The magnetic data suggest that a block of anomalous magnetic basement rocks underlies much of Cache Valley.

The gravity lows along the western side of the Wasatch fault are segmented, and these segments reflect the total accumulation of sediment since the start of the subsidence of the structural lows, presumably in Miocene time (fig. 4*B*). The southern segment (A) is defined by a low-amplitude gravity low between Nephi and Santaquin in Juab Valley, which is adjacent to the highest part of the Wasatch Range and is the valley area of thinnest sediment west of the range. Segment B is Utah Valley, which contains the largest gravity low of any of the Wasatch Front valleys and probably the thickest

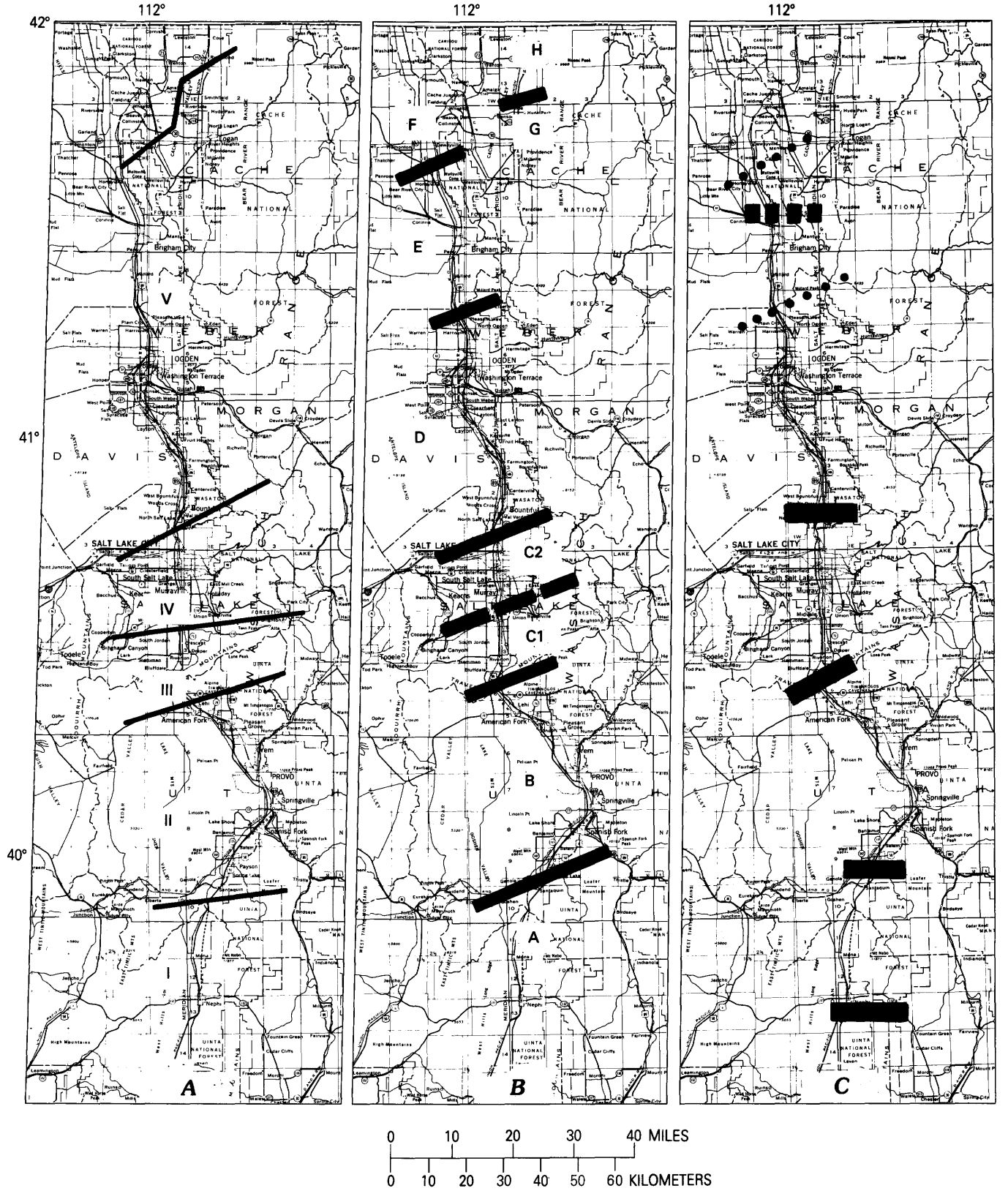

FIGURE 4.—*A*, Blocks of contrasting lithology (I–V) inferred from magnetic anomalies; *B*, boundaries of areas of contrasting gravity anomalies (A–H); *C*, fault-rupture segment boundaries from Schwartz and Coppersmith (1984) (solid and dashed bars) and additional boundaries inferred from geophysical data (dotted lines) for the Wasatch Front.

ments. This segment is bounded on the north by a high gravity trend approximately coincident with the Traverse Range. Segment C is Salt Lake Valley. The southern part of Salt Lake Valley (designated C–2) contains an approximately equidimensional gravity low that is different in shape from any other lows immediately west of the Wasatch fault zone. This low may be in part produced by rocks of Oligocene age or older. In northern Salt Lake Valley (C–1), there is a low-amplitude gravity low east of the axis of the valley. The two gravity segments of Salt Lake Valley are separated by a major gravity gradient that extends across the valley and into the ranges on each side of the valley. The northern edge of segment C–1 is defined by a high-gravity trend coincident with the City Creek spur. Segment D is a pronounced gravity low in the eastern part of the valley area extending from Bountiful to a gravity high over the Pleasant View spur north of Ogden. Segment E is flanked by a relatively narrow gravity low along the front of the range between the Pleasant View spur and the largely concealed spur near Honeyville (Madsen spur). The northern segment (F) is a moderately complex low on the eastern side of the valley. Two segments of the East Cache fault zone on the eastern side of Cache Valley are suggested by the gravity data. In Cache Valley south of Smithfield, segment G is along a pronounced gravity low approximately coincident with the valley. North of Smithfield in segment H, the gravity low is confined to the western side of the valley.

Combining the segments inferred from the gravity and magnetic data suggests six segments of the Wasatch fault zone between Nephi and the Utah-Idaho border. The three southern segments agree well with the segments defined by Schwartz and Coppersmith (1984) (fig. 4*C*). The geophysical data suggest that the Ogden segment as defined by Schwartz and Coppersmith may be terminated on the north by the Pleasant View spur. A division of the fault zone north of the Pleasant View spur into two segments is suggested by relatively subtle features in the gravity and magnetic anomalies. Rather than segment boundaries near Brigham City (dashed bar, fig. 4*C*) as Schwartz and Coppersmith concluded, interpretations of the geophysical data suggest a segment boundary at the largely concealed Madsen spur near Honeyville. The boundaries proposed here reduce the length of the Ogden segment from over 80 km to less than 60 km and leave the Provo segment, at about 60 km, as the longest segment of the Wasatch fault zone.

CONCLUSIONS

Geophysical data combined with borehole data and surface geologic mapping can make substantial contributions to understanding the Wasatch fault zone. Gravity data in the Wasatch Front valleys indicate that the valleys are underlain by low-density sediments that are commonly more than 1,000 m thick and locally more than 3,000 m thick. Data from drill holes and from other geophysical surveys indicate that most of these rocks are Miocene or Pliocene in age. The thickest accumulations of these rocks are in grabens that are usually centered east of the centers of the valleys. The geophysical data are generally consistent with the Wasatch fault's dipping rather gently to the west, except at the ends of spurs, where the faults dip steeply to the west. Faults on the western sides of the grabens within the valleys generally dip steeply to the east. The gravity and magnetic data can be used to define crustal blocks of contrasting lithology along the Wasatch fault, and the boundaries of these blocks may correspond to segment boundaries of the fault. The Wasatch Range and adjacent highlands to the east are in approximate isostatic balance with the lower areas to the west. This contrast with normal ranges in the Basin and Range province suggests that isostatic forces are partly responsible for the uplift of the Wasatch Range.

REFERENCES CITED

Arnow, T., and Mattick, R.E., 1968, Thickness of valley fill in the Jordan Valley east of the Great Salt Lake, Utah, *in* Geological Survey research 1968: U.S. Geological Survey Professional Paper 600–B, p. B79–B82.

Arnow, T., Van Horn, R., and LaPray, R., 1970, The pre-Quaternary surface in the Jordan Valley, Utah, *in* Geological Survey research 1970: U.S. Geological Survey Professional Paper 700–D, p. D257–D261.

Bjorklund, L.J., and McGreevy, L.J., 1971, Ground-water resources of Cache Valley, Utah and Idaho: Utah Department of Natural Resources Technical Publication 36, 72 p.

Bryant, B., 1984, Reconnaissance geologic map of the Precambrian Farmington Canyon complex and surrounding rocks in the Wasatch Mountains between Ogden and Bountiful, Utah: U.S. Geological Survey Miscellaneous Investigations Map I–1447, scale 1:50,000.

Case, W.F., 1985, Significant drill holes of the Wasatch Front Valleys including Cache Valley and Tooele Valley: Utah Geological and Mineral Survey Open-File Report 82, 78 p.

Cook, K.L., and Berg, J.W., Jr., 1961, Regional gravity survey along the central and southern Wasatch Front, Utah: U.S. Geological Survey Professional Paper 316–E, p. E75–E89.

Cook, K.L., Berg, J.W., Jr., and Lum, D., 1967, Seismic and gravity profile across the northern Wasatch trench, Utah, *in* Musgrave, A.W., ed., Seismic refraction prospecting: Tulsa, Okla., Society of Exploration Geophysicists, p. 539–549.

Cook, K.L., Bankey, V., Mabey, D.R., and DePangher, M., 1989, Complete Bouguer gravity anomaly map of Utah: Utah Geological and Mineral Survey Map 122, scale 1:500,000.

Crone, A., and Harding, S., 1984, Near-surface faulting associated with Holocene fault scarps, Wasatch fault zone, Utah, *in* Hays, W.W., and Gori, P.L., eds., Proceedings of Conference XXVI; a

workshop on Evaluation of regional and urban earthquake hazards and risk in Utah: U.S. Geological Survey Open-File Report 84–763, p. 242–268.

Davis, D.A., and Cook, K.L., 1983, Evaluation of low-temperature geothermal potential in Utah and Goshen Valleys and adjacent areas, Utah, pt. I, Gravity survey: Utah Geological and Mineral Survey Report of Investigation RI–179, 139 p.

Davis, F.D., 1983a, Geologic map of the southern Wasatch Front, Utah: Utah Geological and Mineral Survey Map 55–A, scale 1:100,000.

———1983b, Geologic map of the central Wasatch Front, Utah: Utah Geological and Mineral Survey Map 54–A, scale 1:100,000.

———1985, Geologic map of the northern Wasatch Front, Utah: Utah Geological and Mineral Survey Map 53–A, scale 1:100,000.

Dustin, J.D., and Merritt, L.B., 1980, Hydrogeology of Utah Lake with emphasis on Goshen Bay: Utah Geological and Mineral Survey Bulletin 23, 50 p.

Eaton, G.P., Wahl, R.R., Prostka, H.J., Mabey, D.R. and Kleinkopf, M.D., 1978, Regional gravity and tectonic patterns: Their relation to the late Cenozoic epeirogeny and lateral spreading in the western Cordillera, *in* Smith, R.B., and Eaton, J.P. eds., Cenozoic tectonics and regional geophysics of the western Cordillera: Geological Society of America Memoir 152, p. 51–91.

Feth, J.H., Barker, D.A., Brown, R.J., Moore, L.G., and Viers, C.E., 1966, Lake Bonneville: Geology and hydrology of the Weber delta district, including Ogden, Utah: U.S. Geological Survey Professional Paper 518, 76 p.

Gilbert, G.K., 1928, Studies of basin-range structure: U.S. Geological Survey Professional Paper 153, 89 p.

Glenn, W.E., Chapman, D.S., Foley, D., Capuano, R.M., Cole, D.R., Sibbett, B., and Ward, S.H., 1980, Geothermal exploration program, Hill Air Force Base, Davis and Weber Counties, Utah: Earth Science Laboratory, University of Utah Research Institute Report 34, 77 p.

Hintze, L.F., 1980, Geologic map of Utah: Salt Lake City, Utah Geological and Mineral Survey, scale 1:500,000.

Hunt, C.B., Varnes, H.D., and Thomas, H.E., 1953, Lake Bonneville: Geology of northern Utah Valley, Utah: U.S. Geological Survey Professional Paper 257–A, 99 p.

Kane, M.F., and Pakiser, L.C., 1961, Geophysical study of subsurface structure in southern Owens Valley, California: Geophysics, v. 26, p. 12–26.

Mabey, D.R., 1960, Gravity survey of the western Mojave Desert, California: U.S. Geological Survey Professional Paper 316–D, p. D51–D73.

Mabey, D.R., and Morris, H.T., 1967, Geologic interpretation of gravity and aeromagnetic maps of Tintic Valley and adjacent areas, Tooele and Juab Counties, Utah: U.S. Geological Survey Professional Paper 516–D, p. D1–D10.

Mabey, D.R., Crittenden, M.D., Jr., Morris, H.T., Roberts, R.J., and Tooker, E.W., 1964, Aeromagnetic and generalized geologic map of part of north-central Utah: U.S. Geological Survey Geophysical Investigations Map GP–422, scale 1:250,000.

Mattick, R.E., 1970, Thickness of unconsolidated to semiconsolidated sediments in Jordan Valley, Utah, *in* Geological Survey research 1970: U.S. Geological Survey Professional Paper 700–C, p. C119–C124.

Peterson, D.L., 1974, Bouguer gravity map of part of northern Lake Bonneville basin, Utah and Idaho: U.S. Geological Survey Miscellaneous Field Studies Map MF–627, scale 1:250,000.

Peterson, D.L., and Oriel, S.S., 1970, Gravity anomalies in Cache Valley, Cache and Box Elder Counties, Utah, and Bannock and Franklin Counties, Idaho, *in* Geological Survey research 1970: U.S. Geological Survey Professional Paper 700–C, p. C114–C118.

Scheu, S.R., 1985, A gravity and magnetic investigation east of Preston, Idaho: Pocatello, Idaho State University unpublished M.Sc. thesis, 77 p.

Schwartz, D.P. and Coppersmith, K.J., 1984, Fault behavior and characteristic earthquakes: Examples from the Wasatch and San Andreas fault zones: Journal of Geophysical Research, v. 89, no. B7, p. 5681–5698.

Smith, R.B., and Bruhn, R.L., 1984, Intraplate extensional tectonics of the eastern Basin-Range: Inferences on structural style from seismic reflection data, regional tectonics, and thermal-mechanical models of brittle-ductile deformation: Journal of Geophysical Research, v. 89, no. B7, p. 5733–5762.

Stanley, W.D., 1971, An integrated geophysical study related to ground-water conditions in Cache Valley, Utah and Idaho: Salt Lake City, University of Utah, unpublished Ph.D. thesis, 142 p.

Stewart, J.H., 1978, Basin-range structure in western North America: A review, *in* Smith, R.B., and Eaton, J.P. eds., Cenozoic tectonics and regional geophysics of the western Cordillera: Geological Society of America Memoir 152, p. 1–32.

Stokes, W.L., 1977, Subdivisions of the major physiographic provinces in Utah: Utah Geology, v. 4, no. 1, p. 1–17.

Williams, J.S., 1962, Lake Bonneville: Geology of southern Cache Valley, Utah: U.S. Geological Survey Professional Paper 257–C, p. C131–C152.

Zoback, M.L., 1983, Structure and Cenozoic tectonism along the Wasatch fault zone, Utah: Geological Society of America Memoir 157, p. 3–27.

Zohdy, A.A.R., and Jackson, D.B., 1969, Electrical resistivity profile east of the Jordan Narrows, Utah, *in* U.S. Geological Survey Professional Paper 650–C, p. C83–C88.

Zietz, I., Shuey, R., and Kirby, J.R., Jr., 1976, Aeromagnetic map of Utah: U.S. Geological Survey Geophysical Investigations Map GP–907, scale 1:1,000,000.

Observational Seismology and the Evaluation of Earthquake Hazards and Risk in the Wasatch Front Area, Utah

By W.J. ARABASZ, J.C. PECHMANN, *and* E.D. BROWN,
DEPARTMENT OF GEOLOGY AND GEOPHYSICS, UNIVERSITY OF UTAH

ASSESSMENT OF REGIONAL EARTHQUAKE HAZARDS AND RISK ALONG THE WASATCH FRONT, UTAH

U.S. GEOLOGICAL SURVEY PROFESSIONAL PAPER 1500–D

CONTENTS

	Page
Abstract	D1
Introduction	1
Acknowledgments	3
Earthquake Data Base	3
Seismotectonic Framework	5
General Setting and Characteristics	5
Late Quaternary Faulting	8
The 1959 Hebgen Lake and 1983 Borah Peak Earthquakes	10
Threshold of Surface Faulting	10
Seismicity	11
Seismotectonic Framework—Continued	
Earthquake Focal Depths	D13
Problematic Correlation of Seismicity with Geologic Structure	19
Seismic Source Zones and Seismicity Parameters	20
General Remarks	20
Recurrence Modeling	20
Fault-Specific Sources	24
Ground-Shaking Hazard	26
Current Seismicity and the Wasatch Fault	28
References Cited	33

ILLUSTRATIONS

		Page
FIGURE 1.	Flow chart outlining steps in a formalized earthquake hazard analysis and interrelated aspects of observational seismology	D2
2, 3.	Maps showing:	
2.	Distribution of seismograph stations in the Utah region at four different times between 1955 and 1985	4
3.	Setting of the Wasatch Front study area with respect to the Intermountain Seismic Belt and epicenters of historical earthquakes of magnitude 6.0 and greater	6
4.	Schematic block diagram illustrating selected aspects of the seismotectonic framework of the Wasatch Front area	7
5.	Index map of the Wasatch Front study area showing traces of late Quaternary faulting	9
6–9.	Epicenter maps of:	
6.	Utah region, showing all independent main shocks of M_L 4.0 or greater, 1850–1986, and Quaternary faults	12
7.	All earthquakes located by the University of Utah Seismograph Stations in the Utah region, July 1, 1962, to December 31, 1986	14
8.	All earthquakes located by the University of Utah Seismograph Stations in the Wasatch Front area, October 1, 1974, to June 30, 1978	16
9.	All earthquakes located by the University of Utah Seismograph Stations in the Wasatch Front area, July 1, 1978, to December 31, 1986	17
10.	Epicenter map and corresponding vertical sections of earthquakes in the Wasatch Front area located with reliable focal depths, October 1974 through December 1986	18
11.	Schematic geologic cross section illustrating the complex association of seismicity in the upper crust with geological structure in the Intermountain Seismic Belt	19
12.	Map showing epicenters of independent main shocks in the Wasatch Front area from July 1, 1962, through December 31, 1985	22
13, 14.	Graphs showing:	
13.	Recurrence data for independent main shocks in the Wasatch Front area from July 1962 through December 1985	23
14.	Probability of exceedance per year for peak horizontal ground accelerations on soil at the intersection of I–15 and I–80 in South Salt Lake at approximately 40°43.1′ N., 111°54.2′ W.	27
15.	Strip map showing the Wasatch fault, segment boundaries and names, and all earthquakes located by the University of Utah Seismograph Stations during the period July 1962 through December 1986	29
16, 17.	Composite figures showing:	
16.	Cross sections keyed to the boxes in figure 15	30
17.	Space-time diagrams of earthquake occurrence keyed to figure 15	32

TABLES

		Page
TABLE 1.	Largest earthquakes in the Utah region, 1850 through December 1986	D13
2.	Independent main shocks of magnitude (M_L) 4.0 or greater in the Utah region, July 1962 through December 1986	15
3.	Average recurrence intervals for earthquakes in the Wasatch Front region	23
4.	Information for selected fault-specific sources	25

ASSESSMENT OF REGIONAL EARTHQUAKE HAZARDS
AND RISK ALONG THE WASATCH FRONT, UTAH

OBSERVATIONAL SEISMOLOGY AND THE EVALUATION OF EARTHQUAKE HAZARDS AND RISK IN THE WASATCH FRONT AREA, UTAH

By W.J. ARABASZ, J.C. PECHMANN, and E.D. BROWN

ABSTRACT

This chapter presents and considers in a systematic way up-to-date information from observational seismology that is basic to evaluating earthquake hazards and risk in the Wasatch Front area. We present fundamental information relating to (1) the earthquake data base, (2) the seismotectonic framework, (3) seismic source zones and seismicity parameters, (4) the ground-shaking hazard, and (5) current seismicity and the Wasatch fault.

Important features of the seismotectonic framework of the Wasatch Front include (1) a threshold magnitude for surface faulting of M_L 6.0 to 6.5, (2) a maximum magnitude of M_S 7.5 to 7.7, (3) the absence of any large surface-faulting earthquakes and the notable paucity of smaller earthquakes on the Wasatch fault during historical time, and (4) the problematic correlation of background seismicity with mapped Cenozoic faulting. In light of this framework, we consider seismic hazards in the Wasatch Front region to arise from two fundamental sources: (1) the occurrence of infrequent large (M_S 6.3±0.2–7.5±0.2) surface-faulting earthquakes on identifiable faults having evidence of late Quaternary displacement and (2) small- to moderate-sized (up to M_L 6.5) earthquakes that are not constrained in location to mapped faults and may occur anywhere throughout the region. The small to moderate earthquakes dominate the historical earthquake record and, at most localities, are the largest contributor to the probabilistic ground-shaking hazard for exposure periods of 50 years or less. Recurrence modeling using independent main shocks from the 23.5-year instrumental catalog from July 1962 through 1985 predicts an average recurrence interval of 24^{+16}_{-10} years for potentially damaging earthquakes of magnitude 5.5 or greater in the Wasatch Front area. The occurrence of eight such shocks from 1850 through 1987 gives an observed average recurrence interval of 17 years.

INTRODUCTION

The record of earthquake activity since 1850, together with geologic observations dating from more than a century ago, firmly establishes the danger of earthquakes in Utah's Wasatch Front area. This chapter presents and considers in a systematic way information from observational seismology that is basic to evaluating earthquake hazards and risk in the Wasatch Front area.

We follow usage urged by the Earthquake Engineering Research Institute and distinguish a seismic hazard from seismic risk in the following way. A seismic hazard is "any physical phenomenon...associated with an earthquake that may produce adverse effects on human activities," whereas seismic risk is "the probability that social or economic consequences of earthquakes will equal or exceed specified values at [one or more sites] during a specified exposure time" (Earthquake Engineering Research Institute Committee on Seismic Risk, 1984, p. 38). The most notable seismic hazards are the geologic processes of ground shaking, ground failure, surface faulting, tectonic deformation, and inundation.

Insofar as the evaluation of earthquake hazards involves recognition of the location, frequency, and severity of these hazards, observational seismology is generally relied upon to characterize the space, time, and size distribution of the earthquakes giving rise to them. This procedure might involve little more than a qualitative consideration of the available earthquake record and the spatial pattern of earthquake occurrence. On the other hand, more rigorous evaluations of seismic hazard and risk rely on observational seismology to specify quantitative models of earthquake behavior and mechanics, so that either the level of a hazard (for example, a nonexceedance value of ground motion) or the level of risk can be computed at one or more sites for some exposure time. Either a deterministic or a probabilistic approach may be used. In the former case, each independent variable has a single value, and a model predicts a specific value for the dependent variable. For example,

Manuscript approved for publication November 20, 1990.

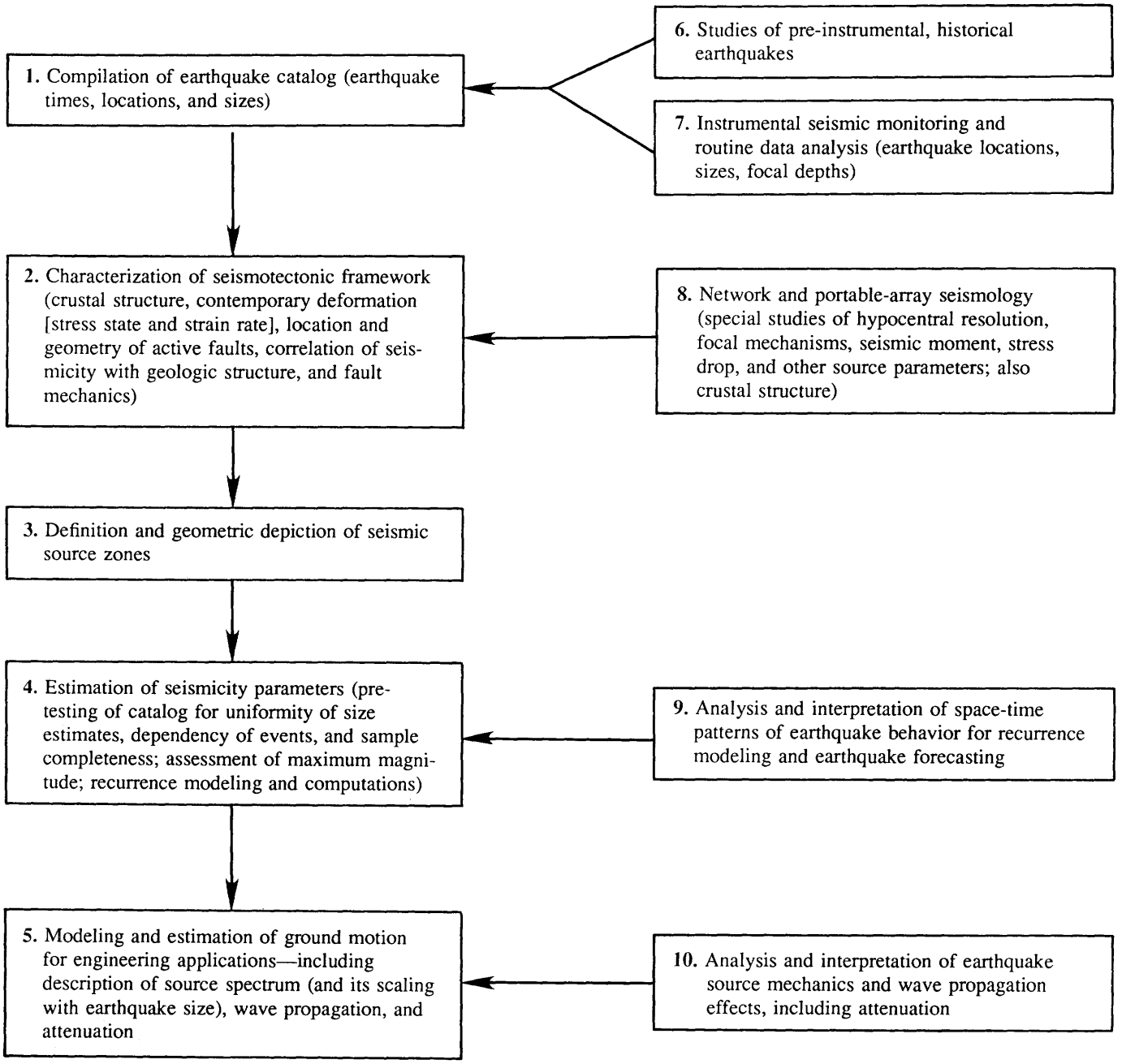

FIGURE 1.—Steps in a formalized earthquake hazard analysis (left column) and interrelated aspects of observational seismology (right column).

the maximum ground shaking expected at a site might be estimated from the comparative effects of nearby earthquake source zones, each of which is assigned a maximum-size event and a minimum distance to the site, along with a corresponding upper limit of predicted ground motion. In the case of a probabilistic approach, uncertainties arising from natural variations or incomplete knowledge are taken into account, and probability theory is used for the analysis (for example, Youngs and others, in press; Algermissen and others, this volume).

The flowchart shown in figure 1 outlines the basic elements of a modern seismic hazard analysis (for example, Savy and others, 1986; Electric Power Research Institute, 1988), using as an example the objective of estimating the hazard of ground motion. (Seismologic input to a risk analysis would be similar.) The sequence of necessary procedures is shown by steps 1 through 5 in the left-hand column; interrelated aspects of observational seismology are shown in the right-hand column. Figure 1 is a useful guide to our presentation as we give

an overview of fundamental information from observational seismology in the Wasatch Front area contributing to steps 1 through 4. Sequentially, we consider (1) the earthquake data base, (2) the seismotectonic framework, and (3) seismic source zones and seismicity parameters. We then discuss a selected aspect of the ground-shaking hazard, referring the reader to Chapter M (in the second volume of this report) by R.R. Youngs and others for an example of the fully completed process of step 5 in which probabilistic estimates of ground motion are made. In the final section, we address the question, "What does observational seismology tell us about the behavior of the Wasatch fault?"

ACKNOWLEDGMENTS

The data in this manuscript implicitly reflect substantial efforts by numerous individuals associated with the University of Utah Seismograph Stations. We thank D. Veneziano of the Massachusetts Institute of Technology for providing data on independent main shocks for the recurrence modeling and for assisting with the probabilistic hazard methodology. We also thank J.A. Barlow, L.B. Burnett, P.A. Onstott, K.J. Quigley, and J.E. Shemeta, all of the University of Utah, for their assistance in the manuscript preparation. Critical reviews were provided by R.L. Wheeler and C.J. Langer of the U.S. Geological Survey. The research arises from ongoing support by the U.S. Geological Survey, Department of the Interior, currently under award numbers 14–08–0001–G1349 and 14–08–0001–A0265, and from support by the State of Utah.

EARTHQUAKE DATA BASE

The catalog of documented earthquakes in the Utah region[1] (step 1, fig. 1) is, as it is elsewhere in the Western United States, a mixed one, relying initially on reports and newspaper accounts of felt earthquakes and later on seismographic recordings made during several stages of evolving instrumental coverage (Arabasz and others, 1979, 1980) (see fig. 2). The historical earthquake record effectively dates from 1850, when the first newspaper was published in the region, shortly after Mormon pioneers began to settle the area in 1847. Instrumental earthquake locations in the region, based on regional seismographic recordings in the Western United States, date from about 1938, with the exception of the 1934 M_S 6.6 Hansel Valley earthquake and its larger aftershocks.

The most prominent sources of earthquake data for the Utah region are compilations made by the University of Utah Seismograph Stations (UUSS) (Arabasz and others, 1979; Richins and others, 1981, 1984; Brown and others, 1986; unpublished data of various workers) and data files of the National Geophysical Data Center, National Oceanic and Atmospheric Administration (NOAA). Other earthquake summaries include a recent compilation for the State of Utah by Stover and others (1986),[2] a data file compiled by Askew and Algermissen (1983) for the Basin and Range province, a Western U.S. data file produced by Eddington and others (1987) for a study of Basin and Range geodynamics, and a continental-scale data file produced by Engdahl and Rinehart (1988) for the "Decade of North American Geology" publication series.

Ideally, the establishment of a master "consensus" catalog would involve the coordinated and formalized efforts of numerous individuals having relevant data and expertise, as was recently done for the entire Central and Eastern United States (Electric Power Research Institute, 1988). The required efforts relate to establishing catalog completeness, uniform estimates of earthquake size, and preferred epicentral locations and origin times and to documenting uncertainties. Similarly rigorous and formal scrutiny of a data base for the Utah region remains to be made. In this chapter, we rely upon the University of Utah's data base, which represents the primary source of instrumental earthquake data since mid-1962 for the Utah region and which includes a comprehensive listing of historical seismicity for which only minor variance from other catalogs should be found. For 1962 through 1986, the UUSS catalog contains an order-of-magnitude more earthquakes than the NOAA data file for the Utah region (for example, 6,994 versus 342 earthquakes for the Wasatch Front area alone).

Although seismographs were first installed on the University of Utah campus in 1907, contributions to the instrumental location of regional earthquakes postdate 1939, when photographic records from modern seismographs began to be routinely forwarded from Salt Lake City to the U.S. Coast and Geodetic Survey. Systematic computerized locations based on local seismographic coverage in the Utah region by the University of Utah date from mid-1962. From mid-1962 through late 1974, a skeletal statewide network of several widely spaced stations was in operation (fig. 2, upper right). Instrumental earthquake data for the period 1962 through 1974 were systematically reanalyzed and revised in a major study by the UUSS (Arabasz and others, 1979). Since late 1974, the University of Utah has operated a modern telemetered network of high-gain short-period seismo-

[1]Our usage of the term "Utah region" is defined in figure 2.

[2]This compilation omits significant earthquakes in Utah that occurred on November 10, 1884, July 21, 1959, and August 30, 1962 (table 1) (Coffman and others, 1982).

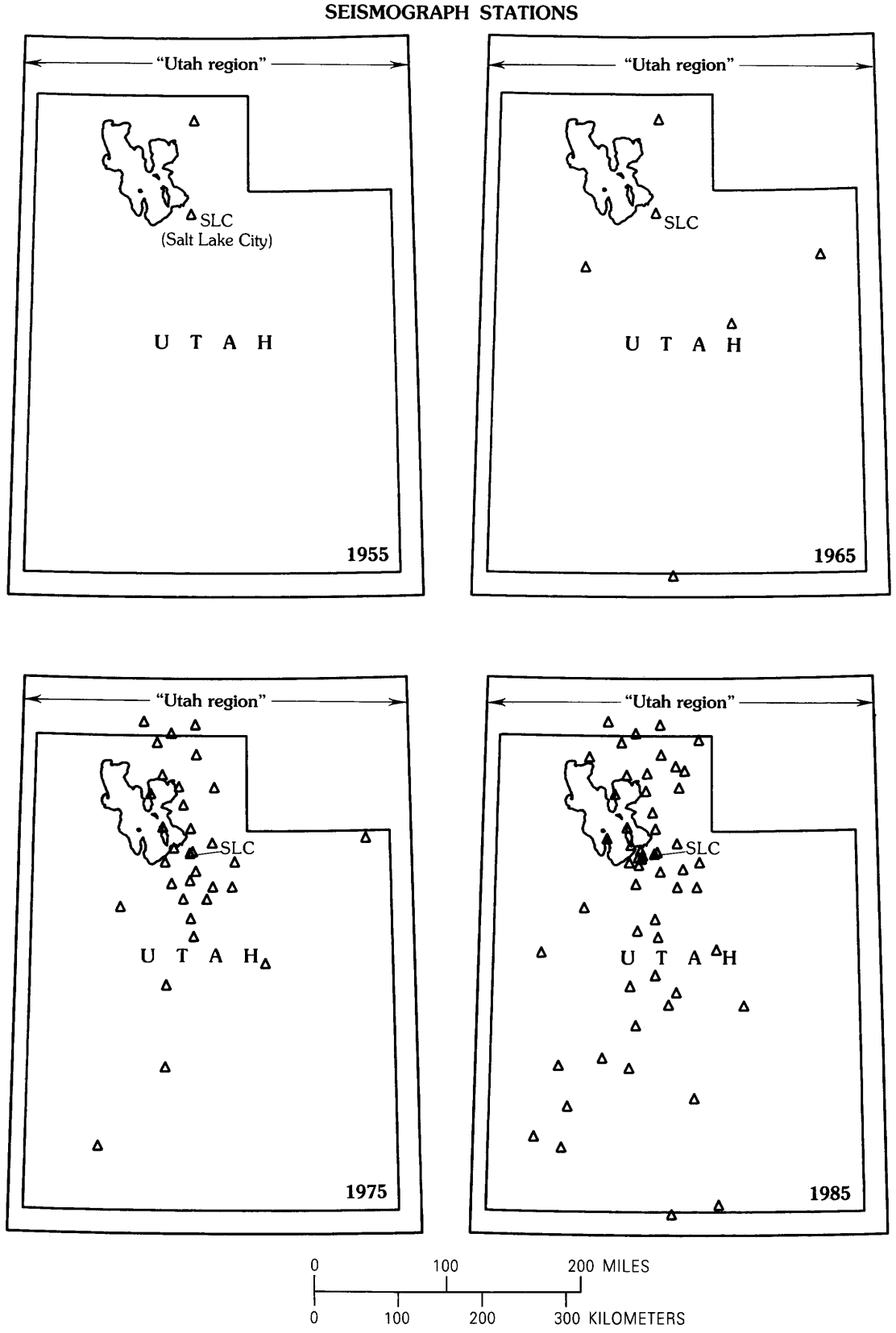

FIGURE 2.—Distribution of seismograph stations (triangles) in the Utah region at four different times between 1955 and 1985. The Utah region, corresponding to a specific domain of the University of Utah's earthquake catalog, extends from latitude 36°45′ N. to 42°30′ N. and from longitude 108°45′ W. to 114°15′ W.

graphic stations in the Intermountain region. About two-thirds of the current network's 85 stations lie within the Utah region (fig. 2, lower right). The seismographic data are centrally recorded at the University of Utah in Salt Lake City. From 1974 through 1980, data were recorded in analog form; since January 1, 1981, recordings have been in digital form.

The UUSS catalog for the Utah region currently contains 9,561 earthquakes for the period from 1850 through 1986, including 413 (chiefly noninstrumental) earthquake locations from 1850 through June 1962 and 9,148 (instrumental) locations from July 1, 1962, to December 31, 1986. Magnitudes given in the UUSS catalog are estimates of local Richter magnitude (M_L) based on systematic procedures described, for example, by Brown and others (1986). Such estimates may differ significantly from values of magnitude in the NOAA catalog, which are typically body-wave magnitude (m_b) and known to be commonly as much as one magnitude unit larger than M_L for small ($m_b \leq 4.0$) earthquakes (Dewey, 1987). We refer the reader to special publications of the UUSS (for example, Arabasz and others, 1979; Brown and others, 1986) for other details of the UUSS data base.

SEISMOTECTONIC FRAMEWORK

The characterization of the seismotectonic framework of any seismically active region (step 2, fig. 1) basically involves an understanding of its geologic and geophysical makeup, its earthquake-generating faults, and the operative deformational processes that lead to earthquake occurrence. Previous studies that have developed such a framework for the Wasatch Front area and its surrounding region include those by Smith and Sbar (1974), Smith (1978), Arabasz and others (1980), Zoback (1983), Smith and Bruhn (1984), and Arabasz and Julander (1986). We will not attempt a complete review of previous studies here. Our intent is (1) to summarize some essential characteristics of the seismotectonic framework of the Wasatch Front area and (2) to emphasize new information acquired from observational seismology by researchers at the University of Utah. Information from network and portable-array seismology (element 8, fig. 1) includes precise earthquake locations, earthquake focal mechanisms and source properties, strain rate tensors from seismic moment release, and models of crustal structure.

GENERAL SETTING AND CHARACTERISTICS

The Wasatch Front area, synonymous herein with the rectangular area outlined in figure 3, is located along the eastern boundary of the Basin and Range province. This boundary coincides with a prominent west-facing topographic escarpment that follows the 380-km-long Wasatch normal fault zone. The Wasatch Front area is traversed by the Intermountain Seismic Belt, a coherent belt of intraplate earthquake activity extending more than 1,500 km from southern Nevada and northern Arizona to northwestern Montana (Smith and Sbar, 1974; Smith, 1978; Stickney and Bartholomew, 1987; Smith and Arabasz, 1991). In general, the Intermountain Seismic Belt is characterized by late Quaternary normal faulting, diffuse shallow seismicity (focal depths of less than 15–20 km), and episodic scarp-forming earthquakes ($M_S \sim 6.5$–7.5), all associated with intraplate deformation within the western North American plate.

Since 1850, at least 16 independent earthquakes (aftershocks excluded) of magnitude 6.0 or greater have occurred within the Intermountain Seismic Belt (fig. 3). Three of these historical earthquakes were associated with documented surface faulting. Normal fault scarps having maximum surface displacements of 0.5, 5.5 ± 0.3, and 2.7 m, respectively, were produced by the M_S 6.6 Hansel Valley, Utah, earthquake of March 1934 (Shenon, 1936), the M_S 7.5 Hebgen Lake, Mont., earthquake of August 1959 (Bonilla and others, 1984), and the M_S 7.3 Borah Peak, Idaho, earthquake of October 1983 (Crone and others, 1987).

The Intermountain Seismic Belt within the Utah region is notably characterized by (1) a general predominance of normal faulting, which reflects an extensional stress regime (although young strike-slip deformation has recently been recognized from seismologic and geologic studies in central Utah (Arabasz and Julander, 1986; Anderson and Barnhard, this volume)); (2) moderate background seismicity, which is lower by about a factor of 4 in comparison with that along the western North American plate boundary (Smith and Arabasz, 1981); (3) diffuse seismicity having weak correlation with major active faults and with focal depths almost exclusively shallower than 15 to 20 km; (4) relatively long (approximately 1,000 years or more), and perhaps temporally variable, average recurrence intervals for surface faulting on individual fault segments (Schwartz and Coppersmith, 1984; Wallace, 1987; Machette and others, this volume); (5) slip rates of late Quaternary faulting of about 1 mm/yr or less, one to two orders of magnitude lower than those on major plate-boundary faults (Schwartz, 1987); and (6) the historical absence of any surface-faulting earthquake larger than the M_S 6.6 Hansel Valley earthquake of 1934, despite the presence of abundant late Quaternary and Holocene fault scarps.

Figure 4 illustrates some important aspects of the seismotectonic framework of the Wasatch Front area. (Letters in parentheses here are keyed to the figure.)

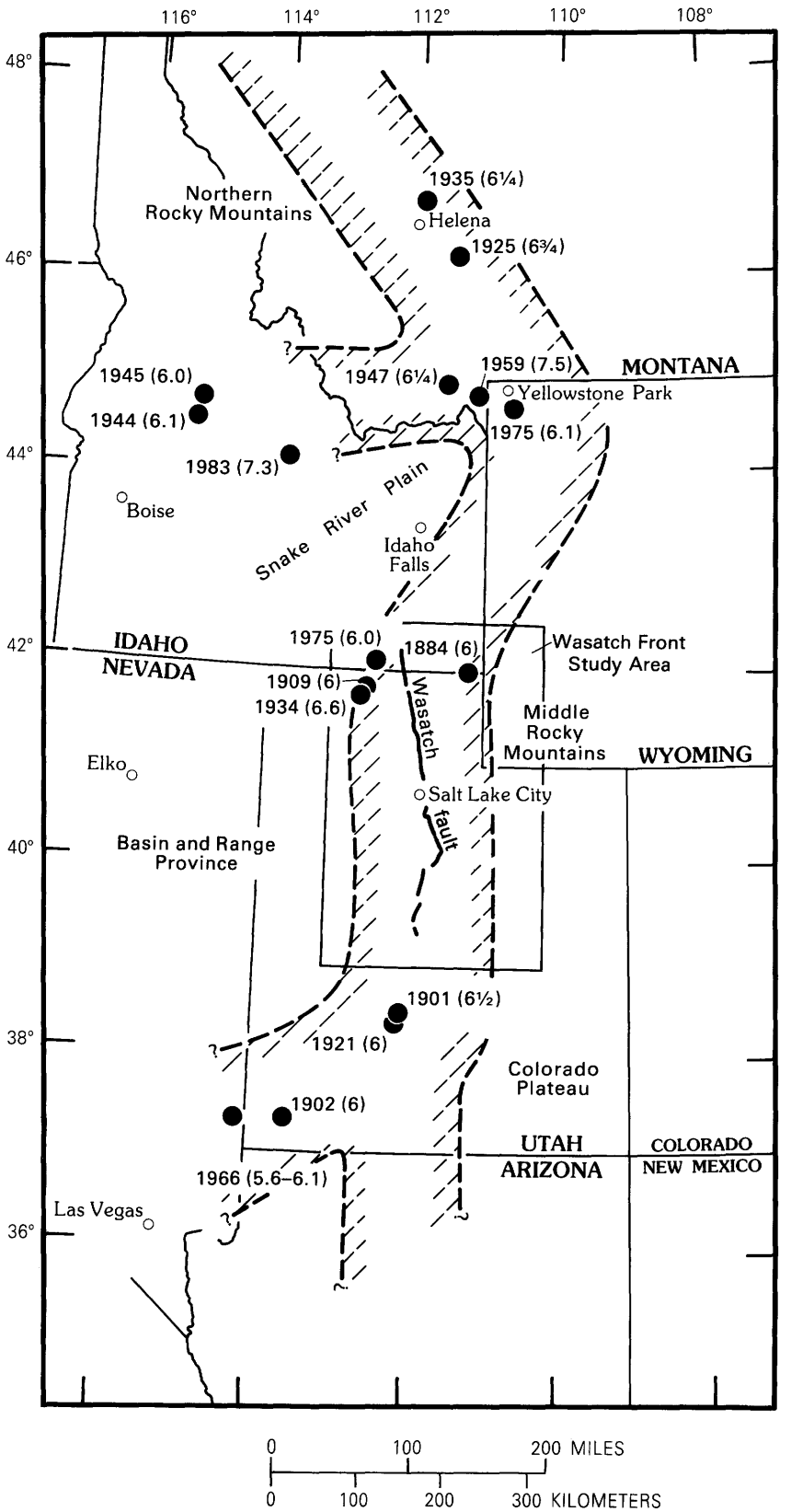

FIGURE 3.—Setting of the Wasatch Front study area with respect to the Intermountain Seismic Belt (hachured zone) and the epicenters of historical earthquakes of magnitude 6.0 and greater (solid circles) (adapted and updated from Arabasz and Smith, 1981). Year and magnitude are labeled for each earthquake.

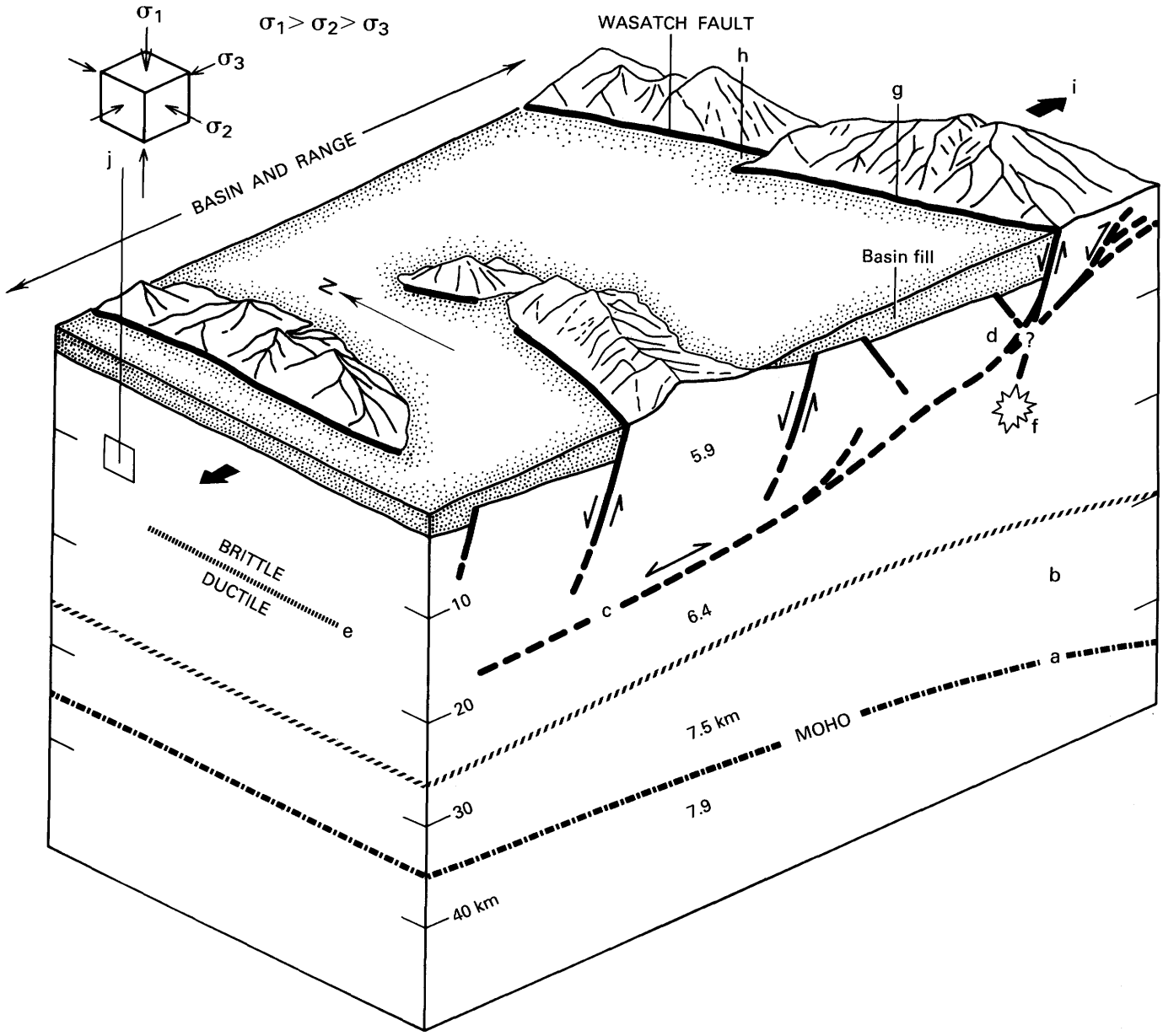

FIGURE 4.—Selected aspects of the seismotectonic framework of the Wasatch Front area (vertical exaggeration approximately 1.0–1.5). Heavy lines with arrows (directions of displacement) represent fault traces. Lowercase letters indicate elements discussed in the text: a, the base of the crust defined by the Moho; b, lower crustal material; c, low-angle detachments; d, listric fault geometry; e, the brittle-ductile transition; f, the nucleation zone of a large earthquake; g, surface-fault scarps; h, a fault segment boundary; i, the direction of crustal extension; j, the orientation of principal stresses (σ_1, σ_2, σ_3), compression being positive.

Total crustal thickness (a) increases eastward from about 36 to 44 km across the transitional boundary between the eastern Basin and Range and the Middle Rocky Mountain-Colorado Plateau provinces (Loeb and Pechmann, 1986; Loeb, 1986). Total lithospheric thickness similarly increases from about 65 km beneath the Basin and Range to more than 80 km beneath the Colorado Plateau (Smith and others, 1987). A wedge of material (b) having a P-wave velocity of approximately 7.5 km/s, formerly thought to be upwarped mantle, has been mapped by J.C. Pechmann and D.T. Loeb (Pechmann and others, 1984; Loeb, 1986) as lying above the 7.9-km/s Moho, on the basis of an analysis of traveltimes from local earthquakes and blasts recorded by the University of Utah's regional seismic network. The importance of low-angle detachments (c) and listric fault geometries (d) in upper crustal structure beneath the eastern Basin and Range appears well established from data from the Consortium for Continental Reflection Profiling (Allmendinger and others, 1983, 1987) and from interpretation of industry

seismic reflection data at the University of Utah (Smith and Bruhn, 1984) (see also Smith and others (1989) for a summary of multiple studies).

The brittle-ductile transition (e) marking the base of the seismogenic layer has been modeled rheologically by Smith and Bruhn (1984) to be transitional, perhaps as shallow as approximately 8 km but probably about 10 to 15 km deep beneath the Wasatch Front area. Large surface-faulting earthquakes in the Wasatch Front area are expected to nucleate (f) at that depth on penetrative planar faults of moderate dip (Smith and Richins, 1984; Doser, 1985a) somehow connected to surface fault scarps (g). As we will discuss later, most of the small- to moderate-sized background seismicity in the area is not directly associated with the first-order faults. Variability in slip, rupture velocity, and fault orientation during large normal-faulting earthquakes can be expected to produce locally complex ground motions (Benz and Smith, 1987). Segmentation (h) of first-order faults such as the Wasatch fault (Swan and others, 1980; Schwartz and Coppersmith, 1984; Machette and others, 1991, this volume) places important constraints on rupture length, maximum earthquake size, and rupture dynamics.

The Wasatch Front area is characterized by roughly east-west extensional deformation (i), as earthquake focal mechanisms and slickenside data indicate (Smith and Lindh, 1978; Arabasz and others, 1980; Zoback and Zoback, 1980; Zoback, 1983). Twenty-four single-event focal mechanisms recently determined by Bjarnason and Pechmann (1989), representing the best focal mechanism data to date for the Wasatch Front area, have an average tension axis azimuth of 96°±12° s.d. Extension calculated by Eddington and others (1987) from moment tensors of historical earthquakes (see also Doser and Smith, 1982) implies an average strain rate of about 2×10^{-16}/s for the Wasatch Front area and a total extension rate of 1 to 2 mm/yr across the study area.

The stress tensor in the upper crust (j) implied by earthquake focal mechanisms and other stress indicator data (for example, Zoback, 1983) has a vertical maximum principal stress axis and intermediate and minimum principal stress axes lying in the horizontal plane, the latter being oriented in an east-west (±20°) direction. Zoback (1984) has argued that both horizontal principal stresses are approximately equal in magnitude along the Wasatch Front, implying the potential for slip on normal faults of varying strike. Earthquake focal mechanisms, however, display strong clustering of tension axes in an east-west direction (Arabasz and Julander, 1986; Bjarnason and Pechmann, 1989). Focal mechanisms for earthquakes in the Wasatch Front region south of about 40° N. show a mixture of normal, oblique-normal, and strike-slip faulting, in contrast to those north of 40° N., which show predominantly normal faulting. This observation suggests that, in the southern Wasatch Front region, the maximum and intermediate principal stresses may be of similar magnitude (Bjarnason and Pechmann, 1989).

LATE QUATERNARY FAULTING

In the absence of a definitive map of known and suspected active faults throughout the Wasatch Front area, efforts were made to compile a base map of late Quaternary faulting for comparison with instrumental seismicity. The resulting map (fig. 5), which relies chiefly on published sources, includes the traces of fault displacements of late to middle Pleistocene (10,000 to about 500,000 yr B.P.) and Holocene (less than 10,000 yr B.P.) age.

A number of sources were used to compile the digitized base map in figure 5. The trace of the Wasatch fault is based chiefly on detailed mapping done by Cluff and others (1970, 1973, 1974) and was taken, in part, from subsequent compilations by Davis (1983a, b, 1985). Depiction of the West Valley fault zone near Salt Lake City is from Keaton and others (1986). Faulting to the east of the Wasatch fault in Utah is from detailed maps by Sullivan and others (1988) and Foley and others (1986); that in Wyoming is from Gibbons and Dickey (1983). The trace of the East Great Salt Lake fault, lying within the bounds of the Great Salt Lake, was taken from Cook and others (1980) and Viveiros (1986). West of 112° W., we relied heavily on maps of fault scarps in unconsolidated sediments published by Bucknam (1977) and Bucknam and Anderson (1979). Some additional faults in the "Western Desert" region of Utah included in the compilation of Anderson and Miller (1979) were added for completeness. Finally, faulting to the north of 42° N. in Idaho, other than the northern extension of the Wasatch fault, was taken from Witkind (1975).

There is some inhomogeneity in figure 5 in that some of the fault traces to the west of the Wasatch fault within the Basin and Range province reflect only the extent of mapped fault scarps in unconsolidated deposits and not necessarily the entire length of a seismogenic range-front fault. Fluctuation of ancient Lake Bonneville, especially between about 25,000 and 13,000 years ago (Currey and others, 1984), could have obliterated evidence of late Quaternary surface faulting in many places.

The Wasatch fault is by far the best-studied fault depicted in figure 5. We refer the reader to other papers in this volume for summaries of up-to-date paleoseismologic information on its segmentation and slip rate and on the timing and size of prehistoric earthquakes. A major active fault to which little attention has heretofore been paid is one beneath the Great Salt Lake that Cook and others (1980) named the "East Great Salt Lake fault zone" and whose slip rate and earthquake potential have

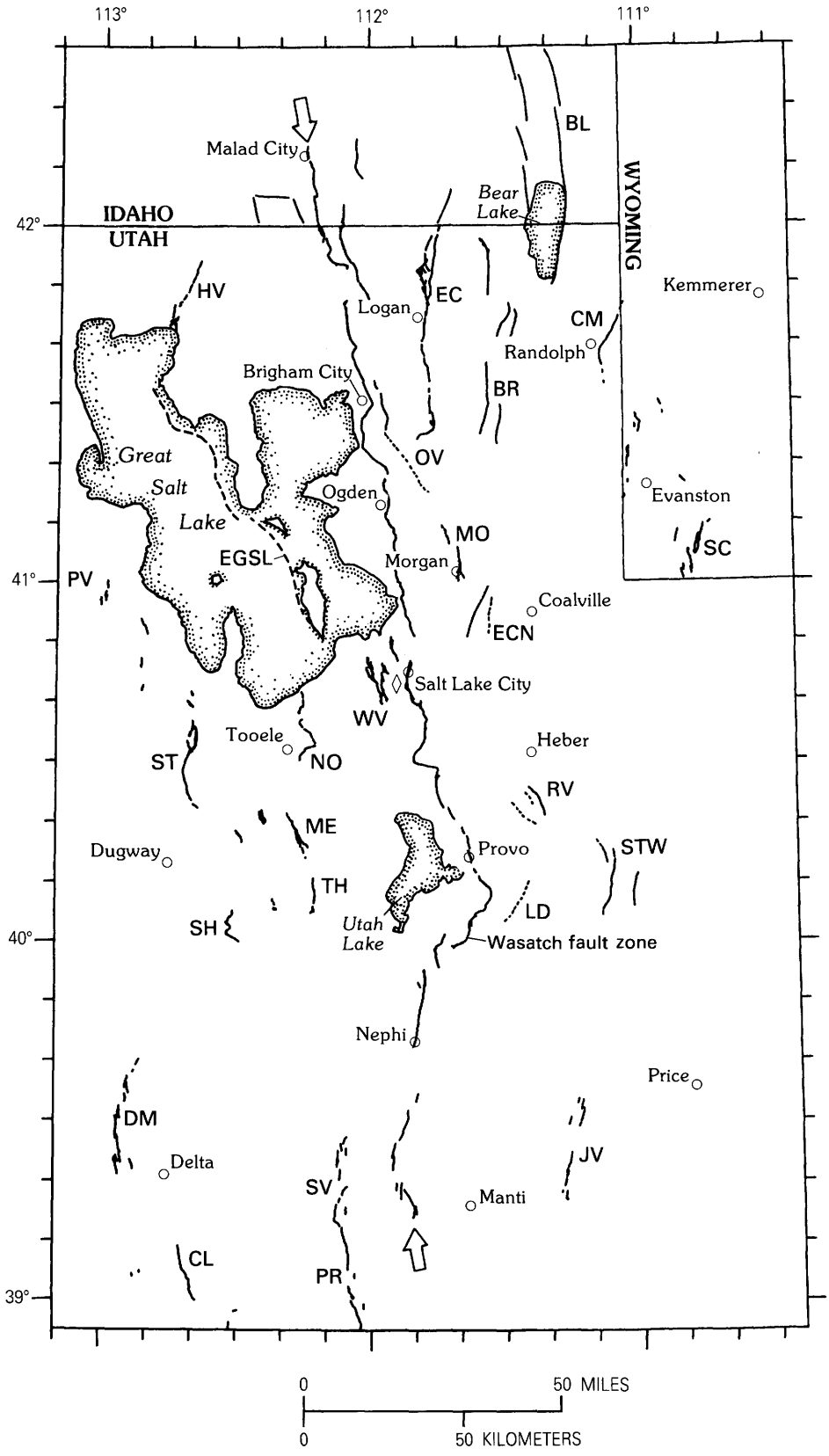

FIGURE 5.—Traces of late Quaternary faulting in the Wasatch Front study area (see text for sources). Large arrows delimit the extent of the Wasatch fault zone. Other faults labeled for general orientation include BL, Bear Lake; BR, Bear River Range; CL, Clear Lake; CM, Crawford Mountains; DM, Drum Mountains.; EC, East Cache; ECN, East Canyon; EGSL, East Great Salt Lake (dashes indicate approximate); HV, Hansel Valley; JV, Joes Valley; LD, Little Diamond Creek; ME, Mercur; MO, Morgan; NO, Northern Oquirrh; OV, Ogden Valley; PR, Pavant Range; PV, Puddle Valley; RV, Round Valley; SC, Sulphur Creek; SH, Sheeprock Mountains; ST, Stansbury Mountains; STW, Strawberry Valley; SV, Scipio Valley; TH, Topliff Hill; WV, West Valley. The diamond near Salt Lake City marks the site for which we performed a probabilistic calculation of the ground-shaking hazard (see fig. 14).

been investigated recently by one of us (J.C. Pechmann, unpub. report, 1987; Pechmann and others, 1987). This fault zone can be seen clearly in seismic reflection profiles across the lake (Mikulich and Smith, 1974; Smith and Bruhn, 1984; Bortz and others, 1985; Viveiros, 1986). Reflection data and well data indicate that the sedimentary basin underlying the lake deepens eastward and is bounded on the east by the East Great Salt Lake fault. The deepest part of the basin contains more than 3,048 m of post-Miocene sedimentary rocks (Mikulich and Smith, 1974; Bortz and others, 1985; Viveiros, 1986), an indication that major subsidence has occurred during the past 24 m.y.

The East Great Salt Lake fault cuts sediments identified as Quaternary on the basis of well data (Mikulich and Smith, 1974; Viveiros, 1986) and must be considered active. Seismic reflection data (Mikulich and Smith, 1974; Viveiros, 1986) indicate that the East Great Salt Lake fault appears to offset sediments to within at least 0.015 to 0.025 s two-way traveltime beneath the lake bottom, corresponding to an approximate depth of less than 10 to 20 m, which implies that slip has occurred in the recent geologic past. Viveiros (1986, p. 72) estimated fault slip rates on the East Great Salt Lake fault of 0.96 mm/yr during the Pliocene and 1.48 mm/yr during the Quaternary from the thicknesses of sedimentary deposits (dependent on an interpreted geometry of faulting). Pechmann and others (1987) interpreted average Quaternary slip rates of 0.4 to 0.7 mm/yr, taking subsurface fault dip into account and assuming that rates of sedimentation adjacent to the fault are controlled by subsidence on the fault. These slip rates are about half the recent slip rates along central segments of the Wasatch fault (Schwartz and Coppersmith, 1984).

THE 1959 HEBGEN LAKE AND 1983 BORAH PEAK EARTHQUAKES

The only historical earthquake in the Utah region known to have produced surface faulting occurred on March 12, 1934, in Hansel Valley just north of the Great Salt Lake (figs. 3, 5). This earthquake was assigned a magnitude of 6.6 by Gutenberg and Richter (1954) and is the largest earthquake to have occurred in the Utah region since 1850. Geologic evidence indicates that earthquakes having surface displacements much larger than the 0.5 m of the 1934 earthquake are expected to occur in Utah in the future, so information from large surface-faulting earthquakes elsewhere in the Intermountain Seismic Belt and in the Basin and Range province is important for evaluating their likely magnitudes and other characteristics.

In the Intermountain Seismic Belt, there have been two large, historical normal-faulting earthquakes greater than magnitude 7.0, both of which produced surface rupture: the October 28, 1983, M_S 7.3 (U.S. Geological Survey determination) Borah Peak earthquake in central Idaho and the August 18, 1959 (GMT), M_S 7.5 Hebgen Lake earthquake in southern Montana (fig. 3). These two earthquakes are generally considered to be good models for future large earthquakes on the Wasatch fault and other major faults in Utah (Smith and Richins, 1984; Doser, 1985a). The surface-wave magnitude (M_S) of 7.5 for the Hebgen Lake event is from Abe (1981) and is probably more accurate than a previous estimate of 7.1, attributed by Murphy and Brazee (1964) to Pasadena. The Hebgen Lake earthquake was accompanied by 35 km of surface faulting along the Red Canyon and Hebgen faults, vertical displacements of up to 5.5 ± 0.3 m (Bonilla and others, 1984; Witkind, 1964), and an average displacement of 2.1 m (Hall and Sablock, 1985). The Borah Peak earthquake produced 36 km of surface faulting along the Lost River and Arentson Gulch faults, vertical displacements of up to 2.7 m, and an average displacement of 0.8 m (Crone and Machette, 1984; Crone and others, 1987). Both earthquakes nucleated at depths of about 15 to 16 km and ruptured upward along faults dipping at 45° to 60° (Doser, 1985a, b; Doser and Smith, 1985).

The most reliable and physically meaningful measurement of earthquake size is the seismic moment, M_0 (Aki, 1966), given by

$$M_0=\mu Sd$$

where μ is the shear modulus, S is the area of the rupture surface, and d is the average displacement along the rupture surface. From the seismic moment, a moment magnitude, M_w (Kanamori, 1977; Hanks and Kanamori, 1979), can be calculated from the definition

$$M_w=(2/3)\log M_0-10.7$$

M_w should be comparable to M_S for earthquakes of $5.0\leq M_w\leq 7.5$ (Hanks and Kanamori, 1979). The Hebgen Lake earthquake had a seismic moment of 1.0×10^{27} dyne-cm (Doser, 1985b), which converts to a moment magnitude of 7.3. The Borah Peak earthquake had a moment of 2.1×10^{26} (Doser and Smith, 1985) to 3.1×10^{26} (Ekstrom and Dziewonski, 1985), which gives a moment magnitude of 6.8 to 7.0.

THRESHOLD OF SURFACE FAULTING

Various authors (for example, Arabasz, 1984; Doser, 1985a; Arabasz and Julander, 1986) have suggested that the threshold magnitude for surface faulting in Utah is approximately 6.0 to 6.5. On the basis of the historical

record of earthquakes in the Intermountain Seismic Belt and in the Basin and Range province, this conclusion appears to be well founded. Bucknam and others (1980) noted that all seven historical earthquakes of $M_L>6.3$ in the Great Basin have produced surface faulting, including the 1934 M_S 6.6 Hansel Valley, Utah, event. In their tabulation of 11 earthquakes that produced historical surface faulting in the Basin and Range province, all five events of $M_L<6.8$ had maximum displacements of less than 1 m. The tabulation includes one California normal-faulting earthquake of M_L 5.6 in 1950 that had 0.2 m maximum displacement and a Nevada earthquake of M_L 6.3 in 1934 that had 0.1 m maximum displacement. In the Intermountain Seismic Belt, Doser (1985a) pointed out that neither the 1975 M_L 6.0 Pocatello Valley earthquake nor the 1975 M_L 6.1 Yellowstone Park earthquake (fig. 3) had identifiable surface faulting, although both earthquakes were accompanied by an apparently coseismic subsidence of up to 12 to 13 cm (Bucknam, 1976; Pitt and others, 1979). On the basis of the historical record, we adopt M_L 6.3±0.2 as a reasonable estimate for the threshold of surface faulting in the Utah region. The implication of this threshold is that one can argue that earthquakes up to this size could occur anywhere in the Wasatch Front region within the main seismic belt, even where there is no geologic evidence for Quaternary surface faulting. We will elaborate in a later section.

SEISMICITY

Figure 6 shows the distribution of all historical main shocks of estimated Richter magnitude 4.0 or greater (or maximum Modified Mercalli intensity V or greater) in the Utah region. The historical sample includes at least 15 independent main shocks that have had an estimated Richter magnitude of 5.5 or greater (or a Modified Mercalli intensity VII or greater). These earthquakes are listed in table 1, and their epicenters are shown as solid circles in figure 6. At the scale of figure 6, apparent correlations of historical seismicity with specific faults must be considered with care. For example, many of the epicenters located along the Wasatch fault are noninstrumental and correspond to locations where effects were felt most strongly for a particular shock, typically in an established city or town. Hence, the coincidence of historical epicenters with the Wasatch fault reflects the locations of settlements along the Wasatch Front and is not necessarily indicative of earthquake activity on the Wasatch fault itself. It is arguable whether the earthquakes of about magnitude 5.5 in 1910 near Salt Lake City and in 1914 near Ogden occurred directly on the Wasatch fault (Arabasz and others, 1980). Thus, as many as two—or perhaps no—earthquakes of magnitude 5 or greater have occurred on the Wasatch fault in historical time. The average interevent time since 1884 of the moderate to large main shocks listed in table 1 is about 6.5 years. There was, however, one unusually long 25-year interval between 1934 and 1959 in which no earthquake of magnitude 5.5 or greater occurred.

Figure 7 shows the pattern of instrumental seismicity for the Utah region determined by University of Utah monitoring since mid-1962 (element 7, fig. 1). The epicentral distribution of small- to moderate-sized background earthquakes is generally similar to that of figure 6. The sample shown in figure 7 includes 9,148 earthquakes of all sizes up to magnitude 6.0 and 2,152 earthquakes of magnitude 2.0 or greater. Table 2 lists independent main shocks of magnitude 4.0 and greater in the sample. Focusing attention on the Wasatch Front study area, figures 8 and 9 show the patterns of instrumental seismicity from October 1, 1974, through June 30, 1978 (2,480 events), and from July 1, 1978, through December 31, 1986 (3,936 events), respectively. The first sample is the same as that described in detail by Arabasz and others (1980) for the initial 3.75 years of detailed monitoring by the University of Utah's telemetered seismic network. The second sample allows an updated comparison for the subsequent 8.5-year period. The earthquake samples in figures 8 and 9 are probably complete above about magnitude 2.0 (discussed later). The extent of seismographic coverage, relevant to inferences of epicentral precision, is shown in figure 2.

The patterns of seismicity shown in figures 8 and 9 are remarkably similar, and comparison with the pattern for 1962 through 1974 (Arabasz and others, 1980, fig. 4) indicates general stability in the pattern of seismicity throughout the period of instrumental monitoring. One notable difference in the seismicity before and after 1974 is the aftershock activity that followed the 1975 M_L 6.0 Pocatello Valley earthquake on the Idaho-Utah border (upper left-hand parts, figs. 8, 9). The pattern of most recent seismicity in the Wasatch Front area illustrated in figure 9 includes several notable features, described from north to south:

1. At the northern extremity of figure 9, earthquake clusters are part of a northeast-trending belt of seismicity that continues to the Jackson-Yellowstone Park region. This trend includes episodic swarm seismicity in the Soda Springs area of Idaho (approximately 42°30′ N., 111°30′ W.). A swarm beginning as early as December 1981 peaked with an M_L 4.7 earthquake in October 1982 (Richins and others, 1983), and seismicity continues in that area.
2. Earthquake activity in the Idaho-Utah border area west of the Wasatch fault has been prominent ever since the 1975 M_L 6.0 Pocatello Valley earthquake (Arabasz and others, 1981). Small- to moderate-sized earthquakes extending southward from the State

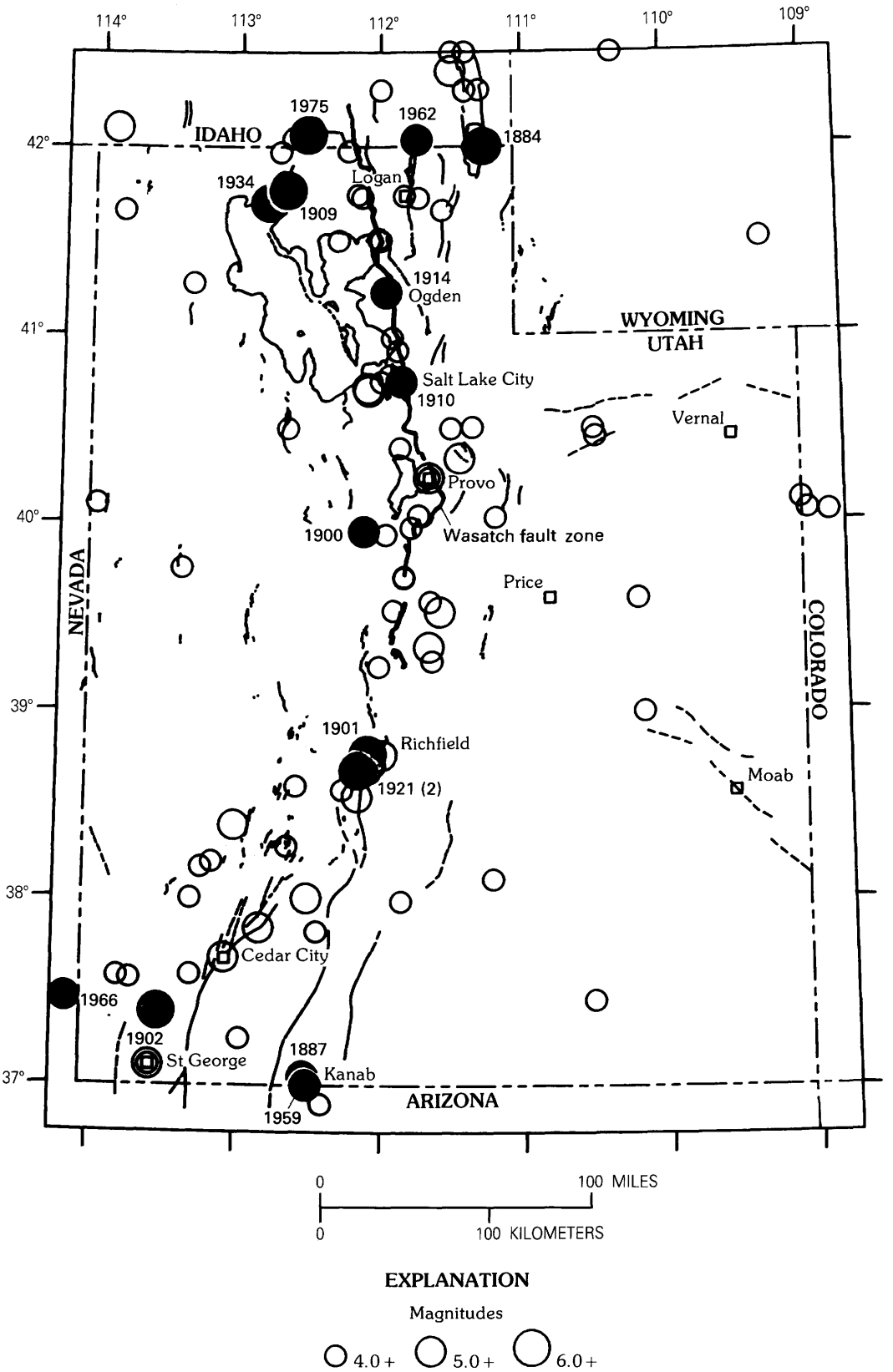

FIGURE 6.—Epicenters of all independent main shocks of M_L 4.0 or greater (or Modified Mercalli intensity V or greater) in the Utah region, 1850–1986, and Quaternary faults. Earthquakes of estimated M_L 5.5 or greater are indicated by solid circles, labeled with date. Data from University of Utah Seismograph Stations.

TABLE 1.—*Largest earthquakes in the Utah region, 1850 through December 1986*

[Modified from Arabasz and others (1979). Includes earthquakes of maximum Modified Mercalli intensity VII or greater or of Richter magnitude 5.5 or greater. Aftershocks excluded. Magnitudes in parentheses are estimated from intensity. Sample area (Utah region): 36.75° N.–42.50° N., 108.75° W.–114.25° W. (fig. 6). Italics denote earthquakes within the Wasatch Front study area: 38.92° N.–42.50° N., 110.42° W.–113.17° W. (fig. 3)]

Local date	Lat, °N.	Long, °W.	Location	Modified Mercalli intensity	Magnitude (M_L)	Moment[1] ($\times 10^{24}$ dyne-cm)
1884, Nov. 10	*42.0*	*111.3*	*Bear Lake Valley*	*8*	*(6)*	
1887, Dec. 5	37.1	112.5	Kanab	7	(5½)	
1900, Aug. 1	*40.0*	*112.1*	*Eureka*	*7*	*(5½)*	
1901, Nov. 13	38.8	112.1	Richfield	9	(6½+)	
1902, Nov. 17	37.4	113.5	Pine Valley	8	(6)	
1909, Oct. 5	*41.8*	*112.7*	*Hansel Valley*	*8*	*(6)*	
1910, May 22	*40.8*	*111.9*	*Salt Lake City*	*7*	*(5½)*	
1914, May 13	*41.2*	*112.0*	*Ogden*	*7*	*(5½)*	
1921, Sept. 29	38.7	112.2	Elsinore	8	(6)	
1921, Oct. 1	38.7	112.2	Elsinore	8	(6)	
1934, Mar. 12	*41.7*	*112.8*	*Hansel Valley*	*9*	*[2]6.6*	*77.0*
1959, July 21	37.0	112.5	Utah-Arizona border	6	5.5+	
1962, Aug. 30	*42.04*	*111.74*	*Cache Valley*	*7*	*5.7*	*7.0*
1966, Aug. 16	37.46	114.15	Nevada-Utah border	6	5.6	1.1
1975, Mar. 27	*42.06*	*112.52*	*Pocatello Valley*	*8*	*6.0*	*18.6*

[1]Doser and Smith (1982).

[2]Richter (1935, p. 24) estimated an M_L value of 7.0. The value of 6.6 comes from Gutenberg and Richter (1954) and appears to be a surface-wave magnitude.

border form an inverted Y pattern, which began to form several months after the March 1975 main shock and in which seismicity persists to the present. At the southwestern extremity of the Y pattern, scattered small earthquakes beneath the northern part of the Great Salt Lake previously have appeared to be part of a broad northeast-trending belt. The sample in figure 9, however, suggests a northwest-trending pattern of epicenters in the vicinity of the East Great Salt Lake fault.

3. Densely clustered earthquakes occurring roughly 10 to 40 km east of the Wasatch fault define a linear belt extending southward from about 41°50′ N. to at least 41° N. and perhaps as far south as 40° N. Earthquakes in the northern part of this belt lie east of the west-dipping East Cache and Wasatch faults and occur within a volumetric zone beneath the Bear River Range, whose western boundary is formed by the East Cache fault. To the south of 41° N., earthquake clusters within this belt to the east of the Wasatch fault follow a zone of northerly trending valleys within the so-called Wasatch Hinterland (Sullivan and others, 1988).
4. Clusters of seismicity appear close to or just west of the trace of the Wasatch fault—near Honeyville at about 41°40′ N., in the vicinity of Salt Lake City at about 40°45′ N., at the northern end of Utah Valley at about 40°20′N., in the vicinity of Goshen Valley at about 40°00′ N., and in a broadly scattered zone at the southern end of the Wasatch fault. We will return to these observations when we consider the Wasatch fault in greater detail in a later section.
5. In the lower right-hand part of figure 9, a prominent feature of the seismicity of east-central Utah is an inverted U-shaped pattern of persistent shallow seismicity that corresponds to underground coal mining along the eastern side of the Wasatch Plateau (between about 39°15′ N. and 39°35′ N.) and along the arcuate Book Cliffs escarpment (east of about 39°45′ N., 111°00′ W.). The seismicity is well known to be mining related and appears to correlate with mining areas where annual rates of extraction exceed 500,000 tons (see summary by Arabasz and Julander, 1986). Results of a recent study of mining-related seismicity in the eastern Wasatch Plateau have been reported by Williams and Arabasz (1989).

EARTHQUAKE FOCAL DEPTHS

This section examines seismic network data from the Wasatch Front region for focal-depth information. It is an unfortunate fact that the computed focal depths of most earthquakes located with the regional seismic network are unreliable because of the large station spacings of 15 to 35 km in the immediate Wasatch Front area and 35 to 100 km elsewhere (fig. 2). As a partial solution to this problem, temporary arrays of portable seismographs are routinely deployed by the University of Utah in selected target areas (element 8, fig. 1) and have provided some of the best data for correlating seismicity with structure (for example, Arabasz and Julander, 1986). It remains useful, nonetheless, to evaluate the regional network data for focal-depth information.

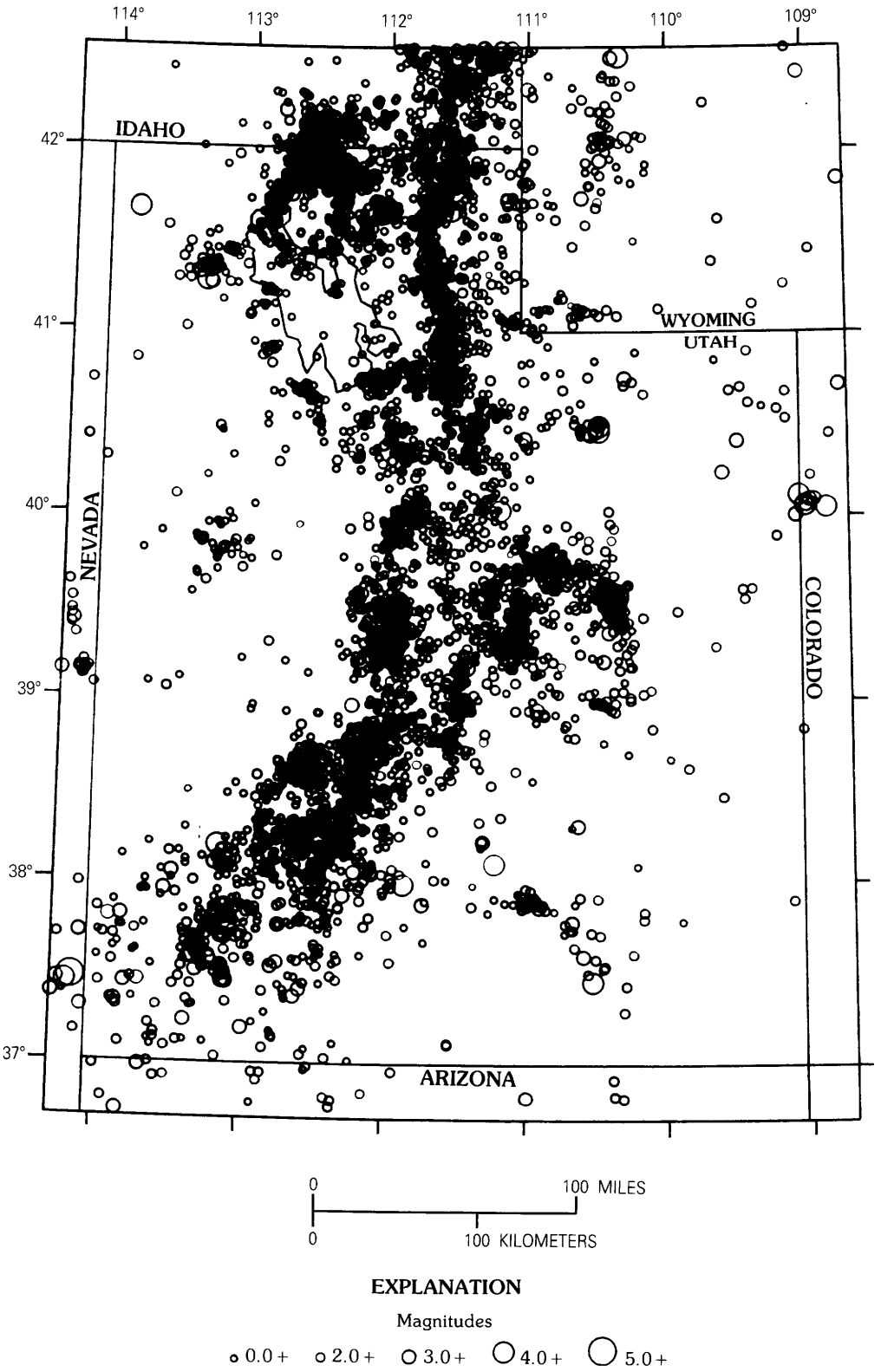

FIGURE 7.—Epicenters of all earthquakes located by the University of Utah Seismograph Stations in the Utah region, July 1, 1962, to December 31, 1986.

TABLE 2.—*Independent main shocks of magnitude (M_L) 4.0 or greater in the Utah region, July 1962 through December 1986*

[Italics denote earthquakes within the Wasatch Front study area (see table 1 for boundaries of the Utah region and Wasatch Front area)]

Local date	Lat, °N.	Long, °W.	Magnitude (M_L)	Location
1962, Aug. 30	*42.04*	*111.74*	*5.7*	*Cache Valley (Logan)—damage.*
1962, Sept. 5	*40.72*	*112.09*	*5.2*	*Magna—damage.*
1963, July 7	*39.53*	*111.91*	*4.4*	*Juab Valley (Levan/Nephi)—damage.*
1963, July 9	*40.03*	*111.19*	*4.0*	*Soldier Summit area.*
1963, Sept. 30	38.10	111.22	4.3	Capitol Reef area.
1964, Oct. 18	*41.73*	*111.73*	*4.1*	*Cache Valley.*
1966, Mar. 17	*41.66*	*111.56*	*4.6*	*Logan.*
1966, May 20	37.98	111.85	4.1	Aquarius Plateau area.
1966, Aug. 16	37.46	114.15	5.6	Nevada-Utah border.
1966, Oct. 21	38.20	113.16	4.2	Escalante Valley.
1967, Feb. 14	40.11	109.05	4.0	Utah-Colorado border.
1967, Feb. 16	41.27	113.33	4.0	Newfoundland Mountains area.
1967, Oct. 4	38.54	112.16	5.2	Marysvale—damage.
1970, Mar. 29	41.66	113.84	4.7	Grouse Creek area.
1970, Apr. 21	40.06	109.01	4.0	Colorado-Utah border.
1971, Dec. 3	42.50	110.34	4.1	Southwestern Wyoming.
1972, Jan. 3	38.65	112.17	4.4	Elsinore—damage.
1972, June 1	38.67	112.07	4.0	Southwestern Sevier County.
1972, Oct. 1	*40.51*	*111.35*	*4.3*	*Heber City—damage.*
1973, Apr. 13	*42.04*	*112.63*	*4.2*	*Pocatello Valley.*
1975, Mar. 27	*42.06*	*112.52*	*6.0*	*Pocatello Valley—damage.*
1976, Nov. 4	*41.81*	*112.70*	*4.0*	*Hansel Valley*[1].
1977, Sept. 30	*40.46*	*110.48*	*4.5*	*Northwestern Duchesne County—damage.*
1978, Nov. 29	*42.10*	*112.49*	*4.6*	*Pocatello Valley.*
1979, Mar. 19	40.04	108.86	4.1	Colorado-Utah border.
1980, May 24	*39.94*	*111.96*	*4.4*	*Goshen Valley.*
1981, Apr. 4	37.59	113.30	4.6	Kanarraville.
1982, May 24	38.71	112.04	4.0	Sevier Valley (Annabella).
1983, Oct. 8	*40.75*	*111.99*	*4.3*	*Northern Salt Lake Valley.*
1986, Mar. 24	*39.24*	*112.01*	*4.4*	*Japanese Valley.*
1986, Aug. 22	37.45	110.53	4.0	Southeastern Utah (near Bullfrog Basin).

[1]Identified by Shimizu (1987) as a dependent event related to the March 1975 Pocatello Valley earthquake and included here for the sake of argument.

It is commonly assumed that the presence of a recording station within one focal depth of an earthquake's epicenter provides good depth control. To test this assumption, K.J. Quigley (unpub. report, 1986) performed numerical experiments on synthetic P-wave arrival-time data for the Wasatch Front seismic network to determine statistical criteria for focal-depth reliability. On the basis of his results, 485 earthquakes out of 6,416 from the 1974–86 UUSS catalog for the Wasatch Front area were judged to have reliable focal depths. The criteria were as follows: (1) distance to the nearest station was less than or equal to the focal depth or 5 km, whichever was larger, and (2) standard vertical hypocentral error (ERZ) was 2 km or less, as calculated by the location program HYPOELLIPSE (1974–80) or HYPOINVERSE (1981–86). Quigley's results verified theoretical expectations that there is a 68 percent probability that the computed focal depth for such events is within 1.0 ERZ of the true focal depth and a 98 percent probability that it is within 2.4 ERZ.

Figure 10 shows the best-resolved foci in map and cross-section view. The selection criterion of having a close station may filter out shallow events in some areas, but deeper events will be less affected. In general, the east-west cross sections do not appear to be particularly informative in terms of significant variations in the east-west distribution of maximum focal depths or spatial association with the Wasatch fault. The north-south cross section, however, suggests that there may be variations in maximum earthquake depth along the Wasatch Front. For example, there are no earthquakes deeper than 17 km in the central part of the cross section, whereas there are earthquakes deeper than 17 km and as deep as 25 km at the northern and southern ends. We caution, however, that the apparent variation in maximum focal depth may be an artifact of sampling because

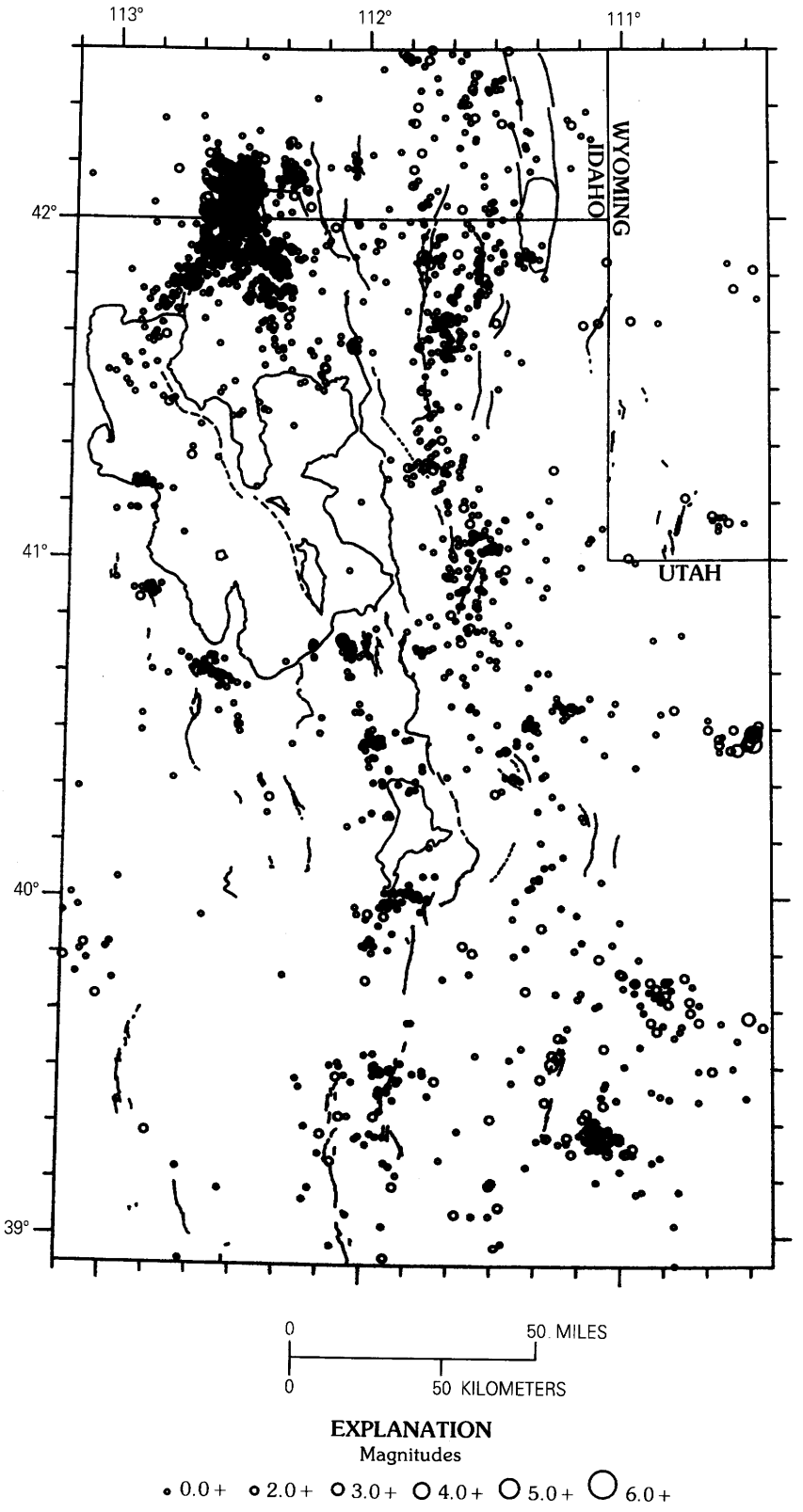

FIGURE 8.—Epicenters of all earthquakes located by the University of Utah Seismograph Stations in the Wasatch Front area, October 1, 1974, to June 30, 1978. Base map is as shown in figure 5.

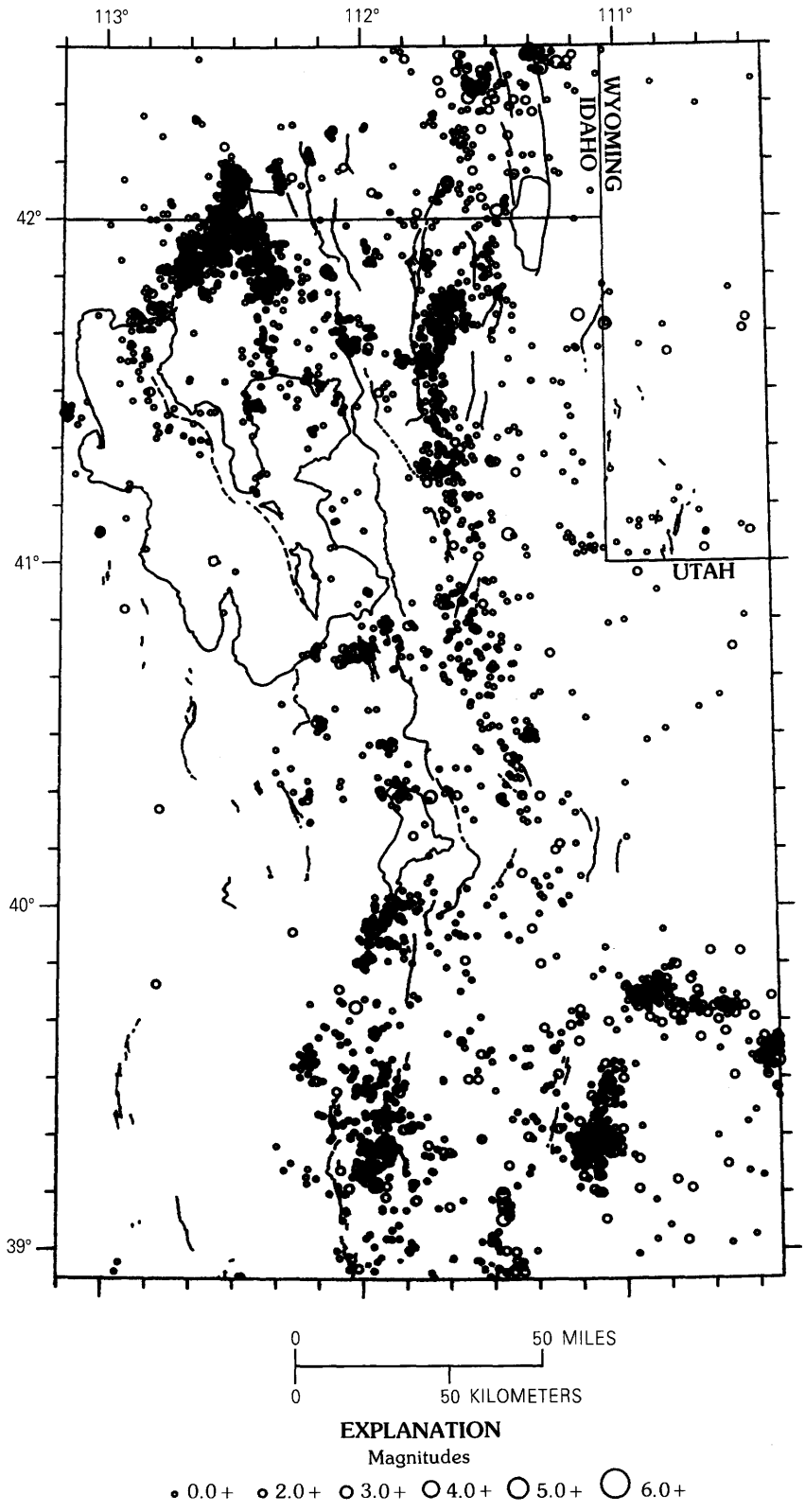

FIGURE 9.—Epicenters of all earthquakes located by the University of Utah Seismograph Stations in the Wasatch Front area, July 1, 1978, to December 31, 1986. Base map is as shown in figure 5.

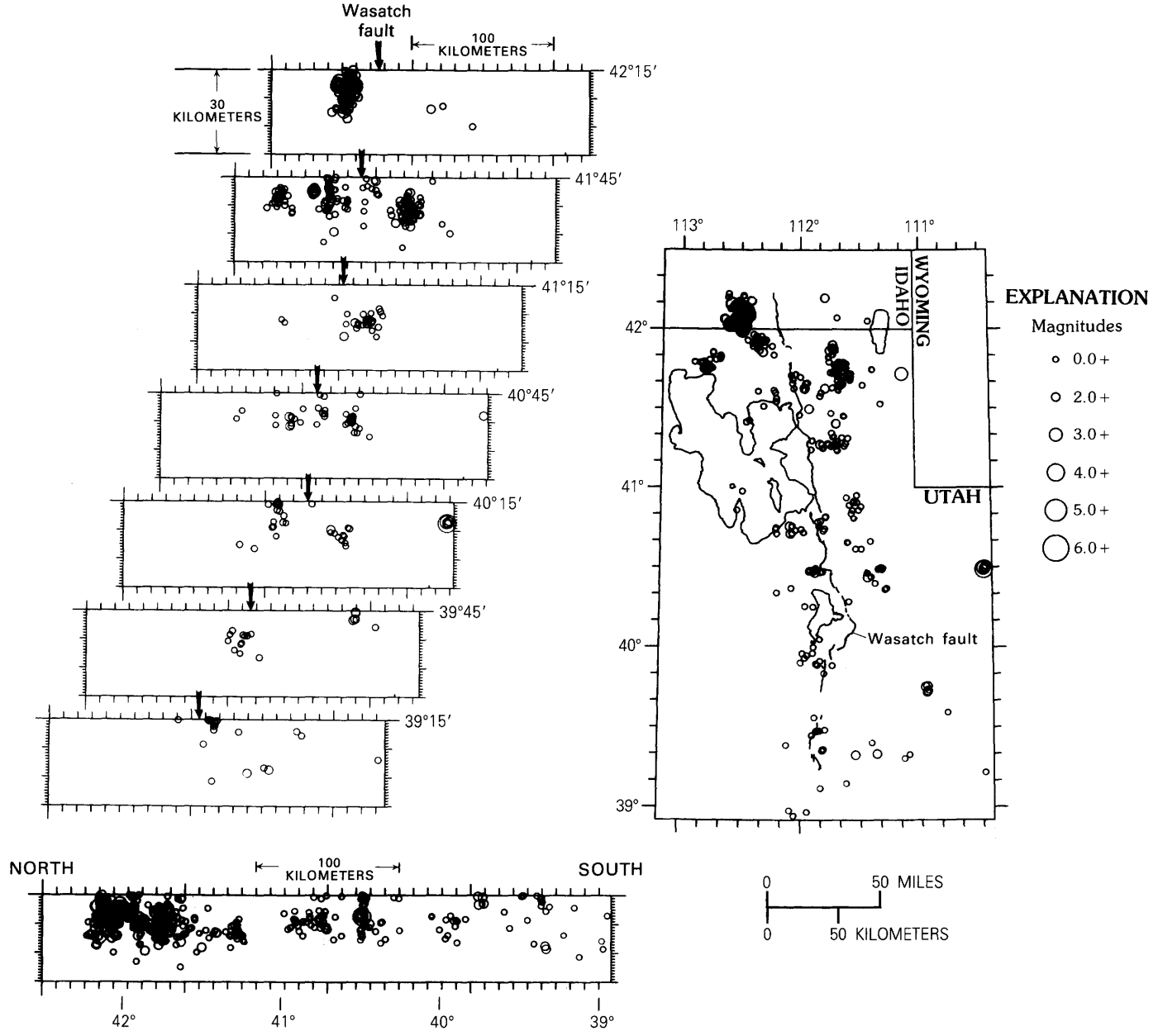

FIGURE 10.—Epicenters (right) and corresponding vertical sections (left) of earthquakes in the Wasatch Front area located with reliable focal depths, October 1974 through December 1986. Sample includes only earthquakes located with a standard vertical hypocentral error of 2 km or less and with the distance to the nearest recording station being less than or equal to the focal depth or 5 km, whichever is larger. Each vertical section includes foci whose epicenters lie within 15′ latitude of the line of section.

there are relatively few events in the central and southern parts of the section. The larger any sample of earthquakes, the more likely it is to contain extreme values of focal depths. To evaluate the influence of north-south variations in the number of earthquakes sampled on the observed maximum focal depths, we determined, for various latitude bands, the focal depth above which 90 percent of the earthquakes lie. These 90th-percentile depths are as follows: 17 km between 38°55′ N. and 40° N. latitude, 13 km between 40° N. and 41° N. latitude, 15 km between 41° N. and 42° N. latitude, and 11 km from 42° N. to 42°30′ N. latitude (where the sampling is dominated by aftershocks of the M_L 6.0 Pocatello Valley earthquake of 1975). These results suggest the possibility of variations in maximum focal depth on the order of 2 to 6 km.

Maximum earthquake focal depths bear directly on crustal rheology, the depth of nucleation of large earth-

quakes, and maximum fault-rupture dimensions. Accordingly, the north-south variations of maximum focal depth suggested in figure 10 should be investigated further. Figure 10 emphasizes the sparseness of three-dimensional information available from the thousands of earthquakes located by the permanent regional network. Consequently, only limited information is available to address the association of seismicity with subsurface structure, as we discuss next.

PROBLEMATIC CORRELATION OF SEISMICITY WITH GEOLOGIC STRUCTURE

Fundamental problems in correlating diffuse seismicity with mapped Cenozoic faulting and subsurface geologic structure in the Utah region have been discussed at length by Arabasz (1984) and by Arabasz and Julander (1986). These discussions are repeated here because of their continued relevance. Problems include (1) uncertain subsurface structure, which typically is more complex along the main seismic belt than surface geology would indicate, (2) observations of discordance between surface fault patterns and seismic fault slip at depth (Arabasz and others, 1981; Zoback, 1983), (3) a paucity of historical surface faulting, and (4) inadequate focal-depth resolution from regional seismic monitoring.

Crustal structure along the eastern Great Basin is known to involve vertically stacked plates separated by low-angle detachments resulting from relict pre-Neogene thrust-belt structure and (or) Neogene extension (Allmendinger and others, 1983; Smith and Bruhn, 1984; Smith and others, 1987). Smith and Bruhn (1984) presented a summary of seismic reflection data that indicate the widespread presence of low-angle and downward-flattening faults in the subsurface and an intimate relationship between pre-Neogene thrust-belt structure and young normal faults along the eastern Basin and Range margin. Seismologic evidence to date indicates that, at least for small to moderate earthquakes, seismic slip in this region predominates on faults having moderate (≥30°) to high-angle dip (Zoback, 1983; Arabasz and Julander, 1986; Bjarnason and Pechmann, 1989).

Given the relatively high magnitude threshold of surface faulting and observations of discordance between surface-fault patterns and seismic slip at depth, one can argue that—with the sole exception of the 1934 Hansel Valley earthquake—no other of Utah's 15 historical earthquakes of M_L 5.5 or greater (table 1) can be confidently associated with a mapped surface fault. Within the domain of Utah's main seismic belt, future seismicity below the threshold of surface faulting (M_L 6.3±0.2) thus cannot be confidently precluded by knowledge of the surface geology alone. Where subsurface structure is complex, moderate-sized earthquakes may occur on blind subsurface structures that have no direct surface expression.

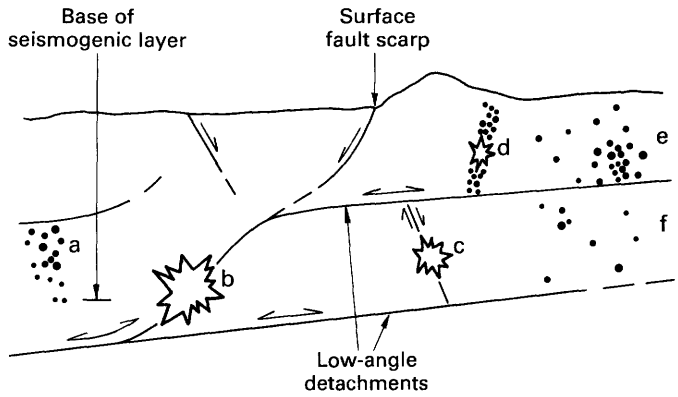

FIGURE 11.—Schematic geologic cross section illustrating the complex association of seismicity in the upper crust with geological structure in the Intermountain Seismic Belt (from Arabasz, 1984; Arabasz and Julander, 1986). Starbursts indicate foci of moderate to large earthquakes; solid circles, microseismicity; lines in subsurface, faults. Arrows indicate sense of slip on faults; two-directional arrows show extensional backsliding on preexisting low-angle faults possibly formed as thrust faults. The base of the seismogenic layer is at a depth of approximately 10 to 15 km. Lowercase letters identify aspects (not exhaustive) of observations and a working hypothesis relating seismicity to structure: a, local predominance of seismicity within a lower plate; b, nucleation of a large normal-faulting earthquake near the base of the seismogenic layer, hypothetically on an old thrust ramp, with linkage or an established rupture pathway to a major surface fault; c, occurrence of a moderate-sized earthquake within a lower plate, without linkage to a shallow structure; d, occurrence of a moderate-sized earthquake and aftershocks on a secondary fault where an underlying detachment restricts deformation to the upper plate; e, diffuse block-interior microseismicity predominating within an upper plate, perhaps responding to extension enhanced by gravitational backsliding on an underlying detachment; f, diffuse block-interior microseismicity within a lower plate where frequency of occurrence is markedly lower than it is in the overlying plate.

On the basis of special earthquake studies in the southern Wasatch Front area, neighboring parts of central Utah, and southeastern Idaho, the following working hypothesis was offered by Arabasz (1984) (see also Arabasz and Julander, 1986) to explain observations of diffuse background seismicity. Background seismicity, it was suggested, is fundamentally controlled by variable mechanical behavior and the internal structure of individual horizontal plates within the seismogenic upper crust. Diffuse epicentral patterns may then result from the superposition of seismicity occurring within individual plates and also perhaps from favorable conditions for block-interior rather than block-boundary microseismic slip. Figure 11 schematically shows some aspects of this working hypothesis.

SEISMIC SOURCE ZONES AND SEISMICITY PARAMETERS

GENERAL REMARKS

Two key steps in any analysis of earthquake hazards or risks are (1) the identification and geometric depiction of seismic source zones within which earthquakes are likely to originate (step 3, fig. 1) and (2) the estimation of seismicity parameters for these source zones (step 4, fig. 1). The important seismicity parameters are the maximum magnitude, the expected earthquake distribution as a function of size, and the rate of activity. Both earthquake catalog data and geologic data on active faults can be used to identify and characterize seismic source zones.

Our current understanding of the seismotectonic framework of the Wasatch Front region, as summarized above, leads to the position that seismic hazards arise from two fundamental classes of earthquakes: (1) infrequent, large ($M_S \geq 6.3 \pm 0.2$) surface-faulting earthquakes on identifiable faults showing evidence of late Quaternary displacement and (2) small- to moderate-sized (up to M_L 6.5) earthquakes, below the threshold of surface faulting, that are not constrained in location to mapped faults and may occur randomly in space throughout broadly defined regions. This position is a consequence of detailed studies that show clear evidence for large prehistoric earthquakes on faults in the region (for example, Swan and others, 1980; Schwartz and others, 1984; Machette and others, 1991, this volume), the diffuse scatter of small- to moderate-sized earthquakes (illustrated in figs. 7, 8, 9), and the problematic correlation of seismicity and geologic structure discussed above. It therefore seems reasonable to distinguish two different types of seismic source zones: (1) fault-specific sources for which the evidence is primarily geologic and (2) areal source zones that are based on the historical and instrumental earthquake record and have a maximum magnitude of 6.5. These two types of source zones have been used in several studies of seismic hazard in the Wasatch Front region, including the elaborate probabilistic analysis of the ground-shaking hazard by Youngs and others (in press), a study of the "Wasatch Hinterland" by Sullivan and others (1988), and a study by Arabasz and others (1987) of the region surrounding the sites that Utah proposed for the Superconducting Supercollider, which are located southwest of the Great Salt Lake along the western boundary of the Wasatch Front region.

In this section, we treat the entire Wasatch Front study area as one areal source zone and use the instrumental earthquake record to model the recurrence of earthquakes within the area of up to magnitude 6.5. Although the available data suggest that seismicity rates may vary somewhat within this region, there are not enough earthquakes in the record to reliably estimate seismicity parameters for subsets of this region. Furthermore, the 25-year record of instrumental seismicity is simply too short to allow extrapolation into the future of spatial variations of the seismicity rate within the Wasatch Front area. We first present results from recurrence modeling for the Wasatch Front area and then briefly discuss the fault-specific sources in this region and the maximum earthquake size that can be expected to occur on them.

RECURRENCE MODELING

Earthquake catalog data provide the only means of determining the rate of occurrence and the size distribution of earthquakes smaller than the threshold of surface faulting. A standard way to characterize seismicity in any seismically active region is with the Gutenberg-Richter exponential frequency-magnitude relationship, given by

$$\log_{10} N = a - b\mathrm{M}$$

where N is the average number of independent events per year of magnitude M or greater and a and b are constants appropriate for the particular region. The a value is a measure of the overall rate of earthquake activity. The b value is a measure of the relative proportion of small events to large events; higher b values indicate relatively more small events. If we define A as the average number of events per year of $\mathrm{M} \geq 3.0$ (that is, $A = 10^{a-3.0b}$), then the above equation can be rewritten as

$$N = A\ 10^{-b(\mathrm{M}-3.0)}$$

To obtain meaningful estimates for the seismicity parameters a (or A) and b from earthquake catalog data, it is first necessary to remove from the catalog all dependent events such as aftershocks, foreshocks, and secondary events in swarm sequences. Shimizu (1987) identified dependent and independent events in the University of Utah catalog for the period July 1962 through December 1985 by applying the local clustering method of Veneziano and Van Dyck (1985, 1986). This method uses statistical tests to identify earthquake clusters, which Veneziano and Van Dyck defined as space-time windows in which the rate of earthquake activity is significantly greater than the estimated local background rate. One or more of the earthquakes within each cluster are then classified as main shocks, and the rest are classified as dependent events. This procedure is repeated until no additional events are identified as dependent. The primary advantage of the local clustering method in comparison with other methods of identifying

dependent events is that it allows for variations in the spatial and temporal extents of clusters of dependent events associated with different main shocks of the same magnitude.

Shimizu's listing of independent events of $M_L \geq 2.0$ in the catalog for this period was supplied to us on computer tape by D. Veneziano. This listing contained 571 main shocks within the study area. The epicenters of these events are plotted in figure 12. For purposes of recurrence modeling, we eliminated the 126 events in the study area south of 39°50′ N. and east of 111°15′ W. (dashed box, fig. 12), where the seismicity is predominantly mining related. This elimination left 445 independent main shocks of $2.0 \leq M_L \leq 6.0$ in the remaining 85,000 km^2 of the study area. These main shocks form the basic data set for our recurrence modeling of the Wasatch Front area.

Figure 13 is a cumulative recurrence plot (log N versus M) for the 445 independent main shocks. The observed number of $M_L \geq 2.0$ events per year is equal to or greater than the number expected from a linear extrapolation of the data for the larger magnitude cutoffs. In fact, the recurrence curve formed by connecting the data points in figure 13 even appears to have a steeper slope for $M_L \leq 3.0$. This observation suggests that the University of Utah catalog contains a reasonably complete listing of main shocks of $M_L \geq 2.0$ in the Wasatch Front region after July 1962. However, the precise threshold magnitude of completeness for the catalog varies with time and with location within the region, depending on station coverage (fig. 2).

The apparent change in slope of the recurrence curve near magnitude 3 may be an artifact of the way that magnitudes are assigned in the University of Utah catalog. The catalog magnitudes for most earthquakes in the Wasatch Front region over magnitude 3 are true local magnitudes calculated from peak amplitudes measured on seismograms from low-gain Wood-Anderson-type instruments. The magnitudes listed for most of the smaller earthquakes are coda magnitudes calculated from signal durations measured on records from various types of higher gain instruments (for details, see Arabasz and others, 1979; Richins and others, 1981, 1984; Brown and others, 1986). The coda magnitude scales were calibrated against Wood-Anderson M_L measurements and should therefore give compatible results. Nevertheless, there may be some small, systematic differences between the two types of estimates. Research on refined methods of magnitude determination using digital waveform data is currently under way at the University of Utah.

The heavy line in figure 13 shows a straight-line fit to the recurrence data above M_L 3.0, determined by using the maximum-likelihood technique of Weichert (1980) and an assumed maximum magnitude of 7.5. The best-fit line has a slope of $b = 0.71 \pm 0.09$. The lighter lines are drawn with lower bound and upper bound slopes of 0.62 and 0.80, respectively. All three lines are constrained to pass through the data point for the minimum magnitude of 3.0. The lighter lines appear to bound the range of possible slopes quite well if a magnitude cutoff of 3.0 is used. However, the b value is unfortunately very sensitive to the cutoff magnitude. Cutoff magnitudes of 2.0 and 2.5 give b values of 0.82 ± 0.04 and 0.88 ± 0.07, respectively. We chose the cutoff magnitude of 3.0 because of possible problems with the smaller magnitudes discussed above and because the lines calculated by using this cutoff provide a better fit to the data for the larger earthquakes, which are of primary concern for seismic hazards.

The recurrence relationship given by our preferred maximum likelihood fit to the data shown in figure 13 is

$$N = (2.51)10^{-(0.71 \pm 0.09)(M_L - 3.0)}$$

or, alternatively,

$$\log N = 2.53 - 0.71\ M_L$$

Table 3 lists average recurrence intervals for earthquakes in the Wasatch Front region calculated from the first of these equations.

As a check on table 3, consider the number of earthquakes of estimated magnitude 5.5 or greater in the Wasatch Front region from 1850 to 1987. The occurrence of eight such earthquakes (table 1, fig. 6) gives an average recurrence interval of 17 years. This average falls within the lower end of our estimated range of recurrence intervals for $M_L \geq 5.5$ earthquakes, which is 14 to 40 years. If, following Arabasz and others (1980), we assume that the catalog is complete at the $M_L \geq 5.5$ level only since 1878, the average recurrence interval shortens to 14 years. The interevent times for the eight $M_L \geq 5.5$ earthquakes range from 0.6 to 28.5 years, the mean being 12.9 years.

The recurrence intervals calculated for earthquakes greater than magnitude 6 represent an extrapolation beyond the limits of the data shown in figure 13. Nevertheless, it is interesting to compare our predicted recurrence interval for $M_L \geq 7.0$ events with estimates of the recurrence interval for $M_L \geq 7.0$ events on the Wasatch fault, given that the Wasatch fault is the dominant source of earthquakes of magnitude 7.0 and greater in the region. The average recurrence interval for $M_L \geq 7.0$ surface-faulting earthquakes on the Wasatch fault has been estimated to be 400 to 666 years by Schwartz and Coppersmith (1984), 330 ± 90 years by Youngs and others (in press), and 220 to 395 years by Machette and others

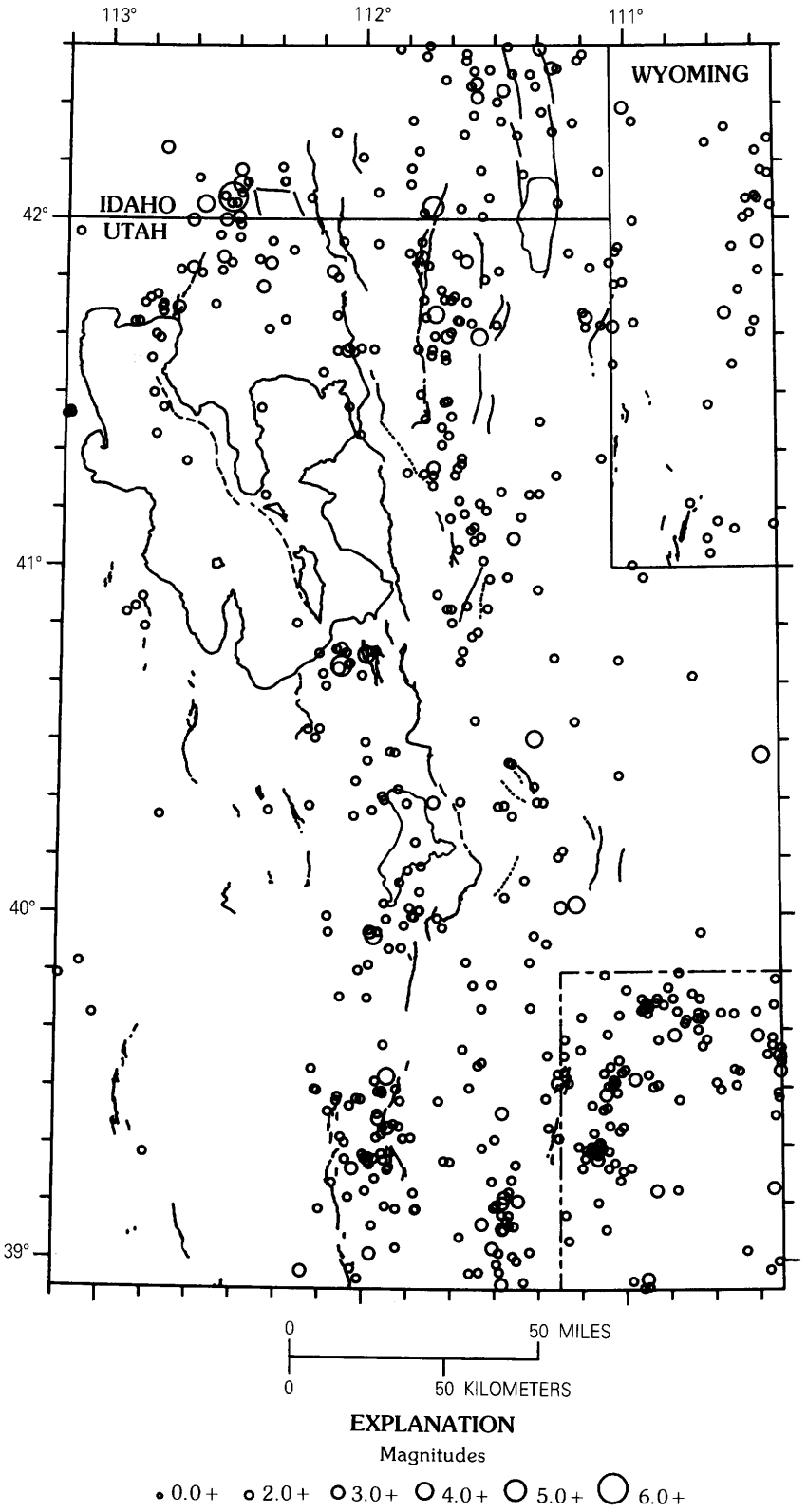

FIGURE 12.—Epicenters of independent main shocks in the Wasatch Front area from July 1, 1962, through December 31, 1985, plotted on the map of late Quaternary faulting shown in figure 5. The dashed box in the lower right-hand corner indicates an area of mining-induced seismicity that was excluded from the recurrence analysis.

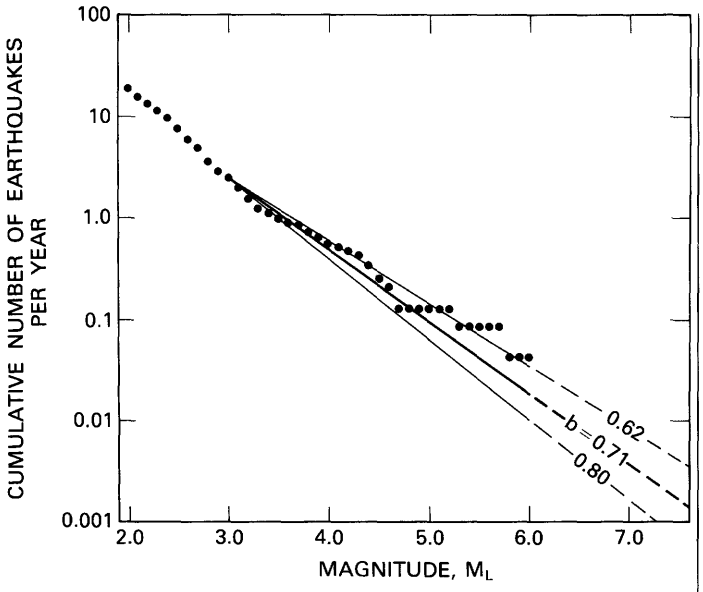

FIGURE 13.—Recurrence data for independent main shocks in the Wasatch Front area from July 1962 through December 1985. Solid circles show the cumulative number of earthquakes per year greater than or equal to the local magnitude (M_L), given on the horizontal axis. The circles are spaced 0.1 magnitude unit apart. The heavy line through the circles for $M_L \geq 3.0$ indicates the preferred maximum-likelihood fit having a slope b of 0.71, calculated by using the method of Weichert (1980). The lighter lines indicate the lower and upper bound slopes of 0.62 and 0.80, respectively. The area used for the recurrence modeling is 85,000 km^2 (area shown in fig. 12, minus the dashed box).

TABLE 3.—*Average recurrence intervals for earthquakes in the Wasatch Front region*

[38°55′ N.–42°30′ N., 110°25′W.–113°10′ W., excluding mining-related seismicity in the southeastern corner of the area. Area equals 85,000 km^2]

Magnitude range	Average recurrence interval (years)	
	Preferred estimate[1]	Range of estimates[2]
$M_L \geq 3.0$	0.40	
$M_L \geq 3.5$	.90	0.81–1.0
$M_L \geq 4.0$	2.0	1.7–2.5
$M_L \geq 4.5$	4.6	3.4–6.3
$M_L \geq 5.0$	10	7–16
$M_L \geq 5.5$	24	14–40
$M_L \geq 6.0$	54	29–100
$M_L \geq 6.5$	120	60–250
$M_L \geq 7.0$	280	120–630
$3.0 \leq M_L \leq 3.5$	71	.66–.78
$3.5 \leq M_L \leq 4.0$	1.6	1.6–1.7
$4.0 \leq M_L \leq 4.5$	3.7	3.3–4.2
$4.5 \leq M_L \leq 5.0$	8.3	6.6–10
$5.0 \leq M_L \leq 5.5$	19	14–26
$5.5 \leq M_L \leq 6.0$	42	28–66
$6.0 \leq M_L \leq 6.5$	96	57–170
$6.5 \leq M_L \leq 7.0$	220	120–420
$7.0 \leq M_L \leq 7.5$	490	240–1,000

[1]Calculated by using a b value of 0.71.

[2]Lower and upper limits calculated by using the limiting b values of 0.62 and 0.80, respectively.

(1991). These estimates are consistent with our predicted average recurrence interval of 120 to 630 years (the preferred value being 280 years) for $M_L \geq 7.0$ events in the Wasatch Front region as a whole.

Arabasz and others (1980) modeled earthquake recurrence for the Wasatch Front region by using independent main shocks from the University of Utah catalog of Modified Mercalli intensity V or greater (approximately $M_L \geq 4$) from 1850 through 1978. They obtained the equation

$$\log N = 2.98 - 0.72M_L$$

Their b value of 0.72 is essentially the same as our b value of 0.71±0.09. However, their a value of 2.98 is larger than our value of 2.53. This difference corresponds to a difference in seismicity rates of a factor of 2.8. Two possible explanations for this disparity are that (1) the seismicity from 1962 through 1985 was low in comparison with the seismicity from 1850 through 1961 or that (2) the magnitudes of the pre-1962 events were overestimated by about 0.6 magnitude unit by Arabasz and others (1980).

Our preferred b value of 0.71 is lower than the b values obtained in most previous studies of earthquake recurrence along the Wasatch Front that made major or exclusive use of the post-1962 instrumental University of Utah catalog. Arabasz and others (1980) determined a b value of 0.95±0.15 by using all magnitude 2.3 and greater earthquakes in the catalog from July 1962 through June 1978 within a subarea of the Wasatch Front region between 111°15′ W. and 112°15′ W. Youngs and others (in press) obtained b values ranging from 0.75±0.03 to 0.83±0.03 (depending on the criteria used to remove dependent events) by using catalog data from 1850 through March 1986 above the uniform detection thresholds that they had estimated. The north-south extent of the study area of Youngs and his co-workers is from 39° N. to 42°30′ N., nearly the same as that of our study area, but their area has a narrower east-west extent. Finally, Shimizu (1987) obtained a b value of 1.1 by using independent main shocks from July 1962 through December 1985 for a region extending from 39° N. to 42.5° N. and 108°45′ W. to 114°15′ W. (excluding mining-related seismicity in east-central Utah), which he calls the "Central-Northern Utah" region.

The higher b value obtained by Arabasz and others (1980) for the post-1962 instrumental catalog can be attributed to the fact that they did not remove dependent events from the catalog before calculating their b value. The differences between the b values of 0.75 to 0.83 determined by Youngs and others (in press) and our

value of 0.71 appear to result primarily from differences in the methods employed to remove dependent events. The higher b value of 1.1 obtained by Shimizu (1987) cannot be explained in this way, since we used his listing of independent events for our recurrence modeling. The higher b value obtained by Shimizu results from his use of a minimum magnitude of 2.5 in his recurrence analysis and, to a lesser extent, from his use of the maximum-likelihood method of Utsu (1965) to fit a straight line to the data. In the method of Utsu (1965), the b value is calculated from the equation

$$b = \log_{10} e/(\overline{M} - M_0)$$

where $\overline{M}$ is the mean magnitude of all events of magnitude greater than or equal to M_0. The b values given by Utsu's method tend to be higher than those given by the more elaborate method of Weichert (1980), which was used both by us and by Youngs and others (in press). Applying Utsu's method to the data in figure 13 for $M_L \geq 2.5$ gives a b value of 0.98, which is in reasonable agreement with Shimizu's value, considering that his calculation included data from a larger area.

FAULT-SPECIFIC SOURCES

Although the 1934 M_S 6.6 Hansel Valley earthquake is the largest historical earthquake to have occurred in the Wasatch Front region, there is good geologic evidence that larger earthquakes can be expected to occur on the Wasatch fault and other active faults in the region. All of the faults showing evidence of late Quaternary (less than 500,000 years) movement (fig. 5) are considered to be potential sources of earthquakes larger than M_L 6.3±0.2, the likely threshold for surface faulting. Maximum earthquake magnitudes for these fault-specific sources can be assessed from estimates of the rupture length, area, and displacement for the maximum size event. Average recurrence intervals for surface-faulting events can, at least in some cases, be determined from geomorphic observations or from the stratigraphy of deposits near the fault trace exposed by trenching (see Allen (1986) and Schwartz and Coppersmith (1986) for reviews of these techniques). A detailed description of all the fault-specific sources shown in figure 6 is beyond the scope of this paper. We refer the reader to Chapter M of this report (Youngs and others, in press) for a thorough summary of available information on the major faults in the Wasatch Front region and a determination of seismicity parameters for these faults. Here we present information on four fault-specific sources that we use below in some probabilistic hazard calculations, consider the maximum probable earthquake for the whole Wasatch Front area, and briefly discuss the issue of frequency-magnitude relationships for individual faults.

Table 4 presents basic information for the four most prominent fault-specific sources near Salt Lake City: the Wasatch fault, the West Valley fault zone, the East Great Salt Lake fault, and the North Oquirrh Mountains fault (fig. 5). The faulting parameters for the Wasatch fault are taken from segmentation model B of Youngs and others (in press). (Minor differences with subsequent segmentation models—for example, that of Machette and others (1991)—are unimportant for our purposes here.) The maximum magnitude listed for each segment is a mean estimate calculated from the set of possible values and their assigned weights listed in table 1 of Youngs and others (in press). The recurrence intervals for maximum earthquakes are mean estimates taken directly from table 3 of Youngs and others (in press). For the West Valley fault zone, the maximum magnitude of 6.5 is also a mean value calculated from table 1 of Youngs and others (in press). The average recurrence interval of 2,000 years is inferred from the observation of six to seven discrete faulting events on the fault zone within the last 13,000 years (S.J. Olig, written commun., 1987). The segmentation of the East Great Salt Lake fault is very uncertain, but it appears to be divided into at least two segments, each about 50 km long (fig. 5) (Pechmann and others, 1987). The maximum magnitude of 7.2 assigned to each segment is based on a simple analogy with the Weber and Salt Lake City segments of the Wasatch fault, which are of comparable length. The average recurrence interval for maximum earthquakes on each segment of the East Great Salt Lake fault is judged to be about 4,000 years, on the basis of the fact that the observed slip rates are about half of those measured for the central segments of the Wasatch fault, which have recurrence intervals of about 2,000 years (Pechmann and others, 1987). For the North Oquirrh Mountains fault, the maximum magnitude of 7.0 is from table 1 of Youngs and others (in press). The average recurrence interval of about 10,000 years or more is inferred from the observation that the most recent surface-faulting event on this fault occurred between 8,000 and 13,500 years ago (Youngs and others, in press), together with generic arguments made by Arabasz and others (1987). For all of the faults in table 4, the annual probability of the maximum earthquake is taken to be the inverse of the average time interval between maximum earthquakes, since, in most cases, the time elapsed since the last large earthquake is poorly known.

Estimates of the maximum earthquake size on any particular fault are subject to the uncertainties inherent in both the prediction of future rupture characteristics and the conversion of those rupture characteristics to magnitude estimates. For this reason, it is useful to

TABLE 4.—*Information for selected fault-specific sources*

Fault source	Approximate length (km)	Maximum magnitude (M_S)	Mimimum distance to site[1] (km)	Interval for maximum earthquake (years)	Annual probability of maximum earthquake (10^4/year)
Wasatch fault segments:[2]					
Collinston	60	7.3	110	8,800	1.1
Brigham City	40	7.1	70	7,250	1.4
Weber	57	7.2	15	1,350	7.4
Salt Lake City	45	7.2	0	2,550	3.9
American Fork	18	6.8	25	1,900	5.3
Provo	19	6.8	40	1,900	5.3
Spanish Fork	32	7.0	60	2,050	4.9
Nephi	40	7.1	80	1,750	5.7
Levan	35	7.1	120	7,100	1.4
Fayette	14	6.6	155	10,000	1.0
West Valley fault zone[3]	18	6.5	0	2,000	5.0
East Great Salt Lake fault segments:[4]					
Promontory	50	7.2	70	4,000	2.5
Antelope Island	50	7.2	20	4,000	2.5
Northern Oquirrh Mountains fault[5]	35	7.0	30	10,000	1.0

[1]The site used for the calculation of the hazard curves is the intersection of I–15 and I–80 in South Salt Lake, at approximately 40°43.1′ N., 111°54.2′ W. (diamond, fig. 5).

[2]Youngs and others (in press), Machette and others (1986).

[3]Young and others (in press), S.J. Olig (written commun., 1987).

[4]Pechmann and others (1987), Viveiros (1986).

[5]Youngs and others (in press), T. Barnhard (personal commun., 1987).

consider, from a historical point of view, the maximum earthquake size that is likely to occur anywhere within the Wasatch Front region.

The 1959 M_S 7.5 Hebgen Lake earthquake is considered by some to represent the maximum earthquake for the Intermountain Seismic Belt (for example, Doser, 1985a). However, larger earthquakes than this have occurred in the western Basin and Range province. Slemmons (1980) listed 13 historical surface-faulting earthquakes in the western Great Basin, including two events having magnitudes greater than 7.5: the March 26, 1872, Owens Valley, Calif., earthquake of estimated magnitude 8.0 and the October 3, 1915, Pleasant Valley, Nev., earthquake of magnitude 7.75. Slemmons (1980) listed a rupture length of 110 km and a maximum displacement of 6.44 m for the Owens Valley event and a rupture length of 62 km and a maximum displacement of 5.6 m for the Pleasant Valley event. Thus, both of these earthquakes have a maximum displacement comparable to that of the Hebgen Lake event but significantly longer rupture lengths. The magnitude of 7.75 for the Pleasant Valley event is from Gutenberg and Richter (1954) and is nearly identical to the surface-wave magnitude of 7.7 calculated by Abe (1981). The magnitude of the Owens Valley event is more controversial, owing to the lack of seismographic instruments at the time. Magnitude estimates for this earthquake, based on felt reports, range from 8.3 (Oakeshott and others, 1972) to 7.2 (Evernden, 1975). From the surface faulting, Beanland and Clark (1987) estimated a moment magnitude of 7.5 to 7.7.

The slip that occurred during the 1872 Owens Valley earthquake had a large strike-slip component to it (Richter, 1958; Oakeshott and others, 1972) and may even have been dominantly strike slip (Beanland and Clark, 1987). Faults in the Wasatch Front region show predominantly normal slip, although there is abundant evidence of strike-slip faulting in south-central Utah (Anderson and Barnhard, 1984, this volume). Thus, the Pleasant Valley and Hebgen Lake earthquakes may be better models for the maximum credible Wasatch Front earthquake than the Owens Valley earthquake. The characteristics of the Pleasant Valley and Hebgen Lake earthquakes suggest that future Wasatch Front earthquakes could have surface-wave magnitudes of up to 7.5 to 7.7, rupture lengths of up to 35 to 65 km, and maximum vertical displacements of up to about 6 m.

One interesting question concerning fault-specific sources is the extent to which they act as sources for small- to moderate-sized earthquakes, excluding foreshocks and aftershocks of large events. The Gutenberg-Richter exponential frequency-magnitude relationship usually fits the size distribution of earthquakes over large regions quite well. However, in general, this relationship does not apply to individual faults (Wesnousky and others, 1983; Singh and others, 1983; Youngs and Coppersmith, 1985). Youngs and others (in press) modeled the magnitude distribution of independent earthquakes on individual faults in the Wasatch Front region in two different ways: (1) by using a standard exponential magnitude distribution and (2) by using the

"characteristic" magnitude distribution proposed by Youngs and Coppersmith (1985). In both cases, only earthquakes of $M_L \geq 6.0$ were included in their analysis. The characteristic distribution is a modification of the exponential distribution that incorporates a decrease in *b* value at magnitudes approaching the maximum magnitude for the fault. Thus, the characteristic magnitude distribution includes relatively more larger earthquakes. A third possible model to consider is the "maximum magnitude" model, which holds that each fault or fault segment produces only maximum-size earthquakes, together with their associated aftershocks and possible foreshocks (Wesnousky and others, 1983; Wesnousky, 1986). In tectonic regions where the repeat time for large earthquakes is relatively short, the available data favor either the characteristic or the maximum magnitude model. In the Wasatch Front region, major faults such as the Wasatch fault have not been important sources of small to moderate background earthquakes over the 25-year record of instrumental seismicity. This observation tends to favor the characteristic and maximum magnitude earthquake models, but the period of observation is too short relative to the repeat times for large earthquakes to allow any definite conclusions to be drawn.

GROUND-SHAKING HAZARD

The final step in the seismic hazard analysis outlined in figure 1 is the estimation of ground motion for engineering applications. Predictions of ground motions from future earthquakes can be arrived at in many different ways and presented in a variety of different forms. One especially popular approach to the problem is the probabilistic methodology for estimating peak ground motions first outlined by Cornell (1968). Algermissen and others (1982) used this basic methodology to derive maps of probabilistic ground-motion estimates for the contiguous United States, including Utah. Youngs and others (in press) used a similar methodology to carry out a detailed probabilistic analysis of the ground-shaking hazard for the Wasatch Front region. In this section, we use Cornell's method to perform some simple probabilistic calculations of maximum ground acceleration for a representative site in the Salt Lake Valley, halfway between the Wasatch and West Valley faults. Our intent here is not to duplicate the extensive work of Youngs and others (in press) but rather to illustrate the relative contributions of various seismic sources to the ground-shaking hazard. In particular, we investigate the relative importance to seismic hazard of small to moderate ($M_L \leq 6.5$) earthquakes, which dominate the historical earthquake record.

The site that we chose for our calculation is the intersection of Interstates 15 and 80 in the city of South Salt Lake at approximately 40°43.1′ N., 111°54.2′ W. (diamond, fig. 5). Our calculation incorporated two fundamental types of earthquake sources, as discussed above: (1) small to moderate ($3.0 \leq M_L \leq 6.5$) earthquakes within a circular source area having a 100-km radius centered on the site and (2) the fault-specific sources listed in table 4, which have maximum magnitudes of 6.5 to 7.3. Although we have not included all of the possible earthquake sources in the Wasatch Front region in our calculations, we believe that we have included all of the major contributors to the ground-shaking hazard in the Salt Lake Valley. Earthquakes within the circular source area are assumed to be independent in size and location, to have a spatially uniform probability of occurrence, and to have an exponential magnitude distribution. We used the seismicity parameters estimated in the section on recurrence modeling to characterize this source area. For the fault-specific sources, only the contribution of the maximum earthquake to the hazard was included in the computation. For these maximum earthquakes, the contribution to the annual probability of exceedance of a given peak acceleration value is the product of two factors: (1) the annual probability of occurrence of the earthquake and (2) the probability that the given peak acceleration level will be exceeded if an earthquake of the specified magnitude and distance occurs.

Peak horizontal acceleration as a function of magnitude and distance was calculated by using the constrained relationship of Campbell (in press). Campbell actually presented a range of median acceleration estimates to reflect uncertainties in how stress regime, fault type, anelastic attenuation, and local site conditions could affect ground motion in Utah. We performed our calculations by using both his upper bound curves and his lower bound curves, which differ in their predictions of peak horizontal accelerations by about a factor of 2. In both cases, the natural log of the peak acceleration was assumed to be normally distributed about the predicted median value, the standard deviation being 0.3 (the standard error given by Campbell).

Some assumption about the depths of the earthquakes was necessary, since Campbell defines source-to-site distance as the shortest three-dimensional distance between the site and the zone of seismogenic rupture. For the earthquakes in his data set, Campbell identified this zone from the aftershock distribution, when possible. We assumed that the zone of seismogenic rupture penetrates to within 4 km of the surface for all earthquakes included in the computation, on the basis of the observation that the tops of the aftershock zones for the 1962 Cache Valley earthquake (Smith and Sbar, 1974), the 1975 Pocatello Valley earthquake (Arabasz and oth-

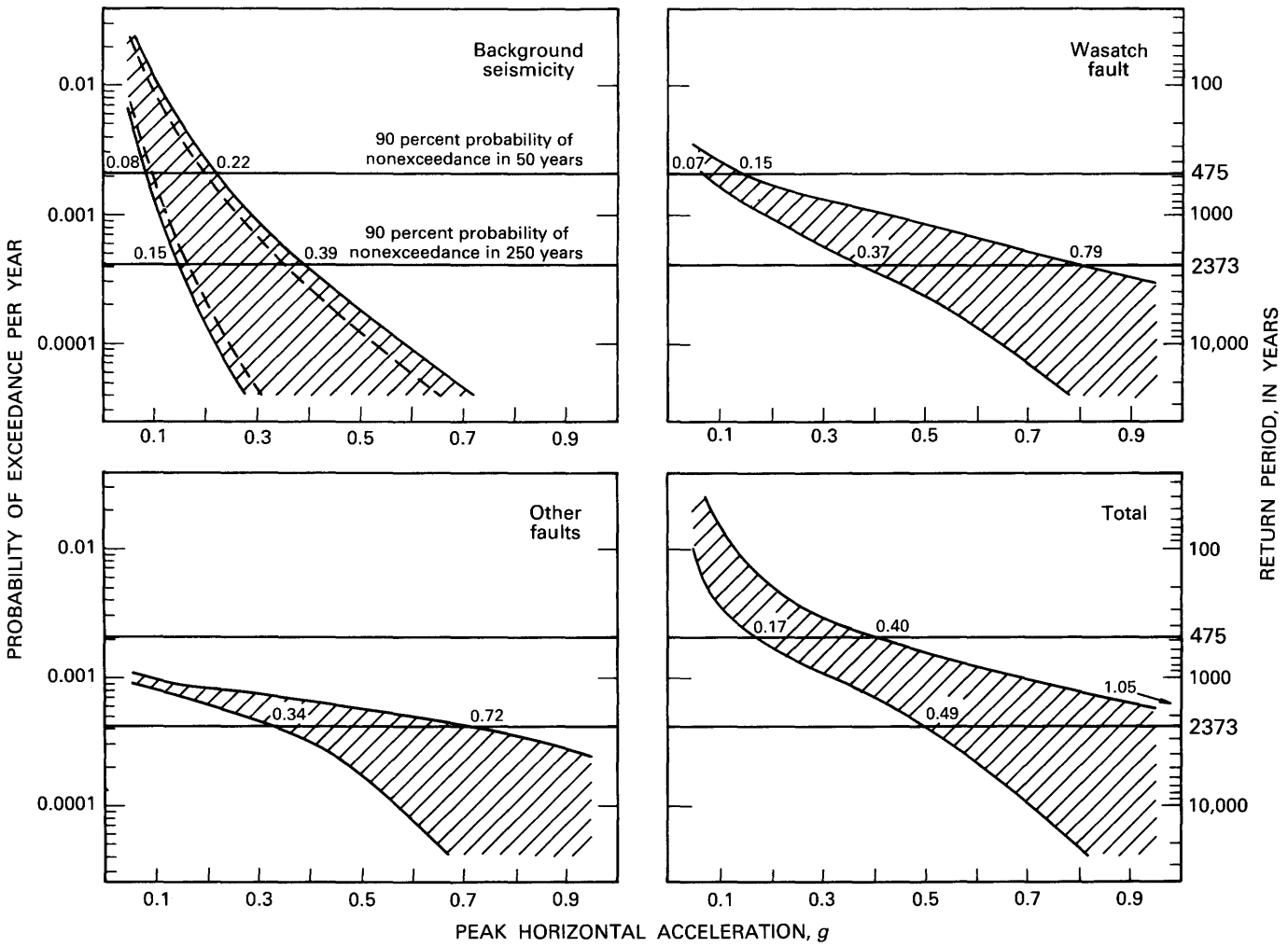

FIGURE 14.—Probability of exceedance per year for peak horizontal ground accelerations on soil at the intersection of I–15 and I–80 in South Salt Lake at approximately 40°43.1′ N., 111°54.2′ W. (diamond, fig. 5). The hachured zones represent the range of values calculated by using the range of median attenuation curves for peak horizontal acceleration presented by Campbell (in press). The results of separate calculations for the background seismicity, the Wasatch fault, other faults (the West Valley, East Great Salt Lake, and North Oquirrh Mountains faults), and all of these sources together are shown. On the graph for background seismicity, the dashed curves bound the range of values obtained by using the preferred *b* value of 0.71. The lower solid curve was calculated by using the upper bound *b* value of 0.80 and Campbell's lower bound acceleration estimates, whereas the upper solid curve was calculated by using the lower bound *b* value of 0.62 and Campbell's upper bound acceleration estimates. The vertical axes at the right show the average return period in years (the inverse of the annual probability).

ers, 1981) and the 1983 Borah Peak earthquake (Richins and others, 1987) were all at depths of 3 to 4 km. However, the assumed minimum depth is important only for earthquakes very near the site. The site is located about 4 km east of the surface trace of the West Valley fault and 4 km west of the surface trace of the Wasatch fault. Because the West Valley fault dips to the east and the Wasatch fault dips to the west, both faults probably extend directly beneath the site. If fault dips of 45° to 70° are assumed, the distance to the seismogenic rupture for a surface-faulting event on either fault would be about 3 to 4 km, which is consistent with the assumption that we made about seismogenic depth.

Figure 14 presents four graphs showing the probability of exceedance per year versus peak horizontal ground acceleration at our representative Salt Lake Valley site. The four graphs illustrate contributions to the ground-shaking hazard from (1) background seismicity, (2) earthquakes on the Wasatch fault, (3) earthquakes on the other three faults listed in table 4, and (4) all of these sources together. The solid curves bordering the shaded regions on each graph were calculated by using Camp-

bell's lower and upper bound peak acceleration relationships. The shaded regions between these curves indicate the range of annual probabilities for any given peak horizontal acceleration. On the graph for the background seismicity, the two dashed curves were calculated by using the preferred b value of 0.71, whereas the upper and lower solid curves were calculated by using the lower and upper limit b values of 0.62 and 0.80, respectively.

If earthquake occurrence is assumed to be a Poisson process, peak acceleration values having a 90 percent probability of nonexceedance in 50 years have an annual probability of 0.0021 or a return period of 475 years (upper horizontal lines, fig. 14). On the graph that includes all of the sources, the acceleration value corresponding to this return period lies between 0.17 and 0.40 g, as the plot indicates. For comparison, the value obtained by Algermissen and others (1982) is 0.20 to 0.28 g, and the value obtained by Youngs and others (in press) is 0.3 g. Peak acceleration values having a 90 percent probability of nonexceedance in 250 years have an annual probability of 0.00042 or a return period of 2,373 years (lower horizontal lines, fig. 14). The acceleration value corresponding to this return period is 0.49 to 1.05 g (fig.14). For comparison, the value obtained by Algermissen and others (1982) is 0.60 to 0.70 g, and the value obtained by Youngs and others (in press) is 0.7 g. Thus, the results of Algermissen and others (1982) and Youngs and others (in press) fall within the range of probabilistic acceleration values that we have calculated for both the 475- and the 2,373-year return periods.

Figure 14 implies that the background source is the largest contributor to the ground-shaking hazard at the site for return periods shorter than 500 years and accelerations less than 0.1 to 0.2 g, depending on the ground-motion model used. The Wasatch fault is the largest contributor to the hazard at longer return periods and higher accelerations. However, other faults, particularly the West Valley fault, are also quite important. Our calculation assumes that earthquakes on the West Valley fault are independent earthquakes, even though there is some possibility that they represent subsidiary fault movements associated with earthquakes on the Wasatch fault (S.J. Olig, personal commun., 1987). At locations farther away from the West Valley and Wasatch faults, the contribution of these faults to the ground-shaking hazard will be less than figure 14 indicates. At locations less than 4 km from the Wasatch fault or near segments whose recurrence intervals are shorter than the recurrence interval of the Salt Lake City segment (table 4), the contribution of the Wasatch fault to the ground-shaking hazard will be slightly greater than figure 14 indicates. The hazard curves for the background source, on the other hand, are applicable throughout most of the interior of the Wasatch Front region. Thus, we can infer from figure 14 that, at most localities, the background source will be the largest contributor to the ground-shaking hazard for return periods of 475 years or less (exposure periods of 50 years or less).

CURRENT SEISMICITY AND THE WASATCH FAULT

In this final section, we wish to consider the question, separate from the systematics of a hazard or risk analysis, "What does observational seismology tell us about the behavior of the Wasatch fault?" We then summarize our perspective on evaluating earthquake hazards and risk in the Wasatch Front area from the viewpoint of observational seismology.

Let us first consider instrumental earthquake locations. Figure 15 shows a detailed plot of instrumental seismicity that might, on the basis of epicentral locations alone, be associated with the Wasatch fault zone. The data include 1,538 earthquake locations from the UUSS catalog for the period July 1962 through December 1986. The largest earthquake included is the M_L 5.2 Magna, Utah, earthquake of September 1962, located in the northwestern corner of box B–B'. Earthquakes were sampled from 30-km-wide zones extending 10 km east of the surface trace of the Wasatch fault to allow for epicentral errors and 20 km west of the fault to allow for both epicentral errors and reasonable downdip projection of the fault. Figure 16 shows complementary cross-section views for those foci in figure 15 that meet the rigorous criteria for focal-depth reliability specified in figure 10. Epicentral precision of ± 5 km would be conservative for the data in figure 15, but errors as large as ± 10 km cannot be ruled out for a very minor fraction of the sample. Because the vast majority of the data postdate 1974, when modern network recording began, most of the epicenters probably have a precision of ± 2 to 3 km (Brown and others, 1986; Arabasz and Julander, 1986).

The cross sections in figure 16 suggest that very few of the well-located foci sampled from the vicinity of the Wasatch fault could be interpreted to lie on the fault—if one believes that the fault is a planar penetrative structure of moderate dip. Although the subsurface geometry of the Wasatch fault is not generally well known, Zoback (this volume) interpreted a planar, relatively steeply dipping (50°–55° W.) subsurface geometry for the Wasatch fault near Nephi. Smith and Bruhn (1984) interpreted a subsurface fault dip of ~34° for the Wasatch fault near Levan.

The best available data for determining whether small earthquakes might be occurring on a listric Wasatch fault

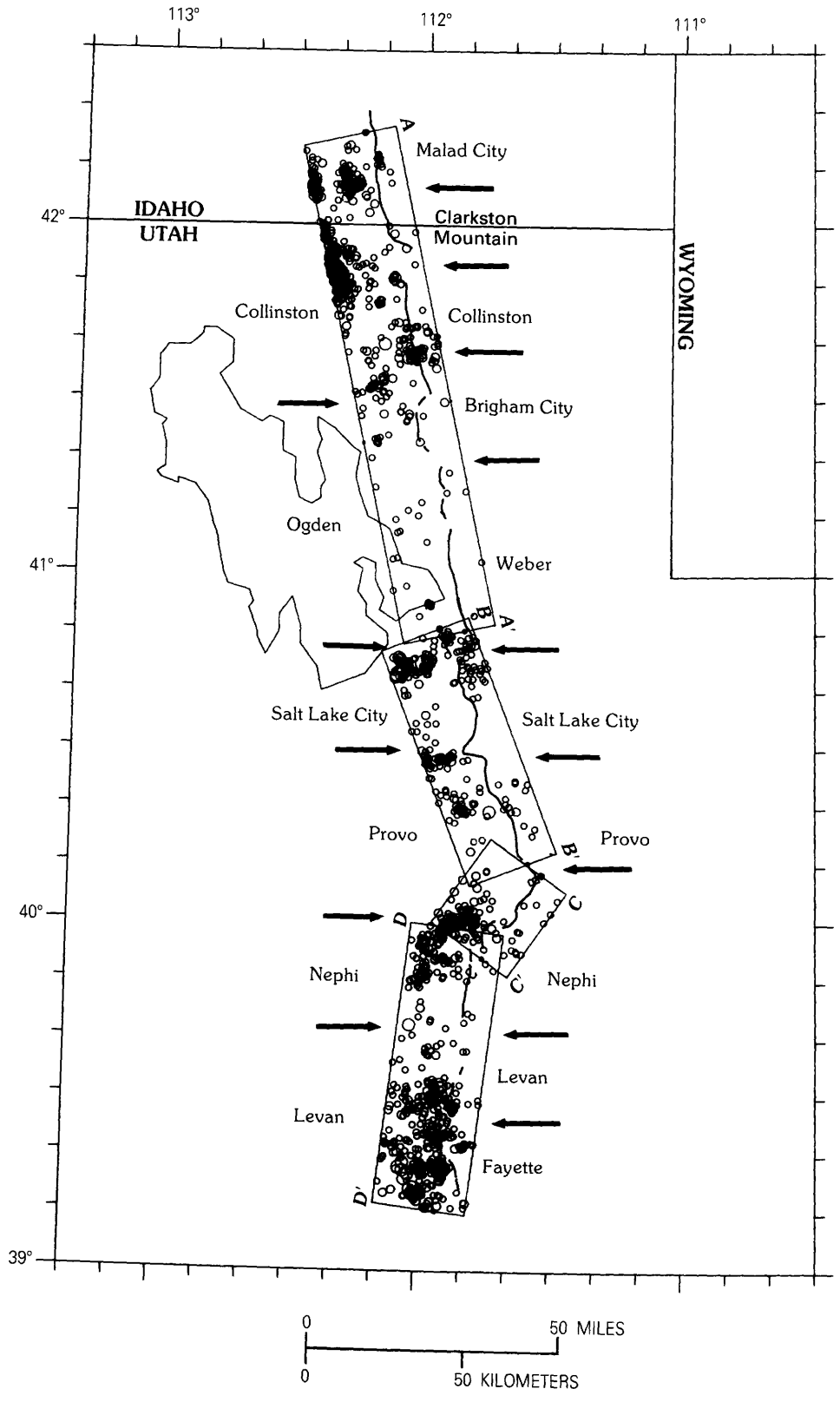

FIGURE 15.—Wasatch fault, segment boundaries and names [according to Machette and others (this volume), right-hand side; Schwartz and Coppersmith (1984), left-hand side], and all earthquakes located by the University of Utah Seismograph Stations during the period July 1962 through December 1986. Circle sizes indicate the relative magnitudes of events.

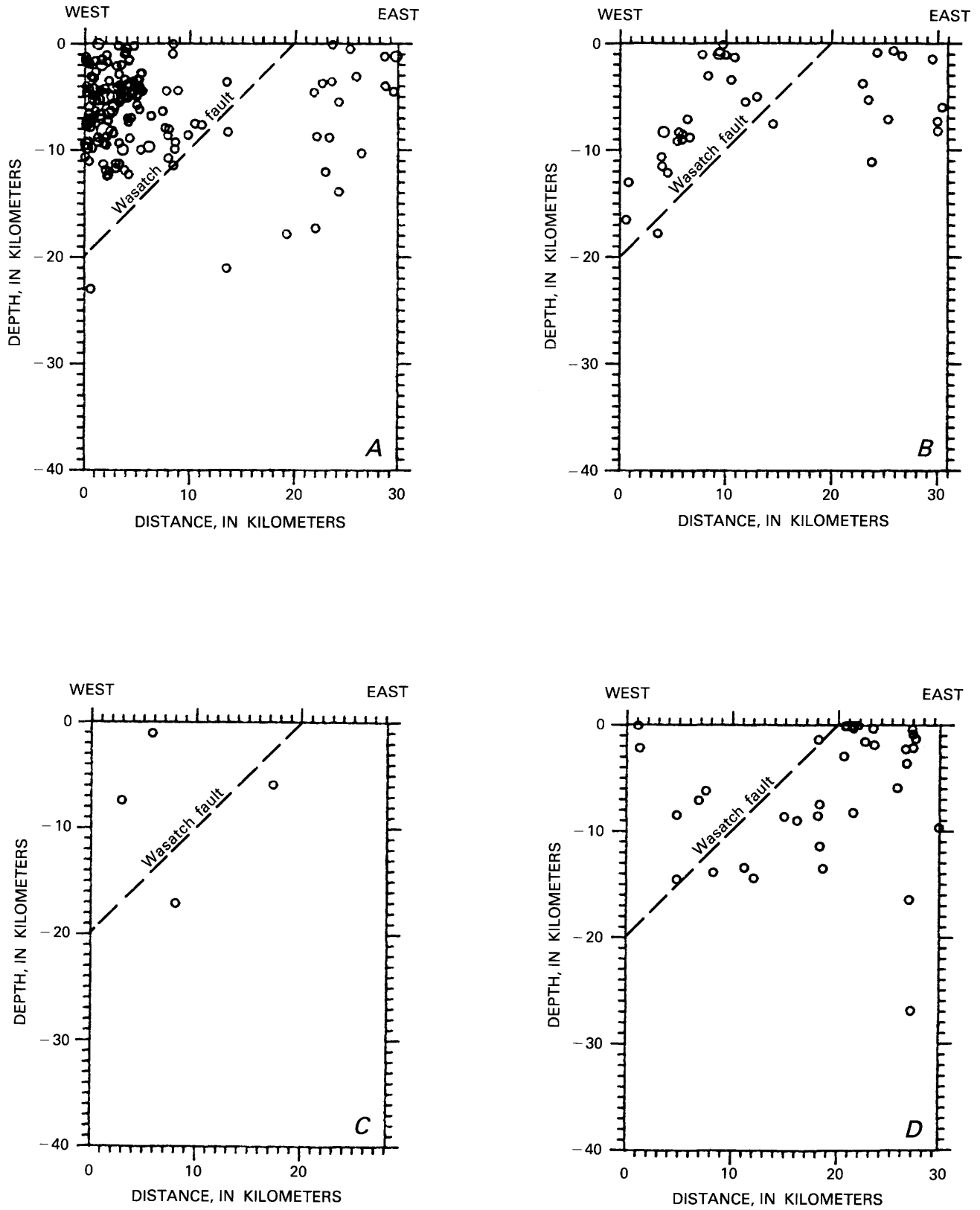

FIGURE 16.—Cross sections keyed to the boxes in figure 15. The Wasatch fault is arbitrarily depicted by a plane dipping 45° to the west from its surface trace. Only foci meeting criteria for reliable focal depths (see fig. 10) are included.

are those from portable-array studies reported by Arabasz and Julander (1986). At the southern end of the Wasatch fault, in both the northern and the southern parts of box *D–D'*, these data show that earthquake foci and corresponding focal mechanisms are incompatible with seismic slip on either a listric or a simple planar projection of the Wasatch fault. Rather, the background seismicity appears to be occurring on secondary structures of moderate (greater than 30°) to high-angle dip. Elsewhere along the Wasatch fault, existing data for earthquakes downdip of the fault are either inadequate or ambiguous (for example, Pechmann and Thorbjarnardottir, 1984) for interpreting subsurface association with a listric projection of the fault.

Comparing figure 15 with figures 8 and 9 indicates a remarkable paucity of microseismicity along the Wasatch fault within the broadly active earthquake belt of the Wasatch Front. Some specific features of small-earthquake occurrence in the vicinity of the fault are targets of ongoing investigation, such as epicentral clustering along the fault trace at the northern end of the Brigham City segment and clustering to the west of the Collinston and Salt Lake City segments. The episodic nature of the earthquake activity, however, handicaps the studies.

Figure 17 shows the space-time distribution of the earthquake sample included in figure 15. Such data might appear attractive for relating seismicity to the segmentation of the Wasatch fault, but caution is clearly appropriate, given the problematic relationship between the seismicity and the fault.

The following general observations can be made from figure 17. Seismicity north of Brigham City provides a clear contrast with seismicity between Brigham City and Bountiful. Ironically, the northernmost segments of the Wasatch fault show no evidence of latest Quaternary movement (Machette and others, 1991, this volume). There is a clear onset of the northern seismicity at about 1975, which corresponds both to the timing of the 1975 M_L 6.0 Pocatello Valley earthquake and the approximate beginning of operation of the UUSS telemetered seismic network. The case for seismic quiescence before the 1975 earthquake was made by Arabasz and Smith (1981). Activation of regional seismicity west of the Wasatch fault after the Pocatello Valley earthquake (discussed earlier) would be consistent with the interpretation that most of the northern seismicity in figure 17 is not on the Wasatch fault itself, although the episodic clustering of earthquakes near Honeyville at the boundary between the Brigham City and Collinston segments (fig. 15) is indeed suggestive of at least partial association.

Seismicity near the northern end of the Salt Lake City segment (northern end of box *B–B'*), both west and east of the Wasatch fault, has long been recognized, as has quiescence to the south. Other apparent features of the space-time diagrams in figure 17 are the post-1974 appearance of scattered earthquakes near the general latitude of American Fork and temporally persistent seismicity near Santaquin and along the southernmost Wasatch fault. There is minimal microseismicity along a 30-km-long section of the Wasatch fault north of Levan, including at least the southern half of the Nephi segment, which has one of the youngest (≥400 years) surface ruptures on the Wasatch fault (Machette and others, 1991). Depending on the structural association of earthquakes west of the Wasatch fault along much of its course, the Wasatch fault itself could conceivably be aseismic throughout most of the space-time diagram in figure 17 (see Arabasz and others, 1980). Thus, figure 17 may not provide simply a side view of seismicity on the Wasatch fault. To what extent seismicity in the vicinity of the fault might be reflecting segmented behavior of the fault must be investigated further (see Wheeler and Krystinik, this volume).

As Arabasz and Smith (1981) argued, apparent seismicity gaps along the Wasatch fault are not necessarily indicative of a late (that is, pre-earthquake) stage of a seismic cycle. Temporal decreases in seismicity ambiguously characterize both the early post-aftershock stage and the late pre-main-shock stage of a seismic cycle (for example, Ellsworth and others, 1981). Veneziano and others (1987) have recently analyzed the UUSS earthquake catalog between 1962 and 1985 to identify independent main events and the hierarchical clustering of secondary events. One result of their statistical analysis was documentation that between roughly 40° N. and 41.5° N.—along an area encompassing most of the Wasatch fault—dependent events are systematically suppressed in comparison with earthquake behavior in neighboring areas. The significance of this suppressed earthquake clustering is the subject of current study. The Wasatch Front area is a classic example of a seismically active region in which the historical and instrumental earthquake record provides an inadequate guide to assessing earthquake potential. The absence of any surface-faulting earthquakes on the Wasatch fault in historical time, the problematic correlation of background seismicity with mapped Cenozoic faulting, and the notable paucity of contemporary earthquakes along the Wasatch fault all combine to enhance the importance of paleoseismologic information. The potential for large surface-faulting earthquakes effectively must be considered independently of observed seismicity. The occurrence of the 1983 M_S 7.3 Borah Peak, Idaho, surface-faulting earthquake in an area of low historical seismicity (Richins and others, 1987; Dewey, 1987)—but in an area of clearly recognizable late Quaternary faulting—is a case in point.

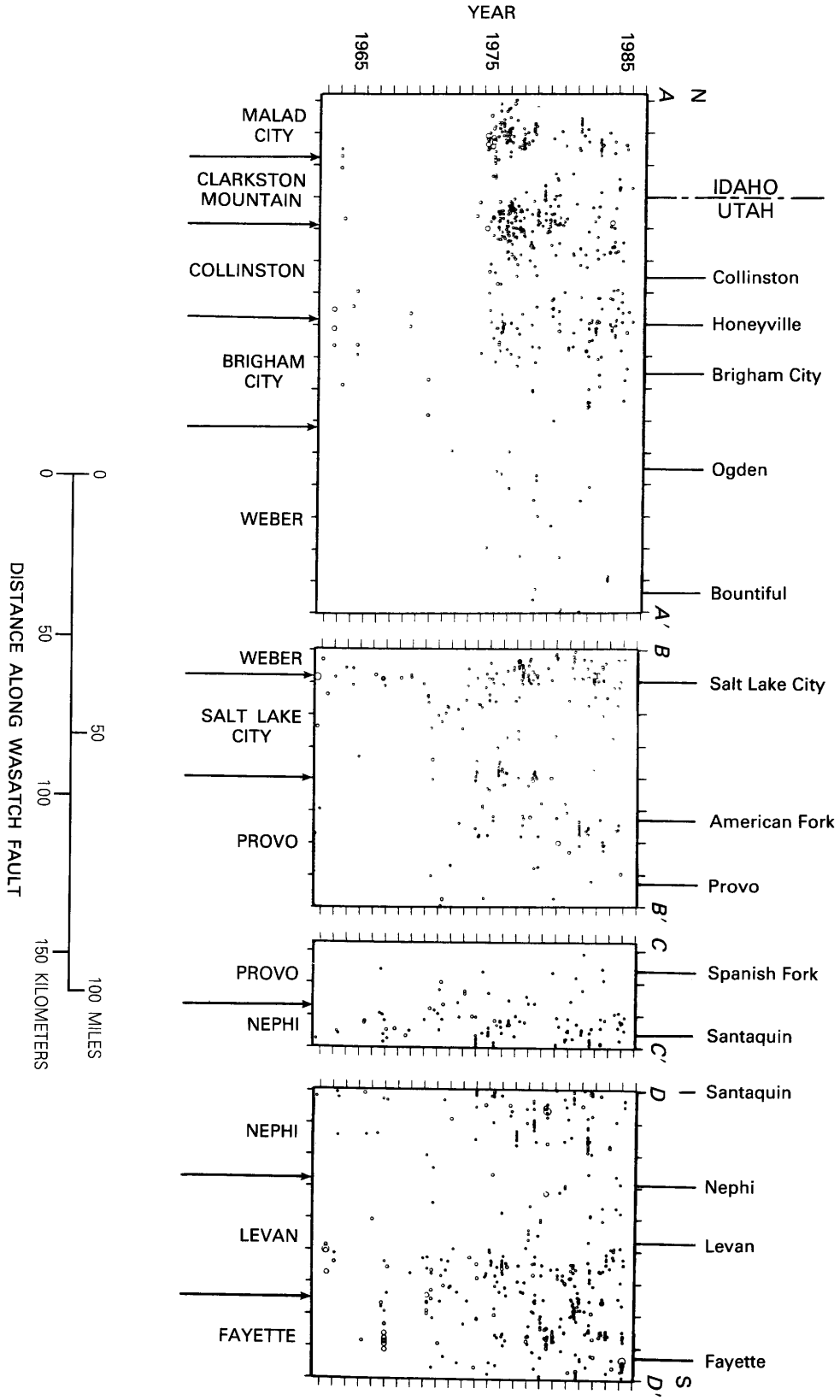

FIGURE 17.—Space-time diagrams of earthquake occurrence keyed to figure 15. Circle sizes indicate relative magnitudes of events. Shown for reference are the locations of selected cities and towns along the Wasatch fault (above) and the boundaries and names of segments of the Wasatch fault delineated by Machette and others (1991, this volume) (below).

Our closing perspective is that observational seismology contributes essential information—much of it still to be refined—for accurate estimations of earthquake hazards and risk in the Wasatch Front area. Background seismicity currently predominates on second-order faults in the Wasatch Front area and is the largest contributor to the probabilistic ground-shaking hazard for exposure periods of 50 years or less. From a seismotectonic point of view, background seismicity poses a major challenge in terms of understanding its association with geologic structure and its information content about deformation on individual segments of the Wasatch fault. Beyond providing essential input to analyses of hazards and risk for engineering applications and decisionmaking, observational seismology remains a critical tool for probing the deformational state of segments of the Wasatch fault and for monitoring changes in their behavior.

REFERENCES CITED

Abe, K., 1981, Magnitudes of large shallow earthquakes from 1904 to 1980: Physics of the Earth and Planetary Interiors, v. 27, p. 72–92.

Aki, K., 1966, Generation and propagation of G waves from the Niigata earthquake of June 16, 1964: Bulletin of the Earthquake Research Institute, Tokyo University, v. 44, p. 23–88.

Algermissen, S.T., Perkins, D.M., Thenhaus, P.C., Hanson, S.L., and Bender, B.L., 1982, Probabilistic estimates of maximum acceleration and velocity in rock in the contiguous United States: U.S. Geological Survey Open-File Report 82–1033, 107 p.

Allen, C.R., 1986, Seismological and paleoseismological techniques of research in active tectonics, *in* Active tectonics: Washington, D.C., National Academy Press, p. 148–154.

Allmendinger, R.W., Hauge, T.A., Hauser, E.C., Potter, C.J., Knuepfer, P., Nelson, K.D., and Oliver, J.E., 1987, Overview of the COCORP 40° N Transect western U.S.A.: The fabric of an orogenic belt: Geological Society of America Bulletin, v. 98, p. 308–319.

Allmendinger, R.W., Sharp, J.W., Von Tish, D., Serpa, L., Brown, L., Kaufman, S., Oliver, J., and Smith, R.B., 1983, Cenozoic and Mesozoic structure of the eastern Basin and Range province, Utah, from COCORP seismic reflection data: Geology, v. 11, p. 532–536.

Anderson, L.W., and Miller, D.G., 1979, Quaternary fault map of Utah: Long Beach, Calif., Fugro, Inc., technical report, 35 p., 1 pl.

Arabasz, W.J., 1984, Earthquake behavior in the Wasatch Front area: Association with geologic structure, space-time occurrence, and stress state, *in* Hays, W.W., and Gori, P.L., eds., Proceedings of Conference XXVI; a workshop on Evaluation of regional and urban earthquake hazards and risk in Utah: U.S. Geological Survey Open-File Report 84–763, p. 310–339.

Arabasz, W.J., and Julander, D.R., 1986, Geometry of seismically active faults and crustal deformation within the Basin and Range-Colorado Plateau transition in Utah, *in* Mayer, L., ed., Extensional tectonics of the southwestern United States: A perspective on processes and kinematics: Geological Society of America Special Paper 208, p. 43–74.

Arabasz, W.J., and Smith, R.B., 1981, Earthquake prediction in the Intermountain seismic belt—An intraplate extensional regime, *in* Simpson, D.W., and Richards, P.G., eds., Earthquake prediction—An international review: American Geophysical Union Maurice Ewing Series, no. 4, p. 248–258.

Arabasz, W.J., Smith, R.B., and Richins, W.D., eds., 1979, Earthquake studies in Utah, 1850 to 1978: Salt Lake City, University of Utah Seismograph Stations Special Publication, 552 p.

———1980, Earthquake studies along the Wasatch Front, Utah: Network monitoring, seismicity, and seismic hazards: Bulletin of the Seismological Society of America, v. 70, p. 1479–1499.

Arabasz, W.J., Richins, W.D., and Langer, C.J., 1981, The Pocatello Valley (Idaho-Utah border) earthquake sequence of March to April 1975: Bulletin of the Seismological Society of America, v. 71, p. 803–826.

Arabasz, W.J., Pechmann, J.C., and Brown, E.D., 1987, Evaluation of seismicity relevant to the proposed siting of a Superconducting Supercollider (SSC) in Tooele County, Utah: Salt Lake City, Utah, technical report prepared for Dames and Moore, Utah, University of Utah Seismograph Stations, SSC Proposal Team, 107 p. (Reprinted in 1989 by Utah Geological and Mineral Survey as Miscellaneous Publication 89–1, 107 p.)

Askew, B., and Algermissen, S.T., 1983, An earthquake catalog for the Basin and Range province, 1803–1977: U.S. Geological Survey Open-File Report 83–86, 42 p.

Beanland, S., and Clark, M.M., 1987, The Owens Valley fault zone, eastern California, and surface rupture associated with the 1872 earthquake: Seismological Research Letters, v. 58, p. 32.

Benz, H.M., and Smith, R.B., 1987, Kinematic source modelling of normal-faulting earthquakes using the finite element method: Geophysical Journal of the Royal Astronomical Society, v. 90, p. 305–325.

Bjarnason, I.T., and Pechmann, J.C., 1988, Contemporary tectonics of the Wasatch front region, Utah, from earthquake focal mechanisms: Bulletin of the Seismological Society of America, v. 79, no. 3, p. 731–755.

Bonilla, M.G., Mark, R.K., and Lienkaemper, J.J., 1984, Statistical relations among earthquake magnitude, surface rupture length, and surface fault displacement: Bulletin of the Seismological Society of America, v. 74, p. 2379–2411.

Bortz, L.C., Cook, S.A., and Morrison, O.J., 1985, Great Salt Lake area, Utah, *in* Gries, R.R., and Dyer, R.C., eds., Seismic exploration of the Rocky Mountain region: Denver, Colo., Rocky Mountain Association of Geologists and the Denver Geophysical Society, p. 275–281.

Brown, E.D., Arabasz, W.J., Pechmann, J.C., McPherson, E., Hall, L.L., Oehmich, P.J., and Hathaway, G.M., 1986, Earthquake data for the Utah region—January 1, 1984 to December 31, 1985: Salt Lake City, University of Utah Seismograph Stations Special Publication, 83 p.

Bucknam, R.C., 1976, Leveling data from the epicentral area of the March 27, 1975, earthquake in Pocatello Valley, Idaho: U.S. Geological Survey Open-File Report 76–52, 6 p.

———1977, Map of suspected fault scarps in unconsolidated deposits, Tooele 1°×2° sheet, Utah: U.S. Geological Survey Open-File Report 77–495, 2 p., 1 pl.

Bucknam, R.C., and Anderson, R.E., 1979, Map of fault scarps on unconsolidated sediments, Delta 1°×2° sheet, Utah: U.S. Geological Survey Open-File Report 79–366, 21 p.

Bucknam, R.C., Algermissen, S.T., and Anderson, R.E., 1980, Patterns of late Quaternary faulting in western Utah and an application in earthquake hazard evaluation, *in* Evernden, J.F., comp., Proceedings of Conference X; Earthquake hazards along the Wasatch and Sierra Nevada frontal fault zones: U.S. Geological Survey Open-File Report 80–801, p. 299–314.

Campbell, K.W., in press, Predicting strong ground motion in Utah, *in* Chap. L, Gori, P.L., and Hays, W.W., eds., Assessment of

regional earthquake hazards and risk along the Wasatch Front, Utah: U.S. Geological Survey Professional Paper 1500.

Cluff, L.S., Brogan, G.E., and Glass, C.E., 1970, Wasatch fault, northern portion: Earthquake fault investigation and evaluation: Oakland, Calif., Woodward-Clyde and Associates, technical report prepared for Utah Geological and Mineral Survey, 27 p.

———1973, Wasatch fault, southern portion: Earthquake fault investigation and evaluation: Oakland, Calif., Woodward-Lundgren and Associates, technical report prepared for Utah Geological and Mineral Survey, 79 p.

———1974, Investigation and evaluation of the Wasatch fault north of Brigham City and Cache Valley faults, Utah and Idaho: A guide to land-use planning with recommendations for seismic safety: Oakland, Calif., Woodward-Lundgren and Associates, technical report prepared for U.S. Geological Survey under contract 14–08–001–13665, 147 p.

Coffman, J.L., von Hake, C.A., and Stover, C.W., 1982, Earthquake history of the United States: Boulder, Colo., National Oceanic and Atmospheric Administration and U.S. Geological Survey Publication 41–1, 208 p. (with supplement).

Cook, K.L., Gray, E.F., Iverson, R.M., and Strohmeier, M.T., 1980, Bottom gravity meter regional survey of the Great Salt Lake, Utah, *in* Gwynn, J.W., ed., Great Salt Lake, a scientific, historical, and economic overview: Utah Geological and Mineral Survey Bulletin 116, p. 125–143.

Cornell, C.A., 1968, Engineering seismic risk analysis: Bulletin of the Seismological Society of America, v. 58, p. 1583–1606.

Crone, A.J., and Machette, M.N., 1984, Surface faulting accompanying the Borah Peak earthquake, central Idaho: Geology, v. 12, p. 664–667.

Crone, A.J., Machette, M.N., Bonilla, M.G., Lienkaemper, J.J., Pierce, K.L., Scott, W.E., and Bucknam, R.C., 1987, Surface faulting accompanying the Borah Peak earthquake and segmentation of the Lost River fault, central Idaho: Bulletin of the Seismological Society of America, v. 77, p. 739–770.

Currey, D.R., Atwood, G., and Mabey, D.R., 1984, Major levels of Great Salt Lake and Lake Bonneville: Utah Geological and Mineral Survey Map 73, scale 1:750,000.

Davis, F.D., 1983a, Geologic map of the southern Wasatch Front, Utah: Utah Geological and Mineral Survey Map 55–A, scale 1:100,000.

———1983b, Geologic map of the central Wasatch Front, Utah: Utah Geological and Mineral Survey Map 54–A, scale 1:100,000.

———1985, Geologic map of the northern Wasatch Front, Utah: Utah Geological and Mineral Survey Map 53–A, scale 1:100,000.

Dewey, J.W., 1987, Instrumental seismicity of central Idaho: Bulletin of the Seismological Society of America, v. 77, p. 819–836.

Doser, D.I., 1985a, The 1983 Borah Peak, Idaho, and 1959 Hebgen Lake, Montana, earthquakes: Models for normal fault earthquakes in the Intermountain Seismic Belt, *in* Stein, R.S., and Bucknam, R.C., eds., Proceedings of Workshop XXVIII—On the Borah Peak, Idaho, earthquake: U.S. Geological Survey Open-File Report 85–290–A, p. 368–384.

———1985b, Source parameters and faulting processes of the 1959 Hebgen Lake, Montana, earthquake sequence: Journal of Geophysical Research, v. 90, no. B6, p. 4537–4555.

Doser, D.I., and Smith, R.B., 1982, Seismic moment rates in the Utah region: Bulletin of the Seismological Society of America, v. 72, p. 525–551.

———1985, Source parameters of the 28 October 1983 Borah Peak, Idaho, earthquake from body wave analysis: Bulletin of the Seismological Society of America, v. 75, p. 1041–1051.

Earthquake Engineering Research Institute Committee on Seismic Risk, 1984, Glossary of terms for probabilistic seismic-risk and hazard analysis: Earthquake Spectra, v. 1, p. 33–40.

Eddington, P.K., Smith, R.B., and Renggli, C., 1987, Kinematics of Basin-Range intraplate extension, *in* Coward, M.P., Dewey, J.F., and Hancock, P.L., eds., Continental extensional tectonics: Geological Society of London Special Publication 28, p. 371–392.

Ekstrom, G., and Dziewonski, A.M., 1985, Centroid-moment tensor solutions for 35 earthquakes in western North America (1977–1983): Bulletin of the Seismological Society of America, v. 75, p. 23–39.

Electric Power Research Institute, 1988, Seismic hazard methodology for the central and eastern United States, v. 1, pt. 2, Methodology (revision 1): Palo Alto, Calif., technical report NP–4726 prepared for Seismicity Owners Group and Electric Power Research Institute under Research Projects P101–38, P101–45, P101–46, 2356, and 2256–14, 194 p.

Ellsworth, W.L., Lindh, A.G., Prescott, W.H., and Herd, D.G., 1981, The 1906 San Francisco earthquake and the seismic cycle, *in* Simpson, D.W., and Richards, P.G., eds., Earthquake prediction—An international review: American Geophysical Union Maurice Ewing Series, no. 4, p. 209–216.

Engdahl, E.R., and Rinehart, W.A., 1988, Seismicity map of North America: Geological Society of America Continent-Scale Map–004, scale 1:5,000,000.

Evernden, J.F., 1975, Seismic intensities, "size" of earthquakes, and related parameters: Bulletin of the Seismological Society of America, v. 65, p. 1287–1313.

Foley, L.L., Martin, R.A., and Sullivan, J.T., 1986, Seismotectonic study for Joes Valley, Scofield, and Huntington North Dams, Emery County and Scofield Projects, Utah: U.S. Bureau of Reclamation Seismotectonic Report 86–7, 132 p.

Gibbons, A.B., and Dickey, D.D., 1983, Quaternary faults in Lincoln and Uinta Counties, Wyoming, and Rich County, Utah: U.S. Geological Survey Open-File Report 83–288, scale 1:100,000.

Gutenberg, B., and Richter, C.F., 1954, Seismicity of the earth and associated phenomena (2d ed.): Princeton, N.J., Princeton University Press, 310 p.

Hall, W.B., and Sablock, P.E., 1985, Comparison of the geomorphic and surficial fracturing effects of the 1983 Borah Peak, Idaho, earthquake with those of the 1959 Hebgen Lake, Montana, earthquake, *in* Stein, R.S., and Bucknam, R.C., eds., Proceedings of Workshop XXVIII—On the Borah Peak, Idaho, earthquake: U.S. Geological Survey Open-File Report 85–290, p. 141–152.

Hanks, T.C., and Kanamori, H., 1979, A moment magnitude scale: Journal of Geophysical Research, v. 84, no. B5, p. 2348–2350.

Kanamori, H., 1977, The energy release in great earthquakes: Journal of Geophysical Research, v. 82, no. 20, p. 2981–2987.

Keaton, J., Currey, D.R., and Olig, S.J., 1986, Paleoseismicity and earthquake hazards evaluation of the West Valley fault zone, Salt Lake City urban area: Technical report prepared for U.S. Geological Survey under contract 14–08–0001–22048, 18 p.

Loeb, D.T., 1986, The P-wave velocity structure of the crust-mantle boundary beneath Utah: Salt Lake City, University of Utah, unpublished M.Sci. thesis, 126 p.

Loeb, D.T., and Pechmann, J.C., 1986, The P-wave velocity structure of the crust-mantle boundary beneath Utah from network travel time measurements [abs.]: Earthquake Notes, v. 57, p. 10.

Machette, M.N, Personius, S.F., and Nelson, A.R., 1986, Late Quaternary segmentation and slip-rate history of the Wasatch fault zone, Utah [abs.]: E⊕S, Transactions of the American Geophysical Union, v. 67, p. 1107.

Machette, M.N., Personius, S.F., Nelson, A.R., Schwartz, D.P., and Lund, W.R., 1991, The Wasatch fault zone, Utah—Segmentation and history of Holocene earthquakes: Journal of Structural Geology, v. 13, p. 137–149.

Mikulich, M., and Smith, R.B., 1974, Seismic reflection and aeromagnetic surveys of the Great Salt Lake, Utah: Geological Society of America Bulletin, v. 85, p. 991–1002.

Murphy, L.M., and Brazee, R.J., 1964, Seismological investigations of the Hebgen Lake earthquake: U.S. Geological Survey Professional Paper 435–C, p. C13–C17.

Oakeshott, G.B., Greensfelder, R.W., and Kahle, J.E., 1972, The great Owens Valley earthquake of 1872...one hundred years later: California Geology, v. 25, p. 55–62.

Pechmann, J.C., and Thorbjarnardottir, B., 1984, Investigations of an M_L 4.3 earthquake in the western Salt Lake Valley using digital seismic data, *in* Hays, W.W., and Gori, P.L., eds., Proceedings of Conference XXVI; a workshop on Evaluation of regional and urban earthquake hazards and risk in Utah: U.S. Geological Survey Open-File Report 84–763, p. 340–365.

Pechmann, J.C., Richins, W.D., and Smith, R.B., 1984, Evidence for a double Moho beneath the Wasatch Front, Utah [abs.]: E⊕S, Transactions of the American Geophysical Union, v. 54, p. 988.

Pechmann, J.C., Nash, W.P., Viveiros, J.J., and Smith, R.B., 1987, Slip rate and earthquake potential of the East Great Salt Lake fault, Utah [abs.]: E⊕S, Transactions of the American Geophysical Union, v. 68, p. 1369.

Pitt, A.M., Weaver, C.S., and Spence, W., 1979, The Yellowstone Park earthquake of June 30, 1975: Bulletin of the Seismological Society of America, v. 69, p. 187–205.

Richins, W.D., Arabasz, W.J., Hathaway, G.M., Oehmich, P.J., Sells, L.L., and Zandt, G., 1981, Earthquake data for the Utah region—January 1, 1978 to December 31, 1980: Salt Lake City, University of Utah Seismograph Stations Special Publication, 125 p.

Richins, W.D., Arabasz, W.J., and Langer, C.J., 1983, Episodic earthquake swarms ($M_L \leq 4.7$) near Soda Springs, Idaho, 1981–82: Correlation with local structure and regional tectonics [abs.]: Earthquake Notes, v. 54, p. 99.

Richins, W.D., Arabasz, W.J., Hathaway, G.M., McPherson, E., Oehmich, P.J., and Sells, L.L., 1984, Earthquake data for the Utah region—January 1, 1981 to December 3, 1983: Salt Lake City, University of Utah Seismograph Stations Special Publication, 111 p.

Richins, W.D., Pechmann, J.C., Smith, R.B., Langer, C.J., Goter, S.K., Zollweg, J.E., and King, J.J., 1987, The 1983 Borah Peak, Idaho, earthquake and its aftershocks: Bulletin of the Seismological Society of America, v. 77, p. 694–723.

Richter, C.F., 1935, An instrumental earthquake magnitude scale: Bulletin of the Seismological Society of America, v. 25, p. 1–32.

———1958, Elementary seismology: San Francisco, W.H. Freeman, 768 p.

Savy, J.B., Bernreuter, D.L., and Mensing, R.W., 1986, Seismic hazard characterization for the eastern United States: Nuclear Safety, v. 27, no. 4, p. 476–487.

Schwartz, D.P., 1987, Earthquakes of the Holocene: Reviews of Geophysics, v. 25., p. 1197–1202.

Schwartz, D.P., and Coppersmith, K.J., 1984, Fault behavior and characteristic earthquakes: Examples from the Wasatch and San Andreas fault zones: Journal of Geophysical Research, v. 89, no. B7, p. 5681–5698.

———1986, Seismic hazards: New trends in analysis using geologic data, *in* Active tectonics: Washington, D.C., National Academy Press, p. 215–230.

Schwartz, D.P., Swan, F.H., III, and Cluff, L.S., 1984, Fault behavior and earthquake recurrence along the Wasatch fault, *in* Hays, W.W., and Gori, P.L., eds., Proceedings of Conference XXVI; a workshop on Evaluation of regional and urban earthquake hazards and risk in Utah: U.S. Geological Survey Open-File Report 84–763, p. 113–125.

Shenon, P.J., 1936, The Utah earthquake of March 12, 1934 (extracts from unpublished report), *in* Neumann, F., United States earthquakes, 1943: U.S. Coast and Geodetic Survey Serial 593, p. 43–48.

Shimizu, Y., 1987, Earthquake clustering in the Utah region: Cambridge, Massachusetts Institute of Technology, unpublished M.Sci. thesis, 149 p.

Singh, S.K., Rodriguez, M., and Esteva, L., 1983, Statistics of small earthquakes and frequency of occurrence of large earthquakes along the Mexican subduction zone: Bulletin of the Seismological Society of America, v. 73, p. 1779–1796.

Slemmons, D.B., 1980, Design earthquake magnitudes for the western Great Basin, *in* Evernden, J.F., comp., Proceedings of Conference X; Earthquake hazards along the Wasatch and Sierra Nevada frontal fault zones: U.S. Geological Survey Open-File Report 80–801, p. 62–85.

Smith, R.B., 1978, Seismicity, crustal structure, and intraplate tectonics of the interior of the western Cordillera, *in* Smith, R.B., and Eaton, G.P., eds., Cenozoic tectonics and regional geophysics of the western cordillera: Geological Society of America Memoir 152, p. 111–144.

Smith, R.B., and Arabasz, W.J., in press, Seismicity of the Intermountain Seismic Belt, *in* Slemmons, D.B., Blackwell, D., Engdahl, E.R., and Zoback, M., eds., Neotectonics of North America: Boulder, Colo., Geological Society of America Decade Map Volume.

Smith, R.B., and Bruhn, R.L., 1984, Intraplate extensional tectonics of the eastern Basin-Range: Inferences on structural style from seismic reflection data, regional tectonics, and thermal-mechanical models of brittle-ductile deformation: Journal of Geophysical Research, v. 89, no. B7, p. 5733–5762.

Smith, R.B., and Lindh, A., 1978, A compilation of fault plane solutions of the western United States, *in* Smith, R.B., and Eaton, G.P., eds., Cenozoic tectonics and regional geophysics of the western cordillera: Geological Society of America Memoir 152, p. 107–110.

Smith, R.B., and Richins, W.D., 1984, Seismicity and earthquake hazards of Utah and the Wasatch Front: Paradigm and paradox, *in* Hays, W.W., and Gori, P.L., eds., Proceedings of Conference XXVI; a workshop on Evaluation of regional and urban earthquake hazards and risk in Utah: U.S. Geological Survey Open-File Report 84–763, p. 73–112.

Smith, R.B., and Sbar, M.L., 1974, Contemporary tectonics and seismicity of the western United States with emphasis on the Intermountain Seismic Belt: Geological Society of America Bulletin, v. 85, p. 1205–1218.

Smith, R.B., Nagy, W.C., Julander, K.A., Viveiros, J.J., Barker, C.A., Bashore, W.W., and Gants, D.G., 1989, Geophysical and tectonic framework of the Basin Range-Colorado Plateau-Rocky Mountain transition, *in* Pakiser, L.C., and Mooney, W.D., eds., Geophysical framework of the continental United States: Geological Society of America Memoir 172, p. 205–233.

Stickney, M.C., and Bartholomew, M.S., 1987, Seismicity and late Quaternary faulting of the northern Basin and Range province, Montana and Idaho: Bulletin of the Seismological Society of America, v. 77, p. 1602–1625.

Stover, C.W., Reagor, B.G., and Algermissen, S.T., 1986, Seismicity map of the State of Utah: U.S. Geological Survey Miscellaneous Field Studies Map MF–1856, scale 1:1,000,000.

Sullivan, J.T., Nelson, A.R., LaForge, R.C., Wood, C.K., and Hansen, R.A., 1988, Central Utah regional seismotectonic study for USBR dams in the Wasatch Mountains: U.S. Bureau of Reclamation Seismotectonic Report 88–5, 365 p.

Swan, F.H., III, Schwartz, D.P., and Cluff, L.S., 1980, Recurrence of moderate to large magnitude earthquakes produced by surface faulting on the Wasatch fault zone, Utah: Bulletin of the Seismological Society of America, v. 70, p. 1431–1462.

Utsu, T., 1965, A method for determining the value of b in the formula $\log n = a - bM$ showing the magnitude-frequency relation for earthquakes: Hokkaido University Geophysical Bulletin, v. 13, p. 99–103.

Veneziano, D., and Van Dyck, J., 1985, Statistical discrimination of "aftershocks" and their contribution to seismic hazard, appendix A–4, *in* Seismic hazard methodology for nuclear facilities in the eastern United States: Golden, Colo., report prepared for Electric Power Research Institute under Research Project P101–29, Dames and Moore, v. 2, p. A121–A186.

———1986, Statistical analysis of earthquake catalogs for seismic hazard, *in* International Symposium on Engineering Geology Problems in Seismic Areas, Bari, Italy, 1986, Proceedings: 43 p.

Veneziano, D., Shimizu, Y., and Arabasz, W.J., 1987, Suppressed earthquake clustering in the Wasatch Front region, Utah [abs.]: EOS, Transactions of the American Geophysical Union, v. 68, p. 1368–1369.

Viveiros, J.J., 1986, Cenozoic tectonics of the Great Salt Lake from seismic reflection data: Salt Lake City, University of Utah, unpublished M.Sci. thesis, 81 p.

Wallace, R.E., 1981, Active faults, paleoseismology, and earthquake hazards in the western United States, *in* Simpson, D.W., and Richards, P.G., eds., Earthquake prediction—An international review: American Geophysical Union Maurice Ewing Series, no. 4, p. 209–216.

———1987, Grouping and migration of surface faulting and variations in slip rates on faults in the Great Basin Province: Bulletin of the Seismological Society of America, v. 77, p. 868–876.

Weichert, D.H., 1980, Estimation of the earthquake recurrence parameters for unequal observation periods for different magnitudes: Bulletin of the Seismological Society of America, v. 70, p. 1337–1346.

Wesnousky, S.G., 1986, Earthquakes, Quaternary faults, and seismic hazard in California: Journal of Geophysical Research, v. 91, no. B12, p. 12587–12631.

Wesnousky, S.G., Scholz, C.H., Shimazaki, K., and Matsuda, T., 1983, Earthquake frequency distribution and the mechanics of faulting: Journal of Geophysical Research, v. 88, no. B11, p. 9331–9340.

Williams, D.J., and Arabasz, W.J., 1989, Mining-related and tectonic seismicity in the east mountain area, Wasatch Plateau, Utah, *in* Gibowicz, S.J., ed., Seismicity in mines: PAGEOPH (Journal of Pure and Applied Geophysics), v. 129, nos. 3/4, p. 345–368.

Witkind, I.J., 1964, Reactivated faults north of Hebgen Lake: U.S. Geological Survey Professional Paper 435–G, p. G37–G50.

———1975, Preliminary map showing known and suspected active faults in Idaho: U.S. Geological Survey Open-File Report 75–278, 71 p.

Youngs, R.R., and Coppersmith, K.J., 1985, Implications of fault slip rates and earthquake recurrence models to probabilistic seismic hazards estimates: Bulletin of the Seismological Society of America, v. 75, p. 939–964.

Youngs, R.R., Swan, F.H., Power, M.S., Schwartz, D.P., and Green, R.K., in press, Probabilistic analysis of the earthquake ground-shaking hazard along the Wasatch Front, Utah, Chap. M *of* Gori, P.L., and Hays, W.W., eds., Assessment of regional earthquake hazards and risk along the Wasatch Front, Utah: U.S. Geological Survey Professional Paper 1500.

Zoback, M.L., 1983, Structure and Cenozoic tectonism along the Wasatch fault zone, Utah: Geological Society of America Memoir 157, p. 3–27.

———1984, Constraints on the in-situ stress field along the Wasatch Front, *in* Hays, W.W., and Gori, P.L., eds., Proceedings of Conference XXVI; a workshop on Evaluation of regional and urban earthquake hazards and risk in Utah: U.S. Geological Survey Open-File Report 84–763, p. 286–310.

Zoback, M.L., and Zoback, M.D., 1980, State of stress in the conterminous United States: Journal of Geophysical Research, v. 85, no. B11, p. 6113–6156.

Superimposed Late Cenozoic, Mesozoic, and Possible Proterozoic Deformation Along the Wasatch Fault Zone in Central Utah

By MARY LOU ZOBACK

ASSESSMENT OF REGIONAL EARTHQUAKE HAZARDS AND RISK ALONG THE WASATCH FRONT, UTAH

U.S. GEOLOGICAL SURVEY PROFESSIONAL PAPER 1500–E

CONTENTS

	Page
Abstract	E1
Introduction	1
Acknowledgments	1
Local Geologic Setting	1
Gravity and Density Data	5
Seismic Reflection and Velocity Data	5
Interpreted Subsurface Structure	10
Basin Geometry and Shallow Structure of the Wasatch Fault Zone	10
Deep Structure	14
Geologic Interpretation of Deep Structure	16
Discussion	18
Conclusions	18
References Cited	19

ILLUSTRATIONS

		Page
FIGURE	1. Index map of central Utah showing late Cenozoic normal faults and Sevier frontal thrust faults	E2
	2, 3. Maps showing:	
	2. Generalized geology of the study area	3
	3. Complete Bouguer gravity data for the Nephi area	6
	4. Seismic reflection profile	7
	5. Line drawing of the seismic reflection profile and true-depth migrated cross section of selected reflectors	8
	6. Detail of seismic reflection profile in Juab Valley showing basin fill and true-depth cross section of prominent reflectors in basin	11
	7. Diagram showing gravity models of basin fill in Juab Valley	13
	8. Cross section showing geologic interpretation of the western half of the true-depth line drawing shown in figure 5*B*	16

TABLES

	Page
TABLE 1. Log-determined densities and sonic velocities of significant wells in the region of the Wasatch fault zone	E9

ASSESSMENT OF REGIONAL EARTHQUAKE HAZARDS
AND RISK ALONG THE WASATCH FRONT, UTAH

SUPERIMPOSED LATE CENOZOIC, MESOZOIC, AND POSSIBLE PROTEROZOIC DEFORMATION ALONG THE WASATCH FAULT ZONE IN CENTRAL UTAH

By Mary Lou Zoback

ABSTRACT

Surface geology, gravity data, and information from petroleum exploration wells have been used to constrain the subsurface structure along a 30-km-long seismic reflection profile across the Wasatch fault zone in central Utah near the town of Nephi. In this region, late Cenozoic normal faulting along the Wasatch fault zone is superimposed on the frontal portion of the Mesozoic Sevier fold and thrust belt. Juab Valley, which is bounded on the east by the Wasatch fault zone, is interpreted as an asymmetric sag; beds on both sides tilt toward the axis of the valley, and a central graben defines the deepest part of the basin. Maximum valley thickness is about 1.6 km, based on a combined interpretation of the gravity and seismic reflection data. Possible displacement of a buried thrust(s), truncation of deep reflectors, and the absence of reverse drag in the basin sediments suggest a planar, relatively steeply dipping (50°–55°) geometry for the Wasatch fault zone at this locality. Because of complex subsurface structure, however, the lack of reverse drag in the basin sediments is probably the strongest evidence against a listric geometry for the Wasatch. Within the study area, both a major Sevier frontal thrust (the Nebo thrust) and possible deeper thrust(s) appear to ramp up in the vicinity of the Wasatch fault zone. A similar correlation of major thrust ramps occurring along several other segments of the Wasatch fault zone was noted by R.B. Smith and R.L. Bruhn in 1984. It is suggested here that both the thrust ramping and the late Cenozoic normal faulting may be localized by a major west-dipping normal fault zone formed during the early phases (pre-drift) of late Precambrian rifting of the western Cordillera.

INTRODUCTION

In central Utah, late Cenozoic extensional faulting along the Wasatch fault zone and other normal fault zones is superimposed on the frontal portion of the Mesozoic Sevier fold and thrust belt (fig. 1), which deforms sediments deposited on a passive margin formed by late Precambrian rifting (Stewart, 1972; Stewart and Poole, 1974). Many of the rocks exposed in the modern range blocks are remnants of laterally extensive thrust sheets transported 100 km or more from the west during the Sevier orogeny (Crittenden, 1961).

This chapter used gravity data and well data, together with a 30-km-long seismic reflection profile across the Wasatch fault zone near its intersection with one of the frontal sole thrust faults, to detail the structural style of late Cenozoic extension superimposed on Mesozoic compressional deformation. Particular emphasis is placed on understanding the subsurface geometry of Cenozoic normal faulting and its relationship to earlier low-angle thrust faults, ramps, and decollement surfaces, as well as to possible normal faults in the crystalline basement formed during Precambrian rifting.

ACKNOWLEDGMENTS

This manuscript was substantially improved by critical, thoughtful reviews by Anthony Crone and Thomas Brocher (U.S. Geological Survey). Discussion with Douglas Sprinkel (Utah Geological and Mineral Survey), Timothy Lawton (New Mexico State University), William Jefferson (Amoco Production Company), and Hal Morris (U.S. Geological Survey) greatly increased my understanding of the structure and tectonics of the region. However, any shortcomings of the interpretations presented here are my own responsibility.

LOCAL GEOLOGIC SETTING

The area of study is centered on the town of Nephi in central Utah, a region of complex, superimposed compressional and extensional deformation of several ages.

Manuscript approved for publication November 20, 1990.

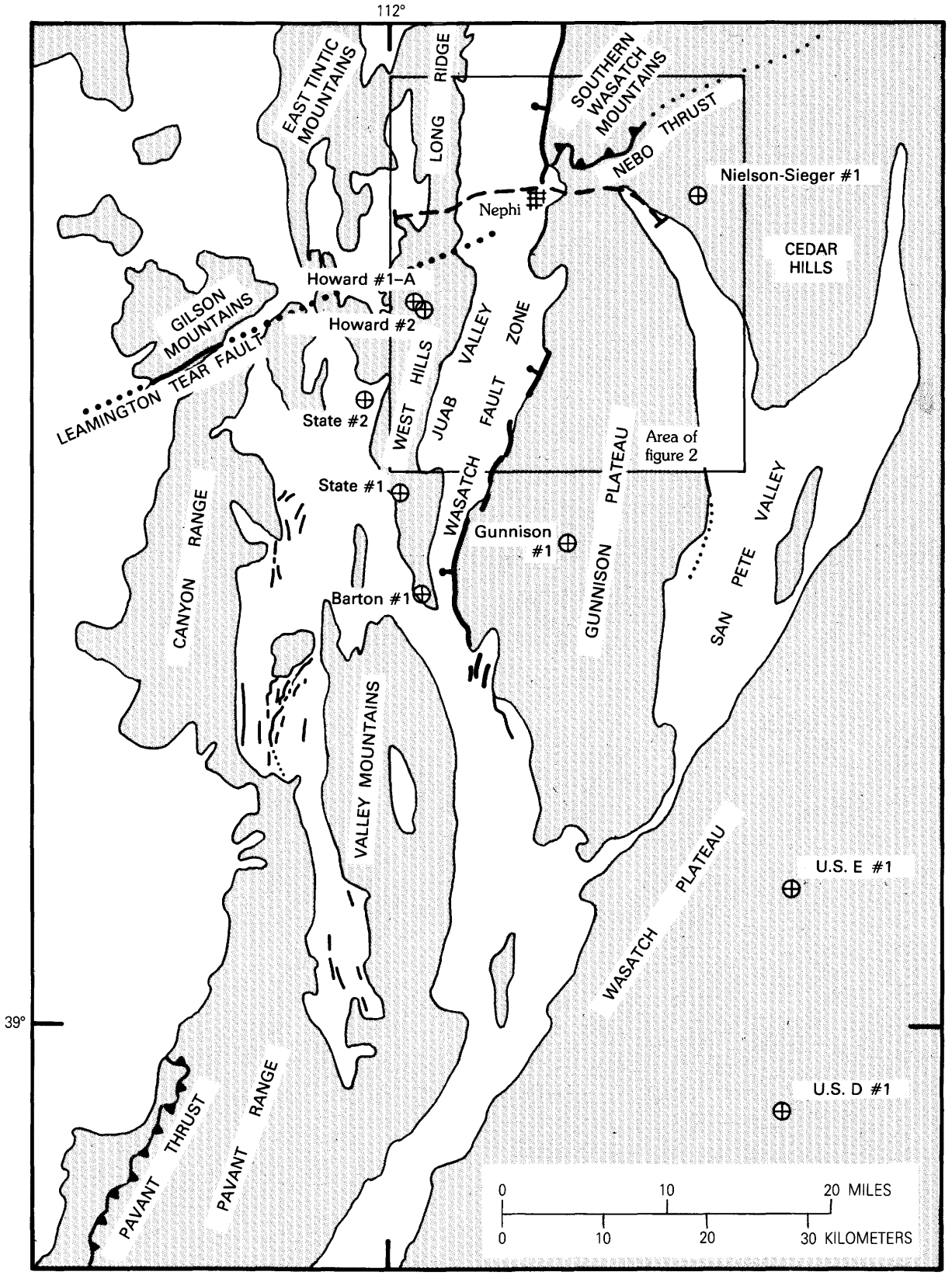

FIGURE 1.—Late Cenozoic normal faults (heavy lines, bar and ball on downthrown side) and Sevier frontal thrust faults (barbed) in central Utah. Ranges are shaded. The Leamington tear fault is shown as a heavy solid line (inferred buried extension shown as a dotted line). Locations of petroleum exploration wells are also indicated. Box shows location of figure 2.

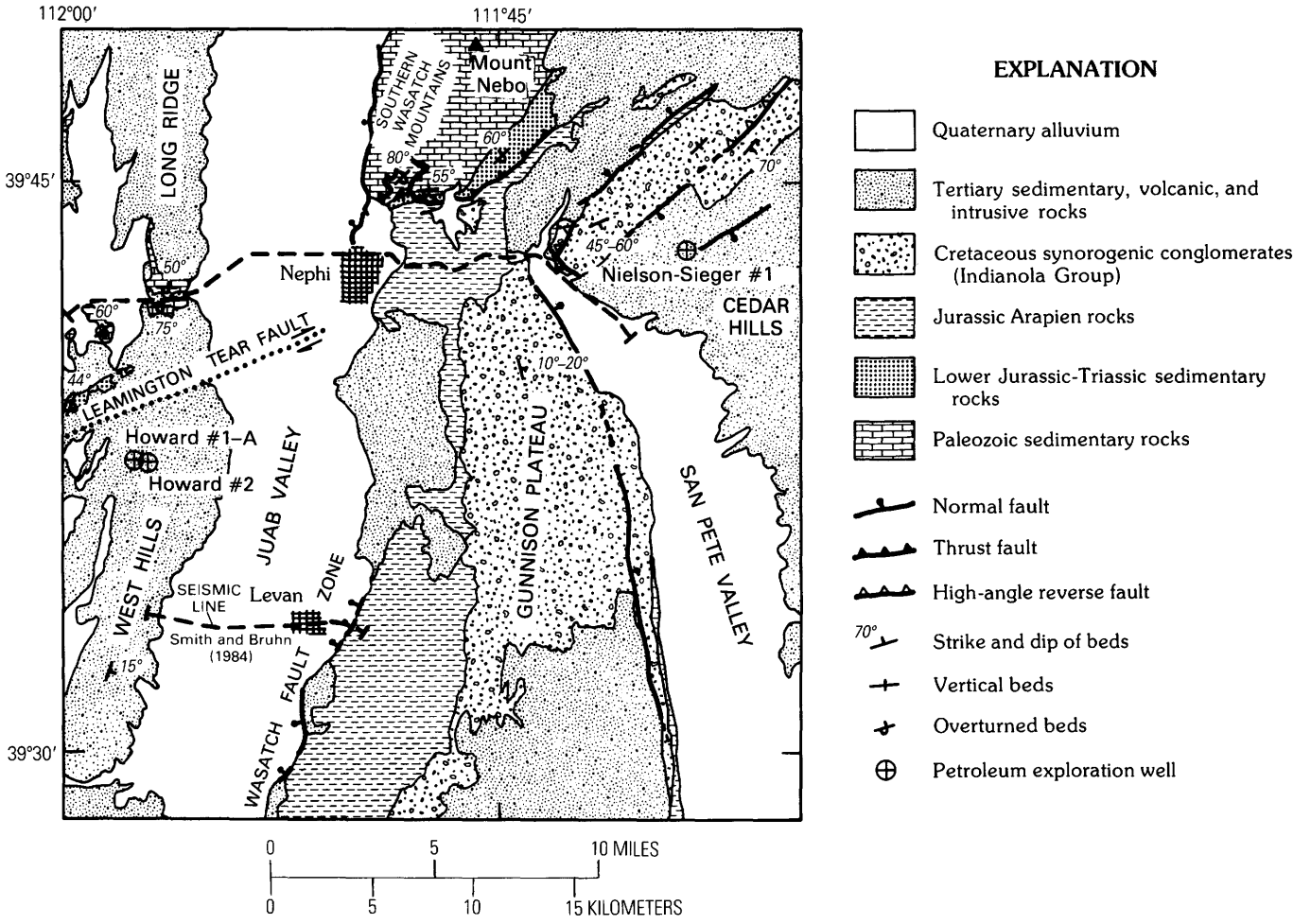

FIGURE 2.—Generalized geology of the study area (see fig. 1 for location). The inferred buried extension of the Leamington tear fault is shown by a heavy dotted line. Locations of seismic reflection profiles near Nephi and to the south (Smith and Bruhn, 1984) are indicated by dashed lines.

The Wasatch fault zone separates the southern Wasatch Mountains and Gunnison Plateau on the east from Juab Valley on the west (fig. 2). Approximately 5 km wide, Juab Valley is bordered on the west by Long Ridge and West Hills.

A late Precambrian (younger than 850 Ma) rifting event (Stewart, 1972) formed a north-trending, west-facing passive margin through western Utah and eastern Nevada (Stewart and Poole, 1974). The study area lies along the inferred hinge line (boundary between shelf and miogeocline) of this margin. In central Utah, deposition on the passive margin continued until the inception of Sevier compressional deformation, which began in latest Jurassic or possibly middle Cretaceous and continued to at least Paleocene time (Standlee, 1982; Lawton, 1982; Heller and others, 1986). During this time, widespread low-angle eastward-directed thrusting occurred in central Utah, concurrent with deposition of synorogenic clastic sediments. The Sevier frontal thrust system is considered the basal and most far-traveled thrust sheet and typically places Paleozoic rocks on Mesozoic rocks. Thrust relations interpreted as part of the frontal thrust zone have been mapped in the Mount Nebo area of the southern Wasatch Mountains, 3.5 km north of the seismic line (fig. 2). The Nebo thrust has been correlated with the Charleston thrust to the north (Crittenden, 1961) and occupies a structural level similar to that of the Pavant thrust to the south (Burchfield and Hickcox, 1972); however, Morris (1983) inferred a major discontinuity in thrust sheet geometry between the Nebo and the Pavant thrusts. Morris interpreted a major tear fault—the Leamington fault—as separating these two frontal thrust systems.

The southern edge of the Nebo thrust, which is exposed in the Mount Nebo area, contains steeply dipping Paleozoic through early Mesozoic rocks deformed into an overturned anticline (Black, 1965). The Nebo allochthon is thrust over the Jurassic Arapien Shale, a

sequence of highly disturbed calcareous mudstone and siltstone units that locally contain significant quantities of salt and anhydrite. A lively controversy exists over the stratigraphic definition and nomenclature of Jurassic marine rocks in central Utah (Spieker, 1946; Hardy, 1952; Witkind, 1982, 1983; Sprinkel, 1982; Lawton, 1985). These disputes over nomenclature are of little importance here; hence, an informal usage describing all the Jurassic shale, silt, and limestone rocks above the Jurassic-Triassic Navajo Sandstone as Arapien rocks (or simply Arapien) has been adopted. This usage includes all of the Arapien Shale as originally named and described by Spieker (1946), including his upper Twist Gulch Member and the underlying Twelve-Mile Canyon Member. Sprinkel (1982) subdivided the Jurassic rocks into two units on the basis of well-log data—the Arapien Shale (calcareous mudstone, shaly siltstone, arenaceous limestone, and evaporites) and the underlying Twin Creek Limestone (limestone and minor amounts of siltstone, sandstone, gypsum, and anhydrite), which rests directly on the Navajo Sandstone. The Twin Creek Limestone has not been identified in surface exposure in central Utah. Twin Creek Limestone is used in this report as the lowermost part of Arapien rocks, as identified in well data.

The Wasatch fault zone truncates the Nebo allocthon along the western edge of the southern Wasatch Mountains and presumably has downdropped the thrust sheet beneath Juab Valley. Exposures of overturned Paleozoic and early Mesozoic rocks in the vicinity of and just south of where the seismic line crosses West Hills and Long Ridge probably represent the western continuation of the Nebo thrust (fig. 2).

The probable southern boundary of the Nebo thrust, the N. 60° E.-trending Leamington tear fault, is exposed 22 km southwest of the end of the seismic line (fig. 1). Where exposed, the fault dips steeply, and the dominant sense of motion is strike slip (Morris, 1983). Its projected trace through the study area is constrained by the exposures of overturned Paleozoic and early Mesozoic rocks in the northern part of West Hills and by two wells in West Hills drilled 8 km south of the seismic line (Placid Oil Howard #1–A and Howard #2) (see figs. 1, 2). Both wells penetrate a normal stratigraphic section of Tertiary through late Mesozoic sedimentary rocks and a section of Jurassic Arapien rocks and bottom in the Jurassic-Triassic Navajo Sandstone (Howard #2, total depth of 3,282 m) or the Triassic Chinle(?) (Howard #1–A, total depth of 3,704 m).

The eastern half of the seismic line crosses the Gunnison Plateau, which is composed primarily of Arapien rocks and overlying synorogenic conglomerates (the Cretaceous Indianola Group), both of which are deformed into a broad asymmetric syncline whose axis generally parallels the modern range. Deformation of these synorogenic conglomerates, particularly along the steep eastern limb of this syncline, has been attributed to simple folding (Spieker, 1946), Laramide compression (Gilliland, 1963), and extensive salt diapirism (Witkind, 1983). However, recent mapping combined with extensive well data and seismic profiling indicates that much of the geometry of deformation within the Gunnison Plateau can be attributed to late-stage Sevier compression and superimposed Tertiary normal faulting. Specifically, the deformation has been related to thrusting beneath the Gunnison Plateau that culminates either in a complex system of west- and east-verging thrusts (Standlee, 1982) or in a triangular zone (Lawton, 1985), both along the eastern margin of the Gunnison Plateau. Well data indicate that the Arapien rocks beneath both the Gunnison Plateau and areas to the west are complexly deformed and tectonically thickened, probably by bedding-plane thrusts (Standlee, 1982; Lawton, 1985). The thrusting beneath the Gunnison Plateau probably has minor displacement and may not have reached the synorogenic erosion surface; Lawton (1985) estimated only 5 to 6 km of shortening in his interpreted triangular zone along the eastern margin of the Gunnison Plateau.

On the basis of repeated and overturned stratigraphic sections in wells along the western margin of the Gunnison Plateau, both Standlee (1982) and Lawton (1985) concluded that bedding-plane thrusts within the Arapien rocks ramped upward in the vicinity of the modern Wasatch fault. An increase in the westward dip of the Nebo basal thrust from an essentially flat attitude on the eastern edge of its exposure in the southern Wasatch Mountains (fig. 2) to a dip of 23° W. near the range-front fault also suggests a ramp structure near the Wasatch fault. Evidence of similar structural styles within thrust sheets to the north presented by Smith and Bruhn (1984) suggests that the modern Wasatch fault is located near the sites of major ramps in Sevier-age thrust faults.

In summary, the seismic line is located in a complex structural setting. The eastern part of the line crosses Arapien rocks that have been tectonically thickened by bedding-plane thrusts and folding and locally disturbed by salt diapirism. These bedding-plane thrusts are below the "basal" Nebo thrust and probably involve only minor transport (approximately 5 km). Upper plate rocks of the Nebo thrust are exposed on the westernmost part of the line; thus, both the Nebo and the lower minor thrust(s) are likely present in the subsurface in this area. The line probably obliquely cuts the southern edge of the Nebo thrust beneath Juab Valley. Geologic and well data suggest a ramp in both the Nebo and the deeper, minor thrust(s) near the modern location of the Wasatch fault zone. Because of the complex subsurface structure,

additional geophysical data were collected to aid in the interpretation of the seismic profile.

GRAVITY AND DENSITY DATA

Existing gravity data in the study area were supplemented by over 200 new stations (fig. 3). As expected, a broad gravity low is associated with Juab Valley. The data suggest a maximum anomaly of about −20 mGal in the valley south of the town of Nephi.

Quantitative modeling of the observed gravity field requires information on the subsurface geometry of the basin and also on the rock densities. Constraints on the subsurface geometry come from the seismic reflection profile and are described later in the interpretive section, together with a quantitative model of valley fill in Juab Valley. Density data from density logs of significant wells in the region are summarized in table 1. In general, rock density increases with age. Despite the complex internal structure of the Arapien rocks and reported large lateral variations in lithology (particularly in salt-anhydrite content), this unit has only a moderate variation in density (2.54–2.64 g/cm^3). However, these values are substantially greater than the values of the density of Arapien rocks reported by Brown and Cook (1982) from logs of the Phillips U.S. D #1 well located 90 km south of the seismic line (see fig. 1). Brown and Cook (1982) recognized three distinct lithologic units within the Arapien-age rocks having mean densities of 2.11, 2.54, and 2.01 g/cm^3 and a weighted mean density of 2.41 g/cm^3. For this study, a mean density for the Arapien-age rocks (including the Twin Creek Limestone of Sprinkel (1982)) of 2.55 g/cm^3 is preferred because it is more representative of the values given in table 1 for wells located close to the seismic profile, particularly Howard #1–A, State #1, and State #2 (figs. 1, 2).

The Jurassic-Triassic Navajo Sandstone underlying the Arapien rocks has approximately the same mean density (2.55 g/cm^3) as the Arapien rocks, whereas the Triassic rocks are slightly more dense (2.63 g/cm^3). Rock units within the Paleozoic have primarily limestone lithologies and a mean density of about 2.73 g/cm^3, the result being a density contrast of +0.10 to +0.18 g/cm^3 with the overlying Triassic and Jurassic rocks.

In addition to the main basin fill anomaly, the gravity data also reveal a relative gravity high within the basin that separates the closed low directly southwest of Nephi from the closed low about 15 km to the north (fig. 3). The source of this relative gravity high may be a transverse structure separating a shallow basin to the north from a deeper basin to the south. Similar transverse structures have been inferred from gravity and geologic data for many of the basins bounded by the Wasatch fault zone (Zoback, 1983). Alternatively, because the east-west-trending gravity high separating the two gravity lows generally coincides with the southern termination of the Nebo allochthon in the range to the east, the gravity high may be caused in part by lateral variations in bedrock density. In this case, the gradient may define the buried extension of the Lemington tear fault, which forms the southern edge of the Nebo thrust plate. The decrease in gravity values south of this gravity high would thus be attributed to the +0.10- to +0.18-g/cm^3 density contrast between the primarily limestone lithologies of Paleozoic rocks within the thrust plate and the predominantly shale and siltstone lithologies of the Arapien rocks on which it rests. This interpretation supports an inferred buried connection between the overturned Paleozoic rocks forming the Nebo allochthon and the overturned Paleozoic and Mesozoic rocks exposed in and just south of the pass between Long Ridge and West Hills (figs. 2, 3). The gentle slope of the gravity gradient may indicate that, in this area, the tear fault may have a shallow dip to the north. Wallace and Morris (1979) reported that tear faults commonly flatten in dip to merge with the bounding thrust. The shape of the gravity gradient, particularly the closed low southwest of Nephi, suggests that this transverse relative gravity high may be related to both effects described above, in which case the southern edge of the Nebo allochthon (Leamington tear fault) may have acted to segment the extensional fault structure in the hanging wall and thereby produce a variation in fill thickness between the northern and southern portions of the basin.

SEISMIC REFLECTION AND VELOCITY DATA

A standard 24-fold Vibroseis (trademark of Conoco, Inc.) profile was shot across the Wasatch fault zone through the town of Nephi in 1975 (fig. 2). The data were collected by a private contractor, United Geophysical, and purchased by the U.S. Geological Survey. Group and shot point intervals were 220 ft, and the data were recorded on a split spread having a near offset of 880 ft and a far offset of 5,940 ft. The standard processing sequence included demultiplexing, velocity analysis, elevation and residual statics, stacking, and filtering. The automatic residual statics produced a very poor quality record section in which there was little continuity of reflectors. The contractor then used an "in-house" statics routine and hand picked some refraction arrivals, a procedure that greatly improved the data quality and yielded the section shown in figure 4. A floating datum used to display the data is generally 30 to 70 m below the ground surface and has a constant value in the basin.

The 30-km-long profile begins in San Pete Valley on the east and follows the divide separating the southern

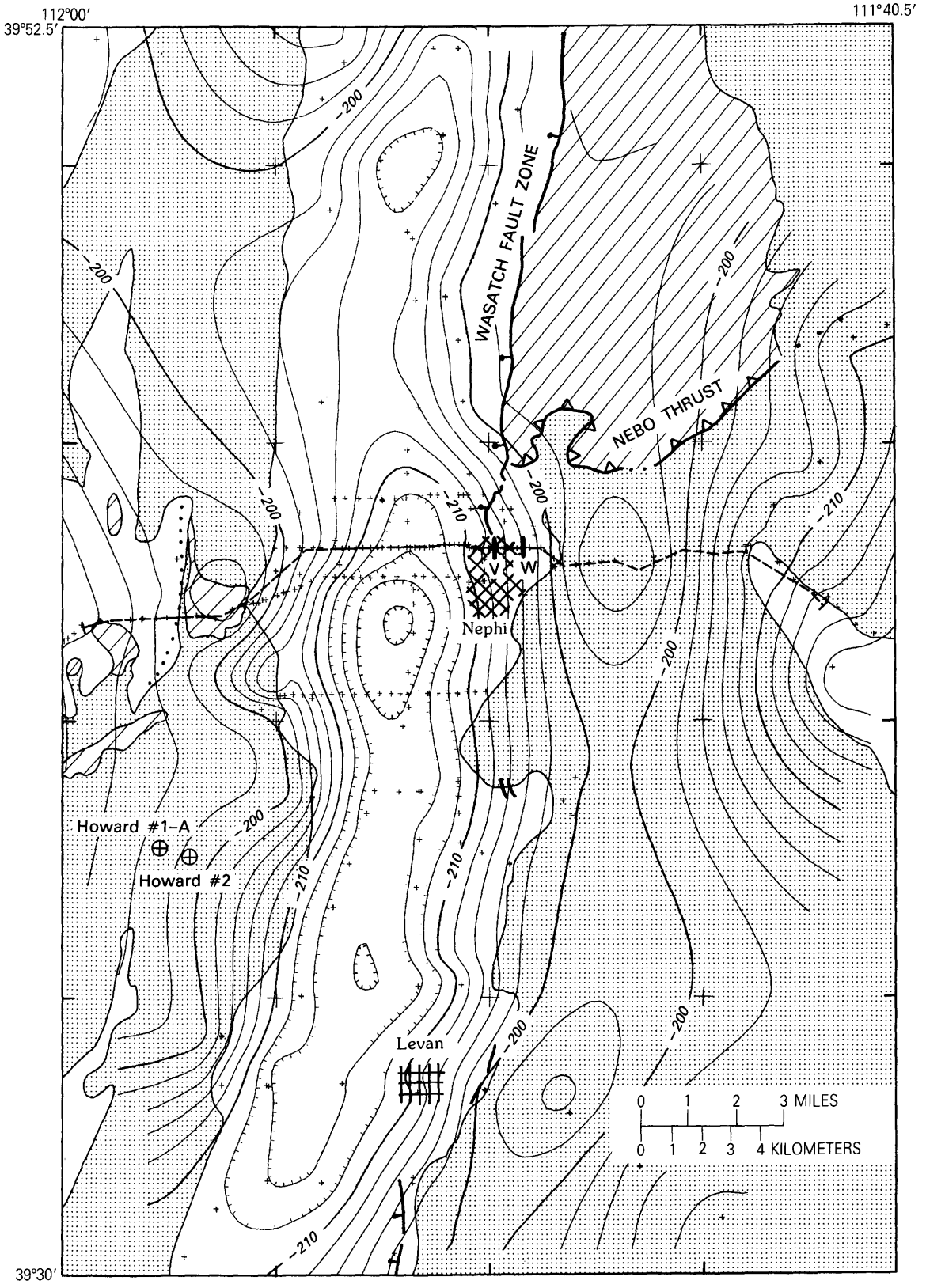

FIGURE 3.—Complete Bouguer gravity data for the Nephi area (contour interval 2 mGal). Gravity stations are shown by plus signs. Ranges are shaded. Rocks inferred to be part of the Nebo thrust sheet are hachured. The dashed line is the location of the reflection profile. The Wasatch fault is indicated by a heavy solid line (bar and ball on downthrown side).

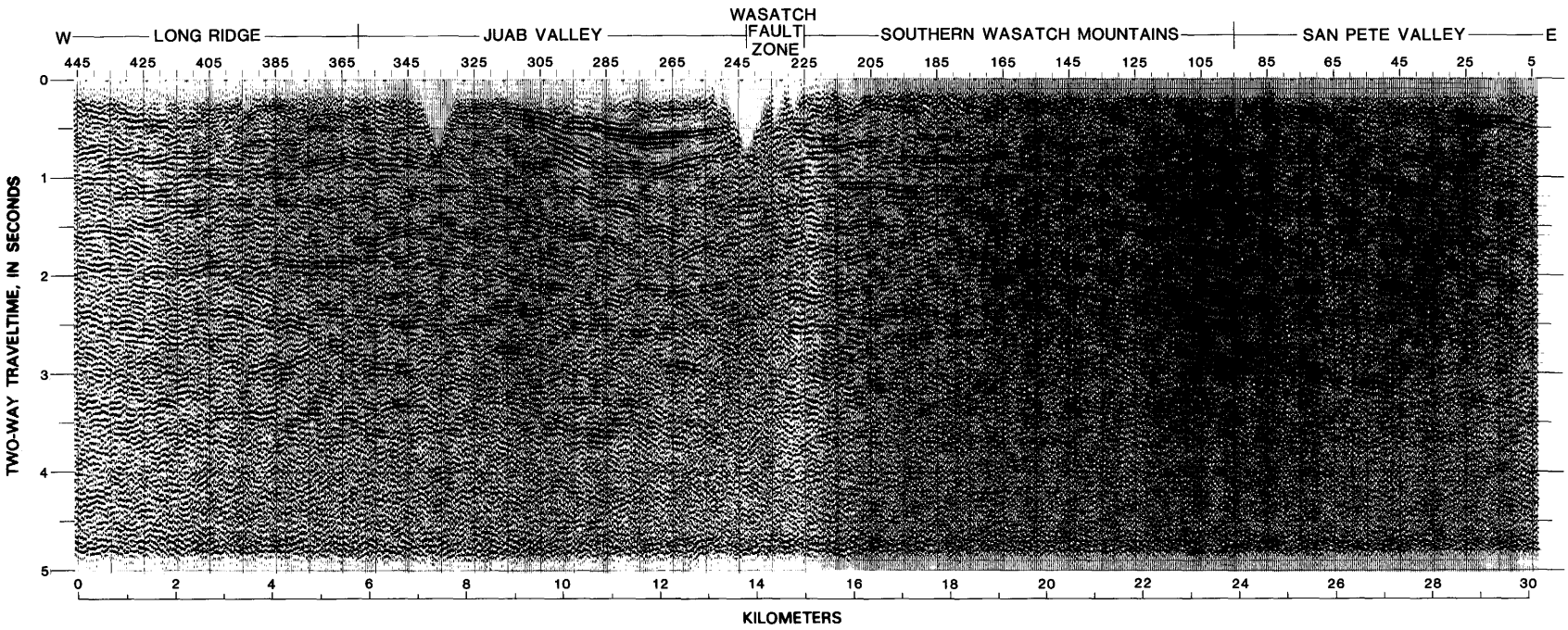

FIGURE 4.—Seismic reflection profile (see fig. 2 for location). Vibrator points are numbered across the top of the profile.

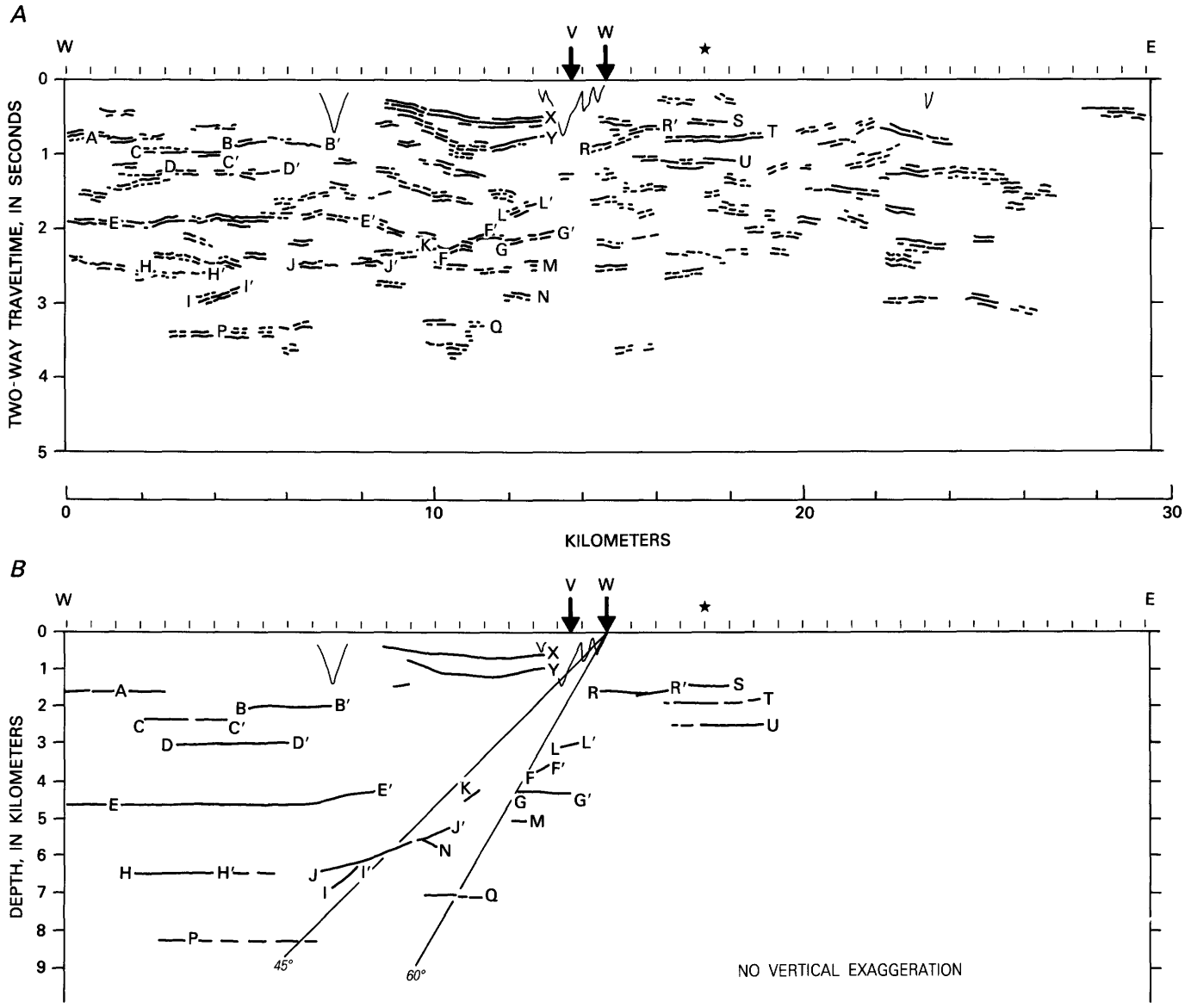

FIGURE 5.—*A*, Seismic reflection profile. Reflectors discussed in the text are lettered. *B*, Selected reflectors on line drawing (true-depth migrated cross section). V and W indicate limits (discussed in text) on the surface projection of the Wasatch fault. The star indicates the axis of a proposed major diapiric fold crossing the seismic line.

Wasatch Mountains from the Gunnison Plateau (fig. 2). It crosses the Wasatch fault zone at Nephi, continues westward across Juab Valley, through the pass between Long Ridge and West Hills, and ends in Dog Valley. There are several large data gaps on the section; the one in the western half of the section is caused by a stream and the one near the center of the section by a major highway and Nephi city streets. Despite folded and steeply dipping to overturned beds exposed in the ranges, the profile is dominated by horizontal and subhorizontal reflectors beneath both the basin and the ranges.

A line drawing of the prominent reflectors on the section is given in figure 5*A*. A discussion of the lettered reflectors and their geologic interpretation will be presented later. First, velocity data are needed to estimate the depth and apparent dip of reflectors on the time section. Some velocity information is derived from the processing of the reflection data; these "stacking velocities" are best determined in areas of strong subhorizontal continuous reflectors. An additional source of velocity data is sonic logs of exploration wells. Sonic velocities and rock densities obtained from logs of nearby wells are summarized in table 1.

TABLE 1.—*Log-determined densities and sonic velocities of significant wells in the region of the Wasatch fault zone*

[Locations of wells shown in fig. 1. —, no data]

	Howard #1-A		Nielson-Singer #1		Gunnison #1		State #1		State #2		Barton #1		U.S. E #1	
	Density	Velocity	Density	Velocity	Density	Velocity	Density	Velocity	Density	Velocity	Density	Velocity	Density	Velocity
Tertiary volcanic rocks											—	[1]2.93		
Eocene Flagstaff Limestone			—	[1]3.05			2.55	[1]3.93						
Cretaceous Indianola Group	[1]2.57	[1]4.88	2.55	[1]4.47	[1]2.68	[1]5.65	2.54	[1]4.97					—	[1]4.76
Jurassic Arapien rocks	2.54	5.04			[1]2.59	4.97	[1,3]2.60	[1,3]5.72	[1]2.63	[1]4.27	—	4.82		
							[1,4]2.64	[1,4]5.61						
Ja[2]	2.54	4.95					[3]—	[3]5.63			—	4.70		
							—	[1,4]5.23						
Jtc[2]	2.54	5.40					—	[1,3]5.95			—	[1]5.54		
							—	[1]6.25						
Jurassic-Triassic Navajo Sandstone	2.60	5.12			[1]2.58	[1]5.23	[1]2.60	[1]6.16	2.56	4.97	—	5.09	2.53	—
Triassic shales	[1]2.63	[1]5.44							2.60	5.03	—	[1]5.21	2.65	—
Permian limestones									[1]2.69	[1]5.35			2.75	5.94
Paleozoic shelf section (Permian-Cambrian)													[1]2.73	[1]5.95

[1]Only part of the unit was sampled owing to logging difficulties or structure encountered in the well.

[2]Division of Arapien-age rocks into Arapien (Ja) and Twin Creek Limestone (Jtc) equivalents (after Sprinkel, 1982).

[3]Above a thrust fault believed to have been encountered in the well.

[4]Below a thrust fault believed to have been encountered in the well.

The well log velocities show a significant amount of scatter for individual units; this scatter may reflect real variations in lithology between wells or may be because of poor log quality caused by borehole irregularities or geologic structure in the well, which led to incomplete sampling. The velocity values in table 1 represent reasonable ranges for the lithologies of the units of interest. The velocity ranges for the Mesozoic have considerable overlap among units (Indianola, 4.47–5.65 km/s; Arapien, 4.70–6.25 km/s; Navajo, 4.97–6.16 km/s; Triassic rocks, 5.03–5.44 km/s). In those wells where Sprinkel (1982) subdivided Arapien-age rocks into Arapien and Twin Creek equivalents, there is generally a large velocity increase between the calcareous mudstones and shaly siltstones of the Arapien rocks and the limestones that dominate the underlying Twin Creek equivalents.

Since seismic reflectance depends on impedance contrasts (velocity times density), the density and velocity data in table 1 indicate numerous potential reflecting horizons throughout the section. Clearly, the Mesozoic-Paleozoic boundary has a large impedance contrast. There is also a considerable impedance contrast between the Arapien Shale and the Twin Creek Limestone in wells where these units are differentiated (Sprinkel, 1982). This impedance contrast within Arapien-age rocks is greater than that between the base of the Twin Creek Limestone and the underlying Navajo Sandstone. The velocity and density data from the Paleozoic shelf rocks drilled in the U.S. E #1 well on the Wasatch Plateau (fig. 1) also indicate significant impedance contrasts between individual units in the Paleozoic section. Thus, numerous potential reflectors occur in the Mesozoic and Paleozoic rocks owing to stratigraphic and lithologic contrasts. In addition, structural features, including thrust-juxtaposed units of high impedance contrast as well as low-angle fault zones (Jones and Nur, 1984), may produce some of the reflections.

Comparison of these well log velocities with stacking velocities obtained during processing of the seismic section indicates that the stacking velocities in general are unrealistically low, except for those in the basin fill region, where the reflectors are strong and very continuous. In particular, the stacking velocities from a velocity analysis near the center of the Gunnison Plateau, where Arapien rocks are exposed and are probably at least 2,000 m thick, indicate a velocity of 3.8 km/s at 1.0 s two-way traveltime and a velocity of 4.27 km/s at 2.0 s two-way traveltime. In contrast, the sonic-log-determined velocities for Arapien rocks, although variable, range between 4.70 and 6.25 km/s (table 1). Similarly, stacking velocities on the western end of the line, where overturned Paleozoic limestones are exposed at the surface, are low in comparison with sonic log velocities. The log velocity of the Paleozoic rocks is quite high (approximately 5.95 km/s) in comparison with several stacking velocities between 3.66 and 3.81 km/s for the prominent reflector (E–E′) at about 1.9 s two-way traveltime. The Paleozoic rocks at the surface are presumed to be part of the Nebo thrust, which probably rests on rocks of Jurassic Arapien age or older; nonetheless, these stacking velocities are unrealistic, even if there is only a thin plate of Paleozoic rocks and much of the section is lower plate Mesozoic rocks. Low stacking velocities may sometimes indicate the presence of multiple reflections in the section. The simplest multiple path predicts a second reflection at twice the two-way traveltime and twice the dip and a stacking velocity of one-half the true root-mean-square velocity. However, there are no obvious shallower reflectors that may have generated multiples, particularly in the case of the laterally continuous reflector E–E′. Because of the inconsistencies between the sonic log velocities and the stacking velocities, the interpretation of the seismic reflection time section in the next section generally relies on the well log velocities (except within the basin fill section) to calculate depth to observed reflectors.

INTERPRETED SUBSURFACE STRUCTURE

BASIN GEOMETRY AND SHALLOW STRUCTURE OF THE WASATCH FAULT ZONE

The most prominent and continuous reflectors on the seismic profile are from the late Cenozoic basin fill section (figs. 4, 5). Figure 6*A* presents a detailed view of this part of the seismic line and a possible interpretation of reflectors across minor faults within the basin. Figure 6*B* is a one-to-one schematic depth cross section of several prominent reflectors showing the depth and dip of these reflectors as inferred from stacking velocities. Stacking velocities within the basin fill section compare quite favorably with velocity data from other basins (for example, Okaya and Thompson, 1985); because the reflectors are so strong and continuous, the stacking velocities were considered valid for this part of the line. The best-constrained reflectors are marked X and Y; three separate velocity analyses detail their depths. Depths of other reflectors shown on figure 6*B* were obtained by interpolation.

The Wasatch fault zone bounds the basin on the east, and the internal structure of the basin is a gentle synclinal sag displaying dips of 7° to 20° on the western flank and 5° to 7° on the eastern flank. On the time section (fig. 6*A*), the basinward dips on the eastern flank are exaggerated because of a velocity increase (suggested by stacking velocities) eastward toward the Wasatch fault zone.

The base of the valley fill section is not marked by a single well-defined reflector. In the western half of the

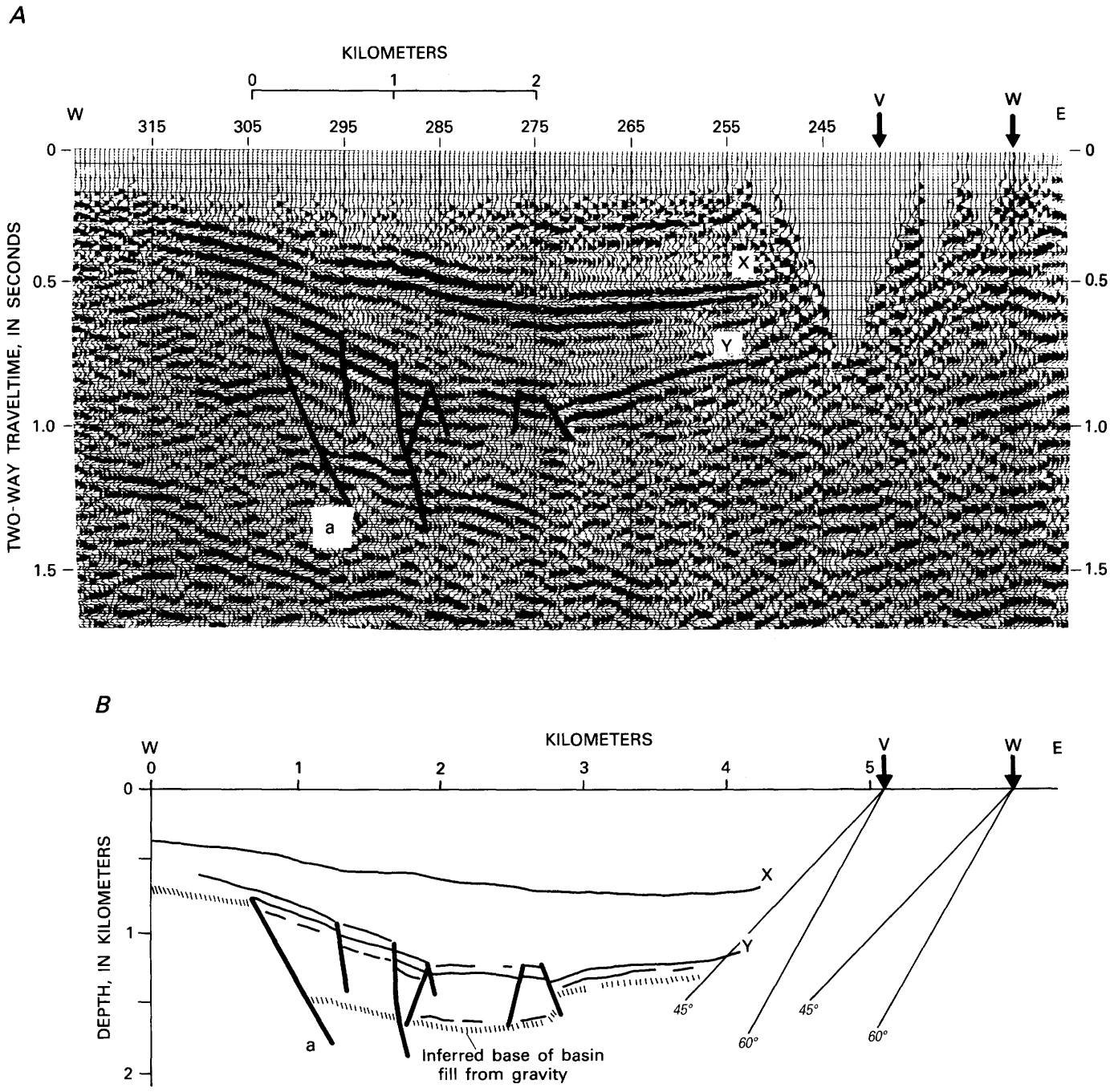

FIGURE 6.—*A*, Detail of seismic reflection profile in Juab Valley showing basin fill. V and W mark possible surface locations of the Wasatch fault zone described in text. Vibrator points are numbered across the top of the section. A major fault on the western side of the basin is labeled a. Reflectors X and Y are discussed in the text. Heavy solid lines are interpreted faults. *B*, Prominent reflectors in basin (true-depth cross section). Projections of planar faults having dips of 45° and 60° and reaching the surface at locations V and W are shown. Vertical and horizontal scales are equal.

basin, the base of the valley fill is inferred to lie between the discontinuous basal synclinal sag (reflectors) and the deeper discordant reflectors (fig. 5*A*). The deepest part of the basin has a grabenlike structure, bounded on the west by a normal fault (fault a, fig. 6) having about 700 m of displacement. There are no obvious subjacent discordant reflectors directly beneath the eastern half of the basin, so only a minimum thickness of valley fill can be determined there. Mean velocities for the basin fill obtained from three stacking velocity analyses on reflectors near the base of the synclinal sag vary between 2.74 and 2.97 km/s, the lower velocity being from the center of

the valley and the slightly higher values being near the margins. Interval velocities between reflectors in the lower part of the basin fill exceed 3.2 km/s and may represent early Tertiary volcanic or sedimentary rocks (see table 1). The thickest section of basin fill is interpreted to lie beneath VP 285, where the fill is estimated to be 1.60 km thick.

The eastern margin of the basin is marked by a broad zone of little or no reflectance. Interpretation of this part of the section is hampered by a data gap caused by cultural noise associated with the town of Nephi. The eastward termination of the basin reflectors in this region may be owing to the data gap and the reduction in fold as the gap is approached but may also be owing in part to a general decay in reflector continuity in the poorly sorted, poorly stratified coarse clastics that comprise the alluvial fans adjacent to major range-front faults. This decay of coherent reflectors within the fan region (as opposed to the uniform reflectors from the finer grainer basinal facies) is typical of many basins within the Basin and Range province (Anderson and others, 1983; Zoback and Anderson, 1983; Okaya and Thompson, 1985).

Prominent multiple-event Holocene scarps mark the trace of the Wasatch fault zone directly north of the study area (Schwartz and Coppersmith, 1984) (see fig. 2); the scarps extend southward to within about 2 km of the seismic line. A curved scarp, located basinward of the main zone of range-front scarps, has been identified by Cluff and others (1973) just north of the seismic profile (fig. 2). The surface location of the main Wasatch fault zone along the profile is believed to lie between the southerly projection of the large Holocene scarps to the north (W, fig. 6) (Schwartz and Coppersmith, 1984) and young faulting exhibiting a net vertical displacement of 11 m at depths of about 150 m (V, fig. 6) inferred from a shallow high-resolution seismic reflection profile run along the same road as the industry reflection profile (Crone and Harding, 1984). The zone of shallow faulting at V is near the southern end of the curved scarp of Cluff and others (1973). However, minor fault displacements were also observed by the high-resolution seismic survey near W, the southward projection of the range-front scarp.

Projections of faults that dip between 45° and 60° are shown on figure 5*B* at localities V and W. The eastward extent of reflector Y places a minimum dip of about 52° for a bounding fault having a surface trace at V. Locating the major bounding fault trace at V assumes that some coherent basin reflectors extend through any fan wedge that might have built up along such a bounding fault; it also assumes that there was no decay of the reflector signal by the data gap. Interestingly, high-quality reflection data possessing good surface-faulting control in a comparable basin (Dixie Valley, Nevada) indicate a 1.0- to 1.25-km fan wedge adjacent to the range-bounding fault (Okaya and Thompson, 1985); this hypothesis would favor location W as the major bounding-fault zone. Of course, there may well be a broad fault zone having displacement distributed across it, the youngest offset apparently being near V, as the high-resolution seismic data (Crone and Harding, 1984) indicate.

Gravity data can help to constrain the geometry of the basin margin. As described earlier, gravity data were collected at more than 200 stations in the vicinity of and along the seismic profile. Gravity measurements were made approximately every 170 m along most of the reflection line. These data are plotted in cross section in figure 7. Several two-dimensional gravity models were computed for the basin fill assuming a -0.4 g/cm^3 density contrast with adjacent bedrock. The only difference between the three models in figure 7 is the location of the eastern margin of the basin. The maximum fill thickness in the center of the basin for all models is about 1.6 km, consistent with the interpretation of the reflection data. A notable feature of the models is a central graben, inferred from the reflection data. The configuration of and vertical displacement on the fault bounding the western side of the graben are taken directly from the reflection data. The modeled base of the basin closely matches the base inferred from the seismic data, except along the eastern margin of the basin.

In model 1 (fig. 7), the Wasatch fault zone is located at W, along the southern projection of the range-front fault, and has a dip of 60° W. This model matches the gravity gradient directly above the fault quite well but greatly overestimates the gravity values east of the fault. Model 2 places the main Wasatch fault zone at V, the most basinward position of young faulting inferred from the high-resolution seismic reflection described by Crone and Harding (1984). This position for the bounding fault clearly provides a very poor fit to the observed gravity data for almost the entire eastern part of the basin.

In an attempt to model the low gravity values east of the fault zone, an easternmost limit for faulting (model 3) was generated from the surface location of bedrock in the range and from the western truncation of reflector R–R′ on the footwall block (fig. 5*B*). This model overpredicts the anomaly to the west of the fault (although the fit would improve if a higher density alluvial wedge were added to the model). Once again, although the fit to the gravity data east of the fault is improved, the computed values are still too large in a 2-km-wide zone east of the easternmost possible fault location. This poor fit suggests that the source of the observed gravity low east of the fault is the result of less dense bedrock (Arapien rocks) of the footwall.

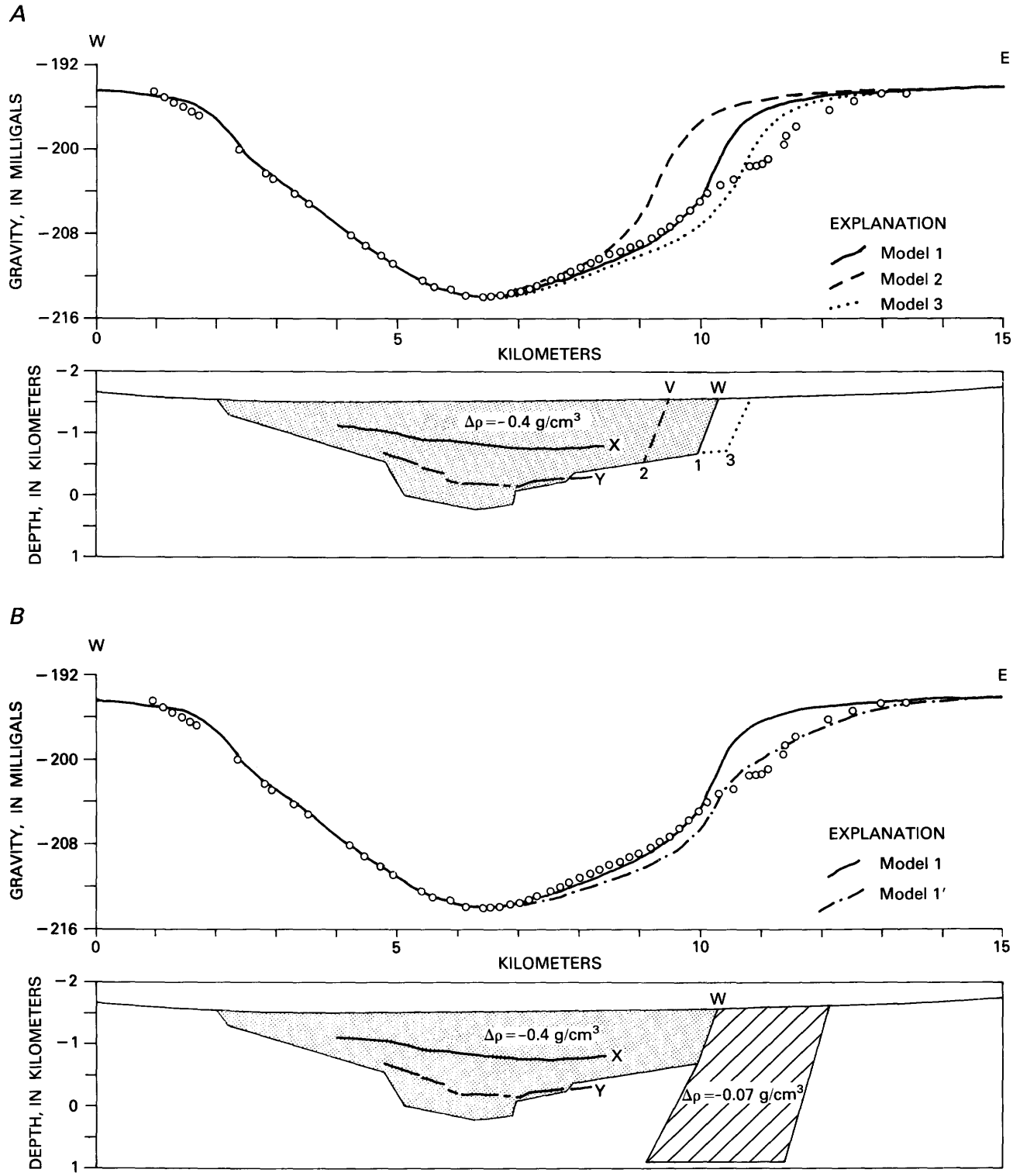

FIGURE 7.—*A*, Gravity models of basin fill in Juab Valley. Open circles are observed gravity values; solid, dashed, and dotted lines give computed values based on the geometries indicated. V and W mark possible surface locations of the Wasatch fault zone described in text. A constant density contrast $\Delta\rho$ of -0.4 g/cm^3 between basin fill and surrounding bedrock was assumed for all models. Reflectors X and Y from figure 6 are shown for reference. *B*, Same as model 1 in *A*, except a low-density tabular body ($\Delta\rho=-0.07$) has been added to the footwall of the Wasatch zone.

In all three models in figure 7*A*, the inferred base of the basin contradicts the position of the intrabasin reflector Y whose depth was determined from an Advanced Interpretative Modeling Systems (AIMS, Geoquest) migration using stacking velocities on the seismic section. One explanation of this discrepancy between the gravity-inferred and seismically inferred basin geometries just west of the bounding-fault zone may be the assumption of a single density contrast for the entire basin. As previously mentioned, alluvial fans along major basin-bounding normal faults produce a wedge of higher velocity, higher density sediment adjacent to the fault zone. Okaya and Thompson (1985) used a fan wedge having a density 0.2 to 0.3 g/cm^3 higher than that of the rest of the basin to reconcile gravity and reflection data from Dixie Valley, Nev. Although using a higher density fan wedge would increase the gravity values west of the fault (and thus improve the fit in model 3), the fan wedge was not included in these simple models, since it would not explain the low gravity values east of the fault zone. Because the initial objective in modeling the gravity data was to constrain both the location and the shallow geometry of the Wasatch fault zone, several possible surface traces for the main bounding-fault zone (using the simple but probably unrealistic assumption of a constant density for the basin) were examined to determine the effects of different fault locations on the gravity field east of the fault.

Figure 7*B* shows a modified simple model that is generally consistent with the observed gravity values east of the fault. Here the main Wasatch fault zone is positioned at W, and a tabular low-density body roughly 2 km wide has been included east of the fault zone. The geometry of this low-density body was chosen simply to provide a reasonable fit to the gravity data. Inclusion of a higher density clastic wedge west of the fault zone (discussed above) could provide a near-perfect fit to the data; however, in the absence of additional constraints on the geometries of these bodies, any near-perfect fit would be nonunique and not particularly instructive. The presence of a low-density body just east of the Wasatch fault zone is supported by the geology along the western edge of the Wasatch Range in the area of the seismic line. Here the seismic line passes an open-pit mine where large quantities of gypsum have been removed from the Arapien rocks. Possibly, the low-density body in the model represents a concentration of diapiric gypsum that rose along or just east of the Wasatch fault zone when the major bedrock offset occurred.

Thus, because of complicated structure within the footwall, the gravity data cannot tightly constrain the near-surface location of the Wasatch fault zone. The gravity data do appear to exclude location V as the position of the main Wasatch fault. On the basis of the geology and the high-resolution seismic work, location W seems to be the most likely position for the main fault zone at the time of the major bedrock offset.

DEEP STRUCTURE

Prominent reflectors on the seismic profile are shown on the line drawing in figure 5*A*. Each of the lettered reflectors was represented by a straight-line segment or a series of straight-line segments and was migrated by means of an AIMS migration scheme and a very simple velocity model. Velocities in Juab Valley were obtained from the stacking velocities; elsewhere, a constant velocity of 5 km/s was assumed, because, as discussed earlier, stacking velocities were generally unrealistically low. A velocity of 5 km/s is probably somewhat low for the deeper portions of the section where Paleozoic rocks are probably present; thus, the depths given for the deep events are only minimum depths.

Figure 5*B* shows the approximate true-depth positions (obtained from the AIMS migration) of the lettered reflectors in figure 5*A*. The outline of the inferred basin structure (from the gravity and seismic interpretation in fig. 6*B*) is indicated, as are projections of planar faults dipping 45° and 60° from the preferred near-surface fault location W. The relationship and position of the lettered reflectors are discussed below, and their geologic interpretation is described in the next section.

Subhorizontal reflectors are common throughout the profile to depths of 2.5 to 3.0 s, and there are several strong and relatively continuous reflectors (marked P and Q) at two-way traveltimes of 3.3 to 3.7 s on the western half of the profile. If the velocity model described above is used, the depth to the top of the P reflectors is greater than 8.3 km. Relatively shallow reflectors in the western half of the seismic profile include the events marked A, B–B′, C–C′, and D–D′. These events are beneath the pass between Long Ridge and West Hills, where overturned, steeply dipping Paleozoic rocks believed to be part of the upper plate of the Nebo thrust are exposed at the surface. The complex band of reflectors marked A, B–B′, and C–C′ lacks significant lateral continuity. Events A and B–B′ are at a depth of 1.65 to 2.0 km (if a mean near-surface velocity of 5.0 km/s is assumed). Event C–C′ occurs at a depth of about 2.3 km, and a slightly deeper zone of subhorizontal reflectors (D–D′), laterally continuous for 6 km, is at a depth of about 3.0 km.

Where the Nebo thrust is exposed in the southern Wasatch Mountains on the eastern side of the basin, Paleozoic limestones in the upper plate of the Nebo thrust are emplaced on Arapien rocks, which, on the basis of the velocities and densities given in table 1, should produce a significant impedance contrast. How-

ever, the lack of a single continuous, well-defined reflector marking the Nebo thrust fault on the western half of the profile is not surprising and is probably due to the complex structure of the overturned anticline forming the upper plate. The Paleozoic rocks are overturned at the surface and dip to the north 50° to 75°. An additional complicating structural feature along this portion of the line is the apparent eastward tilt of the entire Long Ridge-West Hills range complex. Oligocene volcanic and volcanic-sedimentary rocks capping these two ranges are rather uniformly tilted 15° to 30° to the east. The steeply dipping, overturned Paleozoic limestones (inferred to be part of the Nebo thrust) that are exposed in the pass between these two ranges presumably also have been eastward tilted. However, none of the subhorizontal reflectors A, B–B′, C–C′, or D–D′ have eastward dips. Either structural accommodation of the tilting seen at the surface occurs at depths of less than 1.5 to 2.0 km, or else those shallow reflectors had a westward dip before tilting. Thus, because of the complex internal structure of the thrust sheet and post-thrust tilting of the range, as well as the possibility of a ramp in the thrust near the Wasatch fault (discussed previously), not even an approximate thickness of the Nebo plate can be used to constrain which of the reflections A, B–B′, C–C′, or D–D′ might be from the actual Nebo thrust plane.

The most continuous zone of deep reflectors is E–E′, a nearly horizontal band of reflectors that extends across the western half of the section at 1.8 to 2.0 s two-way traveltime (fig. 5*A*). These reflectors are laterally continuous for at least 10 km and possibly for as much as 15 km (to G–G′). An average (root mean square) velocity of about 5.0 km/s for this part of the profile yields a depth of 4.7 km for this prominent reflector. The eastward continuation of reflector E–E′, which appears to exhibit velocity "pulldown" beneath the basin, is obscured by crosscutting events, including west-dipping events K and F–F′. However, on the migrated depth section shown in figure 5*B*, the eastern end of event E–E′, when corrected for velocity pulldown, actually dips to the west beneath the western part of the basin.

On the time section (fig. 5*A*), it appears that events E–E′ and G–G′ might be laterally continuous. However, on the migrated depth section, the events appear unrelated. Reflector G–G′ becomes subhorizontal, shifts eastward, and would be located in the footwall block of a fault dipping 60° and having a surface trace at W. Significantly, west-dipping events L–L′ and F–F′ (which appear to cut events E–E′ and G–G′ on the time section and could be interpreted as possible reflections from a listric fault plane) migrate, according to the simple velocity model described above, updip and are located, along with G–G′, in the footwall block of a 60° (or shallower) fault plane. The apparent dips, in the plane of the profile, of reflectors L–L′ and F–F′ are 11° W. and 30° W., respectively (true dips may be steeper). Event M also appears to be in the footwall block of a 60° fault, whereas the top of the deep events marked Q would be within the footwall block of a west-dipping planar fault of 55° or less. Similarly, the top of the subhorizontal deep event P constrains a planar fault dip to be greater than 47°.

The reflectors deeper than E–E′, including those marked H–H′, I–I′, J–J′, and K, are rather complex, consisting of west-dipping, east-dipping, and crosscutting events. Westward-dipping event J–J′, beneath the western side of the basin, moves considerably upon migration and has an apparent dip of 22° W. East-dipping event N migrates updip and appears to be truncated by event J–J′. Similarly, event I–I′ also migrates to event J–J′ and appears truncated. The migrated position and geometry of event J–J′ are highly suggestive of a reflection from a listric fault plane possibly flattening and merging with event H–H′. However, there is no suggestion on the actual reflection data of continuity between J–J′ and H–H′.

The general character of the seismic profile changes near the Wasatch fault zone. The eastern half of the profile, beneath the Gunnison Plateau, is characterized by a thick sequence of short, discontinuous subhorizontal reflectors. With the exception of the reflectors marked R–R′, S, T, and U on figure 5*A*, no attempt has been made to interpret these numerous discontinuous reflectors. Seismic reflection and well data along the western margin of the Gunnison Plateau 15 to 20 km south of the profile indicate a complicated structure within the Arapien rocks, including multiple thrust faults and overturned to recumbent folds (Standlee, 1982; Lawton, 1985). The west-dipping reflector R–R′ on the time section is one of the stronger reflectors east of the Wasatch fault zone and appears to truncate overlying horizontal reflectors. Upon migration, the western portion of event R–R′ becomes subhorizontal and appears to be cut by the west-dipping eastern limb of R–R′. This eastern limb may also truncate subhorizontal reflectors S, T, and U.

Prominent subhorizontal reflectors beneath the Gunnison Plateau argue against large-scale deep-seated salt diapirism along the axis of the Gunnison Plateau, as Witkind (1982, 1983) suggested. In fact, the axis of a proposed major diapiric fold interpreted to extend for at least 38 km along strike (Witkind, 1983) crosses the seismic line approximately at the location of the star on figure 5*A* and *B*. Reflectors in the shallowest part of the time record (fig. 5*A*) here are slightly upwarped; however, the deeper reflectors (S, T, and U), at approximate depths of 1.5, 2.0, and 2.75 km, respectively (assuming a velocity of 5.0 km/s), are subhorizontal beneath this presumed anticlinal axis and thus suggest

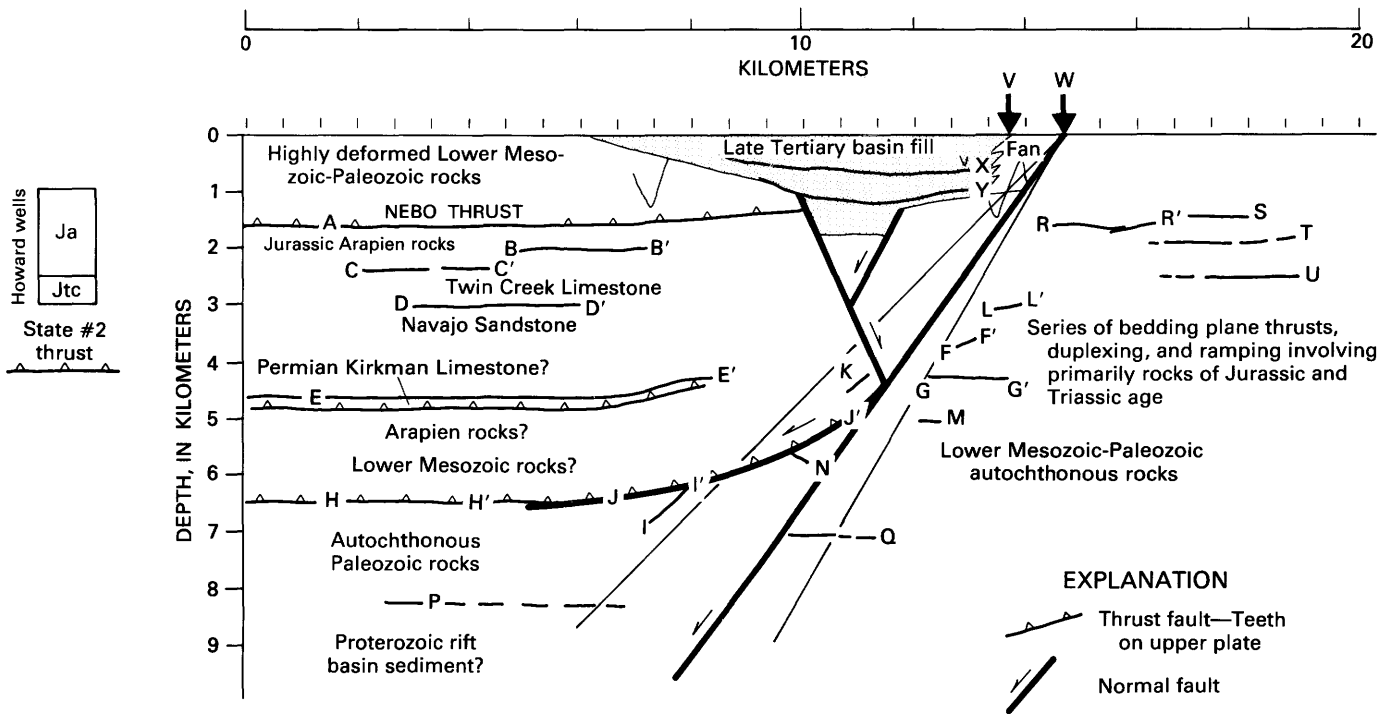

FIGURE 8.—Geologic interpretation of the western half of the true-depth line drawing shown in figure 5*B*. Heavy lines are seismic reflections. Inferred stratigraphic contacts are indicated.

that the diapirism may be a localized shallow phenomena rather than a major deep-seated feature.

GEOLOGIC INTERPRETATION OF DEEP STRUCTURE

One possible geologic interpretation of the subsurface structure on the western half of the seismic profile consistent with subsurface data and regional geologic structure is shown on the true-depth line drawing in figure 8 and described below. Reflector A and short west-dipping reflectors located just west of graben fault a (fig. 6) are interpreted to be the base of the Nebo thrust, which rests on the lower part of the Arapien section. The seismic profile is interpreted to obliquely cut the southern edge of the Nebo thrust near a ramp in the thrust inferred from surface exposures of the thrust just east of the Wasatch fault zone. As discussed earlier, none of the reflectors in this area display the westward dip expected for a thrust fault ramping up to the east; however, the younger eastward tilt of the Long Ridge-West Hills range no doubt complicates and obscures the earlier thrust geometry.

Reflectors B–B′, C–C′, and D–D′ are interpreted as stratigraphic boundaries, possibly within Arapien rocks or from the base of Arapien rocks resting on Jurassic-Triassic Navajo Sandstone. This interpretation is based in part on well data from the Howard #1–A and Howard #2 wells drilled 8 km south of the seismic line (figs. 1, 2). Both wells were positioned south of the southern edge of the Nebo thrust (Leamington tear fault) and were spud in Tertiary sedimentary rocks, drilled through Cretaceous synorogenic conglomerates into the Jurassic Arapien rocks (thicknesses of 2,082 and 1,977 m, respectively), and bottomed in Jurassic and Triassic rocks. The absolute depth range at which the Arapien rocks were encountered in these two wells is indicated on the left-hand side of figure 8. Sprinkel (1982) designated the lower 431 m of the Arapien section of Howard #1–A as the limestones of the Jurassic Twin Creek; he did not report on the data from Howard #2. Thus, interpretation of B–B′, C–C′, and D–D′ as being from within or from the base of the Jurassic rocks is consistent with the depth levels of Arapien rocks south of the Nebo thrust.

The State #2 well, located approximately 28 km south of the seismic line (fig. 1), was drilled through a thin section of Arapien rocks and apparently a complete section (1,383 m thick) of Jurassic-Triassic (Navajo Sandstone) and Triassic rocks testing on 672 m of Permian rocks (Diamond Creek Sandstone and Kirkman Limestone) (D.A. Sprinkel, oral commun., 1984). The Permian rocks were truncated by a thrust fault that emplaced the overlying rocks on the Navajo Sandstone. The absolute depth of this thrust of Permian over Jurassic-Triassic rocks was 2,542 m below sea level, which corresponds roughly to a depth (from the surface) along the seismic profile of about 4.15 km (see left-hand

side of fig. 8). Thus, if D–D′ is interpreted as the top of the Navajo Sandstone, then the prominent, nearly horizontal reflector E–E′ is in a similar position with respect to the Permian limestones encountered just above the thrust in State #2. Beneath the Cenozoic basin, reflector E–E′ begins to dip westward and is interpreted to be part of a ramp anticline above this inferred blind thrust fault. The blind thrust is shown as emplacing Permian on early Mesozoic, possibly Arapien rocks. The section between D–D′ and E–E′ is about 1.58 km thick, comparable to the 1.38-km-thick section of Jurassic-Triassic rocks beneath the Arapien rocks and above the Permian in State #2.

Reflectors H–H′ are interpreted as a deeper blind thrust that ramps up (J–J′) and possibly splays (K). Events I–I′ and N appear truncated by J–J′. The section beneath E–E′ and above H–H′ probably represents Jurassic and Triassic rocks; the section is probably not a complete section, however, because Standlee (1982) estimated a 1,702-m thickness of Arapien rocks alone beneath the Gunnison Plateau, and the State #2 well encountered an additional 1.38 km of Jurassic and Triassic rocks beneath the Arapien rocks. The impedance contrast at H–H′ is interpreted to be due to the thrust juxtaposition of lower Mesozoic rocks on Paleozoic limestones. The 1.8-km-thick section between H–H′ and P is interpreted as autochthonous Paleozoic rocks. A nearly complete section of autochthonous Paleozoic rocks (approximately 1,280 m thick) was drilled in U.S. E #1, located approximately 30 km east of the western end of the seismic line. Along most of its length, the Wasatch fault zone is close to and generally parallels the "Wasatch line" (Kay, 1951), the hinge line that marks the transition from shelf to basinal facies of the Cordillera geosyncline (that is, the zone of dramatic westward thickening of strata deposited on the late Precambrian rifted margin (Stewart, 1972). Thus, the 1,280 m encountered in U.S. E #1 probably represent a minimum thickness for the autochthonous Paleozoic rocks. H–H′ may mark a thrust occurring near the top of the Paleozoic section. Both of the inferred blind thrust faults (below E–E′ and H–H′) may be cut and offset by the Wasatch fault zone and may be correlative with the bedding plane thrust(s) inferred beneath the southern Wasatch Mountains just north of the seismic profile by Jefferson (1982) and Lawton (1985).

The band of reflectors defined by P are interpreted as late Proterozoic sediments. Thrust ramps have been interpreted near the location of the modern Wasatch fault in several localities (for example, Smith and Bruhn, 1984). These ramps may have developed over abrupt changes in basement geometry (that is, preexisting structural discontinuities). Specifically, it is proposed that the thrust ramps may have developed over west-dipping normal faults that formed during the initial Precambrian rifting event in the Precambrian crystalline basement. In this scenario, the reflectors marked by P may be sediments deposited in such a rift basin.

Well data along the westernmost edge of the Gunnison Plateau 25 km to the south (Gunnison #1, fig. 1, and other wells not shown) indicate a very complicated shallow structure beneath the plateau, including recumbent and overturned folds and numerous bedding-plane thrusts involving Arapien rocks and Jurassic-Triassic rocks (Standlee, 1982; Lawton, 1985). The possible thrust splay K and reflectors R–R′ and F–F′ may be related to such deformation.

Two possible subsurface geometries for the Wasatch fault zone are indicated in figure 8. The position and westward dip of reflectors E–E′ and J–J′ beneath the Cenozoic basin strongly suggest a listric geometry for the main Wasatch fault zone. In particular, reflection J–J′, which appears to flatten and merge with inferred blind thrust H–H′, is an excellent candidate for listric backsliding on a preexisting thrust. The symmetric, saglike geometry of the Cenozoic basin and, specifically, the lack of growth faulting and reverse drag (for example, Anderson and others, 1983) argue against such a sharply curved listric geometry (flattening at depths of only 4.5–6.5 km). The alternate interpretation—a planar dip of 54° for the main fault zone—is constrained by the eastern end of reflectors J–J′ and the western truncation of reflector Q. The synclinal saglike geometry of the basin is produced by beds dipping away from the boundary fault zone and appears related to the development of the small central graben. Analysis of a number of seismic reflection profiles in the Great Basin area led Anderson and others (1983) to suggest that the saglike geometry is commonly associated with a steep, relatively planar bounding-fault zone. Dixie Valley, Nev., is a well-documented example of such a basin and steep planar fault geometry (Okaya and Thompson, 1985). Microearthquake studies in central Utah also support a high-angle fault interpretation, indicative of seismic strain release on relatively steep (approximately 33°–90°) planes (Arabasz, 1983).

Distinguishing between the two alternate models for the Wasatch fault geometry is complicated by a possible earlier episode of extensional tectonism responsible for the 15° to 30° eastward tilt of the Oligocene volcanic and sedimentary rocks capping Long Ridge and West Hills. An inferred angular unconformity between these rocks and the oldest basin fill sediments on the western end of the seismic line (maximum dips of 20° E.) suggests possible listric or block-tilt faulting before the development of the modern basin. As mentioned earlier, the lack of eastward-tilted reflectors at depth may indicate a relatively shallow depth or a complex geometry for accommodation of this earlier tilting.

Both the listric and the planar fault models suggest a markedly asymmetric fault pattern for the development of Juab Valley. The west-dipping Wasatch fault zone is the master fault, and internal basin structure is related to formation of a central graben. There is a net topographic decrease across the Wasatch fault zone, as range heights on either side of Juab Valley indicate (range height is also moderated by bedrock lithology of the ranges). The elevation of Long Ridge (1,800–2,130 m) and West Hills (1,800–1,900 m) are 500 to 800 m lower than those of the southern Wasatch Mountains (2,440–3,600 m) and the Gunnison Plateau (2,440–2,700 m) east of the Wasatch fault zone. This net topographic offset could be accommodated by either the listric or the planar fault model.

DISCUSSION

It is apparent that there is no unique interpretation of the reflection section, despite constraints imposed by the gravity data and the high-resolution seismic profiling of Crone and Harding (1984). The complex and superposed Mesozoic and Cenozoic deformation as well as the lack of any drill-hole data along the profile permits only inferences on the subsurface thrust geometry. As noted above, if several of the reflectors are interpreted as thrust faults, simple listric backsliding on these faults fails to explain the basin fill geometry.

The steep-fault interpretation presented here contrasts with Smith and Bruhn's (1984) interpretation for the Wasatch fault zone 18 km to the south near Levan. From a Vibroseis profile across the fault near Levan (see fig. 2), Smith and Bruhn interpreted a planar fault zone having a 34° dip and penetrating only 5 km deep. Reverse drag and growth faulting are observed in the subsurface structure of the basin along their profile. Schwartz and Coppersmith (1984) inferred a segment boundary along the Wasatch fault zone between the two reflection profiles, allowing the possibility that both subsurface geometries might be correct and applicable to different major fault segments.

As described in the section on geologic setting, the Nebo thrust and a deeper thrust(s) within the study area may ramp up in the vicinity of the Wasatch fault zone. Smith and Bruhn (1984) concluded that, along several of the segments (including the segment in the study area), the Wasatch fault zone is located above inferred west-dipping Sevier thrust fault ramps. They suggested that, along several segments, the Wasatch fault may overlie and utilize the thrust fault ramps and merge with subhorizontal thrusts at depth. This conceptual model strongly influenced their and Standlee's (1982) interpretations of the subsurface geometry of the Wasatch fault zone for the Levan seismic profile mentioned above.

As Smith and Bruhn suggested, the general correlation between the Wasatch fault zone and the inferred thrust ramps in the subsurface can be used to argue for a relationship between the location of late Cenozoic normal faults and the geometry of older thrust faults. Alternatively, an even older structure may have controlled the development of both the thrust ramps and the Wasatch fault zone. The location of thrust fault ramps can be controlled by facies changes along the decollement horizon or by interruptions of the decollement by basement offsets such as normal fault zones (Suppe, 1985, p. 282). It is suggested here that west-dipping normal fault zones that formed in the Precambrian crystalline basement during the early phases (pre-drift) of Precambrian rifting (Stewart, 1972) may have provided the structural relief responsible for the formation of the thrust ramps.

The modern passive margin along the Atlantic coast of the United States contains numerous examples of major Triassic basins that formed on the shelf near the contemporary hinge line (for example, Klitgord and Behrendt, 1979; Hutchinson and others, 1986). Since the Wasatch fault zone developed near the Paleozoic hinge line, similar Precambrian rift basins may be located at depth near the trace of the modern Wasatch fault. Interestingly, the lengths of these Atlantic shelf basins are similar to the length of the basin structure along the modern Wasatch fault. Hence, it is suggested here that the location of both the thrust ramps and the modern Wasatch fault ultimately may have been controlled by the location of a Precambrian normal fault zone bounding a basin or series of rift basins along the developing continental shelf.

Wheeler and Krystinik (1988) independently suggested that Precambrian extensional faults may help localize the Wasatch fault zone and control its geometry. They discussed geologic and stratigraphic data that suggest the presence of these late Precambrian normal faults and cited several examples of reactivation of such subthrust faults. The critical test of this hypothesis would be the identification of the sedimentary sections filling the basins of Late Precambrian-early Paleozoic age that were bounded by these faults. Unfortunately, the thick cover of Mesozoic thrust sheets has deeply buried these basins, and, as is obvious from the present study, the complex superposed Mesozoic and late Cenozoic structure makes it difficult to identify these older, deeper structures. The identification here of reflector P as a sequence of Proterozoic sediments is purely speculative and intended to provoke further studies.

CONCLUSIONS

Seismic reflection and gravity data suggest that the overall structure of Juab Valley near the town of Nephi

is an asymmetric sag, in which beds on both sides of the valley tilt toward the axis of the valley. A central graben defines the deepest part of the basin. Anderson and others (1983) and Zoback and Anderson (1983) have identified this type of basin as commonly being bounded by one or more major, planar, steep normal faults. The maximum valley fill thickness is about 1.60 km, on the basis of interpretation of both the reflection and gravity data (if a density contrast for basin sediments of -0.4 g/cm^3 is assumed). Possible displacement of a buried thrust(s), truncation of deep reflectors, and the absence of reverse drag in basin sediments suggest that the Wasatch fault zone has a planar, high-angle dip of 50° to 55° (as opposed to a listric or low-angle geometry). However, the lack of reverse drag within basin sediments is the strongest evidence against a listric geometry.

On a more regional note, structural data suggest the presence of major ramps in the Mesozoic thrust system near the trace of the modern Wasatch fault at several localities along its length. One possible source for this ramping may be major basement displacements on normal faults formed along a north-trending, west-facing passive margin that developed through the region in Late Proterozoic time (Stewart, 1972). Thus, the Wasatch fault zone may be localized by a zone of preexisting extensional faulting in Precambrian crystalline rocks.

REFERENCES CITED

Anderson, R.E., Zoback, M.L., and Thompson, G.A., 1983, Implication of selected subsurface data on the structural form and evolution of some basins in the northern Basin and Range Province, Nevada and Utah: Geological Society of America Bulletin, v. 94, p. 1055–1072.

Arabasz, W.J., 1983, Geometry of active faults and seismic deformation within the Basin and Range-Colorado Plateau transition, central and SW Utah: Earthquake Notes, v. 54, no. 1, p. 48.

Black, B.A., 1965, Nebo overthrust, southern Wasatch Mountains, Utah: Brigham Young University Geology Studies, v. 12, p. 55–89.

Brown, R.P., and Cook, K.L., 1982, A regional gravity of the Sanpete-Sevier Valley and adjacent areas in Utah, *in* Nielson, D.L., ed., Overthrust belt of Utah: Utah Geological Association Publication 10, p. 121–136.

Burchfiel, B.C., and Hickcox, C.W., 1972, Structural development of central Utah, *in* Baer, J.L., and Callaghan, E., eds., Plateau-Basin and Range transition zone, central Utah: Utah Geological Association Publication 2, p. 55–66.

Cluff, L.S., Brogan, G.E., and Glass, E.E., 1973, Wasatch fault, southern portion, earthquake fault investigation and evaluation—A guide for land use planning: Oakland, Calif., report prepared by Woodward-Lundgren Associates for Utah Geological and Mineralogical Survey under Project G-12069A, 33 p.

Crittenden, M.D., Jr., 1961, Magnitude of thrust faulting in northern Utah: U.S. Geological Survey Professional Paper 424-D, p. D128–D131.

Crone, A.J., and Harding, S.T., 1984, Near-surface faulting associated with Holocene fault scarps, Wasatch fault zone, Utah—A preliminary report, *in* Hays, W.W., and Gori, P.L., eds., Proceedings of Conference XXVI; a workshop on Evaluation of regional and urban earthquake hazards and risk in Utah: U.S. Geological Survey Open-File Report 84-763, p. 241–265.

Gilliland, W.N., 1963, Sanpete-Sevier Valley anticline of central Utah: Geological Society of America Bulletin, v. 74, p. 115–124.

Hardy, C.T., 1952, Eastern Sevier Valley, Sevier and Sanpete Counties, Utah, with reference to formations of Jurassic age: Utah Geological and Mineral Survey Bulletin 43, 98 p.

Heller, P.L., Bowdler, S.S., Chambers, H.P., Coogan, J.C., Hagen, E.S., Shuster, M.W., Winslow, N.S., and Lawton, T.F., 1986, Time of initial thrusting in the Sevier orogenic belt, Idaho-Wyoming and Utah: Geology, v. 14, p. 388–391.

Hutchinson, D.R., Klitgord, K.D., and Detrick, R.S., 1986, Rift basins of the Long Island platform: Geological Society of America Bulletin, v. 97, p. 688–702.

Jefferson, W.S., 1982, Structural and stratigraphic relations of Upper Cretaceous to Lower Tertiary orogenic sediments in the Cedar Hills, Utah: Utah Geological Association Publication 10, p. 65–80.

Jones, T.D., and Nur, A., 1984, The nature of seismic reflections from deep crustal fault zones: Journal of Geophysical Research, v. 89, no. B5, p. 3153–3171.

Kay, M., 1951, North American geosynclines: Geological Society of America Memoir 48, 143 p.

Klitgord, K.D., and Behrendt, J.C., 1979, Basin structure of the U.S. Atlantic margin, *in* Watkins, J.S., Montadert, L., and Dickerson, P.W., eds., Geological and geophysical investigations of continental margins: American Association of Petroleum Geologists Memoir 29, p. 85–112.

Lawton, T.F., 1982, Lithofacies correlations within the Upper Cretaceous Indianola Group, central Utah, *in* Nielson, D.L., ed., Overthrust belt of Utah: Utah Geological Association Publication 10, p. 199–213.

———1985, Style and timing of frontal structures, thrust belt, central Utah: Bulletin of the American Association of Petroleum Geologists Bulletin, v. 69, p. 1145–1159.

Morris, H.T., 1983, Interrelations of thrust and transcurrent faults in the central Sevier orogenic belt near Leamington, Utah, *in* Miller, D.M., Todd, V.R., and Howard, K.A., eds., Tectonic and stratigraphic studies in the Eastern Great Basin: Geological Society of America Memoir 157, p. 75–82.

Okaya, D.A., and Thompson, G.A., 1985, Geometry of Cenozoic extensional faulting: Dixie Valley, Nevada: Tectonics, v. 4, p. 107–126.

Schwartz, D.P., and Coppersmith, K.J., 1984, Fault behavior and characteristic earthquakes: Examples from the Wasatch and San Andreas fault zones: Journal of Geophysical Research, v. 89, no. B7, p. 5681–5698.

Smith, R.B., and Bruhn, R.L., 1984, Intraplate extensional tectonics of the eastern Basin-Range: Inferences on structural style from seismic reflection data, regional tectonics, and thermal-mechanical models of brittle-ductile deformation: Journal of Geophysical Research, v. 89, no. B7, p. 5733–5762.

Spieker, E.M., 1946, Late Mesozoic and early Cenozoic history of central Utah: U.S. Geological Survey Professional Paper 205-D, p. D117–D161.

Sprinkel, D.A., 1982, Twin Creek Limestone-Arapien Shale relations in central Utah, *in* Nielson, D.L., ed., Overthrust belt of Utah: Utah Geological Association Publication 10, p. 169–180.

Standlee, L.A., 1982, Structure and stratigraphy of Jurassic rocks in central Utah: Their influence on tectonic development of the Cordilleran foreland thrust belt, *in* Powers, R.B., ed., Geologic

studies of the Cordilleran thrust belt: Denver, Colo., Rocky Mountain Association of Geologists, p. 357–382.

Stewart, J.H., 1972, Initial deposits in the Cordilleran geosyncline: Evidence of a Late Precambrian (850 m.y.) continental separation: Geological Society of American Bulletin, v. 83, p. 1345–1360.

Stewart, J.H., and Poole, F.G., 1974, Lower Paleozoic and uppermost Precambrian Cordilleran Miogeocline, Great Basin, western United States, *in* Dickinson, W.R., ed., Tectonics and sedimentation: Society of Economic Paleontologists and Mineralogists Special Publication 22, p. 28–57.

Suppe, J., 1985, Principles of structural geology: Englewood Cliffs, N.J., Prentice-Hall, 537 p.

Wallace, R.E., and Morris, H.T., 1979, Characteristics of fault and shear zones as seen in mines at depths as much as 2.5 km below the surface, *in* Speed, R., and Sharp, R., co-organizers, and Evernden, J.F., convenor, Proceedings of Conference VIII—Analysis of actual fault zones in bedrock: U.S. Geological Survey Open-File Report 79–1239, 599 p.

Wheeler, R.L., and Krystinik, K.B., 1988, Segmentation of the Wasatch fault zone, Utah—Summaries, analyses, and interpretations of geological and geophysical data: U.S. Geological Survey Bulletin 1827, 47 p.

Witkind, I.J., 1982, Salt diapirism in central Utah, *in* Nielson, D.L., ed., Overthrust belt of Utah: Utah Geological Association Publication 10, p. 13–30.

———1983, Overthrusts and salt diapirs, central Utah: Geological Society of America Memoir 157, p. 45–59.

Zoback, M.L., 1983, Structure and Cenozoic tectonism along the Wasatch fault zone, Utah: Geological Society of America Memoir 157, p. 3–27.

Zoback, M.L., and Anderson, R.E., 1983, Style of Basin-Range faulting as inferred from seismic reflection data in the Great Basin, Nevada and Utah: Geothermal Resources Council Special Report 13, p. 363–381.

Neotectonic Framework of the Central Sevier Valley Area, Utah, and Its Relationship to Seismicity

By R. ERNEST ANDERSON *and* THEODORE P. BARNHARD

ASSESSMENT OF REGIONAL EARTHQUAKE HAZARDS AND RISK ALONG THE WASATCH FRONT, UTAH

U.S. GEOLOGICAL SURVEY PROFESSIONAL PAPER 1500–F

CONTENTS

	Page
Abstract	F1
Introduction	2
Acknowledgments	6
Procedure	6
Structural History and Setting	7
Results from Fault-Slip Sample Areas	10
Clear Creek Downwarp	10
Pavant Range	18
Joseph Flats to Richfield	18
Richfield to Willow Creek	20
Sevier Fault	21
Monroe Segment	23
Results from Fault-Slip Sample Areas—Continued	
Sevier Fault—Continued	
Annabella Segment	F25
Anticline Sample	29
Northern Antelope Range	30
Seismicity and Late Quaternary Deformation	32
Northeast of Annabella	34
Southwest of Elsinore	37
Summary and Discussion	40
Role of Diapirism	44
Speculations on Crustal-Scale Deformation	44
References Cited	45

ILLUSTRATIONS

		Page
FIGURE	1. Index map showing location of the central Sevier Valley study area relative to the structural transition zone and bordering provinces	F2
	2. Map showing distribution of earthquake epicenters in Utah for the period July 1962 through September 1984	3
	3. Geologic map and section of the central Sevier Valley area	4
	4. Generalized stratigraphic column for the central Sevier Valley area	6
	5–8. Photographs showing:	
	5. Dry Wash fault	11
	6. View to the northwest from Dry Wash fault across Clear Creek to the trace of the sinistral strike-slip fault	12
	7. Northeast-trending sinistral-slip fault shown in figure 6	13
	8. Well-exposed, large, smooth, striated surface of small sinistral-slip fault in the Joe Lot Tuff Member of the Mount Belknap Volcanics	14
	9. Schematic representation in block diagram form showing a fold cut by a sinistral fault and two dextral faults	14
	10. Histograms of strike, dip, and rake and lower hemisphere stereographic plots of computed paleostress axes for faults from the Clear Creek sample area in the easternmost part of the Clear Creek downwarp	15
	11. Photograph looking northwest at the excavated surface of a steep planar fault that cuts transversely through northeast-tilted beds of the Sevier River Formation at locality A in figure 3	15
	12. Lower hemisphere stereographic plot of the main fault and 16 subsidiary northeast-trending faults at locality A in figure 3	16
	13. Photograph showing view looking north along the well-exposed Joe Lott Tuff Member of the Mount Belknap Volcanics in the footwall of a north-northwest-striking normal fault at locality B in figure 3	16
	14. Lower hemisphere plots of fault-slip and bedding data at localities along Interstates 70 and 15	17
	15. Histograms of strike, dip, rake, and sense of fault slip for faults along the southeastern margin of the Pavant Range between Joseph Flats and Richfield	19
	16. Photograph showing west-looking view in Flat Canyon north of Elsinore showing the offset contact between smooth- and rough-weathering beds of gently southwest-dipping sandstone, siltstone, and claystone belonging to the formation of Aurora of late Eocene age	20
	17. Lower hemisphere stereographic plot of poles to bedding along the flank of the Pavant Range between Joseph Flats and Richfield	20
	18. Map showing generalized geology of the northwestern part of the Aurora 7½-min quadrangle	22
	19. Cross-sectional sketch showing the typical fault offsets seen in the monoclinally flexed margin of the Pavant Range	23

Page

FIGURE 20. Histograms of strike, dip, and rake, lower hemisphere stereographic plot of faults, striae, and computed paleostress axes, and plot of slip sense for faults along the eastern margin of the Pavant Range between Richfield and Willow Creek F24
21. Histograms of strike, dip, and rake, lower hemisphere stereographic plots of computed paleostress axes, and plot of dip-slip versus strike-slip components of fault slip for faults in the western margin of the Sevier Plateau in the Monroe area 25
22. Lower hemisphere plot of poles to bedding in bedrock along the Annabella segment of the Sevier fault 26
23. Geologic map and cross section of the Annabella-Glenwood area 27
24. Histograms of faults and striations from Tertiary volcanic and sedimentary rocks along the Annabella segment of the Sevier fault (Annabella sample area) 28
25. Lower hemisphere stereographic plot of a subsample of predominantly strike-slip faults derived from the sample shown in figure 24*A* 29
26. Histograms of faults and striations from the Tertiary cover rocks of the Sanpete-Sevier anticline (anticline sample) 31
27. Stereographic plots of faults that cut Tertiary rocks at or above the contact with the mechanically weak Arapien Formation along the southern part of the Sanpete-Sevier anticline 32
28. Histograms of strike, dip, and rake and plot of dip-slip versus strike-slip components of fault slip for faults in the northern part of the Antelope Range 33
29. Photograph showing west-looking view at the surface trace of a high-angle fault in the Antelope Range at locality F in figure 3 33
30. Map and diagrams showing aspects of seismicity in the transition zone 34
31. Photograph looking south across the northeast-trending main strand of the Sevier fault toward the Glenwood Mountain part of the western Sevier Plateau 36
32. Profiles across scarps formed on late Quaternary alluvium and debris flows in the Annabella area 37
33. Diagrams showing spatial distributions of aftershock foci in the Annabella area and focal mechanisms for the 1982 magnitude 4.0 main shock and magnitude 2.7 aftershock 38
34. Geologic map showing south-central part of the Monroe Northwest 7½-min quadrangle showing geology by Steven (1979), modified and augmented in the present study 39
35. Photograph looking south and showing terraces that have progressively greater height and greater eastward tilts with greater age 40
36. Drawing showing channel pattern of the Sevier River between Joseph and Elsinore in relationship to an axis of relative uplift and hypothetical model of the time-sequential response of the slope and channel pattern to uplift across the course of a mixed-load meandering river 41
37. Map showing structural characterizations of the central Sevier Valley area 42

TABLE

Page

TABLE 1. Fault-slip data and computational results F8

ASSESSMENT OF REGIONAL EARTHQUAKE HAZARDS
AND RISK ALONG THE WASATCH FRONT, UTAH

NEOTECTONIC FRAMEWORK OF THE CENTRAL SEVIER VALLEY AREA, UTAH, AND ITS RELATIONSHIP TO SEISMICITY

By R. Ernest Anderson and Theodore P. Barnhard

ABSTRACT

The central Sevier Valley is one of the most seismically active parts of the Intermountain Seismic Belt. Two areas of concentrated seismicity in the valley coinciding with anomalous concentrations of late Quaternary deformation suggest a genetic relationship. Both areas contain late Quaternary fault scarps suggestive of normal faulting and microseismicity suggestive of strike-slip faulting, and each is broadly consistent with east-west extension. Both areas are located at complex structural junctures where the geometries and vergence directions of major structures show dramatic on-strike contrast. Transverse zones of structural accommodation in which stress is likely to be concentrated are required in both areas and probably explain the concentration of seismicity and late Quaternary deformation. Strain rates, faulting histories, rupture lengths, and other deformational aspects of these zones that might be relevant to earthquake hazards assessments are not characteristic of the major structures that extend away from them and are therefore of little value in regional assessments. Geologic mapping and detailed fault-slip studies of areas directly adjacent to the areas of concentrated seismicity show that the youngest deformation is dominated by strike-slip faulting and associated folding of apparent compressional origin in one area, by extreme extension and structural attenuation in another area, and by mixtures of strike-slip and normal faulting with or without monoclinal flexuring in still other areas. Thus, the areas of concentrated seismicity not only are localized at complex structural junctures but also are surrounded by complexly variable neotectonic structures.

Major features of the seismicity include (1) a mixture of strike-slip and normal faulting focal mechanisms in the transition zone; (2) a predominance of strike-slip microseismal focal mechanisms having a conspicuous element of slip incompatibility, the P axes of some mechanisms being parallel to the T axes of others; and (3) hypocenter frequencies that fall off sharply at depths of 5 to 6 km and thus suggest deformation above planes of structural compensation. To explain the mechanics and kinematics of neotectonic deformation in the central Sevier Valley and the way in which that deformation relates to the neotectonic framework of the region requires not only the integration of these major features of the seismicity but also the integration of an extremely varied and complex group of structures, including folds of contrasting orientation and conjugate, nonconjugate, and incompatible types of strike-slip faults, normal faults, mixtures of normal and strike-slip faults, and known or inferred attenuation-type detachment faults. These structures must be understood in the contextual framework of an extensional tectonic regime superposed on an area characterized by a long and complex history of earlier deformation and a strong preexisting northeast-trending structural fabric. Although it would appear impossible to develop a tectonic model capable of explaining all these complexities, one model does seem to satisfy most. The five critical elements of this model are as follows:

1. Extensional deformation in which σ_3 is oriented approximately east-west is distributed very unevenly in space and ranges in magnitude from extreme local attenuation to mountain-sized blocks having less than 5 percent internal extension.
2. Either complementary to or in competition with the extension is an element of lateral tectonic transport resulting either from interchanges in the position of σ_1 and σ_2 or from shear tractions applied to the base of structural blocks at a high angle to the direction of extension (aproximately north-south).
3. There is a strong element of strain gathering by preexisting steeply dipping northeast-trending zones of structural weakness and by gently dipping mechanically weak clay-rich or evaporite-rich strata or preexisting thrust faults. The former results in zones of concentrated extension or strike-slip faulting and the latter in detachment or decoupling of the internally deformed plates.
4. Mechanically resistant structural entities such as the Marysvale volcanic pile and its plutonic root interfere with and produce internal deformation within laterally migrating thin-skinned structural plates.
5. Facing monoclinal folds of the type bordering the Sevier Valley result from extension superposed on lateral shear and resemble divergent strike-slip and oblique-slip mobile zones.

The inferred structural style of extension applied to laterally displaced blocks bounded by strike-slip faults and driven by tractions or drag on their basal detachments is consistent with seismic evidence for strike-slip faulting, slip incompatibility, and hypocenters above distinct planes of structural compensation. Because the deformational style is basically thin-skinned detachment, the potential for large earthquakes on faults in the upper plate is low. Our recognition that some of the largest and youngest exposed faults in the area are strike-slip faults does not significantly increase seismic hazard above what would be estimated for normal faults. Normal faults such as the Sevier fault, because they bound 15- to 20-km-wide blocks that are uniformly tilted, probably cut one or more levels of potential structural detachment and penetrate to the base of the seismogenic part of the crust. Such faults

Manuscript approved for publication November 20, 1990.

are more likely to be the source of infrequent large earthquakes than are faults in the complex structural junctures where late Quaternary deformation is concentrated.

INTRODUCTION

The central Sevier Valley study area is located in the High Plateaus of the Utah section of the Colorado Plateaus in a structural and physiographic transition zone between the Basin and Range on the west and the Colorado Plateaus on the east (fig. 1). The area straddles the Intermountain Seismic Belt, as figure 2 shows. Although most of the study is focused in the central Sevier Valley, the study extends westward to Dog Valley (fig. 3).

This report has a threefold purpose: (1) to present the results of a study of fault-slip characteristics and associated folding in the central Sevier Valley area, (2) to interpret those results in the context of the diverse structural history and historical earthquake record of the region, and (3) to evaluate their relevance to the neotectonic framework and their impact on earthquake hazards. The initial intent of the investigation was to search for geologic evidence of strike-slip faulting in areas where W.J. Arabasz and his students from the University of Utah had provided us with advance reports of earthquakes having a strike-slip mode. The search was successful, and it is now clear that the geologic record contains abundant evidence of Neogene and Quaternary strike-slip faulting in the region. The success of our search (Anderson and Barnhard, 1984a, b) led us to expand the scope of our investigation to include a synthesis of Pliocene and Pleistocene deformation in the area. The range margins along the central Sevier Valley were examined for geologic evidence of late Tertiary and Quaternary deformation, and we herein integrate those findings with our earlier results.

Fault-slip data were collected from parts of the Pavant Range, the Tushar Mountains, the Antelope Range, the Sevier Plateau, and the Sanpete-Sevier anticline, all of which flank the Sevier Valley (fig. 3). The comprehensiveness of our investigation varies greatly from area to area. Accordingly, only a general description of fault slip is given for some areas, quantitative fault orientation and fault-slip data are given for other areas, and a comprehensive account of paleoslip and, where the data are sufficiently coherent, the results of paleostress analysis are given for still other areas. Only from the Clear Creek area do the fault-slip data provide paleostress results that can be confidently related to mapped structural patterns. However, data from the other areas provide valuable insight into the distribution of strike-slip faulting as well as an opportunity for qualitative comparison with the results from the Clear Creek area.

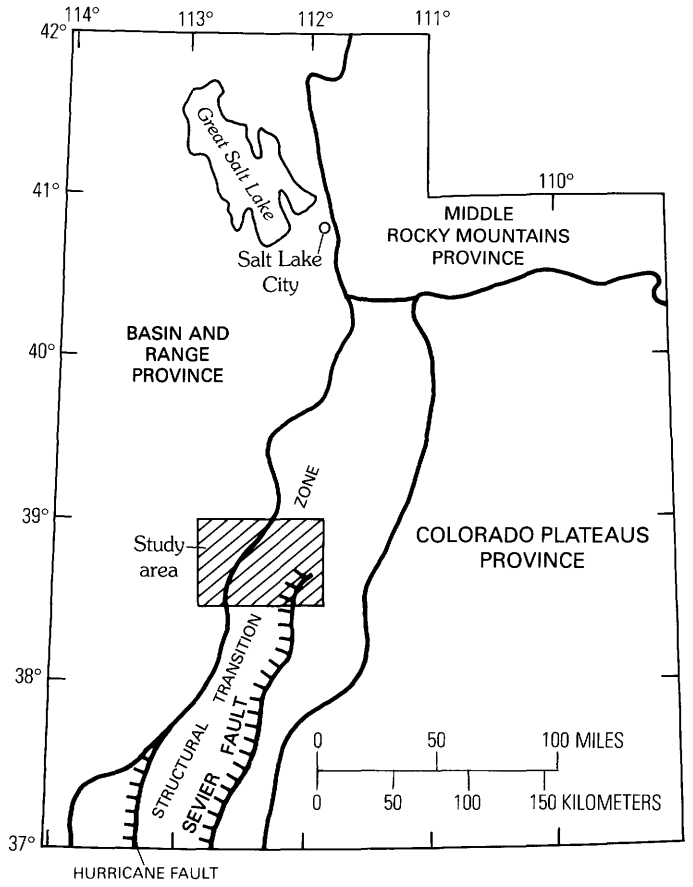

FIGURE 1.—Location of the central Sevier Valley study area relative to the structural transition zone and bordering provinces. The Hurricane and Sevier faults are shown by hachures on the downthrown sides.

A long and complex structural history has been recognized in the study area. It includes compressional thrusting and folding and related foreland deposition ranging in age from latest Jurassic to Paleocene (Standlee, 1982), block uplift and basin formation of Paleocene and Eocene age (Stanley and Collinson, 1979), igneous activity and associated intense volcano-tectonic activity of Oligocene and Miocene age (Rowley and others, 1979), basin development and associated sedimentation of late Miocene age (Callaghan and Parker, 1962; Rowley and others, 1979), and Pliocene and Pleistocene deformation, volcanism, and landsliding that have shaped some of the most conspicuous structural and physiographic features of the area. Although it is the last part of this structural history that is of central importance to this study, the possible influence of old structures on young structures must be considered. We therefore include a section on structural history and setting in which we review what is known about the early deformations, especially those events that left a major imprint on the structural fabric of the area. We do not discuss the stratigraphy or provide

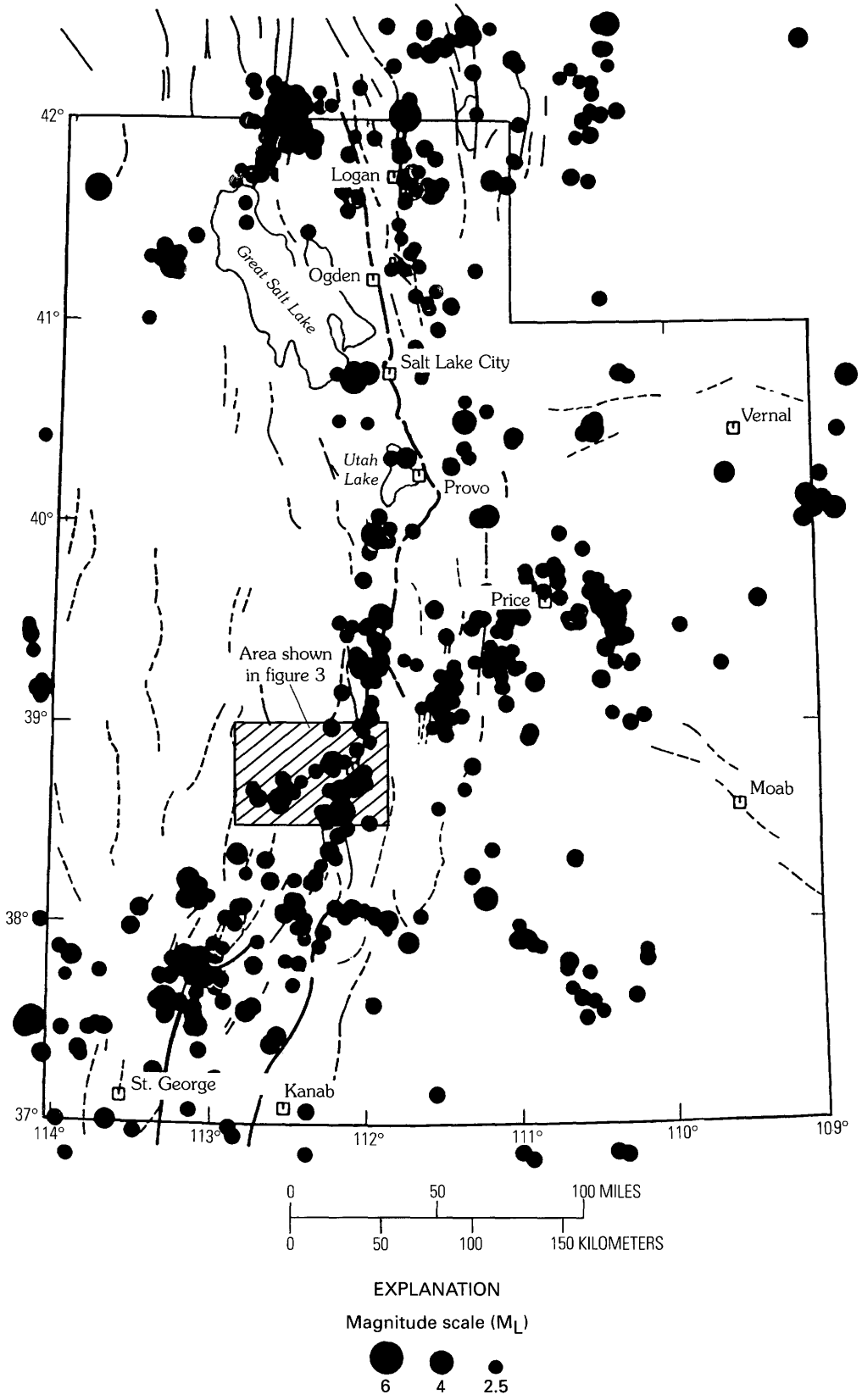

FIGURE 2.—Distribution of earthquake epicenters in Utah for the period July 1962 through September 1984 (from Smith and Richins, 1984). The central north-south zone of abundant seismicity is called the Intermountain Seismic Belt.

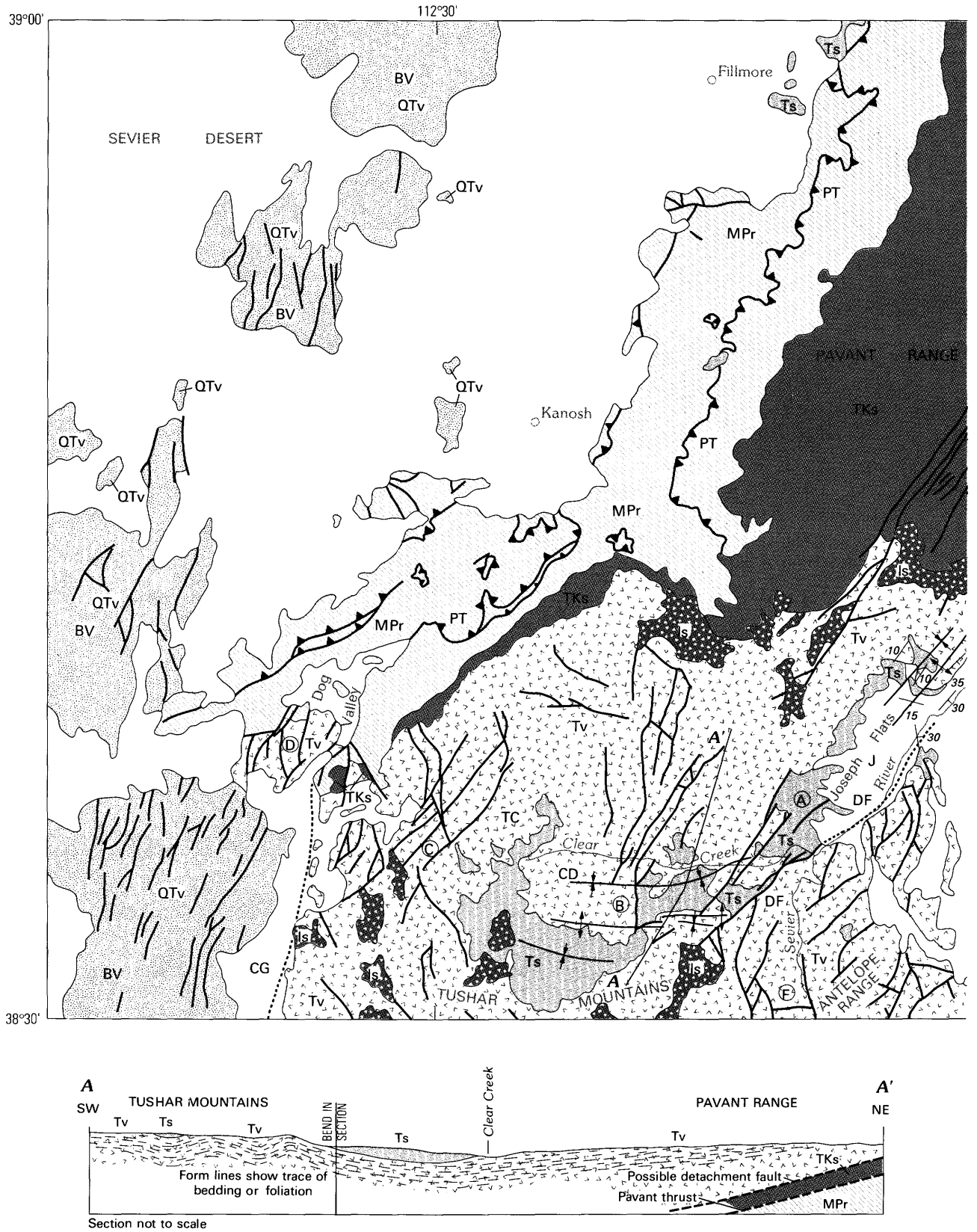

FIGURE 3.—Geology and section of the central Sevier Valley area, after Cunningham and others (1983), Steven and Morris (1983b), and Williams and Hackman (1971). BV, Black Rock volcanic field; CD, Clear Creek downwarp; CG, Cove Fort graben; DF, Dry Wash fault; MC, Monroe Peak caldera; PT, Pavant thrust; SA, Sanpete-Sevier Valley anticline; EF, Elsinore fault; SF, Sevier fault; TC, Three Creeks caldera; J, Joseph; BCH, Bull Claim Hills; TL, Thompson Creek landslide. Circled letters are localities referred to in the text.

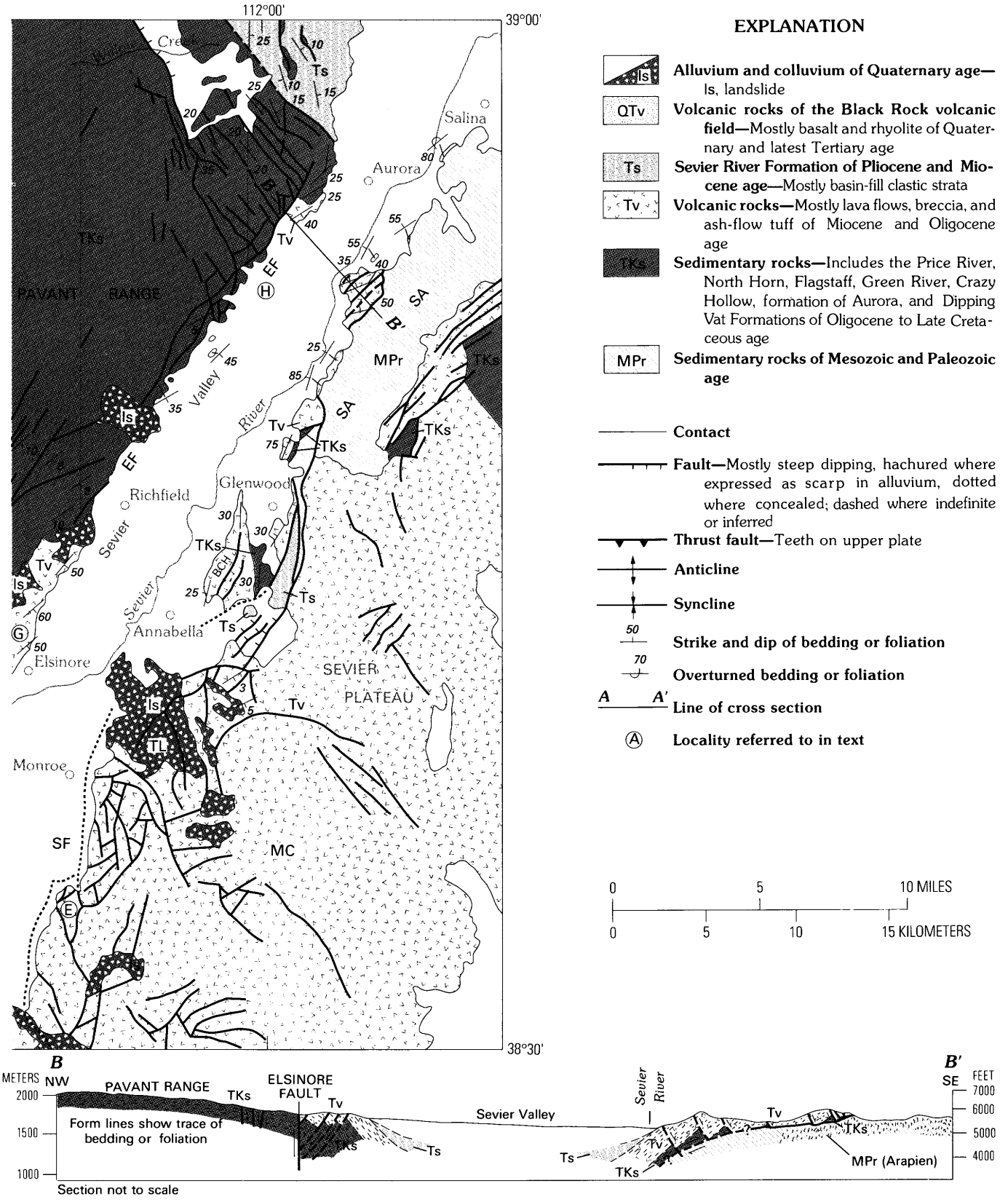

FIGURE 3.—Continued.

detailed information about the lithology of the deformed rocks. The stratigraphic sequence is summarized in figure 4.

ACKNOWLEDGMENTS

We are grateful to Walter Arabasz (University of Utah) for providing us with prepublication drafts of reports in which the ocurrence of strike-slip focal mechanisms in cental Sevier Valley was highlighted and for taking the time to visit us in the field. Field visits by Grant Willis (Utah Geological and Mineral Survey) and Peter Rowley (U.S. Geological Survey) helped us to understand some stratigraphic relationships. We thank Jacques Angelier (University of Paris) for providing us with computer programs for paleostress analysis, Mary Lou Zoback (U.S. Geological Survey) for help in using the programs, and Steve Harmsen (U.S. Geological Survey) for help in developing computer graphics. The report was improved substantally as a result of critical reviews by Dwight Schmidt and Peter Rowley (U.S. Geological Survey) and Grant Willis (Utah Geological Survey).

PROCEDURE

Field procedure for this study consisted of measuring the orientations of fault surfaces and movement-related striae on those surfaces and determining the sense of slip for motions parallel to those striae. These fault measurements were made in specific small sample areas within the Sevier Valley study area. Each sample area is either named for a nearby geographic locality or identified by a locality letter (fig. 3). In the absence of evidence to the contrary, the striae are assumed to represent the youngest deformation on a fault. On some faults, polyphase slip is indicated by two or more sets of striae; for some of these sets, it is possible to determine their sequence of development. The sequential aspects of faulting also can be determined by studying fault intersections or by inferring the angular relationship between faults of contrasting orientation and slip and the directions of bedding tilt. The data are classified according to the displacement amount and the certainty with which the sense of slip was determined. Data analysis consists of a preliminary separation into faulting mode; faults whose rake angles exceed 45° are separated into a dip-slip mode, and those whose rake angles are less than 45° are separated into a strike-slip mode. For most data sets, oblique-slip faults are relatively uncommon, so computations can be performed without separate treatment. Paleostress orientations and various paleostress parameters are computed by using methods similar to those described by Angelier (1979) and are performed on data representing both strike-slip and dip-slip modes.

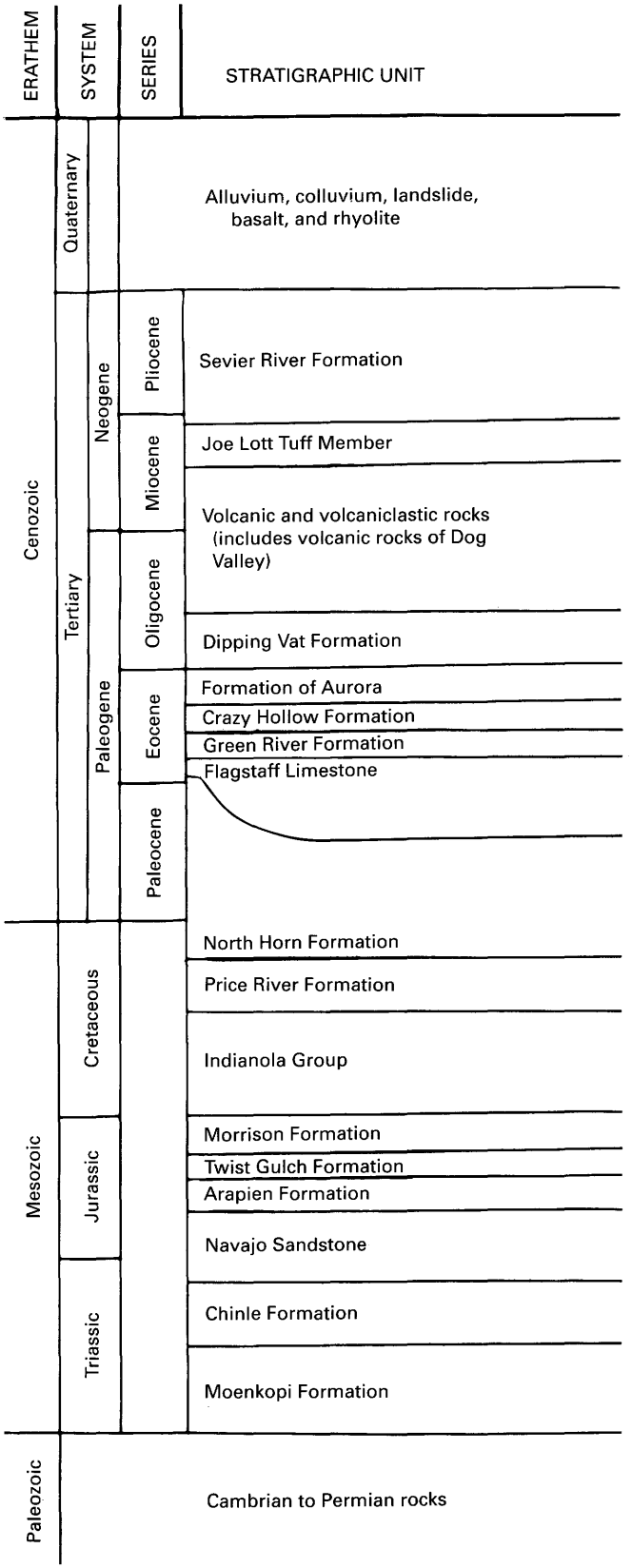

FIGURE 4.—Generalized stratigraphic column for the central Sevier Valley area.

Displacement amount in this report is classified as follows. Small-displacement faults have known or estimated offsets ranging from a few centimeters to a few meters, and large-displacement faults have known or inferred displacements greater than 30 m; the remainder are referred to as intermediate-displacement faults. Many of the large- and intermediate-displacement faults are shown in figure 3; small-displacement faults cannot be shown at the scale of figure 3. In each of the sample areas investigated, we attempted to determine the orientation and sense of slip on mapped faults. This strategy leads inevitably to gathering large amounts of data from small faults having small displacement; this report is based in large part on data from such faults.

Three large-displacement north- to northeast-striking faults were previously named and interpreted as normal faults—the Sevier, Dry Wash, and Elsinore faults (Callaghan and Parker, 1961, 1962; Cunningham and others, 1983). Of these, only the Sevier and Dry Wash faults are shown in figure 3. Except for the southern part of the Dry Wash fault, these two faults are buried by range-flanking alluvium. The strategy used to evaluate the slip characteristics of the large-displacement faults was to search for clues on small- and intermediate-scale faults in the bedrock adjacent to the large faults.

Large-displacement faults in a sample area possibly reflect stress states of a different vintage, a more fundamental rank or order, more regional extent, or a more deeply penetrating tectonic realm than do small-displacement faults. Because of these possibilities, in each sample area where paleostress studies are conducted, small-displacement faults must be determined to have orientations and slip characteristics similar to those of large-displacement faults. To make this determination, two separate computations are generally performed—one on the raw data and one on data that are weighted according to the amount of displacement on each fault as described by Angelier and others (1985). The numerical weights given in table 1 represent a crudely logarithmic scale from 1 to 9, category 1 displacements being less than 10 cm or unknown and category 9 displacements being greater than 100 m. Because exposures of large faults are uncommon in nature, most data sets reported herein consist only of small-displacement faults or contain a very small sample of larger faults; thus, a direct evaluation of the effect of fault size on paleostress is precluded. As an exception, however, slip data gathered from many moderate- and large-displacement faults in the Clear Creek area provide an excellent opportunity to test for the effect of fault size on paleostress. The test shows no significant shift in the position of the paleostress axes or the quality of the limited tensor (table 1). Paleostress computations using data from sample areas where only small faults were found yield results similar to those obtained by using the Clear Creek data, the suggestion being that fault size is not an important factor in determining paleostress in the central Sevier Valley study area.

STRUCTURAL HISTORY AND SETTING

The oldest structural feature in the study area is the Cordilleran hinge line that separates upper Proterozoic to Triassic Cordilleran miogeoclinal rocks on the west from platform facies rocks on the east (Armstrong, 1968; Burchfiel and Hickcox, 1972). Although the hinge, probably initially a zone several tens of kilometers wide, is tectonically and depositionally covered in the study area by thrusts and sediments, it probably trended northeast through the area and could have exerted a control on subsequent fold and thrust structures. Deposition in the miogeocline was interrupted by compressional deformation of the Sevier orogeny possibly as early as latest Jurassic and extending through Late Cretaceous (Campanian) (Armstrong, 1968). The northeast-trending Pavant thrusts shown in the western part of the Pavant Range (fig. 3) were formed during this compressional deformation. The principal compressional structure is a thrust-faulted recumbent fold formed in the Paleozoic miogeoclinal or shelf carbonate rocks and Mesozoic clastic rocks. Associated tear faults suggest thrusting to the southeast (Davis, 1982). A total of 10 km of displacement is inferred for the exposed thrusts (Baer and others, 1982). A buried thrust of unknown displacement beneath the Pavant thrust at a depth of 4 to 5 km is inferred from seismic reflection data referred to by Arabasz and Julander (1986). On the basis of drill-hole data, thrusts and folds that developed during the Sevier orogeny are interpreted to extend east of the Pavant Range beneath the Sevier Valley and probably beneath the northernmost Sevier Plateau (Standlee, 1982). They may also extend southward beneath the thick volcanic cover of the Tushar Mountains, but that possibility is less certain (Richard Kennedy, oral commun., 1984; T.A. Steven, oral commun., 1985).

The folds and thrusts of the Sevier orogeny were erosionally truncated and depositionally overlain by thick continental clastic and chemical (lacustrine) strata and some marine strata ranging in age from latest Cretaceous (Price River Formation) (Spieker, 1946) through late middle Eocene (Green River Formation) (Willis, 1985) to late Eocene (Crazy Hollow Formation and formation of Aurora) (Willis, 1985, 1986). The distribution and depositional history of the uppermost Cretaceous through lower Eocene strata in the region reflect the trend and location of the Cordilleran hinge line and the Sevier fold and thrust belt but are considered by

TABLE 1.—*Fault-slip data and computational results*

[—, no data in these weight categories]

	Clear Creek area		Richfield to Willow Creek	Monroe segment, Sevier fault		Annabella segment, Sevier fault	Anticline sample
	Strike slip	Dip slip		Strike slip	Dip slip	Dip slip	
Number of samples (N)	149	60	33	36	13	90	49
Principal compressional stress:							
Maximum (σ_1)	4, 3	265, 84	147, 88	173, 3	183, 73	166, 86	170, 87
Intermediate (σ_2)	163, 87	170, 1	45, 1	24, 87	347, 17	13, 4	12, 3
Minimum (σ_3)	274, 1	80, 6	315, 2	263, 2	79, 4	282, 2	282, 1
Stress ratio (Φ)	0.16	0.04	0.06	0.12	0.26	0.03	0.05
Mean angular difference (Δ),[1] in deg	23	23	12	19	15	20	15
Discordant data[2]	5	4	1	1	1	2	0
Weight[3]	1 (116)	1 (59)	1 (25)	1 (34)	1 (10)	1 (86)	1 (31)
	3 (25)	3 (1)	2 (1)	5 (2)	5 (3)	4 (1)	2 (4)
	5 (3)	—	3 (1)	—	—	5 (2)	3 (3)
	9 (5)	—	5 (3)	—	—	9 (1)	7 (1)
	—	—	7 (3)	—	—	—	9 (1)
Sense of slip[4,5]	D=58			D=20			
	S=91			S=16			
Strike ranges[6]	D=275°–000°			D=279°–352°			
	S=001°–85°			S=358°–065°			
Degree of certainty[7]	C=57	C=15	C=12	C=2	C=4	C=7	C=24
	P=75	P=40	P=21	P=0	P=8	P=60	P=24
	S=17	S=4	S=0	S=34	S=1	S=23	S=1

[1]Difference between actual striae and the theoretical maximum shear stress on the fault plane.

[2]Identified as striae that form an angle greater than 45° with the theoretical maximum shear stress.

[3]Crudely logarithmic function of fault displacement. 1, less than 50 cm; 3, 2 to 5 m; 5, 10 to 20 m; 7, 50 to 75 m; 9, 100 to 200 m. Number of faults in each weight category is given in parentheses.

[4]Number of dextral strike-slip faults (D) and sinistral strike-slip faults (S).

[5]Anticline sample is too mixed (heterogeneous) for this categorization to have meaning.

[6]Dextral (D) and sinistral (S) faults.

[7]Determination of the sense of slip. C, certain; P, probable; S, supposed. Number is number of faults in each category.

some to be post-orogenic (Stanley and Collinson, 1979). Conglomeratic and other coarse clastic facies in these strata are related, instead, to localized uplifts resembling those of the Laramide orogeny. In central Utah, and especially along the Sanpete and Sevier Valleys, many deformational events, some perhaps very localized, were spread over much of the latest Cretaceous through late Eocene depositional interval (Spieker, 1949; Gilliland, 1963; Standlee, 1982). The regional state of stress accompanying this "post-orogenic" deformation is not obvious. A long-standing controversy concerns the relative roles of vertical tectonics versus compressional tectonics in shaping early Tertiary structures in much of central Utah (see Witkind (1982), Standlee (1982), and Lawton (1985) for dramatically differing interpretations). The area of controversy extends southward into the central Sevier Valley at least as far south as Richfield (fig. 3). Structural trends involved are predominantly northeast and thus parallel the Cordilleran hinge line as well as the Sevier thrust front-foreland boundary. The potential for influencing young structural patterns through inheritance is high in this area.

The late Eocene Crazy Hollow Formation and the formation of Aurora (fig. 4) contain lithologic evidence of syndepositional volcanism probably to the north of the area of figure 3 (Willis, 1985). As part of the province-wide southerly progression of middle Tertiary volcanism (Stewart and others, 1977), the Tushar Mountains area became the locus of major volcanic activity beginning about 35 Ma (the Marysvale volcanic field of Rowley and others (1979)). Airfall tuffs in the Dipping Vat Formation in the central Sevier Valley dated isotopically at 34.2 Ma apparently record volcanism that occurred in the Marysvale field in the southern part of and south of the area of figure 3 (Willis, 1985). The calc-alkaline volcanic rocks of the Marysvale field—mostly lava flows, volcaniclastic sedimentary rocks, and ash-flow tuffs—thin northward through the area and lap onto pre- and lower Tertiary sedimentary rocks (fig. 3). They range to as late as 16 Ma (Rowley and others, 1979). Volcanotectonic structures such as domes, sags, and caldera walls related to their eruption are recognized in the southern part of and south of the area covered in figure 3 (Cunningham and others, 1983). Those structures are largely or completely earlier than the faults that we studied, and we therefore do not show their outlines in figure 3.

Neogene deformation that included faulting and folding occurred along the flanks of the Sanpete-Sevier anticline from Glenwood northeastward (Spieker, 1949; Gilliland, 1963) contemporaneous with and outlasting the volcanism. The paleostress conditions that existed during this Neogene deformation are as uncertain as those that deformed the same area on similar trends during the early Tertiary. Gilliland (1963) studied the part of the anticline that extends into the area that we studied (from Glenwood to Salina, fig. 3). He suggested that it formed no later than during Late Cretaceous time under lateral compressional stresses and that those stresses played a role in its long history of deformation, presumably extending well into the Neogene.

The southern Pavant Range is separated from the structurally elevated volcanic edifice of the Tushar Mountains to the south by a broad, open, east-trending synclinal sag named the Clear Creek downwarp (fig. 3) by Callaghan and Parker (1962). The latest stratigraphic unit that appears to be fully involved with the formation of the downwarp is a 19-Ma ash-flow tuff, the Joe Lott Tuff Member of the Mount Belknap Volcanics (Callaghan and Parker, 1962; Steven and others, 1979). That unit crosses the downwarp but exhibits no conspicuous thickening in the axial part of the downwarp. It exhibits almost 2 km of structural relief where it crosses the downwarp (Callaghan and Parker, 1962), and we assume that relief to be an approximation of the magnitude of downwarping.

Between 16 and 14 Ma, conditions in the southern part of the area changed from predominantly volcanic to basin-fill sedimentation (Callaghan and Parker, 1962; Steven and others, 1979). Callaghan and Parker referred to the sediments as Sevier River Formation, and their general distribution is shown in figure 3. These strata range from basin-margin coarse conglomeratic facies to basin-medial silt and clay and are as young as 5.6 Ma on the basis of a K-Ar age from a tuff bed exposed east of Annabella (H.H. Mehnert and P.D. Rowley, written commun., 1982).

The Clear Creek downwarp may have influenced the local depositional history and distribution of the Sevier River Formation, but, to a large extent, those strata are involved in the downwarping and in subsidiary parallel folding on the southern flank of the downwarp (fig. 3).

Over a stratigraphic interval of several tens of meters, the middle part of the Sevier River Formation directly southwest of Joseph Flats contains an upward transition from pale salmon, fluvial, coarse- to medium-grained sand and gravel to a sequence of pastel yellowish-gray and yellowish-green fluviolacustrine beds. A strikingly similar transitional sequence exposed 30 km northeast in the area south of Glenwood suggests deposition in a single basin of unknown size or shape. In neither area does the lithology of the transitional sequence suggest close proximity to a rising mountain flank. The paleogeographic implication is that neither the Pavant Range, the Sevier Plateau, nor the Sevier Valley existed when those beds were deposited. The tectonic implication is that the present system of structurally controlled mountains and valleys had not yet formed, and, by our definition, the neotectonic realm had not yet begun.

Because the Sevier River Formation represents the youngest well-exposed deformed strata in the area, we concentrated much of our study on the neotectonic structures that deform them. We emphasize that the basalt-rhyolite Black Rock volcanics in the western part of the study area are generally younger than the Sevier River Formation and are highly faulted (Clark, 1977), but they provide little opportunity for gathering fault-slip data and have not been studied for this report.

The study area is located in the structural transition zone between the Basin and Range and Colorado Plateaus provinces—a location that we believe is fundamental to any understanding of neotectonic deformation. Three major transition-zone faults are reported in the area. The Sevier fault, which has a conspicuous zigzag trace and an overall northerly trend, separates the Sevier Valley from the uplifted Sevier Plateau. The fault is one of several major plateau-margin faults between which structural blocks approximately 30 km wide are tilted gently eastward within the regional extent of the transition zone. The Dry Wash fault strikes northeast and is located at the northwestern base of the topographically subdued northern part of the Antelope Range, from where it extends southwestward into the northern flank of the Tushar Mountains. Callaghan and Parker (1961, 1962) and Cunningham and others (1983) mapped it as a normal fault in that area. As it is traced to the southwest, striations on it show that it is chiefly a sinistral strike-slip fault. The third major fault, the Elsinore fault, is essentially a northeastern extension of the Dry Wash fault. Callaghan and Parker (1961) mapped it as a major buried northeast-trending normal fault separating the Sevier Valley from the Pavant Range in the Elsinore area.

Rowley and others (1979) concluded that the major faulting in the Clear Creek downwarp took place after 7 Ma, and Rowley and others (1981a, b) concluded that the main uplift of the Sevier Plateau (about 1.5 km) took place in less than 2.5 m.y. between 7.6 and 4.8 Ma. Anderson and Bucknam (1979) noted fault scarps of probable late Pleistocene age along the Sevier fault near Anabella and along the Elsinore fault near Elsinore. Callaghan and Parker (1961) noted that Quaternary river terraces northeast of Joseph appear to be tilted eastward by displacement on the Dry Wash fault. Thus, the major faulting probably extends from latest Miocene through Pleistocene.

RESULTS FROM FAULT-SLIP SAMPLE AREAS

We present the results of our fault-slip studies geographically by sample areas, beginning in the Clear Creek downwarp, where we collected our most homogeneous and interpretable data. The next sample areas discussed are located northward along the eastern margin of the Pavant Range, where we have evidence of diachronous Neogene deformation, then eastward to the margin of the Sevier Plateau, where our study relies heavily on minor structures, and from there northeastward along the Sanpete-Sevier anticline, where Neogene rocks are mildly to strongly tilted. We present last the results from a reconnaissance in the northern Antelope Range, where we collected our most inhomogeneous and uninterpretable data.

CLEAR CREEK DOWNWARP

Field studies of exposed structures were made in four sample areas along the Clear Creek downwarp. The easternmost area is referred to as the Clear Creek sample area, which contains the specific locality A (fig. 3). Westward, other sample areas are designated B through D (fig. 3).

In the Clear Creek sample area, deep erosion by Clear Creek and its tributaries has produced excellent exposures of the Joe Lott Tuff Member and the overlying Sevier River Formation. Callaghan and Parker (1962) mapped several upright, open, east-trending folds in the rocks on the southern flank of the downwarp. These folds have very narrow hinge zones, amplitudes of about 200 m, and wavelengths of about 2 km (cross section *A–A'*, fig. 3). Callaghan and Parker (1961, 1962) also mapped several northeast-striking faults, the largest of which is the Dry Wash fault. The Dry Wash fault is a critical structure because the Clear Creek downwarp and the subsidiary folds on its southern flank terminate against it, showing a genetic and mechanical interrelationship between folding and faulting. Our study shows that the Dry Wash fault has major sinistral slip where it cuts the axis of the Clear Creek downwarp, as indicated by common subhorizontal striations and corrugations and the geometry and stratigraphic position of rock slabs that are distributed along it (fig. 5). Net displacement on the fault in that area could be several kilometers on the basis of structural and stratigraphic terminations (Cunningham and others, 1983) and stratigraphic contrasts across it (T.A. Steven, oral commun., 1983). In the vicinity of Joseph Flats, it has important dip-slip displacement. Directly northwest of the Dry Wash fault, two additional northeast-striking map-scale faults display abundant evidence of sinistral slip and have net slip of as much as 1 km (figs. 6, 7). Some of their displacement is probably accommodated by the east-trending folds that are located near their southwestern terminations (fig. 3).

The east-trending folds also are cut by many small-displacement steep strike-slip faults, many of which are well exposed in cliffs held up by the Joe Lott Tuff

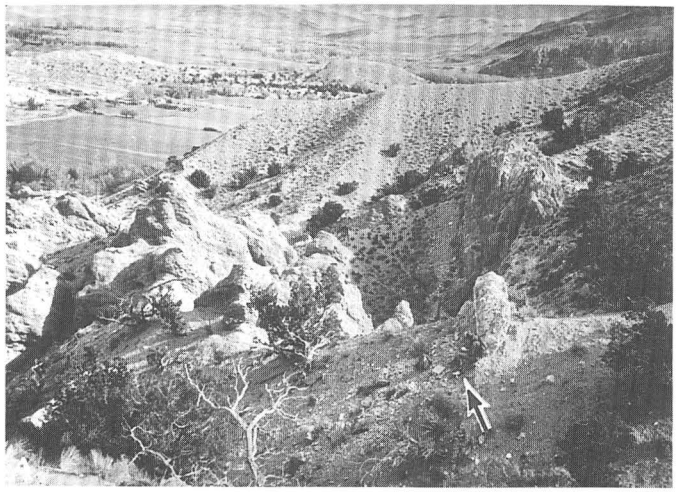

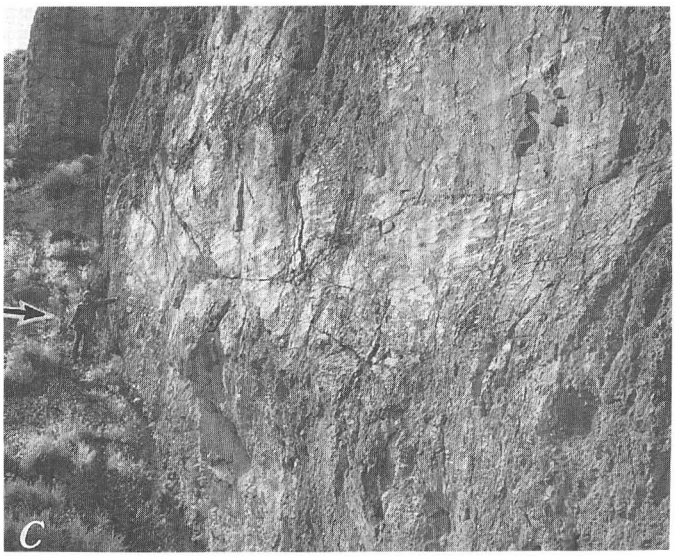

FIGURE 5.—Dry Wash fault. *A*, View looking northeast along the trace of the fault showing slivers of the Joe Lott Tuff Member of the Mount Belknap Volcanics (at and beyond the geologist at arrow) displaced to exotic positions and separating younger coarse clastic sediments of the Sevier River Formation (exposed beds to left of the geologist and unexposed beds in covered slope to his right). The clastic strata dip about 35° away from the camera, so that the slivers of tuff that mark the trace of the fault resemble dikes that crosscut the sediments. The dikelike juxtapositioning results from strike-slip displacement of a previously fault-tilted and fault-repeated sequence of strata. *B*, View looking southeast at a location marked by the geologist in *A* showing a horizontally striated fault surface on the Joe Lott Tuff Member where the cemented gravel of the Sevier River Formation of the hanging wall (lower part of photograph) has spalled away along the fault plane. Compass for scale. *C*, View looking southwest along the main trace of the Dry Wash fault showing gently plunging striations developed on brecciated Joe Lott Tuff Member. Note the geologist at the arrow to the left and below the center of the photograph for scale.

Member (fig. 8). In the welded ash-flow tuffs of the Joe Lott, many of these faults utilized preexisting cooling joints and represent displacements of a few centimeters or less. Detailed study of 81 of these faults in axial and opposed-limb positions in the folded Joe Lott Tuff and Sevier River Formation shows that they comprise northeast-striking sinistral (N=33) and northwest-striking dextral (N=48) sets that (1) offset one another, (2) have broad ranges in strike and no overlap, and (3) contain striations whose rake angles are independent of position on the fold (fig. 9). These relationships indicate that the sinistral and dextral sets are conjugate. Mohr-Coulomb theory (Anderson, 1951) would predict that they formed under conditions of north-south compression. The relationship of their striae to position on the folds (fig. 9) suggests that the last motion on them occurred late in the folding history or perhaps after folding.

We also identified sparse small-displacement dextral faults adjacent to the sinistral Dry Wash fault. These faults have the same range of strike as those that cut the folds and exhibit mutually offsetting characteristics similar to those of the larger displacement sinistral faults of the Dry Wash system. These small dextral faults are clearly synthetic to the Dry Wash fault.

FIGURE 5.—Continued.

Fault-slip data were gathered from 209 faults in the Clear Creek sample area. The determination of sense of slip is classified as certain or probable on 89 percent of the faults, and 16 percent have displacements of 1 m or more. The sample is large but by no means represents all faults in the sample area. We arbitrarily omit data from a northeast-striking oblique dextral fault zone southwest of Joseph Flats (specifically at locality A, fig. 3) because the slip sense is obviously discordant to that of the other northeast-trending faults in the area. The possible structural significance of the oblique-dextral fault at locality A is discussed below. For the 209 faults, dips are distrib-

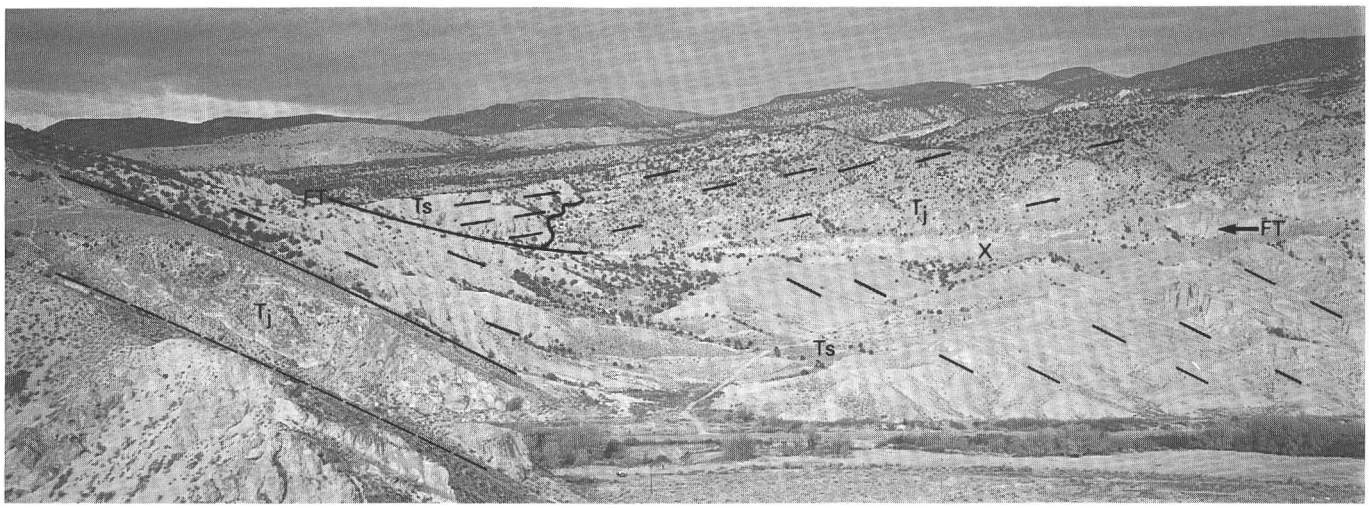

FIGURE 6.—View to the northwest from the Dry Wash fault across Clear Creek (foreground) to the trace (horizontal scar at X) of the sinistral strike-slip fault (FT) (middle distance). The fault parallels the Dry Wash fault and juxtaposes south-dipping rocks of the northern flank of the Clear Creek downwarp beyond the trace against north-dipping rocks of the southern flank of the downwarp on the photographer's side of the trace. Tj, Joe Lott Tuff Member of the Mount Belknap Formation; Ts, Sevier River Formation. Heavy irregular line is the contact between Tj and Ts; light dashed lines accentuate bedding traces. Linear skyline elements and vegetation stripes below the skyline show the extent of the south-dipping flank of the downwarp. Figure 7 shows closeup views of the fault, which is very well exposed in the area of the scar.

uted in a remarkably tight, steep pattern (fig. 10), and rakes show a strong bimodal distribution in which low values (strike-slip faulting) predominate. Fault strikes are mostly north-northwest, north-northeast, and northeast. There is a complete separation of dextral and sinistral fault-strike fields. The separation would, of course, be incomplete if data from the omitted dextral fault were included. The bimodal rake distribution provides a rationale for separating the data into strike-slip and dip-slip subsets for computational purposes. For the strike-slip subset, north-south maximum compressive stress is indicated (fig. 10) consistent with the stress state inferred for the east-west folds and the small faults that cut them. The value for Φ of 0.16 suggests that σ_1 is well constrained and that σ_2 and σ_3 are moderately well constrained. Mapped structures show that the deformation is strongly asymmetric and dominated by sinistral slip on northeast-striking faults and by folding. The analysis of small-displacement faults does not explain the strain asymmetry but shows that it is consistent with north-south compression.

Dip-slip striations were measured on 60 small-displacement faults in the Clear Creek sample area (fig. 10). Five of these faults show evidence of polydirectional slip. The dip slip is younger than the strike slip on three of those five faults and older on two. Thus, no evidence is provided for a temporal separation of strike-slip and dip-slip faulting.

Dip-slip faults that dip greater than 80° and less than 20° are not as compatible with a normal faulting regime as are those that dip between 80° and 20°. Also, faults exhibiting moderate and shallow rake angles are not likely to contribute as much to extensional deformation as are faults displaying steep rakes. To test the importance of normal faulting in the Clear Creek sample area, we eliminated steep- and shallow-dipping faults and those displaying moderate and shallow rakes and computed the paleostress characteristics from the remaining data (31 of the original 60 faults). We do not report the computational results because they do not reflect a lessening of angular discordance between the measured striae and the theoretical maximum shear stress, nor does the value of Φ (0.05) indicate a significantly better constrained σ_3 axis than the one computed from all dip-slip data (0.04, table 1). We conclude from these relationships, together with the overwhelming evidence that the dominant faulting mode in the Clear Creek area is strike slip, that dip-slip faulting in the area is not of first-order structural significance. Alternatively, the dip-slip faulting may provide weak evidence of a temporal interchanging of σ_1 and σ_2 in a stress field dominated by north-south compression and σ_3 oriented approximately east-west.

The northeast-trending oblique-dextral fault at locality A (fig. 3) that is eliminated from the Clear Creek area computations dips 80° to 85° southeast, is sharp and planar (fig. 11), and juxtaposes contrasting facies of basin-fill sediments of the Miocene and Pliocene Sevier River Formation (Callaghan and Parker, 1962). It strikes transverse to bedding, which dips 20° to 30°

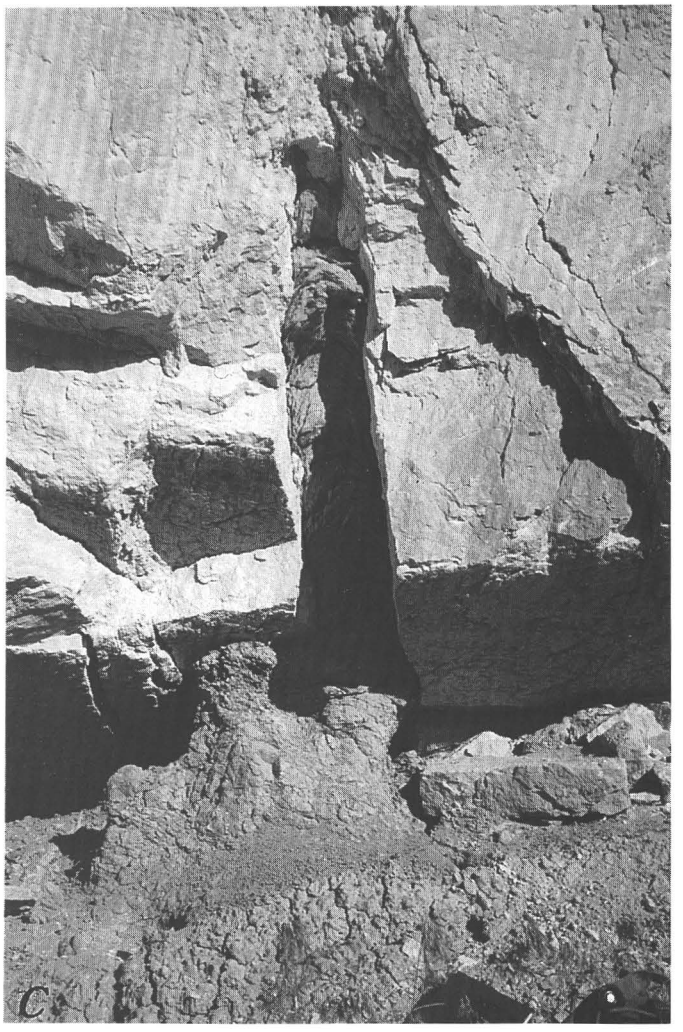

FIGURE 7.—Northeast-trending sinistral-slip fault shown in figure 6. *A*, View looking southwest showing large striated grooves on the Joe Lott Tuff Member of the Mount Belknap Volcanics, where coarse cemented gravels of the Sevier River Formation (visible in the lower part of the scarp) have spalled away from the fault surface. *B*, Closeup view of striations on a large groove shown in *A*. The arrow drawn on the fault surface in the center of the view is 3 cm long and shows the motion direction of the block as required by the streamlining of gouge deposits to the right of the small, mechanically resistant lithic inclusions in the tuff above the arrow. *C*, View looking down at the fault surface (in shade) separating the clayey sands of the Sevier River Formation in the foreground from the Joe Lott Tuff Member. The mechanically weak clayey sands are squeezed like toothpaste into a conspicuous tension gash about 20 cm wide in the mechanically resistant Joe Lott Tuff. Although they are not visible, the conspicuous striations on the shaded fault surface show that the Joe Lott block moved to the left (sinistral).

northeast (figs. 11, 12). Stratigraphic offset and sense of drag show that throw is down to the southeast, and the net displacement is more than 100 m. Fault-slip data were collected from the main fault and 16 additional northeast-striking surfaces having displacements as little as 20 cm. The main fault and the adjacent small-displacement faults presumably constitute a single fault zone. Twelve of the 17 faults have a dextral-slip component, and 11 of those 12 plot within 30° of the pole to bedding (fig. 12). This predominantly oblique dextral slip probably represents the principal displacement on this fault zone. Because the slip direction is consistently about parallel to the pole to bedding, the striae on the fault planes presumably were caused by rotation of a fault block containing the tilted beds. For this fault zone, the data set does not meet the criterion of independence required for the paleostress inversion procedure (Angelier, 1979). However, not all of the data are consistent with such an interpretation. Five of the northeast-striking minor faults have sinistral-slip components that suggest an incompatible element of slip in the fault zone. Similar slip incompatibility is seen in other fault-slip data samples from the central Sevier Valley study area and suggests that slip incompatibility is a common feature. It could result either from block motions driven by trac-

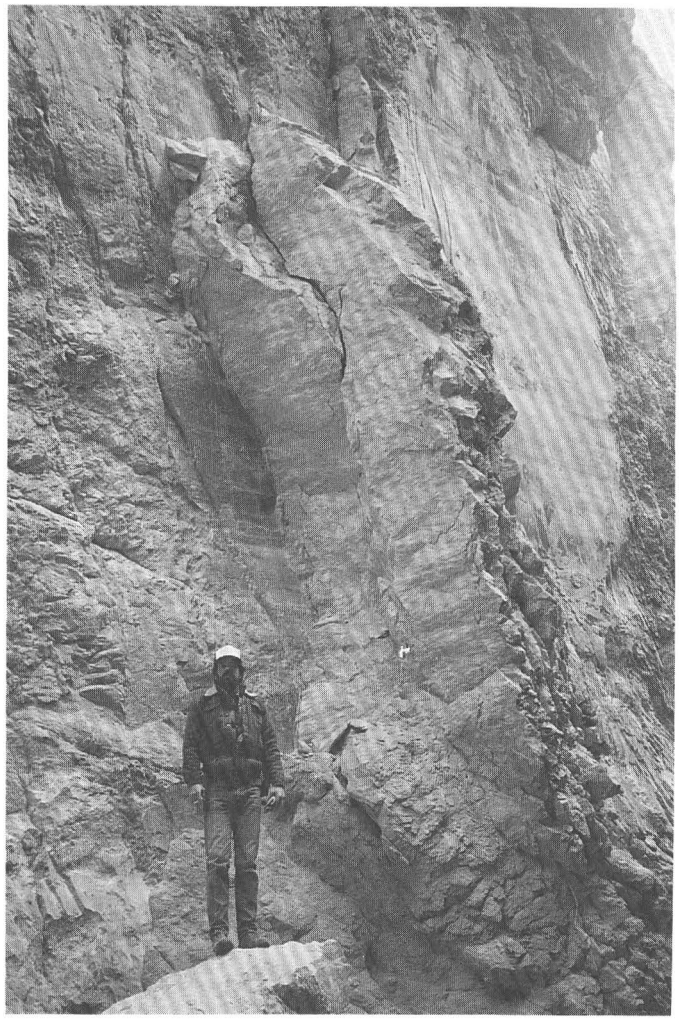

FIGURE 8.—Well-exposed, large, smooth, striated surface of a small sinistral-slip fault in the Joe Lott Tuff Member of the Mount Belknap Volcanics. Rough surfaces (near the top of the photograph) that extend out from and offset the large, smooth surface also contain gently plunging striae (not obvious in the photograph). Dextral displacement on the rough-surface fractures shows that they are conjugate to the large, smooth surface. Two-meter geologist for scale.

tional forces applied to the base of the blocks or from transient stress states generated during recovery phases following major faulting events.

At sample area B (fig. 3), sedimentary strata of the Sevier River Formation are downfaulted to the east against Miocene ash-flow tuffs on a well-exposed striated surface having a local attitude of 345°, 72° NE. (fig. 13). An average rake of about 90° indicates normal faulting. Over a distance of 5 km to the north along the same fault zone, striae on 19 subparallel subsidiary faults have rake angles that range from 68° to 90° and average 82°, providing confirmation that the last major movement on this fault zone is normal dip slip. South of locality B, bedrock in the footwall block is cut by numerous striated

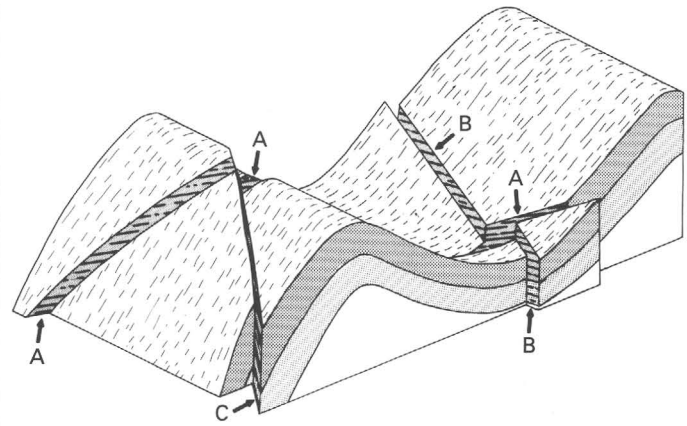

FIGURE 9.—Schematic representation of a fold cut by a sinistral fault (A) and two dextral faults (B, C). The short, heavy lines symbolize striae on fault surfaces. Fault C offsets fault A, and fault A offsets fault B, an indication of conjugate behavior. Also, the rake of striae on the faults is independent of position in the fold.

small-displacement faults exhibiting dextral slip and rake angles as low as 3°. One of those fault surfaces contains intersecting striae indicating both dextral and normal displacements, of which the normal motion is the youngest. These relationships suggest that rocks in this fault zone experienced an early episode of Neogene strike-slip displacement but that the latest and principal displacement is dip slip.

At sample area C, several roadcuts along a 1.5-km stretch of Interstate 70 provide good exposures of transversely faulted Oligocene and Miocene volcanic and sedimentary rocks. The faulted rocks consist of tuffaceous sandstone and gravel, sandstone and cobbly sandstone of probable fluvial origin, ash-flow tuff, and dacite and andesite flows. They dip east to southeast 15° to 30° and are cut by numerous steep, northeast-striking faults. At and around locality C, bedding repetition and physiography suggest simple normal faulting (Cunningham and others, 1983), but the fault-plane striae tell a much different story. Slip orientations and senses were measured on 20 faults ranging in displacement from about 20 cm to more than 100 m. One fault strikes north and is dextral. The remaining 19 faults strike northeast; 17 are sinistral, and 2 are normal (fig. 14*A*). The degree of certainty of the sense of slip was determined as certain on 14 and as probable for the remainder of the faults. The large-displacement faults have gouge zones as wide as 50 cm. The gouge has a strong internal shear fabric whose geometry and orientation are consistent with the orientation and sense of displacement measured on the planar walls of the shear zone, suggesting an unusually high degree of uniformity of fault motion. Eight of the 20 faults have measured or estimated displacements of 10 m or more. The cumulative displacement is not known but could easily be more than 1 km. These excellent expo-

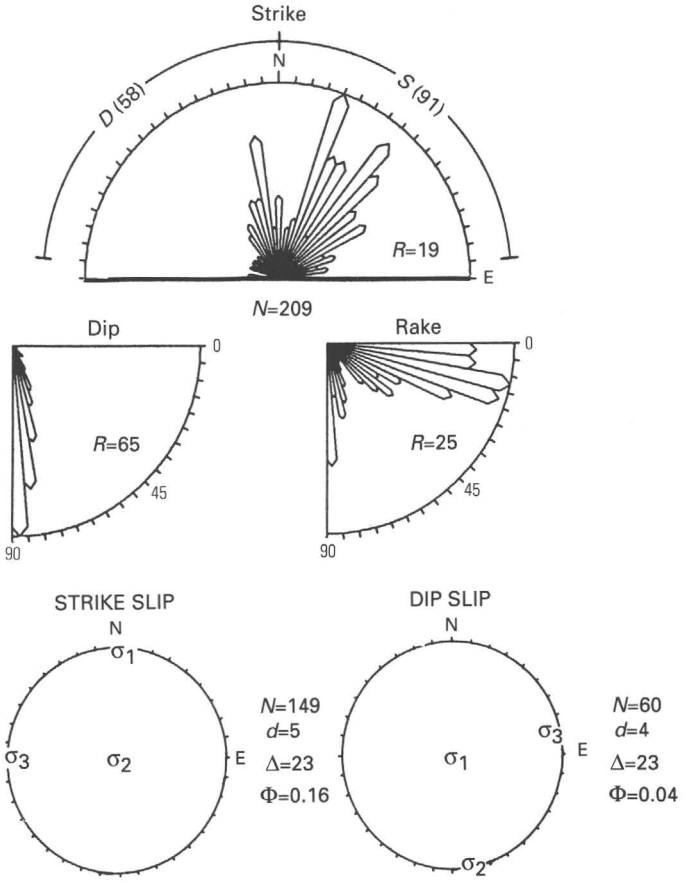

FIGURE 10.—Histograms of strike, dip, and rake and lower hemisphere stereographic plots of computed paleostress axes for faults from the Clear Creek sample area in the easternmost part of the Clear Creek downwarp. N, sample size; R, radius of the histogram, in number of measurements; D, azimuthal range of dextral faults (number of faults in parentheses); S, azimuthal range of sinistral faults (number of faults in parentheses); σ_1, σ_2, and σ_3, maximum, intermediate, and minimum principal compressional stresses, respectively; d, number of striae that form an angle greater than 45° with the theoretical maximum shear stress; Δ, mean angular difference between the actual striae and the theoretical maximum shear stress on the fault plane; $\Phi=(\sigma_2-\sigma_3)/(\sigma_1-\sigma_3)$.

sures show that fault deformation along the 1.5 km of cross-strike distance is predominantly on northeast-striking sinistral faults and that no significant difference exists between the slip on large- and small-displacement faults. The contrast between the paleoslip of the youngest observed striae in sample area B and that in sample area C is dramatic.

Sample area D is along the northbound and southbound lanes of Interstate 15 about 6 km north of the junction with Interstate 70; this area is a few kilometers west of the Basin and Range boundary. Roadcuts along Interstate 70 expose strongly fractured Oligocene volcanic rocks that strike west-northwest and dip gently south-southwest. The average strike of faults in the area is 015° (Cunningham and others, 1983). Because the

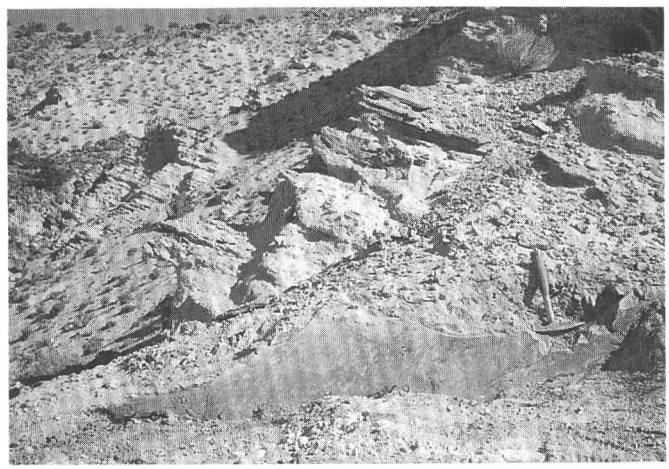

FIGURE 11.—View to the northwest of the excavated surface of a steep planar fault that cuts transversely through northeast-tilted beds of the Sevier River Formation at locality A in figure 3. Figure 12 shows a stereographic plot of the fault and other data. The photographer is standing on clayey and sandy sediments (not visible) that are downthrown by oblique dextral slip against coarse clastic gravel and conglomerate across the fault. Hammer for scale.

faults strike at a high angle to the strike of the beds, the faults are either unrelated to and presumably younger than the stratal tilting or are transverse block-bounding structures that were active during stratal tilting. In either case, we infer that the latest movement on these faults is late Quaternary, because the faults are coextensive with faults that cut nearby volcanic rocks dated radiometrically at about 0.5 Ma (Steven and Morris, 1983; Best and others, 1980). The amount of displacement on an individual fault is not known but is assumed, on the basis of fracture appearances, to range from a few centimeters to a few meters. Steven and Morris (1983) mapped a fault striking 045° along Interstate 15 between the two roadcuts, and unpublished mapping by one of us (R.E. Anderson, 1982) showed that the rocks in the eastern cut are displaced in an oblique sinistral sense at least 150 m relative to the rocks in the western cut. The orientation and sense of slip were measured on six faults in the eastern cut and nine in the western cut. These faults, which range in strike from 345° through 0° to 085° and in dip from 28° to 85°, are probably representative of the range of principal fault orientations near the cuts. Polyphase slip is indicated on 4 of the 15 faults that we studied. Of the 15 faults, 3 northward-striking ones are predominantly dextral, 9 northeastward-striking ones are predominantly sinistral, and the remaining 3 show a predominance of dip slip (fig. 14*B*). These faults, inferred by us to reflect neotectonic deformation, are similar to those in the Clear Creek sample area because they display a mixture of strike slip and dip slip, showing a preference for sinistral strike slip on northeasterly strik-

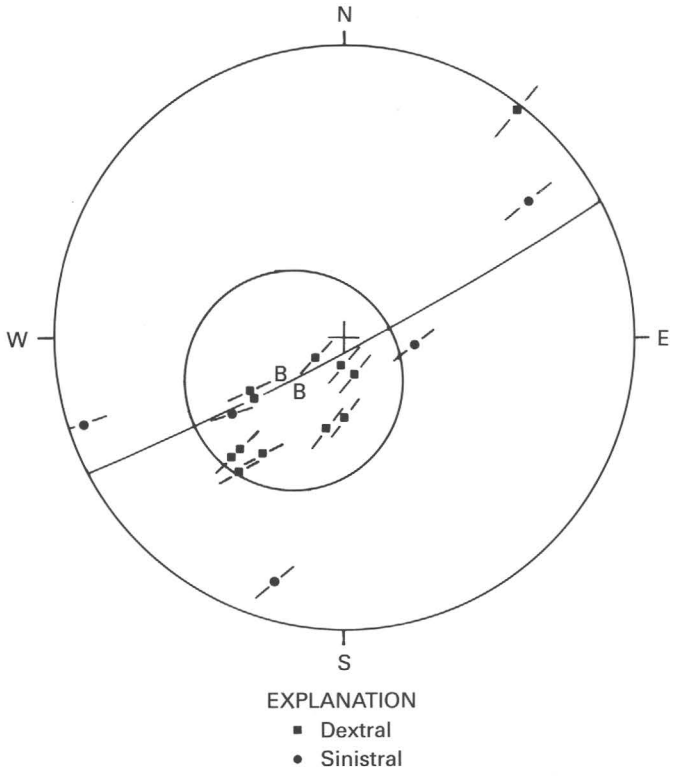

FIGURE 12.—Lower hemisphere stereographic plot of the main fault (great-circle arc) and 16 subsidiary northeast-trending faults (segments of great circles) at locality A in figure 3. Striae on fault planes are distinguished according to the type of slip. Poles to bedding are indicated by the letter B. The circle shows a 30° cone having an axis near the poles to bedding. The concentration of striae within the cone is consistent with an interpretation that most of the faulting is caused by transverse block-boundary displacements related to stratal tilting.

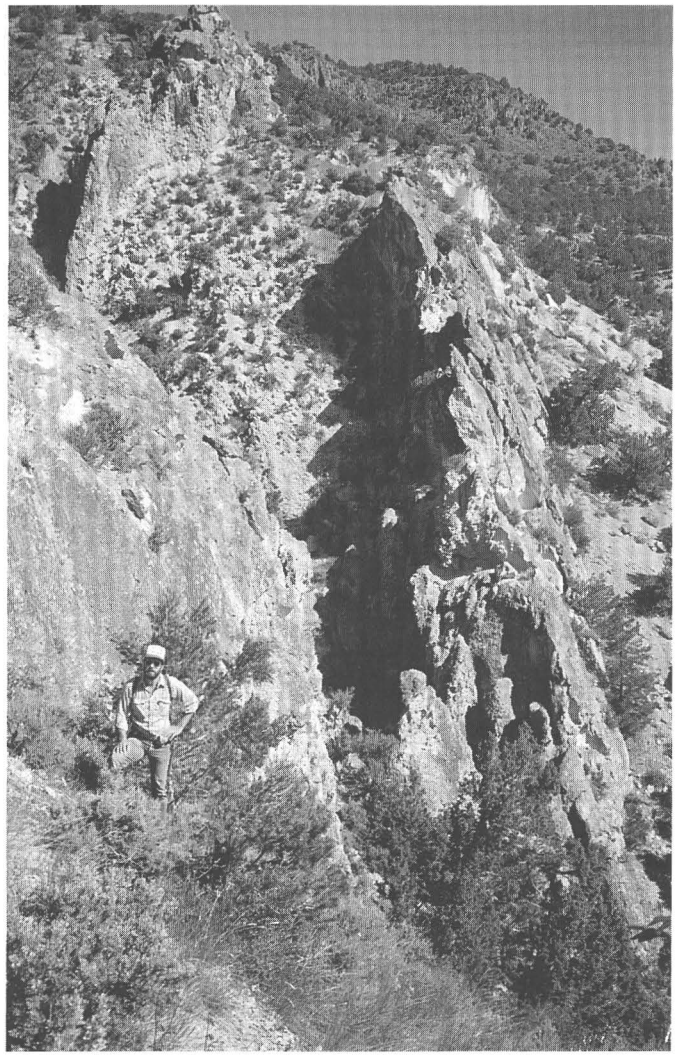

FIGURE 13.—View looking north along the well-exposed Joe Lott Tuff Member of the Mount Belknap Volcanics in the footwall (left and center) of a north-northwest-striking normal fault at locality B in figure 3. The hanging-wall block (right-hand edge of photograph) consists of poorly exposed Sevier River Formation. Two-meter geologist for scale.

ing planes. They indicate that the style of faulting in the Clear Creek area extends westward into the Basin and Range. A limited stress tensor (σ_1, σ_2, and σ_3) computed from the 15 faults (using the youngest motions on those having two sets of striae) is shown on figure 14*B*.

In summary, our study of four sample areas along the Clear Creek downwarp on both sides of the boundary between the Basin and Range province and the transition zone illustrates that the neotectonic deformational mode differs greatly from the simple extensional mode generally assumed for the late Cenozoic deformation in this part of Utah. In two of the four sample areas that we studied, highway-related excavations revealed both the presence and the predominance of late compression-related structures, about which nothing would be known were it not for the excavations. One of these areas is, at first glance, an excellent structural and physiographic candidate for simple late Cenozoic extension. A high probability of error exists in determining the sense of slip of faults shown on geologic maps of this region unless specific data on the orientation and sense of slip are available. In particular, we suspect that several faults mapped as scissors faults in nearby parts of the Pavant Range, the Tushar Mountains, and the Sevier Plateau (see Cunningham and others (1983), for example) are actually faults exhibiting a high proportion of strike-slip displacement and that the scissors mode is an apparent feature arising from the juxtapositioning of strata that have been gently to moderately deformed before strike-slip faulting. Although strike-slip faulting and associated folding predominate in the Clear Creek area, we emphasize that late Cenozoic dip-slip faulting does exist, and we describe a good example at and north of sample area B. Also, in a highway excavation near Cove Fort, at least 20 m of late Pleistocene dip slip is indicated on the principal

east-bounding normal fault of the Cove Fort graben (Anderson, 1980). The presence of dip-slip faults, some of large displacement, intermixed with strike-slip faults of similar orientation suggests complex fault linkages of the type proposed by Gibbs (1987).

Studies along the Clear Creek downwarp show that strike-slip faulting is genetically and mechanically associated with east-trending folds whose axes parallel the axis of the downwarp. Faults and folds in this area give the appearance of having formed in response to late Miocene and (or) later subhorizontal maximum compressive stress oriented approximately north-south. Because sinistral slip on northeast-striking faults dominates, the overall displacement of blocks bounded by these faults is southwesterly. If the entire fault system could be imagined to be simultaneously active, the result would be a positive velocity gradient from east to west. The integrated fault-fold system in the eastern part of the Clear Creek downwarp probably reflects a resistance to this southerly motion by the buttressing effect of the enormous Marysvale volcanic field and its associated plutonic root inferred from gravity modeling (Halliday and Cook, 1980). Structures produced by such a resistance could appear to result from simple, local north-south compression.

Strike-slip faults cutting the Clear Creek downwarp may have resulted from a thin-skinned deformational mode, because available geologic maps provide no evidence that they can be projected northeast along strike into the pre-Cenozoic rocks of the Pavant Range. This dramatic Neogene strain contrast between the two areas of contrasting rock types requires some form of structural accommodation or detachment at a stratigraphic level near the base of the Neogene volcanogenic sedimentary rocks. Detachment would also explain the strong contrast in faulting mode northeast and southwest of Richfield (noted in a subsequent section). The surface trace of the low-angle fault detachment would be largely masked by the large areas mapped as landslide at or near the contact between Neogene volcanic rocks and older rocks in the Pavant Range (fig. 3). Within the landslides southwest of Richfield, we recognize major attenuation of stratigraphic sequences above the Flagstaff Lime-

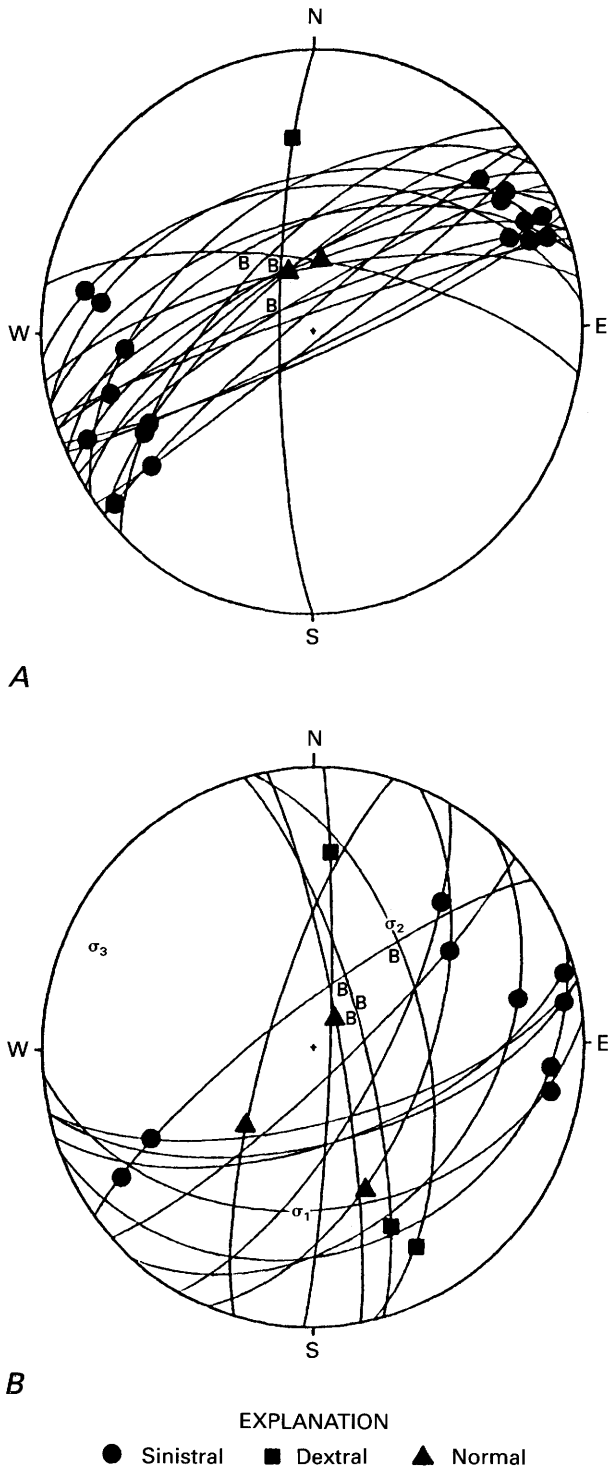

◀ FIGURE 14.—Lower hemisphere plots of fault-slip and bedding data at localities along Interstates 70 and 15. Faults are shown as great-circle arcs, and the striae in those faults are distinguished according to the type of slip. Poles to bedding are shown by the letter B. *A*, Faults at locality C (fig. 3). Most are sinistral, except for one north-trending dextral fault and two dip-slip faults. The poles to bedding plot near the normal-faulting striae and thus suggest an association between the stratal tilting and the dip-slip components of faulting. *B*, Faults at locality D (fig. 3). Those that strike between 015° and 085° are all sinistral or normal sinistral. The remaining are dextral, except for a normal fault exhibiting a steep rake. The faults do not appear to have any simple genetic relationship to stratal tilting. The computed stress axes σ_1, σ_2, and σ_3 (maximum, intermediate, and minimum principal compressional stresses, respectively) are poorly constrained because of the small sample size and the predominance of sinistral slip. Nevertheless, the position of σ_3 is reasonable in comparison with other computed orientations reported herein (table 1). The moderate inclination of σ_1 could result from late-stage rotation of the faults and bedding.

stone. We suspect that much of the attenuation there and to the southwest results from tectonic processes that left the area highly susceptible to landsliding or is simply the direct result of landsliding. One possible interpretation is that the Clear Creek downwarp, which has a structural relief of about 2 km, provided the gravitational potential for producing the detachment and southward sliding, whereas the Tushar Mountains served to buttress the sliding. Deformation could result from updip attachment in the updip area and from downdip buttressing analogous to similar attributes of landslides in the downdip area (Kehle, 1970). This interpretation embodies the unlikely gravitational transport of rocks across the axis of the downwarp, where they crumpled into folds on the northern flank of the Tushar Mountains (cross section *A–A'*, fig. 3). In a more favored interpretation, the compressional structures (folds and strike-slip faults) result from the scraping off of the volcanic cover rocks from a south-moving structural block that thrust under the northern flank of the Tushar Mountains.

PAVANT RANGE

The folds and thrusts of the Sevier orogeny in the southern Pavant Range are onlapped along a northeast-trending unconformity by southeast-dipping fluvial, lacustrine, and volcanic rocks ranging in age from Paleocene to Oligocene (Callaghan and Parker, 1962; Hickcox, 1971). The southeastward dip of the unconformity, of the strata above the unconformity, and of the Pavant thrust beneath the unconformity is caused by southeastward rotational uplift of the Pavant Range block during Neogene time. Concentration of maximum uplift along the western side of the range may result from structural rebound associated with tectonic unloading in the breakaway zone of the west-vergent late Cenozoic Sevier Desert detachment fault (Allmendinger and others, 1983; Wernicke, 1985). Map-scale high-angle faults are conspicuously sparse in the western part of the range (fig. 3), suggesting that the block remained intact during uplift and tilting. We conducted a reconnaissance study of the slip characteristics of large- to small-displacement high-angle faults and measured numerous stratal attitudes along the eastern flank of the range. For purposes of discussion, results from the northern and southern parts of the eastern flank are presented separately, the division being made approximately at the latitude of Richfield (fig. 3). This division has structural significance because vertical displacement of the Pavant Range north-northeast of Richfield relative to that of the Sevier Valley was accomplished through a combination of monoclinal flexing and normal faulting, whereas we recognize no evidence of range-bounding normal faulting south-southwest of Richfield.

JOSEPH FLATS TO RICHFIELD

The Pavant Range between Joseph Flats and Richfield consists of ash-flow tuff and lava flows of Oligocene age sandwiched between variegated sandstone, siltstone, shale, and limestone below and basin-fill clastic strata belonging to the Sevier River Formation above. Although structural complications make it difficult to assess stratigraphic thicknesses, the volcanic rocks are at least 400 m thick. Their stratigraphic relationship to regionally distributed volcanic rocks has been shown by Cunningham and others (1983). Callaghan and Parker (1961) showed that the structure of this part of the range is a northeast-trending syncline-anticline pair in the area south of the latitude of Elsinore grading toward Richfield into a single east-southeast-facing monocline. In detail, the structure is complex and includes a few small-scale folds and many previously unmapped faults. To document it adequately would require detailed mapping at a scale of no less than 1:12,000. Our approach, instead, was to measure many stratal, fault, and striation orientations, record them on aerial photographs, and use the photogeologic compilation as an adjunct to interpreting the published geologic maps. The abundant small structures are too small to depict in figure 3. Instead, figure 3 emphasizes the anticline-syncline pair and southeastern dips in the monocline. Figure 3 shows, as Callaghan and Parker's (1961) map did, that the Miocene-Pliocene Sevier River Formation is involved in the folding.

The complex structure of the Joseph Flats to Richfield segment of the range flank led Cunningham and others (1983) to depict it as dominated by the effects of landsliding. Although landsliding was certainly a factor in shaping the complexity, we conclude that most of it is caused by at least two superposed episodes of deformation, each including faulting and stratal tilting.

Data gathered from 59 intermediate- and small-displacement faults (fig. 15) show that most have moderate to steep dips and strike north to northwest. Their strikes are transverse or acute to that of the range margin, which trends about N. 35° E. Directly west and northwest of Elsinore, ash-flow tuffs that correlate with the Needles Range Group of Oligocene age (Steven, 1979) strike chiefly northwest and are repeated by numerous northwest-striking faults. The average angle between bedding and faults of about 90° suggests that the faults formed as tension fractures before the strata were tilted. Most fault-plane striae show dip slip. The tension fractures were probably reactivated as normal faults and were rotated as the beds rotated, a structural history similar to that described by Angelier and Colletta (1983). The exposed bedding and fault pattern suggests northeast-southwest extension. Some striae on these same faults or on parallel faults have low-angle rakes, possibly suggestive of late-stage reactivation as strike-

slip faults. In Flat Canyon directly north of Elsinore (locality G, fig. 3), the formation of Aurora of late Eocene age is cut by conjugate sets of northwest-trending normal faults having a symmetry axis normal to bedding. These faults also suggest northeast-southwest extension. These strata are also cut by steep north- and northeast-trending strike-slip faults (fig. 16), some of which have large displacements, and by small-displacement reverse faults that offset the conjugate normal faults. The reverse faults are apparently associated with eastward tilting of the early conjugate normal faults. We infer that the north- to northeast-striking strike-slip faults formed in response to the same forces that produced similar faulting in the Clear Creek sample area and at sample area C described earlier (see also fig. 16). We also infer that these faults postdate the early normal faulting in the area. This inference is strongly supported at a few localities between Joseph Flats and Richfield where fault-tilted northwest-striking strata can be traced to the edge of the range, where they bend sharply into the southeast-dipping monocline and strike northeast, indicating that the monocline is superposed on the previously block-faulted strata. This superposed deformation is reflected in figure 17 by the concentration of northwest-plunging poles to bedding. Also, the northeast- and southwest-plunging poles to bedding do not lie along a vertical northeast-striking plane (fig. 17). Instead, they are displaced slightly to the northwest, probably as a result of superposed moderate southeastward tilting in the monocline.

Several faults in the Joseph Flats to Richfield sample area have striae exhibiting a bewildering variety of rake angles and polyphase slip. Qualitative analysis of the oblique-slip and strike-slip motions on similarly oriented faults shows slip incompatibility. The data are not uniquely consistent with either a landslide interpretation or an interpretation based on a compressional stress field analogous to the one that controlled late Cenozoic structural development in the Clear Creek sample area. Although the cause of the slip complexity and incompatibility is not known, we suspect that much of it results from polyphase deformations in a tectonic regime where uplift caused by tectonic unloading competes with lateral shearing caused either by north-south compression, wrench faulting, or tectonic rafting of structural blocks in a highly mobile shear zone. It is unfortunate that the fault-slip data that we gathered are too few to use as a basis for understanding polyphase deformation.

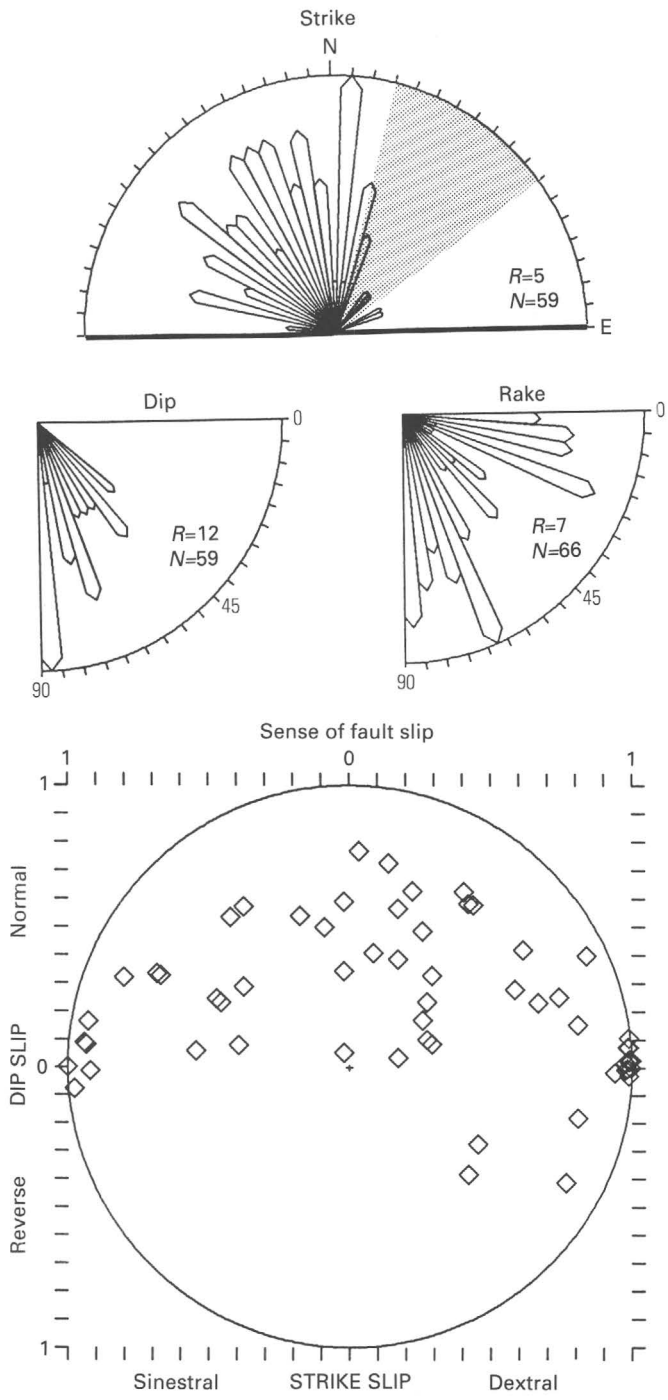

FIGURE 15.—Histograms of strike, dip, rake, and sense of fault slip for faults along the southeastern margin of the Pavant Range between Joseph Flats and Richfield. *R*, radius of the histogram, in number of measurements; *N*, sample size. The contrast between distributions of strike, dip, and rake in this area and those in the nearby Clear Creek area is strong (fig. 10). In the diagram showing the sense of fault slip, the ratio of strike slip to net slip is plotted along the abscissa, and the ratio of the dip-slip component to net slip is plotted along the ordinate. This plot reveals the complex mixture of strike-slip, dip-slip, and oblique-slip faulting that characterizes this sample area. Compare this fault-slip diagram with the simple pattern of dip-slip faulting along the same range front to the northeast of Richfield (fig. 20). The patterned sector on the strike plot shows the average trend, 35°±15°, of the Pavant Range front. Very few faults have that trend. Symbols are the same as for figure 10.

FIGURE 16.—View looking west in Flat Canyon north of Elsinore showing the offset contact between smooth- and rough-weathering beds of gently southwest-dipping sandstone, siltstone, and claystone belonging to the formation of Aurora of late Eocene age (Willis, 1986). The fault that separates the offset sections is approximately vertical, strikes 005°, and has an estimated down-to-the-east throw of 10 m. At first glance, this fault and another nearby fault of similar orientation and displacement but out of camera view appear to be steep dip-slip faults that repeat the strata by down-to-the-east (lower right) displacements. However, as is the case with the faults at locality C (fig. 3) along the Clear Creek downwarp, these faults are sinistral strike-slip faults having rakes of 3° and 13° to the south.

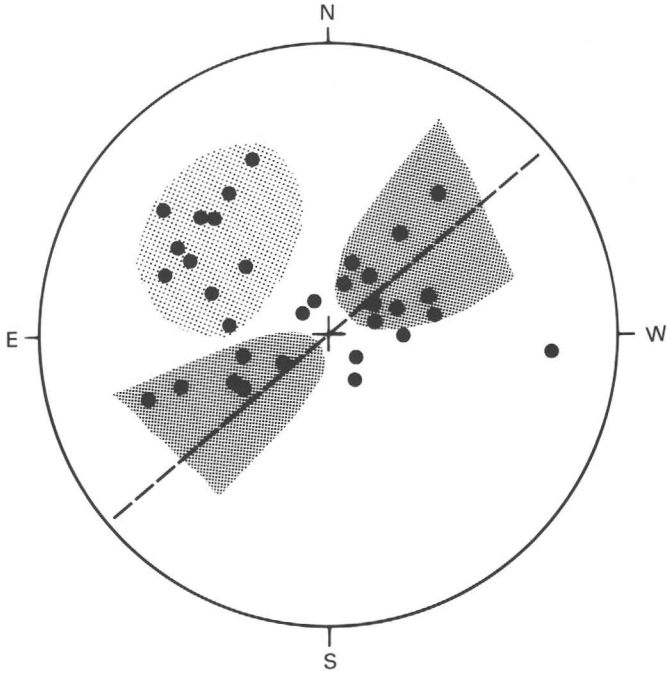

FIGURE 17.—Lower hemisphere stereographic plot of poles to bedding along the flank of the Pavant Range between Joseph Flats and Richfield. The dark shaded areas embrace poles that represent first-phase stratal tilting to the northeast and southwest on generally northwest-trending faults. The light shaded areas embrace poles representing second-phase monoclinal tilting to the southeast. Locally, the northeast-dipping block-faulted strata in the range can be traced continuously into the monocline.

Of the 59 small- and intermediate-displacement faults observed along the range front between Joseph Flats and Richfield, only 6 strike within ±20° of the N. 35° E. trend of the range front; of these 6, only 3 dip southeast—the dip direction that one would expect if the faults are part of a range-front fault system. Of the three, two show sinistral strike-slip striae, and one shows normal slip. Thus, only 1 of 59 faults has an orientation and slip sense similar to what would be expected for a range-front normal fault system that might be inferred from the geology and present-day physiography.

Previous workers have inferred a major normal fault, the Elsinore fault, to be the range-front structure along the Joseph Flats to Richfield segment of the range front (Callaghan and Parker, 1961; Cunningham and others, 1983). Our identification of the chief range-front structure as a monocline and, more specifically, our failure to identify minor structures related to a range-front normal fault suggest that, if a fault exists, it is either (1) buried beneath the monocline and genetically related to it, (2) buried beneath alluvium at some distance east of the range front, or (3) a continuation of the sinistral-slip Dry Wash fault, which, if projected northeastward, should lie along the range front (fig. 3).

RICHFIELD TO WILLOW CREEK

The eastern part of the Pavant Range between a line extending southwest from Richfield northward to Willow Creek (fig. 3) is underlain by lower Tertiary sedimentary rocks. In that area, the eastern margin of the main range block extends northeast from Richfield to approximately the locality marked by H in figure 3. From there, it bends sharply northwest toward Willow Creek, where it is marked by a fault scarp of probable Holocene age (Anderson and Bucknam, 1979). The range margin structure is complex because of (1) the sharp bend, (2) possible diachronous deformation, (3) a mixture of faulting and monoclinal flexing, and (4) a mixture of down-to-valley and down-to-mountain faulting.

The lobe of bedrock that extends toward Aurora from the main range block is dominated by a series of northeast-tilted fault-repeated blocks of Green River Formation but also contains a major and controversial fold structure that wraps around the northeastern extreme of the range and involves the Green River and younger Tertiary rocks (fig. 18). Our early reconnaissance mapping of that area led us to interpret the faulting and tilting on northwestward trends as an early

episode of deformation related to northeast-southwest extension and the wraparound fold as a subsequent episode of monoclinal fold deformation related to formation of the Sevier Valley—a structural history very analogous to that described in the previous section for the Elsinore area. On the basis of 1:24,000-scale quadrangle mapping, Willis (1988) interpreted most major folding and faulting in that area to be genetically and temporally related to a single deformational episode and suggested that the deformation could be as late as Pliocene. His interpretation was strongly influenced by mapping indicating that most of the northwest-striking faults terminate southeastward at the Elsinore fault and thus are contemporaneous with or younger than the Elsinore fault. We maintain that the quality of exposures and lack of marker beds east of the northeast-striking Elsinore fault do not preclude small faults extending into that area and suggest that some large faults do, on the basis of Willis' mapping (fig. 18). We therefore adhere to our initial interpretation of diachronous deformation.

Along the Sevier Valley between Richfield and Aurora, a few hills of dark-colored volcanic rocks of Oligocene age protrude through the alluvium. Most of these volcanic rocks dip moderately to steeply toward the valley, showing that Neogene monoclinal flexing plays an important role in producing the vertical structural relief of that part of the range front. Displacements on subvertical northeast-striking faults also contribute to or, in some places, are the dominant elements in producing the vertical structural relief. Mapping by Willis (1988) showed that these faults can be traced northeast to the latitude of Aurora, northeast of which displacement transfers completely to a southeast-facing monocline (fig. 18). We interpret the entire wraparound fold as part of that monocline and, therefore, as part of the range-flank structure.

Directly west of Richfield, well-exposed monoclinally flexed rocks belonging to the Flagstaff Limestone and the Colton and Green River Formations in the upthrown block of the range-front fault are cut by numerous small- to intermediate-displacement down-to-the-mountain normal faults. About 6 km north of Richfield, similarly flexed equivalent strata dipping valleyward from 15° to 60° on the downthrown side of the range-front fault are cut by intermediate- to large-displacement down-to-the-mountain normal faults. Directly southwest of Aurora, we infer from an anomalously large breadth of outcrop and steep valleyward dips reported by Willis (1988) that the Tertiary volcanic rocks are displaced by as-yet-unrecognized down-to-the-mountain faults (fig. 18). The exposures west of Richfield reveal that the down-to-the-mountain faults tend to cut the tilted strata at approximately 90° to bedding, whereas faults of the main range-front system are subvertical (fig. 19).

Rocks of the Flagstaff Limestone in the upthrown block of the northwest-striking main range front in the vicinity of Willow Creek form a faulted monocline very similar in cross sectional form to the monocline west of Richfield (fig. 19) but having a dramatically different orientation. Despite their different orientation, we infer that these structures are coeval and that, together with the structures of the downthrown block, they adequately characterize the style of range-margin deformation. Little, if any, net extension can be attributed to the near-vertical down-to-valley faults. Stratal flexing tends to subtract from—and may completely negate—extension on down-to-range faults. Therefore, there may be little or no net extension associated with the uplift across these range-margin structures. If so, the range margins are very different from the bedrock lobe west of Aurora, where fault repetition suggests moderate northeast-southwest extension that we believe predates formation of the Pavant Range.

Fault-slip data were gathered from 33 small-, intermediate-, and large-displacement faults belonging to the range-margin system, 20 from the northeast-trending segment west of Richfield and 13 from the northwest-trending segment near Willow Creek. Strike distributions presented in figure 20 show the contrasting northeastern and northwestern trends of the range-margin segments.

A paleostress computation using the 20 faults from the northeast-trending segment yields almost the same orientation for σ_3 (316°) as a computation using all 33 faults (315°). At first, this coincidence seems inconsistent with the contrasting strikes of the range-margin structures. We note, however, that most of the northwest-striking faults in the Willow Creek area, instead of being pure dip-slip faults, are actually oblique-slip faults exhibiting rakes consistently to the northwest, as the stereoplot in figure 20 shows.

We have no direct evidence of strike-slip faulting along the Richfield to Aurora segment of the Pavent Range margin. This lack contrasts greatly with the abundant evidence of strike-slip faults in the volcanic rocks from Richfield southwest. This dramatic contrast may result from structural decoupling or detachment of the volcanic rocks from the underlying sediments, as outlined in "Summary and Discussion."

SEVIER FAULT

The Sevier fault is one of the major structures of the transition zone. It forms the western boundary of the 25- to 30-km-wide east-tilted Sevier Plateau block and locally has at least 1.5 km of down-to-the-west throw. In most places, uplift of the Sevier Plateau is probably distributed over a broad zone of faults that we collectively refer

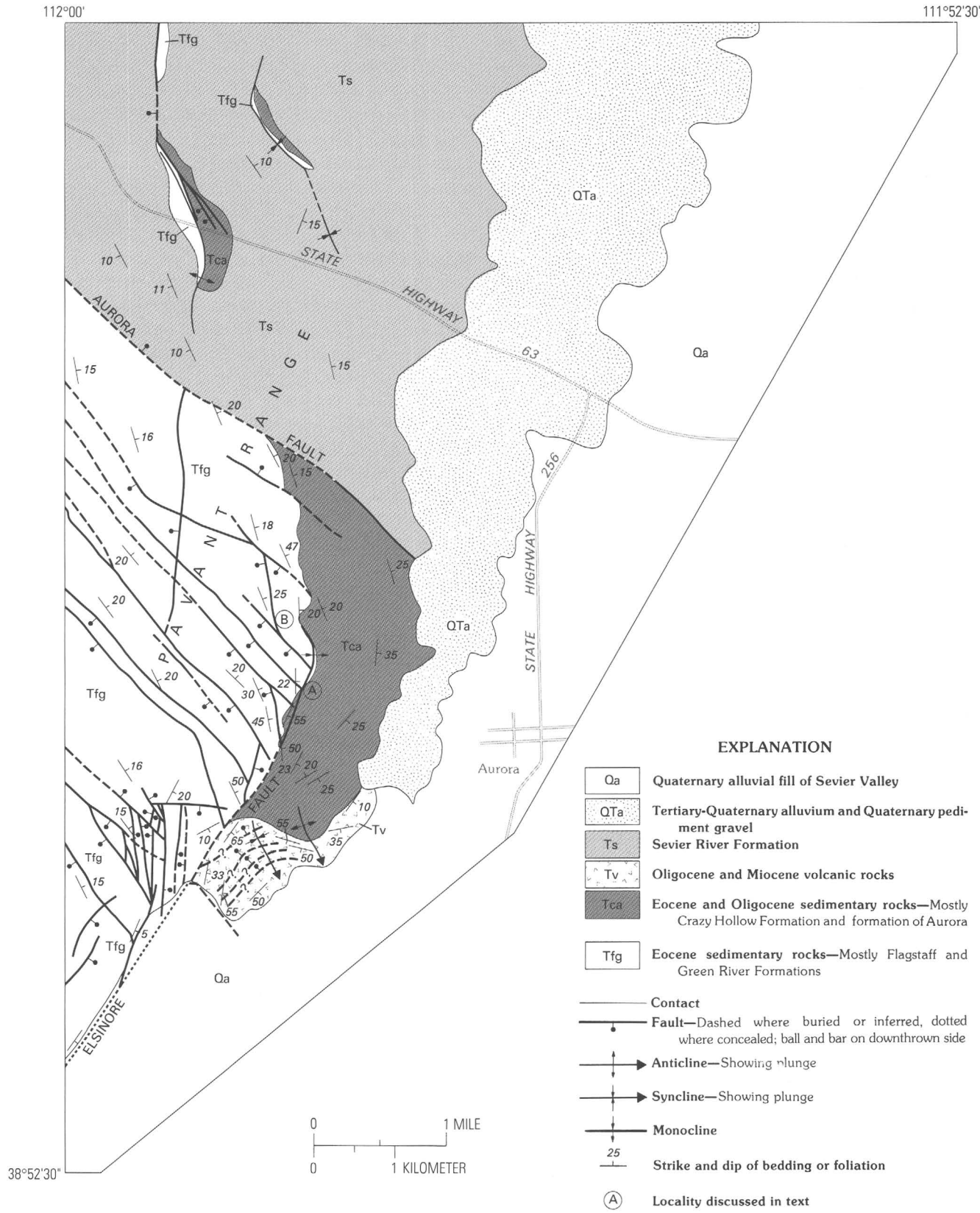
112°00'
111°52'30"
38°52'30"
Tfg
Ts
Tca
Tv
QTa
Qa
AURORA
STATE HIGHWAY 63
STATE HIGHWAY 256
WASATCH RANGE
FAULT
FAULT
ELSINORE
Aurora
A
B
0 1 MILE
0 1 KILOMETER
EXPLANATION
Qa Quaternary alluvial fill of Sevier Valley
QTa Tertiary-Quaternary alluvium and Quaternary pediment gravel
Ts Sevier River Formation
Tv Oligocene and Miocene volcanic rocks
Tca Eocene and Oligocene sedimentary rocks—Mostly Crazy Hollow Formation and formation of Aurora
Tfg Eocene sedimentary rocks—Mostly Flagstaff and Green River Formations
Contact
Fault—Dashed where buried or inferred, dotted where concealed; ball and bar on downthrown side
Anticline—Showing plunge
Syncline—Showing plunge
Monocline
25 Strike and dip of bedding or foliation
A Locality discussed in text

to as the Sevier fault. The Sevier fault extends from near Annabella south about 120 km to near Panguitch, Utah, but consists of several north-, northeast-, and northwest-striking segments that give the fault a conspicuous zigzag trace (Rowley, 1968; Rowley and others, 1979; Cunningham and others, 1983). The northern Sevier fault is well defined, although buried, south of Monroe, where it apparently controls the N. 5° E. trend of the range for about 6 km (fig. 3). Its trace north of Monroe is conjectural because the range-front escarpment bends sharply eastward, and it is uncertain whether the main trace of the Sevier fault follows that bend or, as Callaghan and Parker (1961) indicated, strikes 035° beneath a thick mantle of landslide and alluvial debris to reemerge at the western base of the Bull Claim Hills northeast of Annabella. Whether its main trace north of Monroe strikes northeast or east-northeast (fig. 3), its contrast in strike north and south of Monroe serves as a basis for discussing those segments separately.

MONROE SEGMENT

The Monroe segment of the Sevier fault is defined as the 6-km-long north-trending part south of Monroe (fig. 3). Although modeling of detailed geophysical data and interpretation of drill-hole data at the Monroe geothermal area yield conflicting results, together they indicate that the Sevier fault is a zone of several major north-trending step faults that dip valleyward 80° (Mase and others, 1978; Chapman and Harrison, 1978). In our study, the Sevier fault was observed at only one exposure (directly northeast of locality E, fig. 3). At this locality, a fault having an attitude 007°, 70° W. cuts sharply through conspicuously unbrecciated and unfractured Oligocene andesite and is marked by a 1- to 2-m-wide rib of massive silica that has been prospected locally. Striations on and within the secondary silica have gentle northern plunges indicating late-stage strike-slip motion. Neither the sense nor the amount of displacement is known. Directly northwest of locality E (fig. 3), the mapped trace of a fault that separates calc-alkalic andesite of Oligocene age from downdropped rhyolitic ash-flow tuffs of Miocene age strikes N. 55° E., dips steeply northwestward, and has a stratigraphic separation of at least 1 km (Cunningham and others, 1983). Six steeply dipping gouge-coated surfaces hand excavated in fractured andesite breccia of the footwall block strike within ±15° of the mapped fault and show normal dip slip. Although this fault is not part of the Monroe segment as defined herein, it is a main strand of the Sevier fault. On the basis of these limited data, we infer that the Sevier fault, although predominantly dip slip, has some strike-slip components of displacement along north-striking segments. This inference is consistent with observations of bimodal dip-slip and strike-slip striae seen on the southernmost part of the Sevier fault (R. Krantz, written commun., 1986).

Stratal strikes in Oligocene volcanic rocks along the 005°-striking Monroe segment are varied, and dips average only about 10°. Study of 62 small- and intermediate-displacement faults in these gently tilted and faulted rocks shows fault strikes having northeastern and northwestern maxima and no tendency for fault strikes to parallel the range front (fig. 21). Of 14 faults whose strikes fall within 20° of the range-front trend, only 3 dip toward the valley and show normal displacement. Of the 62 faults, 36 have rakes less than 45°, and 26 have rakes greater than 45°. The data indicate heterogenous slip on faults that have attitudes conspicuously different from the attitude of the Monroe segment of the Sevier fault. Because they contribute little to extension, dip-slip faults having dips greater than 80° were eliminated for computational purposes. The remaining subset of dip-slip faults

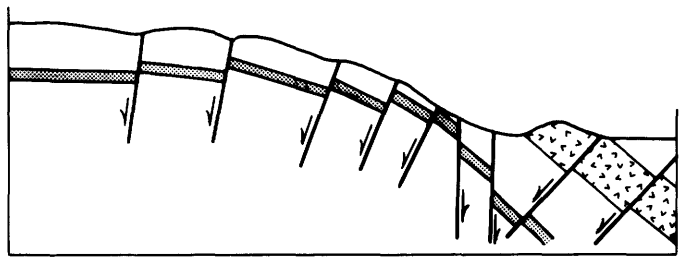

FIGURE 19.—Typical fault offsets seen in the monoclinally flexed margin of the Pavant Range. Fault offsets are similar to those described and analyzed by Thompson and White (1984); patterned beds are hypothetical. Down-to-range faults cut bedding at approximately right angles, and bedding is not rotated by the steep down-to-valley faults.

◀ FIGURE 18.—Generalized geology of the northwestern part of the Aurora 7½-min quadrangle. With the exception of the highly interpretive fault-and-fold pattern in volcanic rocks southwest of Aurora, the data are taken from Willis (1988). The Elsinore fault terminates near a point marked by A, where its displacement is transferred to a southeast-facing monocline that, in turn, bends westward and loses expression near a point marked B. Loss of expression is in large part due to its mergence with the homoclinally northeast-tilted Eocene strata. To the east of the Elsinore fault and its coextensive monocline, the Eocene and Oligocene sedimentary rocks and overlying volcanic rocks wrap neatly around the northwest-trending series of fault-repeated blocks of Eocene sedimentary rocks. This wrap-around structure is herein interpreted to postdate the faulting and tilting on northwestern trends. The down-to-the-northwest series of inferred faults shown cutting the volcanic rocks southwest of Aurora represents a stylized attempt to resolve an anomalously great stratal thickness of volcanic rocks suggested by the moderate to steep dips over a cross-strike distance of more than 1 km. The faulting style follows that seen to the southwest in the downthrown block of the Elsinore fault. The folds are based on stratal strike variations mapped by Willis (1988).

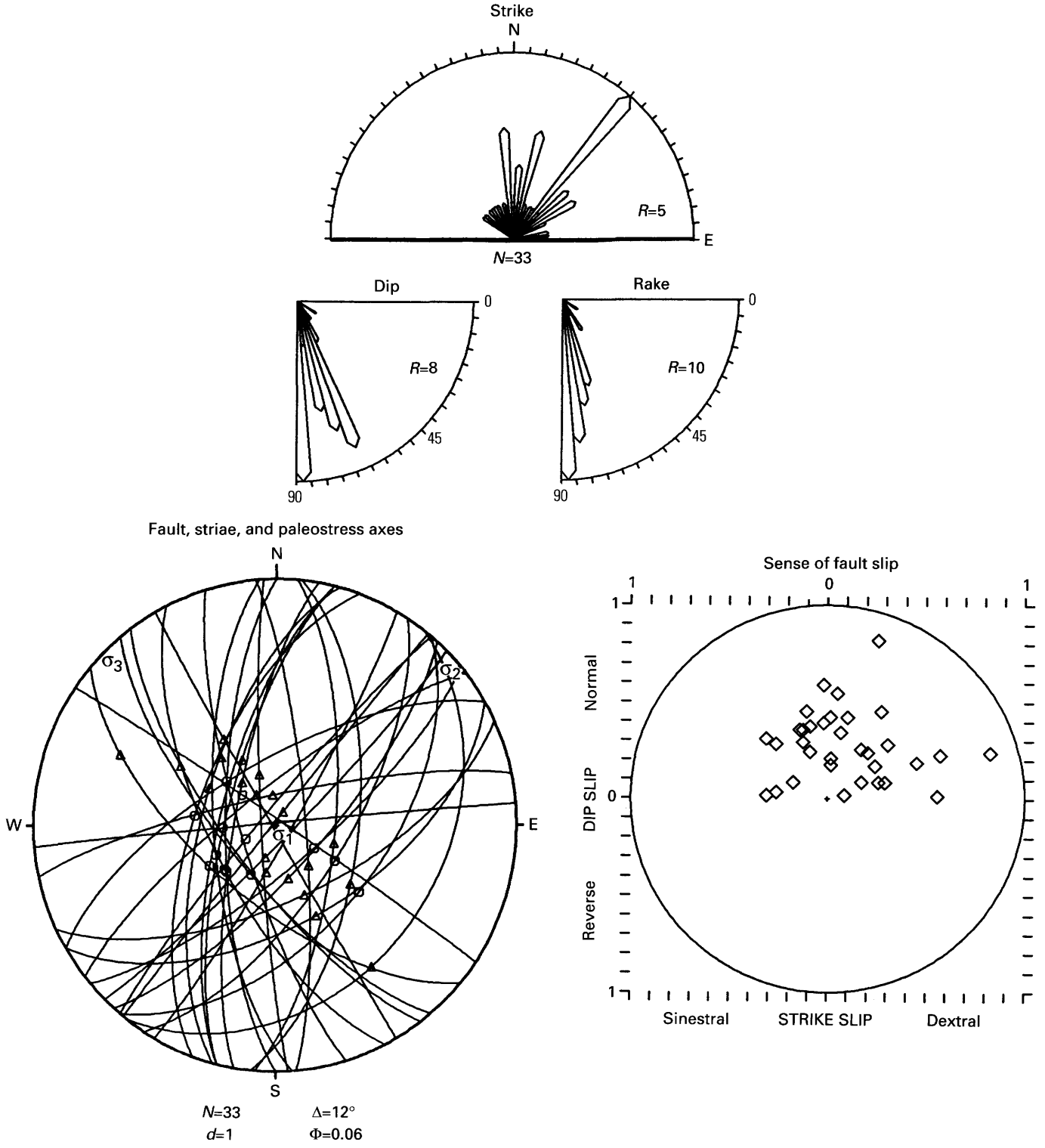

(N=13, table 1) is of marginally small size for paleostress computation. As expected, the dip-slip and strike-slip subsets yield paleostress axes having subvertical σ_1 and σ_2, respectively (fig. 21). Subhorizontal σ_3 axes from the dip-slip and strike-slip subsets are within 12° of each other, suggesting that the two modes of faulting are parts of a single deformational process. The computational results as well as the data distributions are quantitatively similar to those from the Clear Creek sample area. We find this similarity astonishing in view of the

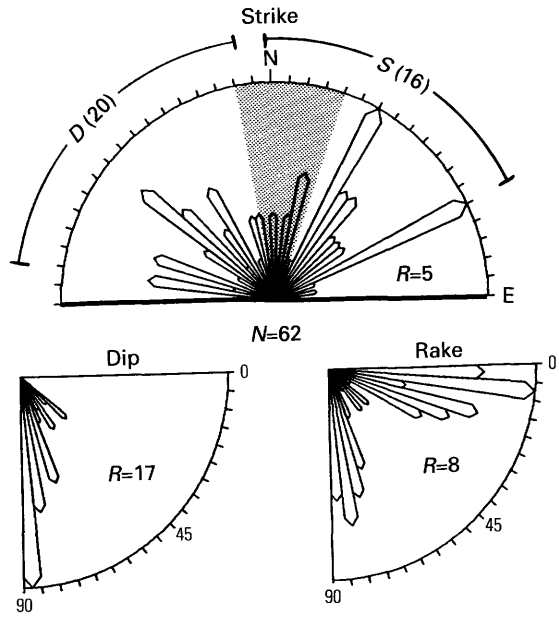

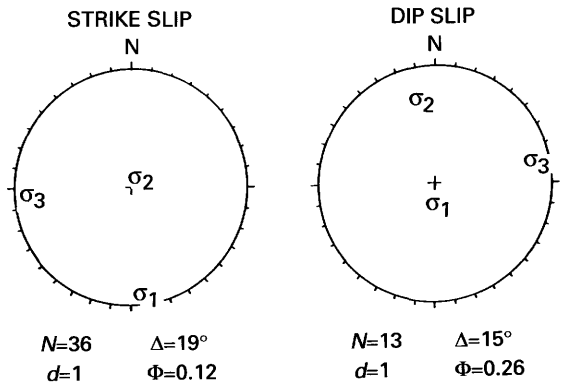

N=36 Δ=19° d=1 Φ=0.12

N=13 Δ=15° d=1 Φ=0.26

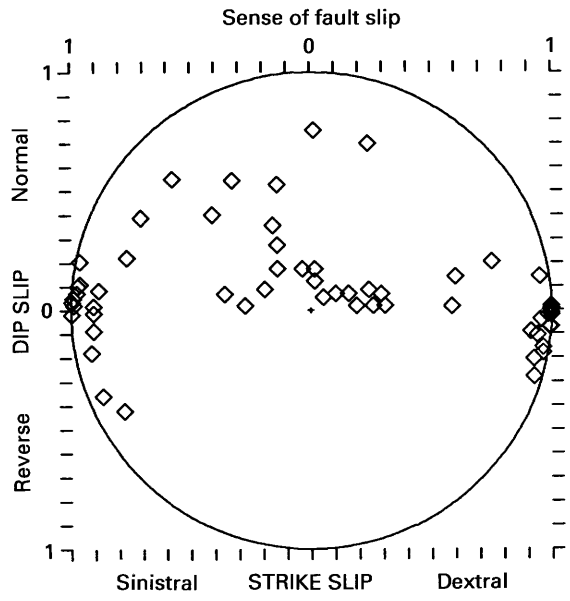

FIGURE 20.—Histograms of strike, dip, and rake, lower hemisphere stereographic plot of faults, striae, and computed paleostress axes, and plot of slip sense for faults along the eastern margin of the Pavant Range between Richfield and Willow Creek. *R*, radius of the histogram, in number of measurements; *N*, sample size; *d*, number of striae that form an angle greater than 45° with the theoretical maximum shear stress; Δ, mean angular difference between the actual striae and the theoretical maximum shear stress on the fault plane; $\Phi=(\sigma_2-\sigma_1)/(\sigma_3-\sigma_1)$; σ_1, σ_2, and σ_3, maximum, intermediate, and minimum principal compressional stress, respectively. The contrast between strike and rake distributions for these data and for those shown in figure 15 is strong. The dip distribution shows two maxima; the 85° to 90° spike represents mostly down-to-valley faults, and the 65° to 70° node represents mostly down-to-mountain faults. Two types of striae are differentiated in the stereographic plot of the fault planes (lower left); squares indicate normal sinistral, and triangles indicate normal dextral. The fault-slip plot shows a preference for oblique dextral slip. The oblique dextral separations are mostly on northwest-striking faults believed to have been early dip-slip faults reactivated in the stress field shown on the stereographic plot. The coordinates in the slip-sense plot are the same as those in figure 15.

very strong contrast between the local structural settings of the two areas. However, we emphasize that the determination of slip sense for strike-slip faults along the Monroe segment is very poorly constrained (table 1).

ANNABELLA SEGMENT

The Annabella segment of the Sevier fault is herein defined as the range-front fault extending east-northeast from the Thompson Creek landslide (fig. 3). For 2.2 km east of the landslide, the trace of the Annabella segment is clearly marked by a precipitous straight bedrock escarpment trending 075°. Stratal attitudes of volcanic and sedimentary bedrock in the escarpment are highly variable, and dips are mostly less than 30° (figs. 22, 23). The escarpment projects eastward toward the lower reaches of Cliff Canyon, where excellent exposures reveal that volcanic rocks in the hanging wall block are

FIGURE 21.—Histograms of strike, dip, and rake, lower hemisphere stereographic plots of computed paleostress axes, and plot of dip-slip versus strike-slip components of fault slip for faults in the western margin of the Sevier Plateau in the Monroe area. The patterned sector on the strike plot is the average range-front trend, 005°±15°. *R*, radius of the histogram, in number of measurements; *N*, sample size; *D*, azimuthal range of dextral faults (number of faults in parentheses); *S*, azimuthal range of sinistral faults (number of faults in parentheses); *d*, number of striae that form an angle greater than 45° with the theoretical maximum shear stress; Δ, mean angular difference between the actual striae and the theoretical maximum shear stress on the fault plane; $\Phi=(\sigma_2-\sigma_3/(\sigma_3-\sigma_1)$; σ_1, σ_2, and σ_3, maximum, intermediate, and minimum principal compressional stresses, respectively. The coordinates in the slip-sense plot are the same as those in figure 15.

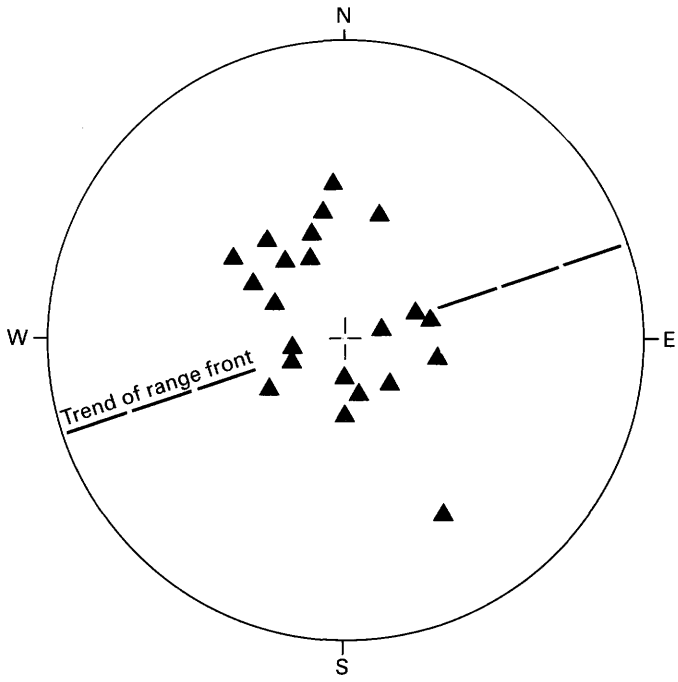

FIGURE 22.—Lower hemisphere plot of poles to bedding in bedrock along the Annabella segment of the Sevier fault. Poles that plot in the southeastern sector mostly represent rocks in the monoclinally flexed or fault-dragged beds of the hanging-wall block, where flexing is away from the range trend (dashed line).

bent down toward the north, suggestive of a large drape fold or possibly normal drag (fig. 23). The Annabella segment extends up Cliff Canyon, exhibiting possibly as much as 400 m of down-to-the-north stratigraphic offset of Oligocene volcanic rocks (Rowley and others, 1981a). A thick sequence of well-exposed Oligocene volcanic rocks in the plateau block south of that part of the fault is very mildly deformed. The rocks are horizontal to gently southeastward dipping and are cut by sparse small-displacement faults (fig. 23).

A total of 235 fault-slip measurements were made on moderately to steeply dipping faults in the upthrown and downthrown blocks along the approximately 4-km-long trace of the Annabella segment (fig. 24). Fault strikes in this sample area are varied, and the histogram of strike distributions shows a minor concentration in the 30° sector centered on the 075° average trend of the Annabella segment. Dip directions for these faults, however, are skewed to the southern hemisphere (that is, toward the uplifted plateau block). Oblique slip is common. The histogram of rake distributions shows a clearly defined minimum at 30°. Dip-slip and oblique-slip faults predominate over strike-slip faults.

To evaluate the role of dip-slip faulting in plateau uplift, we present data-distribution histograms for dip-slip faults having rakes greater than 60° (90 faults) (fig. 24). As did the entire data set, this subsample shows varied strikes and a strongly skewed pattern of dip directions toward the southern hemisphere. Of particular significance is the paucity of dip directions toward the 330° to 360° sector (that is, toward the downdropped block of the Annabella segment). This paucity cannot be ascribed to post-faulting rotation in the draped or folded hanging-wall block because much of the data is from the uplifted footwall block, which shows no consistent pattern of stratal rotation (fig. 22). We did not observe the main fault of the Annabella segment and therefore do not know its true dip. We emphasize that many of our measurements were taken from faulted rocks within a few meters of the main fault. The data suggest that the main fault is a sharp break and that normal faults associated with it drop strata down toward the uplifted plateau. The data show that most of the dip-slip faults in this sample area are not part of a range-front fault system and may not contribute significantly to plateau uplift. In this respect, the Annabella segment is similar to the Monroe segment as well as to the eastern margin of the Pavant Range.

The sense of slip was determined with certainty or reasonable probability on only about 15 percent of the oblique-slip and strike-slip faults along the Annabella segment. A lower hemisphere stereographic plot of faults in this 15-percent subsample is shown in figure 25. For predominantly strike-slip faults, the subsample shows an unusually wide range of attitudes (especially dip values). Despite the attitude variability, slip lines show a strong preference for dispersion around a north-south azimuth, but sinistral and dextral faults are not concentrated in separate strike sectors, as they are in the Clear Creek sample area. We infer from dip variability, north-south dispersed slip lines, and lack of sinistral-dextral partitioning that faulting in a predominantly strike-slip mode does not represent a conjugate-shear response to remote stress. Therefore, quantitative attempts to resolve paleostress characteristics by using strike-slip faults should not be made.

We computed a paleostress orientation from the dip-slip faults exhibiting rakes greater than 60° (N=90). It shows σ_3 at 282°, but the low value of Φ (0.03, table 1) suggests that moderately to steeply dipping faults of any strike are appropriately oriented for dip-slip movement. Although the computed σ_3 orientation is clearly not a reflection of principal extension normal to the Annabella segment of the range front, the low value of Φ and the fact that oblique-slip and strike-slip faults are excluded in its computation lessens its paleostress significance. The dip-slip faulting may be analogous to the strike-slip faulting and may not represent a response to applied remote stresses. Alternatively, a complex and unresolvable history of polyphase deformation could be recorded by the striae that we measured.

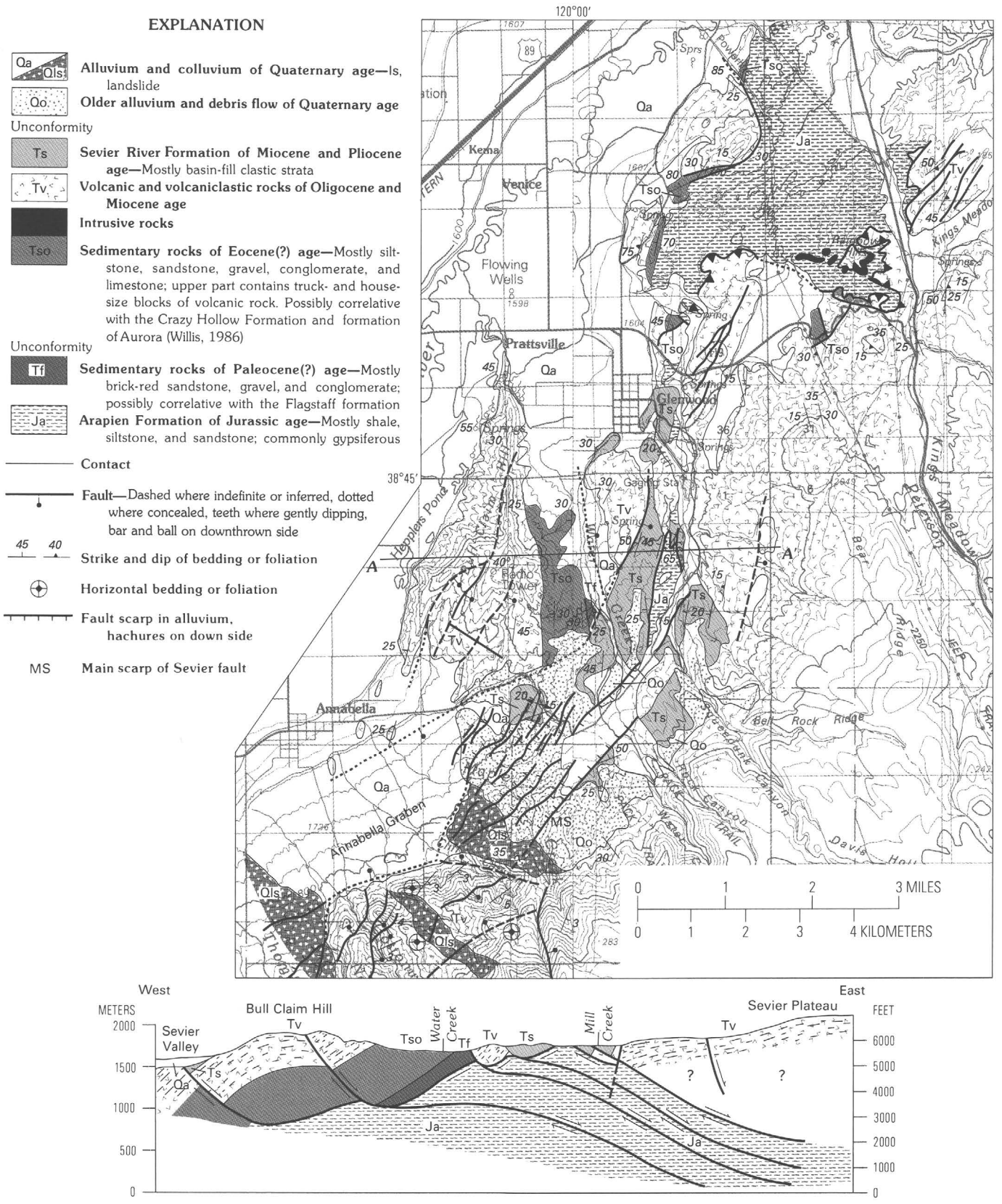

FIGURE 23.—Geology and cross section of the Annabella-Glenwood area. Low-angle faults in the Arapien Formation in the section schematically depict semiductile "flowage" of that mechanically incompetent unit out from beneath the Sevier Plateau. A large down-to-the-west fault analogous to the Sevier fault at the latitude of the cross section is not required. Except for beneath the Sevier Valley, areas underlain by Quaternary deposits are not shown on the cross section.

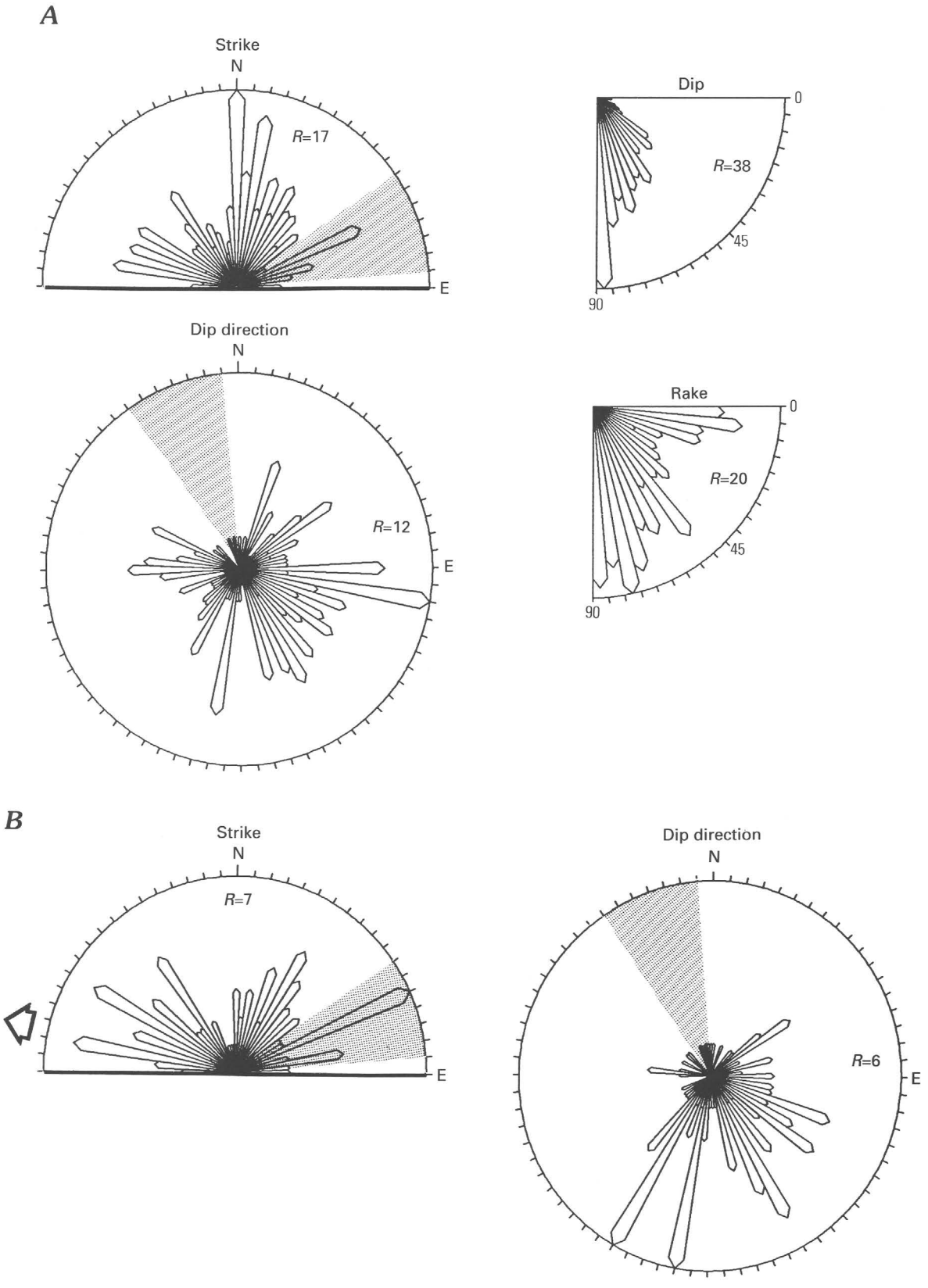
A
Strike
N
R=17
E
Dip
0
R=38
45
90
Dip direction
N
R=12
E
Rake
0
R=20
45
90
B
Strike
N
R=7
E
Dip direction
N
R=6
E

ANTICLINE SAMPLE

The southern part of the Sanpete-Sevier Valley anticline, cored by mechanically weak rocks of the Arapien Formation, is an important structural element in the central Sevier Valley area. For about 20 km south-southwest of Salina, a 5-km-wide core zone of Arapien rocks is exposed, and the adjacent Tertiary rocks tend to dip moderately to steeply (locally overturned) away from the core rocks. By contrast, in the area east of Glenwood and northeast of Annabella, Arapien rocks are exposed only locally in a narrow band, and Tertiary rocks dip uniformly westward, as depicted in cross section (fig. 23). We conducted reconnaissance fault-slip studies in Tertiary rocks at and above the contact with the Arapien. Those rocks contain abundant evidence of extensional deformation and structural attenuation at widely ranging scales and magnitudes. In many places, structural attenuation is so extreme that hundreds of meters of strata are reduced to broken or shattered layers a few meters thick. The ultimate contact with the Arapien is shown on published maps as depositional. We recognize it as a fault in most places. Although it ranges widely in dip direction and magnitude, it dips gently and is discordant to bedding in overlying rocks in many places and over wide areas.

Although we gathered fault-slip data as far north as Salina, the area of greatest interest is to the south, where it is clear that the upper Miocene and Pliocene basin-fill sediments of the Sevier River Formation are intensely involved in the deformation. Our studies in that area demonstrate that extensional deformation, locally of large magnitude and including severe structural attenuation, dominates the late Cenozoic structural record. Our results preclude a major role for the type of compressional tectonics suggested by Gilliland (1963).

Seventy-two fault-slip measurements were made on 69 faults in rocks at and above the contact between Arapien rocks and cover rocks. Although most faults strike northeast, parallel to the Sanpete-Sevier anticline, many have a more northerly strike (fig. 26*A*). Rake angles are varied but mostly steep, and the faults dip more moderately than those in any of the other areas that we sampled. The moderate dips probably result from rotation of faults during extension. On faults displaying polyphase slip, striae having the shallowest rake angles are the youngest on 2 of the 69 faults; data are thus insufficient to establish whether dip-slip faulting is older or younger than strike-slip faulting.

To evaluate the significance of dip-slip faulting separately from that of strike-slip faulting, we present strike- and dip-direction histograms for a subsample of 49 normal faults taken from the entire 69-fault sample (fig. 26*B*). The data distributions are similar to those of the entire sample and show that many normal faults strike more northerly than the anticline and that there is a strong tendency for the faults to dip easterly, consistent with our qualitative field observation that Tertiary rocks dip uniformly westward and are downdropped uniformly eastward across the southernmost part of the anticline. Taken together, these relationships suggest that some process other than anticlinal folding was active during

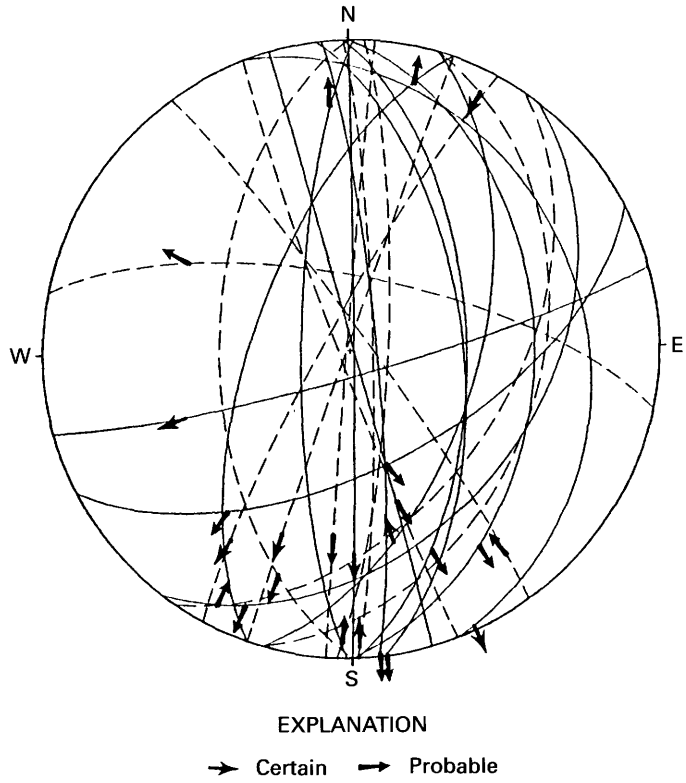

FIGURE 25.—Lower hemisphere stereographic plot of a subsample of predominantly strike-slip faults derived from the sample shown in figure 24*A*. Only faults displaying certain and probable slip-sense determinations are shown, and they are distinguished by different types of arrows. The bases of the arrow shafts mark lineations, and arrows point in the directions of motion of hanging-wall blocks. Solid lines are dextral faults, and dashed lines are sinistral faults.

◀ FIGURE 24.—Histograms of faults and striations from Tertiary volcanic and sedimentary rocks along the Annabella segment of the Sevier fault (Annabella sample area). *R*, radius of the histogram, in number of measurements. Patterned sectors on the strike plots and the dip-direction plots show the average trend of the range front and the facing direction of the range front, respectively (±15°). *A*, Strike, dip, rake, and dip-direction distributions for 235 faults. Very few faults strike parallel to the range front, and there is no tendency for faults to dip toward the downthrown block of the Sevier fault. *B*, Strike and dip-direction distributions for a subsample of 90 normal faults derived from the sample represented in *A*. Even the normal faults show no tendency to dip toward the downthrown block of the Sevier fault. The arrow shows the computed azimuth of σ, the minimum principal compressional stress.

extension and that the anticline did not exert a strong influence on fault kinematics during the extension. This suggestion is supported by a weakly constrained least principal stress direction of 282° computed from the subsample of 49 normal faults (fig. 26*B*, table 1). This orientation is closer to the orientations computed from other sample areas than it is to a direction perpendicular to the anticline. It is almost identical to the orientation computed for the Annabella segment to the south (fig. 24) (also weakly constrained), even though the two sample areas have dramatically differing structural settings. We conclude that regionally significant extensional faulting and associated structural attenuation are the dominant deformational mode in the cover rocks of the southern part of the anticline. Where the Sevier River Formation is exposed, it is involved in the full range of this deformation and thus leads us to conclude that the deformation is neotectonic.

To evaluate the significance of strike-slip faulting separately from dip-slip faulting, we present a lower hemisphere stereographic plot of those faults and striations (fig. 27*A*). This subsample of 29 faults shows orientation diversity similar to that seen in the strike-slip subsample of faults from the Annabella segment directly to the south (fig. 25). This similarity is remarkable in light of the highly contrasting structural settings of the two areas. In particular, there is no tendency of the diversely dipping north- to northeast-striking faults to divide into sinistral and dextral fields, as one would expect if they were conjugate faults. Data gathered from individual exposures (fig. 27*B*, *C*) indicate that faults having generally east-west strikes are probably block-bounding structures genetically linked to systems of predominantly normal faults whose motions are a response to generally east-west extension. Neither these faults (because of their lack of slip independance (Angelier, 1979)) nor the north- to northeast-striking ones (because of their slip incompatibility) are candidates for paleostress analysis. Perhaps the components of strike-slip motion on north- and northeast-trending faults are a response to north-south shortening or to tractions imparted to the base of an extending slab by lateral flowage of subjacent rock. Either possibility is consistent with a strong component of anticline-parallel shortening suggested in north-trending cross sections drawn by Hardy (1952). The possibility of basal tractions is explored more fully in a subsequent section on seismicity and Quaternary deformation.

NORTHERN ANTELOPE RANGE

The part of the Antelope Range adjacent to the Dry Wash fault consists of a fault-repeated sequence of Oligocene and Miocene flows and tuffs displaying east to northeast dips ranging from 5° to 45° (Cunningham and others, 1983). Mapped faults strike mostly north to northeast and drop strata down to the west. No evidence was found for the east-trending folds that are common in the Clear Creek area across the Dry Wash fault. Because the northern Antelope Range consists of a more orderly arrangement of fault-tilted blocks than most other areas in the region, it was hoped that a straightforward relationship between fault slip, block tilting, and extensional deformation consistent with the mapped structural pattern could be discerned. Instead, a reconnaissance of fault slip reveals a complex mixture of strike slip, oblique slip, and dip slip that cannot be understood in terms of a single deformational event or any simple structural pattern.

Paleoslip was measured on 135 faults. Displacement on 108 of them is known or estimated to be less than 1 m; on the remaining 27, it ranges from 1 to more than 100 m. Most measurements were made within 3 km of the trace of the Dry Wash fault. Of the 135 faults, 17 contain polydirectional striae; on all but 1, the oldest slip event has the lowest rake. This indication that dip-slip faulting is consistently younger than strike-slip faulting agrees with observations near locality B (fig. 3) in the Clear Creek downwarp but is not a feature recognized in all other areas that we studied.

Some major dip-slip faults in the northern Antelope Range displace the sparsely preserved Sevier River Formation by at least 100 m. We assume that the strike-slip displacements also postdate the Sevier River Formation because they do so in the adjacent Clear Creek area.

Fault strikes are mostly north and northeast, and sinistral slip predominates over dextral slip in the strike-slip subset, similar to the faults in the Clear Creek sample area (figs. 10, 28). The proportion of faults having rake angles greater than 30° and a component of reverse slip is larger in this sample area than it is in the others. As is the case with a major, steeply north-dipping,

FIGURE 26.—Histograms of faults and striations from the Tertiary cover rocks of the Sanpete-Sevier anticline (anticline sample). *R*, radius of the histogram, in number of measurements. *A*, Strike, dip, rake, and dip-direction distributions for 72 faults; the solid arrow marks the approximate trend of the axis of the Sanpete-Sevier anticline. *B*, Strike and dip-direction distributions for a subset of 49 normal faults derived from the sample represented in *A*. The open arrow shows the computed azimuth of σ_3, the minimum principal compressional stress. The anticline trend approximately bisects the dispersion pattern of fault strikes. This occurrence, together with the moderate fault dip, computed σ_3, and abundant field evidence for large-magnitude fault-related attenuation, shows important extension at a high angle to the trend of the anticline. Some of the strike-slip faults (eliminated from *B*) are block-boundary faults coupled to the normal faults as shown in figure 27.

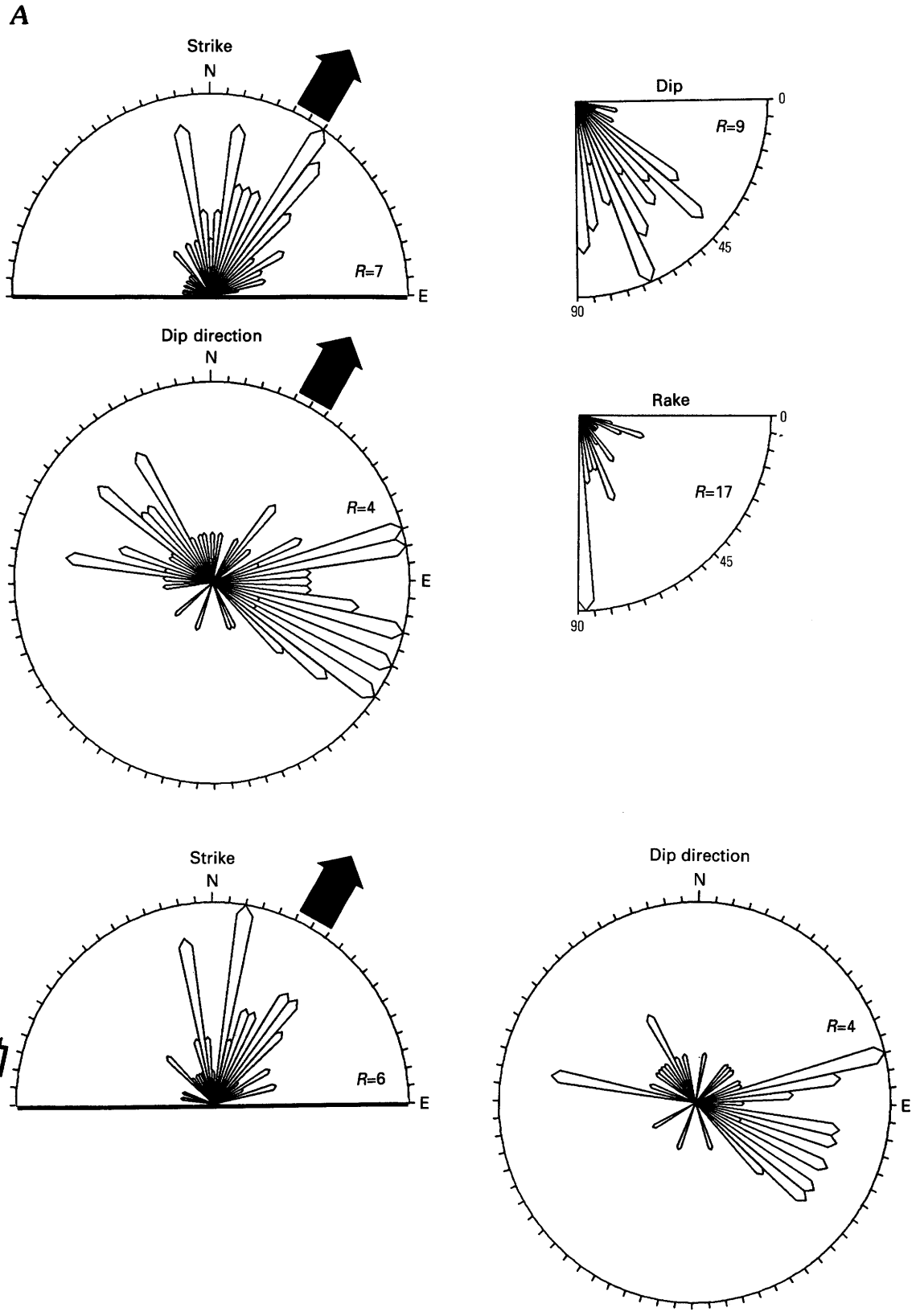
A
Strike
N
R=7
E
Dip
0
R=9
45
90
Dip direction
N
R=4
E
Rake
0
R=17
45
90
B
Strike
N
R=6
E
Dip direction
N
R=4
E

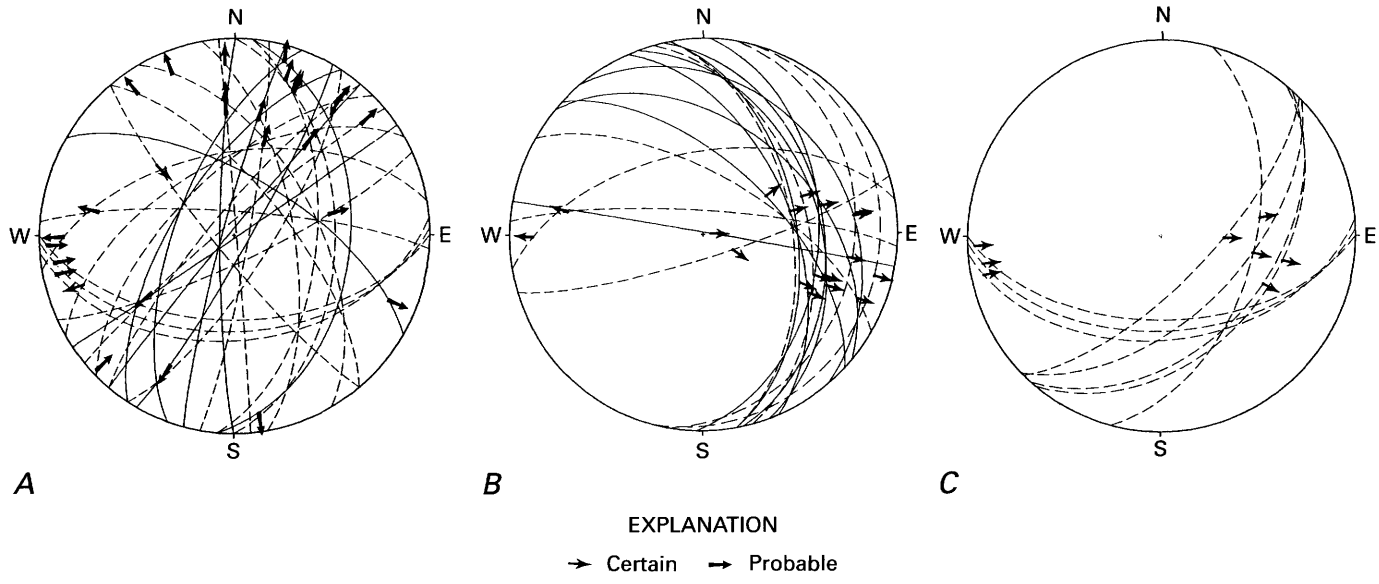

FIGURE 27.—Stereographic plots of faults that cut Tertiary rocks at or above the contact with the mechanically weak Arapien Formation along the southern part of the Sanpete-Sevier anticline. Solid lines are dextral faults; dashed lines are sinistral faults. *A*, Subsample of 29 predominantly strike-slip faults derived from the sample shown in figure 26*A*. *B*, Faults and striae from a group of closely spaced exposures of highly fractured welded ash-flow tuffs on the eastern flank of the anticline. The bases of arrow shafts mark lineations, and arrows point in directions of motion of hanging-wall blocks. *C*, Faults and striae from an exposure on the western flank of the anticline. The bases of arrow shafts mark lineations, and arrows point in directions of motion of hanging-wall blocks. Strike-slip faults in *B* and *C* are also shown in *A*. That group of strike-slip faults is interpreted as block-boundary structures genetically and mechanically related to the dip-slip and oblique-slip motions represented by the easterly directed clusters of arrows in *B* and *C*.

east-striking sinistral and reverse-sinistral fault at locality F (near the southern boundary of fig. 3) (fig. 29), it is generally not possible to distinguish between true reverse faults and subsequent rotation by later faulting. Of the 92 measurements made on faults having rake angles greater than 30°, the slip sense on 17 indicates reverse slip. Neither these 17 measurements nor the 56 measurements of strike-slip striae having rake angles of 30° or less are qualitatively consistent with the mapped pattern of fault-repeated and fault-tilted blocks.

In summary, a reconnaissance investigation of fault slip in the northern Antelope Range reveals complex data distributions, many aspects of which are qualitatively inconsistent with what would be expected from the mapped structural patterns. The structural significance of the complexities is not understood. Also, the data provide no basis for meaningful paleostress computations. Nevertheless, the common occurrence of reverse-slip and strike-slip displacements represented by the striae that we observed indicates that the faults clearly did not result from straightforward application of extensional stresses in which σ_1 was in an approximate vertical position. As is the case with the other areas that we studied, a horizontal maximum compression or a lateral tectonic transport of blocks, possibly caused by tractional forces applied from below, or both are required to produce some of the deformation.

SEISMICITY AND LATE QUATERNARY DEFORMATION

Seismicity studies in the Intermountain Seismic Belt by W.J. Arabasz and his students at the University of Utah, using a combination of permanent regional and temporary local seismic networks, have established the distribution of earthquake epicenters and have yielded an extensive sample of earthquake hypocenters and fault-plane solutions (Arabasz and Julander, 1986). Earthquake epicenters in western Utah tend to form clusters, and there is, in general, no clear-cut spatial association between those clusters and fault scarps formed on Quaternary alluvium. In the central Sevier Valley, however, two areas of concentrated seismicity do coincide with areas of late Quaternary surface deformation. One, a magnitude 4.0 main shock and aftershock sequence, occurred in 1982 in the area northeast of Annabella, where late Quaternary fault scarps are common. (All magnitudes reported herein are local Richter magnitudes taken from Arabasz and Julander (1985).) The other is directly southwest of Elsinore, where we recognize tilted Quaternary geomorphic surfaces, late Quaternary fault scarps, and possible deformation-related anomalies in the channel pattern of the Sevier River. In both areas, complex junctures between major mapped structures are logical candidates for localization

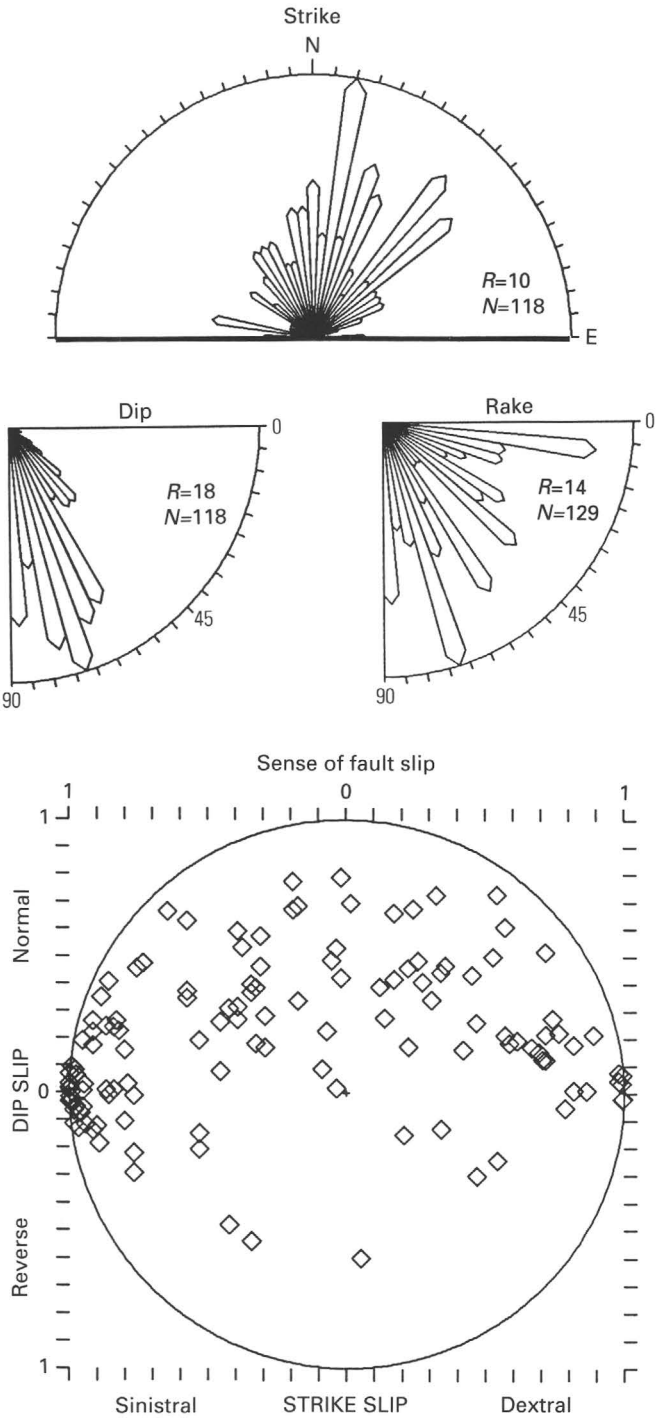

FIGURE 28.—Histograms of strike, dip, and rake and plot of dip-slip versus strike-slip components of fault slip for faults in the northern part of the Antelope Range. *R*, radius of the histogram, in number of measurements; *N*, sample size. Note the wide distribution of rake angles, the significant number of reverse-slip faults, and the strong bias for sinistral slip. Only in the distribution of strike and the bias for sinistral slip do these data distributions resemble those from the adjacent Clear Creek sample area (fig. 10).

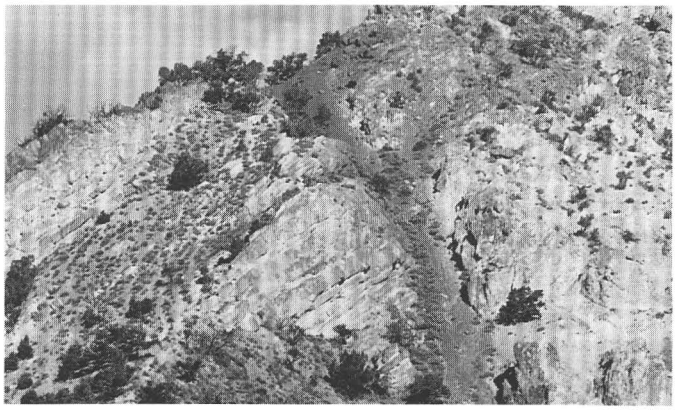

FIGURE 29.—View looking west at the surface trace of a high-angle fault in the Antelope Range at locality F in figure 3. Hydrothermally altered and fractured rocks of the Bullion Canyon volcanics form the upthrown hanging wall on the right, and stratigraphically higher, unaltered volcanic sediments in the lower part of the Mount Belknap Volcanics (Cunningham and others, 1983) form the footwall block. Bedding in the footwall dips about 40° south, whereas the fault dips 60° to 80° north. Striations and stratigraphic separation indicate reverse and reverse sinistral movement on the fault. However, it is not known whether the bedding and the fault were tilted after faulting, an occurrence that would make the structure a tilted normal-sinistral fault.

of the seismicity—the Sevier fault system east of Annabella and the northeasternmost extent of the Dry Wash fault in the Elsinore area. These two coincidences are very unusual in the Intermountain Seismic Belt, where generally an association between seismicity and known mapped structures is not possible (Smith, 1978; Arabasz and Smith, 1981). Because the coincidence of seismicity with mapped faults offers an opportunity for improving understanding of the relationship between mapped faults, surface deformation, and seismicity, we will discuss each area in some detail. But first, we will make some general comments on the seismicity of the region.

Analysis of 53 fault-plane solutions by Arabasz and Julander (1986) shows that seismic slip in the transition zone is characterized by a mixture of strike-slip and normal faulting, as the summary of those results shows in figure 30. They suggested that this mixture results from interchanges in the positions of σ_1 and σ_2, whereas σ_3 remains stationary and approximately horizontal at about 102°.

In three areas in the Intermountain Seismic Belt, Arabasz and Julander (1986) recognized that horizontally bounded zones of microearthquake hypocenters correlate with known or inferred subhorizontal thrust faults. On the basis of this correlation, they hypothesized that the depth distribution of background seismicity is controlled by the internal structure and variable mechanical behavior of horizontal plates bounded by major low-angle faults within the seismogenic upper crust (fig. 30). They stated

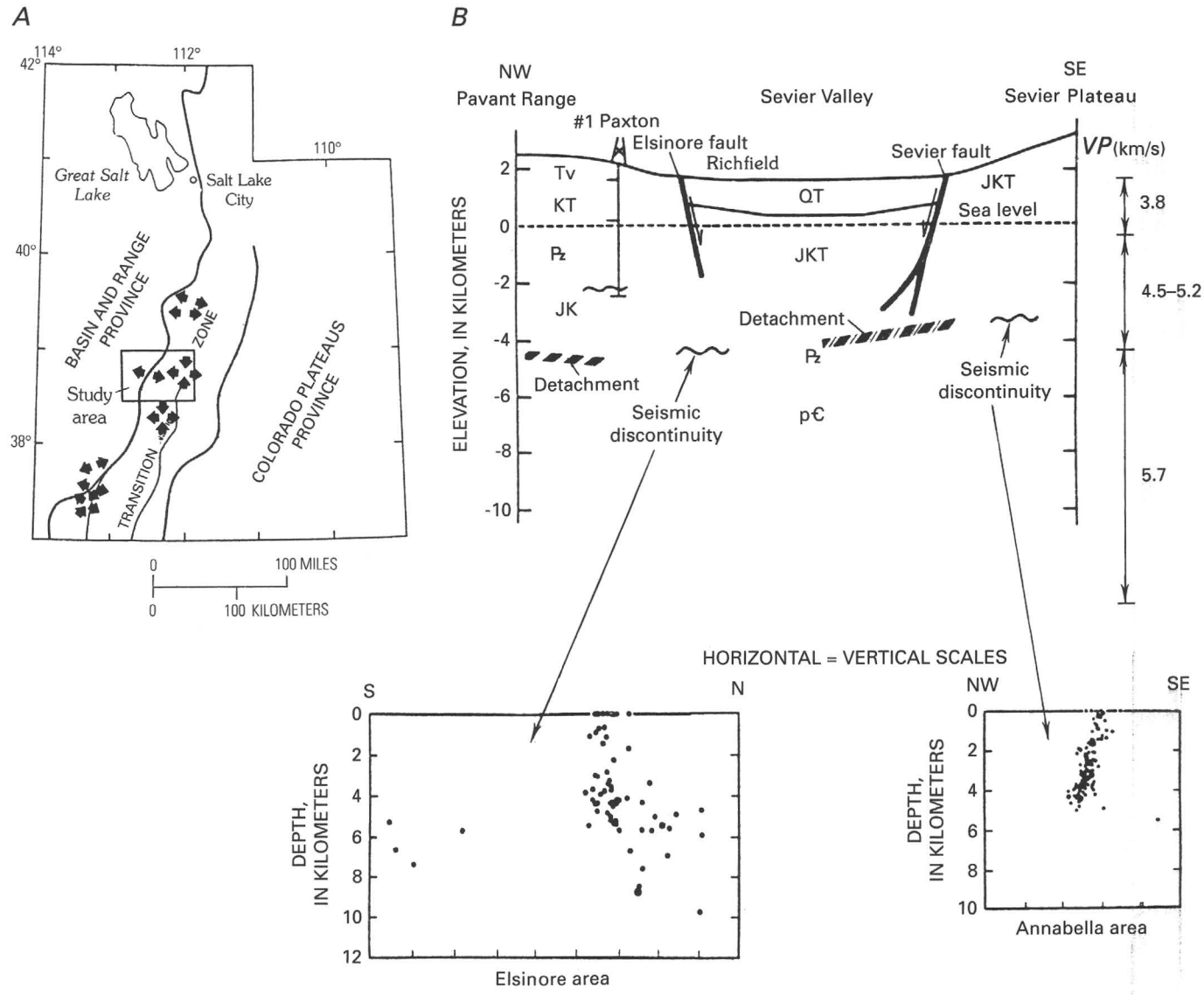

FIGURE 30.—Aspects of seismicity in the transition zone. *A*, Map showing sample of current stress orientations inferred from earthquake focal mechanisms for the transition zone. The single outward-directed arrows are least-compressive-stress directions inferred from dip-slip focal mechanisms; the combined inward- and outward-directed arrows are maximum- and least-compressive-stress directions inferred from strike-slip focal mechanisms. *B*, The lower part shows depth distribution of microseisms in the Elsinore and Annabella areas, and the upper part shows the correlation in schematic cross section between the seismic discontinuities suggested by the depth distributions and detachment faults inferred from reflection seismicity. V_P, P-wave velocity. p€, Precambrian rocks; Pz, Paleozoic rocks; JK, Jurassic and Cretaceous rocks; JKT, Jurassic, Cretaceous, and Tertiary rocks; KT, Cretaceous and Tertiary rocks; Tv, Tertiary volcanic rocks; QT, Tertiary and Quaternary basin-fill sedimentary rocks.

that this heterogeneity, which influences the depth distribution of earthquakes, was produced by vertical stacking of thrust plates during Sevier-age overthrusting. Seismic slip on the bounding low-angle faults in any of the three areas or elsewhere in the Intermountain Seismic Belt is not evident and led Arabasz and Julander to speculate that such faults may move aseismically. The central Sevier Valley, including the concentrated seismicity in the Annabella and Elsinore areas, is one of the three areas in which Arabasz and Julander (1986) suggested the correlation between horizontal seismicity zones and low-angle faults (fig. 30).

NORTHEAST OF ANNABELLA

The part of the Sevier Plateau bounded on the west by the Monroe segment and on the north by the Annabella segment of the Sevier fault is best characterized as a weakly deformed, generally east-tilted, relatively intact structural block of Tertiary igneous rocks uplifted 0.5 to

2 km above its surroundings. In sharp contrast, the part of the Sevier Plateau north of the Annabella segment, including the Bull Claim Hills, is best characterized as a highly deformed series of west-tilted blocks of volcanic and sedimentary rocks that are repeated eastward by faults that drop strata down toward the east and southeast (toward the uplifted Sevier Plateau) (fig. 23). That area is also characterized by strong structural attenuation of the stratigraphic section, especially in the vicinity of the exposed Arapien Formation. The tilting, stratal repetition, and attenuation involve strata of the upper Tertiary Sevier River Formation to the same extent that they involve older Tertiary rocks, the suggestion being that the deformation is neotectonic. Between the two areas of highly contrasting internal structure and neotectonic structural vergence and tucked into the large physiographic embayment in the plateau margin is a northeast-trending graben that we refer to as the Annabella graben (fig. 23). Downdropped strata of the Sevier River Formation are preserved in the graben and are overlain unconformably by Quaternary landslides, debris flows, and coarse alluvial deposits that accumulated during graben formation. The Sevier River Formation in this area predates graben formation and plateau uplift. A K-Ar age of 5.6±0.4 Ma was determined by H.H. Mehnert on a sample of volcanic ash from the Sevier River Formation east of Annabella (H.H. Mehnert and P.D. Rowley, written commun., 1982).

An anomalous concentration of northeast-trending fault scarps ranging in height from less than 1 to more than 100 m is formed on the Quaternary deposits of the Annabella graben. These scarps are concentrated in an area of only 15 km^2. Individual fault-scarp lengths are less than 5 km. Some of the scarps are high and contain evidence for recurrent movement as late as the time of the Pleistocene-Holocene boundary (Anderson and Bucknam, 1979). The main fault in this area appears to be the fault labeled MS in figure 23. This fault bounds the graben on the southeast. The surface scarp that marks the trace of this fault not only reveals strong evidence of recurrent late Quaternary movement, but it also has a large cumulative displacement of upper(?) Quaternary deposits of about 109 m; it is thus one of the highest fault scarps in alluvial deposits in Utah (figs. 31, 32). Its midslope section is 90 m long and has a slope of about 35°. To maintain such a large, steep slope resulting from slip events equivalent in size to the youngest event (fig. 31) requires about 25 small slip events spaced closely in time. Owing to complexities resulting from landsliding, it is uncertain how this fault connects with the Annabella segment of the Sevier fault (fig. 23).

A magnitude 4.0 main shock and an extensive aftershock sequence in 1982 are centered on the Annabella graben (Arabasz and Julander, 1986). First-motion data for the main shock are inconsistent with the focal mechanism characteristics of and planar distribution of the aftershock sequence (fig. 33). Of several nodal planes allowed by first-motion data of the main shock, a northeast-striking southeast-dipping plane displaying predominantly normal slip would correspond well with the fault that bounds the Annabella graben on the northwest. Alternatively, hypocenter distributions resulting from detailed aftershock studies define a northeast-trending envelope dipping about 75° NW. (fig. 33). The envelope is only about 5 km long by 3 km wide and 5 km deep (fig. 33). Although such an envelope agrees well with any of several similarly oriented faults marked by Quaternary scarps in the Annabella graben, the aftershocks that define it yield focal mechanisms indicating predominantly strike slip on steeply dipping faults, and the envelope does not match any of the main shock's nodal planes. Thus, the faulting kinematics indicated by this seismicity are internally enigmatic, and their relationship to mapped faults is unresolved. Nevertheless, the spatial coincidence of this seismicity and the area of anomalously disrupted upper Quaternary deposits suggests to us a genetic relationship between the seismicity and scarp-producing faults.

The aftershocks of the 1982 seismicity define two types of focal mechanisms having approximately interchangeable pressure (P) and tension (T) axes (Arabasz and Julander, 1986). The preferred orientation for the T axes is approximately east-west, similar to the orientation indicated by the main shock (Arabasz and Julander, 1986). If the T axes are inferred to be colinear with the extension direction, a simple interchange between σ_1 and σ_2 satisfies most of the data. The internally incompatible strike-slip events can be related to the oblique-slip main shock by assuming that release of extensional stress creates a secondary compensatory motion of blocks parallel to the preexisting northeast-trending dominant structural fabric. In the case of the 1982 aftershocks, we would choose the northeast-striking dextral and sinistral nodal planes and would assume a southwest-directed tectonic transport of blocks bounded by faults analogous to these nodal planes. Such deformation would have to result from some secondary system of basal tractions or horizontally layered stress gradients felt by the blocks as extension progresses. This conjectured deformation is consistent with our fault-slip data, which indicate a mixture of dip slip and strike slip, and, in particular, with the tectonic transport parallel to the axis of the Sanpete-Sevier anticline indicated by the incompatible strike-slip striae from the Annabella segment and the southern Sanpete-Sevier Valley anticline. It is also consistent with the pattern of north-south shortening shown by folds

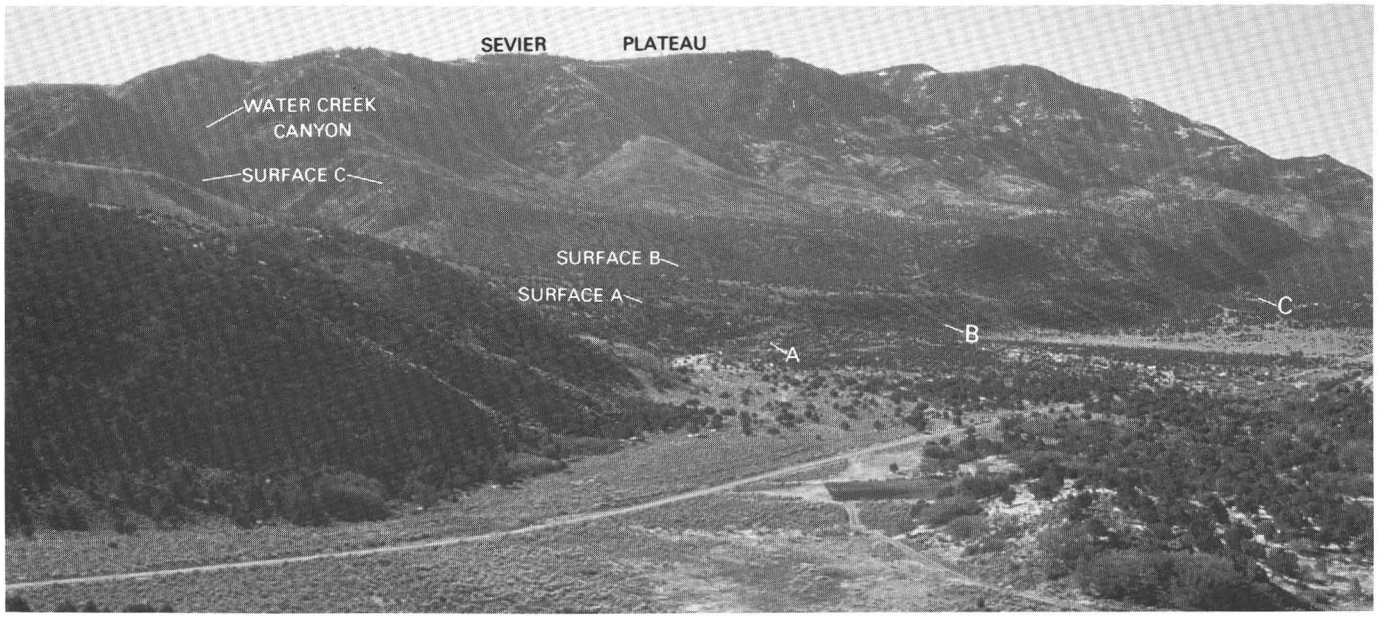

FIGURE 31.—View to the south across the northeast-trending main strand of the Sevier fault toward the Glenwood Mountain part of the western Sevier Plateau. Geomorphic surfaces labeled A, B, and C terminate to the northwest against conspicuous scarps that mark the trace of the Sevier fault. Lettered lines A, B, and C below the respective surfaces point to localities where the scarp profiles shown in figure 32 are measured. The irregularly forested area beneath the scarps is part of a structurally complex graben containing clastic sediments of Miocene to Quaternary age. In contrast, linear elements of the Glenwood Mountain skyline as well as crudely banded vegetation patterns beneath the skyline reflect the structural simplicity of that structural block. The uplifted remnants of surface C that are found on both sides of Water Creek Canyon are interpreted to be parts of a once-continuous surface that predates cutting of the canyon. That surface is smoothly graded across the alluvium-bedrock contact high in the plateau margin, and there is no suggestion there of displacements by young faults.

between Glenwood and Salina (Hardy, 1952). We return to this notion of basal tractions in "Summary and Discussion."

Late Quaternary faulting and seismicity may be concentrated in the Annabella graben, because a structural juncture exists here between the down-to-the-west and down-to-the-northwest faults related to the Sevier fault and the dramatically different set of down-to-the-east structures along the northern and northeastern projection of the Sevier fault. An east-northeast-trending transverse zone of structural accommodation seems to be required beneath the graben. Concentration of stress in such a zone would be expected. The short length of fault scarps, the fact that they do not rupture contemporaneously, and the small size of the area containing them does not portend large-magnitude (6.5–7.5) earthquakes associated with their development. In particular, there is no justification for assuming that the concentrated young deformation is characteristic of the Sevier fault. Slip events on the Sevier fault from the graben southward are likely to be associated with larger earthquakes having much longer return periods than the earthquakes that produced the scarps.

Witkind (1982) noted the colinearity of the Sanpete-Sevier Valley anticline and the Sevier fault and suggested a genetic relationship between the two. Within this same context, we suggest an alternative interpretation for the concentration of seismicity and young deformation. The concentration could be related to lateral movement of the relatively ductile rocks of the Arapien Formation. The southernmost exposures of the Arapien are directly northeast of the graben, and equivalent rocks could exist in the shallow subsurface beneath the graben. Perhaps Arapien rocks have flowed into the extensional regime of the northeasterly projection of the Sevier fault where, because of a reduction in confining pressure, they tend to spread laterally. As Witkind (1982) suggested, movement of the Arapien could be stimulated by displacements on buried faults. Arapien rocks could be supplied to the fault zone from beneath the Sevier Plateau. This possibility is consistent with our observations in the vicinity of exposed Arapien rocks, where there is an indication that these rocks have been drawn out from beneath the Sevier Plateau (fig. 23). Such flowage would tend to remove most or all surface and near-surface traces of the Sevier fault. Although this hypothesis is an attractive alternative for explaining the thin-skinned extensional attenuation in rocks above the Arapien, it does not explain fault-slip and seismicity data indicating that strike-slip motions are common on north-

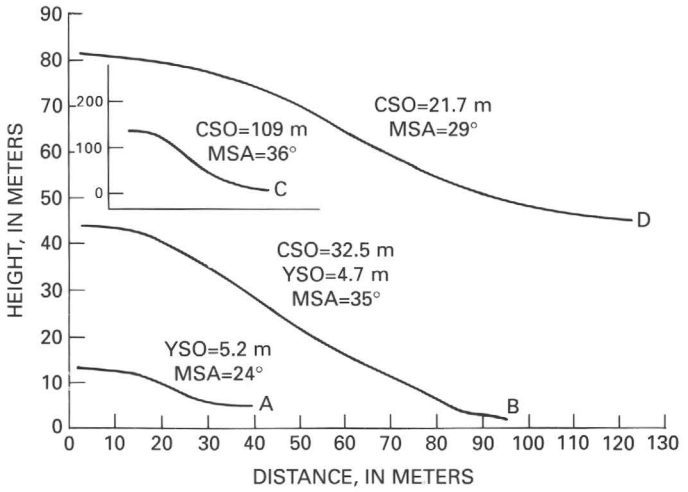

FIGURE 32.—Profiles across scarps formed on late Quaternary alluvium and debris flows in the Annabella area. Profiles A, B, and C cross the main strand of the Sevier fault at localities identified by corresponding letters in figure 31. CSO, cumulative surface offset; YSO, young surface offset; MSA, maximum slope angle. Profiles A and B were measured with a clinometer. At profile A, the fault offsets the youngest terrace above the modern stream bed at the mouth of Water Creek Canyon, whereas the same fault at profile B offsets an older and higher terrace a short distance to the south of A. The young surface-faulting event represented by profile A produced a surface offset of 5.2 m. That surface-faulting event, which probably occurred close in time to the Pleistocene-Holocene boundary, is shown in profile B by a 20-m-long scarp midsegment displaying an average slope near the angle of repose at 35°. This oversteepened part of the compound scarp yields a young surface offset of about 4.7 m, similar to that of the single-event scarp at A. This young faulting event is probably also expressed in the high compound scarp at locality C (note the tenfold scale difference), but it cannot be discriminated, because that profile was constructed from data on the 1:24,000-scale topographic map (Water Creek Canyon, Utah) and therefore only approximates the true surface profile. A remarkably large planar part of the scarp at C stands approximately at the angle of repose (compare profile C with the photograph in fig. 31), indicating numerous late Quaternary faulting events. With a surface offset of about 130 m, it is probably the highest late Quaternary fault scarp in alluvial deposits in Utah. Profile D was measured with a clinometer on a northeast-striking fault scarp 1.5 km northwest of the scarp at locality C. It is included to show that other scarps in the Annabella area do not reflect the same high rates of activity that are found on the main strand of the Sevier fault.

and northeast-trending faults and that lateral motions have occurred parallel to the principal fault-fold trend. These factors introduce complexities that seem to require competing deformational processes.

SOUTHWEST OF ELSINORE

The Elsinore area is one of the most seismically active areas in Utah. Five earthquakes of magnitude 5 or greater are assigned to the area—two in 1910 and three in 1921 (Williams and Tapper, 1953; Arabasz and McKee, 1979). An intense cluster of microseisms ($M \leq 1.9$) recorded in 1981 about 4 km southwest of Elsinore (Julander, 1983) is centered at the alluviated gap connecting Joseph Flats with the broad Sevier Valley. The envelope containing the densest part of the cluster dips steeply and has an east-west strike. Eight focal mechanisms all indicate predominantly strike-slip faulting (Julander, 1983). As is the case with the aftershocks northeast of Annabella, the focal mechanisms divide into two types having approximately interchangeable P and T axes and are indicative of strong slip inhomogeneity and incompatibility.

North of the alluvial gap at Joseph Flats, at a locality marked X on figure 34, faulted and tilted Sevier River Formation is unconformably overlain by Quaternary alluvium. A fault at this locality having an attitude of 054°, 76° SE. and an estimated displacement of 30 m contains striated clay suggestive of a 34° rake to the southwest. The predominately strike-slip component is dextral. Although we have no direct evidence of the direction and sense of slip on the Dry Wash fault in the vicinity of the alluvial gap, its strike-slip component elsewhere is known to be sinistral. Therefore, the geologic record suggests incompatible strike slip on northeast-striking faults; this suggestion is geometrically and mechanically consistent with the microseismic data. Our preference is to interpret such incompatible slip as an indication of lateral block motion, as we have done with the faults northeast of Annabella.

A northwest-southeast gravity profile across Joseph Flats and the Dry Wash fault shows no significant anomaly at the fault (Halliday and Cook, 1978). Instead, a 10-mGal gravity low is located beneath Joseph Flats, its axis being about 2 km northwest of the fault trace. These data are consistent with our interpretation that the Dry Wash is primarily a strike-slip fault and that the alluvial basin beneath Joseph Flats results mainly from the southerly projection of an open south-southwest-plunging syncline (fig. 3).

Steven (1979) mapped north- to northeast-striking faults whose traces are well marked by scarps in Quaternary alluvium on the northern and southern flanks of the alluviated gap separating Joseph Flats from the Sevier Valley. A northeast-trending fault scarp about 3 m high is formed on a gently inclined river terrace (terrace 4, fig. 34), south of which are remnants of three additional geomorphic surfaces showing southward-increasing erosional dissection and southward-increasing eastward inclinations (fig. 35). The relationships suggest increasing eastward tilts on increasingly older Quaternary surfaces. The faulting, which appears to be mostly normal sense, and the tilting, which may be on the eastern flank of an anticline, paired with the syncline beneath Joseph Flats, seem to represent rates of Qua-

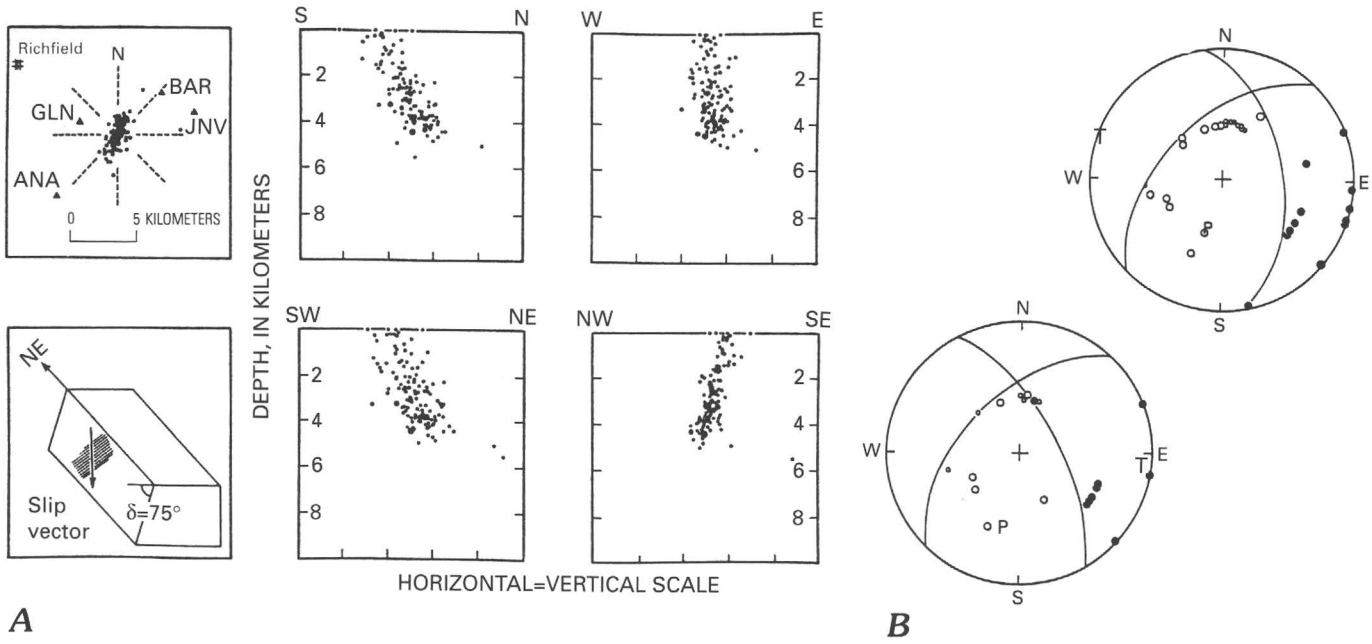

FIGURE 33.—*A*, Spatial distributions of aftershock foci in the Annabella area (lettered triangles represent seismograph stations). *B*, Focal mechanisms for the 1982 magnitude 4.0 main shock (upper stereogram) and magnitude 2.7 aftershock (lower stereogram) (from Julander, 1983). The earthquake foci are shown in map view (upper left-hand square) and cross section (center and right-hand squares). The block diagram (lower left-hand square) shows the planar orientation of clustered foci and slip direction from the main shock. For focal mechanisms, the solid circles represent compression, and open circles represent tension. P and T are pressure and tension axes. δ, dip of fault; shaded area, fault surface.

ternary deformation higher than those seen along major structures extending away from the alluviated gap.

Within the alluviated gap, the channel pattern of the Sevier River appears to have responded to young deformation. Along the 3.5-km reach downstream from Joseph, the channel pattern changes from sinuous to reticulate. Where the river crosses the projection of the Dry Wash fault (fig. 36*A*), the pattern changes abruptly from reticulate to a sinuous or island-braided pattern. This abrupt change is analogous to an experimentally supported model of a meandering river carrying a combination of suspended- and bed-load sediment (like the Sevier River) that has had to adjust to an anticlinal uplift across its course (fig. 36*B*) (Ouchi, 1985). The east-side-up fault displacement in the alluviated gap is analogous to an uplift axis at the fault trace. The reticulate pattern results from the damming effects of the uplift, which enhances flood-plain deposition upstream. The sinuous or island-braided pattern downstream of the uplift axis is a feature that results from the cutoff of intensified meander loops that develop first as the river attemps to lengthen its course to maintain its gradient across the oversteepened terrain. Although sufficient time has presumably lapsed since deformation for the Sevier River to reach this stage, the lapsed time is insufficient for the river to reestablish an equilibrium channel pattern analogous to the final stage shown in figure 36*B*. Although it is not possible to estimate these lapsed times, the fluvial patterns clearly support late Quaternary displacement on the Dry Wash fault system in this area. About 90 km northwest of Elsinore, we recognize an analogous anomaly in the channel pattern of the Sevier River where it flows southwest across the southern projection of the Drum Mountains fault scarp system of Holocene age southwest of Delta, Utah. The

FIGURE 34.—South-central part of the Monroe Northwest 7½-min quadrangle showing geology by Steven (1979), modified and augmented in the present study. Shaded and numbered areas are the four terraces first identified by Callaghan and Parker (1961) within which we estimate the average slope directions and values (arrows with numbers). The slope values represent best-fit planes through a series of highest-possible (ridge crests in dissected areas) points (number of points in parentheses) within the patterned areas. A computer-assisted stereometric procedure was used. The northernmost terrace (number 4) is represented by two areas separated by a fault scarp. Ts, Sevier River Formation; Tv, volcanic rocks of Tertiary age. Heavy lines, faults (dashed where buried, ball and bar on downthrown sides). A representative sample of attitudes in the Sevier River Formation shows that the gravels forming the geomorphic surfaces overlie unconformably tilted and erosionally truncated Sevier River Formation. The three high terraces (1 through 3), fault scarp, and two low-terrace elements (4) are identified in a south-looking photograph in figure 35. Young deformation in this area is probably responsible for an anomaly in the channel pattern of the Sevier River, as figure 36 shows. X indicates the locality referred to in the text. ▶

young deformation there appears to have affected a 35-km-long reach of the river and is suggestive of a basin-range-scale structural disturbance.

The displacement sense inferred from the stream-pattern anomaly near Elsinore is consistent with the pattern of eastern to northeastern tilting of geomorphic surfaces and the underlying Sevier River Formation in the area east of the northernmost Dry Wash fault (figs. 34, 35). If a range of ages is assigned to these east-tilted elements and if a specific size and geometry are assigned to the structural block containing them, it is possible to compute a range of uplift rates for the terrace-bearing block. The computed range can then be compared with uplift rates on faults in the eastern Great Basin region.

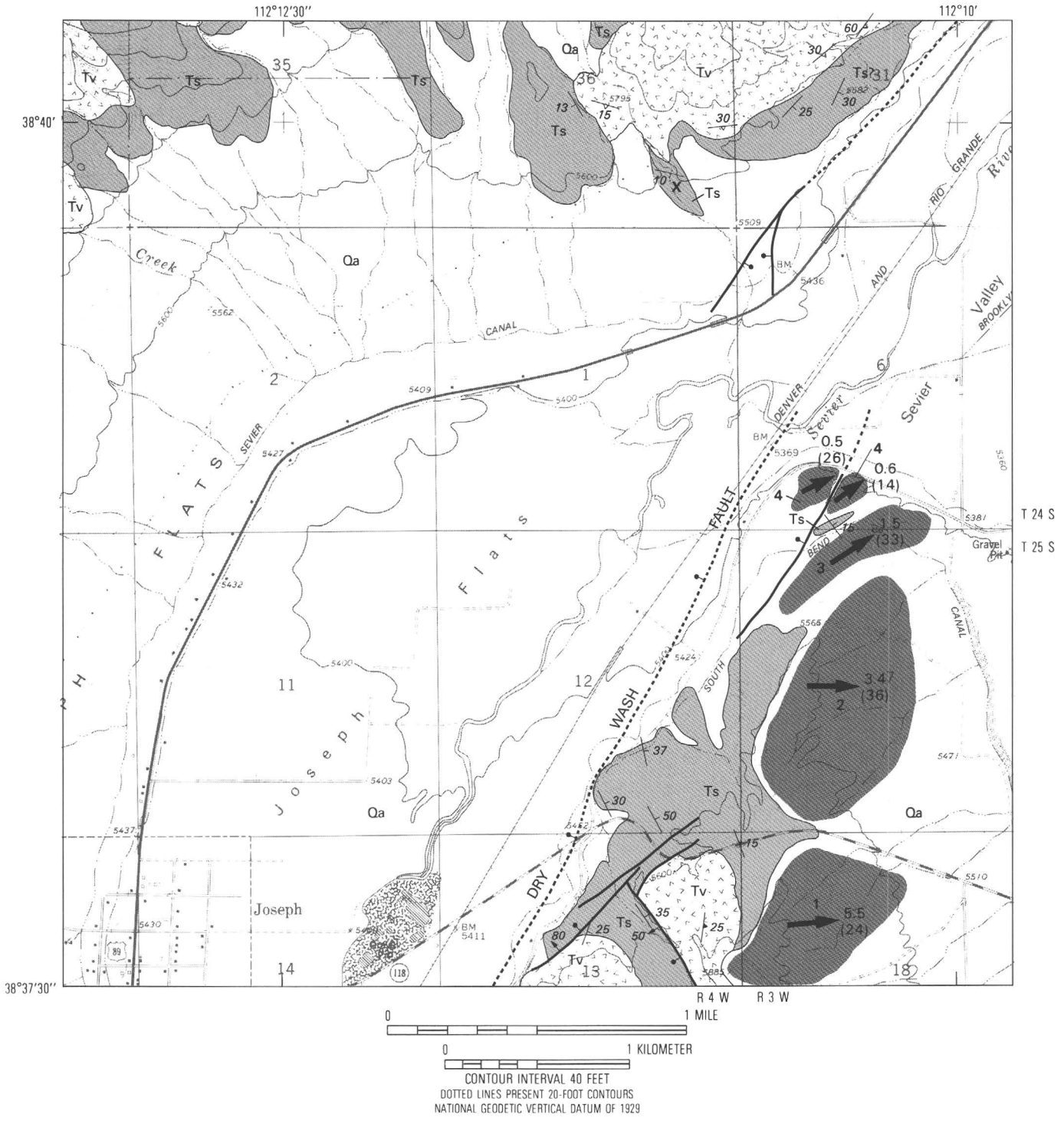

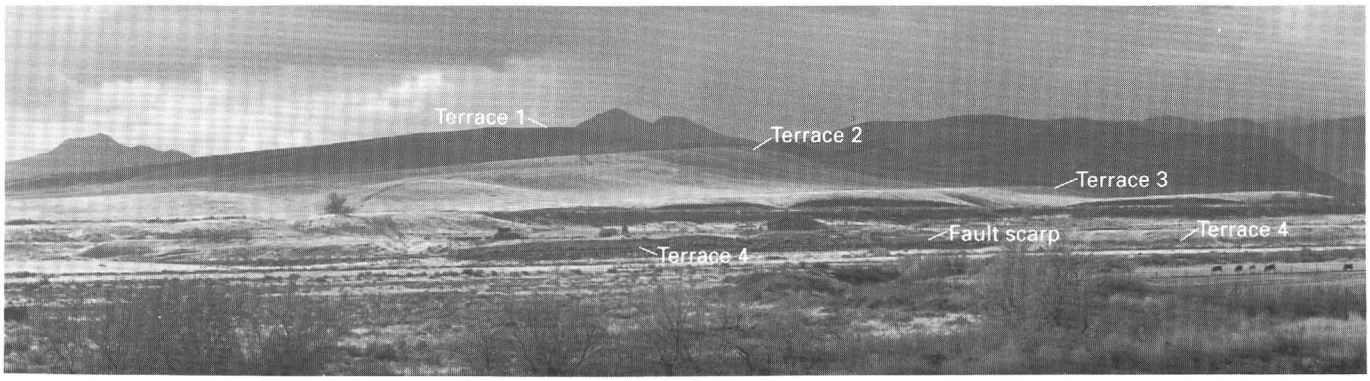

FIGURE 35.—View looking south showing terraces that have progressively greater height and greater eastward tilts with greater age. Age is inferred from the height above the grade of the Sevier River and the degree of erosional dissection. The conspicuous shaded scarps below terrace 3 are excavations for an irrigation ditch; those below terrace 4 result from erosional trimming by the Sevier River. Slopes of the terraces are given in figure 34. Access was denied to the area where fault scarp could be studied. Only the relative ages of the terraces are known.

We assume that the slope angles shown in figure 32 represent structural tilts of a block 2 km wide and that the block is bounded by the gravity step beneath Joseph Flats on the west and is hinged along its eastern edge. We assign age ranges of 2 to 5×10^4 years for the 0.5°-tilted surface, 2 to 5×10^5 years for the 5.5°-tilted surface, and 1 to 5×10^6 years for the duration of tilting of the 15°-tilted Sevier River strata. The rate of uplift required to produce those tilts in the assumed time slots ranges from about 0.4 to 1.0 mm/yr for the two geomorphic surfaces and from 0.1 to 0.6 mm/yr for the Sevier River Formation. The range of lower rates (0.1–0.4 mm/yr) seems to us to be more reasonable than the range of higher rates because it falls below the approximately 0.4-mm/yr long-term rates of uplift on the Wasatch and Hurricane faults (Anderson and Mehnert, 1979).

Because of large uncertainties in the epicentral locations of the magnitude 5 or greater 1910 and 1921 earthquakes near Elsinore, no direct association can be made between known Quaternary surface deformation and those earthquakes. Also, only a spatial association can be made between known Quaternary surface deformation and the microseismic record.

The geologic setting of the surface scarps and seismicity near Elsinore is complex. The northeastward projection of the Dry Wash fault (and the inferred flexure cut by it) beyond the alluvial gap between Joseph Flats and the Sevier Valley encounters the monoclinal flexure along the southeastern base of the Pavant Range. The fact that these two structures have opposite senses of vertical displacement suggests that such a projection is not reasonable in terms of dip-slip components. If both structures terminate in the vicinity of the alluvial gap, there is a need for a buried transverse structural zone to accommodate the dramatically contrasting along-strike deformational styles. Strain is likely to be concentrated in such a transverse zone. We infer that the concentration of seismicity and Quaternary surface deformation is related to this zone. If the predominantly sinistral-slip Dry Wash fault terminates at the alluvial gap, sagging might be expected in an area of extension northwest of the terminal segment, and uplift might be expected in an area of compression southeast of the terminal segment (Segall and Pollard, 1980). Uplift of the block containing the tilted terraces and depression of the block containing Joseph Flats could represent a highly imperfect distribution of extensional and compressional deformation related to the fault termination.

In summary, concentrations of seismicity and Quaternary deformation in the Elsinore and Annabella areas appear to be related to strong along-strike disparities in the geometry and vergence of major structures extending away from those areas. These disparities are probably sites of transverse zones of structural accommodation and strain concentration. They are located on opposite sides of the Sevier Valley and could, in fact, be parts of a single transverse zone. Strain rates, displacement histories, or other features that are relevant to earthquake hazards in those zones should not be assumed to be typical of the major structures extending from them or of the central Sevier Valley in general.

SUMMARY AND DISCUSSION

Multiphase deformation, possibly beginning with events related to the evolution of the Paleozoic miogeocline and extending through the compressional events of the Mesozoic and early Cenozoic Sevier and Laramide orogenies, fashioned a strong northeast-trending structural fabric in the central Sevier Valley study area. The compressional events probably also left the crust of the area structurally layered as a result of thrusting. The

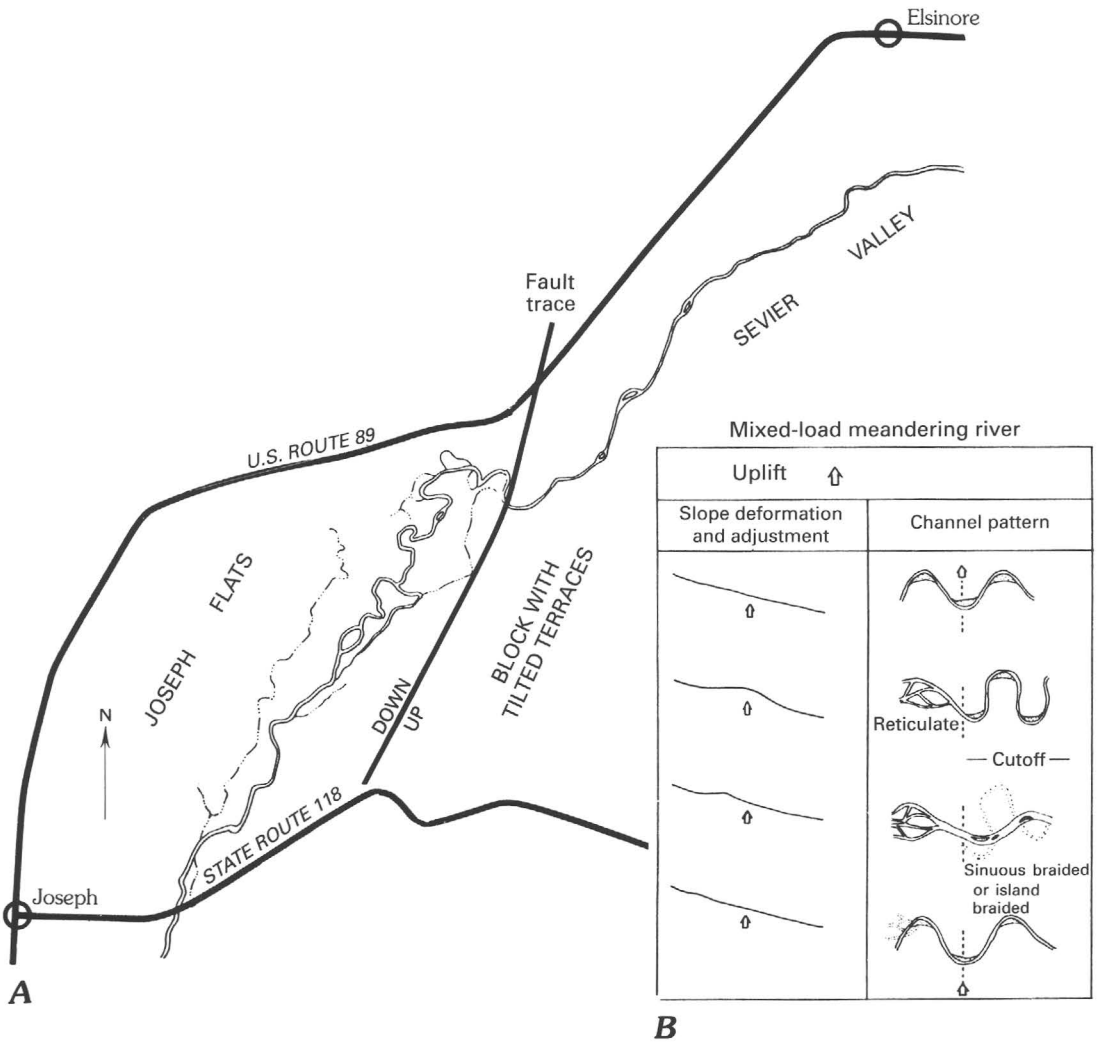

FIGURE 36.—*A*, Channel pattern of the Sevier River between Joseph and Elsinore (from the Monroe 15-min quadrangle, 1:62,500 scale, 1940) in relationship to an axis of relative uplift. *B*, Hypothetical model of the time-sequential response (age increases downward) of the slope and channel pattern to uplift across the course of a mixed-load (bed-load and suspended-load sediments) meandering river (from Ouchi, 1985). Note the similarity between the channel pattern of the Sevier River and the third stage of channel-pattern response.

control that these early structures exerted on the location, trend, and form of late Cenozoic structures is least in the southern part of the study area, probably because of crustal welding associated with large middle and late Cenozoic volcanic centers and their inferred subjacent plutons. Subsequent to the igneous activity and a phase of basin-fill sedimentation, the entire area became the structural transition zone between the Basin and Range and the Colorado Plateaus—an event that we identify as ushering in the neotectonic regime. Our structural studies, chiefly in the part of the area where the potential for control by preexisting structure is high, reveal the previously unappreciated importance of late Cenozoic folding, strike-slip faulting, and, locally, structural attenuation within this part of the transition zone. Thus, the fundamentally extensional neotectonic framework of the central Sevier Valley area must be examined not only in terms of the long and complex and sometimes controversial history of early events occurring in diverse tectonic settings but also in terms of the newly revealed evidence for neotectonic folding, strike-slip faulting, and detachment faulting. The magnitude and style of neotectonic deformation vary dramatically and portend strong strain inhomogeneity that introduces additional complications into analyses of neotectonic deformation. The main elements of the variations are shown in figure 37. They include sharp constrasts in (1) the amount of extension and structural attenuation, (2) the amount of strike-slip faulting, (3) the amount of monoclinal flexing associated with block-bounding structures, and (4) the

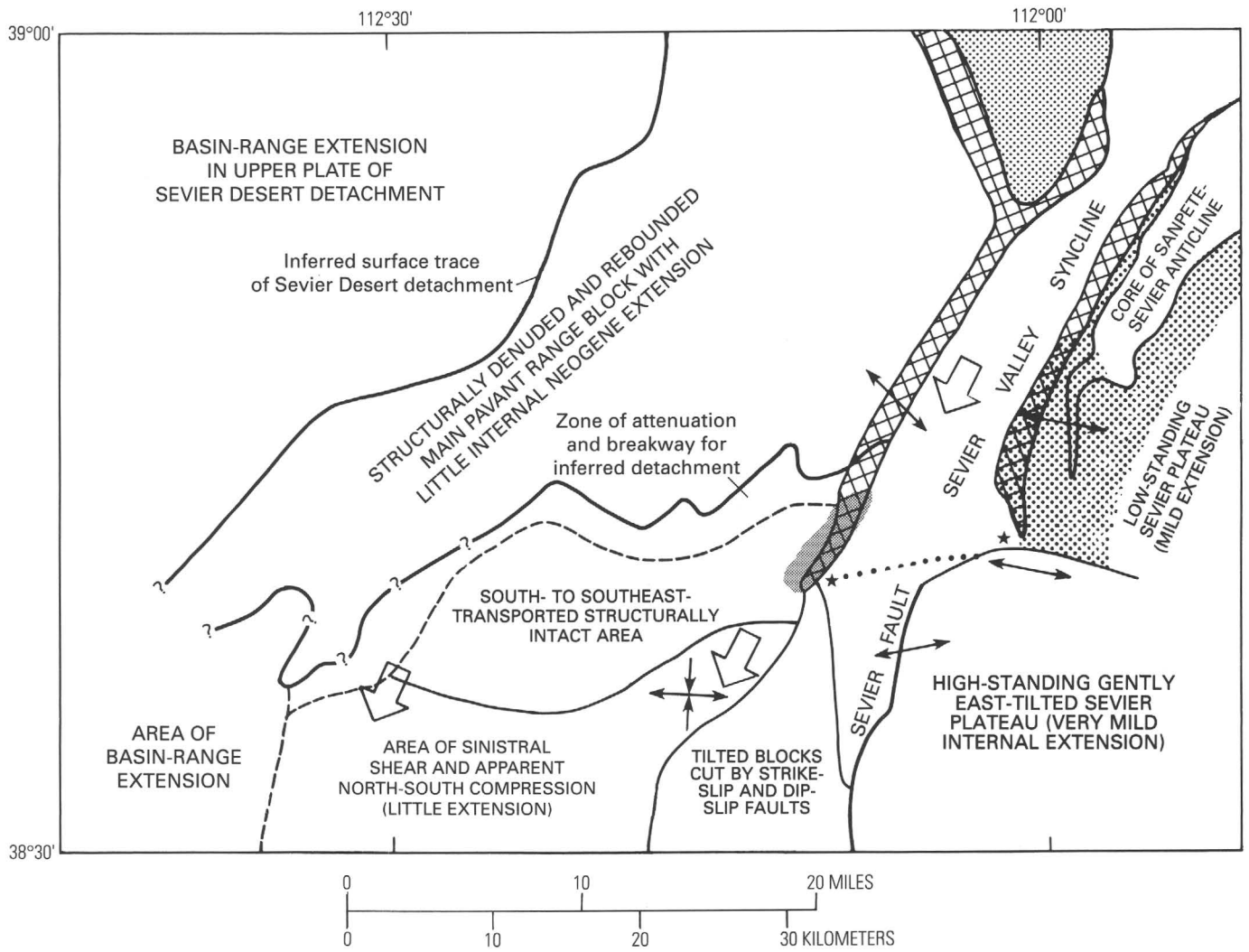

FIGURE 37.—Structural characterizations of the central Sevier Valley area. Resolved paleostress directions (outward-pointing double-headed arrows show σ_3 for dip-slip solutions, inward- and outward-pointing arrows show σ_1 and σ_3, respectively, for strike-slip solution); directions of principal tectonic transport (large open arrows, inferred for Sevier Valley); possible cross-valley transverse structure (dotted line); faulted monoclines bordering uplifted blocks (cross hatching); area of major extension and structural attenuation (stipple); areas of northwest-striking faults interpreted to represent a preneotectonic stage of northeast-southwest extension (shaded); and sites of coincident earthquake clustering and anomalously intense late Quaternary surface deformation (stars).

vergence direction of on-strike range-bounding structures.

Seismic hazards assessments in the central Sevier Valley area are closely linked to our understanding of the depth of penetration of faults. The main Pavant Range block is divided into a northern part, which lacks evidence of significant internal deformation, and a deformed southern part, which is further divided into a northern (updip) area of structural(?) attenuation and landsliding and a southern (downdip) area deformed in apparent north-south compression that produced mechanically coupled neotectonic folds and strike-slip faults (fig. 37). Horizontal deformation is concentrated on northeast-striking sinistral-slip faults on which displacements range from a few centimeters to a few kilometers. The abundance of these faults in excavations and excellent natural exposures suggests localized sinistral shear strain approaching unity, much more than in any other part of the study area. The net sinistral-slip displacement could approach 10 km. This concentration of horizontal displacement and compressional structures could reflect a tendency for the south-moving Pavant Range block to buttress against and slip southeastward around the igneous "spot weld" represented by the huge Marysvale volcanic-plutonic complex. Alternatives to this interpretation of thick-skinned denudation include (1) gravity-driven thin-skinned tectonic denudation of the uplifted Pavant Range block and (2) scraping off from a

southward-moving structural block that thust under the Tushar Mountains. Either alternative requires shallow detachment, albeit displaying an opposite sense of slip. Either can explain why northeast-striking sinistral-slip faults are not found in the main part of the Pavant Range to the northeast. Choosing between a thick-skinned interpretation and a thin-skinned one would seriously impact estimates of the depth to which faults extend and, in turn, estimates of earthquake hazards. In separate reports (Anderson and Barnhard, 1984a, 1987), we have favored separate interpretations. We choose here to straddle the fence.

The chief element of structural consistency in the Pavant Range is the lack of evidence of significant neotectonic extensional deformation even in the deformed southern part and along the range-bounding structures on its eastern flank. Evidence for an earlier episode of extension is found in restricted areas west of Aurora and near Elsinore (fig. 37). As does the main Pavant Range structural block, the part of the Sevier Plateau that we studied south of the Annabella segment of the Sevier fault lacks evidence of significant extensional deformation, even in areas within a few meters of the main "extensional" plateau-bounding faults. These faults are, by definition, neotectonic structures. Because they bound broad, evenly tilted blocks displaying little internal deformation, we assume that they extend to the base of the seismogenic crust.

In sharp contrast to the large blocks of weak internal extension, rocks adjoining and lying atop the Arapien-cored Sanpete-Sevier anticline are highly extended and, locally, severely attenuated. The southernmost exposures reveal persistent down-to-the-east throw across the anticline and a strong tendency for the extensional strain to be absorbed at the contact zone with the mechanically weak underlying Arapien Formation. Deformational kinematics suggest that Arapien rocks are withdrawn from beneath the northernmost part of the Sevier Plateau as an integral part of the extensional and attenuation process. As with the deformed southern part of the Pavant Range, this deformation has strong thin-skinned attributes. The Arapien apparently serves as a decollement zone characterized by relatively low-viscosity rock flowage below a cover-rock sequence that deforms by brittle failure. Such a zone is capable of vertically partitioning deformation and providing the kind of mechanical layering in the upper crust that gives rise to depth partitioning of small and moderate earthquakes (Arabasz, 1984; Arabasz and Julander, 1986).

The north-trending Monroe segment of the Sevier fault appears to break cleanly through gently east-tilted Tertiary strata, giving no suggestion of monoclinal flexing toward the Sevier Valley. Apart from this example, our studies show that the margins of uplifted blocks in the central Sevier Valley area are mostly or partly monoclinal flexures cut by one class of faults that displace rocks down toward the uplifted block and another class of very steep faults that displace rocks down toward the valley. The net extension may be small in some monoclines. Where monoclines are well developed in range-margin structural settings, such as in the Pavant Range, the possibility exists that this deformational style reflects draping over major buried faults that dip toward the valley at steep or moderate angles. There may be a component of lateral spreading or mushrooming as blocks lose lateral confinement during uplift. Such spreading may be a factor in the large-scale extension and structural thinning seen in the southernmost part of the Sanpete-Sevier anticline. This deformational style is dominated by faults that drop strata down toward the axes of the monoclines. It qualifies as thin skinned, although it may portend deeply penetrating buried structures. Because it is common, it is important that this style be understood and that this understanding be integrated with our understanding of seismicity. This topic is vital for future research. Currently, we believe that very few mapped faults in the central Sevier Valley area penetrate more than a few kilometers and that only range-bounding faults such as the Sevier fault and inferred faults beneath range-front monoclines have the potential for large damaging earthquakes related to their probable penetration to the base of the seismogenic crust.

The coincidence of clustered seismicity and surface deformation in the central Sevier Valley area can be explained in terms of localized zones of high strain that develop where there is a need to compensate for strongly contrasting along-strike style and vergence of range-front structures. We do not claim to understand the dynamics of faulting and seismicity in these zones. We assert, however, that fault recurrence times and slip rates estimated from the high-strain zones do not characterize the major structures that extend away from them and therefore should not be used to characterize earthquake hazards beyond the zones themselves.

In the central Sevier Valley area, geologic fault-slip and earthquake focal-mechanism data are generally similar in (1) the approximate east-west orientation of inferred least compressive stress (figs. 30, 37), (2) the widespread distribution of mixed-mode dip-slip and strike-slip faulting (figs. 30, 37), and (3) the common presence of slip incompatibility for strike-slip faults. The slip incompatibility indicates significant amounts of block-boundary faulting that cannot be interpreted in terms of applied remote stress. Unfortunately, we know of no straightforward way to separate block-bounding strike-slip faults from other strike-slip faults. In addition to the slip incompatibility, there is a paradox inherent in

the results of our fault-slip studies. Four of the five Φ values for dip-slip faulting (table 1) are very low (less than 0.1), and the other is low (0.26). If, for the purpose of discussion, strike-slip faulting is disregarded, the low Φ values suggest that σ_2 and σ_3 are close in value and that moderately dipping faults of any orientation are favorably oriented for dip slip. If strike-slip faulting is regarded, its intermixture with dip-slip faulting suggests that σ_1 and σ_2 are capable of interchanging their positions and are therefore close in value. We make no attempt to resolve this paradox.

ROLE OF DIAPIRISM

Witkind (1982) suggested that Cenozoic folding resulted from episodes of salt diapirism triggered by movement on deep-seated faults. Diapirism has great appeal because either compressional or extensional regional stresses acting on deep-seated faults will produce the same deformational style associated with diapirism. It explains how, in an extensional environment, Neogene folds can form parallel to or superposed on and having geometry similar to that of earlier folds resulting from compression. It does not seem adequate to explain the uniform down-to-the-plateau faulting in the southern part of the anticline unless the diapiric process is extended to include the lateral withdrawal of rock from beneath the northern Sevier Plateau. Also, the fault contact between the Arapien Formation and superjacent rocks in that area is approximately planar and dips at moderate to low angles over large areas. Diapiric upwelling would be expected to produce a highly irregular and steep to overturned contact (Witkind, 1982).

Geologic mapping (Willis, 1986) and an unpublished cross-valley reflection profile by S.T. Harding (written commun., 1986) have shown that the part of the Sevier Valley bordering the Sanpete-Sevier anticline from Salina to Annabella is underlain by a relatively symmetrical Neogene syncline. Diapirism does not seem adequate to explain the northeast-trending folding and faulting along the Pavant Range-Sevier Valley margin, where the folded rocks are far above the Arapien Formation, which is the causative rock that has been identified for the diapiric process. Because fold-fault patterns involving Neogene rocks are so similar on both limbs of the Sevier Valley syncline (fig. 37), we believe that they result from a single process, which is not likely to be diapirism.

SPECULATIONS ON CRUSTAL-SCALE DEFORMATION

With special reference to thrusts and thrust-related structures, Standlee (1982) emphasized that major blind (unexposed) structures exist in the region and that tectonic interpretations based on surface geology alone can be very equivocal. In areas where deformation is thin skinned and dominated either by lateral spreading of rock at the margins of or from beneath uplifted blocks or by detachment faulting, we further recognize that the location, geometry, and kinematics of major deeply penetrating neotectonic structures could be masked. The alluvial fill of the Sevier Valley precludes knowledge of deep structure from surface studies. Even though these conditions foster equivocation regarding deep structure, it is worthwhile to speculate how the earthquake record, the subsurface geology, and the surface geology, especially that pertaining to widespread neotectonic folding and strike-slip faulting, factor into the regional picture of crustal-scale deformation.

In the Basin and Range, the principal deformational mode is reasonably assumed to be extensional, and the strike-slip faulting either results from extension or is superposed on it from a competing deformational process. In the western part of the Basin and Range, right-lateral shear associated with the plate-margin transform fault system (San Andreas) has been suggested as a deformational process that competes with east-west extension (Atwater, 1970).

The results of this present study and of other studies to the southwest (Anderson, 1973, 1980a; Bohannon, 1983) indicate that the principal horizontal shearing along the southeastern margin of the northern Basin and Range is sinistral on northeast-striking faults. Because such shear cannot be caused by distributed plate-margin transform interaction, other explanations must be sought. The orientation of active extension in the Basin and Range and in the transition zone of west-central and central Utah is interpreted to be about 285° (Zoback and Zoback, 1980; Arabasz and Julander, 1986). Anderson and Barnhard (1986) determined an identical neotectonic paleostress orientation from the eastern part of the transition zone, and similar poorly constrained average paleostress is inferred from the present study (fig. 37) for the western part of the transition zone. These orientations are all approximately normal to the Basin and Range-Colorado Plateau boundary. Extension and accompanying crustal thinning lead to lateral transfer of material at depth either by simple shearing or by ductile flow. For the central Utah transition zone, it is reasonable to assume east-to-west transfer of material within the semiductile or quasiplastic zone of upper crustal (7–15 km) low velocity (Smith and others, 1975; Gants and Smith, 1983) and possibly also at deeper levels. Rocks at these levels are warm and thermally weakened relative to the equivalent-depth lithosphere of the adjacent Colorado Plateau (Thompson and Zoback, 1979). Lateral transfer of thermally weakened material could be significantly retarded by the mechanical resistance of

the thicker, cooler lithosphere beneath the plateau interior. The retardation could translate some of the outward (west-to-east) material transfer into movement parallel to the boundary in the direction of least resistance to such movement (Anderson, 1973). If an avenue of escape exists along the trend of the transition zone, the material would tend to flow or be translated in that direction (that is, subparallel to the province boundary). Specific directions of such translation could be strongly influenced by nonuniform preexisting structural strengths and weaknesses. The result is a local rafting of surficial crustal blocks parallel to the flow direction. If coeval extension on the Basin and Range side of the boundary is uniformly distributed over extensive areas, the rate and magnitude of tectonic transport would increase in the direction of escape because the required compensation for retardation would be cumulative. Very large and episodic motions, such as the 65 km of southwesterly tectonic transport of the Frenchman Mountain block near Las Vegas (Anderson, 1973; Bohannon, 1979), could be predicted as one progressed southwestward from the central Sevier Valley. This tectonic model combines a fundamental aspect of approximately east-west extension with tectonic rafting imposed by a system of basal tractions propagated upward from deep lateral flow of material.

Direct evidence for large-scale strike-slip faulting beneath the Sevier Valley does not exist. The presence of folds that strike approximately parallel to a principal set of strike-slip faults such as the Dry Wash fault and subparallel faults is not an uncommon feature in strike-slip structural settings, although it eludes understanding through structural modeling. For example, Aydin and Page (1984) studied the distribution, geometry, and orientation of folds and other structures related to strike-slip faults in the San Francisco Bay region. They found that the diverse structures collectively are more compatible with a simple shear model than they are with a Mohr-Coulomb model of remote compressive stress. However, even after allowances for structural inhomogeneities, transient influences, and varied degrees of rotation are made, the simple shear model fails to account for folds that commonly parallel shear direction (Aydin and Page, 1984). In the Mercury 7½-min quadrangle of Nevada, Barnes and others (1982) mapped Neogene folds that parallel the principal northeast-trending sinstral-shear direction. In southern Nevada, Bohannon (1983) mapped Neogene folds that parallel the sinistral-slip Lake Mead shear zone. In the Death Valley area, Cemen and others (1984) reported folds that developed parallel to late Cenozoic northwest-striking dextral faults. Those maps and reports show that such Neogene folds exist along strike-slip faults in the Basin and Range and lend confidence to the assumption that a similar association exists in the central Sevier Valley. In the Andaman Sea area, Harding (1985) showed that drape folds, interpreted to be caused by dip-slip components of displacement on predominantly strike-slip faults, have axes that parallel the main wrench faults. In addition, he noted that divergent wrench faults commonly have a pair of drape folds that face each other and parallel the main wrench fault. On the basis of seismic reflection profiles, Howell and others (1980) described synclinal troughs paralleling major faults in the divergent wrench-fault regime off coastal California. Basin margin unconformities attest to repeated tectonism during basin development, possibly analogous to the late-stage unconformities described along the Sevier Valley by Spieker (1946). We interpret the facing monoclinal folds bordering the Sevier Valley as resulting from the superpositioning on the system of east-west extension of a competing system of southwest-directed basal tractions and associated strike-slip faults. Although this model is highly speculative, it is consistent with the slip incompatibility seen in the earthquake and geologic fault-slip records, as well as with observed major components of strike slip on some of the deepest earthquakes of the region (Arabasz and Julander, 1986).

Future geologic studies in this area should focus on evaluating the role of detachment faults in the localization and dynamics of lateral block motions, compressional folding, and shear folding. Because the style of deformation in the central Sevier Valley is dramatically different from that along the Wasatch Front, an effort should be made to locate and characterize the deformational boundary between these two on-strike terrains.

REFERENCES CITED

Allmendinger, R.W., Sharp, J.W., Von Tish, D., Serpa, L., Brown, L., Kaufman, S., Oliver, J., and Smith, R.B., 1983, Cenozoic and Mesozoic structure of the eastern Basin and Range province, Utah, from COCORP seismic-reflection data: Geology, v. 11, p. 532–536.

Anderson, E.M., 1951, The dynamics of faulting (2d ed.): Edinburgh, Oliver and Boyd, 206 p.

Anderson, R.E., 1973, Large-magnitude late Tertiary strike-slip faulting north of Lake Mead, Nevada: U.S. Geological Survey Professional Paper 794, 18 p.

———1980, The status of seismotectonic studies of northwestern Utah: U.S. Geological Survey Open-File Report 80–801, p. 519–547.

Anderson, R.E., and Barnhard, T.P., 1984a, Extensional and compressional paleostress and their relationship to paleoseismicity and seismicity, central Sevier Valley, Utah: U.S. Geological Survey Open-File Report 84–763, p. 515–546.

———1984b, Late Cenozoic fault and fold patterns in Sevier County, Utah, and their relationships to seismicity in the area [abs.]: Geological Society of America Abstracts with Programs, v. 16, no. 6, p. 430.

———1986, Genetic relationship between faults and folds and determination of Laramide and neotectonic paleostress, western Colorado Plateau transition zone, central Utah: Tectonics, v. 5, no. 2, p. 335–357.

———1987, Neotectonic framework of the central Sevier Valley area, Utah, and its relationship to seismicity, *in* Gori, P.L., and Hays, W.W., eds., Assessment of regional earthquake hazards and risk along the Wasatch Front, Utah: U.S. Geological Survey Open-File Report 87–585–F, p. F1–F134.

Anderson, R.E., and Bucknam, R.C., 1979, Map of fault scarps on unconsolidated sediments, Richfield 1°×2° quadrangle, Utah: U.S. Geological Survey Open-File Report 79–1239, 1 sheet, scale 1:250,000, 15-p. text.

Anderson, R.E., and Mehnert, H., 1979, Reinterpretation of the history of the Hurricane fault, *in* Newman, G.W., and Goode, H.D., eds., 1979 Basin and Range Symposium: Denver, Colo., Rocky Mountain Association of Geologists, p. 145–173.

Angelier, J., 1979, Determination of the mean principal stress for a given fault population: Tectonophysics, v. 56, p. T17–T26.

Angelier, J., and Colletta, B., 1983, Tension fractures and extensional tectonics: Nature, v. 301, no. 5895, p. 49–51.

Angelier, J., Colletta, B., and Anderson, R.E., 1985, Neogene paleostress changes in the Basin and Range—A case study at Hoover Dam, Nevada-Arizona: Geological Society of America Bulletin, v. 96, p. 347–361.

Arabasz, W.J., 1984, Earthquake behavior in the Wasatch Front area: Association with geologic structure, space-time occurrence, and stress state, *in* Hays, W.W., and Gori, P.L., eds., Proceedings of Conference XXVI; a workshop on Evaluation of regional and urban earthquake hazards and risk in Utah: U.S. Geological Survey Open-File Report 84–763, p. 310–339.

Arabasz, W.J., and Julander, D.R., 1986, Geometry of seismically active faults and crustal deformation within the Basin and Range-Colorado Plateau transition in Utah: Geological Society of America Special Paper 208, p. 43–73.

Arabasz, W.J., and McKee, M.E., 1979, Utah earthquake catalog 1850–June 1962, *in* Arabasz, W.J., Smith, R.B., and Richins, W.D., eds., Earthquake studies in Utah 1850 to 1978: Salt Lake City, University of Utah Seismograph Stations, Department of Geology and Geophysics, p. 548.

Arabasz, W.J., and Smith, R.B., 1981, Earthquake prediction in the intermountain seismic belt—An intraplate extensional regime, *in* Simpson, D.W., and Richards, P.G., eds., Earthquake prediction—An international review: American Geophysical Union Maurice Ewing Series, v. 4, p. 238–258.

Armstrong, R.L., 1968, Sevier orogenic belt in Nevada and Utah: Geological Society of America Bulletin, v. 79, p. 429–458.

Atwater, T., 1970, Implications of plate tectonics for the Cenozoic tectonic evolution of western North America: Geological Society of America Bulletin, v. 81, p. 3513–3536.

Aydin, A., and Page, B.M., 1984, Diverse Pliocene-Quaternary tectonics in a transform environment, San Francisco Bay region, California: Geological Society of America Bulletin, v. 95, p. 1303–1317.

Baer, J.L., Davis, R.L., and George, S.E., 1982, Structure and stratigraphy of the Pavant Range, central Utah, *in* Nelson, D.L., ed., Overthrust belt of Utah: Utah Geological Association Publication 10, p. 31–48.

Barnes, H., Ekren, E.B., Rodgers, C.L., and Hedlund, D.C., 1982, Geologic and tectonic maps of the Mercury quadrangle, Nye and Clark Counties, Nevada: U.S. Geological Survey Miscellaneous Investigations Map I–1197, scale 1:24,000.

Best, M.G., McKee, E.H., and Damon, P.E., 1980, Space-time composition patterns of late Cenozoic mafic volcanism, southwestern Utah and adjoining areas: American Journal of Science, v. 280, p. 1035–1050.

Bohannon, R.G., 1979, Strike-slip faults of the Lake Mead region of southern Nevada, *in* Armentrout, J.M., Cole, M.R., and TerBest, H., eds., Cenozoic paleogeography of the Western United States: Pacific Coast Paleogeography Symposium, 3d, Los Angeles, 1979, Pacific Section, Society of Economic Paleontologists and Mineralogists, p. 129–139.

———1983, Geologic map, tectonic map and structure sections of the Muddy and northern Black Mountains, Clark County, Nevada: U.S. Geological Survey Miscellaneous Investigations Map I–1406, scale 1:62,500.

Burchfiel, B.C., and Hickcox, C.W., 1972, Structural development of central Utah, *in* Baer, J.L., and Callaghan, E., eds., Plateau-Basin and Range transition zone, central Utah, 1972: Utah Geological Association Publication 2, p. 55–66.

Callaghan, E., and Parker, R.L., 1961, Geology of the Monroe quadrangle, Utah: U.S. Geological Survey Geologic Quadrangle Map GQ–155, scale 1:62,500.

———1962, Geology of the Sevier quadrangle, Utah: U.S. Geological Survey Geologic Quadrangle Map GQ–156, scale 1:62,500.

Cemen, I., Pickens, T.B., Wright, L.A., Drake, R.E., and Johnson, F.C., 1984, Cenozoic deformation and sedimentation, southeasternmost part of the Furnace Creek fault zone, Death Valley, California: Geological Society of America Abstracts with Program, v. 16, no. 6, p. 466.

Chapman, D.S., and Harrison, R., 1978, Monroe, Utah, hydrothermal system: Results from the drilling of test wells MC–1 and MC–2: Salt Lake City, University of Utah, Department of Geology and Geophysics Topical Report, DOE/DGE contract EY–76–S–07–1601, 26 p.

Clark, E.E., 1977, Late Cenozoic volcanic and tectonic activity along the eastern margin of the Great Basin, in the proximity of Cove Fort, Utah: Brigham Young University Geology Studies, v. 24, pt. 1, p. 87–114.

Cunningham, C.G., Steven, T.A., Rowley, P.D., Glassgold, L.B., and Anderson, J.J., 1983, Geologic map of the Tushar Mountains and adjoining areas, Marysvale volcanic field, Utah: U.S. Geological Survey Miscellaneous Investigations Map I–1430–A, scale 1:50,000.

Davis, R.L., 1982, Geology of the Dog Valley-Red Ridge area, Southern Pavant Mountains, Millard County, Utah: Brigham Young University Geology Studies, v. 30, no. 1, p. 19–36.

Gants, D.L., and Smith, R.B., 1983, Joint interpretation of refraction and reflection data for an area of low-angle faulting in the eastern Basin-Range: EOS, Transactions of the American Geophysical Union, v. 64, p. 763.

Gibbs, A., 1987, Development of extension and mixed-mode sedimentary basins, *in* Coward, M.P., Dewey, J.F., and Hancock, P.L., eds., Continental extensional tectonics: Geological Society of America Special Publication 28, p. 19–33.

Gilliland, W.N., 1963, Sanpete-Sevier Valley anticline of central Utah: Geological Society of America Bulletin, v. 74, p. 15–124.

Halliday, M.E., and Cook, K.L., 1978, Gravity and ground magnetic surveys in the Monroe and Joseph KGRA's and surrounding region, south-central Utah: Salt Lake City, University of Utah, Department of Geology and Geophysics Report, DOE/DGE contract EY–76–S–07–1601, 164 p.

———1980, Regional gravity survey, northern Marysvale volcanic field, south-central Utah: Geological Society of America Bulletin, v. 91, p. 502–508.

Harding, T.P., 1985, Seismic characteristics and identification of negative flower structures, positive flower structures, and positive structural inversion: Bulletin of the American Association of Petroleum Geologists, v. 69, no. 4, p. 582–600.

Hardy, C.T., 1952, Eastern Sevier Valley, Sevier and Sanpete Counties, Utah: Utah Geological and Mineralogical Survey Bulletin 43, 93 p.

Hickcox, C.W., 1971, The geology of a portion of the Pavant Range allochthon, Millard County, Utah: Houston, Tex., Rice University, unpublished Ph.D. dissertation, 67 p.

Howell, D.G., Crouch, J.K., Greene, H.G., McCulloch, D.S., and Vedder, J.G., 1980, Basin development along the late Mesozoic and Cenozoic California margin: A plate tectonic margin of subduction, oblique subduction and transform tectonics, *in* Ballance, P.F., and Reading, H.G., eds., Sedimentation in oblique-slip mobile zones: International Association of Sedimentologists Special Publication 4, p. 43–62.

Julander, D.R., 1983, Seismicity and correlation with fine structures in the Sevier Valley area of the Basin and Range-Colorado Plateau transition, south-central Utah: Salt Lake City, University of Utah, unpublished M.Sci. dissertation, 142 p.

Kehle, R.O., 1970, Analysis of gravity sliding and orogenic translation: Geological Society of America Bulletin, v. 81, p. 1641–1664.

Lawton, T.F., 1985, Style and timing of frontal structures, thrust belt, central Utah: Bulletin of the American Asociation of Petroleum Geologists, v. 69, no. 7, p. 1145–1159.

Mase, C.W., Chapman, D.S., and Ward, S.H., 1978, Geophysical study of the Monroe-Red Hill geothermal system: Salt Lake City, University of Utah, Department of Geology and Geophysics Topical Report, DOE/DGE contract 78–C–07–1701, 99 p.

Ouchi, S., 1985, Response of alluvial rivers to slow active tectonic movement: Geological Society of America Bulletin, v. 96, no. 4, p. 504–515.

Rowley, P.D., 1968, Geology of the southern Sevier Plateau, Utah: Austin, University of Texas, unpublished Ph.D. dissertation, 385 p.

Rowley, P.D., Steven, T.A., Anderson, J.J., and Cunningham, C.G., 1979, Cenozoic stratigraphic and structural framework of southwestern Utah: U.S. Geological Survey Professional Paper 1149, 22 p.

Rowley, P.D., Steven, T.A., and Kaplan, A.M., 1981a, Geologic map of the Monroe NE quadrangle, Sevier County, Utah: U.S. Geological Survey Miscellaneous Field Studies Map MF–1330, 1 sheet, scale 1:24,000.

Rowley, P.D., Steven, T.A., and Mehnert, H.H., 1981b, Origin and structural implications of upper Miocene rhyolites in Kingston Canyon, Piute County, Utah: Geological Society of America Bulletin, v. 92, p. 590–602.

Segall, P., and Pollard, D.D., 1980, Mechanics of discontinuous faults: Journal of Geophysical Research, v. 85, no. B8, p. 4337–4350.

Smith, R.B., 1978, Seismicity, crustal structure, and intraplate tectonics of the Western Cordillera: Geological Society of America Memoir 152, p. 111–144.

Smith, R.B., and Richins, W.D., 1984, Seismicity and earthquake hazards of Utah and the Wasatch Front: Paradigm and paradox, *in* Hays, W.W., and Gori, P.L., eds., Proceedings of Conference XXVI; a workshop on Evaluation of regional and urban earthquake hazards and risk in Utah: U.S. Geological Survey Open-File Report 84–763, p. 73–112.

Smith, R.B., Braile, L.W., and Keller, G.R., 1975, Crustal low velocity layers: Possible implications of high temperature at the Basin and Range-Colorado Plateau transition: Earth and Planetary Science Letters, v. 28, p. 197–204.

Spieker, E.M., 1946, Late Mesozoic and early Cenozoic history of central Utah: U.S. Geological Survey Professional Paper 205–D, p. D117–D161.

———1949, The transition between the Colorado Plateaus and the Great Basin in central Utah: Utah Geological Society Guidebook to the Geology of Utah, no. 4, 106 p.

Standlee, L.A., 1982, Structure and stratigraphy of Jurassic rocks in central Utah: Their influence on tectonic development of the Cordilleran foreland and thrust belt, *in* Powers, R.B., ed., Geologic studies of the Cordilleran thrust belt: Denver, Rocky Mountain Association of Geologists, v. 1, p. 357–382.

Stanley, K.O., and Collinson, J.W., 1979, Depositional history of Paleocene-lower Eocene Flagstaff Limestone and coeval rocks, central Utah: Bulletin of the American Association of Petroleum Geologists, v. 63, no. 3, p. 311–323.

Steven, T.A., 1979, Geologic map of the Monroe NW quadrangle, west-central Utah: U.S. Geological Survey Miscellaneous Field Studies Map MF–107, scale 1:24,000.

Steven, T.A., and Morris, H.T., 1983a, Geologic map of the Cove Fort quadrangle, west-central Utah: U.S. Geological Survey Miscellaneous Investigations Map I–1481, 1 sheet, scale 1:50,000.

———1983b, Geologic map of the Richfield 1°×2° quadrangle, west-central Utah: U.S. Geological Survey Open-File Report 83–583, scale 1:250,000.

Steven, T.A., Cunningham, C.G., Naeser, C.W., and Mehnert, H.H., 1979, Revised stratigraphy and radiometric ages of volcanic rocks and mineral deposits in the Marysvale area, west-central Utah: U.S. Geological Survey Bulletin 1469, p. 1–40.

Stewart, J.H., Moore, W.J., and Zietz, I., 1977, East-west patterns of Cenozoic igneous rocks, aeromagnetic anomalies, and mineral deposits, Nevada and Utah: Geological Society of America Bulletin, v. 88, p. 67–77.

Thompson, G.A., and White, D.E., 1964, Regional geology of the Steamboat Springs area, Washoe County, Nevada: U.S. Geological Survey Professional Paper 458–A, 52 p.

Thompson, G.A., and Zoback, M.L., 1979, Regional geophysics of the Colorado Plateau: Tectonophysics, v. 61, no. 1/2, p. 149–181.

Wernicke, B., 1985, Uniform-sense normal simple shear of the continental lithosphere: Canadian Journal of Earth Sciences, v. 22, no. 1, p. 108–125.

Williams, J.S., and Tapper, M.L., 1953, Earthquake history of Utah, 1850–1949: Bulletin of the Seismological Society of America, v. 43, p. 191–218.

Williams, P.L., and Hackman, R.J., 1971, Geology, structure, and uranium deposits of the Salina quadrangle, Utah: U.S. Geological Survey Miscellaneous Geologic Investigations Map I–591, scale 1:250,000.

Willis, G.C., 1985, Revisions to the geochronology and source areas of Early Tertiary formations in the Salina area of Sevier Valley, central Utah [abs.]: Geological Society of America Abstracts with Program, v. 17, no. 4, p. 272.

———1986, Geology of the Salina quadrangle, Sevier County, Utah: Utah Geological and Mineral Survey Map 83, scale 1:24,000.

———1988, Geology of the Aurora quadrangle, Sevier County, Utah: Utah Geological and Mineral Survey Map 112, scale 1:24,000.

Witkind, I.J., 1982, Salt diapirism in central Utah, *in* Nielson, D.L., ed., Overthrust belt of Utah: Utah Geological Association Publication 10, p. 13–30.

Zoback, M.L., and Zoback, M.D., 1980, State of stress in the conterminous United States: Journal of Geophysical Research, v. 85, no. B22, p. 6113–6156.

Neotectonics of the Hansel Valley-Pocatello Valley Corridor, Northern Utah and Southern Idaho

By JAMES McCALPIN, DEPARTMENT OF GEOLOGY, UTAH STATE UNIVERSITY,
ROBERT M. ROBISON, UTAH COUNTY PLANNING DEPARTMENT, *and*
JOHN D. GARR, EARTHFAX ENGINEERING, INC.

ASSESSMENT OF REGIONAL EARTHQUAKE HAZARDS AND RISK ALONG THE WASATCH FRONT, UTAH

U.S. GEOLOGICAL SURVEY PROFESSIONAL PAPER 1500–G

CONTENTS

	Page
Abstract	G1
Introduction	1
Acknowledgments	3
Neotectonic Features in Pocatello Valley	4
Tectonic Setting	4
Eastern Margin Fault	4
Stratigraphy at the Range Front	5
Warped Shorelines	7
Western Margin Fault	9
Neotectonic Features in Hansel Valley	G9
Tectonic Setting	9
Eastern Margin Fault	10
Northwestern Margin Fault	11
Southwestern Margin Fault	11
Late Quaternary Tectonic History	15
Pocatello Valley	15
Hansel Valley	16
Conclusions	16
References Cited	17

ILLUSTRATIONS

		Page
FIGURES 1–3.	Maps showing:	
	1. Earthquake epicenters of the Hansel Valley-Pocatello Valley corridor for the period March 28, 1975, to June 30, 1985	G2
	2. Location and general geology of the Hansel Valley-Pocatello Valley corridor	3
	3. Bouguer gravity anomalies of the Hansel Valley-Pocatello Valley corridor and adjacent areas	3
4.	Index map of the Pocatello Valley area, Idaho-Utah	4
5, 6.	Logs of:	
	5. Trench 1, excavated across the Lake Utaho shoreline on the eastern valley margin	5
	6. Trench 2, located at the base of a faceted spur on the eastern valley margin	6
7, 8.	Diagrams showing:	
	7. Comparison of soil profile properties	7
	8. Method used in estimating actual elevations of pluvial lake shorelines covered by Holocene colluvium	8
9.	Profiles of Lake Utaho shoreline elevations	10
10.	Graph of scarp surface offset plotted against the tangent of the maximum scarp slope angle for Hansel Valley fault scarps and other dated scarps within Utah	11
11.	Sketch showing the fault exposed on the southern side of the Rattlesnake Pass (Interstate 84) roadcut	11
12.	Map showing profile locations, scarp heights, and surface offsets on the Hansel Valley southwestern margin fault scarp	12
13.	Conceptual model showing how fault scarps on the southwestern margin fault might be heightened by a coseismic rotational slump	13
14.	Sketches showing the geomorphic setting of a fault scarp formed during a lacustrine transgression and regression	13
15.	Wall log of the West Gully showing fault patterns	14
16.	Composite stratigraphic section of Quaternary deposits exposed in the West Gully	15

TABLE

		Page
TABLE 1.	Surveyed elevation data for the Lake Utaho shoreline, Pocatello Valley, Idaho	G9

ASSESSMENT OF REGIONAL EARTHQUAKE HAZARDS
AND RISK ALONG THE WASATCH FRONT, UTAH

NEOTECTONICS OF THE HANSEL VALLEY-POCATELLO VALLEY CORRIDOR, NORTHERN UTAH AND SOUTHERN IDAHO

By JAMES MCCALPIN, ROBERT M. ROBISON,[1] and JOHN D. GARR

ABSTRACT

The Hansel Valley-Pocatello Valley corridor on the Utah-Idaho border has experienced intense historical earthquake activity, including damaging earthquakes in 1934 (M_L 6.6) and in 1975 (M_L 6.0). Range fronts flanking both valleys display youthful morphology, yet valleys contain few well-preserved fault scarps in Quaternary deposits that might allow reconstruction of fault histories. Range-front trenching, pluvial lake shoreline surveying, and arroyo wall mapping were used to reconstruct the neotectonic history of each valley. In Pocatello Valley, 15-ka shorelines are locally warped vertically as much as 6.4 m where they cross en echelon splays of the eastern range front fault, but no scarps in unconsolidated deposits are found. A trench at the range front exposes unfaulted colluvial wedges up to 95 ka old that may have been rotated down toward the valley center and locally warped. The absence of either fault scarps or liquefaction features in late Quaternary deposits implies that displacement on the range-front fault in eastern Pocatello Valley occurs by creep or by small displacements that do not propagate as discrete fractures to the surface.

Two short fault scarps on the eastern range-front fault of Hansel Valley indicate that four to five surface-faulting events have occurred in the last 65 to 140 ka. A splay fault in an Interstate 84 roadcut shows only one recent 2.6-m displacement in the last 100 ka, not compatible with the scarp evidence. Along the southwestern valley margin, one of several scarps created by the 1934 earthquake merges with an 8-km-long prehistoric scarp up to 9 m high that displaces Lake Bonneville shoreline gravels. Scarp profiles and geomorphic relations with shorelines indicate that the scarp was formed by one or two subaqueous displacements totaling 1.3 to 2.5 m between 26 and 12 ka. Supporting evidence of recurrent faulting based on gully exposures and five thermoluminescence dates show that deposits have been multiply faulted between 138 and 72 ka; no events occurred from 72 to 58 ka, one event occurred between 58 and 26 ka (nearer the latter), one event occurred around 15 to 21 ka, and a possible event occurred at 13 ka. Displacements of up to 2.5 m seem to be clustered in time when large pluvial lakes existed in the basin (oxygen isotope stages 6 and 2) rather than when either no lake or only shallow lakes existed (oxygen isotope stages 5, 4, and 3). We suggest that the 1934 M_L 6.6 earthquake may be a typical interpluvial maximum event (long recurrence time, small displacement) in comparison with the larger, more frequent surface-faulting events presumably triggered by pluvial lake water loading.

Manuscript approved for publication November 20, 1990.

[1]Now at Sergent, Hauskins, and Beckwith Engineers, 4030 South 500 West, Salt Lake City, UT 84123.

INTRODUCTION

The Hansel Valley-Pocatello Valley corridor on the Utah-Idaho border has been the site of intense historical seismicity, including the 1934 M_L 6.6 and the 1975 M_L 6.0 earthquakes (fig. 1). The 1934 event, the largest in Utah's history, is one of only three historical earthquakes in the Intermountain Seismic Belt to rupture the surface and produce a fault scarp. The high rate of historical seismicity in the corridor contrasts with a scarcity of prehistoric fault scarps offsetting late Quaternary deposits, in spite of the youthful range-front morphology of bounding mountain ranges. The primary objective of this research was to determine why such a seismically active area lacked abundant geologic evidence of late Quaternary surface faulting. A secondary objective was to compare earthquake frequency-magnitude relations deduced from geologic evidence with those from historical time to help assess the current potential of this region to generate large, damaging earthquakes. Finally, if damaging earthquakes are found to have occurred without leaving significant geologic evidence, do the methods currently used on the Wasatch fault need to be modified for estimating earthquake potential?

The study area is located within the Hansel Mountains-West Hills part (Stokes, 1977) of the Great Basin section of the Basin and Range physiographic province (Stokes, 1977) and is composed of north- to northeast-trending valleys separated by linear mountain ranges (fig. 2). The Hansel, North Hansel, and North Promontory Mountains are primarily composed of the Pennsylvanian-Permian Oquirrh Formation (Adams, 1962; Allmendinger, 1983; Jordan, 1985), while Samaria Mountain

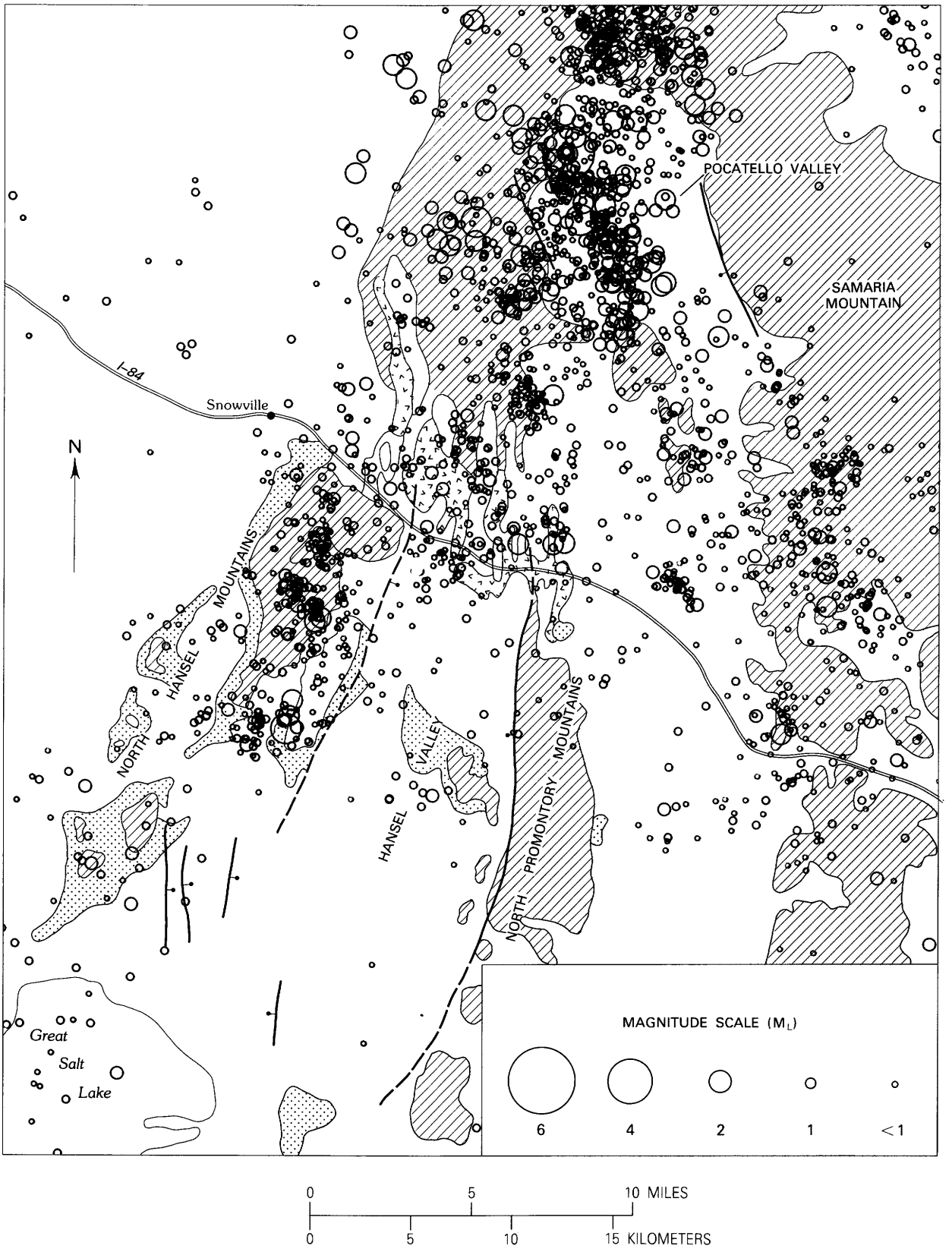
POCATELLO VALLEY
SAMARIA MOUNTAIN
I-84
Snowville
N
NORTH HANSEL MOUNTAINS
HANSEL VALLEY
NORTH PROMONTORY MOUNTAINS
Great Salt Lake
MAGNITUDE SCALE (M_L)
6
4
2
1
<1
0 5 10 MILES
0 5 10 15 KILOMETERS

◀ FIGURE 1.—Earthquake epicenters of the Hansel Valley-Pocatello Valley corridor for the period March 28, 1975, to June 30, 1985. Data provided by the University of Utah Seismograph Stations. Diagonal patterns represent mountain blocks; stippling represents Lake Bonneville shoreline gravels. Normal faults displaying Quaternary displacement are shown by heavy solid lines (bar and ball on downthrown side). Dashed lines show inferred fault locations at the base of steep range fronts.

contains carbonates and clastic rocks of Ordovician through Pennsylvanian age (Beus, 1968; Platt, 1977). In the valleys, Lake Bonneville sediments occur below about 1,585 m; higher valley margins are covered by alluvial fans. The valley fill beneath Lake Bonneville sediments is as much as 570 m thick in Pocatello Valley (estimated from gravity data by Harr and Mabey (1976, p. 6–7)), presumably composed mainly of pre-Bonneville Quaternary deposits and of the Tertiary Salt Lake Formation, which crops out on valley margins. Fill in Hansel Valley is considerably thinner, as shown by smaller gravity anomalies (fig. 3) (from Peterson, 1974) and by outcrops of Paleozoic rock within the valley (Hood, 1971, p. 5).

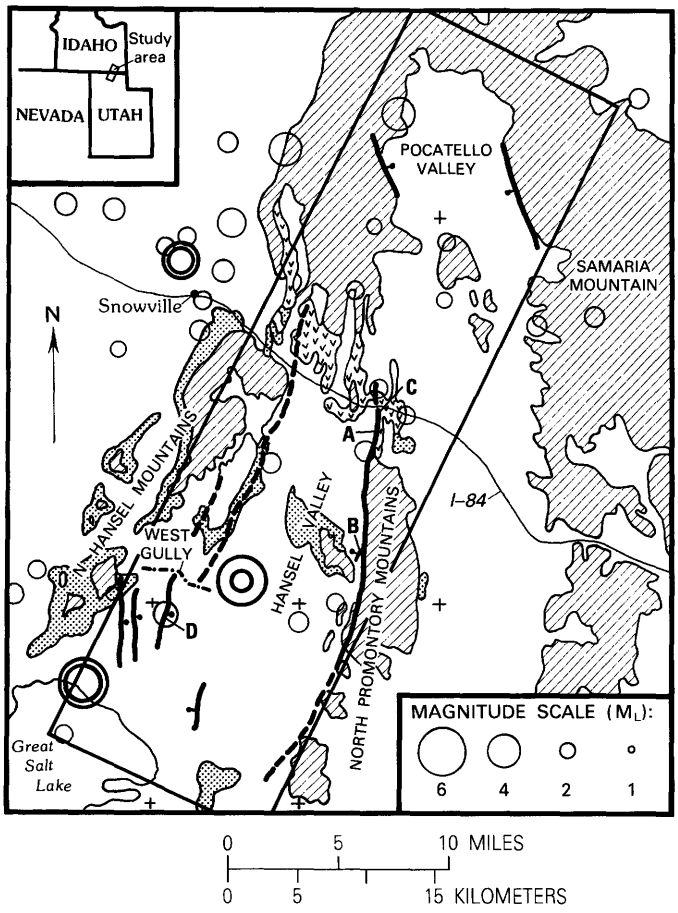

FIGURE 2.—Location and general geology of the Hansel Valley-Pocatello Valley corridor (rectangle). Marginal normal faults discussed in text are shown by heavy lines (dashed where inferred, bar and ball on downthrown side). Earthquake epicenters from 1850 through June 1962 are shown by heavy circles; epicenters from June 1962 through March 27, 1975, are shown by lighter circles. Paleozoic rocks, diagonal pattern; Tertiary volcanic rocks, small v's; Quaternary shoreline gravels, stippling; Quaternary lake-bottom deposits and alluvium, no pattern. A through D locate faults discussed in text.

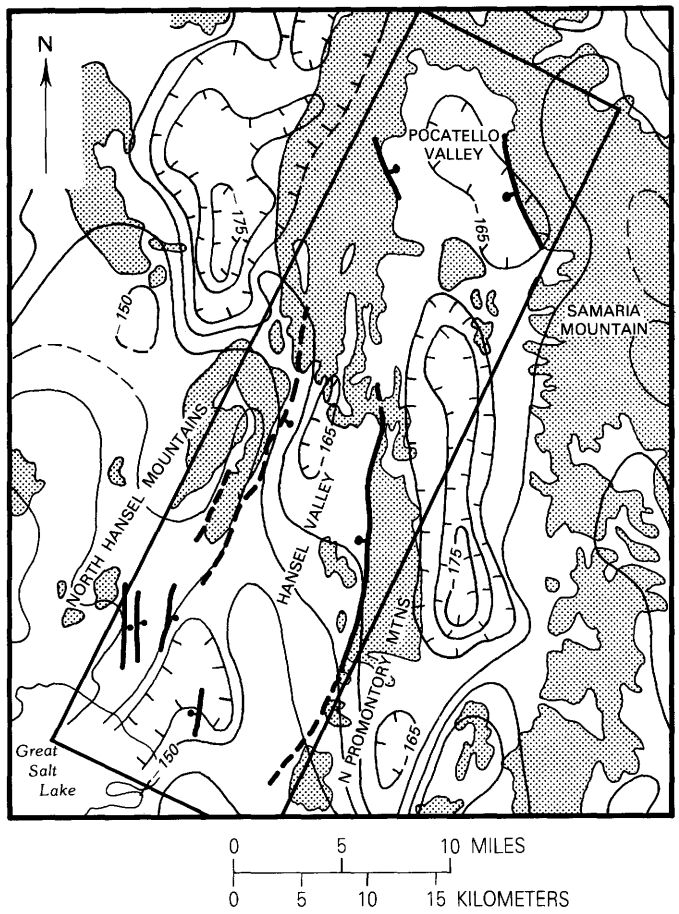

FIGURE 3.—Bouguer gravity anomalies of the Hansel Valley-Pocatello Valley corridor (rectangle) and adjacent areas (from Peterson, 1974). Gravity values are in milligals; contour interval 5 mGal. Stippling represents mountain blocks; heavy lines represent Quaternary faults (dashed where inferred, ball and bar on downthrown side). The gravity low of Pocatello Valley seems to continue southward to Blue Creek Valley rather than southwestward to Hansel Valley.

ACKNOWLEDGMENTS

Richard Forester (U.S. Geological Survey) interpreted the ostracode faunas from the West Gully. Jerry Stipp (Alpha Analytic, Inc.) provided the thermoluminescence dates and valuable advice, and William McCoy (University of Massachusetts) contributed thermoluminescence dates from type localities at Promontory Point. The manuscript benefited from reviews by Alan Nelson and Robert Bucknam (U.S. Geological Survey). Field-

work was supported by U.S. Geological Survey contract 13-08-001-21899.

NEOTECTONIC FEATURES IN POCATELLO VALLEY

TECTONIC SETTING

Pocatello Valley is a topographic and structural depression bounded on the east by Samaria Mountain, on the west by the North Hansel Mountains, and on the north and south by low hills (fig. 4). Cenozoic normal faults bound the eastern side of the valley (Beus, 1968; Platt, 1977) and part of the western side (Allmendinger, 1983). Platt (1975, 1976) inferred late Quaternary activity on the eastern margin fault from indirect geomorphic evidence such as steepness of faceted spurs. Both gravity data and tilt of strata suggest that this fault forms the boundary between two east-tilted blocks. Another inferred north-trending fault may bound the western side of a gravity saddle in the center of the valley (fig. 3). Cenozoic displacement on the eastern margin fault may be up to 1,420 m, as shown by the elevation difference between the top of Samaria Mountain (2,440 m) and the bottom of inferred valley fill (1,020 m) (Harr and Mabey, 1976). A shorter (8 km long) normal fault of lesser displacement bounds the central western margin of Pocatello Valley. Allmendinger (1983, section *C–C'*) showed a down-to-the-east displacement of about 122 m where it offsets Paleozoic rocks on its northern end. The smooth gravity gradients and the lack of large range-front spurs suggest that the western valley margin is dominantly a dip slope of an east-tilted block (Allmendinger and Platt, 1983, fig. 3) marked by a few short, low-displacement normal faults. In late Quaternary time, this topographic depression was occupied by pluvial Lake Utaho (Currey, 1981), a small body of water contemporaneous with but physically separate from Lake Bonneville.

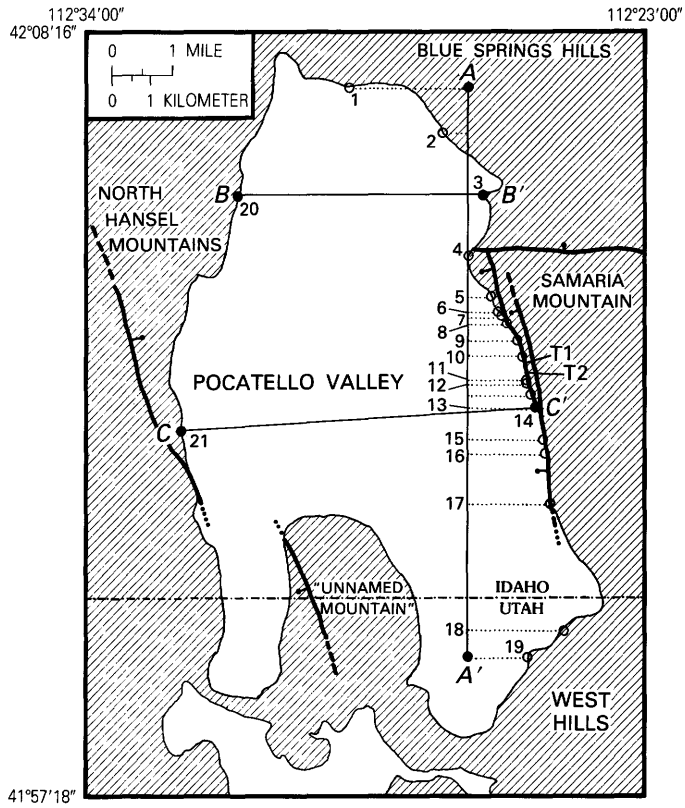

FIGURE 4.—Pocatello Valley area, Idaho-Utah. Diagonal pattern indicates highlands above the Lake Utaho and Lake Bonneville shorelines. Open circles are shoreline elevation data points; solid circles are data points and (or) endpoints of profiles shown in figure 9. Dotted lines indicate the position of shoreline elevation data points used in transect *A–A'* (fig. 9). Normal faults are shown by heavy lines (dashed where inferred, bar and ball on downthrown side). T1 and T2 indicate the locations of trench 1 and trench 2, respectively.

EASTERN MARGIN FAULT

The youthful range-front morphology cited by Platt (1977) as evidence of late Quaternary activity was quantified by using mountain-front sinuosity ratios (S) and ratios of valley floor width to valley height (V_f) (after Bull and McFadden, 1977). S is the ratio of the length of the mountain-piedmont junction to the overall length of the mountain front. Tectonically inactive fronts have high (3.0–7.0) S values caused by extensive embayment and pedimentation, whereas tectonically active fronts have lower values (1.2–1.6). The eastern margin range front has a sinuosity ratio of 1.7, suggestive of slightly active to active tectonism. The ratio of valley floor width to valley height (V_f) gives a general indication of whether streams draining the mountain block are engaged in channel downcutting (high rate of tectonic base-level fall, low value of V_f) or lateral erosion (low rate of base-level fall, high value of V_f). The width of a canyon floor is compared with the mean height of the canyon at a given distance (0.5 km in this study) upstream from the mountain front. Canyons and valleys in several ranges in the northern Mojave desert have V_f values ranging from 0.055 to 47.0 (Bull and McFadden, 1977). Only two canyons along the eastern margin of Pocatello Valley have stream channels long enough to use in calculating ratios of valley floor width to valley height; they yielded low values of 0.22 and 0.24 that indicated active tectonism. The mountain-front sinuosity ratio and the ratios of valley floor width to valley height quantify what can be seen in the field: the mountain front is steep, the canyons are deeply incised and strongly V shaped, and embayment and pedimentation are minimal, all suggestive of a young, active mountain front. In addition, Platt (1976) inferred that subsidence of the valley floor near the base

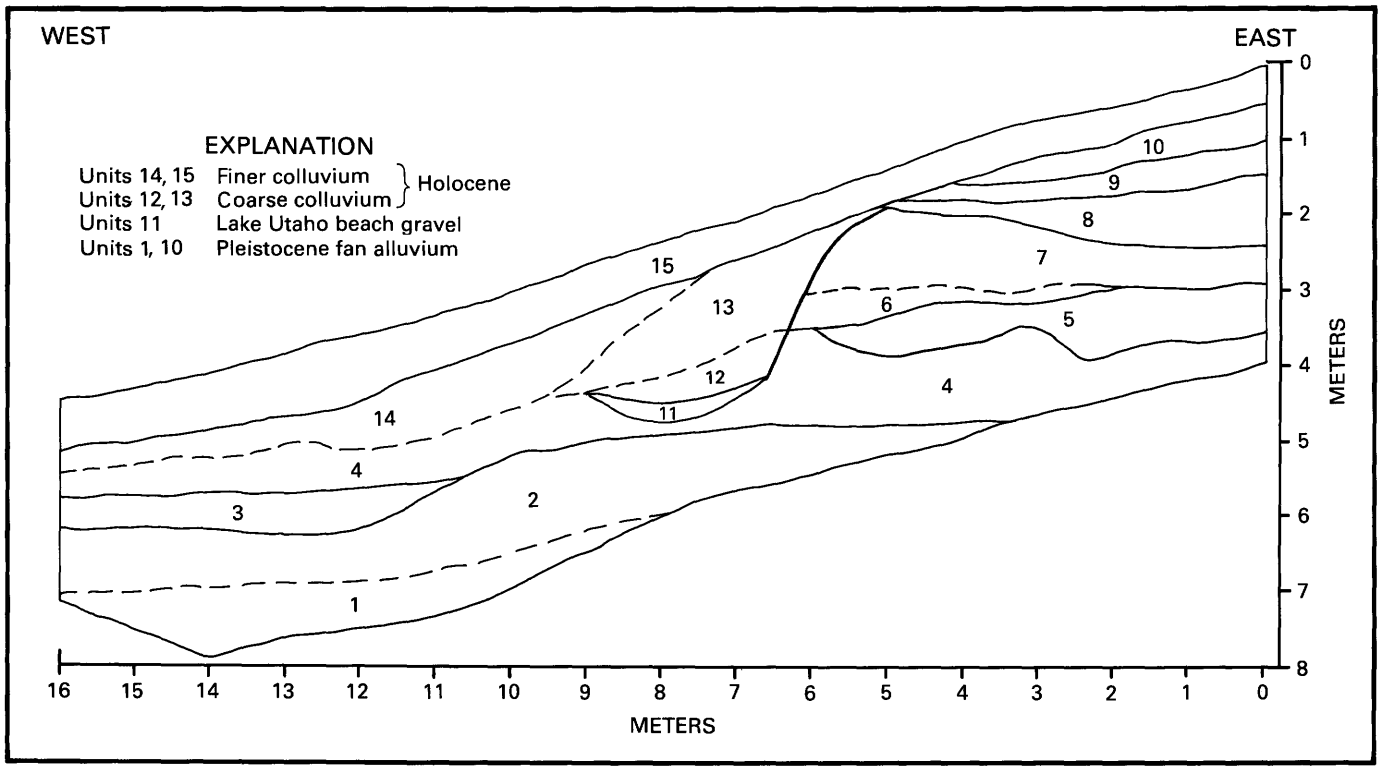

FIGURE 5.—Log of trench 1, excavated across the Lake Utaho shoreline on the eastern valley margin (T1, fig. 4). Lenticular late Pleistocene alluvial-fan gravels (units 1–10) are truncated by an erosional scarp, at the base of which lies Lake Utaho highstand beach gravel (unit 11). Bouldery scarp-derived colluvium (unit 12) is overlain by a wedge of gravelly colluvium (unit 13), the 35° W.-dipping fabric of which suggests a growing colluvial wedge. Finer colluvial unit 14 appears to be mixed with loess (early Holocene?), and unit 15 contains a weak A/Cca soil profile. Alluvial-fan strata beneath the buried scarp face (units 1–4) are not displaced, proof that no surface faulting has occurred at this location in the last 15 ka.

of Samaria Mountain has resulted in alluvial fans of much smaller volume than one would expect, given the size of the canyons from which the alluvium originated. According to gravity data (Harr and Mabey, 1976), the deepest depocenter within the valley (570 m of fill) is adjacent to the southern portion of the Samaria Mountain front. The gravity gradient from the mountain to the depocenter is approximately 3 mGal/km, almost double the gradient around most of the valley margin. Despite this indirect evidence for Quaternary fault activity, no fault scarps displacing Quaternary deposits could be located at the range front, either by earlier workers (Rogers and others, 1975) or in this study.

STRATIGRAPHY AT THE RANGE FRONT

Two trenches were excavated by a large track-mounted backhoe to look for evidence of Quaternary faulting at the range front. Trench 1 was cut across the most prominent scarp in Quaternary deposits along the range front (T1, fig. 4). This scarp was located at the same elevation as the Lake Utaho shoreline and could have been (1) a fault scarp, (2) an abnormally well developed pluvial lake shoreline scarp, or (3) a fault scarp later occupied and reworked by a shoreline. Trench logging revealed a thin lens of beach gravels at the base of the buried scarp free face, overlain by a fining- upward colluvial wedge (fig. 5). Moderately well stratified alluvial fan gravels beneath the beach gravel were continuous across the entire length of the trench, indicating no tectonic offset beneath the scarp and thus disproving a tectonic origin.

Because trench 1 yielded no tectonic information, trench 2 (T2, fig. 4) was cut through a colluvial apron at the base of a faceted spur approximately 400 m south of trench 1. Excavation was begun at the base of the spur directly on an outcrop of Pennsylvanian-Permian Oquirrh Formation limestone, which was encountered at depths ranging from 0 to 1.5 m in the upslope 15 m of the trench (fig. 6). The bedrock contact beneath colluvium then abruptly dropped 3 m into the trench floor at an angle of 63°, beyond the limit of extension of the backhoe. The limestone in and around the inferred range-front fault zone is intensely fractured and locally hydrothermally altered. The oldest colluvial deposit (unit I) carries a paleosol displaying well-developed argillic horizons. Comparison of this soil with a dated buried soil from

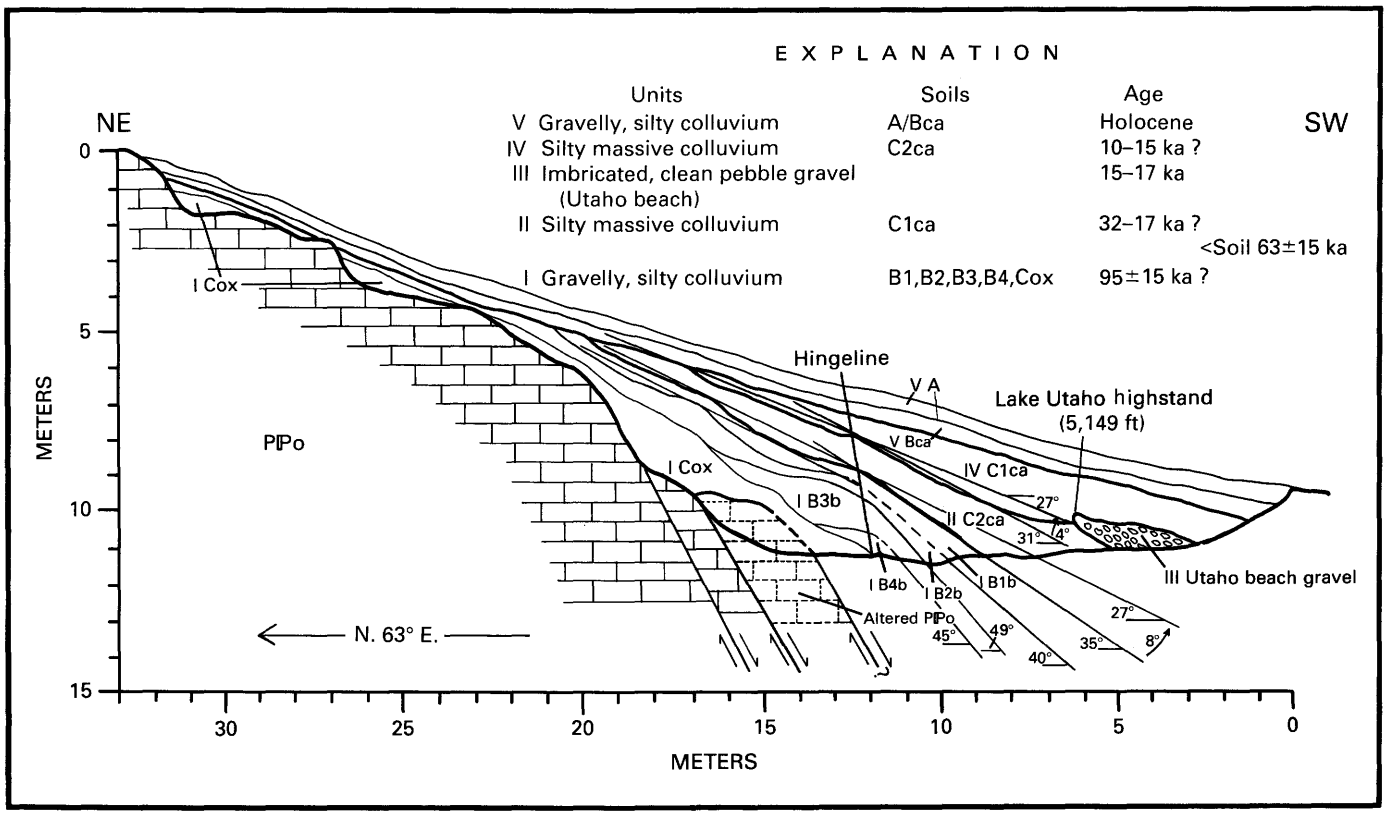

FIGURE 6.—Log of trench 2, located at the base of a faceted spur on the eastern valley margin (T2, fig. 4). Heavy lines separate lithologic units I through V; light lines separate soil horizons. Dips of units II through IV increase downslope of the hinge line by 4° to 8°; dips in unit I soil horizons increase up to 49°. Ages of units are estimated by correlating the Lake Utaho shoreline gravels (unit III) with the Lake Bonneville shoreline and by assessing the degree of soil development (fig. 7). The block pattern represents limestone bedrock (dashed where bedrock has been fractured and hydrothermally(?) altered to a variegated clay).

Jordan Valley, Utah (Scott and others, 1982, p. 42), suggests that this soil represents about 63±15 ka of weathering (fig. 7). Overlying stone-free (loessial?) colluviums (units II and IV) both underlie (unit II) and overlie (unit IV) Lake Utaho highstand beach gravel (unit III), which is assumed to be contemporaneous with the Bonneville shoreline (15.5–17 ka) (Scott and others, 1983). The modern colluvium (unit V) truncates all underlying units.

Although the overall geometry of older, steeper wedges overlain by successively younger, gentler layers is expectable, the very steep tilt of unit I paleosols (up to 49°) is anomalous. Colluvial wedges below fault scarp free faces typically have initial slopes of 35° (Wallace, 1977); this slope is maintained only while deposition is rapid. By the time the slope is declining slowly enough to allow soil formation on the colluvial wedge, the wedge slope is considerably lower (8°–25°) (Wallace, 1977, fig. 3, stage E). Buried soil horizons within unit I must have required slope stability to form, but now dip 35° to 49° west downslope of the hinge line shown in figure 6. The unit II-unit IV contact is bent about 4° along this hinge line, whereas younger units are unbent. The amount of angular change on the unit I-unit II contact (8°, age ~32 ka if deposition occurred early during the Utaho transgression) versus that on the unconformity between units II and IV (4°, age 15–17 ka) suggests progressive monoclinal flexure with time (0.25°/ka). If this rate is applied to the even more steeply dipping buried soil horizons B3b and B4b, an age of approximately 88 ka is obtained. This date is roughly compatible with an age of 95±15 ka for unit I estimated by adding the time of soil formation (63±15 ka) to the inferred age of the unit I-unit II unconformity (fig. 7). There are no discrete faults or shears within the colluvial wedge.

Monoclinal flexure of surficial materials in narrow (2–5 m wide) zones overlying fault traces has been previously described by Clark and others (1972, p. 118) and by Bonilla (1982, p. 18). Although the evidence in trench 2 is not conclusive, it suggests that some kind of progressive flexure has occurred over the last 95 ka within 20 m downslope of the inferred range-front fault in bedrock, unaccompanied by any surface faulting. It is unknown whether the warping resulted from coseismic deformation or aseismic creep, but the absence of fractures supports the latter explanation.

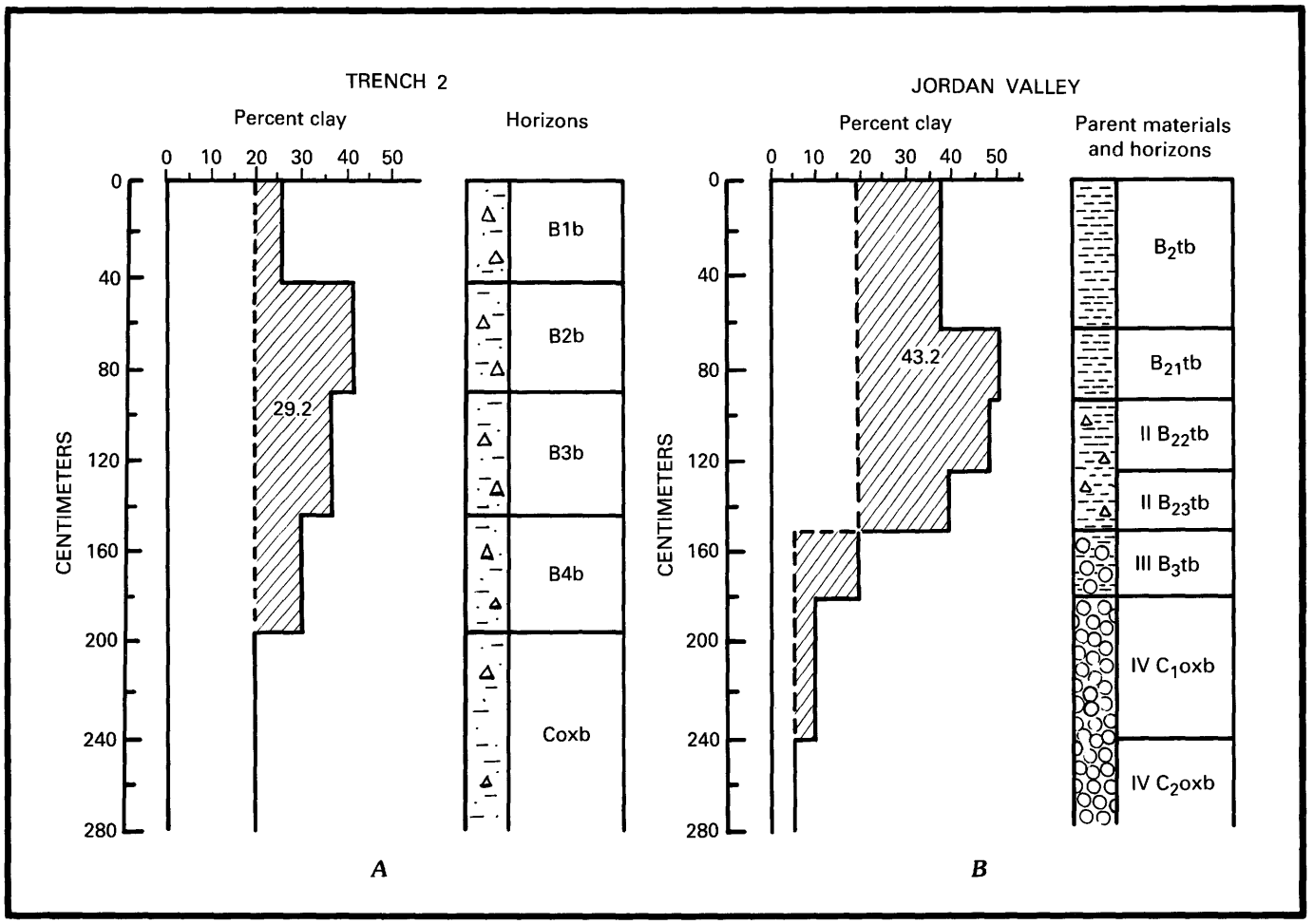

FIGURE 7.—Comparison of soil profile properties between (*A*) the trench 2 paleosol developed on unit I and (*B*) a buried soil developed on pre-Bonneville lacustrine gravel in Jordan Valley, Utah (Scott and others, 1982, table 5, p. 42). Total pedogenic clay in each horizon is shown by the diagonal pattern, computed by multiplying the percentage of pedogenic clay by weight in each soil horizon (heavy lines) by the horizon thickness. Two assumptions are made in the comparison: (1) the original clay content of both parent materials (dashed lines) was about 20 percent for loess and colluvium and 5 percent for lacustrine gravels, and (2) bulk densities of comparable horizons in both soils are similar. Numbers in the patterned areas show dimensionless values for comparing the amount of clay in each soil. The soil shown in *A* contains roughly 67 percent as much pedogenic clay as the soil shown in *B*. If clay formation rates are similar for the soil in *A* (Pocatello Valley) and the soil shown in *B* (Jordan Valley), the soil in *A* should represent roughly 67 percent of the time of soil formation represented by the soil in *B*. Scott and others (1982) calculated the formation time of the calcareous facies of the soil in *B* as 94±22 ka. Comparison of pedogenic clay amounts suggests that the soil in *A* in trench 2 developed over a period equivalent to 67 percent of 94±22 ka or roughly 63±15 ka. Horizontal dashes, silt; dots, sand; triangles, angular pebbles and small cobbles; open circles, rounded pebbles and cobbles. Horizon abbreviations follow U.S. Department of Agriculture conventions (b indicates buried horizons).

WARPED SHORELINES

The elevation of the Lake Utaho shoreline was determined at 46 points around the margin of Pocatello Valley to detect indirect evidence of tectonic deformation. Survey points were concentrated along suspected fault zones at the base of steep mountain fronts to look for anomalous warps or tilts in the originally horizontal shorelines. Surveying was performed with a Leitz TM10E theodolite and Leitz RED–2 electronic distance meter. The meter and the theodolite were set up over a benchmark or spot elevation on the valley floor, and a tripod-mounted reflecting prism was placed at the base of the shoreline scarp. While measurements were taken at the instrument station, a profile of the shoreline scarp was made by using a 4.5-m rod and Abney level (after Bucknam and Anderson, 1979, p. 12). In most instances, the profile measurement was made from 30 m above to 30 m below the shoreline scarp. Typically, three distinct slope components were evident: a beach platform (3°–4°), a colluvial wedge (8°–12°), and a wave-cut scarp (18°–28°) (fig. 8).

Because the Pleistocene lake shorelines were developed in unconsolidated deposits in all but a few locations

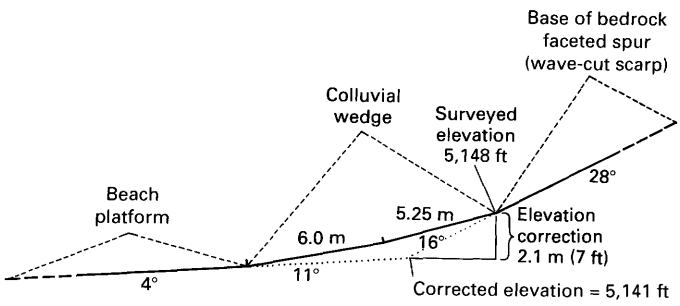

FIGURE 8.—Method used in estimating actual elevations of pluvial lake shorelines covered by Holocene colluvium. The beach platform and wave-cut scarp components are projected beneath the colluvial wedge. The resulting intersection is presumed to be a more accurate representation of the actual shoreline angle.

around the valley margin, the shoreline angle has been covered subsequently by Holocene colluvium. The amount of colluvial cover varies depending on slope, aspect, deposit grain size, and local drainage patterns. To eliminate the effect of colluvial deposition from the surveyed shoreline scarp elevations, the beach platform and wave-cut scarp angles were projected under the colluvial wedge component on the profiles (fig. 8). The intersection of the two angles is assumed to be a more accurate approximation of the shoreline angle. Because trenches 1 and 2 were excavated after the shoreline surveying phase of the study, they provided a means of checking the accuracy of the method; in both instances, the projected beach platform and wave-cut scarp angles intersected within 30 cm of the tops of Lake Utaho beach gravel lenses.

Although the water surface at the Lake Utaho highstand was horizontal, shorelines could have been superelevated, coincident, or subelevated with respect to the formative water plane (Currey, 1982, p. 21–22). All survey points along the eastern range front were in similar drift-aligned gravel beaches; data from Rose (1981, table 5.6) showed that the shoreline angle of such beaches is usually within 0.5 m of the mean water surface. Large waves that might deposit gravel far above the mean water surface would be hard to generate in Lake Utaho, which was only 10 km in diameter at its maximum extent.

The precision of the instrumentation used in this study was calculated to be ±1.31 cm elevation per kilometer of horizontal distance. The longest survey shot made was 1.78 km, and most shots were less than 0.48 km long. The combined uncertainties of surveyed elevation (13 cm), projected shoreline angle (1.0 ft), and relation to water surface (50 cm) yield a ±93-cm uncertainty for each measured shoreline point (table 1).

Figure 9 (transect *A–A′*) shows shoreline elevations that deviate as much as 6.4 m from one another and up to 4.5 m from elevations predicted by Crittenden (1963) on the basis of basin-scale isostatic rebound. The most significant deviations from a smooth profile occur where the north-northwest-trending shoreline crosses the more northerly trending faults at the base of Samaria Mountain. The shoreline at the southern end of the transect (point 17) is cut onto a faceted spur on the upthrown side of the fault, whereas, at points 4, 5, and 6, the shoreline is clearly on the downthrown side of the two parallel range-front faults (fig. 4). Point 17 falls at almost the exact elevation predicted for the Bonneville shoreline by Crittenden (1963, fig. 3), whereas points 4, 5, and 6 on the downthrown block plot 4.2 to 4.5 m, too low in relation to their expected post-rebound elevations. Highly variable shoreline elevations between points 16 and 7 probably result from the sinuous shoreline's repeatedly crossing from the upthrown to the downthrown side of a more linear but buried fault or fold hinge line. For example, point 9 is a shoreline cut onto bedrock at the base of a spur, whereas the shoreline at points 8 and 10 is cut into colluvium farther valleyward. The position of a linear fault paralleling the range front would cross between point 9 and points 8 and 10. Farther north, a parallel branch of the north-trending range-front fault intersects the north-northwest-trending Utaho shoreline somewhere between points 6 and 9 (fig. 9). Within this area, the shoreline loses 6.4 m of elevation in a horizontal distance of 900 m. The great similarity of all shoreline profiles suggests that they were formed with a constant relation to the mean water plane. Importantly, there are no fault scarps visible in this area.

East-west profiles suggest that the Utaho shoreline has been tilted eastward from 1.8 m (fig. 9, transect *B–B′*) to as much as 7.4 m (fig. 9, transect *C–C′*) in the most active-appearing range-front area. Crittenden (1963, fig. 3), showed an expected west-to-east shoreline elevation drop of approximately 1 m across Pocatello Valley resulting from differential isostatic rebound. The small residual displacement on transect *B–B′* (1.8 m−1.0 m=0.8 m) is within the range of surveying error and suggests that no significant tectonic eastward rotation has occurred north of the mapped eastern margin fault. The 6.4-m residual down-to-the-east displacment along transect *C–C′* strongly argues for post-Utaho slip along the central range front.

The overall implication is that late Quaternary slip on the range-front fault has resulted in very little absolute elevation change of the upthrown block, but points on the downthrown block have been lowered 4.5 to 6.4 m, presumably by subsidence of the Pocatello Valley block. Geodetic data collected by Bucknam (1976) after the 1975 M_L 6.0 earthquake showed no absolute uplift of surrounding mountain blocks but a maximum of 13 cm of valley floor subsidence near the epicenter in western

TABLE 1.—*Surveyed elevation data for the Lake Utaho shoreline, Pocatello Valley, Idaho*

Reference elevation[1] (ft a.s.l.)	Shoreline elevation point[2]	Height of shoreline above reference elevation[3] (ft)	Calculated shoreline elevation[4] (ft)	Colluvial wedge correction[5] (ft)	Corrected shoreline elevation[6] (ft a.s.l.)
5,032 (a)	1	110	5,142	−3	5,139
5.022 (b)	2	111	5,133	+3	5,136
	3	105	5,127	+2	5,129
	4	113	5,135	−2	5,133
4,977 (c)	5	157	5,134	0	5,134
	6	161	5,138	−3	5,135
	7	168	5,145	−3	5,142
	8	166	5,143	−2	5,141
	9	182	5,159	−3	5,156
	10	164	5,141	0	5,141
	11	174	5,151	0	5,151
	12	176	5,153	−3	5,150
	13	172	5,149	0	5,149
4,994 (d)	14	148.5	5,142.5	−1.5	5,141
	15	149	5,143	−1.5	5,141.5
	16	146.5	5,140.5	−4	5,136.5
5,063 (e)	17	88	5,151	−2	5,149
	18	98.5	5,159.5	−13	5,148.5
	19	96.5	5,159.5	−10	5,149.5
5,006 (f)	20	127	5,133	0	5,133
4,997 (g)	21	160	5,157	+9.5	5,166.5

[1]Reference points of known elevation where the surveying base station was located: a, SW¼ sec. 16, T. 15 S., R. 34 E.; b, benchmark O'FNL, sec. 26, T. 15 S., R. 34 E.; c, SW¼ sec. 1, T. 16 S., R. 34 E.; d, SW¼ sec. 13, T. 16 S., R. 34 E.; e, SW¼ sec. 30, T. 16 S., R. 34 E.; f, benchmark SE¼ sec. 20, T. 15 S., R. 34 E.; g, NW¼ sec. 17, T. 16 S., R. 34 E.

[2]Shoreline points located on figures 4 and 9.

[3]Calculated by trigonometric leveling from reference elevation; precision 0.5 ft.

[4]Calculated by adding the third column to the first column.

[5]The elevation difference between the projected shoreline angle (see fig. 8) and the point where the shoreline elevation was measured; precision 1.0 ft.

[6]Calculated by adding or subtracting the fifth column from the fourth column. This elevation should be within 1.6 ft of the mean elevation of the formative water plane (Rose, 1981, table 5.6).

Pocatello Valley. The closed topography of the valley suggests that subsidence has been the dominant long-term tectonic trend during the Quaternary, as Harr and Mabey (1976) previously suggested for the late Cenozoic.

WESTERN MARGIN FAULT

Over 30 normal faults have been mapped by Allmendinger (1983) in the portion of the North Hansel Mountains in our study area. The longest fault strikes N. 20° W., is 8 km long (fig. 4), and displaces older Quaternary pediment gravels by at least 55 m down to the east. The S value for the southern portion of the fault is 2.33, indicative of moderate to slightly active tectonism (Bull and McFadden, 1977). The V_f ratios of two gullies along the western margin fault are 5.0 and 4.0, values which are approximately 20 times those calculated for the eastern margin fault. The difference in V_f values suggests that the western margin fault is less active than the eastern margin fault.

NEOTECTONIC FEATURES IN HANSEL VALLEY

TECTONIC SETTING

Hansel Valley, Utah, lies southeast of Pocatello Valley and is bounded on the east by the North Promontory Mountains and on the west by the Hansel (or Summer Ranch) Mountains (fig. 2). The fault at the western base of the North Promontory Mountains has created an extremely linear north-trending range front, complete with faceted spurs, about 25 km long. The eastward tilt of Oquirrh Formation strata on either side of the fault near Bull's Pass suggests eastward rotation of fault blocks (Jordan, 1985). The inferred Cenozoic throw on this fault near Bull's Pass (425 m) (Jordan, 1985, section A–A') is considerably less than the 1,420 m inferred for the eastern fault of Pocatello Valley. The linear range front at the eastern base of the Hansel Mountains is inferred to be underlain by a normal fault (Adams, 1962, pl. 1; Doelling, 1980, pls. 1, 3, section G–G'). However, the fault does not offset Quaternary deposits and has not

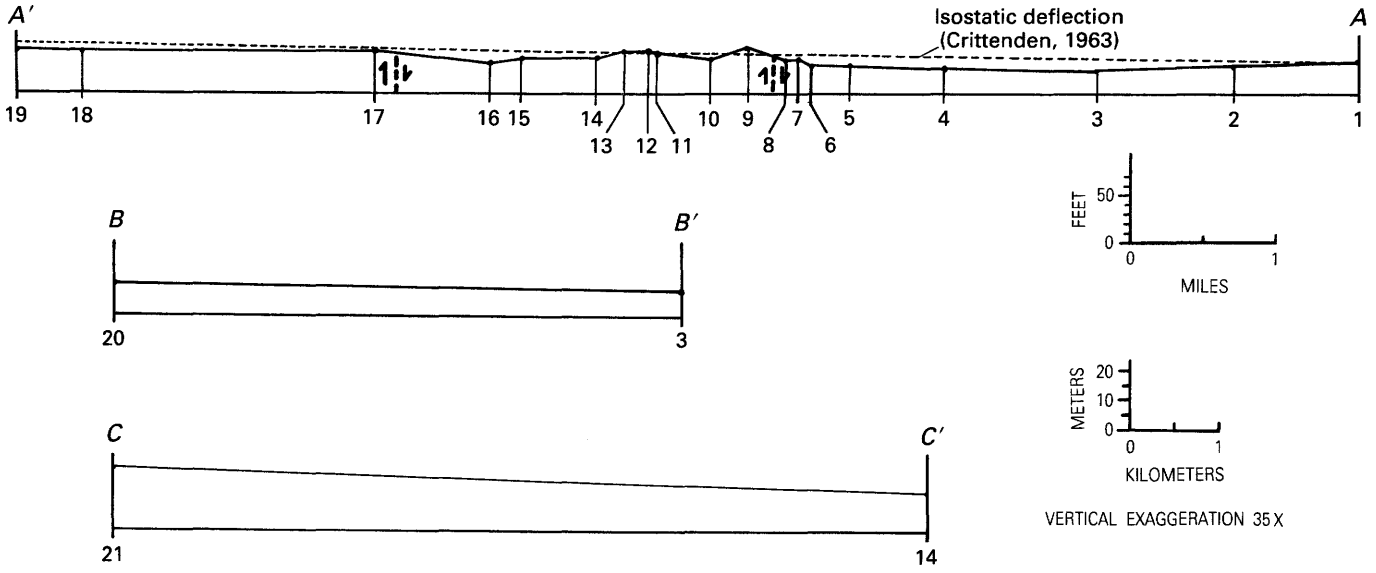

FIGURE 9.—Lake Utaho shoreline elevations. Locations of profiles are shown in figure 4. The amount of error owing to instrument inaccuracies and projecting of the shoreline angle is approximately represented by the width of the profile line (1.4 ft). On profile *A–A'*, significant deviations from the expected elevation occur where the shoreline crosses inferred branches of the range-front fault (points 17–16, points 9–6). Profiles *B–B'* and *C–C'* show slight tilting of shorelines toward the eastern range-bounding fault.

created the sharp faceted spurs that exist on the eastern valley margin. Outcrops of Oquirrh Formation on the valley floor suggest that the throw on this fault is no greater than that on the eastern margin fault; it may be a minor fault on a hinged valley side, similar to the western margin fault in Pocatello Valley. The southwestern margin of Hansel Valley is a subdued and irregular range front veneered by Lake Bonneville deposits. The east-facing 1934 fault scarp and a prehistoric scarp up to 9 m high trend northerly across this zone. Very low gravity gradients in this region (fig. 3) and the lack of appreciable topographic relief suggest that this fault has a low Cenozoic slip rate. Tertiary and early Pleistocene sediments exposed in arroyos on the valley floor are extensively faulted. These faults usually have displacements of less than 5 m and do not displace overlying Lake Bonneville bottom sediments. The segmented linear nature of arroyos in northern Hansel Valley may be controlled by these north- to northeast-trending faults in underlying Tertiary sandstones (Salt Lake Formation). Normal faults of similar strike offset Tertiary basalts immediately north of Interstate 84 and tilt them into a series of east-dipping blocks (Adams, 1962).

EASTERN MARGIN FAULT

Fault scarps occur at only two locations along the eastern margin fault, where the trace is not covered by Holocene talus. At the northern location (A, fig. 2), a 13-m-high scarp offsets a delta graded to the Bonneville shoreline. Farther south, a branch fault (B, fig. 2) diverges southwesterly from the range front and creates a scarp up to 12.9 m high across pre-Bonneville alluvial fans. Both scarps are probably the result of multiple events; because each is limited to a single geomorphic surface and displays no multiple crests, reliable evidence of recurrent movement is lacking. Two profiles across the northern scarp and three across the southern scarp yield scarp surface offsets and maximum scarp slope angles that can be compared with those of dated single-event scarps elsewhere in Utah (fig. 10). The sparse data suggest that the scarps are roughly comparable in age to the Bonneville shoreline (15.5–17 ka) (Scott and others, 1983).

A graben bounded by two high-angle faults in Quaternary deposits is exposed on the southern roadcut of Interstate 84 across Rattlesnake Pass (C, fig. 2). The faults offset seven distinct units of locally derived alluvium and colluvium deposited in a broad swale cut into Tertiary basalts (fig. 11). Of the four paleosols within the sequence, the lowest one is better developed than 140-ka-old noncalcareous soils developed elsewhere in the Bonneville Basin (Scott and other, 1982, p. 42), whereas soils on units II, IV, and VI plus VIII each resemble calcareous soils developed elsewhere on 17-ka deposits (Scott and others, 1982, p. 36). Units I through V are clearly faulted; unit VI may be faulted, whereas soil horizon K1 is clearly superposed across the fault, an indication that faulting occurred between the deposition of unit V and the formation of soil K1 (latest Pleistocene–early Holocene?).

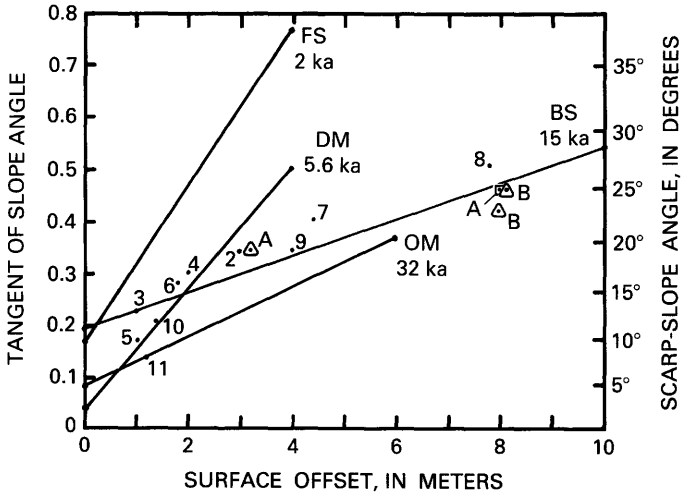

FIGURE 10.—Scarp surface offset plotted against the tangent of the maximum scarp slope angle for Hansel Valley fault scarps and other dated scarps within Utah (modified from Hanks and others, 1984). Solid lines show the relationship between offset and slope angle for scarps at Fish Springs (FS), the Drum Mountains (DM), the Bonneville shoreline (BS, many geographic locations), and the Oquirrh Mountains (OM). Hansel Valley data are shown by open triangles marked B (from scarp area B in fig. 2), an open square marked A (from scarp area A in fig. 2), and numbered solid circles (from the southwestern margin scarp, marked D on fig. 2). Numbers refer to profile locations shown in figure 12. Comparison of Hansel Valley scarp data with other Utah data suggests that (1) the scarp at location A is roughly contemporaneous with the Bonneville shoreline (because this scarp offsets a delta graded to the Bonneville shoreline, faulting must have occurred immediately after construction of the delta); (2) scarps at location B are older than the Bonneville shoreline, which is consistent with their displacing pre-Bonneville alluvial fans above the Bonneville shoreline; and (3) the scarp at location D is slightly younger than the Bonneville shoreline (this age is consistent with age estimates based on geomorphic data (fig. 14) that faulting occurred during the regression from the Provo shoreline before about 12 ka).

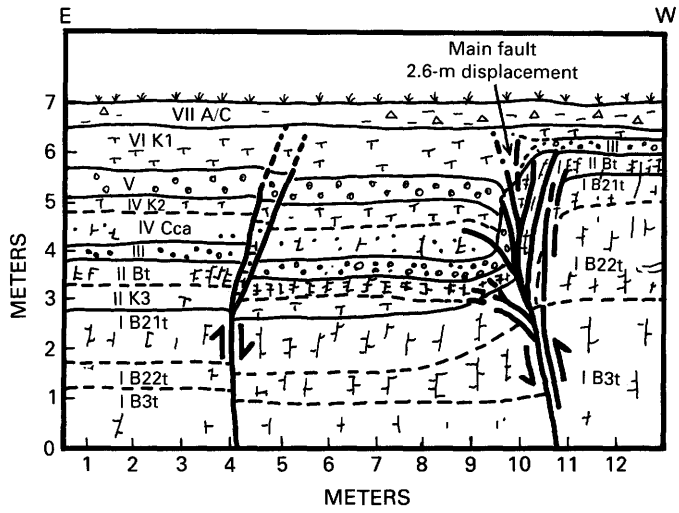

FIGURE 11.—Fault exposed on the southern side of the Rattlesnake Pass (Interstate 84) roadcut (C, fig. 2). Four paleosols are exposed in the eastern two-thirds of the cut, developed on parent materials of unit I (horizons B21t, B22t, and B3t), unit II (horizons Bt and K3), unit IV (horizons K2 and Cca), and unit VII (horizon A/C) plus unit VI (horizon K1). The main fault displaces units I through III by 2.6 m. Units IV and V have evidently been eroded from the upthrown block west of the main fault, and unit VI is considerably thinner on the upthrown block, probably the result of scarp relief. Unit VIII (Holocene? colluvium) is not faulted. Pattern intensity indicates the degree of secondary carbonate or clay enrichment in soil horizons.

NORTHWESTERN MARGIN FAULT

The northwestern margin fault flanks the eastern margin on the Hansel Mountains (fig. 2). The range front is linear and exhibits subdued talus-covered faceted spurs. Bonneville-cycle shoreline deposits abut the range front, but no evidence of surface faulting exists in these sediments. Any fault scarps that may have been formed before the transgression of Lake Bonneville were presumably completely eroded. A shorter fault, about 4 km in length, parallels the northwestern margin fault along the east side of a small valley at the southern end of the Hansel Mountains (fig. 2) (Adams, 1962; Doelling, 1980). This fault forms a horst at the southern end of the mountain and decreases in displacement toward the north. This smaller fault is aligned with the trace of the 1934 scarp and may be an extension of that fault zone.

SOUTHWESTERN MARGIN FAULT

The fault on the southwestern margin of Hansel Valley is markedly different from the valley-bounding faults previously described. Here the mountain block is located 3 to 4 km west of an 8-km-long east-facing fault scarp offsetting Bonneville-cycle shoreline gravels. Eleven profiles across the scarp (fig. 12) reveal an increase in scarp height from 1.7 m to 9.0 m along the central part of the scarp, where it ascends a 60-m-high bedrock-cored escarpment. The increased scarp heights probably result from the addition of a fault scarp plus a landslide scarp produced by syntectonic sliding (fig. 13), as the arcuate plan shape of the scarp suggests. Because the material involved in the sliding (beach gravel) is not particularly susceptible to landsliding when it is unsaturated, we infer that pore pressures were very high at the time that faulting and sliding occurred, either from ground-water saturation or from submersion under Lake Bonneville.

Geomorphic relations (described below) between the fault scarp and the shorelines indicate that the scarp must have formed after the Bonneville transgression rose above 1,402 m (about 26 ka) (Scott and others, 1983, fig. 5) but before the post-Provo regression fell below 1,326 m (about 12 ka). Our reasoning is as follows. During a pluvial lake cycle, surface-faulting events can

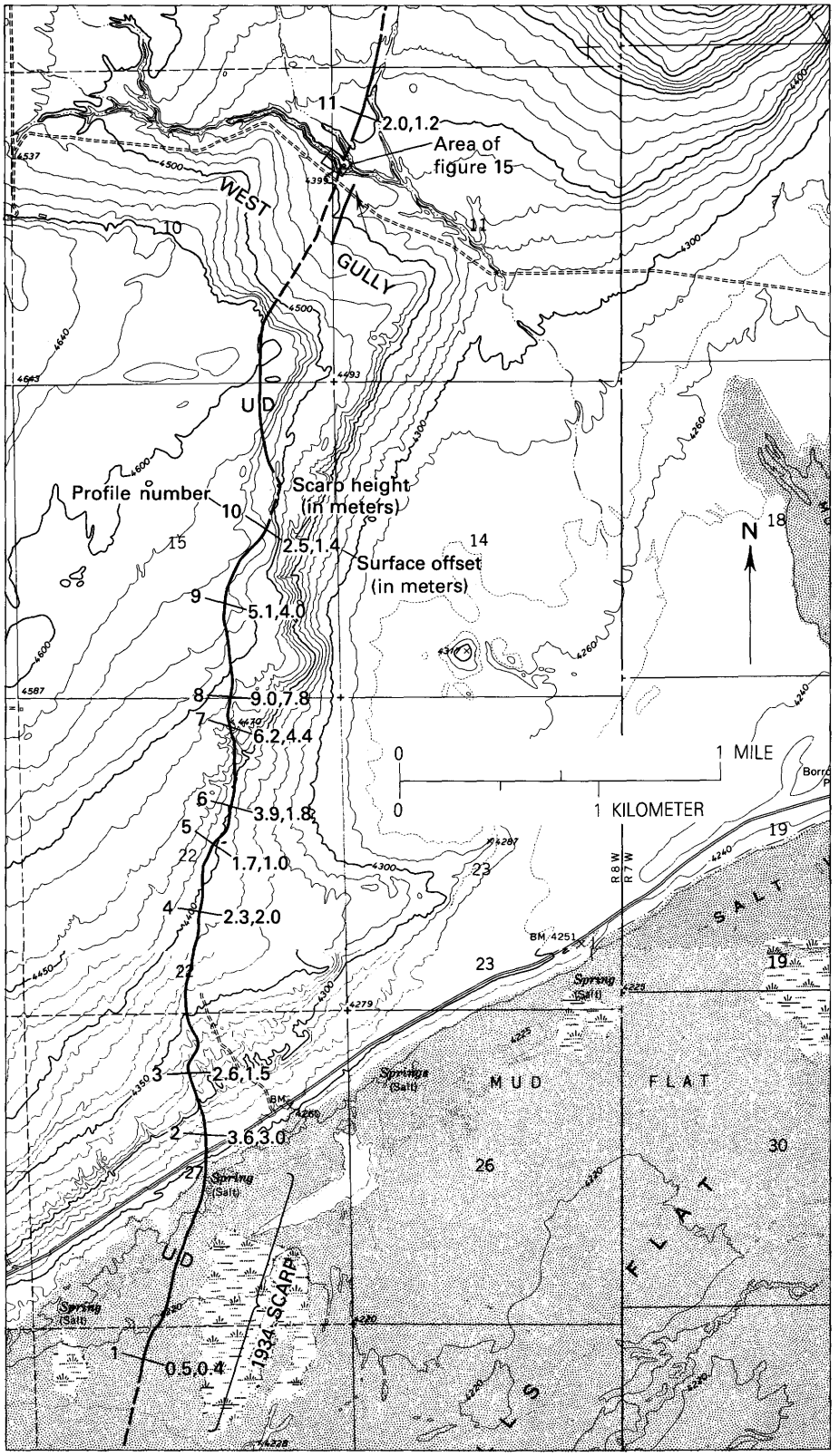

FIGURE 12.—Profile locations, scarp heights, and surface offsets on the Hansel Valley southwestern margin fault scarp (scarp D, fig. 2). The 1934 scarp appears on the southern end of the prehistoric scarp. Scarp heights increase as the scarp ascends a larger escarpment; the arcuate scarp plan shape strongly indicates syntectonic slumping (fig. 13). If slump effects are disregarded, most surface offsets are in the 1.0- to 2.0-m range.

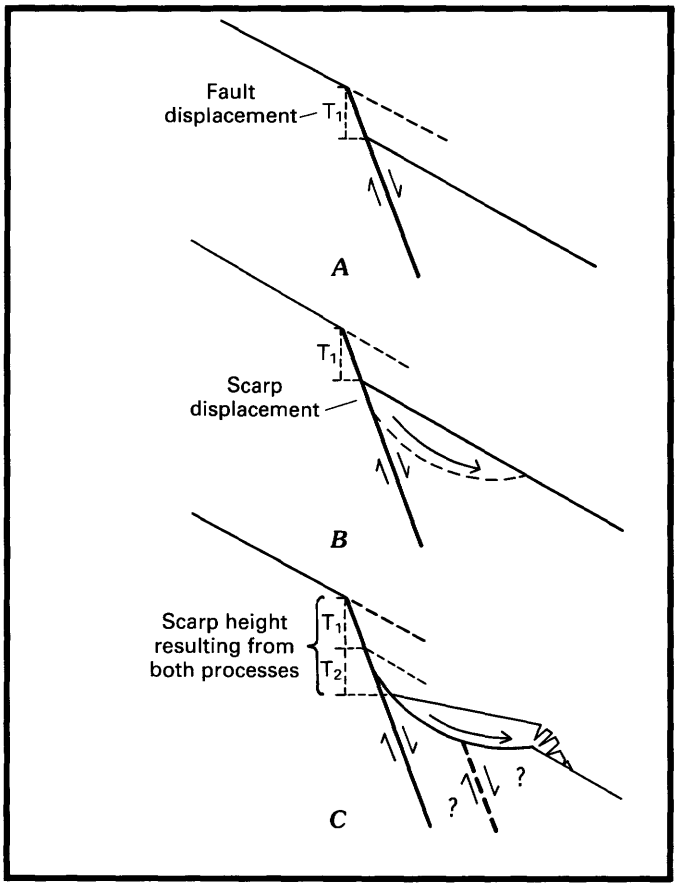

FIGURE 13.—Conceptual model showing how fault scarps on the southwestern margin might be heightened by a coseismic rotational slump. *A*, Initial fault displacement creates a scarp of height T_1. *B*, During seismic shaking, a rotational slump begins to form on the downthrown block. Slumping would be likely if surface materials were saturated (see text). *C*, After slumping, the total scarp height includes components from fault displacement (T_1) and from the slump headscarp (T_2). The dashed and queried fault in *C* indicates that the causative fault may actually underlie the slump, in which case the scarp preserved today is entirely of slump origin. Because slumps were large and slump toes indistinct, profiles used to calculate surface offsets in figure 12 were not extended downslope to include the entire slump deposit.

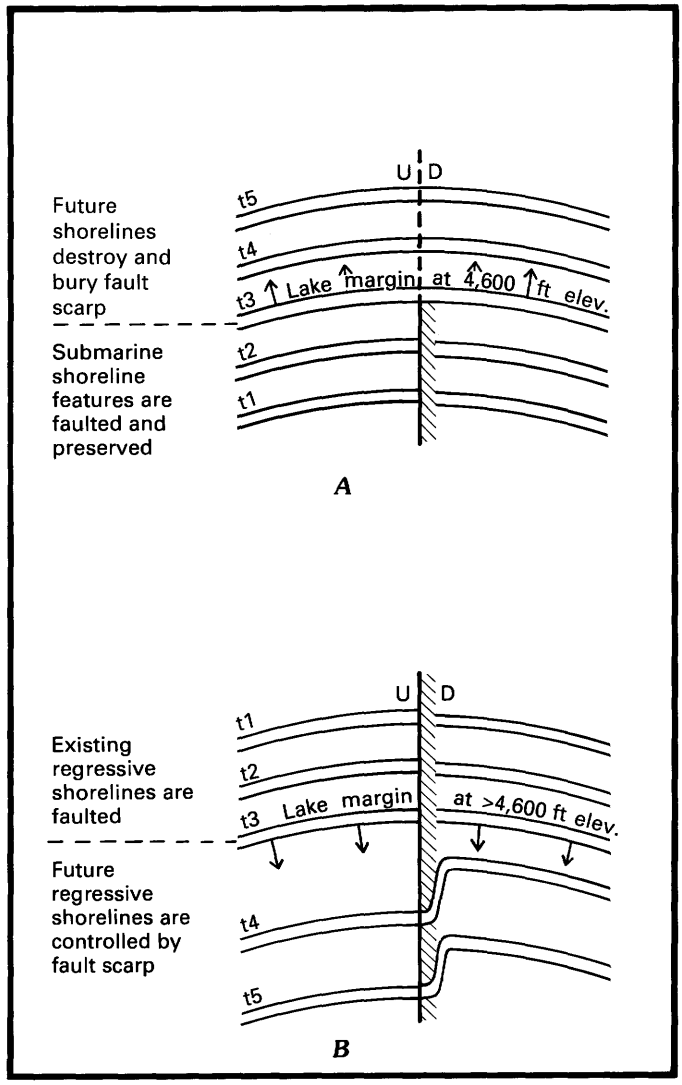

FIGURE 14.—Geomorphic setting of a fault scarp formed during a lacustrine transgression (*A*) and regression (*B*). Time of shoreline occupation is shown by t and progresses from t1 to t5. In both instances, hypothetical faulting occurs when the shoreline is at t3.

occur (1) before the lake rose, (2) during the transgression, (3) during the lake highstand, (4) during the regression, or (5) after the lake had completely receded. Small fault scarps (1–2 m high) that formed before a major transgression would be reworked and destroyed, judging from the thickness (>5 m) and coarseness of Bonneville transgressive bars. Surface faulting during a transgression would displace submerged shorelines already formed; the scarp might be preserved if it were below the effective wave base. That part of the scarp above the shoreline would be destroyed during the continued transgression. A scarp formed during a transgression therefore should displace all shorelines below the one occupied at the time of faulting and terminate at that shoreline, being obscured at higher elevations by wave reworking and longshore deposition (fig. 14*A*). Any fault scarp formed during the lake highstand would displace all transgressive shorelines that it intersected. If faulting occurred during a regression, small regressive shorelines already formed as the lake receded should be displaced. The position of later (lower elevation) regressive shorelines would be controlled by the position of the fault scarp, because only minor deposition (less than 1 m) accompanies regression (except for the Provo shoreline) in the Bonneville Basin. In this case, a scarp would displace regressive shorelines above a certain elevation; below that elevation, shorelines would wrap around or abut a modified scarp of similar height (fig. 14*B*). The

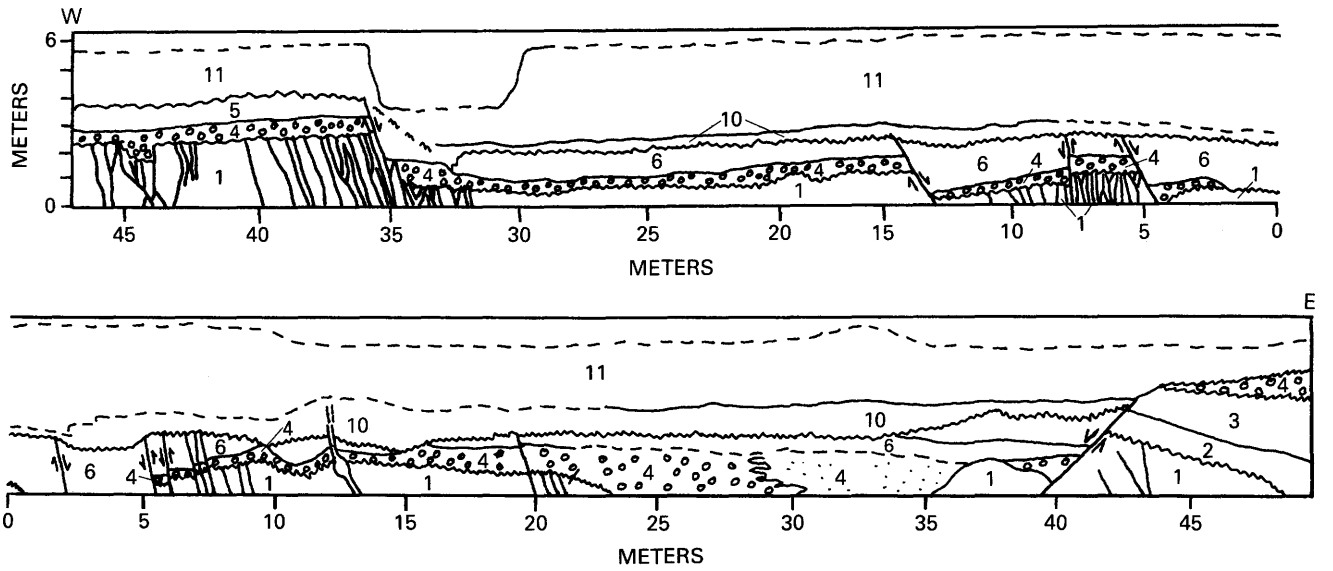

FIGURE 15.—Wall log of the West Gully showing fault patterns. Numbered units 1 through 6 refer to the stratigraphic section in figure 16; units 10 and 11 (not shown in fig. 16) are Holocene alluvium. The zero point on the horizontal scale is the section 10-section 11 boundary, which crosses the arroyo (fig. 12). The chronology of faulting deduced from this log is discussed in the text.

elevation of this transition in morphology marks the position of the shoreline at the time of surface faulting. Surface faulting after the lake had completely receded would result in displacement of all transgressive and regressive shorelines.

Most fault scarps in the Bonneville Basin trend parallel to shorelines near range fronts and therefore are not favorably oriented for intersecting multiple shorelines. The Hansel Valley scarp, however, displaces numerous shorelines as it ascends from the valley-floor (1,286 m) to 1,402 m (fig. 12). The displacement of all transgressive shorelines up to 1,402 m indicates that surface faulting occurred after the Bonneville transgression had risen to this elevation (about 26 ka) (Scott and others, 1983, fig. 5). Small regressive bars at 1,326 m terminate against the scarp, an indication that the scarp was already formed by the time the post-Provo regression reached that elevation (about 12 ka). Therefore, the scarp must have formed after 26 ka but before 12 ka. Scarp surface offset versus tangent of slope angle data suggest that the latest surface-rupture event occurred between roughly 15 and 5.6 ka (closer to the older date) (fig. 10), although scarps formed underwater are not strictly comparable to subaerial scarps. The overlap between these age estimates (12–15 ka) probably closely dates the latest faulting event. If these dates are correct, then the entire southwestern margin scarp was produced by subaqueous displacement of the lake floor.

Near its northern end, the prehistoric scarp is intersected by a 10- to 15-m-deep arroyo (informally termed the West Gully) (figs. 2, 12). Two deformation zones are well exposed on arroyo walls: (1) the main fault zone, consisting of 11 normal faults defining a 90-m-wide graben (fig. 15), and (2) a subsidiary fault zone approximately 100 m to the east, composed of three major normal faults. Detailed logging and sampling of 200 m of arroyo walls reveal that the faults offset a stratigraphic section 19 m thick composed of nine lacustrine units (fig. 16) from three lake cycles. Physical stratigraphy, sedimentology, ostracode assemblages, and thermoluminescence (TL) dating (described by McCalpin, 1986) indicate that deposits of two pre- Bonneville ages are present. The older deposit (unit 1, fig. 16) appears discontinuously in arroyo bottoms, consists of very compact, laminated silt and clay beds, and is disrupted by numerous high-angle fractures and faults of small displacement. Ostracode fauna and a TL date of 138 ka suggest that this lower unit is correlative with the Little Valley deposits described by Scott and others (1983). Unconformably overlying this unit are shoreline gravels and lake-marginal marsh sediments (units 2 and 3), which are also faulted (40–45 m E., fig. 15). TL dates of 76 and 82 ka indicate that these units were deposited during a previously undated lake cycle (informally termed the Hansel Valley cycle) in late oxygen isotope stage 5 or early stage 4 (Morley and Hays, 1981). A lake cycle of similar inferred age has been postulated recently by Oviatt and others (1987). Deposits of the Bonneville cycle (units 4–9) include transgressive gravel and lake-bottom silts and clays. Lake-bottom beds (unit 6) approximately 1.5 m above the transgressive gravel are dated at 14 ka by amino acids and at 15.5 ka by ^{14}C on gastropod shells. Strata 4 m below the top of the stratigraphic section (upper unit 8) are dated at 13 ka by TL. These dates are

roughly correlative with the Bonneville-cycle lake elevation curve of Scott and others (1983, fig. 5).

Although they are not shown on figure 15, faults extend through unit 6 but cannot be traced through units 7 or 8. Both units 6 and 8 are internally deformed, the former by diapirs, roll structures, and convolutions and the latter by rotational faulting of intact blocks along listric faults (lateral spreading?). Although such deformation could be caused by nontectonic mechanisms, the coincidence of discrete deformed beds with a known multiple-event Quaternary fault suggests earthquake-induced liquefaction. The difference in deformation styles may be owing to great difference in water depths (and pore pressures) between the time when unit 6 was deformed (at roughly 245 m) and the time when unit 8 was deformed (at less than 60 m).

Post-Bonneville alluvium (units 10 and 11) truncates all faults exposed in the West Gully, demonstrating that no Holocene events (not even the 1934 earthquake) have induced surface rupture at this location. Although the prehistoric scarp cannot be traced to the edge of the West Gully (because of agricultural disturbances), the net displacement (1.3 m, down to the east) of the transgressive gravel (unit 4) across the graben is similar to scarp heights north and south of the arroyo.

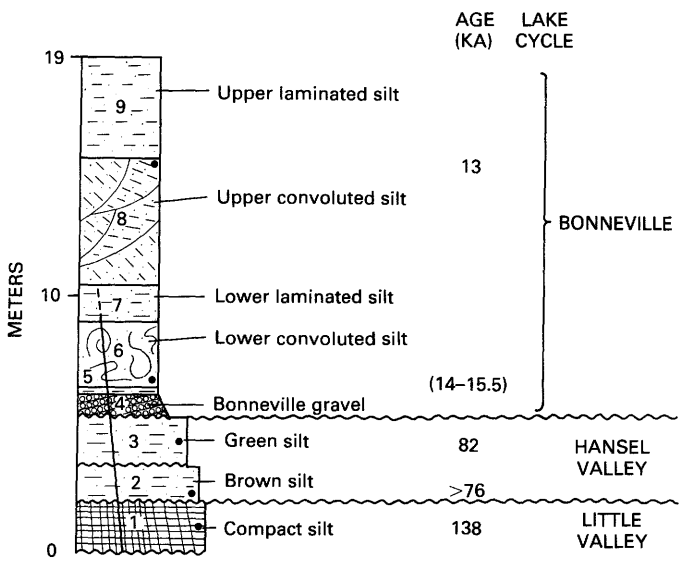

FIGURE 16.—Quaternary deposits exposed in the West Gully. Numbers correspond to those in figure 15, except that post-Bonneville alluvium (units 10 and 11) is not shown. Ages are from thermoluminescence dates on bulk sediment (McCalpin, 1986) or from ^{14}C dates on gastropod shells (in parentheses). Sample locations are shown by solid circles.

LATE QUATERNARY TECTONIC HISTORY

POCATELLO VALLEY

Three lines of indirect evidence suggest a small but measurable amount of late Quaternary displacement on the eastern margin of Pocatello Valley: (1) lack of fault scarps in 15-ka deposits, (2) rapid elevation changes (up to 6.4 m) of a 15-ka shoreline, and (3) tilted but unfaulted Quaternary colluvium at the range front. Shoreline elevation data further suggest that deformation has been dominated by valley subsidence along the 7-km-long central segment of the eastern margin fault. Compilations by Bonilla (1982) and Slemmons (1982) showed that the threshold of surface rupture for shallow-focus earthquakes on normal faults is roughly M_L 6.2 to 6.3. Therefore, it appears that no earthquakes of this magnitude or larger have occurred anywhere along the range-front fault in the last 15 ka. Within 20 m of the inferred range-front fault, the absence of tectonic displacements disrupting 95-ka colluvium suggests that no earthquakes of M_L>6.2 to 6.3 have occurred since that time. If this 7-km-long fault segment is capable of generating surface-faulting earthquakes, then recurrence times between them must be at least 15 ka and possibly as much as 95 ka.

The cause of the rapid 4.5- to 6.4-m vertical changes in shoreline elevation is not fully understood. The magnitude of change appears to be significantly greater than that of the combined surveying errors, whereas the locations of greatest change coincide with shoreline-fault intersections. However, the calculated post-Utaho subsidence rate (4.5 m in 15 ka, or 0.3 mm/yr) seems excessive in light of the overall structural relief and age of the valley. At that rate, the 1,420-m inferred displacement across the fault could have been created in only 475 ka. The presence of Salt Lake Formation (Miocene-Pliocene) within the downthrown block shows that inception of block faulting must be at least Miocene, so the inferred late Quaternary rate must be much higher than the post-Miocene average. This inference is compatible with the observed high rates of historical seismicity.

The 1975 M_L 6.0 earthquake we tentatively assign to the western margin fault, on the basis of epicentral location and focal mechanisms derived by Arabasz and McKee (1979). Like the eastern margin fault, this fault does not displace any Lake Utaho deposits, an indication that no M_L>6.2 to 6.3 events have occurred in the last 15 ka. An early(?) Quaternary pediment (500 ka?) is displaced at least 55 m down to the east, yielding a slip rate of 0.11 mm/yr. This rate is roughly one-third of the slip rate calculated for the eastern margin fault, compatible with the differences in their tectonic geomorphology values quoted earlier.

HANSEL VALLEY

Paleoseismic recurrence and magnitude data from the eastern margin fault are scanty and somewhat contradictory. The 8-m surface offset of the scarp across a 15-ka delta implies multiple ruptures (three to four if displacements per event were 2.0–2.5 m) in the last 15 ka. The resulting recurrence intervals (3.7–5.0 ka) seem too short in view of the total range-front relief and tectonic geomorphology in comparison with those of nearby normal faults such as the Wasatch fault (Machette and others, this volume). Evidence of only a single recent 2.6-m displacement on the Rattlesnake Pass splay fault within the last 100 ka is not compatible with three to four events on the main trace in 15 ka, unless the main fault has ruptured many times without involving this particular splay. However, multiple post-Bonneville displacements are seen nowhere else along the length of the eastern margin, although the inferred fault trace emerges from under its talus cover for several long stretches. Only a single branch fault farther south offsets pre-Bonneville (oxygen isotope stage 4 or 6) alluvial fans 9.5 m. Depending on the age assigned to these fans (roughly 65 or 140 ka), the recurrence intervals for 2.0- to 2.5-m events are between 16 and 35 ka, although not every main trace rupture may have involved this branch. Given the poor geomorphic evidence, all that can be stated with certainty is that this fault has sustained surface rupture at least once since Bonneville time and several times since either oxygen isotope stage 4 or 6.

Although temporal control is better for the well-exposed faulted strata in the West Gully, the inability to trace any subsurface faults to the surface (and thus connect them to the surface scarp) poses a large obstacle to fault-history reconstruction. The older history of faulting is ambiguous; multiple events of unknown displacement occurred along many traces, some of which were truncated by the oxygen isotope stage 4 transgression about 72 ka. On blocks rotated by post-26-ka faulting, the lack of angular unconformity between oxygen isotope stage 6 and 4 deposits indicates that no tectonic rotation occurred there from 72 to 58 ka (35 m E., fig. 15). The 26-ka Bonneville transgression truncates many small-displacement fractures of unknown age in unit 1 but also fills in an open tectonic fissure (42 m W., fig. 15) that could not have remained open for too long after its creation; this fact implies an event not far in advance of 26 ka. Although units 4, 5, and 6 are displaced along major faults, these faults cannot be traced through overlying units owing to poor exposures. The only later evidence of tectonism is the rotated blocks of unit 8, which could be a result of either tectonic or nontectonic lateral spreading. Taken together, the evidence argues for multiple events between roughly 140 and 72 ka, no events from 72 to 58 ka, at least one event between 58 and 26 ka (nearer the latter), an event around 14 to 15 ka (the age of unit 6) and possibly another at 13 ka (unit 8), and a M_L 6.6 event in 1934.

This history implies widely varying recurrence intervals (RI's), from one event from 72 to 26 ka (RI=46 ka) to two events at 14 to 15 ka and 13 ka (RI=1–2 ka). Although the field evidence is ambiguous, it appears that recurrence intervals have been shorter when large lakes existed in the Bonneville Basin (oxygen isotope stages 6 and 2) than they have been during times of small or no lakes (oxygen isotope stages 5, 4, 3). An exception is the 1934 M_L 6.6 earthquake, which occurred in the middle of an interpluvial episode. However, its maximum displacement (0.5 m) is small in comparison with the displacements seen in stage 2 time (2.2–2.6 m, in either one or two events) and may indicate that interpluvial earthquakes are smaller than pluvial earthquakes. Crustal stresses imposed by the rapid filling and draining of pluvial lakes (especially the catastrophic drop from the Bonneville shoreline to the Provo shoreline) may be the main triggering mechanism for the Quaternary surface-faulting events experienced by the southwestern margin fault, as others (Swan and others, 1983; Machette and others, this volume) have suggested for the nearby Wasatch fault.

CONCLUSIONS

Quaternary geologic mapping, shoreline surveying, arroyo wall logging, and trenching indicate that late Quaternary displacements have occurred on both margin faults in Pocatello and Hansel Valleys. The lack of fault scarps in pluvial lake deposits in Pocatello Valley suggests that no surface faulting has occurred in the last 15 ka, yet shorelines and colluvium at the range front appear warped. The 6.4-m maximum vertical shoreline warping may be caused by monoclinal flexure over a buried fault trace; examples of similar warping of surficial deposits near faults have been given by Bonilla (1982, p. 18), although none are for normal faults. Colluvium in a range-front trench appeared warped but unfractured, suggestive of creep flexure rather than flexure around an upward-propagating rupture. Recent trenching on the West Valley fault zone in Salt Lake County, Utah, by Keaton and others (1986) has exposed monoclinal warps along Quaternary normal faults. Given the limited data on hand, it appears that surface flexure could arise from creep or from earthquakes occurring slightly below the threshold magnitude necessary to create a fault scarp. Geomorphic evidence from Pocatello Valley suggests that significant vertical displacements may occur without the creation of fault scarps, over horizontal distances of

hundreds of meters, and that these displacements are not detectable in the field without careful surveying. Such a conclusion has implications for displacement studies on the Wasatch fault, where it has been assumed that most (if not all) cumulative net vertical tectonic displacement can be measured solely by fault-scarp profiling.

Marginal faults bounding Hansel Valley have generated multiple surface-faulting earthquakes in the late Quaternary, despite the seemingly small structural relief of this valley in comparison with that of the Pocatello Valley. Although a few short scarps occur on the steep eastern margin, the best record of activity is on the southwestern margin, where an 8-km-long scarp is intersected by a 15-m-deep arroyo. The multiple events deduced from logging a 90-m-wide complex graben that displaces lacustrine sediments 138 to 13 ka old show that even faults exhibiting minimal topographic and structural expression can have complex recurrence histories. TL dating of silty lacustrine deposits in the graben yielded ages compatible with stratigraphic and paleoecologic evidence and showed that this technique holds promise for dating noncarbonaceous, nonfossiliferous lake beds. Finally, the concentration of deformation in the oldest lacustrine deposit (oxygen isotope stage 6) and in the deposits of the Bonneville cycle (oxygen isotope stage 2) suggests that surface faulting was enhanced when deep pluvial lakes occupied Hansel Valley, as opposed to when no lakes (oxygen isotope stages 3 and 5) or shallow lakes (oxygen isotope stage 4) existed. This temporal clustering has been described by others (Swan and others, 1983) and may result from increased pore pressures and water loading of the crust.

REFERENCES CITED

Adams, O.C., 1962, Geology of the Summer Ranch and North Promontory Mountains, Utah: Logan, Utah State University, unpublished M.Sci. thesis, 57 p.

Allmendinger, R.W., 1983, Geologic map of the North Hansel Mountains, Idaho and Utah: U.S. Geological Survey Miscellaneous Field Studies Map MF–1643, scale 1:24,000.

Allmendinger, R.W., and Platt, L.B., 1983, Stratigraphic variation and low-angle faulting in the North Hansel Mountains and Samaria Mountain, southern Idaho: Geological Society of America Memoir 157, p. 149–163.

Arabasz, W.J., and McKee, M.E., compilers, 1979, Utah earthquake catalog, 1850–June 1962, *in* Arabasz, W.J., Smith, R.B., and Richins, W.D., eds., Earthquake studies in Utah, 1850–1978: University of Utah Seismograph Stations Special Publication, p. 552.

Beus, S.S., 1968, Paleozoic stratigraphy of Samaria Mountain, Idaho-Utah: Bulletin of the American Association of Petroleum Geologists, v. 52, no. 5, p. 782–808.

Bonilla, M.G., 1982, Evaluation of potential surface faulting and other tectonic deformation: U.S. Geological Survey Open-File Report 82–0732, 91 p.

Bucknam, R.C., 1976, Leveling data from the epicentral area of the March 27, 1975, earthquake in Pocatello Valley, Idaho: U.S. Geological Survey Open-File Report 76–52, 6 p.

Bucknam, R.C., and Anderson, R.E., 1979, Estimation of fault-scarp ages from a scarp height-slope angle relationship: Geology, v. 7, p. 11–14.

Bull, W.B., and McFadden, L.D., 1977, Tectonic geomorphology, north and south of the Garlock Fault, California, *in* Doehring, D.O., ed., Geomorphology in arid regions: Annual Geomorphology Symposium, 8th, Binghampton, N.Y., 1977: London, Allen and Unwin, p. 115–138.

Clark, M.M., Grantz, A., and Rubin, M., 1972, Holocene activity of the Coyote Creek fault as recorded in sediments of Lake Cahuilla: U.S. Geological Survey Professional Paper 787, p. 112–130.

Crittenden, M.D., Jr., 1963, New data on the isostatic deformation of Lake Bonneville: U.S. Geological Survey Professional Paper 454–E, 31 p.

Currey, D.R., 1981, Late Quaternary Lake Utaho in southern Idaho-northern Utah: Denver, Colo., Association of American Geographers, Program Abstracts 1981, p. 166–167.

———1982, Lake Bonneville: Selected features of relevance to neotectonic analysis: U.S. Geological Survey Open-File Report 82–1070, 30 p.

Doelling, H.H., 1980, Geology and mineral resources of Box Elder County, Utah: Utah Geological and Mineralogical Survey Bulletin 115, 251 p.

Hanks, T.C., Bucknam, R.C., LaJoie, K.R., and Wallace, R.E., 1984, Modification of wave-cut and faulting-controlled landforms: Journal of Geophysical Research, v. 89, no. B7, p. 5771–5790.

Harr, C.J., and Mabey, D.R., 1976, Gravity survey of Pocatello Valley, Idaho and Utah: U.S. Geological Survey Open-File Report 76–766, 12 p.

Hood, J.W., 1971, Hydrologic reconnaissance of Hansel Valley and Northern Rozel Flat, Box Elder County, Utah: Utah Department of Natural Resources Technical Publication 33, 41 p.

Jordan, T.E., 1985 Geologic map of the Bull's Pass quadrangle, Box Elder County, Utah: U.S. Geological Survey Miscellaneous Field Studies Map MF–1491, scale 1:24,000.

Keaton, J., Currey, D.R., and Olig, S.J., 1986, Paleoseismicity and earthquake hazards evaluation of the West Valley fault zone, Salt Lake City urban area: Contract report prepared for U.S. Geological Survey under contract 14–08–0001–22048, 18 p.

McCalpin, J., 1986, Thermoluminescence (TL) dating in seismic hazard evaluations; an example from the Bonneville Basin, Utah: Annual Engineering Geology and Soils Engineering Symposium, 22d, Boise, Idaho, 1986, Proceedings, p. 156–176.

Morley, J.J., and Hays, J.D., 1981, Towards a high-resolution, global, deep sea chronology for the last 750,000 years: Earth and Planetary Science Letters, v. 15, p. 279–295.

Oviatt, C.G., McCoy, W.D., and Reider, R.G., 1987, Evidence for a shallow early or middle Wisconsin-age lake in the Bonneville Basin, Utah: Quaternary Research, v. 27, p. 248–262.

Peterson, D.L., 1974, Bouguer gravity map of part of the northern Lake Bonneville Basin, Utah and Idaho: U.S. Geological Survey Miscellaneous Field Studies Map MF–627, scale 1:250,000.

Platt, L.B., 1975, Recent faulting at Samaria Mountain, southeastern Idaho: Geological Society of America Abstracts with Programs, v. 7, p. 1224–1230.

———1976, Geologic mapping and earthquakes in southeastern Idaho: Earthquake Information Bulletin, v. 8, p. 8–12.

———1977, Geologic map of the Ireland Springs-Samaria area, southeastern Idaho and northern Utah: U.S. Geological Survey Miscellaneous Field Studies Map MF–890, scale 1:48,000.

Rogers, A.M., Langer, C.J., and Bucknam, R.C., 1975, The Pocatello Valley, Idaho, earthquake; Earthquake Information Bulletin, v. 7, no. 3, p. 16–18.

Rose, J., 1981, Raised shorelines, *in* Goudie, A., ed., Geomorphological techniques: London, Allen and Unwin, p. 327–341.

Scott, W.E., Machette, M.N., Shroba, R.R., and McCoy, W.D., 1982, Guidebook for the 1982 Friends of the Pleistocene Rocky Mountain Cell Field Trip to Central Utah, pt. I, Little Valley and Jordan Valley, Utah: U.S. Geological Survey Open-File Report 82–845, 58 p.

Scott, W.E., McCoy, W.D., Shroba, R.R., and Rubin, M., 1983, Reinterpretation of the exposed record of the last two cycles of Lake Bonneville, Western United States: Quaternary Research, v. 20, p. 241–265.

Slemmons, D.B., 1982, Determination of design earthquakes magnitudes for microzonation, *in* Proceedings of the Third International Earthquake Microzonation Conference, Seattle, WA: Berkeley, Calif., Earthquake Engineering Research Institute, v. 1, p. 110–130.

Stokes, W.L., 1977, Subdivisions of the major physiographic provinces in Utah: Utah Geology, v. 4, no. 1, p. 1–17.

Swan, F.H., III, Hanson, K.L., Schwartz, D.P., and Black, J.H., 1983, Study of earthquake recurrence intervals on the Wasatch fault, Utah: 8th semiannual technical report to U.S. Geological Survey under contract 14–08–0001–19842, 20 p.

Wallace, R.E., 1977, Profiles and ages of young fault scarps, north central Utah: Geological Society of America Bulletin, v. 88, no. 10, p. 1267–1281.

Structure of the Salt Lake Segment, Wasatch Normal Fault Zone: Implications for Rupture Propagation During Normal Faulting

By R.L. BRUHN, P.R. GIBLER, W. HOUGHTON, *and* W.T. PARRY,
DEPARTMENT OF GEOLOGY AND GEOPHYSICS, UNIVERSITY OF UTAH

ASSESSMENT OF REGIONAL EARTHQUAKE HAZARDS AND RISK ALONG THE WASATCH FRONT, UTAH

U.S. GEOLOGICAL SURVEY PROFESSIONAL PAPER 1500–H

CONTENTS

	Page
Abstract	H1
Introduction	1
Acknowledgments	2
Tectonics of the Wasatch Fault Zone	2
Structure of the Salt Lake Segment	4
Paleostress Analysis	4
Fault Zone Structure	10
Traverse Mountains Barrier	10
Fault Zone Structure—Continued	
Southern Fault Sections	H14
Northern Fault Sections	14
Salt Lake Salient	15
Discussion	16
Geometry of Fault Sections	16
Directional Characteristics of Rupture Propagation	17
Conclusions	23
References Cited	24

ILLUSTRATIONS

		Page
FIGURES 1, 2.	Maps showing:	
	1. Tectonics of the Salt Lake rupture segment, Wasatch normal fault zone	H3
	2. Geology and cross section of part of the Wasatch Mountains and the Salt Lake rupture segment	5
3, 4.	Diagrams showing:	
	3. Contoured orientations of poles to fault planes and slickenlines for fault populations in each structural domain in figure 1	8
	4. Paleoprincipal deviatoric stress orientations from each of the four structural domains in figure 1 based on inversion of fault-plane and slickenline data	10
5, 6.	Maps showing:	
	5. Geometry of faulting at the Traverse Mountains barrier and block diagram of the tripartite fault array	11
	6. Geology of the Fort Canyon fault zone in the Fort Canyon structural domain shown in figure 1	12
7.	Stereoprojection showing the orientation of the Fort Canyon fault, the preferred orientation of the Draper fault section at the southern end of the Salt Lake segment, and slip directions for various ϕ values of the paleostress field	13
8.	Map showing surface fault traces in the Salt Lake segment and preferred dip angles based on geometric modeling	14
9.	Stereoplot of north-striking faults having dips between 20° and 80° W. and sliplines for the paleostress field in the Red Butte structural domain	15
10, 11.	Maps showing:	
	10. Trace of the Salt Lake fault segment and estimated dimensions D_b of barriers modeled as equivalent "plastic" deformation zones	19
	11. Normal faults in the northern half of the Red Butte structural domain and cross section illustrating the conjugate geometry of faulting in the footwall	20
12.	Schematic cross sections illustrating possible structure of the branched fault zone in the northern half of the Salt Lake segment	21
13.	Map showing rupture traces of the Borah Peak, Idaho, and Hebgen Lake, Mont., earthquake rupture zones in comparison with the Quaternary trace of the Salt Lake rupture segment	22

TABLES

		Page
TABLE 1.	Barrier classifications	H6
2.	Principal stress data	10

ASSESSMENT OF REGIONAL EARTHQUAKE HAZARDS
AND RISK ALONG THE WASATCH FRONT, UTAH

STRUCTURE OF THE SALT LAKE SEGMENT, WASATCH NORMAL FAULT ZONE: IMPLICATIONS FOR RUPTURE PROPAGATION DURING NORMAL FAULTING

By R.L. BRUHN, P.R. GIBLER, W. HOUGHTON, and W.T. PARRY

ABSTRACT

The Salt Lake fault segment is one of the six independent earthquake rupture segments in the Wasatch normal fault zone of Utah originally proposed by D.P. Schwartz and K.J. Coppersmith in 1984. The Salt Lake segment is about 35 km long and capable of generating earthquakes of M 7.0 to 7.5. The fault segment is defined by a series of Quaternary scarps that form a branched fault trace; a narrow single rupture zone bifurcates into two subparallel rupture zones in the northern half of the segment. The surface rupture trace is subdivided into several linear to curvilinear sections approximately 3 to 12 km in length. The dips of these fault sections are modeled by using information about characteristics of the paleoslip directions and the paleostress field. Estimated dips vary from 45° to 90° depending on the strike of individual fault sections.

A nonconservative rupture barrier is located at each end of the segment, and the zone of fault bifurcation forms a third nonconservative barrier located in the center of the segment. The relative fracture toughness of barriers has been estimated solely on the basis of their cross-sectional dimensions and on the assumption that the barriers are mechanically equivalent to a "plastic tip" deformation zone in fracture mechanics theory.

Two potential sites of rupture initiation for large earthquakes are tentatively proposed on the basis of the structural history and inferred mechanical characteristics of the Salt Lake segment. One site is the nonconservative barrier in the central part of the segment. A rupture initiating there would propagate bilaterally to the north and the south, possibly arresting in the two nonconservative barriers at the ends of the segment. The other likely rupture initiation site is within the nonconservative barrier at the southern end of the fault segment. An earthquake initiating there would rupture unilaterally toward the north, propagating into the bifurcated northern half of the fault segment in a manner similar to the propagations of the Hebgen Lake, Mont. (M_S 7.3), and the Borah Peak, Idaho (M_S 7.3), earthquake ruptures. Evidence of significant lateral variations in the long-term deformation rate within the segment suggests that this latter site may have been the most common position for repetitive rupture initiation during roughly the last 17 m.y.

Manuscript approved for publication November 20, 1990.

INTRODUCTION

Large fault zones are divided into sections that vary in geometry and rupture history. The intersections of adjacent fault sections may form geometric barriers that strongly influence the history of rupturing within the fault zone and play a fundamental role in determining the seismogenic characteristics of the crust (Aki, 1979; King, 1983; King and Yielding, 1984; King and Nabelek, 1985). A propagating rupture may exhibit several different types of behavior upon encountering a barrier. The rupture front may slow down or pause temporarily for periods of seconds or minutes or become permanently arrested. In the latter case, new ruptures may nucleate and propagate into adjacent parts of the fault zone at later times. Consequently, geometric barriers must be considered as potential sites of both rupture arrest and initiation (King, 1983; King and Yielding, 1984; King and Nabelek, 1985).

King and Yielding (1984) defined two fundamental types of geometric barriers—the conservative barrier and the nonconservative barrier. Geometric barriers represent jogs or bends in the main fault zone caused by offset in the fault trace and changes in strike and dip. A conservative barrier is one in which the fault-slip vector is constant on both sides of the barrier and parallels the intersection line between the primary fault planes comprising the adjacent sections of the fault zone. That is, the adjacent sections form a cylindrical surface that can be generated by moving the slip vector parallel to itself. Conversely, a nonconservative barrier develops in regions where the slip vectors differ between two adjacent sections of the fault zone. The structures of these two types of barriers differ significantly. Faulting in the conservative barrier is accommodated within a narrow fault zone and does not require extensive fracturing of

the adjacent country rock to transfer motion between two adjacent sections of the fault zone. Alternatively, rupturing through a nonconservative barrier requires the development of at least one new direction of primary faulting in addition to the directions of the two intersecting fault sections comprising the main fault zone. This process will result in the formation of numerous subsidiary faults that must be activated to allow the transfer of motion between the fault sections. This network of subsidiary faults results in a broad, diffuse zone of deformation in the nonconservative barrier, which has the effect of "blunting" the tip zone of the propagating rupture and diffusing energy into a large volume of rock. Consequently, nonconservative barriers are likely sites for the permanent arrest of a propagating rupture. This process, in turn, may set the stage for the initiation of a subsequent rupture that will propagate into an adjacent section of the primary fault zone (King and Nabelek, 1985). The mutual interference and interlocking of numerous subsidiary faults in the barrier result in the development of asperities, which must be broken in order to establish the full length of the next rupture segment. The breaking of these asperities must be a time-dependent process that is related to (1) rates of deformation that increase stress level through time, (2) fluid chemistry and pressure in the barrier, and (3) material properties in the barrier.

Several criteria exist for identifying geometric barriers in fault zones (King, 19983; King and Yielding, 1984; King and Nabelek, 1985). An abrupt offset, bend, or geometric branching in the trace of a primary fault zone is sufficient to identify the presence of a barrier. The presence of a nonconservative barrier is indicated by a change in the amount or directions of slip on two adjacent sections of the primary fault zone. This phenomenon leads to (1) development of a third direction of faulting in the barrier, (2) breakup of the hanging wall above the barrier in normal fault zones, (3) abrupt changes in the amount of throw across the fault zone between the two primary sections, and (4) the possibility of diffuse seismicity associated with the failure of asperities within the barrier.

This paper presents our study of the geometry and paleostress field of the Salt Lake rupture segment (fig. 1) of the Wasatch fault zone. The Salt Lake segment is one of six large rupture segments within the Wasatch fault zone that were proposed by Schwartz and Coppersmith (1984). This segment extends for about 35 km through the urban corridor of Salt Lake City, along the eastern edge of the Basin and Range province. The fault zone is marked by prominent scarps in Quaternary deposits and has undergone at least two, and probably four, earthquakes of M 7.0 to 7.5 that generated surface scarps during the last 8,000 years (Schwartz and Coppersmith, 1984). Our goal is to determine the geometric and mechanical characteristics of the segment in order to better understand the processes of crustal segmentation and the seismogenic characteristics of the Wasatch fault zone.

ACKNOWLEDGMENTS

This work was part of a program of structural and geochemical studies of the Wasatch fault zone undertaken by R.L. Bruhn and W.T. Parry. P.R. Gibler wrote the stress tensor inversion programs and collected field data for the paleostress analysis. W. Houghton mapped the Fort Canyon fault zone and studied the petrofabrics of the fault rock. This work represents part of Gibler's and Houghton's M.Sci. theses at the University of Utah. Financial support was provided by the U.S. Geological Survey Earthquake Hazards Program grant 14–08–0001–G–886 to Bruhn and Parry, American Chemical Society grant 14179AC to Bruhn, and the Integrated Tectonics and Seismology Program of the University of Utah. We thank W.J. Arabasz and J.C. Pechmann (University of Utah), R.B. Smith (University of Utah), and D.P. Schwartz (U.S. Geological Survey) for discussions concerning the structural and seismogenic characteristics of normal faulting. Thorough reviews of a draft version of the manuscript by P.C. Thenhaus and R.L. Wheeler (U.S. Geological Survey) were very helpful.

TECTONICS OF THE WASATCH FAULT ZONE

The Wasatch normal fault zone extends for 370 km along the eastern edge of the Basin and Range province in southern Idaho and northern Utah (fig. 1). This major fault zone has a pronounced footwall escarpment, displaying up to 3 km of relief, that separates alluvial-filled valleys of the Basin and Range to the west from the Wasatch Mountains to the east (Gilbert, 1928). Total throw across the Wasatch fault zone varies along strike. Estimates from gravity modeling range from 2.6 to 4.0 km (Zoback, 1983). Throw across the fault zone may reach 11 km just south of Salt Lake City, Utah (Parry and Bruhn, 1984, 1986).

Schwartz and Coppersmith (1984) proposed that the Wasatch fault zone is divided into six structural segments defined by differences in the geometry of the fault trace, variations in footwall topography, and earthquake rupture history. Individual segments have strike lengths of 35 to 70 km, and their ends are marked by east-trending faults and basement ridges that subdivide basins in the hanging wall of the fault zone (Zoback, 1983; Schwartz and Coppersmith, 1984; Smith and Bruhn, 1984). This segmentation has been refined further by Machette and others (this volume). Each segment has

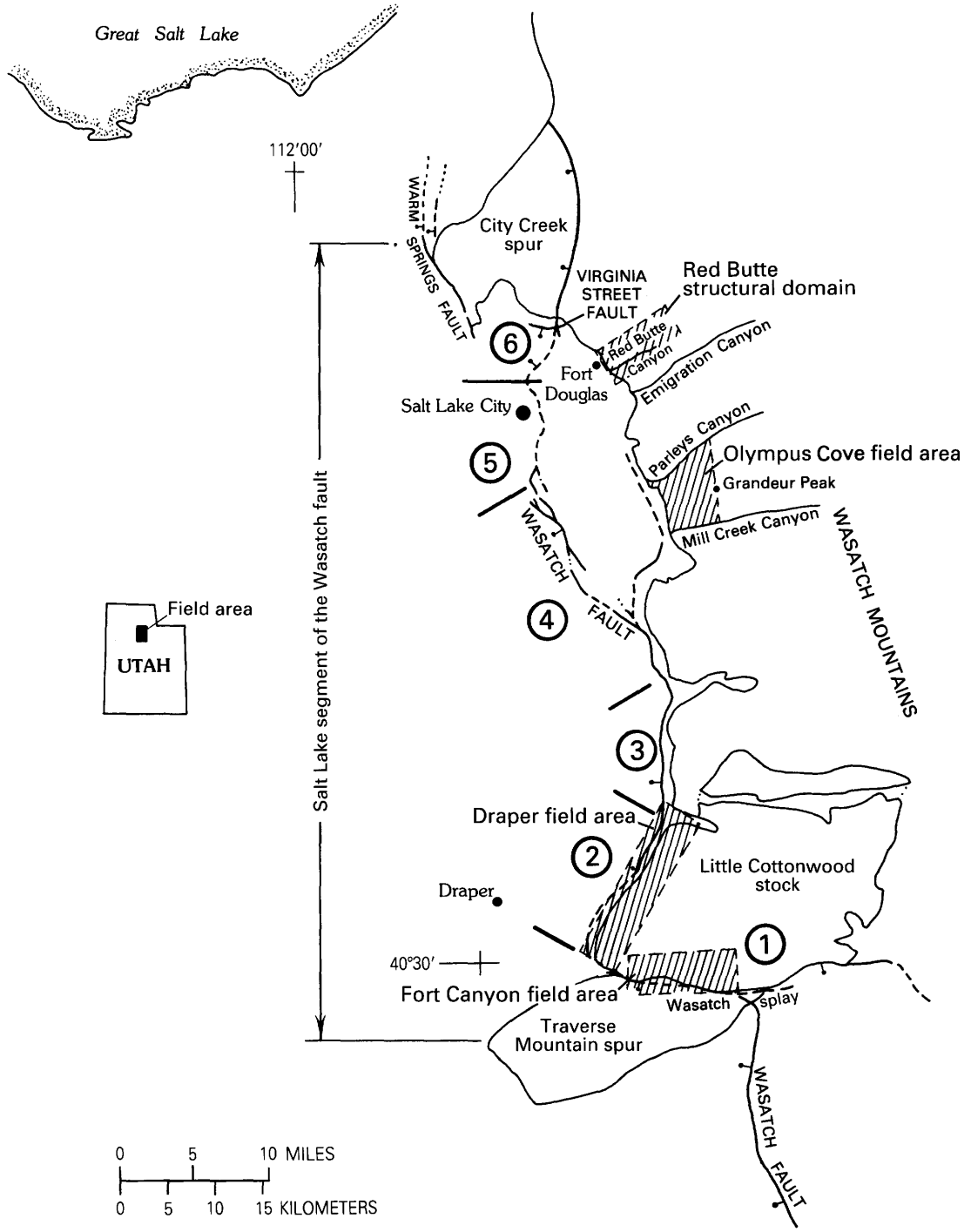

FIGURE 1.—Tectonics of the Salt Lake rupture segment, Wasatch normal fault zone, Utah. Structural domains for paleostress analysis are indicated by hachures. Normal fault is indicated by line with ball and bar on the hanging wall (solid where scarp is exposed, dashed where buried or inferred). Circled numbers are sections of the Salt Lake rupture segment presented in figure 8 and discussed in the text for purposes of inferring the positions of geometric barriers and fault zone orientation.

undergone multiple episodes of surface faulting during the Pleistocene and Holocene and is presumed capable of generating characteristic earthquakes of M 7.0 to 7.5 on the basis of fault displacements measured in trenches placed across Quaternary scarps. The recurrence interval of surface rupturing on individual segments is estimated to be as short as 4,580 years; an average recurrence interval for characteristic earthquakes is 400

to 600 years for the entire Wasatch fault zone (Swan and others, 1980; Schwartz and others, 1983; Schwartz and Coppersmith, 1984).

The Wasatch fault zone is associated with a north-south zone of diffuse seismicity that generally dos not show a strong spatial correlation with the Quaternary fault scarps (Arabasz and others, 1980; Zoback, 1983). Earthquake focal mechanisms, geodetic measurements, and fault-slip vector data taken from Quaternary scarps indicate that, regionally, the crust is extending in a west-southwest–east-northeast direction, at an average orientation of the least principal stress (maximum extension axis) of 073°±15° (Zoback, 1983).

STRUCTURE OF THE SALT LAKE SEGMENT

The Salt Lake segment of the Wasatch fault zone extends for 35 km from the Salt Lake salient on the north to the Traverse Mountain spur on the south (fig. 2) (Gilbert, 1928; Schwartz and Coppersmith, 1984). The footwall of the Salt Lake segment is composed of Proterozoic through Tertiary sedimentary strata, Precambrian schist and amphibolite, and Oligocene quartz monzonite. Precambrian, Paleozoic, and Mesozoic strata generally strike eastward and are folded in the east-trending Uinta arch, a large anticlinorium that developed during the latest Cretaceous and earliest Tertiary (Crittenden, 1976). Quartz monzonite of the Little Cottonwood stock intruded Precambrian and Paleozoic rock along the southern part of the footwall during the Oligocene (Crittenden and others, 1973). The Wasatch fault cuts across these earlier structures at high angle to their strike.

The hanging wall of the Salt Lake segment contains a large Neogene basin containing over 1 km of sedimentary fill. The fill consists of Miocene through Quaternary strata and volcanics (Cook and Berg, 1961; Zoback, 1983). The hanging-wall basin is structurally segmented by an east-trending basement step that separates the deeper southern part of the basin, which is about 1 to 1.5 km deep, from the northern section, where the thickness of the basin fill is generally less than 300 m, according to Zoback (1983).

The history of faulting on the Salt Lake segment is poorly constrained. Normal faulting postdated intrusion of the Little Cottonwood stock, which was intruded 31.1±0.9 m.y. ago (Crittenden and others, 1973). A muscovite concentrate from exhumed fault rock in the Wasatch fault zone along the southwestern margin of the stock was dated as 17.3±0.7 m.y. and represents the age of the earliest observed syntectonic hydrothermal alteration in the fault zone at that locale (Parry and Bruhn, 1986). Consequently, normal faulting in the Salt Lake segment began by latest early Miocene. Relative uplift of the footwall at the southern end of the Salt Lake segment is about 11 km on the basis of fluid pressure estimates from fluid inclusions trapped in cataclasite in the fault zone (Parry and Bruhn, 1984, 1986). A minimum estimate for throw at the northern end of the segment is 2.5 km, based on the geology of the footwall and an estimated 300 m of fill in the hanging-wall basin (Zoback, 1983).

The Quaternary surface trace of the Salt Lake segment consists of several linear to curvilinear fault sections that vary in orientation and range in length from as little as 3 km to as much as 12 km (fig. 2). These sections are separated by significant bends in the trace of the fault zone that define geometric barriers. The bends are classified as either conservative or nonconservative barriers on the basis of the criteria listed in table 1. Several barriers can be readily identified; of these, three are classified as nonconservative barriers—one at each end of the Salt Lake segment (nos. 1 and 9, table 1) and a third composite barrier associated with a branch point in the fault trace located in the central part of the segment (nos. 4, 5a, and 5b, table 1).

The fundamental characteristics of a nonconservative barrier are that the slip directions on the adjacent sections of the primary fault zone are different in orientation or magnitude or both and that at least a third direction of faulting is required to accommodate displacement within the primary fault zone (King, 1983; King and Yielding, 1984). The direction of slip on a series of variably oriented fault sections will depend on the geometry of the sections and on the orientations and relative magnitudes of the principal stresses operating across the fault planes. We first consider the nature of the paleostress and contemporary stress fields in the Salt Lake segment and then discuss the geometric characteristics of the individual fault sections and barriers. Finally, we speculate on the rupture characteristics of the Salt Lake segment.

PALEOSTRESS ANALYSIS

The orientation of the paleostress field in the Salt Lake segment was determined on the basis of a stress tensor inversion analysis of mesoscopic fault populations in the Wasatch fault zone and adjacent parts of the footwall. Four structural domains were chosen for analysis (fig. 1). Each domain was chosen because of its excellent exposure and its structural position within the fault segment. The Red Butte and Olympus Cove domains were located in Paleozoic and Mesozoic strata in the northern and central parts of the segment. The Draper and Fort Canyon structural domains were located in exhumed

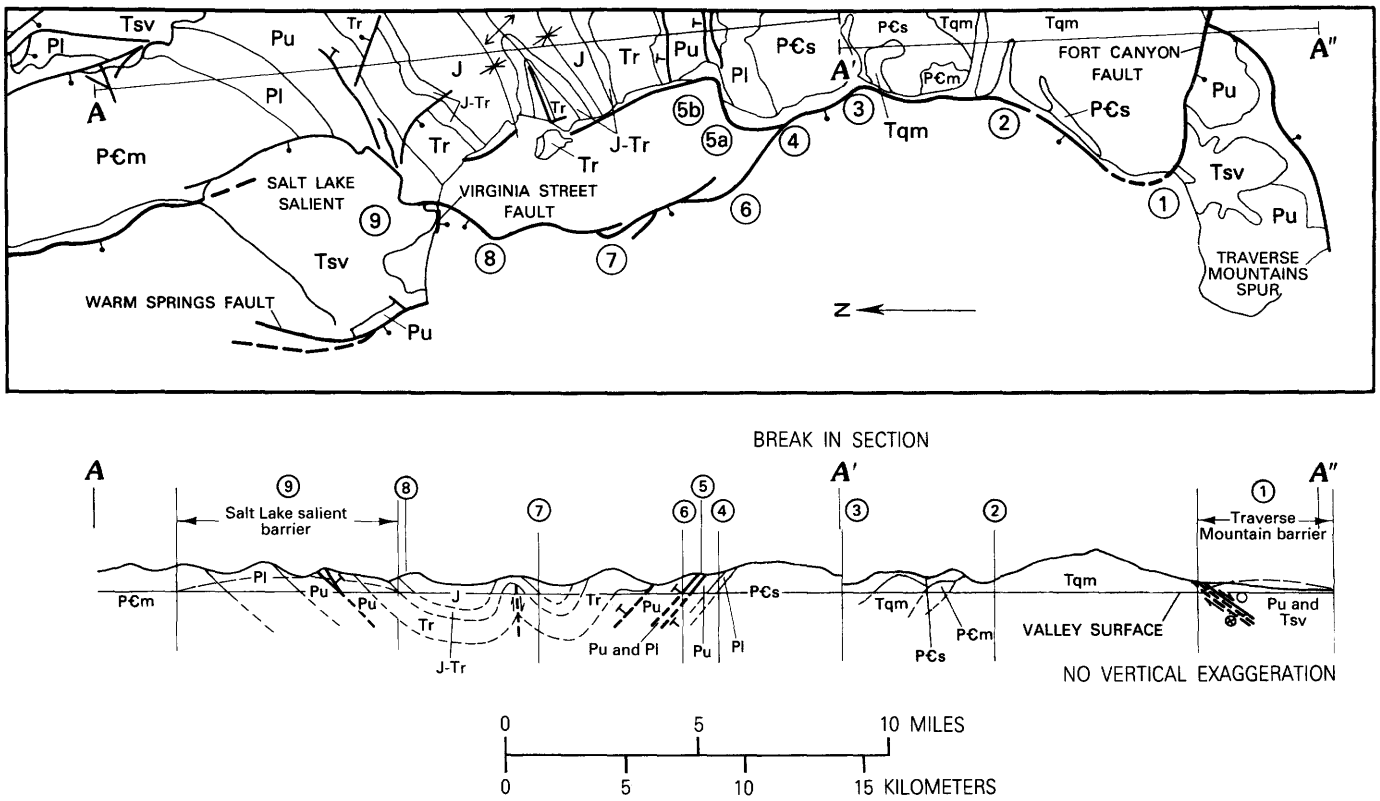

EXPLANATION

- Tsv — Tertiary sedimentary and volcanic rock
- Tqm — Tertiary igneous intrusive rock
- J — Jurassic strata
- J-Tr — Jurassic and Triassic strata
- Tr — Triassic strata
- Pu — Upper Paleozoic strata
- Pl — Lower Paleozoic strata
- P€s — Precambrian strata
- P€m — Precambrian metamorphic rock

- Lithologic contact—Dashed in the subsurface
- Thrust fault—Dashed in the subsurface; (T on upper plate)
- Normal fault—Dashed in the subsurface
- Normal fault—Ball and bar on hanging wall, dashed where buried or inferred
- Projections of barrier (bend in fault zone) on cross section
- Axial trace of anticline
- Axial trace of syncline

FIGURE 2.—Geology and cross section of part of the Wasatch Mountains and the Salt Lake rupture segment. Barriers in the fault zone are numbered and projected onto the footwall cross section. Geology from Davis (1983a, b); Wasatch fault trace from Marsell (1969).

fault rock within the Wasatch fault zone on the western and southern margins of the Little Cottonwood stock. The latter two domains were chosen to provide information about paleostress orientations in the Traverse Mountains barrier at the southern end of the Salt Lake segment.

TABLE 1.—*Barrier classifications*

Barrier no.[1]	Structural characteristics[2]	Barrier type
1	TF, HB, TH, SE, OF	Nonconservative.
2	B	Conservative.
3	B	.....do.
4	BR, TF, HB	Nonconservative.
5a	B, ID	.....do.
5b	B, TF(?), ID	.....do.
6	B	Conservative(?).
7	B	.....do.
8	B	.....do.
9	TF, BR, HB, SE, OF	Nonconservative.

[1]Branch point 4 and bends 5a and 5b are considered one composite nonconservative barrier.

[2]B, bend in trace; BR, branching of fault trace; OF, lateral offset of two primary rupture traces; TF, three directions of large-scale faulting; HB, hanging-wall breakup or basement ridge; TH, abrupt difference in primary fault throw; ID, dip incompatible with conservation of slip on adjacent fault section; SE, diffuse seismicity.

Faults within each domain form several sets that permeate the rock on the meter to centimeter scale. The age of faulting is not well constrained. The Draper and Fort Canyon domains are located in a structural carapace of cataclastic and phyllonitic quartz monzonite that varies from a few meters to about a hundred meters in thickness. This fault rock formed at depth within the Wasatch fault zone beginning about 17 m.y. ago and continued to form during uplift of the footwall relative to the hanging wall of the fault zone (Parry and Bruhn, 1984, 1986).

Faults in the Red Butte and Olympus Cove domains cut Paleozoic and Mesozoic strata in the footwall of the Wasatch fault zone (figs. 1, 2). They are part of a large population of normal to normal-oblique slip faults that occur in the footwall block and increase in number as the Holocene scarps of the Wasatch fault zone are approached. The Red Butte and Olympus Cove domains are both located about 2.5 km east of the youngest Holocene scarp system but lie directly adjacent to an older system of Quaternary scarps along the Wasatch Mountain front (fig. 1) (Van Horn, 1972).

Slickenlines for fault populations from each domain are plotted in figure 3, and, with the exception of those in the Fort Canyon domain, the slickenlines generally form two or more maxima. In the Fort Canyon domain, the slickenlines form a broad partial girdle in the stereoplot, indicative of a diffuse spatial distribution of slip directions. The dominant spatial concentrations in the other domains trend between 230° and 250°; subsidiary maxima plunge at moderate angles into either the northern or the southern quadrant. The fault populations are composed of a mixture of fault types, and slip varies from purely normal through oblique-slip to almost pure strike-slip motion on faults of various orientations.

Slip directions on Quaternary fault surfaces in the Salt Lake segment were reported by Pavlis and Smith (1980) from two faults exposed at the northern end of the segment in the Salt Lake salient (fig. 2). Exposures of the Warm Springs fault, which strikes N. 45° W. and dips 70° W., contained two sets of slickenlines. The older set trended 288°, and the younger trended 239°. The Virginia Street fault located a few kilometers to the southeast strikes N. 80° E. and dips 68° S. Slickenlines on this fault formed two maxima plunging towards the west-southwest. The average trend of the northern maximum was 255°, and that of the southern maximum was 233°. The relative age of the two slickenline sets on the Virginia Street fault could not be determined from field observations.

The slip directions determined by Pavlis and Smith (1980) for Quaternary faulting at the northernmost end of the Salt Lake segment are consistent with the directions of the most prominent slickenline maxima from the paleofault populations in the Red Butte, Olympus Cove, and Draper domains. This observation does not imply that the paleofault populations are Quaternary in age but, rather, raises the contention that extension across the Salt Lake segment may have been oriented consistently toward the west-southwest over an extended period of time. The oldest set of slickenlines on the Warm Springs fault provides an exception, in that this set trends about 20° north of west, whereas the prominent maxima in the paleofault populations trend south of west. However, the remainder of the Quaternary slickenline sets lie within the general trend of the prominent set in each of the paleofault population domains.

The paleostress directions in each domain were determined by using a linear stress tensor inversion method like the one discussed by Michael (1984). This technique provides an estimate of the trend and plunge of the paleoprincipal deviatoric stresses ($S_1 \geq S_2 \geq S_3$) and the stress parameter $\phi = (S_2 - S_3)/(S_1 - S_3)$ for a population of faults. The data input into the inversion routine include the orientation of each fault and the fault's slip direction and sense of slip. The following assumptions are required to generate a system of linear equations for solution:

1. The paleostress tensor remained constant in orientation and magnitude during the deformation event.
2. Slip on an individual fault plane was parallel to the maximum resolved shear stress vector (τ), which paralleled the slickenline directions.
3. Each fault slipped when τ reached a specific magnitude, which was assumed constant for each fault in the population.

These assumptions allow construction of a system of linear equations of the form

$$\tau_i = Sn_i - [(Sn_i) \cdot ni] \cdot n_i$$

where τ_i is the unit shear stress vector parallel to τ on fault i, S is the normalized deviatoric paleostress tensor, and n_i is the unit normal vector to the ith fault plane. This set of i linear equations is then solved for S by using a singular value decomposition procedure described by Lawson and Hanson (1974, subroutine SVA). The normalized principal deviatoric stresses ($S_1 \geq S_2 \geq S_3$) and their orientations are then found as the eigenvalues and eigenvectors of S. The procedure has been discussed in detail by Gibler (1985).

The principal stress directions determined for each domain indicate that the maximum principal stress (S_1) dipped steeply and that the least principal stress (S_3) plunged gently and trended east-northeast (fig. 4, table 2). The preferred trend of S_3 between the four domains varied only 11°, and the average for the set of measurements was 050°±5°. The ϕ values for the domains varied from a high of 0.54 in Red Butte to a low of 0.21 at Fort Canyon (table 2).

The solutions for the paleoprincipal deviatoric stress directions and relative magnitudes must be considered as an approximation of the true characteristics of the stress tensor because of assumptions concerning the temporal and mechanical characteristics of faulting and potential errors in field measurement. The assumption that faults within the population slipped at the same resolved shear stress is a fundamental mechanical constraint on fault behavior that may not be justified, particularly in a volume of rock occupied by numerous intersecting and potentially interlocking faults. However, Michael (1984) compared the results of the linear inversion technique with the nonlinear inversion method of Angelier (1979) and Angelier and others (1982) and found the results to be similar. The nonlinear inversion method does not require the assumption of equal shear strength on each fault plane in the population.

Potential measurement errors include the following:

1. Inadvertently including faults of several different deformational events in the fault population was a potential problem, particularly in the Red Butte and Olympus Cove domains, where Paleozoic and Mesozoic strata were deformed in folds and thrust sheets during the Mesozoic and early Tertiary. However, measurements were confined to faults within zones of extensive north-south-trending normal faulting adjacent to the Wasatch fault zone. This sampling problem was considered less serious for the southern domains, which were located in the Little Cottonwood stock. There, the mesoscopic faults slipped either during or subsequent to the high-temperature hydrothermal alteration event dated at 17.3±0.7 m.y. ago (Parry and Bruhn, 1986). Consequently, faults in these latter two domains must reflect movement in the Wasatch fault zone, although the history of faulting could be protracted, and there is no a priori reason to assume that the stress tensor remained constant in either magnitude or orientation.
2. Random errors in fault plane and slickenline orientation may have been introduced as the result of field measurement. Our measurements were reproducible to within ±5°, and such errors should not affect the results of the analysis because of their random nature.
3. The stress tensor was implicitly assumed to be constant in direction and magnitude throughout the volume of rock occupying a domain. This assumption was verified in a subjective manner only, by noting that faults formed consistently oriented sets displaying consistent slip directions throughout the domain as the measurements were made in the field.

The results of the inversion analysis appear reasonable on the basis of several independent lines of evidence. First, the steeply dipping S_1 attitude is to be expected in the vicinity of a normal fault zone, and the attitude of the least principal stress (S_3), which trends to the west-southwest, is consistent with the trend of the prominent slickenline maxima in each domain except Fort Canyon, where no strong maxima occur in the slickenline orientation data. The trend of S_3 is also consistent with the Quaternary slip directions determined by Pavlis and Smith (1980) on the Warm Spring and Virginia Street faults at the northern end of the Salt Lake segment. Finally, paleostress orientations are very similar in each of the four domains, even though the fault populations vary considerably in their overall geometric characteristics and are located in rocks of different ages and lithologies. Qualitatively, the mixture of normal, oblique, and strike slip faults in the populations from each domain is consistent with $\phi > 0$ and supports the results of the inversion analysis. If $\phi = 0$, then $S_2 = S_3$, and the slickenlines should plunge downdip on all faults within the population, given a nearly vertical S_1. Clearly, these conditions are not met in each of the domains. However, other than this qualitative evaluation based on the geometric characteristics of fault populations, we have no independent means of quantitatively evaluating the accuracy of ϕ as determined in the paleostress inversion analysis.

The average paleo-S_3 trend determined from the stress tensor inversion of fault populations is about 23° north (clockwise) of the regional, contemporary S_3 orientation of 073°±15° determined for the Wasatch Front region by Zoback (1983) on the basis of her analysis of earthquake focal mechanisms, geodetic measurements, in situ stress measurements, and Quaternary fault surfaces. The ϕ value for the contemporary stresses is near 0, according to Zoback (1985), on the basis of stress magnitudes and directions determined from hydrofracture stress tests and well-bore breakouts in areas south

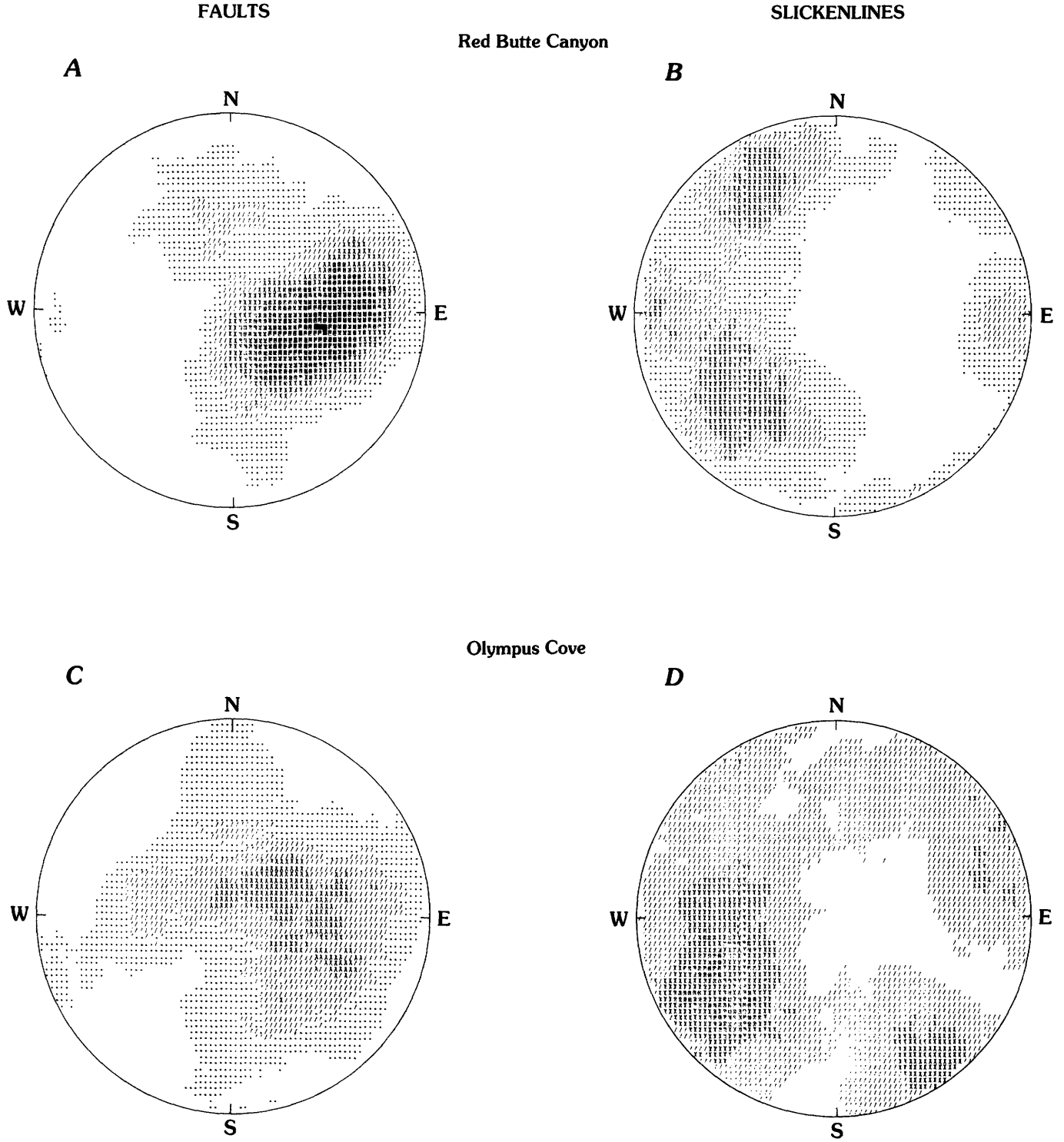

FIGURE 3.—Contoured orientations of poles to fault planes and slickenlines for fault populations in each structural domain in figure 1. Red Butte, 129 measurements of faults (*A*) and slickenlines (*B*); Olympus Cove, 105 measurements of faults (*C*) and slickenlines (*D*); Draper, 110 measurements of faults (*E*) and slickenlines (*F*); Fort Canyon, 106 measurements of faults (*G*) and slickenlines (*H*). Contour intervals are 0, 2, 4, 6, and 8 standard deviations above a random distribution plotted on the lower hemisphere, equal-area projections.

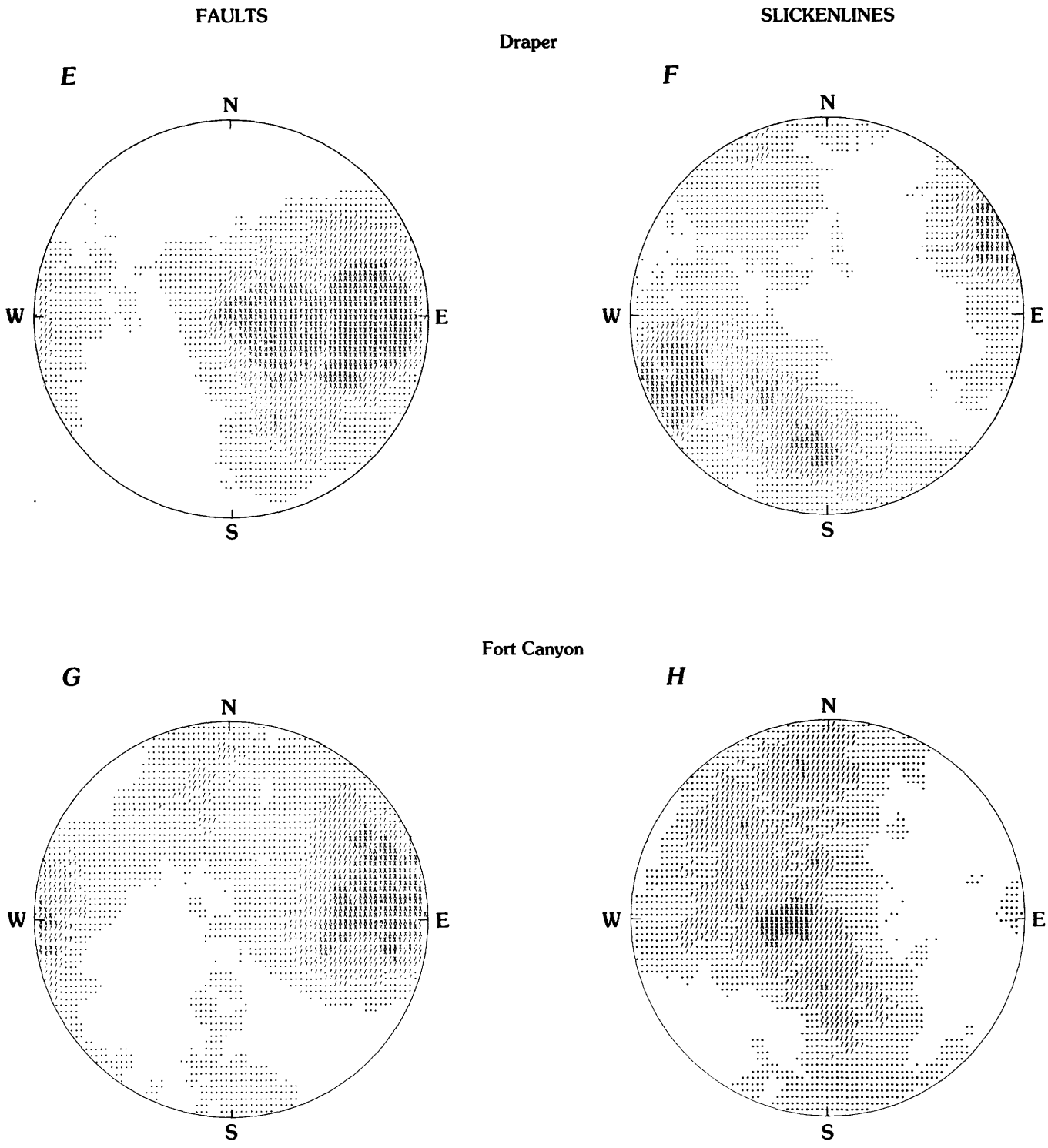

FIGURE 3.—Continued.

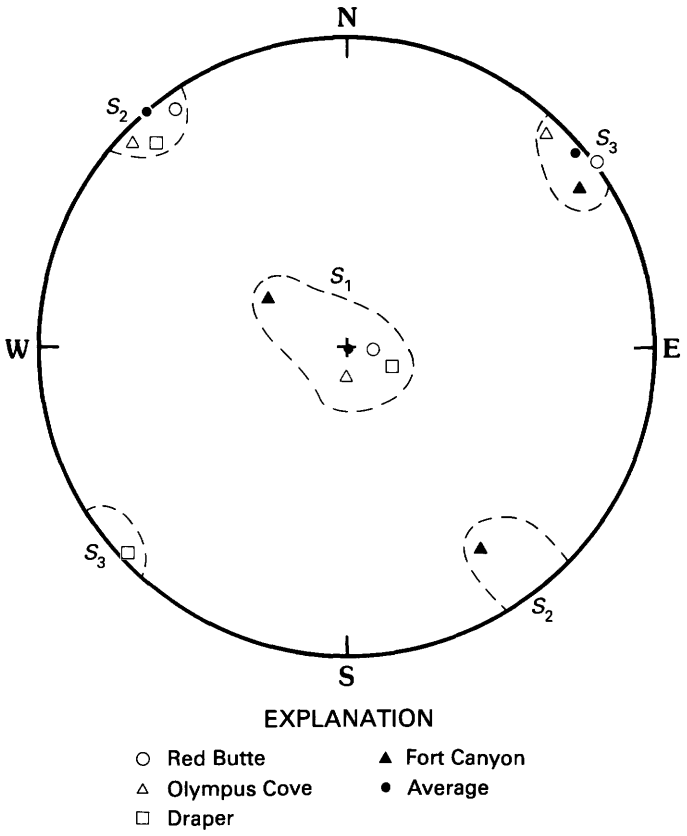

FIGURE 4.—Paleoprincipal deviatoric stress orientations from each of the four structural domains in figure 1 based on inversion of fault-plane and slickenline data. S_1 is the maximum principal compressive stress, S_2 is the intermediate principal stress, and S_3 is the least principal stress. The trend and plunge of each stress axis are shown in table 2.

of the Salt Lake segment in the region surrounding the three southernmost rupture segments defined by Schwartz and Coppersmith (1984). Alternatively, Arabasz (1985) and Arabasz and Julander (1986) concluded that ϕ is close to 1 on the basis of their analysis of earthquake focal mechanisms and hydrofracture tests from the southernmost segment of the Wasatch fault zone and the adjacent Basin and Range-Colorado Plateaus transition zone. Consequently, the contemporary ϕ parameter of the regional stress field remains controversial and poorly defined.

TABLE 2.—*Principal stress data*

Structural domain	Trend/plunge S_1	S_2	S_3	ϕ[1]	No. of faults
Red Butte	095°/83°	324°/07°	054°/00°	0.54	130
Olympus Cove	180°/82°	314°/06°	044°/07°	.50105	
Draper	113°/77°	317°/12°	227°/04°	.42	110
Fort Canyon	301°/66°	146°/21°	056°/10°	.21	106

[1] $\phi=(S_2-S_3)/(S_1-S_3)$.

FAULT ZONE STRUCTURE

TRAVERSE MOUNTAINS BARRIER

A complex zone of faulting forms a nonconservative barrier at the southern end of the Salt Lake fault segment that we have informally named the Traverse Mountains barrier (barrier 1, table 1). The Traverse Mountains are located at the intersection of the Provo and Salt Lake rupture segments as defined by Schwartz and Coppersmith (1984). Here we consider only the northern part of the Traverse Mountains structure. Further work is required to establish the structural relations between the Traverse Mountains and the Ogden segment. The Traverse Mountains barrier is composed of three primary fault sections that form a triple junction comprised of the southern end of the Salt Lake segment, the Fort Canyon section of the Wasatch fault zone, and the west-southwest-trending fault zone along the northern edge of the Traverse Mountains (fig. 5). The southern end of the Salt Lake segment is marked by a major jog in the trace of the Wasatch fault zone, where the Salt Lake and Provo segments are offset about 7.5 km and connected by an east-trending fault zone along the southern margins of the Little Cottonwood stock. We informally refer to this east-trending section of the Wasatch fault zone as the Fort Canyon fault section. The Fort Canyon fault zone lies along the westward projection of the Deer Creek normal fault, which is located in the footwall of the Wasatch fault zone and can be traced eastward through the Wasatch Mountains for a distance of at least 20 km (Baker and Crittenden, 1976). The eastern part of the Traverse Mountains is in the hanging wall of the southward-dipping Fort Canyon fault section, whereas the western part of the mountains forms the footwall of a north-dipping west-southwest-trending normal fault zone at the southern end of Jordan Valley, informally named the Traverse Mountains fault section.

The southern part of the Salt Lake segment (Draper fault section) can be traced as a series of south-southwest-trending scarps that strike 035° in unconsolidated deposits (Gilbert, 1928). These scarps project southward into the exhumed bedrock fault zone along the western edge of the Little Cottonwood stock (quartz monzonite). Here the fault zone curves southward to join the east-trending Fort Canyon normal fault section along the southern margins of the stock and intersects the southwest-striking normal fault zone along the northwestern edge of the Traverse Mountains.

The exhumed bedrock fault zone consists of a cataclastic carapace of faulted quartz monzonite that extends along the western and southern edges of the Little Cottonwood stock (fig. 1) (Gilbert, 1928; Bullock, 1954). The carapace varies in thickness from several tens of

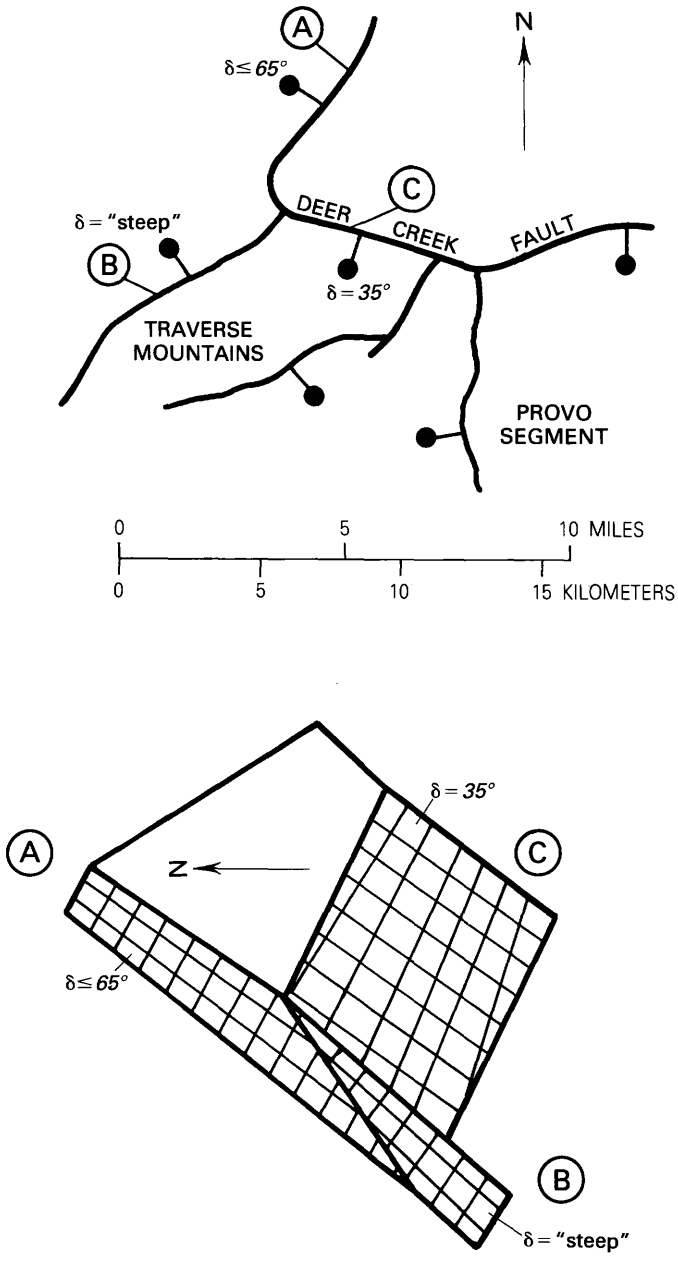

FIGURE 5.—Geometry of faulting at the Traverse Mountains barrier (top) and the tripartite fault array (bottom). Fault A, Draper fault section; fault B, Fort Canyon fault section; fault C, Traverse Mountains fault section. δ is the fault dip angle. Ball and bar are on the hanging wall of normal-oblique slip faults.

meters to hundreds of meters. Progressive uplift of the footwall relative to the hanging wall resulted in overprinting of higher temperature and pressure alteration mineral assemblages by lower temperature and pressure assemblages during faulting (Parry and Bruhn, 1984, 1986). The oldest and highest temperature alteration mineral assemblage in the faulted carapace consists of chlorite, epidote, and muscovite, which occur in relict patches of phyllonite and younger, more broadly distributed cataclasite. Fluid inclusions trapped in microcracks within deformed quartz grains in the cataclasite yield paleofluid temperatures as high as 350 °C and pressures up to 280 MPa, which indicate that this faulted rock originated at depths of 11 km or more in the crust in a fault zone where transient fluid pressures were nearly lithostatic (Parry and Bruhn, 1984, 1986). The formation of this high-temperature alteration in the cataclasite about 17 m.y. ago is indicated by a K-Ar date on hydrothermal muscovite from the fault zone (Parry and Bruhn, 1986). The high-temperature mineral alteration assemblage was subsequently faulted and overprinted by a younger, lower temperature laumontite-prehnite assemblage that is also faulted, suggestive of a decrease in fluid temperature and pressure during progressive uplift and exhumation of the footwall.

The attitude of the Fort Canyon fault section has been determined by detailed mapping of the fault zone along the southern margins of the Little Cottonwood stock (fig. 6). Here Paleocene strata and Oligocene volcanics in the hanging wall are faulted directly against the cataclastic carapace on the margin of the igneous stock, where the fault zone dips 30° to 40° S. Direct measurement of the dip of the cataclastic carapace in the footwall can be made in Fort Canyon, where there is an abrupt transition from essentially undeformed quartz monzonite in the interior of the Little Cottonwood stock into overlying phyllonite and cataclasite in the fault zone. Here we measured the dip as 30° to 35° S., and Gilbert (1928) estimated the dip as 29° S. We will use a strike of N. 80° W. and a dip of 35° S. as a best estimate for the attitude of the Fort Canyon fault section based on the mapping and direct field measurements.

The paleoslip direction on the Fort Canyon fault section has been estimated by using the results of the paleostress tensor analysis on mesoscopic faults within the cataclastic carapace on the southern margin of the Little Cottonwood stock (Fort Canyon domain, table 2). The slip direction on the fault zone was assumed to coincide with the trace of the maximum resolved shear stress vector in the plane of the fault zone (Angelier, 1979). This trace is the projection of the total stress vector (S) onto the fault plane, and the orientation of this trace is uniquely determined by the orientation of the fault, the directions of the principal stresses, and the principal stress parameter (ϕ) (Angelier, 1979). Knowledge of the actual magnitudes of the principal stresses is not required. The range of possible paleoslip vectors in the plane of the fault zone was determined graphically on a stereonet by using a construction proposed by Angelier (1979). If $\phi=0$, then $S_2=S_3$, and the slip direction is defined by the projected trace of S_1 on the fault plane. Conversely, if $\phi=1$, then $S_1=S_2$, and the predicted slip direction coincides with the trace of S_3 on the fault plane.

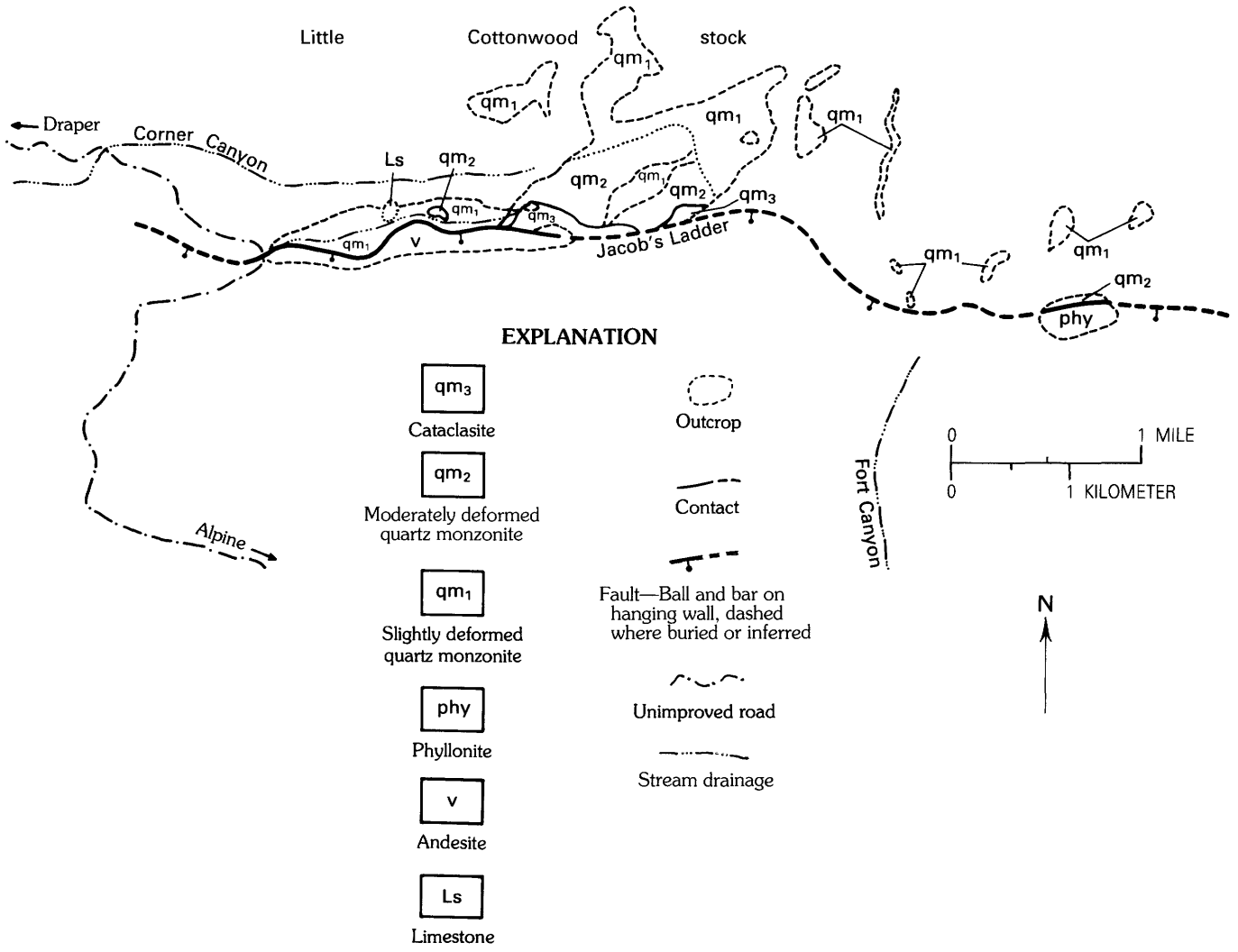

FIGURE 6.—Geology of the Fort Canyon fault zone in the Fort Canyon structural domain shown in figure 1.

Slip directions for $0<\phi<1$ lie in the plane of the fault zone between these two slip directions (fig. 7). The slip direction limits estimated for the Fort Canyon fault zone are 24°/238° for $\phi=0$ to 18°/252° for $\phi=1$. The paleostress tensor inversion estimated that $\phi\simeq0.2$, which defines the preferred estimate for the slip direction as 22°/242°. This slip direction requires dextral-normal movement on the Fort Canyon fault zone.

Structural fabrics of relic phyllonite preserved in the fault zone are also consistent with a component of dextral slip. These fabrics predate the cataclastic deformation (Parry and Bruhn, 1986) that resulted in development of the mesoscopic fault populations used in the stress tensor inversion analysis. The oldest fault rock preserved in the faulted carapace in Fort Canyon consists of isolated outcrops of phyllonite, which contain a penetrative foliation and, in some locales, an extension lineation. Locally, these rocks also contain a mesoscopic shear band fabric (S–C bands of Simpson and Schmidt (1983)) in which the primary foliation is deflected into planar millimeter-wide zones of intensive shearing. The sense of slip on these S–C bands as measured in outcrop is consistent with dextral normal movement on the fault zone and slip directions plunging from 20° to 30° to 210° to 230° (Parry and Bruhn, 1986). Slip directions determined from S–C bands and asymmetric augen in oriented thin sections from the phyllonite also indicate dextral to dextral-normal movement in the fault zone (Houghton, 1985).

The southernmost section of the Salt Lake segment of the Wasatch fault zone—the Draper section—is marked by a discontinuous series of scarps in Quaternary deposits that strike 035° for a distance of about 7 km along the western edge of Little Cottonwood stock. The fault zone is not exposed in bedrock in this area, although numerous discrete normal faults occur in the margins of the stock and presumably represent subsidiary normal faulting associated with the Wasatch fault zone. We have

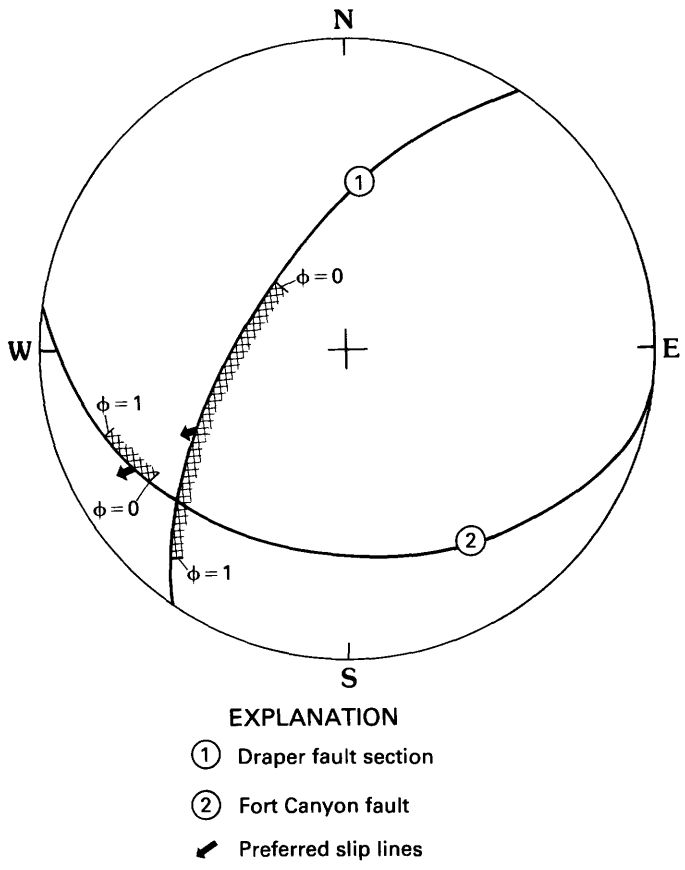

FIGURE 7.—Orientation of the Fort Canyon fault, the preferred orientation of the Draper fault section at the southern end of the Salt Lake segment, and slip directions for various ϕ values of the paleostress field. The preferred slip direction on the Draper fault section is 240° on a fault plane dipping about 65° NW. Lower hemisphere, equal-area projection. See figure 5 for a geometric model of these faults in the Traverse Mountain barrier.

attempted to constrain possible dip angles for this section of the fault zone on the basis of the geometry of faulting within the Traverse Mountain barrier. The approach is based on finding possible slip directions on the Draper section that are consistent with slip directions on the other two primary fault zones in the barrier—namely, the Fort Canyon fault zone and the north-dipping fault zone that extends along the northwestern edge of the Traverse Mountains. The paleoslip direction on the Fort Canyon fault zone has been estimated as about 22°/242°. We have no data bearing on the slip direction on the fault bounding the northern edge of the Traverse Mountains other than the strike of the fault zone, which is approximately N. 60° E. (240°), and drill data and gravity modeling indicating that the fault zone dips steeply northward with a minimum throw of about 1 km (Cook and Berg, 1961; Zoback, 1983). This latter evidence indicates that the fault zone has a normal component of slip, which requires an unknown component of extension perpendicular to strike. This observation, taken in conjunction with the slip direction across the Fort Canyon fault zone, is sufficient to constrain a maximum probable dip on the Draper section of the Wasatch fault zone.

The primary faults in the Traverse Mountain barrier form a tripartite fault array. We do not have complete information concerning the magnitudes of the three slip vectors, but we do know the slip direction on the Fort Canyon section and require that the slip direction across the northern Traverse Mountain fault zone have a normal component of movement. This latter criterion constrains the slip direction on the Draper fault section in that the resultant slip vector between the Fort Canyon and the Draper fault sections cannot cause convergence across the Traverse Mountain fault. Consequently, we seek acceptable solutions for slip directions on the Draper fault section by assuming various dip angles and applying the paleoprincipal stress orientations and a value of $\phi \simeq 0.4$ determined from stress tensor inversion of the mesoscopic fault populations at the southernmost end of the Draper section.

This approach is shown graphically in figure 7. The maximum dip angle (δ) on the Draper fault section that meets the criterion for extension across the fault zone along the northern edge of the Traverse Mountains is 65° (fig. 5). In this case, the difference vector between the Fort Canyon and the Draper fault sections is parallel to the trend of the fault zone along the northern edge of Traverse Mountain. Lesser dip angles on the Draper section are also satisfactory in that the difference vector across the Traverse Mountain fault zone requires extension. Steeper dips on the Draper fault section require convergence across the northern edge of the Traverse Mountains and are therefore unacceptable solutions to the slip direction analysis. Further refinement of the dip estimate of the Draper fault section would require more information on the dip angle and slip vector in the fault zone along the northern edge of the Traverse Mountains.

The structural model for the Traverse Mountains barrier consists of a triple junction formed by a tripartite array of primary fault zones (fig. 5). The northern arm, consisting of the Draper fault section, dips approximately 65° or less toward the west-northwest; the eastern arm, comprised of the Fort Canyon fault section (or western end of the Deer Creek fault), dips approximately 35° S.; the western arm dips steeply northward. The difference in slip between the Draper and the Fort Canyon fault sections is presumably accommodated by sinistral-normal faulting on this third arm of the triple junction. The barrier must plunge toward the southwest into the crust, presumably paralleling the intersection line between the Draper and the Fort Canyon fault sections. This line plunges approximately 28° to 230°, subparallel to the strike (240°) of the third arm of the triple junction. This structure is clearly a nonconserva-

tive barrier and represents a likely site for the arrest and (or) initiation of seismic ruptures within the Wasatch normal fault zone.

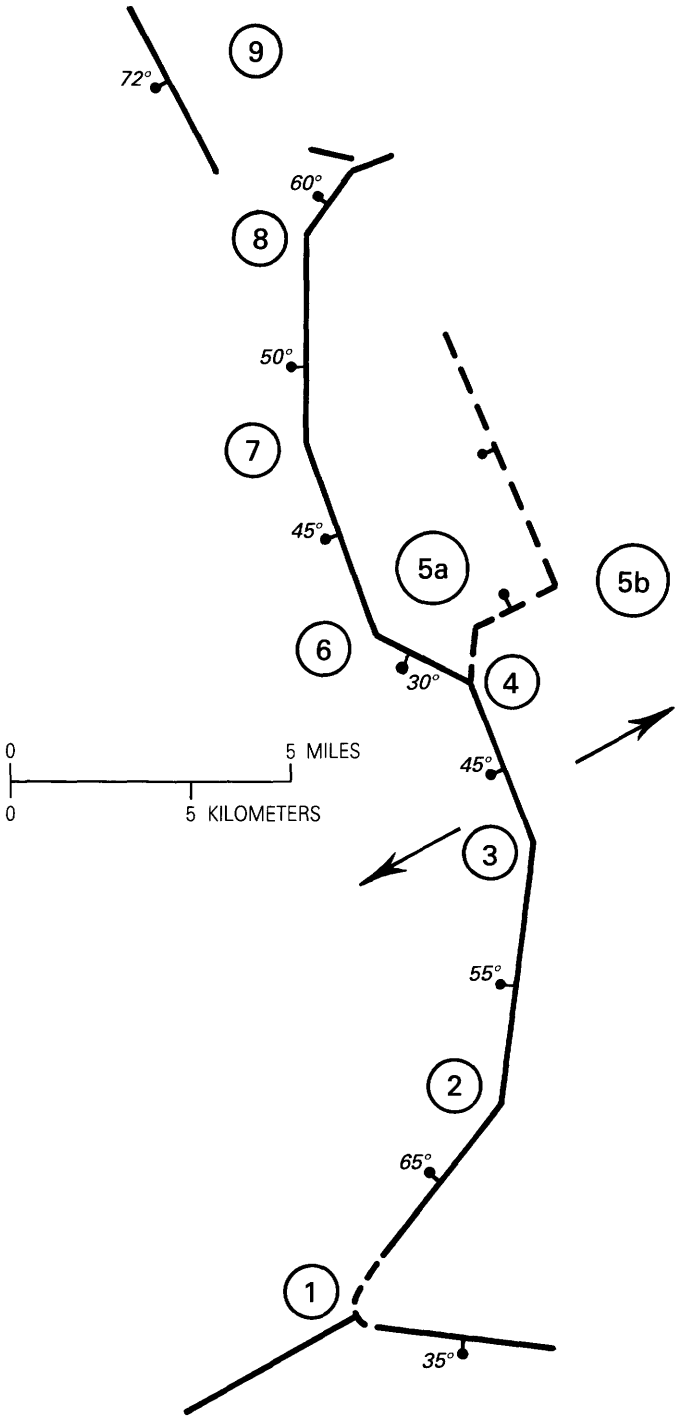

FIGURE 8.—Surface fault traces in the Salt Lake segment and preferred dip angles based on geometric modeling. Numbers of barriers are the same as those in figure 2 and table 1. Solid lines indicate normal faults (ball and bar on hanging wall, dashed where inferred or buried). Large arrows indicate inferred directions of extension. See text for discussion.

SOUTHERN FAULT SECTIONS

The surface trace of the Wasatch fault zone consists of three rectilinear sections between the Traverse Mountain barrier (no. 1) and the bifurcation of the fault trace at branch point 4 (fig. 2). These rectilinear sections are separated by two bends (branch points 2 and 3, fig. 2) that mark significant changes in the strike of the fault zone. These bends are classified as conservative barriers (table 2) because there is no apparent development of a major third direction of faulting in either the hanging walls or the footwalls of the fault zone in the regions of the bends. This absence implies that the slip direction on the Draper fault section parallels the slip directions on the two sections to the north and that the fault zone in this area can be modeled as a cylindrical surface. Consequently, one can use the dip estimate and slip direction (approximately 240° trend) on the Draper fault section to model the dip of these two adjacent sections. The intersection lines between the fault sections must parallel the plunge and trends of the slip vector in the Draper fault section. This problem can be solved on a stereonet by using a geometric construction, which results in estimated dip angles of 55° for the fault section between barriers 2 and 3 and 45° for the section between barriers 3 and 4 (fig. 8). These solutions are directly dependent on our estimate of the dip of the Draper fault section. If the 65° dip estimate in this section is too great, then the remaining sections would have more gentle dips; conversely, if the estimate for the Draper section is too low, the other sections would dip more steeply. A similar type of error would be introduced by the estimated slip direction in the Draper fault section, in that too shallow a plunge would result in underestimating the dip angle of the adjacent fault sections and too steep a plunge would cause an overestimation of the fault dip angles.

An unreversed seismic refraction-reflection profile across the fault zone in the section between barriers 2 and 3 by Bashore and others (1981) provides an independent check on our fault zone modeling in this area. The fault zone was modeled by using two-dimensional synthetic seismograms and gravity data as dipping about 60° W. near the surface and decreasing in dip to between 40° and 50° at a depth of 4 to 5 km. Their result is generally consistent with the 55° westward dip in our model, which is based on a totally different approach and a different set of data.

NORTHERN FAULT SECTIONS

The geometry of the northern half of the Salt Lake fault segment is different than that of the southern part, where the fault zone is delineated by a narrow zone of surface scarps along the Wasatch mountain front. The

northern part of the segment, in contrast to the southern part, is characterized by a major bifurcation of the Quaternary fault trace into a zone about 12 km long by 6 km wide (fig. 2) (Marsell, 1969; Van Horn, 1972) beginning at branch point 4 . This zone extends northward and terminates in the Salt Lake salient, a bedrock ridge that separates the proposed Ogden rupture segment to the north from the Salt Lake segment to the south (Schwartz and Coppersmith, 1984). Two zones of surface scarps delineate an eastern branch extending along the mountain front for 10 km north of the branch point and a western branch that extends about 15 km northward until it curves abruptly eastward and intersects the mountain front at the southern end of the Salt Lake salient (bend 8). Each of these branches is composed of discontinuous, mostly linear zones of surface scarps separated by bends in the fault-zone trace (figs. 2, 8).

According to Van Horn (1972), surface scarps in the eastern branch are older than most of those in the western branch. The eastern scarps presumably formed between 5,000 years and 3 m.y. ago, whereas most scarps in the western branch formed during the last 5,000 years. Greater activity on the western branch of the fault is also indicated by the distribution of Quaternary sediments, which thicken abruptly westward across the western branch of the fault zone, whereas the area in between the two branches is underlain by only a thin veneer of Quaternary deposits overlying bedrock (Marsell, 1969; Crone and Harding, 1985).

The zone of bifurcation in the fault zone between branch point 4 and bends 5a and 5b apparently represents a nonconservative barrier. There are two lines of evidence for this conclusion. First, this region lies along a major east-northeast-trending basement ridge beneath Jordan Valley (Cook and Berg, 1961; Zoback, 1983). This ridge separates the Jordan graben into a deeper southern part and a shallower northern half, according to the gravity modeling of Zoback (1983). Presumably, this ridge reflects structural accommodation of the hanging wall to changes in slip vector direction and (or) magnitude in the vicinity of branch point 4. Second, the fault section between bends 5a and 5b dips steeply northward and trends between 240° and 245°, subparallel to the 240° average slip vector for the Salt Lake segment as a whole. A north-dipping fault section having this strike cannot link with the fault section immediately to the south and conserve a slip vector orientation of 240° around bend 5a. Consequently, bend 5a must be a nonconservative barrier.

The dips of the fault sections between branch point 4 and bend 9 along the western branch of surface faulting have been estimated by assuming that each of these bends represents a conservative barrier. The only support for this assumption is that no major structures have been inferred from the gravity data in Jordan Valley between the basement ridge near branch point 4 and the Salt Lake salient barrier (Cook and Berg, 1961; Zoback, 1983). The preferred dip of the north-trending section between bends 7 and 8 was first found by assuming a slip vector trending 240° and using the paleostress data from the Red Butte domain, where $\phi=0.54$. The solution for the preferred fault plane dip is shown in the stereoplot of figure 9, where the orientation of the maximum shear stress vector for this paleostress system is plotted as a series of three curves for $\phi=0$, 0.5, and 1.0 on faults dipping between 20° and 80° W. The 240° slip line does not intersect the $\phi=0.5$ shear stress vector curve but lies a few degrees to the north of it at the closest point of approach. A fault plane dipping 50° W. lies closest to this maximum resolved shear stress vector; therefore, $\delta=50°$ is the preferred dip estimate for the north-dipping fault section. The dip angles of the remaining fault sections in the western branch of surface rupturing were then found by assuming a cylindrical fault-zone surface. These angles vary between 45° and 72°, as figure 8 shows.

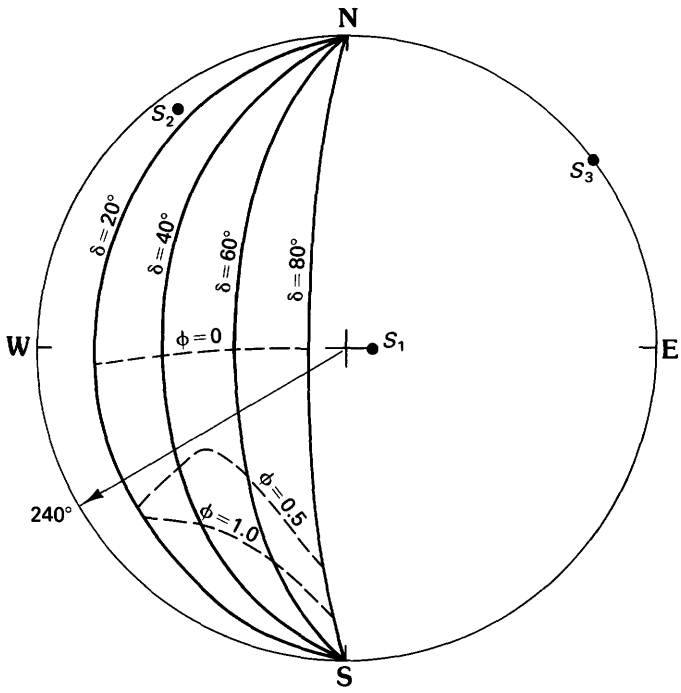

FIGURE 9.—North-striking faults having dips (δ) between 20° and 80° W. and sliplines for the paleostress field in the Red Butte structural domain (fig. 1, table 2). Slip directions for $\phi=0.0$, 0.5, and 1.0 are defined by intersections of great circles defining fault planes having lines of constant ϕ. The best estimate for slip in a 240° direction is a fault plane dipping 50°. See text for discussion.

SALT LAKE SALIENT

The Salt Lake salient is a ridge of Paleozoic and Tertiary bedrock that extends west of the Wasatch

Front at the northern end of the Salt Lake rupture segment (Gilbert, 1928; Schwartz and Coppersmith, 1984). A large west-dipping normal fault having a total throw of about 1.5 km forms the eastern boundary of the salient, where Tertiary strata are faulted against Precambrian metamorphic and Paleozoic sedimentary rock in the footwall (fig. 2) (Gilbert, 1928). The western boundary of the salient is formed by the Warm Springs fault, a north-trending normal fault that dips approximately 70° W. (Gilbert, 1928). Quaternary strata in the hanging wall are faulted directly against Paleozoic rocks in the footwall of the normal fault. We have not mapped the internal structure of the salient in this study, but 1:24,000-scale mapping by Van Horn (1981) shows a number of north-northwest- and northeast-trending normal faults that postdate Oligocene deposits and were probably formed during the late Tertiary.

The geometry of linkage between the main rupture zones in the Salt Lake segment and faults in the interior of the Salt Lake salient is not clear. Surface scarps at the southern margin of the salient are discontinuous but apparently extend into the large normal fault along the eastern boundary of the segment. There is no reported evidence for Quaternary movement on this fault in the interior of the salient, so, presumably, the Quaternary ruptures have not reactivated most of this fault. The Virginia Street fault trends westward along the southern margin of the salient and conceivably represents a bifurcation of the rupture zone, in which displacement is transferred onto the Warm Springs fault at the western boundary of the salient (Pavlis and Smith, 1980; Zoback, 1983).

Gravity and drill data from the valley west of the Salt Lake salient indicate that the salient forms part of a major, west-trending basement ridge and fault zone that extends across the entire width of the valley (Cook and Berg, 1961; Zoback, 1983). This basement ridge is reflected in an elongate gravity high at the northern end of Jordan Valley and by a significant change in the thickness of Tertiary valley fill indicated by drill data and gravity modeling. The fill in the northern end of Jordan Valley is only several hundred meters thick, whereas the fill is in excess of 1 km immediately north of the basement ridge, according to Zoback (1983).

The structure of the Salt Lake salient indicates that it marks the site of a large nonconservative barrier in the Wasatch fault zone. The salient is marked by three primary fault systems—the Salt Lake rupture segment on the south, the Ogden rupture segment to the north, and inferred west-trending fault zone associated with the gravity saddle and modeled basement ridge at the northern end of Jordan Valley. The structure of the Ogden fault segment has not been mapped in this study, but the observation that the Tertiary valley fill is thicker immediately north of the salient relative to the area to the south indicates that throw across the Ogden segment is greater than that in the northern part of the Salt Lake segment. This difference could be owing to several factors, the most likely being (1) that the dip on the Ogden fault segment is steeper than that on the adjacent Salt Lake segment or (2) that extension is greater across the Ogden segment. The resolution of this problem requires further mapping and detailed gravity studies in the Salt Lake salient and the southern part of the Ogden fault segment.

DISCUSSION

GEOMETRY OF FAULT SECTIONS

Our modeling of dips for fault sections in the Salt Lake segment is based on the premise that traces of surface ruptures forming linear to slightly curvilinear patterns 3 km or more in length reflect the strike of fault sections in the subsurface. This premise is supported by (1) the physiography of the Wasatch Front and (2) the overall shape of gravity contours in the hanging-wall basin, both of which partly mimic the geometric pattern of the fault zone (Cook and Berg, 1961; Zoback, 1983).

The estimated dip angles are steeper than those reported by Gilbert (1928), according to measurements of bedrock fault exposures on the southwestern edge of the Little Cottonwood stock at the southern end of our Draper structural domain (fig. 1) and at Mill Creek Canyon in the Olympus Cove domain. Gilbert estimated the dip of the fault zone as 35° in the Draper domain, and we agree that the cataclastic carapace in the fault zone dips 35° to 45° SW. in the same area. However, because this area is located in the curvilinear zone of intersection between the Fort Canyon and the Draper fault sections, it is not representative of the main part of the northeast-trending Draper fault section. Our work predicts a 20° to 30° SW. dip at this locale because of the intersection of the Fort Canyon fault, which dips 35° S., and the Draper section, which dips approximately 65° NW. or less (fig. 5).

We have not estimated the dip of the eastern rupture zone in the Olympus Cove domain because of the nonconservative barrier at bends 5a and 5b. We prefer a dip of about 45° to 50° (fig. 8) for the fault section about 6 km west of the mountain front. This dip is approximately 10° greater than the dip measured in the bedrock by Gilbert (1928).

Fault scarps in Quaternary deposits, which define almost all of the rupture traces in the Salt Lake segment, dip steeply between 60° and 70° (Gilbert, 1928). Our model of the fault zone predicts that these dips do not extend into bedrock at depth in some of the fault sections

but are probably confined to the surficial deposits. This conclusion is similar to the conclusion reached by Bashore and others (1981) on the basis of their seismic reflection-refraction experiment in the southern part of the fault segment. We do not have any evidence as to whether the fault zone is listric or remains planar at depth.

DIRECTIONAL CHARACTERISTICS OF RUPTURE PROPAGATION

Predicting the direction of rupture propagation during a large earthquake in the Salt Lake segment is an important goal in earthquake hazards mitigation. If the position of rupture nucleation within the fault segment can be predicted, this region should be selectively monitored for precursory phenomena. Also, the distribution of strong ground motion during a large earthquake depends on the direction of rupture propagation, which is in turn related to the position of rupture nucleation in the fault segment.

Three types of evidence need to be considered in discussing the possible directions of large-earthquake rupture propagation within the Salt Lake segment—long-term deformation rates, the dimensions of nonconservative barriers, and the overall geometry of Quaternary rupture traces. Here we focus our attention only on large earthquakes of approximately M 7.0 to 7.5, the "characteristic earthquakes" defined by Schwartz and Coppersmith (1984), which would presumably rupture most, if not all, of the segment during a single event. We do not consider the effects of large-earthquake ruptures that could originate in adjacent segments and propagate into the Salt Lake segment. These types of events are beyond the scope of this study.

Large kilometer-scale variations in total displacement along the strike of a normal fault zone provide evidence that average rates of deformation have varied systematically along the length of the zone over extended periods of time. The rationale for relating long-term deformation rates to rupture nucleation is as follows. An increase in deformation rate within a fault zone raises ambient shear stress levels and enhances the transition from quasi-plastic to cataclastic (frictional) deformation. This latter effect may increase the permeability of the fault zone and lead to greater fluid access. Increased shear stress levels and the chemical and physical effects of fluids enhance the nucleation and growth of quasi-static ruptures, which may in turn become unstable and trigger earthquakes (Das and Scholz, 1981). Consequently, we suggest that large variations in displacement along the strike of a rupture segment are one criterion for identifying potential sites of rupture nucleation. This criterion is not necessarily valid for predicting the site of rupture nucleation for each large earthquake but must be used in a long-term statistical sense. That is, we can assume that the greatest frequency of nucleation events, when considered over a large number of M 7.0 to 7.5 earthquakes, is likely to occur in the area where long-term rates of deformation are greatest.

Differential displacement data from the footwall of the Salt Lake segment indicate that the greatest long-term deformation rate has occurred at the southern end of the segment. The amount of net slip across the Salt Lake segment is difficult to quantify because Paleozoic and Mesozoic rocks in the hanging wall are buried beneath upper Cenozoic sedimentary deposits in Jordan Valley (Cook and Berg, 1961; Mattick, 1970; Zoback, 1983). However, there is evidence that the footwall has been warped on a regional scale—a minimum of 5 km and perhaps as much as about 9 km of uplift of the southern end of the footwall with respect to the northern end. The evidence is as follows. The unconformity at the base of the Paleocene-Eocene Wasatch Formation in the northern part of the segment provides a geologic datum; this unconformity marked the surface during Paleocene to Eocene time. This formation is in turn overlain by the Norwood Tuff, Oligocene volcaniclastic deposits that were coeval with emplacement of the Little Cottonwood and Alta stocks at the southern end of the Salt Lake segment (Hintze, 1973). Our studies of fluid inclusions (Parry and Bruhn, 1986) and geobarometry on Oligocene skarn deposits on the margins of the Alta stock (Parry and Bruhn, 1987) in the southern part of the footwall indicate that fault rock now exposed at an elevation of about 1,515 m originated at depths of approximately 11 km, whereas the skarns at an elevation of 3 km formed at depths of approximately 5 km. The fact that the skarn deposits are now at the same elevation as the projected base of the Oligocene tuffaceous deposits (Norwood Tuff) at the northern end of the segment indicates differential warping of the footwall, the southern end being uplifted a minimum of 5 km with respect to the northern end. The maximum value of approximately 9 km is obtained by subtracting the elevation of the Eocene-Oligocene unconformity (approximately 3 km) from the estimated depth of origin of the fault rock (approximately 11 km) now at an elevation of 1,515 m.

Fission-track and K-Ar dating of the uplift history and time of origin of fault rock at the southern end of the segment indicate that faulting had begun by about 17 m.y. ago. The differential uplift rate between the southern and the northern ends of the footwall is approximately 0.3 to 0.5 mm/yr averaged over this time interval. In fact, the fission-track dating of Evans and others (1985) suggests that the greatest rates of footwall uplift occurred in the last 10 m.y. Notably, the long-term average differential uplift or "north-south warping" rate

of the footwall is a significant fraction of estimated net slip rates across the fault zone. Trenching studies done by Swan and others (1980) indicate that these latter rates were between 0.6 and 1.4 mm/yr during the last 19,000 years. Clearly, the southern end of the segment meets our criterion as a probable site for repetitive rupture nucleation on the basis of its long-term differential displacement rates.

The dimensions of nonconservative barriers within the fault segment may be an additional factor in controlling the direction of rupture propagation during large earthquakes (M approximately 7.0–7.5). King and Yielding (1984) suggested that fracture toughness is a geometric property of the fault zone and can be crudely estimated by considering the barrier as a zone of plastic deformation. If several nonconservative barriers are present in a fault zone, rupture nucleation may be favored in the barrier having the least fracture toughness.

The length of a plastic deformation zone can be estimated for an ideal elastic-plastic material from simple fracture mechanics considerations. The length (D_b) of the plastic deformation zone at the tip of a mode III (antiplane shear) crack is given by the Bilby-Cottrell-Swinden model

$$D_b=\pi/8(K^*/S_y) \quad (1)$$

where K^* is fracture toughness and S_y is plastic yield stress (Knott, 1973, p. 70–71). The fracture toughness (K^*) is a stress intensity factor reflecting the stress concentration at the tip of a mode III rupture owing to (1) the regional stress field and (2) crack size. K^* is that stress intensity factor at which the crack can undergo self-extension in the zone of plastic deformation at its tip. K^* increases with increased plastic zone length (D_b). The plastic deformation zone effectively "blunts" the tip of the propagating crack and thus reduces the stress concentration below the concentration for an identical crack having no plastic tip zone.

King and Yielding (1984) suggested that nonconservative barriers act as regions of plastic deformation in fault zones and applied a formula like equation 1 to a study of rupture propagation in the Al Asnam fault zone of Algeria. Here plastic deformation is used in only an approximate sense and implies distortion of a volume of material by contemporaneous movement on a population of broadly distributed fault planes that mutually interfere and interlock. In this sense, a barrier is considered mechanically equivalent to a plastic yield zone in an ideal elastic-plastic material.

The magnitude S_y of the yield stress in equation 1 is unknown. King and Yielding (1984) used a maximum value of 200 MPa, a typical shear strength of intact rock, and a minimum of 20 MPa, a nominal stress drop for large earthquakes in their study of the Al Asnam earthquake fault zone. Two large earthquakes within the Rocky Mountain region have recently occurred in fault segments exhibiting geometries and dimensions similar to those of the Salt Lake segment. The M_S 7.5 Hebgen Lake, Mont., earthquake had a stress drop of approximately 11 MPa, whereas the the stress drop estimated for the Borah Peak, Idaho, earthquake (M_S 7.3) was approximately 1 MPa (Doser, 1985). These stress drops are significantly lower than the nominal values used by King and Yielding (1984).

Here we tentatively evade the problem of the magnitude of S_y by comparing the relative fracture toughnesses of any two nonconservative barriers. The relationship, derived directly from equation 1, is simply

$$(K_1^*/K_2^*)=[D_{b1}/D_{b2}]^{1/2} \quad (2)$$

where the numerical subscripts refer to barriers 1 and 2. Using equation 2 implies that the yield stress (S_y) is the same in all nonconservative barriers within the fault zone. This assumption is partly supported by rock friction experiments, where the static coefficient of sliding friction is essentially constant over a large range of temperatures, strain rates, and effective confining pressures for rocks of many different lithologies (Byerlee, 1967). The situation is similar in a large barrier, where highly fractured rocks of different lithologies extend to depth within the fault zone. However, other factors, such as the geometry of the fault population and fluid pressures and chemistry, may differ significantly between barriers and strongly influence relative yield stresses. At present, we do not have enough data to determine the differences between the overall fault population geometries of the various barriers or whether major differences in fluid pressure or chemistry may occur. These features of barriers are important parameters for further research.

Three large nonconservative barriers have been identified within the Salt Lake segment (1,9, and the composite barrier at 4). The lengths of these barriers can be determined from geologic mapping (fig. 2). D_b for the Traverse Mountain barrier is approximately 8 km, whereas D_b for the Salt Lake salient barrier is approximately 10 km (fig. 10). The difference between the relative fracture toughness of the Salt Lake barrier and that of the Traverse Mountain barrier based on equation 2 is only 10 percent, and, in our opinion, it is not at all certain that such a small difference is meaningful, given the assumptions required in using equation 2.

The structural characteristics of the northern half of the Salt Lake segment, between the Salt Lake salient and branch point 4, can be interpreted in two fundamentally different ways. The zone of branching between

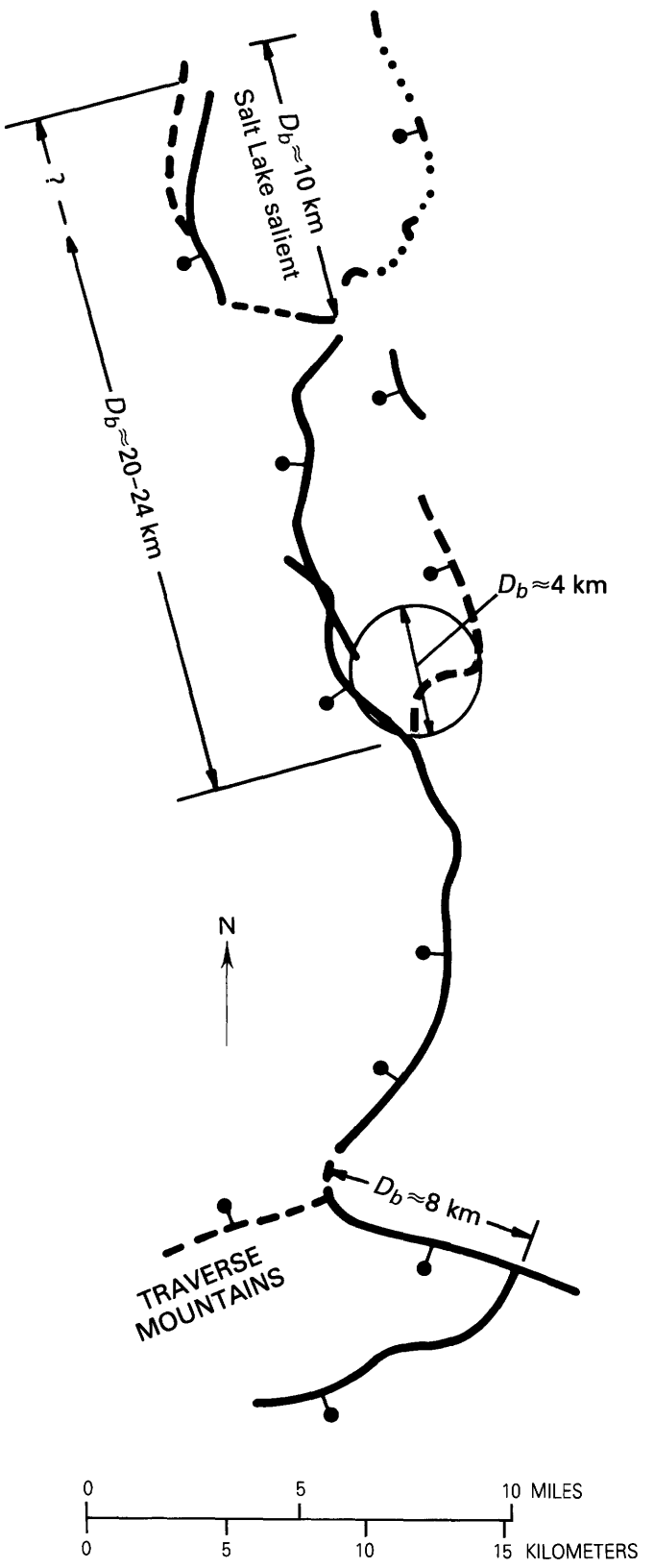

FIGURE 10.—Trace of the Salt Lake fault segment and estimated dimensions D_b of barriers modeled as equivalent "plastic" deformation zones. Solid lines indicate normal faults (ball and bar on hanging wall, dashed where inferred or buried).

branch point 4 and bends 6 on the west and 5b on the east may represent a separate nonconservative barrier. The size of this barrier is estimated by assuming that the barrier can be approximated as a right circular cylinder having an axis dipping 45° W. The estimated diameter of this cylinder is 4 km and is taken to be the effective length (D_b) of the nonconservative barrier. The relative fracture toughness of this barrier is approximately 60 percent less than that of the Salt Lake salient and approximately 40 percent less than that of the Traverse Mountain barrier. Consequently, in this interpretation, the barrier in the center of the segment has the least fracture toughness, and, according to the model of King and Yielding (1984), a large-earthquake rupture is most likely to nucleate from the central part of the segment.

The alternative interpretation of the mechanical characteristics is that the entire northern half of the segment (north of branch point 4) may act as a large nonconservative barrier having length D_b of approximately 20 to 24 km (fig. 10). This interpretation is based on speculation about the geometric and mechanical characteristics of the region between the two primary fault traces north of the branch point (4). Mapping in the footwall of the fault zone shows that the footwall is extensively faulted for a distance of about 1 to 2 km from the trace of the primary fault zone (fig. 11). These faults form a conjugate system of east- and west-dipping normal to oblique-slip faults. We suspect that the region between the two primary fault zones in the northern half of the segment is pervaded by conjugate fault systems like those exhumed in the footwall. This region may then approximate a large "plastic" deformation zone comprised of numerous interlocking and mutually interfering conjugate faults. Two schematic cross sections of this zone are shown in figure 12. In one, the two primary fault traces are shown as parallel fault planes, whereas, in the other, the two primary fault planes intersect at depth. At present, there is insufficient evidence to choose one section over the other. In either case, the zone of highly faulted rock between the two primary faults presumably forms an elongate plastic deformation zone. When this zone is combined with the Salt Lake salient immediately to the north, it has a length D_b of approximately 24 km, much larger than the D_b length of 8 km estimated for the Traverse Mountain barrier. The large length of the former barrier invalidates the small tip zone approximation inherent in the derivation of equation 1, and, therefore, equation 2 cannot be used to estimate the relative fracture toughnesses of this barrier and others. Clearly, the fracture toughness of the northern half of the fault segment is greater than that of the Traverse Mountain barrier. This interpretation of the mechanical characteristics of the Salt Lake segment implies that large-earth-

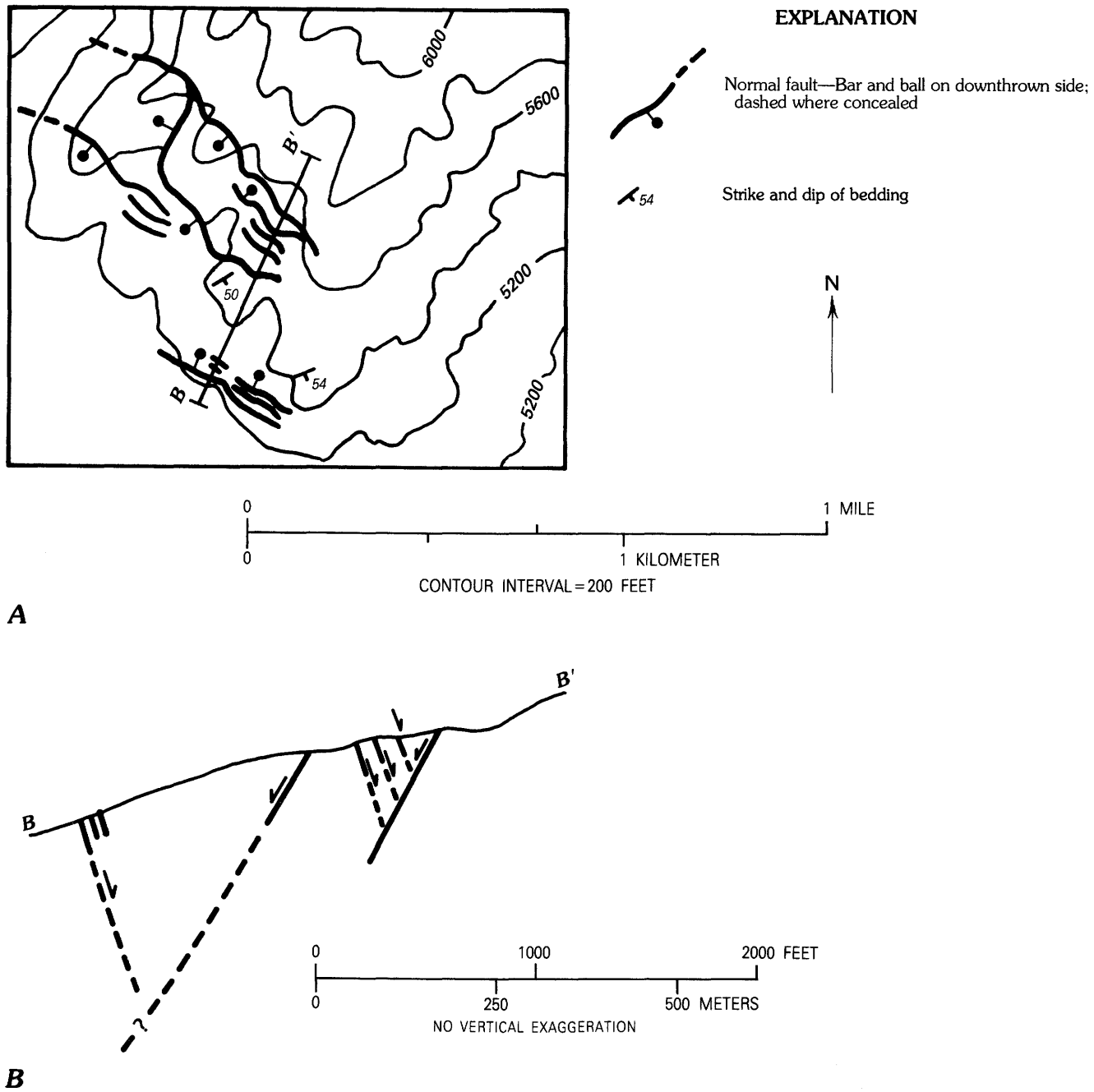

FIGURE 11.—*A*, Normal faults in the northern half of the Red Butte structural domain (fig. 1). *B*, Cross section *B*–*B'* illustrating the conjugate geometry of faulting in the footwall. Dashed and queried lines indicate projected positions in the subsurface.

quake ruptures are most likely to nucleate at the southern end of the segment and propagate northward.

The geometries of two other seismogenic fault zones in the Basin and Range-Rocky Mountain transition zone support the contention that geologic structure may provide information about directions of rupture propagation during large earthquakes. Ruptures in the 1959 Hebgen Lake (M_S 7.5) and the 1983 Borah Peak (M_S 7.3) earthquakes propagated unilaterally in both events, rupturing toward points of structural bifurcation in the fault zone (Smith and others, 1984; Doser, 1985a, b) (fig. 13). At Borah Peak, the bifurcation zone was marked by a major bedrock ridge that extends northwest of the main mountain front (Crone and Machette, 1984), whereas the fault zone at Hebgen Lake bifurcated into two normal fault zones, one extending well into the main mountain range and the other paralleling and locally cutting into the main mountain front along the edge of the hanging-wall valley (Myers and Hamilton, 1964). The structural geometries of both fault zones clearly developed over an extended

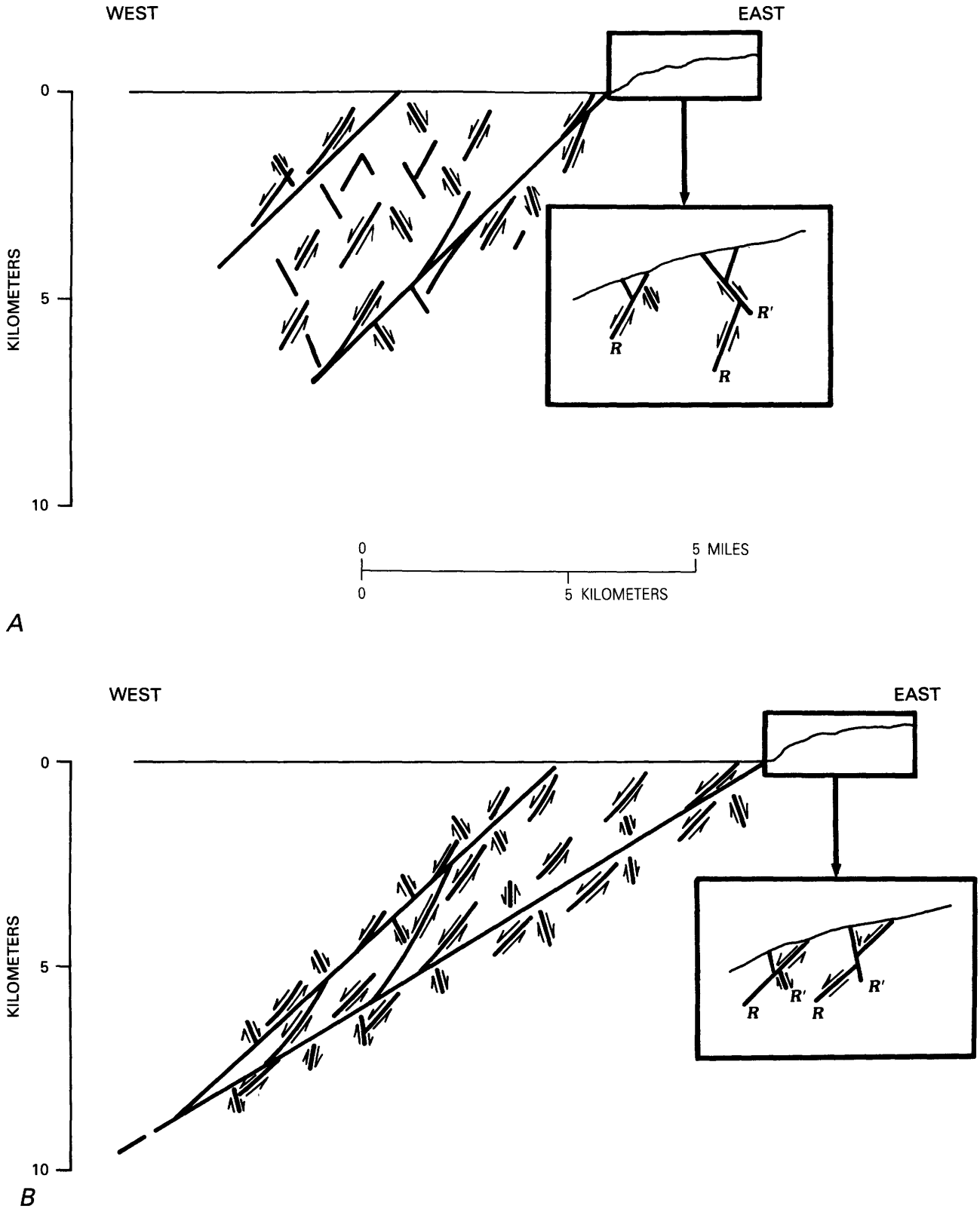

FIGURE 12.—Possible structure of the branched fault zone in the northern half of the Salt Lake segment. Conjugate faults like those in figure 11 are interpreted to pervade the region between the eastern and western primary fault planes. *A*, The two primary fault branches are assumed to dip at the same angle. *B*, The two primary fault branches are assumed to intersect at a depth of several kilometers. Faults labeled *R* and *R'* are Riedel and anti-Riedel shears, respectively.

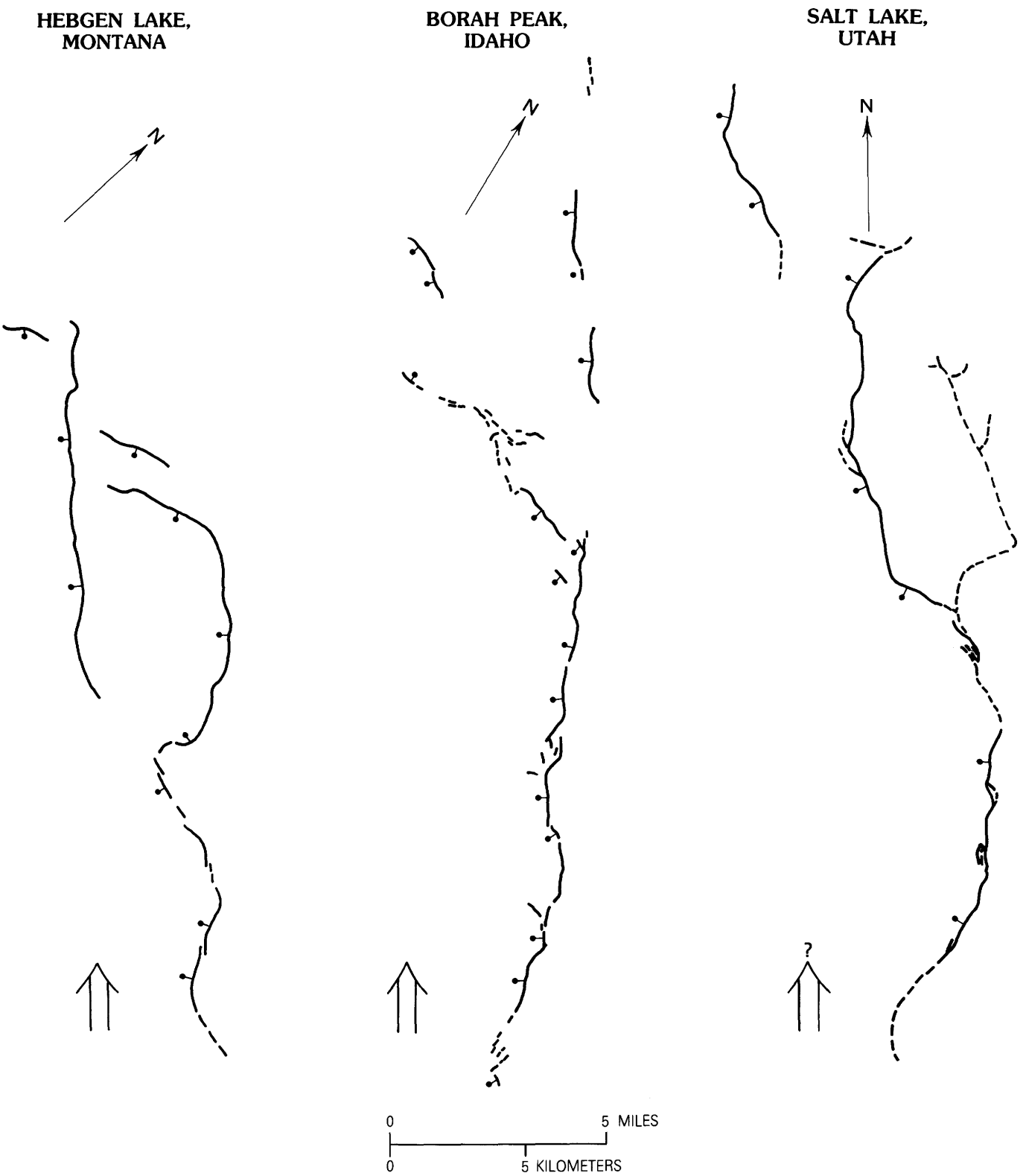

FIGURE 13.—Rupture traces of the Borah Peak, Idaho, and Hebgen Lake, Mont., earthquake rupture zones in comparison with the Quaternary trace of the Salt Lake rupture segment. Solid lines indicate normal faults (ball and bar on hanging wall, dashed where inferred or buried). The large arrows indicate the directions of unilateral rupture propagation for the Borah Peak and Hebgen Lake events. The question mark by the arrow on the Salt Lake rupture zone indicates the inferred rupture direction during most earthquakes. The Borah Peak rupture trace is after Crone and Machette (1984); the Hebgen Lake trace is after Myers and Hamilton (1964).

period of time and presumably reflect the summation of numerous large earthquakes.

The branchlike structures of the Borah Peak and Hebgen Lake earthquake fault zones are characteristic of bifurcated cracks in experiments on crack branching. That is, the direction of propagation in experiments is toward the direction of bifurcation (Broek, 1983), implying that the geometric characteristics of an earthquake fault zone developed as the result of numerous rupturing events and may reflect a consistent directionality of rupture propagation. This rationale is particularly applicable to normal fault zones, where the hanging walls and footwalls remain essentially stationary along the strike of the fault zone during numerous rupturing events. In strike-slip zones, on the other hand, such evidence is likely to be destroyed as the opposite walls of the fault zone are translated into adjacent regions of changing rupture characteristics.

The overall geologic structure of the Salt Lake segment is comparable to the structures of the Borah Peak and Hebgen Lake earthquake fault zones in that it also contains a bifurcation point, where the fault zone divides into two primary branches. However, caution must be taken in making direct comparisons, because there currently is no reported evidence for simultaneous rupturing of both fault branches in the northern half of the Salt Lake segment (Van Horn, 1975). That is, there is a possibility that the eastern branch, which exhibits scarps between 5,000 years and 3 m.y. in age, may have become inactive, and earthquake rupturing may now be confined to the western branch, which displays the youngest scarps. Alternatively, slip may have occurred at depth on the eastern fault branch during the youngest earthquakes without propagation of the rupture to the surface.

Two fundamentally different, but equally important, views of the structural comparison between the Borah Peak, Hebgen Lake, and Salt Lake rupture segments arise from the previous discussion. On one hand, the bifurcated geometry of the Salt Lake segment may still control seismic ruptures, even though the youngest scarps are located on only one branch. In this case, the geometries of the Borah Peak and Hebgen Lake earthquake scarp systems may provide direct analogies for the expected directionality of rupturing within the Salt Lake segment. Notably, the direction of inferred rupture would agree with the direction implied by arguments concerning (1) long-term displacements and (2) the effective fracture toughness model, in which the bifurcated northern half of the fault segment is considered as a large plastic deformation zone. On the other hand, the fact that the youngest surface scarps apparently occur only on the western fault branch of the Salt Lake segment may indicate that the bifurcated fault geometry has been bypassed during the Holocene, as the fault zone continued to evolve structurally. In this case, comparative studies of the three earthquake fault zones may further our knowledge of barrier evolution within seismically active normal fault zones, an important topic in itself.

CONCLUSIONS

The Salt Lake rupture segment (Schwartz and Coppersmith, 1984) is composed of several linear to slightly curvilinear fault sections that intersect in geometric barriers defined by bends and branch points in the trace of the fault zone. The dips of these fault sections vary with the strike of the fault zone, estimated dips ranging between 45° and 90°.

Extension across the normal fault zone was to the southwest, averaging approximately 240°. This extension direction superimposed a component of sinistral slip on individual sections of the rupture segment; this slip varied as a function of the strike and dip of each fault section. The stress parameter (ϕ) varied from a low of approximately 0.2 in the Fort Canyon fault section at the Traverse Mountain barrier to approximately 0.5 in the remainder of the rupture segment.

The Salt Lake segment is bounded on its northern and southern ends by two large nonconservative barriers. A third nonconservative barrier occurs in the central part of the segment, located at the point of bifurcation in the trace of surface ruptures. The mechanical characteristics of this third barrier may be interpreted in two ways. The barrier can be considered as the smallest nonconservative barrier in the segment, possessing the corresponding least effective fracture toughness (K^*). Alternatively, the barrier can be viewed as part of a much larger elongate zone of effective "plastic" deformation comprising the entire northern bifurcated half of the rupture segment. In this case, the Traverse Mountain barrier, at the southern end of the segment, would be the nonconservative barrier having the least K^*.

Long-term deformation rates have been highest at the southern end of the Salt Lake segment and thus provide a rationale for selecting this part of the rupture segment as the most likely site for repetitive initiation of large-earthquake (M approximately 7.0 to 7.5) ruptures. This hypothesis is consistent with the second interpretation of fault zone fracture toughness and, possibly, with observed directions of rupture propagation in the Borah Peak and Hebgen Lake earthquakes. These earthquakes occurred in fault zones displaying overall bifurcated geometries similar to the geometry of the Salt Lake segment, although the latest earthquakes in the Salt Lake segment apparently did not produce surface scarps on both primary fault branches, as those at Borah Peak

and Hebgen Lake did. Whether this absence represents a fundamental difference in the mechanical characteristics of the Salt Lake rupture segment relative to those of the Borah Peak and Hebgen Lake ruptures remains an important and fundamental problem.

REFERENCES CITED

Aki, K., 1979 , Characteristics of barriers on earthquake faults: Journal of Geophysical Research, v. 84, no. B11, p. 6140–6148.

Angelier, J., 1979, Determination of the mean principal directions of stresses for a given fault population: Tectonophysics, v. 56, p. T17–T26.

Angelier, J., Tarantola, A., Valette, B., and Manoussis, S., 1982, Inversion of field data in fault tectonics to obtain the regional stress, pt. I, Single phase fault populations: A new method of computing the stress tensor: Geophysical Journal of the Royal Astronomical Society, v. 69, p. 607–621.

Arabasz, W.J., 1985, Earthquake behavior in the Wasatch front area: Association with geologic structure, space-time occurrence and stress state, *in* Hays, W.W., and Gori, P.L., eds., Proceedings of Conference XXVI; a workshop on Evaluation of regional and urban earthquake hazards and risk in Utah: U.S. Geological Survey Open-File Report 84–763, p. 310–339.

Arabasz, W.J., and Julander, D.R., 1986, Geometry of seismically active faults and crustal deformation within the Basin and Range-Colorado Plateau transition in Utah: Geological Society of America Special Paper 208, p. 43–74.

Arabasz, W.J., Smith, R.B., and Richins, W.D., 1980, Earthquake studies along the Wasatch front, Utah: Network monitoring, seismicity, and seismic hazards: Bulletin of the Seismological Society of America, v. 70, p. 1479–1500.

Baker, A.A., and Crittenden, M.D., Jr., 1961, Geology of the Timpanogos Cave quadrangle, Utah: U.S. Geological Survey Geologic Quadrangle Map GQ–132, scale 1:24,000.

Bashore, W.M., Smith, R.B., Zandt, G., and Ansorge, J., 1981, Upper crustal structure of the Salt Lake Valley and the Wasatch Front from seismic modelling: E⊕S, Transactions of the American Geophysical Union, v. 62, p. 961.

Broek, D., 1983, Elementary engineering fracture mechanics: Boston, Martinus Nijhoff, 469 p.

Bullock, R.L., 1954, The geology of Lehi quadrangle, Utah: Provo, Utah, Brigham Young University, unpublished M.Sci. thesis, 57 p.

Byerlee, J.D., 1968, Brittle-ductile transition in rocks: Journal of Geophysical Research, v. 73, no. B14, p. 4741–4750.

Cook, K.L., and Berg, J.W., Jr., 1961, Regional gravity survey along the central and southern Wasatch Front, Utah: U.S. Geological Survey Professional Paper 316–E, p. E75–E89.

Crittenden, M.D., Jr., 1976, Stratigraphic and structural setting of the Cottonwood area, Utah, *in* Hill, J.G., ed., Geology of the Cordilleran hingeline: Denver, Colo., Rocky Mountain Association of Geologists, p. 281–317.

Crittenden, M.D., Jr., Stuckless, J.S., Kistler, R.W., and Stern, T.W., 1973, Radiometric dating of intrusive rocks in the Cottonwood area, Utah: U.S. Geological Survey Journal of Research, v. 1, p. 173–178.

Crone, A.J., and Harding, S.T., 1985, Near-surface faulting associated with Holocene fault scarps, Wasatch fault zone, Utah: A preliminary report, *in* Hays, W.W., and Gori, P.L., eds., Proceedings of Conference XXVI; a workshop on Evaluation of regional and urban earthquake hazards and risk in Utah: U.S. Geological Survey Open-File Report 84–763, p. 241–268.

Crone, A.J., and Machette, M.N., 1984, Surface faulting accompanying the Borah Peak earthquake, central Idaho: Geology, v. 12, p. 664–667.

Das, S., and Scholz, C.H., 1981, Theory of time-dependent rupture in the earth: Journal of Geophysical Research, v. 86, no. B7, p. 6039–6051.

Davis, F.D., 1983a, Geologic map of the central Wasatch front, Utah: Utah Geological and Mineralogical Survey Map 55–A, scale 1:100,000.

———1983b, Geologic map of the southern Wasatch front, Utah: Utah Geological and Mineralogical Survey Map 55–A, scale 1:100,000.

Doser, D.I., 1985a, The 1983 Borah Peak, Idaho, and 1959 Hebgen Lake, Montana, earthquakes: Models for normal fault earthquakes in the Intermountain Seismic Belt, *in* Stein, R.S., and Bucknam, R.C., convenors, Proceedings of Workshop XXVIII on the Borah Peak, Idaho, earthquake: U.S. Geological Survey Open-File Report 85–290, p. 368–384.

———1985b, Source parameters and faulting processes of the 1959 Hebgen Lake, Montana, earthquake sequence: Journal of Geophysical Research, v. 90, no. B6, p. 4537–4556.

Evans, S.H., Parry, W.T., and Bruhn, R.L., 1985, Thermal, mechanical and chemical history of Wasatch fault cataclasite and phyllonite, Traverse Mountains area, Salt Lake City, Utah: Age and uplift rates from K/Ar and fission track measurements: U.S. Geological Survey Open-File Report 85–22, p. 422–429.

Gibler, P.R., 1985, Bedrock deformation along the Salt Lake segment of the Wasatch fault: Implications for stress magnitudes, stress directions and seismicity: Salt Lake City, University of Utah, unpublished M.Sci. thesis, 60 p.

Gilbert, G.K., 1928, Studies of basin-range structure: U.S. Geological Survey Professional Paper 153, 92 p.

Hintze, L.F., 1973, Geologic history of Utah: Brigham Young University Geology Studies, v. 20, p. 1–181.

Houghton, W., 1986, Structural geology of the Deer Creek and Wasatch faults: Salt Lake City, University of Utah, unpublished M.Sci. thesis, 64 p.

King, G., 1983, The accommodation of large strains in the upper lithosphere of the earth and other solids by self-similar fault systems: The geometrical origin of b-value: Pure and Applied Geophysics, v. 121, p. 761–814.

King, G., and Nabelek, J., 1985, Role of fault bends in the initiation and termination of earthquake rupture: Science, v. 228, p. 987.

King, G., and Yielding, G., 1984, The evolution of a thrust fault system: Processes of rupture initiation, propagation and termination in the 1980 El Asnam (Algeria) earthquake: Geophysical Journal of the Royal Astronomical Society, v. 7, p. 915–933.

Knott, J.F., 1973, Fundamentals of fracture mechanics: London, Butterworth, 273 p.

Lawson, D.L., and Hanson, R.J., 1974, Solving least squares problems: Englewood Cliffs, N.J., Prentice-Hall, 340 p.

Marsell, R.E., 1969, The Wasatch fault zone in north central Utah, *in* Jensen, M.L., ed., Guidebook of northern Utah: Utah Geological and Mineralogical Survey Bulletin, v. 82, p. 125–139.

Mattick, R.E., 1970, Thickness of unconsolidated to semiconsolidated sediments in Jordan Valley, Utah: U.S. Geological Survey Professional Paper 700–C, p. C119–C124.

Michael, A.J., 1984, Determination of stress from slip-data; faults and folds: Journal of Geophysical Research, v. 89, no. B13, p. 11,517–11,526.

Myers, W.B., and Hamilton, W., 1964, Deformation accompanying the Hebgen Lake earthquake of August 17, 1959: U.S. Geological Survey Professional Paper 435, p. 55–98.

Parry, W.T., and Bruhn, R.L., 1984, Pore fluid and seismogenic characteristics of fault rock at depth on the Wasatch fault, Utah:

E⊕S, Transactions of the American Geophysical Union, v. 65, p. 11–14.

———1986, Pore fluid and seismogenic characteristics of fault rock at depth on the Wasatch fault, Utah: Journal of Geophysical Research, v. 91, no. B1, p. 730–744.

———1987, Fluid inclusion evidence for minimum 11 km vertical offset on the Wasatch fault, Utah: Geology, v. 15, p. 67–70.

Pavlis, T.L., and Smith, R.B., 1980, Slip vectors from faults near Salt Lake City from Quaternary displacement and seismicity, *in* Arabasz, W.J., Smith, R.B., and Richins, W.D., eds., Earthquake studies in Utah 1850 to 1978: Salt Lake City, University of Utah Seismograph Stations, p. 378–382.

Schwartz, D.P., and Coppersmith, K.J., 1984, Fault behavior and characteristic earthquake: Examples from the Wasatch and San Andreas fault zones: Journal of Geophysical Research, v. 89, no. B7, p. 5681–5698.

Schwartz, D.P., Hanson, K.L., and Swan, F.H., III, 1983, Paleoseismic investigations along the Wasatch fault zone: An update, *in* Geologic excursions in neotectonics and engineering geology in Utah, Guidebook, pt. IV: Salt Lake City, Utah, Geological Society of America, p. 45–48.

Simpson, C., and Schmid, S.M., 1983, An evaluation of criteria to deduce the sense of movement in sheared rocks: Geological Society of America Bulletin, v. 94, p. 1281–1288.

Smith, R.B., and Bruhn, R.L., 1984, Intra-plate extensional tectonics of the eastern Basin-Range; inferences of structural style from seismic reflection data, regional tectonics and thermal-mechanical models of brittle-ductile deformation: Journal of Geophysical Research, v. 89, no. B7, p. 5733–5762.

Smith, R.B., Richins, W.D., Doser, D.I., Pechmann, J.C., and Langer, C., 1984, The 1983 M 7.3 Borah Peak, Idaho earthquake: A model for active crustal extension: Geological Society of America Abstracts with Programs, v. 16, p. 16.

Swan, F.H., III, Schwartz, D.P., and Cluff, L.S., 1980, Recurrence of moderate-to-large magnitude earthquakes produced by surface faulting on the Wasatch fault zone: Bulletin of the Seismological Society of America, v. 70, p. 1431–1462.

Van Horn, R., 1972, Map showing relative ages of faults in the Sugar House quadrangle, Salt Lake County, Utah: U.S. Geological Survey Miscellaneous Investigations Map I–766–B, scale 1:24,000.

———1981, Geologic map of the pre-Quaternary rocks of the Salt Lake City North quadrangle, Davis and Salt Lake Counties, Utah: U.S. Geological Survey Miscellaneous Investigations Map I–1330, scale 1:24,000.

Zoback, M.L., 1983, Structure and Cenozoic tectonism along the Wasatch fault zone, Utah: Geological Society of America Memoir 157, p. 3–27.

———1985, Constraints on in-situ stress field along the Wasatch Front, *in* Hays, W.W., and Gori, P.L., eds., Proceedings of Conference XXVI; a workshop on Evaluation of regional and urban earthquake hazards and risk in Utah: U.S. Geological Survey Open-File Report 84–763, p. 286–309.

Late Quaternary Displacement on the Morgan Fault, A Back Valley Fault in the Wasatch Range of Northeastern Utah

By J. TIMOTHY SULLIVAN *and* ALAN R. NELSON, U.S. BUREAU OF RECLAMATION

ASSESSMENT OF REGIONAL EARTHQUAKE HAZARDS AND RISK ALONG THE WASATCH FRONT, UTAH

U.S. GEOLOGICAL SURVEY PROFESSIONAL PAPER 1500–I

CONTENTS

	Page
Abstract	I1
Introduction	1
Acknowledgments	1
Back Valleys of the Wasatch Range	1
Morgan Valley	2
Morgan Fault	2
Age of Quaternary Deposits Adjacent to the Central Section of the Morgan Fault	5
Trench Investigations of Quaternary Faulting on the Central Section of the Morgan Fault	12
Stratigraphy in Trench M4	13
Trench Investigations of Quaternary Faulting on the Central Section of the Morgan Fault—Continued	
Ages of Faulted Deposits	I15
Events in Trench M4	15
Other Trenches	16
Slip Rates on the Morgan Fault	16
Quaternary Slip Rates	16
Cenozoic Slip Rates	16
Conclusions	17
References Cited	17

ILLUSTRATIONS

		Page
FIGURES 1, 2.	Maps showing:	
	1. Location of the Morgan fault, the Wasatch fault, and other middle or late Quaternary faults in northeastern Utah	I3
	2. Cenozoic geology of Morgan Valley	4
3.	Generalized topographic profiles and geologic section parallel to the Morgan fault drawn along the crest of the footwall escarpment and along the hanging wall at the base of the escarpment	6
4, 5.	Maps showing surficial geology of:	
	4. Central section of the Morgan fault	7
	5. Southern end of the central section of the Morgan fault, showing locations of trenches at the Robeson Springs trench site and sampling sites	8
6.	Log of trench M4 at the Robeson Springs trench site, showing faulted middle and late Quaternary colluvial deposits at the southern end of the central section of the Morgan fault	14

TABLES

		Page
TABLE 1.	Selected properties of soils on alluvial, colluvial, and lacustrine sediments along the Morgan fault, Morgan Valley, north-central Utah	I10
2.	D-alloisoleucine/L-isoleucine ratios in the total amino acid fraction and calculated ages for *Oreohelix* cf. *strigosa* from alluvial and colluvial sediments along the Morgan fault, Morgan Valley, north-central Utah	12

ASSESSMENT OF REGIONAL EARTHQUAKE HAZARDS
AND RISK ALONG THE WASATCH FRONT, UTAH

LATE QUATERNARY DISPLACEMENT ON THE MORGAN FAULT, A BACK VALLEY FAULT IN THE WASATCH RANGE OF NORTHEASTERN UTAH

By J. TIMOTHY SULLIVAN[1] and ALAN R. NELSON[2]

ABSTRACT

The Morgan fault is a 16-km-long north-trending normal fault bounding the eastern side of Morgan Valley, a back valley of the Wasatch Range. A history of late Cenozoic surface displacements on the Morgan fault is suggested by triangular facets preserved on the footwall escarpment of the fault, back-tilted erosion surfaces adjacent to the fault, and the preservation of a 1,000-m-thick fanglomerate in the hanging wall of the fault. Trenches across the Morgan fault show that middle Pleistocene colluvial deposits are displaced about 4 m and Holocene deposits are displaced about 1 m. Amino acid ratio minimum age estimates on shells, radiocarbon dating of peat deposits, soil development indices, displacement data, and stratigraphic correlations of late Quaternary deposits among the trenches suggest a minimum average middle to late Pleistocene slip rate of about 0.01 to 0.02 mm/yr for the Morgan fault. Stratigraphic relations in one of the trenches suggest that repeated surface displacements on the fault have been about 1 m or less, an indication that paleoearthquakes of magnitude 6½ to 7 have occurred on the fault.

INTRODUCTION

Most neotectonic studies in Utah have emphasized the hazard posed by the occurrence of large-magnitude earthquakes on the Wasatch fault (Swan and others, 1980; Schwartz and Coppersmith, 1984), but fault maps (Anderson and Miller, 1979; Nakata and others, 1982) and other studies show late Quaternary (less than 125 ka) faults east of the Wasatch fault, including those in Cache Valley (Swan and others, 1983; Nelson and Sullivan, this volume), Bear Lake Valley (Williams and others, 1962), the Bear River fault zone (West, 1986), and Strawberry Valley (southeast of Kamas Valley, fig. 1) (Nelson and Martin, 1982; Nelson and Van Arsdale, 1986). A diffuse band of contemporary seismicity including earthquakes as large as magnitude 5.7 and extending through this area about 20 km east of the Wasatch fault (Arabasz and others, 1980, this volume) suggests that additional late Quaternary faults may be present.

ACKNOWLEDGMENTS

This study was part of a regional seismotectonic study for the assessment of seismic hazards to U.S. Bureau of Reclamation dams in the Wasatch Range in central Utah (Sullivan and others, 1986). The staff of the Bonneville Construction Office of the U.S. Bureau of Reclamation in Provo, Utah, provided the logistical support essential to the completion of this work. We especially thank both Leyland Kippen and the Union Pacific Railroad for permission to excavate on private properties. Edward Baltzer and Carol Krinsky (geologists formerly with the U.S. Bureau of Reclamation) assisted in the trench logging. Dean Ostenaa (U.S. Bureau of Reclamation, Denver, Colo.) reviewed early drafts of this manuscript. Soils analyses by Rolf Kihl (Institute for Arctic and Alpine Research (INSTAAR), University of Colorado) are appreciated. Nelson determined amino acid ratios in the INSTAAR Amino Acid Geochronology Laboratory, with the help of Dan Goter and under the direction of Gifford Miller.

BACK VALLEYS OF THE WASATCH RANGE

The back valleys of the northern Wasatch Range are in the transition zone between the eastern Basin and Range

Manuscript approved for publication November 20, 1990.

[1]Now at Yucca Mountain Project Office, U.S. Department of Energy, P.O. Box 539, Las Vegas, NV 89109.

[2]Now at U.S. Geological Survey, Mail Stop 966, Federal Center, Denver, CO 80225.

province and the Middle Rocky Mountains and Colorado Plateaus provinces. This zone is coincident with late Cretaceous and early Paleogene thrust faults of the Sevier thrust belt (Armstrong, 1968). Seismic reflection data generated for oil and gas exploration, locally detailed surface mapping, and seismologic investigations in the transition zone indicate a complex interaction between these stacked thrust faults and younger normal faults (Royse and others, 1975; Lamerson, 1982; McKee and Arabasz, 1982; Smith and Bruhn, 1984). The back valleys are structural and physiographic basins exhibiting less late Cenozoic structural relief than morphologically similar basins in the Basin and Range (Zoback, 1983; Sullivan and others, 1986). Gilbert (1928) suggested recent displacement on some faults in Cache Valley, Ogden Valley, Morgan Valley, and Kamas Valley, structural basins in the Wasatch Range that he termed "back valleys" (fig. 1). Late Quaternary displacement has been inferred on faults in Ogden Valley, near Mantua, and on the East Canyon fault (Sullivan and others, 1986). Other unstudied late Cenozoic normal faults that may have Quaternary displacement are the Crawford Mountains fault and faults in the Bear River Range (Sullivan and others, 1986).

MORGAN VALLEY

Morgan Valley is a 25-km-long, 10- to 15-km-wide, northwest-trending back valley, located 20 km east of the Wasatch fault, that was described by Gilbert (1928) as a structural trough similar to Ogden and Cache Valleys to the north. Eardley (1944) later described Morgan Valley as a syncline but subsequently recognized the role of normal faulting in the development of the valley (Eardley, 1955). Most recently, Morgan Valley has been interpreted as an asymmetric graben bounded on the east by the Morgan fault (Hopkins, 1982; Hopkins and Bruhn, 1983).

Cenozoic deposits of three ages, separated by angular unconformities, are present in Morgan Valley and suggest a deformational history dating from the Eocene. The conglomerates of the Eocene Wasatch Formation, dipping 40° to 65° to the east and northeast, are exposed on the western margin of the valley unconformably overlying Paleozoic and Mesozoic sedimentary rocks (Mullens and Laraway, 1973; Bryant, 1984). The overlying tuffaceous sandstones and conglomerates of the Norwood Tuff, described and dated as late Eocene to early Oligocene by Eardley (1944), are exposed throughout the valley dipping 10° to 40° to the northeast. Schick (1955) and Coody (1957) mapped a fanglomerate unconformably overlying the Norwood Tuff on the eastern side of the valley (Thv, fig . 2) that they informally correlated with the Huntsville fanglomerate (informal name), which is mapped in Ogden Valley and near the East Canyon fault (fig 1).

MORGAN FAULT

The 16-km-long Morgan fault is mapped on the eastern side of Morgan Valley at the base of an escarpment formed in Paleozoic and early Tertiary rocks (Mullens and Laraway, 1973). The escarpment consists of three linear 5- to 8-km-long sections that correspond to en echelon steps in the trace of the fault and to differences in escarpment height and elevation of hanging-wall deposits (figs. 2, 3). There are no fault scarps in unconsolidated deposits along the three sections of the fault. However, triangular facets along the base of the escarpment that are 100 to 250 m high and slope 20° to 25° suggest that Quaternary displacements have occurred on all sections of the fault.

Evidence suggests that Cenozoic displacement may be greatest on the northern section of the fault. On the basis of (1) the correlation of thrust faults mapped on Durst Mountain in the footwall of the Morgan fault with those exposed on the western side of the valley and (2) the thickness of Cenozoic deposits in the valley, Hopkins (1982) concluded that 6,800 m of Cenozoic normal displacement has occurred on the northern section of the fault. Along this section of the fault, tilted late Cenozoic erosion surfaces are cut on the Huntsville fanglomerate (fig. 2), which overlies the Norwood Tuff in the hanging wall of the fault. Schick (1955) concluded that this fanglomerate is of Pliocene(?) age and suggested that it was displaced by the Morgan fault. Recent mapping (Mullens and Laraway, 1973; Hopkins, 1982) indicates that this fanglomerate dips 5° to 38° into the fault and also suggests that the fanglomerate is faulted. Although triangular facets are also present on the southern section of the fault, Cenozoic displacement appears to be less there than it is on the northern section (Hopkins, 1982, p. 35).

Our investigation of the late Quaternary displacement history of the Morgan fault focused on the central section of the fault, where Quaternary alluvial fans (Qaof) set into the Huntsville fanglomerate suggest displacement by the Morgan fault (figs. 2, 3 , 4). We infer this topographic low on the hanging wall of the fault to be a 0.5- to 1-km-wide graben filled with alluvial fan deposits that is bounded on the east by the main scarp of the Morgan fault and on the west by an inferred east-facing antithetic fault (fig. 4). Dissected alluvial fan deposits (Qaof) slope 6° to 9° to the southwest within this inferred graben. The lower 50 m of some of the facets slope 1° to 3° more steeply than their upper portions. Thus, we infer the surface trace of the fault to be at the 50- to 100-m-

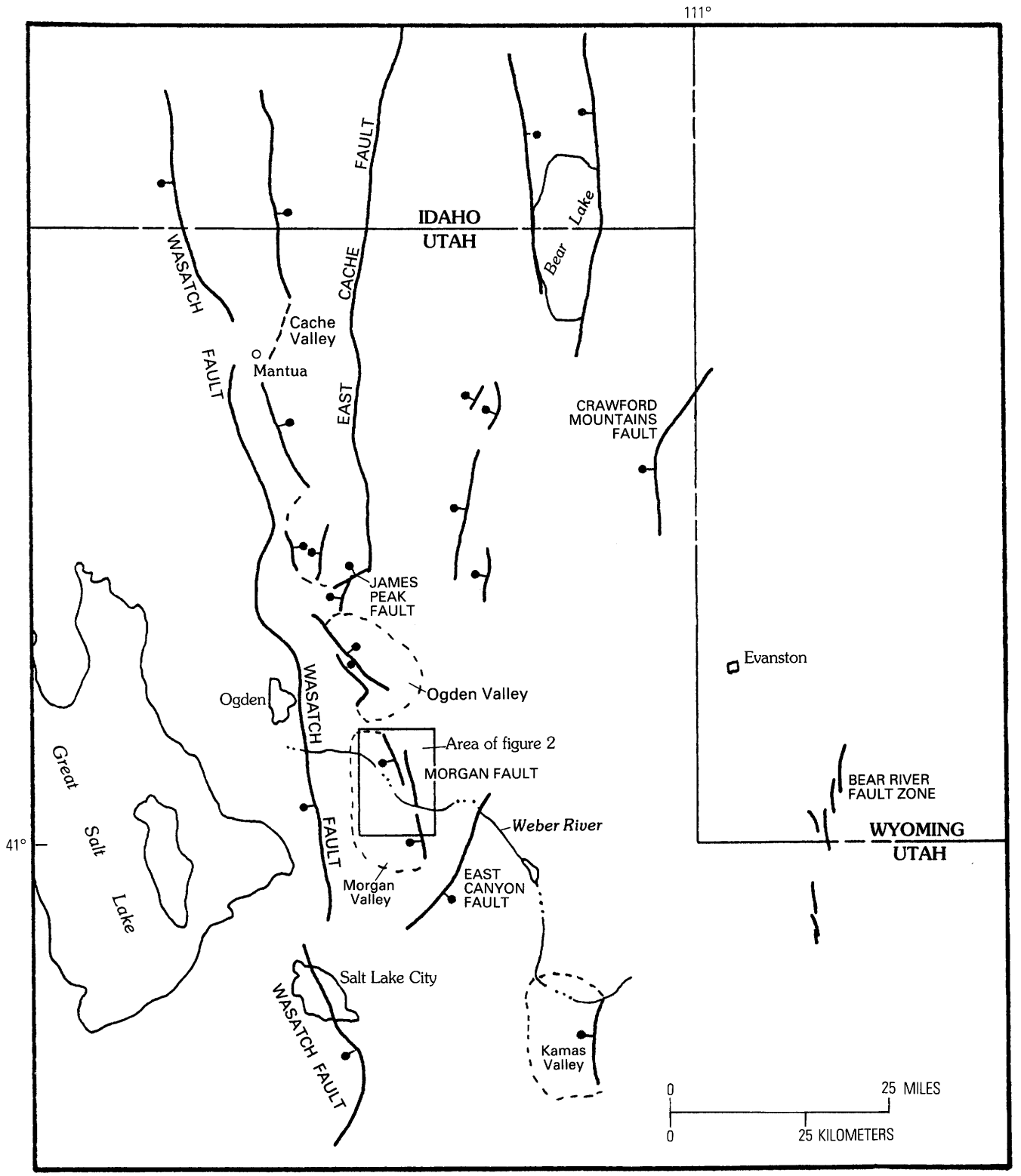

FIGURE 1.—Location of the Morgan fault, the Wasatch fault, and other middle or late Quaternary faults (ball and bar on downthrown side) in northeastern Utah. Outlines of the back valleys of the northern Wasatch Mountains are indicated by dashed lines. The area of figure 2 is shown.

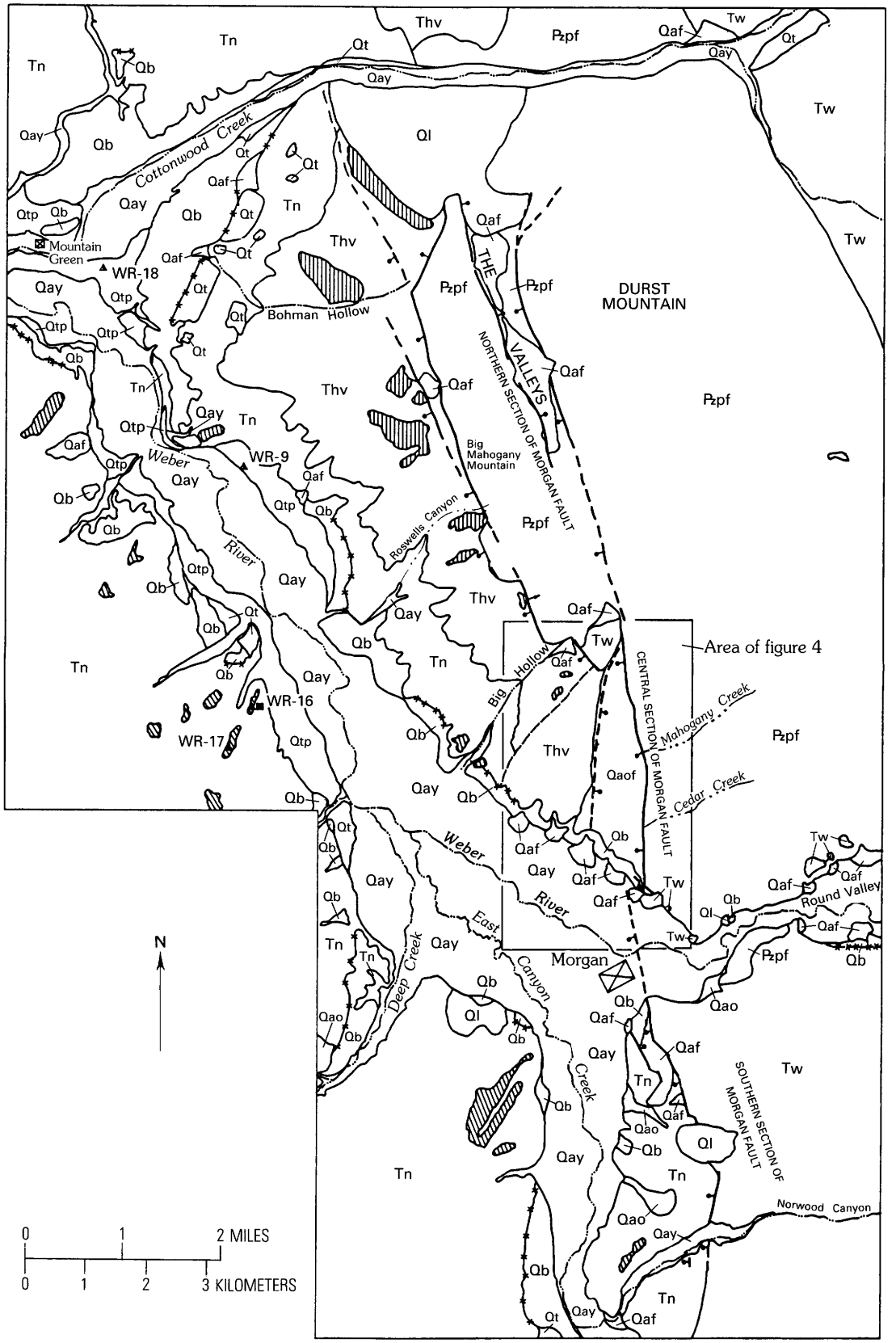
Tn
Qb
Qt
Thv
Pzpf
Qaf
Tw
Qay
Ql
Cottonwood Creek
Mountain Green
WR-18
Bohman Hollow
THE VALLEYS
NORTHERN SECTION OF MORGAN FAULT
DURST MOUNTAIN
Big Mahogany Mountain
Roswells Canyon
Weber River
WR-9
WR-16
WR-17
Big Hollow
CENTRAL SECTION OF MORGAN FAULT
Mahogany Creek
Cedar Creek
Area of figure 4
Round Valley
East Canyon Creek
Deep Creek
Morgan
SOUTHERN SECTION OF MORGAN FAULT
Norwood Canyon
N
0 1 2 MILES
0 1 2 3 KILOMETERS

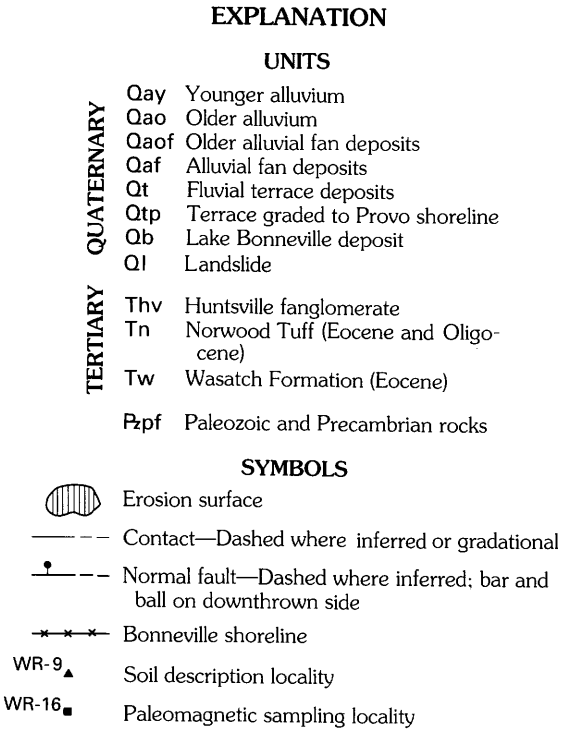

FIGURE 2.—Explanation.

wide break in slope between the facets and the fans. Although a few small, discontinuous Holocene fans along the break in slope in the larger drainages are undissected, channels (some up to 20 m deep) are incised into the surfaces of all the larger alluvial fans along the central section (fig. 4). Longitudinal profiles down these channels show that they are graded to the Bonneville shoreline along all but their lowest reaches. Knickpoints in the profiles caused by the fall of the lake (dated at 15 ka by Scott and others (1983)) do not appear to have migrated more than 100 m up the fan channels. Holocene alluvial fans have been deposited where the channels reach the flood plain of the Weber River. Thus, we conclude that most of the sediment derived from the footwall of the fault is being carried beyond the hanging-wall fan surfaces. Distinguishing tectonic responses from climatic or changing base-level responses in alluvial fan systems is difficult at best (for example, Funk, 1976; Bull, 1977), but the dissection of older fans along the central section suggests that fault slip rates are lower than stream-downcutting rates.

◀ FIGURE 2.—Cenozoic geology of Morgan Valley modified from Mullens and Laraway (1973). Reversely magnetized samples of a silty clay from the B horizon of a soil on an erosion surface west of the Weber River (site WR–16) indicate that this soil, the underlying deposits, and higher erosion surfaces in the valley are older than 730 ka (Sullivan and others, 1988). Most younger alluvium postdates the fall of Lake Bonneville from the Provo shoreline (14 ka). Fluvial terraces are all of Pleistocene age, but several ages are represented, including a terrace graded to the Provo shoreline (Qtp). The area of figure 4 is shown.

AGE OF QUATERNARY DEPOSITS ADJACENT TO THE CENTRAL SECTION OF THE MORGAN FAULT

The Quaternary deposits along the central section of the Morgan fault consist of Holocene alluvium in the major drainages, deposits of Lake Bonneville, and older colluvial and alluvial deposits at elevations above the Bonneville shoreline (fig. 4). Soils developed in the alluvium in the larger drainages (Qay, figs. 4, 5) and in the fans (Qayf, figs. 4, 5) deposited where the drainages reach the floor of Morgan Valley are weakly developed and contain no argillic B horizons. Comparison of these soils with the Holocene soils described by Shroba (1982) indicates that the alluvium is of Holocene age. Soils began forming on the buff-colored sands and silts between the present flood plain and the highest stand of Lake Bonneville in the valley following the fall of the lake about 14 to 15 ka. A soil developed on these deposits near Robeson Springs (M–2) (table 1, fig. 5) lacks an argillic horizon but contains substantial amounts of pedogenic carbonate. A sequence of older fan deposits (Qaof, figs. 3, 4, 5) derived from the mountains to the east is exposed above the Bonneville shoreline. These deposits are overlain by thin (1- to 3-m-thick) hillslope colluvium that thickens to 7 m adjacent to the Morgan fault near Mahogany Canyon. Exposures and test pits (all sampling localities, fig. 4) show thick calcium carbonate soil horizons (stages II and III of Gile and others (1966)) on both the colluvial and alluvial deposits; a 1-m-thick petrocalcic horizon (stage IV) in fan deposits was exposed beneath about 3 m of colluvium near Mahogany Canyon (locality 1, fig. 4). Thus, comparisons with similar soils developed in similar deposits elsewhere in the region (Machette, 1985a) indicate that many of these alluvial and colluvial sediments are probably of middle Quaternary age (125–730 ka). However, the differing degree of carbonate development in units of similar lithology, unconformities between most alluvial and overlying colluvial units, and uncertainty in correlating individual alluvial units in isolated exposures suggest that units deposited during a number of episodes during the Pleistocene may be present.

We used three relative dating methods in an attempt to estimate more accurately the ages of the older colluvial and alluvial sediments along the central section of the Morgan fault—two measures of the degree of soil development and amino acid ratios measured on fossil gastropod shells in the deposits.

Soil development indices (Harden and Taylor, 1983) provide an objective way of comparing the degree of soil

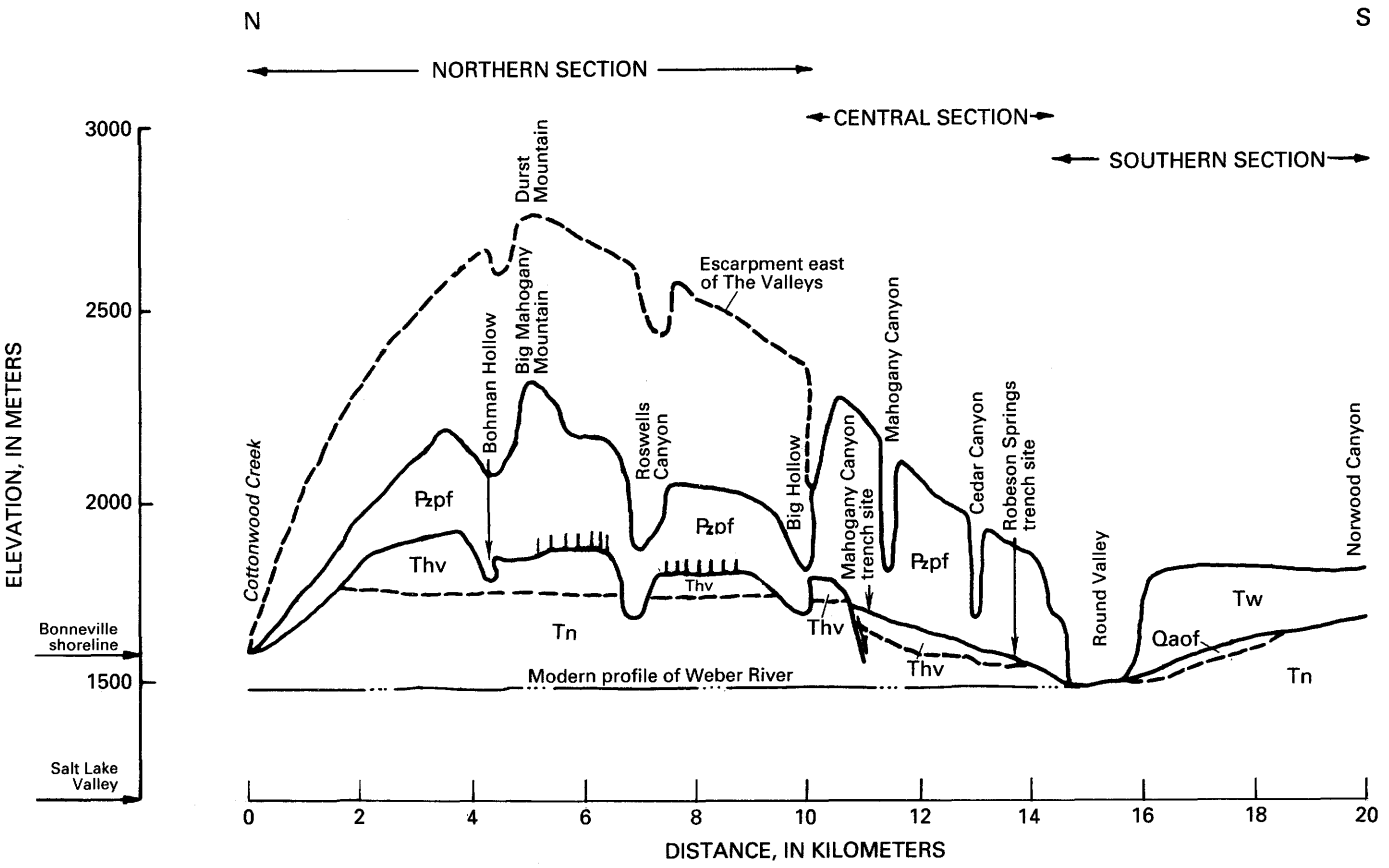

FIGURE 3.—Generalized topographic profiles (solid lines) and geologic section parallel to the Morgan fault drawn along the crest of the footwall escarpment and along the hanging wall at the base of the escarpment. Profiles are from a 1:62,500-scale map having a vertical exaggeration of approximately 6:1. The approximate position of the contact between the Huntsville fanglomerate (Thv) and the Norwood Tuff (Tn) is shown by a dashed line north of Mahogany Canyon. Thv is overlain by older alluvial fan deposits south of the antithetic fault at Mahogany Canyon. The modern profile of the Weber River and the locations of erosion surfaces (hachured lines) are also shown. Geologic units are the same as those used in figure 2.

development on deposits of unknown age with that on deposits of similar lithology in areas where numerical ages are available (Birkeland, 1984). Several calibrated (independently dated) soil profiles available from Morgan Valley (discussed by Sullivan and others (1988)) include soil M–6, which overlies a peat dated at 832±100 ka (Beta–9244) in a trench near Robeson Springs (table 1, fig. 5); soils (M–2, table 1; WR–9, WR–18, fig. 2) on both fine and coarse materials younger than the Bonneville shoreline (14–15 ka); and profile WR–16, which has a reversely magnetized B horizon that shows it to be older than 730 ka (fig. 2). The variable but high carbonate content of the soils described on alluvial and colluvial deposits along the central section of the Morgan fault (table 1, fig. 4) makes the indices of Harden and Taylor (1983) (table 1) less useful in estimating the age of these soils than in estimating the ages of many of the soils elsewhere in the Wasatch Range (Sullivan and others, 1988).

Measuring the rates of total pedogenic carbonate accumulation in soils is another method that has proven useful for estimating the age of soils in a number of areas in the arid and semi-arid Western United States (Machette, 1985a). Age estimates based on total carbonate values cannot be relied on for soils significantly younger than the last interglacial (125 ka) (unless many independent age estimates for similar soils in the region are available) because of probable major changes in carbonate accumulation rates over this period. However, over longer time spans, multiple cycles of climate change tend to attenuate accumulation rate changes; as a result, age estimates for older soils are relatively more accurate

FIGURE 4.—Surficial geology of the central section of the Morgan fault, modified from Mullens and Laraway (1973). See figure 2 for location. Older alluvial fan deposits have an estimated age of more than 400 ka, and colluvial deposits (not shown here) are inferred to range in age from Holocene to older than 400 ka. The upslope inflections in contour lines on unit Qaof mark channels incised into the older alluvial fan deposits. Younger alluvium and alluvial fan deposits postdate Lake Bonneville deposits (16–14 ka) in the valley. Sampling localities and the area of figure 5 at southern end of the central section are shown. ▶

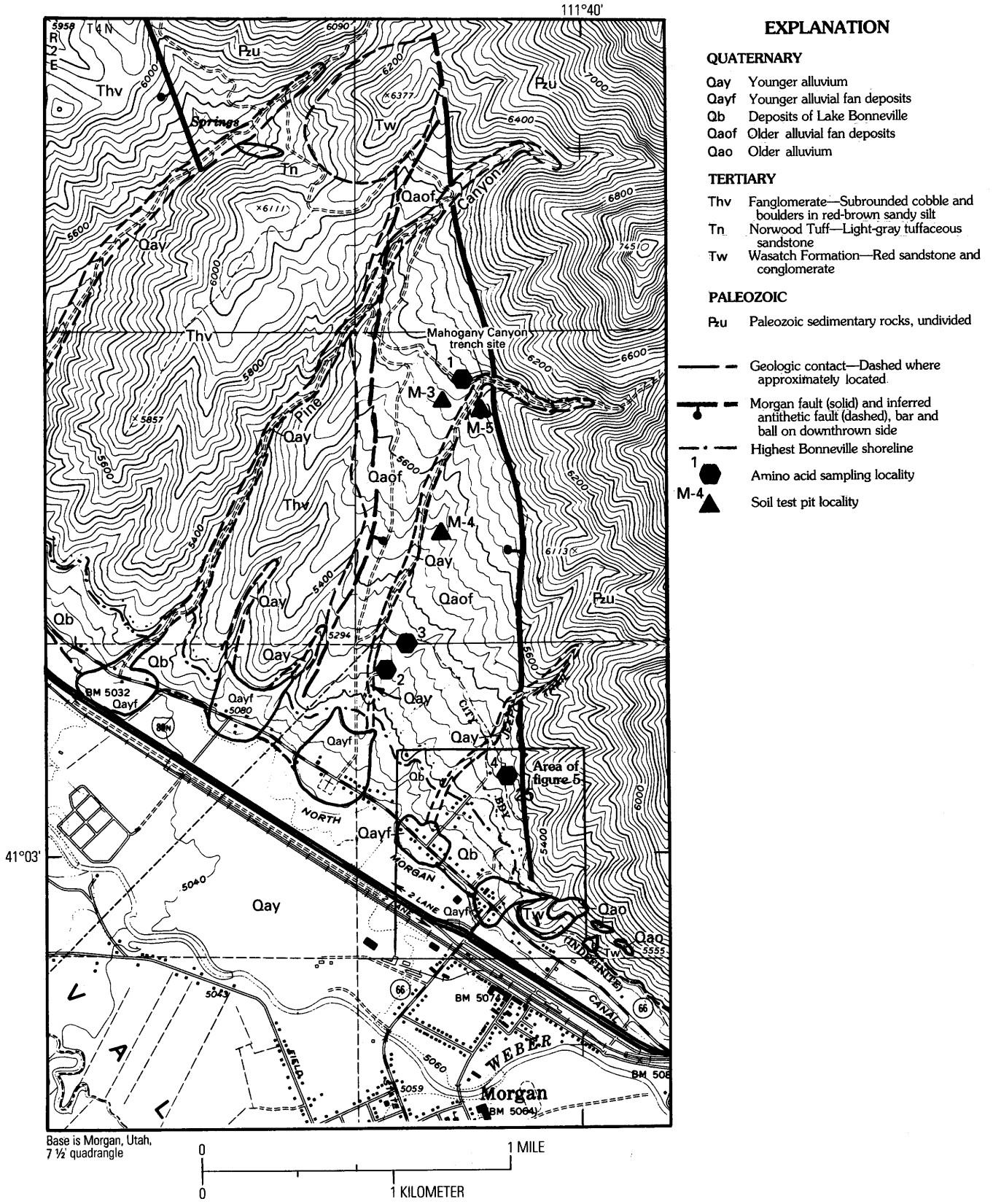

EXPLANATION

QUATERNARY

- Qay Younger alluvium
- Qayf Younger alluvial fan deposits
- Qb Deposits of Lake Bonneville
- Qaof Older alluvial fan deposits
- Qao Older alluvium

TERTIARY

- Thv Fanglomerate—Subrounded cobble and boulders in red-brown sandy silt
- Tn Norwood Tuff—Light-gray tuffaceous sandstone
- Tw Wasatch Formation—Red sandstone and conglomerate

PALEOZOIC

- Pzu Paleozoic sedimentary rocks, undivided

- Geologic contact—Dashed where approximately located
- Morgan fault (solid) and inferred antithetic fault (dashed), bar and ball on downthrown side
- Highest Bonneville shoreline
- 1 Amino acid sampling locality
- M-4 Soil test pit locality

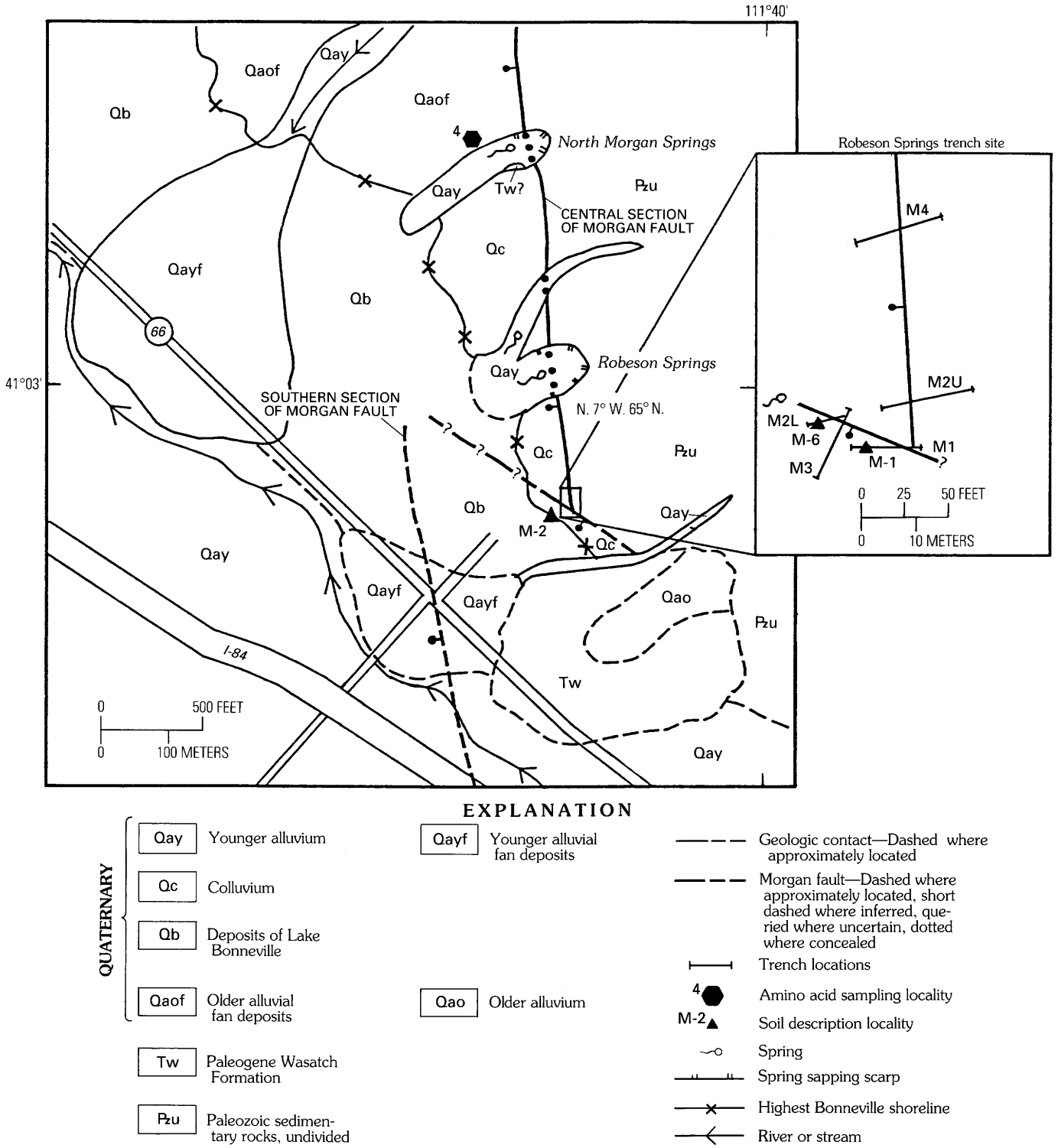

FIGURE 5.—Surficial geology of the southern end of the central section of the Morgan fault, showing locations of trenches at the Robeson Springs trench site and sampling sites.

age estimates for older soils (Machette, 1985b; Colman and others, 1988).

Machette's (1985a) methods were used to calculate amounts of carbonate, in grams per square centimeter, in the total profile for the Morgan soils and to compare them with values for carbonate-rich soils in the northern Wasatch Range having some independent age control. Sullivan and others (1988) calculated latest Pleistocene-Holocene (0–15 ka) carbonate accumulation rates of as much as 1 g/cm^2 per thousand years from two soils (M–2 and M–6, table 1) in Morgan Valley and one soil in Heber Valley (about 65 km to the south). However, ground water may have added carbonate to the soil in profile M–2, and primary carbonate values are difficult to estimate for all soils. The longer term (0–150 ka) rate of Sullivan and others (1988)—0.5 g/cm^2 per thousand years (again based on only three soils along the Weber River, fig. 1)—is roughly half the latest Pleistocene-Holocene rate. Because the back valley soils are located east of the crest of the Wasatch Range, it is unlikely that latest Pleistocene-Holocene carbonate accumulation rates are higher than the 0.5 g/cm^2 per thousand years calculated by Scott and others (1982) for soils of similar age near Salt Lake City. Rates of about 0.15 g/cm^2 per thousand years for Fisher Valley (Colman and others, 1988), 0.14 g/cm^2 per thousand years for the Beaver area (Machette, 1985b), and maximum rates of 0.14 to 0.26 g/cm^2 per thousand years for Spanish Valley (Harden and others, 1985) elsewhere in Utah indicate that middle and late Quaternary rates in the eastern Wasatch Range may well have been less than 0.2 g/cm^2 per thousand years. We use 0.5 g/cm^2 per thousand years as a maximum rate to estimate minimum ages of 70 to 100 ka for the soils in profiles M–3, M–4, and M–5 (table 1). These calculations suggest that soils on the alluvial fans (unit Qaof, fig. 4) are certainly older than 50 ka and probably date to before the last interglacial age (125 ka). Because the fans are being eroded, even finite soil ages would be minimum ages for the fan sediments.

Amino acid ratios derived from analysis of the organic matrix within carbonate fossils have proven useful in the relative dating and correlation of a variety of Quaternary stratigraphic units worldwide (Wehmiller, 1982). This methodology, termed aminostratigraphy by Miller and Hare (1980), is valid within a region as long as all samples have had very similar temperature histories and if the amino acids in the species analyzed racemize at about the same rate (Williams and Smith, 1977). Although most studies have used marine mollusks (Wehmiller, 1982), recent work indicates that amino acid ratios from nonmarine gastropods are useful for relative dating (Miller and others, 1982; Scott and others, 1983; Nelson and others, 1984; Barnes and others, 1986). The Paleozoic carbonates and alluvial fan surfaces having carbonate-rich soils along the central section of the Morgan fault provide a favorable environment for lime-loving terrestrial gastropods. The large terrestrial gastropod *Oreohelix* cf. *strigosa* is abundant in the surface litter along the trace of the fault, and fragments and whole shells of this species were found in the older alluvial fan sediments (Qaof) and overlying colluvium (Qc) at four sites (fig. 4, table 2). Ratios of D-alloisoleucine to L-isoleucine in these samples in the alluvium are greater than 0.4, whereas those in the colluvial units range from 0.20 to 0.57; these ratios suggest that the shells are of several ages.

Accurate numerical age estimates are difficult to obtain from amino acid ratios. Such estimates require accurate kinetic models of amino acid racemization in the mollusk genera of interest, along with estimates of the temperature histories of the fossil samples. A ±1° uncertainty in the effective diagenetic temperature (EDT) (integrated chemical effect of the sample's temperature history) results in a 20 percent uncertainty in the age estimate, and we have no way of estimating the uncertainty in our EDT's. Although the diagenetic models that we used were developed by using different genera (table 2), the models for many genera differ little, and there is no reason to think that these models do not apply to *Oreohelix* shells in Morgan Valley.

We used two kinetic models to calculate (minimum) ages for our samples (table 2). The linear model assumes a constant rate for the isoleucine racemization reaction in shells but probably applies only to our younger samples, because the reaction rate has been shown to decrease markedly in older samples (Wehmiller, 1982). One of several possible nonlinear models suggests much greater ages for the older samples. A few of the samples that were collected less than 2 m below the surface may have been affected by seasonal temperature changes (which would increase their apparent age), but, because the alluvial fan sediments are being eroded, most samples must have been buried more deeply during most of their burial history. If the shallower samples were less than 2 m deep for their entire burial history, the maximum possible surface heating effect would reduce our calculated ages by about half (for example, Wehmiller, 1977). Because of large uncertainties in sample temperature histories and appropriate kinetic models, only the linear-model age estimates (table 2) are used—and they are only minimum age estimates. However, enough is known about EDT's in the region and the reaction rate in gastropods to suggest that the samples from the colluvium exhibiting ratios of 0.20 and 0.27 are less than 200 to 400 ka and less than 300 to 500 ka, respectively.

Thus, on the basis of six samples (table 2), the older alluvial fan deposits are thought to be older than 400 ka. The colluvial deposits overlie these older fan deposits at

TABLE 1.—*Selected properties of soils on alluvial, colluvial, and lacustrine sediments along the Morgan fault, Morgan Valley, north-central Utah*

[—, not detectable]

Horizon[1]	Average depth (cm)	Parent material	Munsell color	Estimated percentage by volume			Percentage by weight[2]			Organic matter[3] (percent)	Carbonate[4] (percent)	Soil profile index[5]	Total pedogenic carbonate[6] (g/cm²)
				Pebbles (0.2–8 cm)	Cobbles (8–25 cm)	Boulders (>25 cm)	Sand (2–0.5 mm)	Silt (50–2 μm)	Clay (<2 μm)				
Profile M–1													
A	0–10	Slopewash colluvium	10YR 6/2	5	0	0	27	56	18	1.7	16.5	15	63
Bwk	10–23	do	10YR 5/3	5	0	0	28	52	21	1.2	24.9		
Bkm	23–50	do	10YR 8/0n	5	0	0	28	58	15	.5	43.7		
Bk1	50–84	do	7.5YR 8/2	5	0	0	18	75	7	.4	48.9		
Bk2	84–161	do	7.5YR 7/3	2	0	0	14	79	7	.3	35.6		
C	161–228+	do	7.5YR 7/3	2	0	0	28	62	11	3.3	—		
Profile M–2													
Ap	0–9	Loess and lake sediments.	7.5YR 5/3	0	0	0	21	73	6	1.5	—	15	19
A	9–20	do	7.5YR 5/3	0	0	0	22	70	9	1.1	—		
Bw	20–42	Lake sediments	7.5YR 6/4	0	0	0	44	43	13	.3	—		
Cox1	42–50	do	7.5YR 7/4	0	0	0	50	40	11	.1	5.5		
Bk1	50–61	do	7.5YR 7/4	0	0	0	44	45	11	.2	13.9		
Bk2	61–71	do	7.5YR 8/3	0	0	0	39	47	15	.4	35.5		
Bk3	71–107	do	7.5YR 8/3	0	0	0	6	81	14	.1	21.7		
Cox2	107–155+	do	7.5YR 7/3	0	0	0	6	82	12	.1	13.0		
Profile M–3													
Ap	0–10	Loess and alluvium	7.5YR 5/3	10	10	2	28	57	15	6.5	—	19	35
Bt	10–32	do	7.5YR 5/3	10	10	2	20	52	28	3.4	14.3		
2Bkm	32–35	Alluvium	7.5YR 8/0	20	5	2	17	66	17	1.2	50.4		
2Bk	35–73	do	7.5YR 8/3	20	5	2	20	66	14	.4	56.0		
2Bt	73–128	do	7.5YR 6/3	5	0	0	19	73	7	.2	21.6		
3Ckm	128–135+	do	7.5YR 8/1	20	10	2	27	41	32	.3	51.0		
Profile M–4													
A1	0–13	Loess and colluvium	7.5YR 4/3	10	5	1	22	57	20	4.5	21.6	12	49
A2	13–37	do	7.5YR 4/3	10	5	1	22	62	16	3.2	28.0		
2BA	37–50	Alluvium	7.5YR 7/3	30	1	0	36	50	15	1.3	53.8		
2Bk	50–71	do	7.5YR 7/4	30	1	0	31	43	26	.7	54.6		
3Ck	71–120	do	7.5YR 8/3	10	5	2	17	73	10	.4	47.6		
3C	120–140+	do	7.5YR 7/3	10	5	2	19	53	29	.2	39.8		

TABLE 1.—*Selected properties of soils on alluvial, colluvial, and lacustrine sediments along the Morgan fault, Morgan Valley, north-central Utah*—Continued

Horizon[1]	Average depth (cm)	Parent material	Munsell color	Estimated percentage by volume			Percentage by weight[2]			Organic matter[3] (percent)	Carbonate[4] (percent)	Soil profile index[5]	Total pedogenic carbonate[6] (g/cm^2)
				Pebbles (0.2–8 cm)	Cobbles (8–25 cm)	Boulders (>25 cm)	Sand (2–0.5 mm)	Silt (50–2 μm)	Clay (<2 μm)				
Profile M–5													
Ap	0–9	Loess and colluvium	7.5YR 5/3	15	10	1	24	58	18	4.7	—	14	40
A	9–30	do	7.5YR 5/4	15	10	1	21	53	26	2.7	12.8		
BA	30–44	do	7.5YR 7/4	15	10	1	29	48	23	1.4	46.1		
2Bkm	44–52	Alluvium	7.5YR 8/2	20	10	0	32	48	20	.4	47.9		
2Bk	52–88	do	7.5YR 8/3	20	10	0	38	43	19	.4	46.6		
3CB	88–138	do	7.5YR 7/4	40	1	0	31	48	21	.2	41.6		
4C	138–149+	do	7.5YR 7/4	5	0	0	34	48	18	.2	46.0		
Profile M–6													
Ap	0–16	Slopewash colluvium	7.5YR 4/2	5	0	0	31	56	13	9.8	10.7	16	7
A	16–37	Colluvium	7.5YR 4/3	5	0	0	28	55	17	3.4	19.8		
Bt	37–69	do	7.5YR 5/3	5	0	0	30	55	14	2.2	25.0		
Ck	69–98	do	7.5YR 7/3	5	0	0	33	57	10	1.4	12.4		
2C1	98–135	do	10YR 7/3	10	0	0	28	49	23	.9	36.4		
2C2	135–175+	do	10YR 7/3	5	2	0	23	50	27	1.0	11.6		

[1]Horizon nomenclature of Guthrie and Witty (1982) and Birkeland (1984), except that the master K horizon is not used.

[2]Particle size distribution of <2-mm fraction obtained by using sieve-pipette methods (for example, Carver, 1971) and a Sedigraph for some silt-clay fractions from which carbonates and organic matter have been removed by Jackson's (1956) method.

[3]Method of Walkley and Black (1934).

[4]Method of Allison and Moodie (1965, p. 1387).

[5]Nonarid index of Harden and Taylor (1983).

[6]Method of Machette (1985a).

TABLE 2.—*D-alloisoleucine/L-isoleucine ratios in the total (free + peptide-bound) amino acid fraction and calculated ages for* Oreohelix *cf.* strigosa *from alluvial and colluvial sediments along the Morgan fault, Morgan Valley, north-central Utah*

[—, age not calculated]

INSTAAR lab no.[1]	Depth below surface (m)	Number of sample preparations	Mean total aIle/Ile ratio[2]	Minimum age estimate (ka)		Location[5]	
				Linear kinetic model[3]	Nonlinear model[4]	Site	Unit
Modern surface float (mean annual temperature 7.2 °C–7.7 °C)							
DAN–194	0	8	0.025±.005	—	—	1	—
North Morgan Springs							
DAN–190	>4	3	0.61±.05	709–777	1,511–1,660	4	Qaof
Gravel pit							
DAN–207	2.3	3	0.27±.06	317–289	—	2	Qc
DAN–209	.7	3	.35±.06	422–386	—	2	Qc
DAN–189	3	2	.41±.06	456–503	—	2	Qaof
DAN–208	5.5	3	.43±.04	485–530	—	3	Qaof
Mahogany Canyon roadcut							
DAN–198	>1.6	3	0.30±.04	337–369	—	1	Qc
DAN–193, 195, 196, 197, 199	>2	8	.49±.06	582–637	861–942	1	Qaof
Trench at site M6, Mahogany Canyon[6]							
DAN–206	1.7	3	0.20±.01	214–234	—	1	Qc
DAN–201	5.0	3	.35±.05	400–438	—	1	Qc
DAN–200	5.1	3	.57±.03	691–757	1,350–1,478	1	Qc
DAN–203	6.0	3	.40±.05	463–508	—	1	Qc
DAN–204	4.8	3	.44±.03	515–564	—	1	Qaof
DAN–205	5.8	3	.46±.03	542–593	677–740	1	Qaof

[1]Institute for Arctic and Alpine Research, University of Colorado, Boulder, Colo.

[2]aIle/Ile ratio (peak area) measured by using methods of Miller and Hare (1980). Mean ratios include one standard deviation. Extraneous values rejected by using methods of Dixon (1965).

[3]Age calculated by using a linear kinetic model of isoleucine racemization (equation 18 of Williams and Smith (1977)), where k=0.77; a modern ratio of 0.025 for *Oreohelix* cf. *strigosa* (A.R. Nelson, unpub. data, 1984); Arrhenius parameters determined for *Vallonia* by Nelson and others (1984); values of constants in the Arrhenius equation (equation 9 of Williams and Smith (1977)); and an effective diagenetic temperature for the late Quaternary in this region of 8 °C less than the present mean annual temperature (Nelson and others, 1984) (for example, Wehmiller and Belknap, 1982). Age range calculated by using ±0.25 °C range in estimated effective diagenetic temperature.

[4]Age calculated by using a nonlinear model, a Quaternary effective diagenetic temperature (see footnote 3) (for example, Wehmiller and Belknap, 1982), and the same relationships used in the linear model, except that the reaction rate is assumed to decrease to one-fifth the initial rate for samples having aIle/Ile ratios greater than 0.4.

[5]As seen in figure 4. Qc not mapped.

[6]Trench discussed in detail by Sullivan and others (1988).

all the sampling sites. The lowest ratio obtained from colluvium, in the trench near Mahogany Canyon, suggests an age of more than 200 ka. Higher ratios from other colluvial units indicate either that these units are older or that shells in the slope colluvium are reworked from the older fan deposits. The minimum age estimates from the soil carbonate data are consistent with these age estimates from amino acid ratios.

TRENCH INVESTIGATIONS OF QUATERNARY FAULTING ON THE CENTRAL SECTION OF THE MORGAN FAULT

The Morgan fault is exposed at the base of the escarpment in 2-m-high exposures at Robeson Springs (fig. 5) as a planar, N. 7° W.-striking, 65° W.-dipping sheared contact between Paleozoic carbonates and light-brown silty colluvium. Sheared and altered dolomite is exposed for a distance of about 15 m to the east in the footwall of the fault, but no other shears are evident in colluvial deposits in the exposure, which extends about 25 m west of the fault. This exposure and additional exposures at North Morgan Springs (fig. 5) showed that unconsolidated deposits, exposed above the Bonneville shoreline, were displaced by the Morgan fault in a narrow zone at the base of the triangular facets on the escarpment.

The Robeson Springs trench site is located at the southern end of the central section of the Morgan fault (fig. 5). The linear trace of the footwall escarpment ends

at a small, east-trending ephemeral drainage south of the trench site. South of this drainage, red sandstone and conglomerate of the Wasatch Formation are exposed dipping 40° to the west and extending across the projection of the central section of the fault. Projecting the southern section of the fault north across the Weber River indicates that the Morgan fault steps westward about 200 m between the southern and central sections (figs. 2, 5).

At the Robeson Springs site, five trenches were excavated at or near the break in slope at the base of the footwall escarpment of the Morgan fault (fig. 5). Two of these trenches (M2U and M4) exposed the main trace of the Morgan fault. Another normal fault trending northwest between the central and southern sections of the Morgan fault is exposed in trenches M2U, M1, and M3. The Cambrian and Devonian dolomite that forms the escarpment is exposed in all the trenches. To the east, it is overlain by Devonian and Mississippian sedimentary rocks that generally dip to the west but that have been complexly folded and faulted (Mullens and Laraway, 1973). In trenches M2U and M4, colluvial deposits overlie the dolomite in the hanging wall of the fault, but, in the exposures at North Morgan Springs, the colluvial deposits overlie older alluvial fan deposits that are correlated with similar deposits exposed at four locations north of the Robeson Springs site (figs. 4, 5).

STRATIGRAPHY IN TRENCH M4

The Morgan fault is clearly expressed in trench M4 as a zone of sheared dolomite and fault gouge from within 1 m of the ground surface to the base of the trench (fig. 6). The fault zone juxtaposes colluvial deposits and bedrock along a N. 7° W.-striking, 50° W.-dipping planar contact. The eastern boundary of the fault zone is an abrupt planar shear separating fractured bedrock (unit 1) from a fine-grained fault breccia (unit 1b) derived from the bedrock. Near the base of the trench, a plastic clay gouge (unit 1c) forms part of the fault zone.

On the western margin of the fault zone, a 4-m-thick sequence of colluvial deposits has been displaced by the fault (units 3, 6, 7a, 7b, fig. 6). The colluvial deposits are all of similar lithology—clayey silts containing variable but small (less than 15 percent) amounts of dispersed angular pebbles of dolomite. Slight differences in color, clay content, carbonate content, and induration have been used to map three main colluvial units (units 3, 6, 7) and to identify separate facies (identified by lower case letters) within two of the units. Unit 3 is massive and moderately indurated and contains upper and lower zones of pedogenic carbonate (stage II). Unit 6 is siltier, lacks carbonate, and is loose and unconsolidated. Modern soil is developed in unit 7, including a cambic B horizon containing weak stage II carbonate in some parts (unit 7a).

Discrete downslope-thinning colluvial wedges that are derived from erosion of the free face of a fault scarp are typically found adjacent to faults displaying scarps more than 1 m high in unconsolidated deposits. The stratigraphy and thickness of these colluvial wedges have been used to estimate the size of the individual surface displacements on faults (for example, Schwartz and Coppersmith, 1984). Near the floor of trench M4, two 0.1-m-thick, 0.5- to 0.8-m-long fingers of fault breccia (unit 1b) are interbedded with colluvial unit 3c (fig. 6). This interbedding of fault breccia and colluvium appears to have resulted from the erosion of fault breccia from the free face of a scarp that was formed during two separate surface displacements on the fault. The colluvium between these fingers of fault breccia is 0.4 m thick, and 0.5 m of colluvium is preserved between the lower finger and the underlying bedrock. These thicknesses provide minimum estimates of the height of the scarp and of the vertical displacement that produced it.

The lack of discrete horizons within unit 3 suggests that it did not accumulate as a succession of scarp-derived colluvial wedges. Unit 3 consists of 2 m of massive pebbly, clayey silt deposited by surface wash and creep from above the trench site. The uniform thickness of fault breccia preserved adjacent to this unit along a planar 50°-W.-dipping contact indicates that unit 3 has been faulted into its present position. We interpret this unit to consist of multiple indistinguishable colluvial units that have been downdropped along the fault during successive small surface displacements and subsequently buried by continuing deposition from the escarpment above the fault. These colluvial units inferred to comprise unit 3 are lithologically identical; unconformities between them or any differences in soil development from one unit to another apparently have been masked by carbonate accumulation. On the basis of the depth of carbonate in the modern soil (unit 7a), it is thought that the pedogenic carbonate zones of unit 3 probably developed 1 to 2 m below the ground surface. The lack of interbedding within unit 3 (other than at the floor of the trench, where fingers of fault breccia divide portions of unit 3c) indicates that the displacements did not expose the fault breccia in the scarp free face. Thus, the individual surface displacements were not significantly greater than the present thickness of slope colluvium (unit 7)—about 0.5 m—on the footwall of the fault. Thus, the displacements were probably about the size of the minimum displacements inferred from the thickness of colluvium preserved below the fingers of fault breccia near the floor of the trench.

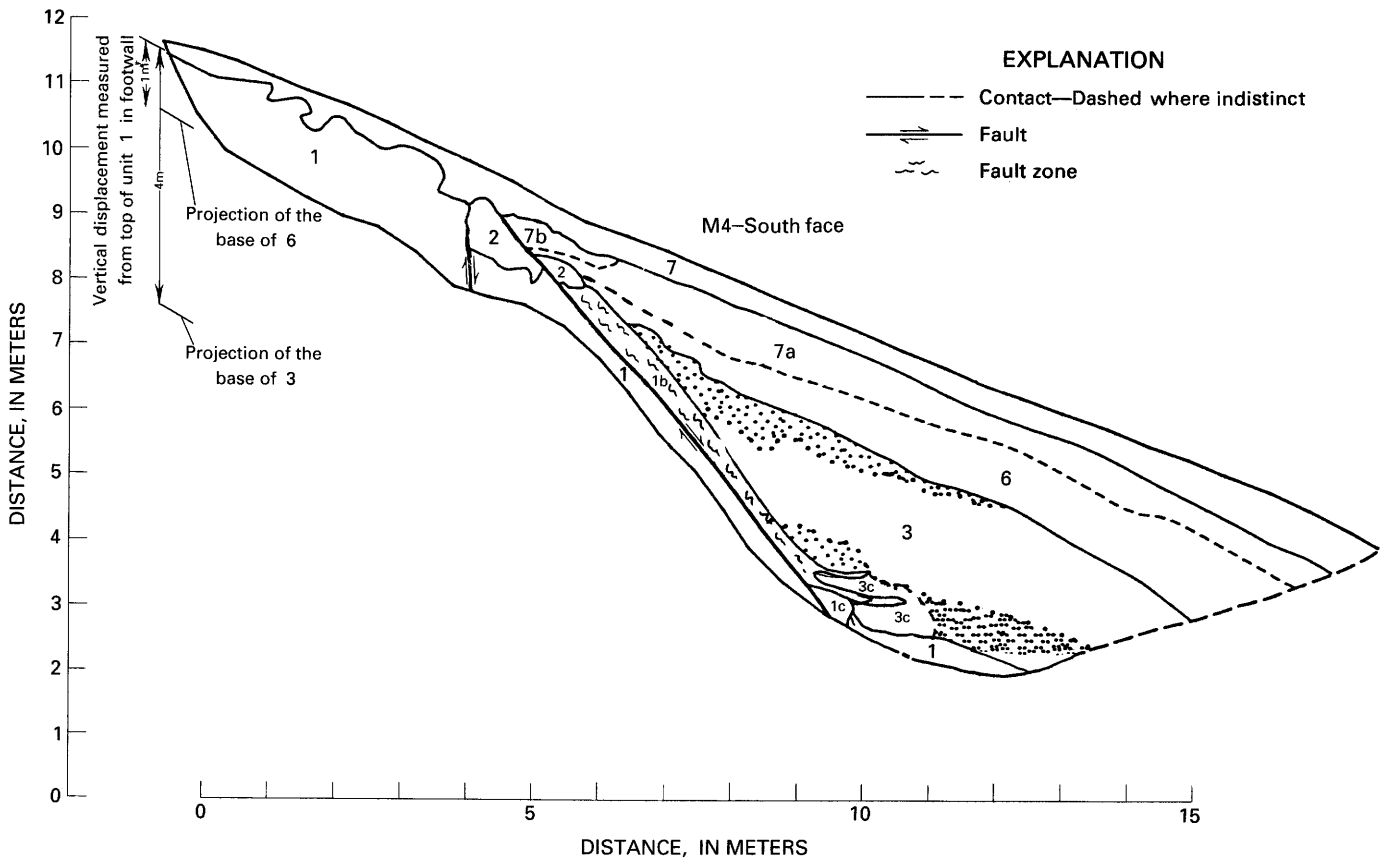

DESCRIPTION OF UNITS

7 Colluvium (HOLOCENE)—Dark brown, loose, pebbly, silt with organic material, A horizon
7b Colluvium (HOLOCENE)—Dark brown, loose, pebbly silt
7a Colluvium (HOLOCENE)—Light brown, moderately indurated, pebbly silt with cambic B and BCa horizon
6 Colluvium (HOLOCENE)—Brown, loose, clayey silt
3 Colluvium (MIDDLE AND LATE QUATERNARY)—Light brown, moderately indurated, pebbly, clayey silt. Upper and lower zones of carbonate accumulation stippled
3c Colluvium (MIDDLE QUATERNARY)—Yellowish-brown, well-indurated, pebbly
2 Colluvium (MIDDLE QUATERNARY)—Yellow, well-indurated, sandy silt
1 Bedrock (PALEOZOIC)—Dark gray, moderately weathered dolomite with no recognizable bedding, DCd of Mullens and Laraway (1973)
1b Fault breccia—Dark grey, uncemented silt-sized dolomite fragments
1c Fault gouge—Yellow plastic clay

FIGURE 6.—Log of trench M4 at the Robeson Springs trench site, showing faulted middle and late Quaternary colluvial deposits at the southern end of the central section of the Morgan fault. Sloping lines at the left are projections of displaced surfaces (the amount of the displacement is indicated).

The total displacement since the deposition of unit 3c has been estimated by projecting the base of unit 3 to the footwall of the fault at the same slope as the ground surface (fig. 6). The measured vertical displacement between the present bedrock surface and the top of unit 3 is about 4.0 m. This estimate, however, is a minimum, because this bedrock surface in the footwall must have been eroded as unit 3 was deposited.

In the upper portion of trench M4, the apparent displacement of the base of unit 6 records the most recent displacement event on the fault at this locality. Unit 6 is a key stratigraphic unit that is present in all of the trenches at the site and that overlies a dated peat deposit in trenches M2L and M3 (discussed below). The amount of this displacement has been estimated by projecting the base of unit 6 to the footwall of the fault and using the slope of the present ground surface (fig. 6). The vertical displacement measured between the bedrock surface and the base of unit 6 is about 1.0 m. The fault plane on which this displacement occurred is preserved in unit 2, a lighter colored, well-indurated pocket of colluvium, as a carbonate-impregnated plane dipping 50° to the west. We assume that this plane approximately represents the actual vertical displacement, not a minimum value, because little erosion of the bedrock surface is presumed to have occurred since the most recent Holocene event.

Estimated displacements of 0.5 to 1 m per event are small in comparison with displacements estimated for other Quaternary faults in Utah (for example, Schwartz and Coppersmith, 1984; Nelson and Van Arsdale, 1986; Nelson and Sullivan, this volume). These small displacements and empirical relationships (for example, Bonilla and others, 1984) between earthquake magnitude and the amount of surface displacement suggest paleoearthquake magnitudes of 6½ to 7 for the 16-km-long Morgan fault, as do similar relationships between earthquake magnitude and fault rupture length.

The preservation of unit 2 directly above the main fault appears to be related to an earlier displacement. A near-vertical carbonate-filled shear extends from the base of unit 2 to the floor of the trench in the bedrock east of the main fault and strikes N. 8° E. across the trench. Unit 7a and its more pebbly upslope facies, unit 7b, are interpreted to be parts of a horizon of slope colluvium downdropped to its present position by the most recent displacement event on the main fault zone. Unit 6 thins upslope to its contact with unit 2 in the hanging wall of the fault, and it is not clear if it ever extended across the fault. The predominance of silt and the lack of induration in unit 6 suggest that it consists principally of loess (or loess redeposited by surface wash) rather than slope colluvium eroded from the escarpment. Because it is the only colluvial unit in this trench and in other trenches that thickens downslope, unit 6 may have been deposited on only the lower parts of the slope and may not have extended across the fault zone.

AGES OF FAULTED DEPOSITS

Estimates of the ages of displaced colluvial deposits at the Robeson Springs trench site are based on radiocarbon dates for peat interbedded with colluvial deposits in trenches M2L and M3 and on amino acid ratios from snails in colluvial and alluvial fan deposits exposed in four other locations along the central segment of the Morgan fault. A small (3×6 m) bog deposit of peat that underlies colluvial unit 6 and overlies bedrock in the hanging wall of the Morgan fault is exposed in trenches M2L and M3. Unit 6 is correlated between trench M4 and the other trenches 32 m to the south (fig. 5) on the basis of similar lithologies and stratigraphic and geomorphic positions (Sullivan and others, 1988). Radiocarbon dates of 8,320±100 ka on peat (Beta–9244) and 9,105±270 ka on wood (GX–9968) from this deposit indicate an early Holocene age for the bog and an early or middle Holocene age for overlying colluvial unit 6.

A post-early Holocene displacement event of 1 m might be expected to have produced scarps along the central section of the fault that would still be visible today. Scarps 1 m high on gently sloping alluvial fans probably would be preserved for tens of thousands of years (Hanks and others, 1984). However, the Morgan fault is mapped at the base of a 20° to 25° sloping escarpment, and figure 6 shows that the 1-m-high scarp has been completely covered since the deposition and faulting of unit 6. Erosion and deposition of younger alluvial deposits apparently obliterated the scarp in drainages crossing the escarpment.

We infer a middle to late Pleistocene age for the older colluvial deposits (unit 3) in trench M4 by using their similar lithologies, degrees of carbonate development, stratigraphic positions, depths, and positions adjacent to the fault to correlate them with the sequence at Mahogany Creek for which we have amino acid age estimates (table 2). At Mahogany Creek, about 2.5 km north of the Robeson Springs trench site (fig. 5), a similar sequence of colluvial deposits varies in thickness from 7 m in a trench at the mountain front to about 1 m in a roadcut 180 m to the west. In the trench at Mahogany Canyon, this colluvium overlies older alluvial fan deposits in which a petrocalcic horizon containing stage IV carbonate is developed. This degree of pedogenic carbonate development suggests that the fan deposits are at least 200 to 300 ka and probably older than 500 ka. Snails from this colluvium at depths of 1 to 5 m and from other sites at similar depths have estimated ages of 200 to 400 ka or more (discussed above, table 2). However, the upper parts of unit 3 may date from the late Pleistocene (10–125 ka) because individual units cannot be correlated from Mahogany Creek to Robeson Springs.

EVENTS IN TRENCH M4

On the basis of the stratigraphic relations in trench M4 and our estimates of the age of the colluvial deposits, we have interpreted the following sequence of events:

1. During the middle and late Pleistocene, units 3 and 3c were deposited as a series of 0.5- to 1.0-m-thick horizons of slopewash that were downdropped and preserved by a series of small-displacement events comprising a minimum of 3 m of displacement on the Morgan fault. Before or during this period, unit 2 was deposited as slopewash across the fault zone and displaced about 1 m on a near-vertical shear; as a result, it was preserved from erosion upslope from the main fault zone.
2. Following an interval of nondeposition of unknown duration, a depression in the hanging wall of the fault exposed in trench M2L (fig. 5) was filled with bog deposits (radiocarbon dates of 8.3 and 9.1 ka).
3. Unit 6 was deposited above unit 3 and the bog deposits principally as loess that may have been derived from exposed Lake Bonneville sediments in the valley.

4. Units 7a and 7b were deposited by surface wash across the fault zone.
5. Units 2, 7a, and 7b were displaced about 1.0 m along the main fault zone.
6. Modern surface wash continued to deposit colluvium (unit 7) on the slope across the fault zone.

OTHER TRENCHES

In trench M2U, about 30 m south of M4 (fig. 5) at the southern end of the central section of the fault, vertical relief on the bedrock surface across the projection of the fault exposed in M4 is about 3.5 m, although the fault plane is not distinct. A 1.5-m-high, near-vertical displacement of the bedrock surface striking N. 7° W. marks the Morgan fault in this trench. This step is overlain by about 1.0 m of undisplaced colluvium having the same lithology and in the same stratigraphic position as units 7 and 7a in trench M4 (Sullivan and others, 1986). If this correlation is correct, it suggests that the most recent surface displacement recorded in trench M4 did not extend south to M2U. However, below this horizon, massive colluvium about 1.5 m thick, equivalent to unit 3 in trench M4, is interpreted to have been displaced during small (less than 1 m) faulting events (Sullivan and others, 1988).

About 10 m south and west of trench M2U, a normal fault striking N. 65° W. and dipping about 50° to the southwest that is exposed in trenches M1, M3, and M2L (fig. 5) displaces fine-grained colluvial deposits equivalent to unit 3, but overlying colluvial units are not displaced. Trench M1 crosses the projection of the N. 7° W.-striking fault exposed in trenches M2U and M4 and shows that the main trace of the Morgan fault has been terminated by this northwest-striking fault, as the bedrock relationships at the trench site (discussed earlier) suggest. Because the base of the colluvium was not exposed in the hanging wall of the fault in trench M1, an estimate of the amount of displacement since the deposition of the colluvial deposits is precluded.

SLIP RATES ON THE MORGAN FAULT

QUATERNARY SLIP RATES

Mapping and trench investigations on the central section of the Morgan fault provided evidence that middle to late Pleistocene and Holocene displacements have occurred on this back valley fault. At the Robeson Springs trench site, two faults were identified: (1) the north-trending central section of the main fault that displaces middle to late Pleistocene and Holocene colluvial deposits a minimum of 4 m and (2) a northwest-trending trace of a subsidiary fault that displaces similar middle to late Pleistocene colluvial deposits. Radiocarbon dates of 8.3 and 9.1 ka provide a maximum age for the younger colluvium that has been displaced about 1 m by the main fault in trench M4. If it is assumed that the lower part of the underlying sequence of colluvial deposits in trench M4 is 200 to 400 ka, a minimum of 4 m of displacement yields a minimum middle to late Pleistocene slip rate of 0.01 to 0.02 mm/yr. Because only one event is recorded, a Holocene slip rate cannot be calculated. These Pleistocene slip rates are an order of magnitude lower than long-term Pleistocene rates on the Wasatch fault (Machette and others, this volume), but some other faults in the region may have rates nearly as low (Nelson and Van Arsdale, 1986; McCalpin and others, this volume; Nelson and Sullivan, this volume).

We interpret the colluvial stratigraphy in trench M4 as suggesting recurrent Quaternary surface displacements of 0.5 to 1.0 m. If 0.5 m most nearly represents the average size of the surface-displacement events that are represented by the 4 m of displacement in at least the last 200 to 400 ka (as the lack of discrete scarp-derived colluvial wedges in the trench suggests), about eight individual events have occurred. These estimates yield a maximum average middle to late Quaternary event recurrence interval of 25 to 50 k.y. If only four events of 1 m displacement have occurred, the maximum average recurrence interval would be 50 to 100 k.y.

CENOZOIC SLIP RATES

The effect of the late Cenozoic uplift of the Wasatch Range on the evolution of landforms in Morgan Valley depends partly on the distribution of late Cenozoic faults. Naeser and others (1983) estimated uplift rates of 0.8 mm/yr over the last 5 Ma and 0.4 mm/yr over the last 10 Ma for the north-central Wasatch Range west of Morgan Valley. As a section constructed across the northern portion of Morgan Valley by Hopkins (1982, fig. 5) shows, the faults bounding the western side of Morgan Valley as mapped by Bryant (1984) have limited displacement, and the structural relief in the valley is primarily caused by Cenozoic displacement on the Morgan fault. If the late Cenozoic slip rate on the Wasatch fault is much greater than that on the Morgan fault, the effect of this relative uplift of the Wasatch Range would be to accelerate late Cenozoic erosion in Morgan Valley. The fact that the Weber River has incised the Norwood Tuff more than 300 m in Morgan Valley (fig. 3) indicates that such erosion has occurred and suggests that the average late Cenozoic slip rate on the Morgan fault is much lower than that on the Wasatch fault.

The accumulated thickness of the Huntsville fanglomerate preserved adjacent to the northern section of the Morgan fault provides a crude estimate of the average

Cenozoic slip rate on the fault. In Hopkins' (1982) cross section, the Huntsville fanglomerate overlies the late Eocene-early Oligocene Norwood Tuff and dips 13° E. into the fault. It has an estimated maximum thickness of 1,000 m, which provides a minimum estimate of displacement since the beginning of deposition of the fanglomerate. The age of this deposit is poorly constrained; previous workers have suggested that it is of Pliocene age (Eardley, 1944; Coody, 1957). However, similar unconsolidated gravel deposits of Oligocene age have been mapped further south in the Wasatch Range overlying and interbedded with the Oligocene Keetley Volcanics (Bromfield and Crittenden, 1971; Sullivan and others, 1988). Using an age range of 5 to 35 Ma for the Huntsville fanglomerate and a minimum displacement estimate of 1,000 m yields an estimated average middle and late Cenozoic slip rate of 0.03 to 0.2 mm/yr.

The tilting of late Cenozoic erosion surfaces adjacent to the northern section of the fault also provides a crude estimate of the average late Cenozoic slip rate on the fault. In this area, locally well-preserved, gently (0.5°–1.7°) east-dipping erosion surfaces, cut on the Huntsville fanglomerate, slope up to 1.7° northeast, into the fault (fig. 2). Our observations in less dissected terrains of the Weber River drainage suggest that these surfaces probably once sloped at least 3° toward the center of the valley; therefore, we interpret the back tilting of these surfaces to have resulted from displacement on the Morgan fault. If the most steeply tilted surface, south of Bohman Hollow and 1.7 km west of the main trace of the fault, has been uniformly rotated from a 3° westerly dip to its present 1.7° easterly dip, then projection of this surface to the fault indicates about 150 m of displacement. If the erosion surface has been downdropped relative to the footwall as well as rotated, total displacement would be greater. These erosion surfaces are probably significantly older than a much lower erosion surface on the western side of the valley (fig. 2) paleomagnetically dated at more than 730 ka. Assuming an age of 1 to 5 Ma for this surface yields an average latest Cenozoic slip rate of 0.03 to 0.15 mm/yr for this section of the fault, which is consistent with the rate estimated from the thickness and age of the Huntsville fanglomerate.

These slip-rate values are poorly constrained and do not take into account probable significant variations in slip rates during the late Cenozoic. Estimates of 0.01 to 0.02 mm/yr determined at the Robeson Springs trench site for the middle to late Quaternary are at the low end of the ranges of late Cenozoic slip rates. Because we infer only one Holocene event and because our estimates of average minimum recurrence intervals range from 25 to 100 ka, we have no way of judging whether the Holocene slip rate or recurrence interval differs from our estimates for the middle to late Quaternary, as Wallace (1984) has suggested for the Great Basin and as Machette and others (1987, this volume) have suggested for the Wasatch fault. Our dating control is too imprecise to determine whether there has been a significant change in slip rates during the late Cenozoic. If there is a difference in rates, rates on the Morgan fault for the middle to late Quaternary are probably lower than those for earlier periods.

CONCLUSIONS

Quaternary surface displacements have occurred on the Morgan fault, a north-trending, range-bounding fault in the back valleys of the Wasatch Mountains. Colluvial deposits having an age of 200 to 400 ka, estimated from amino acid ratios on gastropods found in correlative deposits, are displaced a minimum of 4 m at the Robeson Springs trench site on the central section of the fault. These data yield a minimum average middle to late Pleistocene slip rate of 0.01 to 0.02 mm/yr. The tilting of late Cenozoic erosion surfaces and estimates of the displacement of a Cenozoic fanglomerate along the northern section of the fault suggest that these rates are at the low end of a range of estimates of the average late Cenozoic slip rate on the Morgan fault.

Radiocarbon dates of 8.3 and 9.1 ka on bog deposits underlying displaced alluvial units show that the most recent surface-displacement event (approximately 1 m) occurred during the Holocene. The colluvial stratigraphy in trench M4 is interpreted as showing that earlier individual surface displacements on the fault at this location have also been small (0.5–1.0 m). Because this trench site is near the end of the central segment of the fault, this estimate of individual surface displacements may be somewhat smaller than the maximum surface displacement, which is commonly used to estimate paleoearthquake magnitudes. Empirical relationships between surface displacement and rupture length, however, suggest results that are consistent with the trench data. Maximum surface displacements of 0.5 to 1.0 m are estimated for rupture of the entire 16-km-long fault from the empirical relationships of Bonilla and others (1984). These data suggest that paleoearthquakes in the magnitude range 6½ to 7 have occurred on the Morgan fault.

REFERENCES CITED

Allison, L.E., and Moodie, C.D., 1965 Carbonate, *in* Black, C.A., Methods of soil analysis, pt. 2, Chemical and microbiological properties: Madison, Wis., American Society of Agronomy, p. 1379–1396.

Anderson, L.W., and Miller, D.G., 1979, Quaternary fault map of Utah: Long Beach, Calif., Fugro, Inc., 39 p., scale 1:1,000,000.

Arabasz, W.J., Smith, R.B., and Richins, W.D., 1980, Earthquake studies along the Wasatch Front, Utah—Network monitoring, seismicity, and seismic hazards: Bulletin of the Seismological Society of America, v. 70, p. 1479–1500.

Armstrong, R.L., 1968, Sevier orogenic belt in Nevada and Utah: Geological Society of America Bulletin, v. 79, p. 429–459.

Barnes, D.A., Clark, P.U., and Nelson, A.R., 1986, Preliminary aminostratigraphy of Mississippi Valley loess: American Quaternary Association Biennial Meeting, 9th, Champaign-Urbana, Ill., 1986, Programs and Abstracts, p. 117.

Birkeland, P.W., 1984, Soils and geomorphology: New York, Oxford University Press, 372 p.

Bonilla, M.G., Mark, R.K., and Lienkaemper, J.J., 1984, Statistical relations among earthquake magnitude, surface rupture length, and surface fault displacement: Bulletin of the Seismological Society of America, v. 74, p. 2379–2411.

Bromfield, C.S., and Crittenden, M.D., Jr., 1971, Geologic map of the Park City East Quadrangle, Summit and Wasatch Counties, Utah: U.S. Geological Survey Geologic Quadrangle Map GQ–852, scale 1:24,000.

Bryant, B., 1984, Reconnaissance geologic map of the Precambrian Farmington Canyon Complex and surrounding rocks in the Wasatch Mountains between Ogden and Bountiful, Utah: U.S. Geological Survey Miscellaneous Investigations Map I–1447, scale 1:50,000.

Bull, W.B., 1977, The alluvial-fan environment: Progress in Physical Geography, v. 1, p. 222–270.

Carver, R.E., ed., 1971, Procedures in sedimentary petrology: New York, Wiley-Interscience, 653 p.

Colman, S.M., Choquette, A.F., and Hawkins, F.F., 1988, Physical, soil, and paleomagnetic stratigraphy of the upper Cenozoic sediments in Fisher Valley, southeastern Utah: U.S. Geological Survey Bulletin 1686, 33 p.

Coody, G.L., 1957, Geology of the Durst Mountain-Huntsville area: Salt Lake City, University of Utah, unpublished M.Sci. thesis, 63 p.

Dixon, W.J., 1965, Extraneous values, *in* Black, C.A., Methods of soil analysis, pt. 2, Chemical and microbiological properties: Madison, Wisc., American Society of Agronomy, p. 43–49.

Eardley, A.J., 1944, Geology of the north-central Wasatch Mountains, Utah: Geological Society of America Bulletin, v. 55, p. 819–894.

———1955, Tertiary history of north central Utah, *in* Eardley, A.J., ed., Tertiary and Quaternary geology of the eastern Bonneville Basin: Utah Geological Society Guidebook to the Geology of Utah, no. 10, p. 37–44.

Funk, J.W., 1976, Climatic and tectonic effects on alluvial fan systems, Birch Creek Valley, east central Idaho: Lawrence, University of Kansas, unpublished Ph.D. thesis, 246 p.

Gilbert, G.K., 1928, Studies of Basin and Range structure: U.S. Geological Survey Professional Paper 153, 89 p.

Gile, L.H., Peterson, F.F., and Grossman, R.B., 1966, Morphological and genetic sequences of carbonate accumulation in desert soils: Soil Science, v. 101, p. 347–360.

Guthrie, R.L., and Witty, J.E., 1982, New designations for soil horizons and layers and the new Soil Survey Manual: Soil Science Society of America Journal, v. 46, p. 443–444.

Hanks, T.C., Bucknam, R.C., Lajoie, K.R., and Wallace, R.E., 1984, Modification of wave-cut and faulting-controlled landforms: Journal of Geophysical Research, v. 89, no. B7, p. 5771–5790.

Harden, D.R., Biggar, N.E., and Gillam, M.L., 1985, Quaternary deposits and soils in and around Spanish Valley, Utah, *in* Weide, D.L., ed., Soils and Quaternary geology of the southwestern United States: Geological Society of America Special Paper 203, p. 43–64.

Harden, J.W., and Taylor, E.M., 1983, A quantitative comparison of soil development in four climatic regimes: Quaternary Research, v. 20, no. 3, p. 342–359.

Hopkins, D.L., 1982, A structural study of Durst Mountain and the north central Wasatch Mountains, Utah: Salt Lake City, University of Utah, unpublished M.Sci. thesis, 50 p.

Hopkins, D.L., and Bruhn, R.L., 1983, Extensional faulting in the Wasatch Mountains, Utah [abs.]: Geological Society of America Abstracts with Programs, v. 15, no. 5, p. 402.

Jackson, M.L., 1956, Soil chemical analysis, advanced course: Madison, University of Wisconsin, Department of Soil Science, unpublished laboratory manual, 656 p.

Lamerson, P.R., 1982, Fossil Basin area and its relation to the Absaroka thrust system, *in* Powers, R.B., ed., Geological studies of the Cordilleran thrustbelt: Denver, Colo., Rocky Mountain Association of Geologists, p. 279–340.

Machette, M.N., 1985a, Calcic soils of the southwestern United States, *in* Weide, D.L., ed., Soils and Quaternary geology of the southwestern United States: Geological Society of America Special Paper 203, p. 1–23.

———1985b, Late Cenozoic geology of the Beaver Basin, southwestern Utah: Brigham Young University Studies in Geology, v. 32, pt. 1, p. 19–37.

McKee, M.E., and Arabasz, W.J., 1982, Microearthquake studies across the Basin and Range-Colorado Plateau transition in central Utah, *in* Nielson, D.L., ed., Overthrust Belt of Utah: Utah Geological Association Publication 10, p. 137–149.

Miller, G.H., and Hare, P.E., 1980, Amino acid geochronology: Integrity of the carbonate matrix and potential of molluscan fossils, *in* Hare, P.E., Hoering, T.C., and King, K., Jr., eds., Biogeochemistry of amino acids: New York, John Wiley, p. 415–443.

Miller, G.H., McCoy, W.D., and Nelson, A.R., 1982, Environmental controls in the amino acid racemization rate from continental-interior deposits [abs.]: Geological Society of America Abstracts with Programs, v. 14, no. 7, p. 565.

Mullens, T.E., and Laraway, W.H., 1973, Geologic map of the Morgan 7.5-minute quadrangle, Morgan County, Utah: U.S. Geological Survey Miscellaneous Field Studies Map MF–318, scale 1:24,000.

Nakata, J.K., Wentworth, C.M., and Machette, M.N., 1982, Quaternary fault map of the Basin and Range and Rio Grande Rift provinces, Western United States: U.S. Geological Survey Open-File Report 82–579, scale 1:2,500,000.

Naeser, C.W., Bryant, B., Crittenden, M.D., and Sorenson, M.L., 1983, Fission-track ages of apatite in the Wasatch Mountains, Utah—An uplift study, *in* Miller, D.M., Todd, V.R., and Howard, K.A., eds., Tectonic and stratigraphic studies in the eastern Great Basin: Geological Society of America Memoir 157, p. 29–36.

Nelson, A.R., and Martin, R.A., 1982, Seismotectonic study for Soldier Creek Dam, Central Utah Project: Denver, Colo., Seismotectonic Report 82–1, Engineering and Research Center, U.S. Bureau of Reclamation, 115 p.

Nelson, A.R., and Van Arsdale, R.B., 1986, Recurrent late Quaternary movement on the Strawberry normal fault, Basin and Range-Colorado Plateau transition zone, Utah: Neotectonics, v. 1, p. 1–30.

Nelson, A.R., Madole, R.F., Evanoff, E., Piety, L.A., and Scott, G.R., 1984, Quaternary paleotemperature estimates using amino-acid ratios measured on terrestrial gastropods from fluvial sequences in Colorado: American Quaternary Association Biennial Meeting, 8th, Boulder, Colo., 1984, Program and Abstracts, p. 92.

Royse, F., Jr., Warner, M.A., and Reese, D.L., 1975, Thrust belt structural geometry and related stratigraphic problems,

Wyoming-Idaho-northern Utah, *in* Bolyard, D.W., ed., Symposium on deep drilling frontiers of the central Rocky Mountains: Denver, Colo., Rocky Mountain Association of Geologists, p. 41–54.

Schick, R.B., 1955, Geology of the Morgan-Heneter area, Morgan and Summit Counties, Utah: Salt Lake City, University of Utah, unpublished M.Sci. thesis, 54 p.

Scott, W.E., Shroba, R.R., and McCoy, W.D., 1982, Guidebook for the 1982 Friends of the Pleistocene, Rocky Mountain Cell, field trip to Little Valley and Jordan Valley, Utah: U.S. Geological Survey Open-File Report 82–845, 58 p.

Scott, W.E., McCoy, W.D., Shroba, R.R., and Rubin, M., 1983, Reinterpretation of the exposed record of the last two cycles of Lake Bonneville, western United States: Quaternary Research, v. 20, p. 241–265.

Schwartz, D.P., and Coppersmith, K.J., 1984, Fault behavior and characteristic earthquakes—Examples from the Wasatch and San Andreas fault zones: Journal of Geophysical Research, v. 89, no. B7, p. 5681–5698.

Shroba, R.R., 1982, Soil B-horizon properties as age indicators for late Quaternary deposits along the Wasatch Front, north-central Utah [abs.]: Geological Society of America Abstracts with Programs, v. 14, no. 4, p. 233.

Smith, R.B., and Bruhn, R.L., 1984, Intraplate extensional tectonics of the eastern Basin-Range—Inferences on structural style from seismic reflection data, regional tectonics, and thermal-mechanical models of brittle-ductile deformation: Journal of Geophysical Research, v. 89, no. B7, p. 5733–5762.

Sullivan, J.T., Nelson, A.R., LaForge, R.C., Wood, C.K., and Hansen, R.A., 1988, Central Utah regional seismotectonic study for USBR dams in the Wasatch Mountains: Denver, Colo., Seismotectonic Report 88–5, U.S. Bureau of Reclamation, 269 p.

Swan, F.H., III, Schwartz, D.P., and Cluff, L.S., 1980, Recurrence of moderate- to large-magnitude earthquakes produced by surface faulting on the Wasatch fault zone, Utah: Bulletin of the Seismological Society of America, v. 70, p. 1431–1462.

Swan, F.H., III, Hanson, K.L., Schwartz, D.P., and Black, J.H., 1983, Study of earthquake recurrence intervals on the Wasatch fault, Utah: San Francisco, Calif., Woodward-Clyde Consultants, 8th semi-annual technical report to the U.S. Geological Survey under contract 14–08–0001–19842, 36 p.

Walkley, A., and Black, I.A., 1934, An examination of the Degtjareff method for determining soil organic matter, and a proposed modification of the chromic acid titration method: Soil Science, v. 34, p. 29–38.

Wallace, R.E., 1984, Patterns and timing of late Quaternary faulting in the Great Basin province and relation to some regional tectonic features: Journal of Geophysical Research, v. 89, no. B7, p. 5763–5769.

Wehmiller, J.F., 1977, Amino acid studies of the Del Mar, California, midden site: Apparent rate constants, ground temperature models, and chronological implications: Earth and Planetary Science Letters, v. 37, p. 184–196.

———1982, A review of amino acid racemization studies in Quaternary mollusks—Stratigraphic and chronologic applications in coastal and interglacial sites, Pacific and Atlantic coasts, United States, United Kingdom, Baffin Island, and tropical islands: Quaternary Science Reviews, v. 1, p. 82–120.

Wehmiller, J.F., and Belknap, D.F., 1982, Amino acid age estimates, Quaternary Atlantic coastal plain—Comparison with U-series dates, biostratigraphy, and paleomagnetic control: Quaternary Research, v. 18, no. 3, p. 311–336.

West, M.W., 1986, Quaternary extensional reactivation of the Darby and Absaroka thrusts, southwestern Wyoming and north-central Utah [abs.]: Geological Society of America Abstracts with Programs, v. 18, no. 5, p. 422.

Williams, J.S., Willard, A.D., and Parker, V., 1962, Recent history of Bear Lake Valley, Utah-Idaho: American Journal of Science, v. 260, p. 24–36.

Williams, K.M., and Smith, G.G., 1977, A critical evaluation of the application of amino acid racemization to geochronology and geothermometry: Origins of Life, v. 8, p. 91–144.

Zoback, M.L., 1983, Structure and Cenozoic tectonism along the Wasatch fault zone, Utah, *in* Miller, D.M., Todd, V.R., and Howard, K.A., eds., Tectonic and stratigraphic studies of the eastern Great Basin: Geological Society of America Memoir 157, p. 3–27.

CONTENTS

	Page
Abstract	J1
Introduction	1
Acknowledgments	1
Geologic Setting	2
Structure	2
Quaternary Deposits	4
Scarp and Mountain-Front Morphology	4
Age of Faulted Deposits	J4
Fault-Displacement History	6
Slip Rates and Recurrence	10
Relationship to the East Cache Fault	10
Conclusions	12
References Cited	12

ILLUSTRATIONS

	Page
FIGURES 1, 2. Maps showing:	
1. Location of the southern Cache Valley region	J2
2. Generalized Quaternary geology of the area north of James Peak	3
3. Plot of rubification versus nonarid soil development indices for soils near the trench site	6
4. Log of the eastern wall of the trench across the scarp of the James Peak fault	8

TABLE

	Page
TABLE 1. Selected properties of soils on the northern flank of James Peak, north-central Utah	J7

ASSESSMENT OF REGIONAL EARTHQUAKE HAZARDS
AND RISK ALONG THE WASATCH FRONT, UTAH

LATE QUATERNARY HISTORY OF THE JAMES PEAK FAULT, SOUTHERNMOST CACHE VALLEY, NORTH-CENTRAL UTAH

By ALAN R. NELSON[1] and J. TIMOTHY SULLIVAN[2]

ABSTRACT

The James Peak normal fault is marked by a northeasterly trending 7-m-high scarp that cuts outwash fans of Bull Lake age on the northern flank of James Peak. The occurrence of two surface-faulting events, each having about 2 m of displacement, on the fault in the last 140 ka indicates a late Quaternary slip rate of about 0.03 mm/yr. The degree of soil development on the outwash fans and on fault-related colluvial wedges provides only limited control on the timing of events. Average event recurrence intervals are at least 50,000 years, but recurrence may be nonuniform, and the most recent event may be as young as 30 ka. The amount of displacement during each event suggests that surface breaks may have extended north and ruptured the southern portion of the East Cache fault. If so, the James Peak fault may be a westerly splay of the East Cache fault rather than a separate valley-bounding fault.

INTRODUCTION

Comparing Quaternary fault-slip rates is a widely used means of assessing the earthquake potential of geologically young faults. The Wasatch fault poses the greatest hazard to population centers in north-central Utah because its slip rate may be several times greater and its recurrence of surface faulting 3 to 10 times greater than those of other faults in the Wasatch Mountain region (Schwartz and Coppersmith, 1984). However, other faults in the region may still pose a significant earthquake hazard, although their histories and slip rates have been documented in only a few cases (Nelson and VanArsdale, 1986; Sullivan and Nelson, this volume; McCalpin and others, this volume). Anderson and Miller (1979) and Nakata and others (1982) mapped a number of faults on which significant Quaternary slip had occurred, but other faults in the eastern Wasatch Mountains—some displaying late Quaternary (younger than 125 ka) slip—have only recently been identified (Sullivan and Nelson, 1983; Sullivan and others, 1988). One such fault, the James Peak normal fault, is marked by scarps on bedrock, outwash fans, and other alluvium on the northern flank of James Peak and extends west-southwest from the southern tip of the East Cache fault in southern Cache Valley almost to Ogden Valley (fig. 1). We will summarize trench data used to estimate a slip rate on the James Peak fault and suggest how surface breaks on the fault may relate to ruptures on the adjacent East Cache fault, which is recognized as posing a significant earthquake hazard (Swan and others, 1983).

ACKNOWLEDGMENTS

This study was part of a regional seismotectonic study for the assessment of seismic hazards to large dams in the Wasatch Mountains and was supported by the U.S. Bureau of Reclamation (Sullivan and others, 1988). The staff of the Bonneville Construction Office of the U.S. Bureau of Reclamation in Provo, Utah, provided considerable logistical support. We especially thank Karl A. Jensen of Tremonton, Utah, for permission to excavate on his property. Edward Baltzer (U.S. Bureau of Reclamation, Denver) assisted in mapping and logging the trench. Soil analyses by Rolf Kihl (Institute for Arctic and Alpine Research, University of Colorado) are appreciated. Dean Ostenaa (U.S. Bureau of Reclamation, Denver) reviewed earlier drafts of the manuscript, and Anthony Crone (U.S. Bureau of Reclamation, Denver) and James McCalpin (Utah State University) substantially improved this draft.

Manuscript approved for publication November 20, 1990.

[1]Now at U.S. Geological Survey, Mail Stop 966, Federal Center, Denver, CO 80225.

[2]Now at Yucca Mountain Project Office, Department of Energy, P.O. Box 539, Las Vegas, NV 89109.

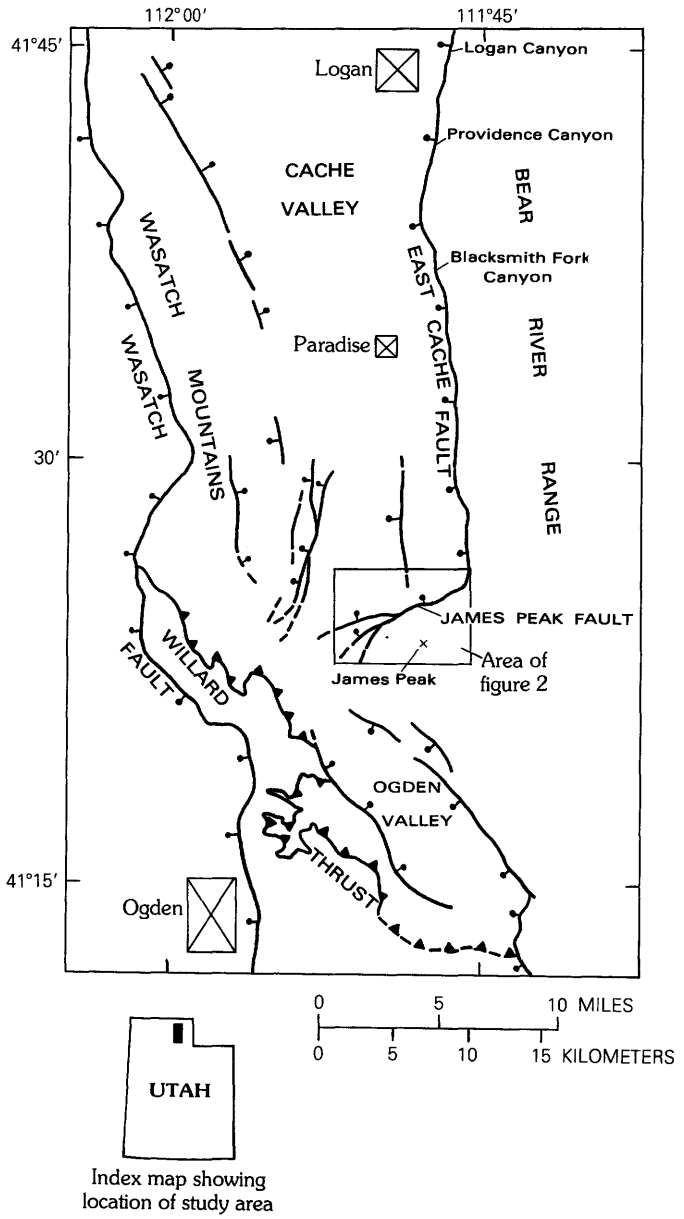

FIGURE 1.—Location of the southern Cache Valley region. Selected late Cenozoic normal faults (modified from Crittenden and Sorensen, 1985a, b) are indicated by heavy lines (bar and ball on downthrown side), dashed where approximately located. The edge of the Willard thrust fault is indicated by sawteeth on the overriding plate.

GEOLOGIC SETTING

Our review of 1:58,000-scale color infrared and 1:15,000- to 1:40,000-scale black-and-white aerial photographs shows that the scarp of the James Peak normal fault is the only previously unreported fault scarp on unconsolidated deposits in the eastern Wasatch Mountains. The scarp marks the southern edge of an unnamed structural and topographic basin between James Peak and Middle Mountain (fig. 2) at the southern end of Cache Valley and 5 km north of Ogden Valley (fig. 1). The basin, about 3 km wide and 9 km long, contains Tertiary Salt Lake Formation covered by Quaternary colluvium and alluvium (Blau, 1975; Hintze, 1980). The basin is bounded on the north by highly dissected Paleozoic limestones, shales, dolomites, and quartzites and on the south by Proterozoic and Paleozoic orthoquartzites, argillites, and volcanic rocks that make up the highlands around James Peak (King, 1965; Blau, 1975; Davis, 1983).

STRUCTURE

Cenozoic structural basins termed "back valleys" occur throughout the Wasatch Mountains east of the Wasatch fault (Gilbert, 1928). Cache Valley is a late Cenozoic structural and topographic basin, bounded by normal faults, that developed in the Cache allocthon, the upper plate of the Willard (fig. 1) and Woodruff thrusts (Bjorkland and McGreevy, 1971; Crittenden, 1972; Hintze, 1980). The East Cache fault, the principal fault in the valley, is marked by triangular facets cut on the east-dipping Proterozoic and Paleozoic rocks at the western base of the Bear River Range. Geophysical data (Stanley, 1972; Peterson, 1974) compiled by Zoback (1983) suggest that the upper Cenozoic basin fill in the valley is 1.7 to 2.1 km thick. A seismic reflection profile across the East Cache fault shows that Cache Valley is an asymmetric basin, deepest on the eastern margin adjacent to the East Cache fault (Smith and Bruhn, 1984). Consistent east dips of reflectors in the late Tertiary basin fill suggest a listric geometry for the East Cache fault, although the fault plane cannot be resolved from the available data.

The James Peak normal fault, at the base of the escarpment in Proterozoic and Paleozoic rocks on the northern side of James Peak (fig. 2), marks the southern boundary of the east-west-trending basin at the southern end of Cache Valley. Isolated outcrops of Paleozoic sedimentary rocks suggest that the Salt Lake Formation may be less than 100 m thick in the basin, an indication

FIGURE 2.—Generalized Quaternary geology of the area north of ▶ James Peak. The James Peak fault scarp (hachures point down the slope of the scarp) trends northeast-southwest in the middle of the figure. An f following the unit symbol indicates that the surficial unit has alluvial fan morphology. A slash within a unit symbol shows a deposit of multiple genesis (for example, Qa/c indicates Quaternary alluvium and colluvium). Qay deposits are primarily of Holocene and latest Pinedale age (younger than 15 ka). Most Qao (Qaof) units are pre-Pinedale (older than 30 ka). Qa and Qc units are undifferentiated on the basis of age. Qc/Tsl marks thin deposits of colluvium and alluvium over Tertiary Salt Lake Formation. Most faults in bedrock south of the James Peak fault scarp are from Blau (1975). Many units (such as Qablf) contain smaller areas of younger and older deposits.

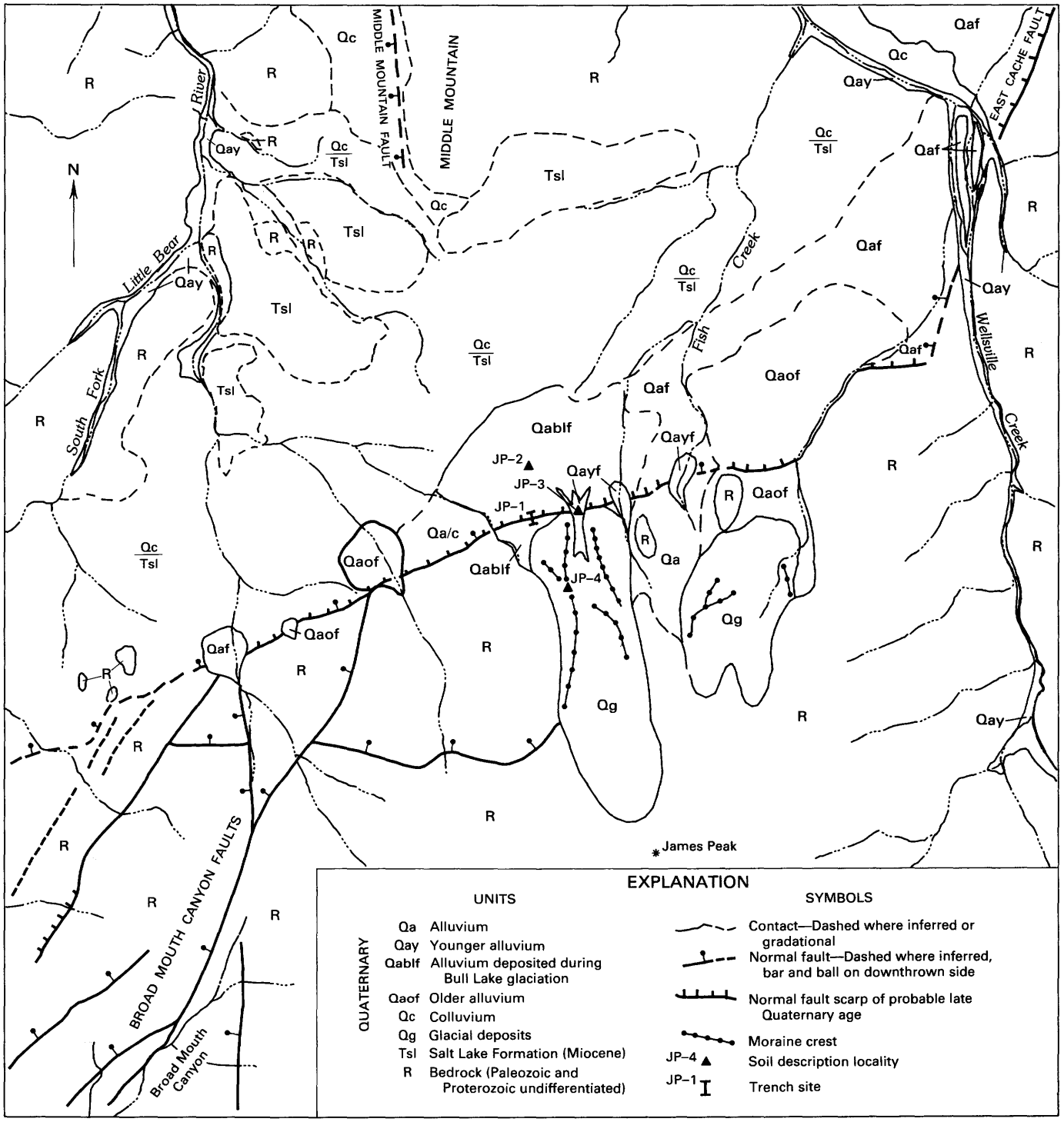
N
Little Bear River
South Fork
MIDDLE MOUNTAIN FAULT
MIDDLE MOUNTAIN
Fish Creek
Wellsville Creek
EAST CACHE FAULT
BROAD MOUTH CANYON FAULTS
Broad Mouth Canyon
James Peak
JP-1
JP-2
JP-3
JP-4
Qa/c
Qaof
Qablf
Qayf
Qa
Qg
Qaf
Qay
Qc
Qc/Tsl
Tsl
R
EXPLANATION
UNITS
QUATERNARY
Qa Alluvium
Qay Younger alluvium
Qablf Alluvium deposited during Bull Lake glaciation
Qaof Older alluvium
Qc Colluvium
Qg Glacial deposits
Tsl Salt Lake Formation (Miocene)
R Bedrock (Paleozoic and Proterozoic undifferentiated)
SYMBOLS
Contact—Dashed where inferred or gradational
Normal fault—Dashed where inferred, bar and ball on downthrown side
Normal fault scarp of probable late Quaternary age
Moraine crest
Soil description locality
Trench site
0 1 MILE
0 1 KILOMETER

that cumulative subsidence is much less here than it is in Cache Valley. North of the basin, north-dipping lower Paleozoic rocks are cut by north-trending normal faults, including the Middle Mountain fault. Near Broadmouth Canyon on the western side of James Peak, Blau (1975) mapped north-trending normal faults having estimated displacements of about 1,500 m that are about on trend with the Middle Mountain fault. Bedrock escarpments mark these north-trending faults, but north-trending scarps are not developed on the sediments in the basin. No east-west-trending faults are mapped along the northern edge of the basin, where fluvial dissection has produced extensive outcrops of the Salt Lake Formation. Thus, the basin appears to be a shallow half-graben connecting the larger and deeper grabens at the southern end of Cache Valley and the northwestern end of Ogden Valley (Zoback, 1983; Sullivan and others, 1988).

QUATERNARY DEPOSITS

Quaternary deposits in the basin consist of locally derived, bouldery colluvial deposits (unit Qc, fig. 2) in the central and northern portions that thicken and are interbedded with fan alluvium to the south. Alluvial fan deposits (Qaf), including two large, bouldery outwash fans (Qaof and Qablf) derived from the quartzites exposed on James Peak, occur along the southern edge of the basin. These fans become larger and appear to thicken from west to east; if so, this thickening may indicate downfaulting, tilting, or deeper erosion of the eastern part of the basin near Wellsville Creek and the East Cache fault. Sandy till (Qg) makes up the high, steep moraines built by the glaciers that deposited the outwash fans in two of the unnamed drainages on the northern flank of James Peak.

SCARP AND MOUNTAIN-FRONT MORPHOLOGY

Mountain-front slopes developed on bedrock along the James Peak fault are steep, especially on James Peak (26°), despite the fact that this side of the peak has been extensively eroded by glaciers. On the lower half of the mountain, eroded spurs (ridge crests) are faceted. Three breaks in slope on the spurs, as well as the north-facing faceted spur (25° slope) just west of Wellsville Creek at the eastern end of the basin (fig. 2), suggest a history of recurrent Quaternary displacements on the fault (for example, Gilbert, 1928; Hamblin, 1976). To the east, the mountain front is lower and more dissected and has gentler slopes, although here, as elsewhere, the steepest facets are at the base of the slopes along the fault. However, by comparison, the facets along the fault are smaller, less continuous, and less steep than those along the East Cache and Wasatch faults. The short (less than 7 km) mountain front along the James Peak fault makes quantitative comparisons with other mountain fronts (for example, Bull and MacFadden, 1977) of little value. Overall, the mountain-front morphology of the northern flank of James Peak suggests that Quaternary slip rates are much lower here than they are on major nearby faults such as the East Cache and Wasatch faults.

The James Peak fault scarp is expressed primarily as a scarp on bedrock over much of its length, but, along the central part of the fault, the scarp offsets alluvial and colluvial deposits and the large alluvial fans (units Qablf and Qaof, fig. 2) issuing from the glaciated drainages on the northern flank of the mountain. The scarp is generally higher (10–30 m) and steeper (20°–35° maximum slope angle) on bedrock (or thin colluvium over bedrock) than it is on fan sediments (1–4 m, 15°–30°). Where the scarp is on alluvium undissected by small drainages, it is uniformly 3 to 4 m high.

An en echelon offset at the eastern end of the scarp forms a junction with the prominent scarp at the southern end of the East Cache fault; the scarps join at about a 110° angle. The eastern half of the scarp is subdued (less than 2 m high, 20° maximum slope angle) where it crosses the apex of the easternmost alluvial fan (Qaof, fig. 2), but the scarp is steeper (20°–25°) in the Cambrian quartzite on the en echelon segment (500 m west of Wellsville Creek). The lower slopes of the Paleozoic limestone and sandstone bedrock facets, 2.7 km to the north on the East Cache fault, are steeper still (25°–30°). Just west of the large alluvial fans, the western half of the scarp is steep (22°–30° maximum slope angle) near the base of dissected facets in quartzite, but, farther west, the scarp is indistinct because the bedrock hills west of James Peak are lower and more rounded than the faceted mountain flanks to the east.

Just south of the western end of the basin, the Broadmouth Canyon normal faults trend about N. 30° E. through low, dissected bedrock hills (Blau, 1975). A major topographic boundary between the western flank of James Peak and the lower hills to the west marks the largest normal fault, which exhibits 1,500 m of throw, that extends into Broadmouth Canyon. One large topographic step (120 m difference in elevation) and several smaller ones (most down to the northwest) (fig. 2) that parallel the largest fault are interpreted as related subsidiary faults.

AGE OF FAULTED DEPOSITS

Our chronology of Quaternary deposits and the scarps bounding or cutting them near James Peak is based on the morphology and relative position of fans, moraines, and scarps and on the data from four soils developed on

deposits in the largest glaciated drainage. Most mapped Quaternary deposits are undifferentiated as to age (fig. 2), but even the oldest are probably no more than a few hundred thousand years old.

The height of topographic scarps along the Broadmouth Canyon faults suggests Pliocene to Quaternary—but not necessarily late Quaternary—displacement. Most of the faults cannot be traced into the Salt Lake Formation in the basin to the north; thus, they appear to be buried by Tertiary sediments. However, in two areas where the Broadmouth Canyon faults meet the James Peak fault, faint lineaments extend into dissected Salt Lake Formation sediments; exposures are not sufficient to resolve the relationships between the lineaments and the faults. Although the Broadmouth Canyon faults may join the James Peak fault, the young scarp on the James Peak fault indicates that the Broadmouth Canyon faults have been displaced by it.

The steep, continuous scarp on the alluvial fans along the central part of the James Peak fault suggests late Quaternary displacement on the fault. However, except for the smallest, youngest fans, which lack scarps where the fault crosses them, fans of significantly different ages (on which to compare scarp heights) were not identified. Topographic profiling across the scarp was difficult because of the thick alder-aspen forest and the soft, loose, organic-rich soil on the surface of the scarp. For this reason, profiling to obtain estimates of displacement and relative age (for example, Bucknam and Anderson, 1979) was not attempted.

Most Quaternary chronology studies in the Rocky Mountain region have divided deposits of the most recent major glaciations between the Bull Lake glaciation and the Pinedale glaciation; older deposits have been designated as pre-Bull Lake (Madole, 1976; Pierce, 1979). These groupings are usually based on relative age data such as relative position in the landform sequence, landform morphology, degree of soil development, and surface-weathering characteristics (Birkeland and others, 1979). Because the data used to subdivide these deposits into relative age groups are usually compared only for sites within a single mountain range or drainage basin, deposits in different ranges or basins elsewhere in the region that have been assigned to the same relative age group may not be the same age (Pierce, 1979; Porter and others, 1983). Colman and Pierce (1981) have identified moraines in Idaho probably dating from about 60 to 70 ka, intermediate in age between the accepted ages of 15 and 25 ka for most Pinedale deposits and 130 and 150 ka for Bull Lake deposits. Thus, deposits placed in the Bull Lake relative age group in some drainages might be as young as 60 to 70 ka. Following Pierce (1979) and Porter and others (1983), we use "Pinedale" and "Bull Lake" to name the more recent major Quaternary glaciations in the Rocky Mountains and assume ages for the deposits of each glaciation by comparing our soils data with similar data from numerically dated glacial deposits (Pierce and others, 1976; Porter and others, 1983; Colman and Pierce, 1986).

Soil development indices are an objective way of comparing the degrees of development of soils (Birkeland, 1984). The soil properties that vary the most systematically with time in the Rocky Mountain region include horizon thickness, color, texture, and calcium carbonate accumulation (Shroba and Birkeland, 1983). Ways to express changes in these properties include simple, widely used soil development indices (for example, depth to base of observable oxidized parent material and increase of maximum percentage of clay), profile summations (Machette, 1985), and the indices of Harden (1982) and Harden and Taylor (1983). Harden's indices refine those of Bilzi and Ciolkosz (1977) and incorporate, in a quantitative way, most of the concepts represented by development indices used previously in the Western United States. The profile development index (Harden, 1982) (fig. 3) is particularly useful because the degree of development of all selected properties can be objectively summarized by a single value.

We followed Harden and Taylor (1983) in using *X–Y* plots to compare indices for the soils that we described and sampled near the trench site (table 1, fig. 2) with those for soils of known age elsewhere in the Wasatch Mountains (fig. 3). Soils on a lateral moraine (JP–4) and on the outwash fan in front of it (JP–2) were described to determine whether the deposits were Bull Lake or Pinedale. For comparison, a Holocene soil (JP–3) was described on very coarse, bouldery alluvium in a narrow channel where the moraines are narrowly breached. The thick soil developed on the colluvial wedges in the trench (JP–1) was also described to help estimate the age of the wedges. Soils JP–1 and JP–2 are developed in deposits of more than one age. To help estimate the time interval represented by the degree of soil development in each of the younger deposits as well as by the degree of development of the whole soil, we calculated soil indices for each depositional unit of these two soils (table 1, fig. 3).

Soil development indices (fig. 3) calculated by using field and laboratory data show that the outwash gravels (unit Qablf, fig. 2) in the lower parts of soils JP–1 and JP–2 are in relative age group (RAG) 2 and are probably chronocorrelative with outwash from the Bull Lake glaciation. Although it is possible that this outwash significantly postdates the last interglacial (about 125 ka) (discussed above), the reddish clay-rich argillic horizons of these soils suggest that they began forming about 140 ka.

Soil JP–4 on the steep, high, left-lateral moraine (fig. 2) is poorly developed, and its soil indices are lower than

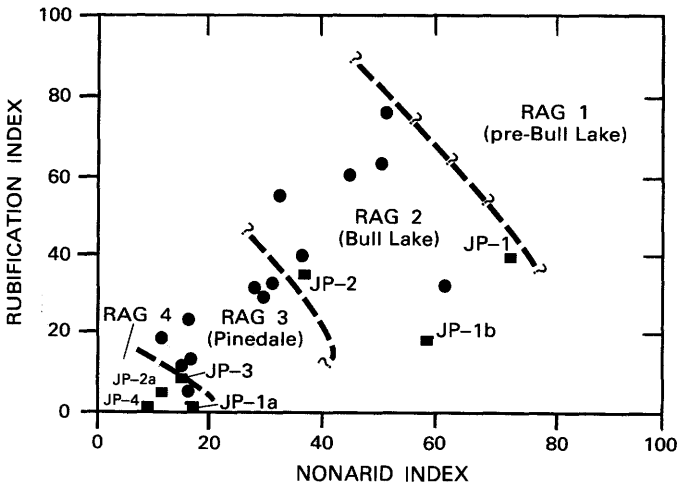

FIGURE 3. —Rubification versus nonarid soil development indices (solid squares) (after Harden, 1982; Harden and Taylor, 1983) for soils near the trench site (fig. 2, table 1). Point JP–1a is a plot of indices for the upper 83 cm of soil JP–1 (unit 4, fig. 4), JP–1b is for the upper 205 cm of the same soil (units 3 and 4), JP–2a is for the upper 53 cm of soil JP–2, and JP–1, JP–2, JP–3, and JP–4 are indices for the entire profiles. Dashed lines divide the diagram into four relative age groups (RAG's) defined by indices from soils of known age (marked by solid circles) elsewhere in the eastern Wasatch Mountains (Nelson and Krinsky, 1982; Sullivan and others, 1988, p. 54). Question marks indicate that we do not know if the dashed lines forming approximate boundaries between RAG's can be extended, because we have no development indices for soils in the areas beyond the dashed lines. Comparing the degree of development of soils in these RAG's with that of soils on glacial deposits elsewhere in the Rocky Mountain region (Madole, 1976; Pierce, 1979; Shroba and Birkeland, 1983; Colman and Pierce, 1986) suggests that soils in RAG 4 are of Holocene age or a little older (younger than 12 ka), those in RAG 3 correlate with glacial deposits of Pinedale age (15–25 ka), those in RAG 2 may be of Bull Lake age (130–150 ka), and those in RAG 1 are older than Bull Lake.

the indices for most soils on tills and outwash of the Pinedale glaciation (fig. 3). However, the till on which the soil is developed is derived entirely from quartzites, which do not weather easily. In addition, the steep slopes and narrow crests of the moraines indicate that this soil may have been partially stripped by erosion on the moraine crest. Thus, both because soil development proceeds so slowly in quartzite-derived tills and because of erosion, the moraine is probably much older than the soil indices suggest.

The bouldery surfaces, narrow crests, and steep slopes of the moraines on the northern flank suggest that they were built during the Pinedale glaciation, but the indices for soils developed on the outwash apron in front of the moraines suggest an older age, probably before the last interglacial (more than 125 ka). The most probable interpretation of the age of the moraines is that the Pinedale and Bull Lake glaciers extended the same distance downvalley but that, during the Pinedale glaciation, high Bull Lake lateral moraines protected all but the center of the fan surfaces from burial by younger outwash. Thus, the outwash fans that are displaced by the James Peak fault (Qablf and Qaof, fig. 2) are probably primarily of Bull Lake age (130–150 ka).

Soil JP–3 and the uppermost parts of JP–1 (JP–1a) and JP–2 (JP–2a) are only weakly developed and fall in RAG 4 (fig. 3). Cambic and weak argillic B horizons have developed in the mixed fine-grained sheetwash and loess deposits in the upper parts of soils JP–1 and JP–2. Soil JP–3 has a weak argillic horizon but no increase in hue or chroma to bright reddish colors (table 1). Soil indices suggest a Holocene or very latest Pleistocene age for this soil, and its position near the main stream channel of the largest drainage basin on the northern flank also suggests that it is of Holocene (probably late Holocene) age. Argillic horizon development in deposits this young is probably caused by a locally high rate of eolian dust influx (fine silt as well as clay) from the large areas of exposed Bonneville lake sediments in southern Cache Valley. Shroba (1980) has also described argillic horizons from deposits of early to middle Holocene age along the Wasatch fault.

FAULT-DISPLACEMENT HISTORY

To estimate the sizes, number, and ages of the more recent surface-displacement events on the James Peak fault, a single trench was excavated across the 7-m-high scarp on the outwash fan 200 m west of the left-lateral moraine (fig. 2). Dense aspen forest and soft soils prevented access to all other promising trench sites. The trench exposed white, coarse, sandy, quartzite-derived outwash (unit 1, fig. 4) on which was developed a reddish argillic horizon (unit 1bB, fig. 4) overlain by bouldery, silty colluvial wedges (unit 2, fig. 4). The wedges were overlain by silty colluvial units (units 3 and 4, fig. 4) marked by thick cambic and argillic B horizons. Despite the slumping and raveling of the very loose, unconsolidated outwash in the lower trench walls, we were able to expose the fault zone and former free face of the scarp at the southern end of the trench. A topographic profile across the scarp indicates that the fan has been displaced about 4.2 +0.6/−0.2 m at this site. The stratigraphic relations, unit contacts, lithologies of the outwash and the colluvial wedges, and soils developed on them do not clearly show whether one event of about 4-m displacement or two events of about 2-m displacement occurred on the same fault in the trench. As we will discuss later, we favor a two-event interpretation.

On the basis of regional correlation of map and trench units as suggested by the soil development indices of figure 3, we infer the following sequence of events:

TABLE 1.—*Selected properties of soils on the northern flank of James Peak, north-central Utah*

Profile	Trench log unit	Horizon[1]	Average depth (cm)	Parent material	Munsell dry color	Estimated percentage by volume			Percentage by weight[2]			Organic matter[3] (percent)
						Pebbles (0.2–8 cm)	Cobbles (8–25 cm)	Boulders (>25 cm)	Sand (2–0.5 mm)	Silt (50–2μm)	Clay (<2 μm)	
JP–1	4b	A1	0–10	Colluvium-loess	7.5YR 2/2	10	2	0	20	57	23	9.4
	4b	A2	10–46	.....do.....	7.5YR 3/2	10	2	0	22	54	24	8.8
	4a	Bw	46–83	.....do.....	7.5YR 5/3	10	5	0	28	51	21	3.2
	3bB	2Bt1	83–100	.....do.....	7.5YR 5/4	10	5	0	26	53	21	2
	3Ba	2Bt2	100–205	.....do.....	7.5YR 6/4	25	15	0	28	48	24	.7
	2	3Cox/3Bt	205–248	Scarp colluvium	7.5YR 7/4	20	20	2	33	45	23	.6
	1bB	4Bt	248–278	Outwash	5YR 4/6	30	30	10	54	18	28	.3
	1	4Cox	248–390+	.....do.....	7.5YR 7/3	30	30	10	90	8	3	.2
Extra samples[4]	2b	3C	260	Scarp colluvium	7.5YR 7/4	10	15	25	36	45	19	.9
	2a	3C	355	.....do.....	7.5YR 6/4	10	20	20	21	39	40	.4
JP–2		Ap	0–10	Sheetwash-loess	10YR 6/3	20	25	0	29	52	19	5.2
		A	10–20	.....do.....	7.5YR 6/4	20	25	0	28	52	20	3.7
		Bt	20–53	.....do.....	7.5YR 6/4	20	25	0	37	37	26	1.4
		2Bt	53–85	Outwash	2.5YR 4/6	50	25	0	72	17	11	.6
		2BC	85–114	.....do.....	5YR 7/4	50	25	0	88	7	5	.2
		2Cox	114–136+	.....do.....	5YR 7/4	40	35	1	84	11	5	.3
JP–3		A1	0–16	Loess-alluvium	7.5YR 4/3	15	20	25	35	53	12	13.4
		A2	16–41	.....do.....	7.5YR 5/3	15	20	25	41	41	19	5.2
		Bt	41–85	.....do.....	7.5YR 5/4	15	20	25	63	27	10	1.2
		2C	85–132+	Alluvium	7.5YR 7/3	25	20	30	82	13	5	.4
JP–4		A1	0–13	Sheetwash-till	7.5YR 3/3	20	5	10	62	31	8	10.4
		A2	13–48	.....do.....	7.5YR 4/3	10	20	10	66	27	6	3.6
		2Bt	48–72	Till	7.5YR 8/1	20	10	10	72	20	9	.4
		2C	72–105+	.....do.....	7.5YR 8/0	20	15	10	81	15	4	.4

[1]Horizon nomenclature of Guthrie and Witty (1982) and Birkeland (1984).

[2]Particle size distribution of <2-mm fraction obtained by using sieve-pipette methods (for example, Carver, 1971) and a Sedigraph for some silt-clay fractions from which organic matter has been removed by Jackson's (1956) method. No samples contained carbonate.

[3]Determined by Walkley and Black's (1934) method.

[4]From center of units 2a and 2b at distance *m* (fig. 4).

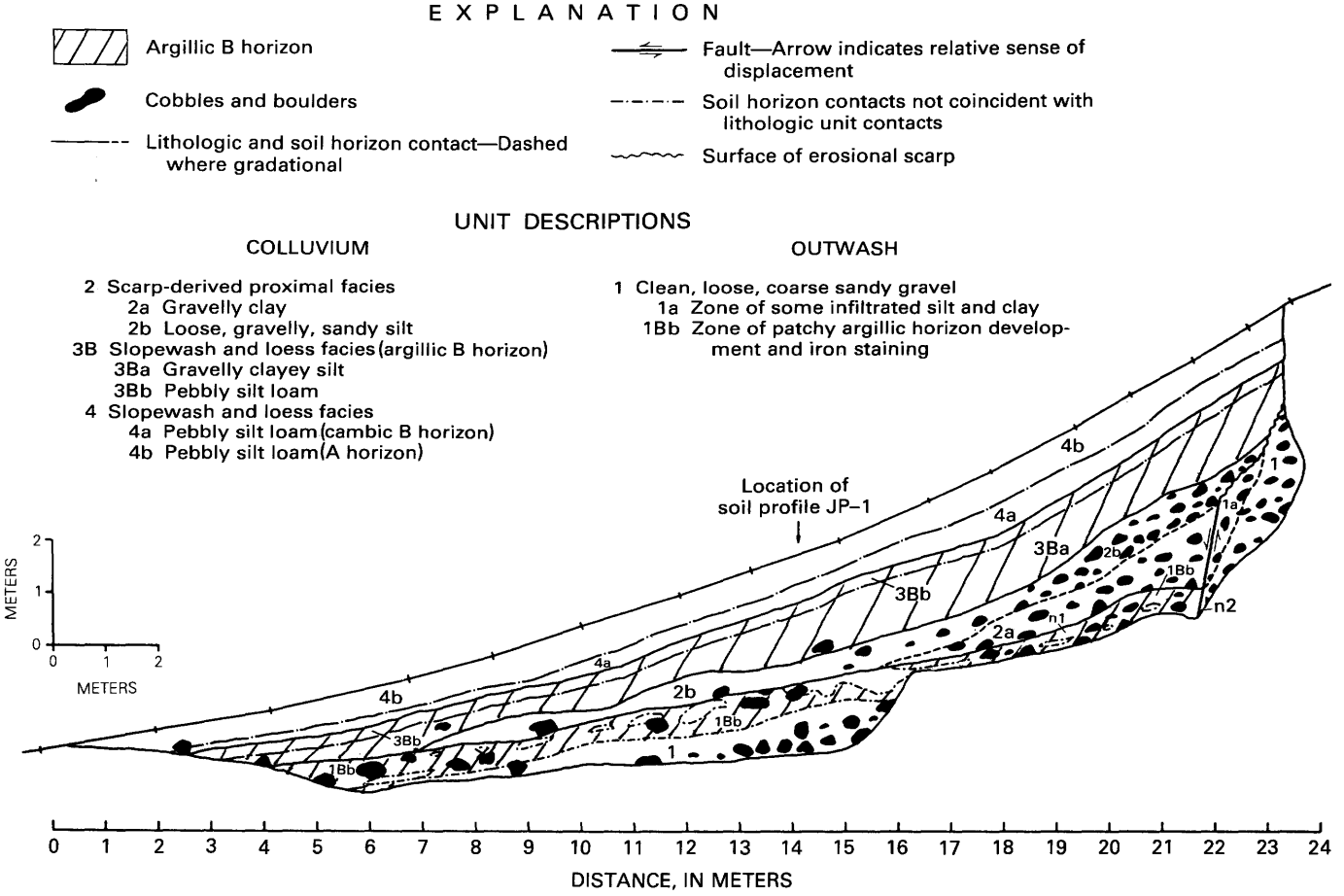

FIGURE 4.—Log of the eastern wall of the trench across the scarp of the James Peak fault (fig. 2). The segmented line at the top of the log is the central portion of topographic profile JP-1 measured across the site by using the methods of Bucknam and Anderson (1979). To trench as high as possible on the scarp, the trench was dug in two parts; the first part (0–12 m in distance) was backfilled before the second part (12–19 m in distance) was dug. Lowercase letters in unit symbols indicate sublithofacies, and B marks argillic B horizons. The lithology of the proximal colluvial wedges—units 2a and 2b—suggests that the scarp was formed by two surface-faulting events (see text).

1. Moraines and an extensive outwash fan were deposited on the northern flank of James Peak, probably during the Bull Lake glaciation (about 130–150 ka). Soils developed on stable areas of moraines and outwash, but gradual erosion prevented well-developed soils from forming on moraine crests. The length of time required to develop the reddish argillic B horizons on the outwash is difficult to estimate, partly because the soil north of the trench site (JP–2) appears to have been stripped. The fact that the argillic horizon and the fine-grained units overlying it are thin suggests that soil JP–2 has been eroded, perhaps by meltwater in braided outwash channels (which did not reach the trench site) during the later Pinedale glaciation. These horizons may have developed rapidly because of high rates of dust influx owing to the silt and clay from lake sediments exposed in Cache Valley to the north. Because the B horizons on these deposits are much more strongly developed than the B horizons on late Pinedale or Holocene deposits, these horizons must have taken at least a few tens of thousands of years to develop, perhaps as long as 70,000 years.
2. Surface faulting vertically displaced the outwash (unit 1, fig. 4) about 1.6 to 2.2 m down to the north. A proximal colluvial debris wedge (unit 2a, fig. 4), formed by spall, slump, and slopewash, rapidly buried the argillic horizon developed on the outwash (unit 1bB, fig. 4) and the lower part of the free face of the scarp. The source of the bouldery debris wedge, which has a matrix of silty clay (table 1), must have been the surface colluvium of similar lithology overlying the outwash on top of the scarp (not exposed in our trench). The uppermost part of unit 1bB near the fault is mapped as part of the soil developed on unit 1. But the thickening of the reddish clayey silt near the

top of unit 1bB (note 1, fig. 4) and the inclusion of reddish clayey peds in the matrix of less reddish clayey silt near the base of unit 2a suggest that material along the contact between units 1bB and 2a may be fragments of an argillic horizon eroded from the crest of the scarp immediately after the event. We infer that none of the loose, sandy outwash (unit 1, fig. 4) was exposed in the free face by this event; if it had been, the free face would have slumped almost immediately after faulting and contributed much coarse sand to the debris wedge. Equilibrium scarp degradation models at gently sloping sites suggest that the maximum fault displacement is about two times the maximum colluvial wedge thickness (for example, Nash, 1981). However, the steep slope above the site and the inferred active surface transport processes (discussed below) suggest that the amount of vertical displacement during this event was probably not much greater than the wedge thickness (1.6 m).

3. After the argillic horizons had formed and probably after the first fault event, soil development on the lower part of the outwash fan continued. However, the steep (20°–25°) slope of the fan above the trench site, the lack of well-developed B horizons on the proximal wedges, and the high clay content of surface colluvium above the scarp suggest that creep and solifluction may have been the dominant slope processes during periods of cold, moist climate (onset of Pinedale glaciation, about 75 ka?) during or after the deposition of the first proximal wedge. These processes may have eroded existing soils or prevented well-developed soils from forming at and above the site.
4. A second displacement event on the same fault moved unit 2a down against the outwash. The loose, sandy lithology of the proximal debris wedge (unit 2b, fig. 4) that was produced following this event indicates that some outwash was exposed in the free face in addition to the bouldery, clayey silt (not exposed in the trench) overlying the outwash. Erosion of the scarp following the first event also probably reduced the proportion of bouldery silt to outwash exposed in the free face during the second event and resulted in a sandy wedge. Slumping of the outwash in the lower part of the free face helped to spread loose debris downslope and buried the debris wedge from the first event. The loose debris produced a thin wedge (unit 2b, fig. 4) that extended farther downslope than the first wedge (unit 2a, fig. 4); this geometry is typical of debris wedges produced by the second and third events on multiple-event scarps (Ostenaa, 1984). Displacement during the second event is more difficult to estimate from the thickness of the debris wedge; it must be close to the difference between the total topographic displacement across the scarp and the displacement of the first event (4.2 m−(1.6–2.2 m)=2.0–2.6 m). We could not measure total throw because the top of the outwash unit in the footwall was not exposed in the trench. The lack of any evidence of soil development on the debris wedge resulting from the first event suggests that the two events may have occurred less than a few tens of thousands of years apart. However, the active surface processes on the steep fan (discussed earlier) could also have eroded a moderately developed soil or prevented one from forming. It is also possible that weak soil development near the top of wedge 2a is masked by later development of more strongly developed soils on units 2b and 3Ba (fig. 4). An alternate interpretation that must be considered is that both units 2a and 2b are proximal debris wedges produced following a single displacement event of about 4 m. This interpretation would explain the absence of (1) an abrupt contact between units 2a and 2b, (2) any evidence of soil development on unit 2a, and (3) deformation of the first debris wedge (unit 2a) during the second event. The apparent overlap of the time estimates for pre-first event and post-second event soil-forming intervals (discussed later) would also be explained by a single event. Clear evidence of shearing along the contact between units 2a and 1a was not observed, but three cobbles were imbricated parallel with the contact near the base of unit 1a, and the outwash is so unconsolidated that evidence of shearing may not have been preserved. Possibly, unit 1a is a fissure that filled with outwash that slumped from the free face after a second event. In any case, the stratigraphic relations near the fault show that most of unit 2a must have been deposited immediately after faulting, and its lithology shows that this unit was derived from units that contained little sand. Because we find it difficult to explain how a thick proximal debris wedge could be deposited adjacent to an almost vertical free face of loose, sandy outwash several meters high in such a way that the outwash contributed no sediment to the wedge, we favor a two-event fault history. In addition, 2-m displacement events are much more typical of faults in the region, even faults that are much longer than the James Peak fault (for example, Schwartz and Coppersmith, 1984).
5. A silty colluvial wedge (unit 3B, fig. 4) was deposited over the proximal debris wedges by wash erosion of the scarp crest and by rill and wash transport of fines from above the site. The thickness and high silt content of the wedge (table 1) suggest that it has a strong eolian component, probably owing to exposed lake sediments in Cache Valley. As the deposition

rate of the colluvial wedge decreased, B horizon development in the upper part of the wedge became more distinct and culminated in a 122-cm-thick argillic horizon (table 1) on the wedge. Because of its position on the scarp slope, this soil is not directly comparable to soils in more stable landscape positions whose age is better known. We interpret this soil as forming in a climate not greatly different from the present; thus, it must either predate the main Pinedale glaciation (18–25 ka) or postdate the fall of Lake Bonneville from its high stand (15 ka) (Scott and others, 1983). The total amount of clay in this soil (9 g/cm^2) in comparison with regional rates of clay accumulation (for example, Colman and others, 1988) and most other soil indices (fig. 3) for this part of the soil on unit 3 suggest an age as great as 100 to 150 ka because these horizons are so thick. However, the limited soil reddening and weak B horizon structure, the probable high rate of dust influx during part of the history of the site, and the likelihood that some of unit 3 is derived from clay-rich soils upslope all suggest a much younger age. Thus, we estimate that this soil, which postdates both fault events, developed over a period of 30,000 to 70,000 years.

6. Finally, an episode of rapid slopewash deposition, probably marked by some eolian influx, produced a silty colluvial unit (unit 4, fig. 4) that is very similar to unit 3. A weak cambic B horizon (unit 4a) and a thick, silty A horizon (unit 4b, fig. 4) on this unit indicate a Holocene age (soil JP–1a, fig. 3). Deposition during the warmer and probably drier Altithermal of the middle Holocene (Baker, 1983) is likely.

SLIP RATES AND RECURRENCE

The topographic profile across the scarp at the trench site (fig. 4) shows that the outwash, most likely about 140 ka, is displaced about 4.2 m for an average late Quaternary vertical slip rate of 0.03 mm/yr on the James Peak fault.

Because the soils developed on the outwash and on the colluvium overlying the faulting-related wedges provide only maximum and minimum age estimates for the wedges, the true intervals of time between surface-faulting events are difficult to estimate. Although displacement data for each of the two fault events are uncertain, scarp erosion models that consider the position of the scarp at the foot of a steep slope, the thickness of the first colluvial wedge, and the volumes and lithologies of both wedges suggest that the second event may have been larger than the first. We estimate average displacements of about 1.8+0.4/−0.2 m for the first event and 2.4+0.8/−0.6 m for the second event. The reddish argillic horizon on the outwash beneath the colluvial wedges probably required at least several tens of thousands of years (we assume more than 30,000 but perhaps even 70,000 years) to develop before burial. This well-developed soil adjacent to the fault shows that no significant displacement occurred on the fault for a long period of time after outwash deposition ceased. Thus, the first event could have occurred as early as 110 ka (140–30 ka) or as late as 70 ka (140–70 ka). The thick argillic horizon on unit 3B (fig. 4), which postdates the second displacement event, also suggests a soil-forming interval of at least 30,000 and perhaps 70,000 years. Given these broad constraints, a time interval of 80,000 years (110–30 ka) is available in which the two events could have occurred. If we take the mean of possible times at which each event occurred (first event 90 ka, second event 50 ka), the events are separated by 40,000 years (90–50 ka). Because the maximum estimates of the length of the soil-forming intervals following each event overlap, no minimum estimate of the length of this period can be made. If the two events were separated by 40,000 years, the recurrence interval between these events and earlier and future events would be more than 50,000 years (50,000+40,000+50,000=140,000 years). Thus, the average recurrence interval for the two events since 140 ka is at least 50,000 years, but the lack of a soil between the two debris wedges suggests nonuniform recurrence. However, if there was only one event (discussed earlier), it probably occurred about 70 ka.

RELATIONSHIP TO THE EAST CACHE FAULT

The location of the James Peak fault at the southern end of the East Cache fault suggests that their surface-rupture histories may be related. Blau's (1975) mapping showed that the East Cache fault is abruptly terminated at its high-angle intersection with the James Peak fault (fig. 2), because no north-trending fault extends up Wellsville Creek. The James Peak fault is also oriented at near-right angles to the contemporary regional extensional stress field (Zoback and Zoback, 1980). However, portions of the Wasatch fault that intersect at high angles have ruptured concurrently during the Holocene (Nelson and Personius, 1990), and similar fault patterns are found along late Quaternary fault zones elsewhere in the Basin and Range (for example, Wallace, 1979). The morphology of the bedrock scarps on the Broadmouth Canyon faults (fig. 2) does not suggest recurrent late Quaternary displacement but also does not preclude some Quaternary slip. These scarps trend southwesterly, nearly parallel to the southern part of the East Cache fault. We speculate that the Broadmouth Canyon faults may be the southernmost part of a Quaternary rupture zone encompassing all three faults.

Some of the larger surface-displacement events on the James Peak fault may have ruptured part of the East Cache fault. Empirical relations between the amount of surface displacement and fault rupture length (Bonilla and others, 1984) suggest that more than 7 km of surface faulting is associated with events that produce the 2 m of displacement that we infer from our trench stratigraphy. On the Wasatch fault, surface displacements of 1.6 to 2.6 m are thought to be associated with ruptures on fault segments 30 to 60 km long (Schwartz and Coppersmith, 1984). The 1983 Borah Peak, Idaho, earthquake had a maximum displacement of about 2.5 m and a total rupture length of 36±3 km (Crone and Machette, 1984). Thus, even if small, unrecognized ruptures occurred on the Broadmouth Canyon faults during the events recorded at James Peak, at least 15 to 20 km of the southern part of the East Cache fault may also have ruptured. Near the southern end of the East Cache fault, Swan and others (1983) could not determine the age of most recent displacement because the main trace of the fault is well above the Bonneville shoreline at the range front and because scarps along the fault are almost completely masked by younger (post-Provo shoreline, younger than 14 ka) (Scott and others, 1983) alluvial fans. Mullens and Izett (1964) also did not find evidence of surface faulting in the Paradise area (fig. 1). Thus, any scarps along the East Cache fault related to the James Peak events are probably covered by younger deposits. Farther north along the East Cache fault near Logan, Utah (fig. 1), Swan and others (1983) concluded that two 1- to 2-m post-Bonneville surface-displacement events have occurred on this part of the East Cache fault for a slip rate of 0.10 to 0.2 mm/yr for the last 15,000 years. The first event occurred between the high stand of Lake Bonneville (15–16 ka) (Scott and others, 1983) and its catastrophic fall to the Provo shoreline (14–15 ka). The second event postdates the Provo level of the lake and predates alluvial fans thought to be about 6 to 10 ka. Excavations at several places along the East Cache fault have also revealed post-Bonneville displacements (B.N. Kaliser, oral commun., 1981), but these investigations are undocumented. Thus, the average recurrence interval on the section of the East Cache fault marked by the post-Provo scarps near Logan since the high stand of Lake Bonneville appears to be about 7,000 years, but the actual interval between events could be as short as 2,000 to 3,000 years (Swan and others, 1983).

Estimates of the thickness of basin fill in southern Cache Valley (Zoback, 1983) and topographic relief on the bedrock escarpment of the East Cache fault, both of which decrease south of Logan, suggest that total displacement on the fault also diminishes to the south. Late Pleistocene scarps are mapped along the fault at least as far south as Blacksmith Fork Canyon (Cluff and others, 1974; Swan and others, 1983), but Swan and others (1983) speculated that the rupture near Logan may die out south of Providence Canyon.

Site-specific fault slip data indicate differing histories for the East Cache and James Peak faults, but little reliable information on the southern half of the East Cache fault is available to distinguish among several possible relations. One possibility is that displacements on the James Peak fault occur near the end of surface ruptures produced by very large but infrequent (average recurrence interval of more than 50,000 years) earthquakes that break a large part (more than 50 km) of the East Cache fault. The length of these ruptures and the fact that the amount of displacement near the center is likely to be greater than that near the end of the rupture segment indicate that these earthquakes would be as large as or larger than those inferred on the central segments of the Wasatch fault (Bonilla and others, 1984; Schwartz and Coppersmith, 1984), a supposition that seems very unlikely. Alternatively, the East Cache fault may consist of unrecognized segments, the recurrence interval on the southern part of the fault (and the James Peak fault) being an order of magnitude longer than that on the East Cache fault near Logan. The southern part of the East Cache fault could also have a slip rate and a recurrence interval similar to those of the central part of the fault; if displacements were occurring near the base of the facets along the range front, on faults buried by the post-Provo alluvial fans along the range front, or on faults basinward of the alluvial fans, scarps on these unrecognized faults would be either buried or quickly eroded.

Although the apparent slip rates on the East Cache and James Peak faults differ by a factor of 3 to 6, it should be emphasized that the ages of the datums used to estimate those rates differ by almost an order of magnitude. A similar situation is reported by Machette and others (this volume), whose mapping suggests that the high slip rates and short recurrence intervals on the central segments of the Wasatch fault zone may apply only to the latest Pleistocene and Holocene; longer term, late Quaternary rates appear to be much lower, closer to those estimated for other faults in the region (for example, Nelson and VanArsdale, 1986; Sullivan and Nelson, this volume). The rapid changes in subsurface pore pressures and the isostatic loading and unloading accompanying the rise and fall of Lake Bonneville about 15 ka may have triggered many earthquakes on the Wasatch and East Cache faults and resulted in a latest Pleistocene and Holocene recurrence rate several times larger than the late Quaternary rate (Swan and others, 1983; Machette and others, this volume). Thus, we speculate that late Quaternary slip rates on the East Cache fault

and the James Peak fault, and perhaps recurrence intervals as well, do not differ nearly as much as the apparent slip rates suggest.

CONCLUSIONS

Two surface-displacement events of about 2 m each have occurred on the James Peak fault in the last 140 ka, indicative of a late Quaternary slip rate of about 0.03 mm/yr. Surface-faulting recurrence intervals are difficult to estimate because of poor age control, but the average interval between events is at least 50,000 years. The fault may be a westerly splay of the East Cache fault rather than a separate valley-bounding fault like the ones to the south. The lack of detailed slip and recurrence data from the southern half of the East Cache fault precludes determining whether the central part of the East Cache fault behaves independent of the southernmost part of the fault and of the James Peak fault or whether all parts of both faults have had a similar late Quaternary history.

REFERENCES CITED

Anderson, L.W., and Miller, D.G., 1979, Quaternary fault map of Utah: Long Beach, Calif., Fugro, Inc., 39 p.

Baker, R.G., 1983, Holocene vegetational history of the western United States, *in* Wright, H.E., Jr., ed., The Holocene, *in* Wright, H.E., Jr., ed., Late Quaternary environments of the United States: Minneapolis, University of Minnesota Press, v. 2, p. 109–127.

Bilzi, A.F., and Ciolkosz, E.J., 1977, Time as a factor in the genesis of four soils developed in recent alluvium in Pennsylvania: Soil Science Society of America Journal, v. 41, p. 122–127.

Birkeland, P.W., 1984, Soils and geomorphology: New York, Oxford University Press, 372 p.

Birkeland, P.W., Colman, S.M., Burke, R.M., Shroba, R.R., and Meierding, T.C., 1979, Nomenclature of alpine glacial deposits—Or what's in a name?: Geology, v. 7, p. 532–536.

Bjorkland, C.J., and McGreevy, C.J., 1971, Geologic map and section of Cache Valley, Utah and Idaho: Utah Department of Natural Resources Publication 36, 1 pl., scale 1:180,000.

Blau, J.C., 1975, Geology of the southern part of the James Peak quadrangle: Logan, Utah State University, unpublished M.Sci. thesis, 55 p.

Bonilla, M.G., Mark, R.K., and Lienkaemper, J.J., 1984, Statistical relations among earthquake magnitude, surface rupture length, and surface fault displacement: Bulletin of the Seismological Society of America, v. 74, p. 2379–2411.

Bucknam, R.C., and Anderson, R.E., 1979, Estimation of fault-scarp ages from a scarp-height–slope-angle relationship: Geology, v. 7, p. 11–14.

Bull, W.B., and McFadden, L.D., 1977, Tectonic geomorphology north and south of the Garlock fault, California, *in* Doehring, D.O., ed., Geomorphology in arid regions: Annual Geomorphology Symposium, 8th, Binghamton, N.Y., 1977, Proceedings, p. 115–138.

Carver, R.E., ed., 1971, Procedures in sedimentary petrology: New York, Wiley-Interscience, 653 p.

Cluff, L.S., Glass, C.E., and Brogan, G.E., 1974, Investigation and evaluation of the Wasatch fault north of Brigham City and Cache Valley faults, Utah and Idaho; A guide to land use planning with recommendations for seismic safety: Oakland, Calif., Woodward-Lundgren and Associates, report to U.S. Geological Survey under contract 14–08–001–13665, 146 p.

Colman, S.M., and Pierce, K.L., 1981, Weathering rinds on andesitic and basaltic stones as a Quaternary age indicator, Western United States: U.S. Geological Survey Professional Paper 1210, 56 p.

———1986, Glacial sequence near McCall, Idaho: Weathering rinds, soil development, morphology, and other relative-age criteria: Quaternary Research, v. 25, p. 25–42.

Colman, S.M., Choquette, A.F., and Hawkins, F.F., 1988, Physical, soil, and paleomagnetic stratigraphy of the upper Cenozoic sediments in Fisher Valley, southeastern Utah: U.S. Geological Survey Bulletin 1686, 33 p.

Crittenden, M.D., Jr., 1972, Willard thrust and Cache allochthon, Utah: Geological Society of America Bulletin, v. 83, p. 2871–2880.

Crittenden, M.D., Jr., and Sorensen, M.L., 1985a, Geologic map of the North Ogden quadrangle and part of the Ogden and Plain City quadrangles, Box Elder and Weber Counties, Utah: U.S. Geological Survey Miscellaneous Investigations Map I–1606, 1 pl., scale 1:24,000.

———1985b, Geologic map of the Mantua quadrangle and part of the Willard quadrangle, Box Elder, Weber, and Cache Counties, Utah: U.S. Geological Survey Miscellaneous Investigations Map I–1605, 1 pl., scale 1:24,000.

Crone, A.J., and Machette, M.N., 1984, Surface faulting accompanying the Borah Peak earthquake, central Idaho: Geology, v. 12, p. 664–667.

Davis, F.D., 1983, Geologic map of the central Wasatch Front, Utah: Utah Geological and Mineral Survey Map 54–A, 2 pls., scale 1:100,000.

Gilbert, G.K., 1928, Studies of Basin and Range structure: U.S. Geological Survey Professional Paper 153, 89 p.

Guthrie, R.L., and Witty, J.E., 1982, New designations for soil horizons and layers and the new Soil Survey Manual: Soil Science Society of America Journal, v. 46, p. 443–444.

Hamblin, W.K., 1976, Patterns of displacement along the Wasatch fault: Geology, v. 4, p. 619–622.

Harden, J.W., 1982, A quantitative index of soil development from field descriptions—Examples from a chronosequence in central California: Geoderma, v. 28, p. 1–28.

Harden, J.W., and Taylor, E.M., 1983, A quantitative comparison of soil development in four climatic regimes: Quaternary Research, v. 20, p. 342–359.

Hintze, L.F., 1980, Geologic map of Utah: Utah Geological and Mineral Survey, 2 pls., scale 1:500,000.

Jackson, M.L., 1956, Soil chemical analysis, advanced course: Madison, University of Wisconsin, Department of Soil Science, unpublished laboratory manual, 656 p.

King, H.D., 1965, Paleozoic stratigraphy of the James Peak quadrangle, Utah: Logan, Utah State University, unpublished M.Sci. thesis, 47 p.

Machette, M.N., 1985, Calcic soils of the southwestern United States, *in* Weide, D.L., ed., Soils and Quaternary geology of the southwestern United States: Geological Society of America Special Paper 203, p. 1–21.

Madole, R.F., 1976, Glacial geology of the Front Range, Colorado, *in* Mahaney, W.C., ed., Quaternary stratigraphy of North America: Stroudsburg, Pa., Dowden, Hutchinson, and Ross, p. 297–318.

Mullens, T.E., and Izett, G.A., 1964, Geology of the Paradise quadrangle, Utah: U.S. Geological Survey Geologic Quadrangle Map GQ–185, 1 pl., scale 1:24,000.

Nakata, J.K., Wentworth, C.M., and Machette, M.N., 1982, Quaternary fault map of the Basin and Range and Rio Grande Rift provinces, Western United States: U.S. Geological Survey Open-File Report 82–579, 2 pls., scale 1:2,500,000.

Nash, D.B., 1981, Fault—A Fortran program for modeling the degradation of active normal fault scarps: Computers and Geosciences, v. 7, p. 249–266.

Nelson, A.R., and Krinsky, C.K., 1982, Late Cenozoic history of the upper Weber and Provo Rivers, NE. Utah [abs.]: Geological Society of America Abstracts with Programs, v. 14, no. 3, p. 344.

Nelson, A.R., and Personius, S.F., 1990, Preliminary surficial geologic map of the Weber segment, Wasatch fault zone, Weber and Davis Counties, Utah: U.S. Geological Survey Miscellaneous Field Studies Map MF–2132, scale 1:50,000.

Nelson, A.R., and VanArsdale, R.B., 1986, Recurrent late Quaternary movement on the Strawberry normal fault, Basin and Range-Colorado Plateau transition zone, Utah: Neotectonics, v. 1, p. 1–30.

Ostenaa, D.A., 1984, Relationships affecting estimates of surface fault displacements based on scarp-derived colluvial deposits [abs.]: Geological Society of America Abstracts with Programs, v. 16, no. 5, p. 327.

Peterson, D.L., 1974, Bouger gravity map of part of the northern Lake Bonneville Basin, Utah and Idaho: U.S. Geological Survey Miscellaneous Field Studies Map MF–627, 1 pl., scale 1:250,000.

Pierce, K.L., 1979, History and dynamics of glaciation in the northern Yellowstone National Park area: U.S. Geological Survey Professional Paper 729–F, 90 p.

Pierce, K.L., Obradovich, J.D., and Friedman, I., 1976, Obsidian hydration dating and correlation of Bull Lake and Pinedale glaciations near West Yellowstone, Montana: Geological Society of America Bulletin, v. 87, p. 703–710.

Porter, S.C., Pierce, K.L., and Hamilton, T.D., 1983, Late Wisconsin mountain glaciation in the western United States, *in* Porter, S.C., ed., The Late Pleistocene, *in* Wright, H.E., Jr., ed., Late Quaternary environments of the United States: Minneapolis, University of Minnesota Press, v. 1, p. 71–111.

Scott, W.E., McCoy, W.D., Shroba, R.R., and Rubin, M., 1983, Reinterpretation of the exposed record of the last two cycles of Lake Bonneville, western United States: Quaternary Research, v. 20, p. 241–265.

Schwartz, D.P., and Coppersmith, K.J., 1984, Fault behavior and characteristic earthquakes—Examples from the Wasatch and San Andreas fault zones: Journal of Geophysical Research, v. 89, no. B7, p. 5681–5698.

Shroba, R.R., 1980, Influence of parent material, climate, and time on soils formed in Bonneville-shoreline and younger deposits near Salt Lake City and Ogden, Utah [abs.]: Geological Society of America Abstracts with Programs, v. 12, no. 6, p. 304.

Shroba, R.R., and Birkeland, P.W., 1983, Trends in late Quaternary soil development in the Rocky Mountains and Sierra Nevada of the western United States, *in* Porter, S.C., ed., The Late Pleistocene, *in* Wright, H.E., Jr., ed., Late Quaternary environments of the United States: Minneapolis, University of Minnesota Press, v. 1, p. 145–156.

Smith, R.B., and Bruhn, R.L., 1984, Intraplate extensional tectonics of the eastern Basin and Range—Inferences on structural style from seismic reflection data, regional tectonics, and thermal-mechanical models of brittle-ductile deformation: Journal of Geophysical Research, v. 89, no. B7, p. 5733–5762.

Stanley, W.D., 1972, Geophysical study of unconsolidated sediments and basin structure in Cache Valley, Utah and Idaho: Geological Society of America Bulletin, v. 83, p. 1817–1830.

Sullivan, J.T., and Nelson, A.R., 1983, Late Cenozoic faulting in Heber and Keetley valleys, northeastern Utah, *in* Gurgel, K.D., ed., Guidebook, pt. IV, *in* Crone, A.J., ed., Field trip 5; Paleoseismicity along the Wasatch front and adjacent areas, central Utah: Geologic excursions in neotectonics and engineering geology in Utah: Utah Geological and Mineralogical Survey Special Studies 62, p. 55–61.

Sullivan, J.T., Nelson, A.R., LaForge, R.C., Wood, C.K., and Hansen, R.A., 1988, Central Utah regional seismotectonic study for USBR dams in the Wasatch Mountains: U.S. Bureau of Reclamation Seismotectonic Report 88–5, 338 p.

Swan, F.H., III, Hanson, K.L., Schwartz, D.P., and Black, J.H., 1983, Study of earthquake recurrence intervals on the Wasatch fault, Utah: San Francisco, Woodward-Clyde Consultants, 8th semiannual technical report to U.S. Geological Survey under contract 14–08–0001–19842, 36 p.

Walkley, A., and Black, I.A., 1934, An examination of the Degtjareff method for determining soil organic matter, and a proposed modification of the chromic acid titration method: Soil Science, v. 34, p. 29–38.

Wallace, R.E., 1979, Map of young fault scarps related to earthquakes in north-central Nevada: U.S. Geological Survey Open-File Report 79–1554, 2 pls., scale 1:125,000.

Zoback, M.L., 1983, Structure and Cenozoic tectonism along the Wasatch fault zone, Utah, *in* Miller, D.M., Todd, V.R., and Howard, K.A., eds., Tectonic and stratigraphic studies in the eastern Great Basin: Geological Society of America Memoir 157, p. 3–29.

Zoback, M.L., and Zoback, M.D., 1980, State of stress in the conterminous United States: Journal of Geophysical Research, v. 85, no. B11, p. 6113–6156.

SELECTED SERIES OF U.S. GEOLOGICAL SURVEY PUBLICATIONS

Periodicals

Earthquakes & Volcanoes (issued bimonthly).
Preliminary Determination of Epicenters (issued monthly).

Technical Books and Reports

Professional Papers are mainly comprehensive scientific reports of wide and lasting interest and importance to professional scientists and engineers. Included are reports on the results of resource studies and of topographic, hydrologic, and geologic investigations. They also include collections of related papers addressing different aspects of a single scientific topic.

Bulletins contain significant data and interpretations that are of lasting scientific interest but are generally more limited in scope or geographic coverage than Professional Papers. They include the results of resource studies and of geologic and topographic investigations, as well as collections of short papers related to a specific topic.

Water-Supply Papers are comprehensive reports that present significant interpretive results of hydrologic investigations of wide interest to professional geologists, hydrologists, and engineers. The series covers investigations in all phases of hydrology, including hydrogeology, availability of water, quality of water, and use of water.

Circulars present administrative information or important scientific information of wide popular interest in a format designed for distribution at no cost to the public. Information is usually of short-term interest.

Water-Resources Investigations Reports are papers of an interpretive nature made available to the public outside the formal USGS publications series. Copies are reproduced on request unlike formal USGS publications, and they are also available for public inspection at depositories indicated in USGS catalogs.

Open-File Reports include unpublished manuscript reports, maps, and other material that are made available for public consultation at depositories. They are a nonpermanent form of publication that may be cited in other publications as sources of information.

Maps

Geologic Quadrangle Maps are multicolor geologic maps on topographic bases in 7.5- or 15-minute quadrangle formats (scales mainly 1:24,000 or 1:62,500) showing bedrock, surficial, or engineering geology. Maps generally include brief texts; some maps include structure and columnar sections only.

Geophysical Investigations Maps are on topographic or planimetric bases at various scales; they show results of surveys using geophysical techniques, such as gravity, magnetic, seismic, or radioactivity, which reflect subsurface structures that are of economic or geologic significance. Many maps include correlations with the geology.

Miscellaneous Investigations Series Maps are on planimetric or topographic bases of regular and irregular areas at various scales; they present a wide variety of format and subject matter. The series also includes 7.5-minute quadrangle photogeologic maps on planimetric bases that show geology as interpreted from aerial photographs. Series also includes maps of Mars and the Moon.

Coal Investigations Maps are geologic maps on topographic or planimetric bases at various scales showing bedrock or surficial geology, stratigraphy, and structural relations in certain coal-resource areas.

Oil and Gas Investigations Charts show stratigraphic information for certain oil and gas fields and other areas having petroleum potential.

Miscellaneous Field Studies Maps are multicolor or black-and-white maps on topographic or planimetric bases for quadrangle or irregular areas at various scales. Pre-1971 maps show bedrock geology in relation to specific mining or mineral-deposit problems; post-1971 maps are primarily black-and-white maps on various subjects such as environmental studies or wilderness mineral investigations.

Hydrologic Investigations Atlases are multicolored or black-and-white maps on topographic or planimetric bases presenting a wide range of geohydrologic data of both regular and irregular areas; principal scale is 1:24,000, and regional studies are at 1:250,000 scale or smaller.

Catalogs

Permanent catalogs, as well as some others, giving comprehensive listings of U.S. Geological Survey publications are available under the conditions indicated below from the U.S. Geological Survey, Book and Open-File Report Sales, Federal Center, Box 25425, Denver, CO 80225. (See latest Price and Availability List.)

"Publications of the Geological Survey, 1879–1961" may be purchased by mail and over the counter in paperback book form and as a set of microfiche.

"Publications of the Geological Survey, 1962–1970" may be purchased by mail and over the counter in paperback book form and as a set of microfiche.

"Publications of the U.S. Geological Survey, 1971–1981" may be purchased by mail and over the counter in paperback book form (two volumes, publications listing and index) and as a set of microfiche.

Supplements for 1982, 1983, 1984, 1985, 1986, and for subsequent years since the last permanent catalog may be purchased by mail and over the counter in paperback book form.

State catalogs, "List of U.S. Geological Survey Geologic and Water-Supply Reports and Maps For (State)," may be purchased by mail and over the counter in paperback booklet form only.

"Price and Availability List of U.S. Geological Survey Publications," issued annually, is available free of charge in paperback booklet form only.

Selected copies of a monthly catalog "New Publications of the U.S. Geological Survey" are available free of charge by mail or may be obtained over the counter in paperback booklet form only. Those wishing a free subscription to the monthly catalog "New Publications of the U.S. Geological Survey" should write to the U.S. Geological Survey, 582 National Center, Reston, VA 22092.

Note.—Prices of Government publications listed in older catalogs, announcements, and publications may be incorrect. Therefore, the prices charged may differ from the prices in catalogs, announcements, and publications.


U. S. DEPARTMENT OF THE INTERIOR
March 3, 1849